Lawrence Berkeley National Laboratory

Title
DECOVALEX-THMC Task D: Long-Term Permeability/Porosity Changes in the EDZ and Near Field
due to THM and THC Processes in Volcanic and Crystaline-Bentonite Systems, Status Report October
2005

Permalink
https://escholarship.org/uc/item/5g66807g

Authors
Birkholzer, J.
Rutqvist, J.
Sonnenthal, E.
et al.

Publication Date
2005-11-01
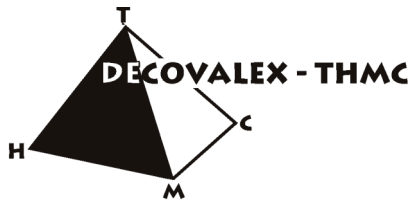
DECOVALEX-THMC Task D:

Long-Term Permeability/Porosity Changes in the EDZ and Near Field due to THM and THC Processes in Volcanic and Crystalline-Bentonite Systems

October 2005

Authors:

J. Birkholzer (Contact), J. Rutqvist, E. Sonnenthal
Lawrence Berkeley National Laboratory, USA

and D. Barr
Office of Repository Development, DOE, USA

With Contributions From:

J. Birkholzer, J. Rutqvist, E. Sonnenthal, LBNL, USA
Y. Oda, T. Fujita, M. Chijimatsu, JAEA, Japan
M. Xie, W. Wang, T. Nowak, H. Kunz, H. Shao, O. Kolditz, BGR, Germany
L. Quansheng, Z. Chengyuan, L. Xiaoyan, CAS, China

Berkeley, October 31, 2005

I

Summary

The DECOVALEX project is an international cooperative project initiated by SKI, the Swedish Nuclear Power Inspectorate, with participation of about 10 international organizations. The name DECOVALEX stands for **DE**velopment of **CO**upled models and their **VAL**idation against **Ex**periments. The general goal of this project is to encourage multidisciplinary interactive and cooperative research on modeling coupled processes in geologic formations in support of the performance assessment for underground storage of radioactive waste.

Three multi-year project stages of DECOVALEX have been completed in the past decade, mainly focusing on coupled thermal-hydrological-mechanical processes. Currently, a fourth three-year project stage of DECOVALEX is under way, referred to as DECOVALEX-THMC. THMC stands for **T**hermal, **H**ydrological, **M**echanical, and **C**hemical processes. The new project stage aims at expanding the traditional geomechanical scope of the previous DECOVALEX project stages by incorporating geochemical processes important for repository performance. The U.S. Department of Energy (DOE) leads Task D of the new DECOVALEX phase, entitled "Long-term Permeability/Porosity Changes in the EDZ and Near Field due to THC and THM Processes for Volcanic and Crystalline-Bentonite Systems." In its leadership role for Task D, DOE coordinates and sets the direction for the cooperative research activities of the international research teams engaged in Task D.

The research program developed for Task D of DECOVALEX-THMC involves geomechanical and geochemical research areas. THM and THC processes may lead to changes in hydrological properties that are important for performance because the flow processes in the vicinity of emplacement tunnels will be altered from their initial state. Some of these changes can be permanent (irreversible), in which case they persist after the thermal conditions have returned to ambient; i.e., they will affect the entire regulatory compliance period. Geochemical processes also affect the water and gas chemistry close to the waste packages, which are relevant for waste package corrosion, buffer stability, and radionuclide transport.

Research teams participating in Task D evaluate long-term THM and THC processes in two generic geologic repositories for radioactive waste, with the ultimate goal of determining the impact of geomechanical and geochemical processes on hydrologic properties and flow patterns. The two repositories are simplified representations of possible repository sites and emplacement conditions considered by the participating countries. One repository is a simplified model of the Yucca Mountain site, featuring a deep unsaturated volcanic rock formation with emplacement in open gas-filled tunnels. The second repository is located in saturated crystalline rock; emplacement tunnels are backfilled with a bentonite buffer material.

During the past year, four international research teams from China, Germany, Japan, and USA have started research activities for the geomechanical and geochemical scenarios of Task D. As shown in the table, these teams are using different simulators with different model capabilities. Thus, good agreement of model results between the different teams

(that use different simulators) would provide valuable supporting evidence for the validity of the various predictive models simulating THM and THC processes. Since all research teams model the same task configuration, research results from the participating teams can be compared.

Numerical simulator	Coupling	Research Team	Mechanical/ chemical model	Hydraulic and transport model
TOUGH-FLAC	THM	DOE/LBNL	Elastic Elastoplastic Viscoplastic	Single or dual continuum; multiphase liquid and gas flow
ROCMAS	THM	DOE/LBNL	Elastic Elastoplastic Viscoplastic	Single continuum; unsaturated liquid flow; thermal vapor diffusion
GeoSys/ Rockflow	THM	BGR Center for Applied Geosciences	Elastic Elastoplastic Viscoplastic	Single continuum; unsaturated liquid flow; thermal vapor diffusion
FRT-THM	THM	CAS Chinese Academy of Sciences	Elastic Elastoplastic Viscoplastic	Single continuum; unsaturated liquid flow; thermal vapor diffusion
THAMES	THM	JAEA Japan Atomic Energy Agency*	Elastic Elastoplastic Viscoplastic	Single continuum; unsaturated liquid flow; thermal vapor diffusion
TOUGHREACT	THC	DOE/LBNL	Equilibrium and kinetic reactions, using HKF activity model	Single or dual continuum; multiphase liquid and gas flow; advection/ diffusion of total concentrations (sequential)
GeoSys/ Rockflow with PHREEQC	THC	BGR Center for Applied Geosciences	PHREEQC	Single continuum; unsaturated liquid flow; thermal vapor diffusion; advection/ diffusion of total concentrations (sequential)
COUPLYS with THAMES, Dtransu-3D-EL and PHREEQC	THMC	JAEA Japan Atomic Energy Agency*	PHREEQC	Single continuum; unsaturated liquid flow; thermal vapor diffusion; advection/ diffusion of total concentrations (sequential)

* The Japanese organization was recently renamed from JNC to JAEA. We have not been able to update the report parts accordingly; thus the text and figure references in this report still use the old name JNC.

The research work is performed in a collaborative manner with close interaction between the international research teams during meetings, visits, via email, and per telephone. This close collaboration among international top scientists and engineers is one of the major benefits from participation in DECOVALEX-THMC. First, interaction with top international scientists helps to further the understanding of geomechanical and geochemical processes related to geologic storage of radioactive waste. Second, the cooperative research work conducted in the field of THMC modeling provides valuable peer-review of the modeling analyses in this field.

The international research teams involved in Task D have made significant progress during the past year. At the current project stage, the geomechanical and geochemical modeling studies are conducted separately. (In later stages, the separate THM and THC model analyses may be integrated to a fully coupled geomechanical and geochemical analysis.) The teams working on THM processes finalized the model development work, and all four teams presented results of the first modeling phase (assuming simplified geomechanical processes). Comparison of these results indicates a good overall agreement between the research teams (see example for comparative evaluation in below figure). The research teams participating in the geochemical tasks have mostly been working on code and model development during the last year. Preliminary simulation results showed good agreement for a simplified geochemical system. Results from both geomechanical and geochemical simulations provide a good basis for adding another layer of complexity in the next project phases, e.g., evaluating the changes in hydrological processes due to geomechanical and geochemical changes, developing alternative model approaches, and estimating conceptual as well as data uncertainties.

This status report summarizes the research activities conducted within Task D of the international DECOVALEX project (status October 2005). Additional information is provided in the attached CD, which includes various appendices. The appendices comprise a detailed description of the DECOVALEX THMC Task D definition, three meeting summaries from workshops in Kunming, Berkeley, and Ottawa, as well as separate status reports on research results provided by the participating research teams. To bring out similarities and discrepancies, the LBNL research team has conducted a comparative evaluation of all status reports with regards to the conceptual models used and the simulation results. This comparative evaluation is provided in Sections 4 and 5 of this report.

Summary (in Swedish)

To be added.

TABLE OF CONTENTS

APPENDICES

(provided in attached CD)

Appendix A: Draft Description for DECOVALEX THMC Task D (Status August 2005)

Appendix B: Meeting Summaries for Task Force Meetings in Kunming, China,
February 20, 2005, Berkeley, CA, July 21-22, 2005, and Ottawa, Canada,
October 4, 2005

Appendix C: Status Report for D_THM DOE Team

Appendix D: Status Report for D_THM JNC Team (Japan)

Appendix E: Status Report for D_THM BGR Team (Germany)

Appendix F: Status Report for D_THM CAS Team (China)

Appendix G: Status Report for D_THC DOE Team

Appendix H: Status Report for D_THC JNC Team (Japan)

Appendix I: Status Report for D_THC BGR Team (Germany)

FIGURES

FIGURES (Continued)

TABLES

1. INTRODUCTION

This status report summarizes the research activities of several international research teams with respect to Task D of the international DECOVALEX project. The DECOVALEX project is an international cooperative project initiated by SKI, the Swedish Nuclear Power Inspectorate, with participation of several international organizations. The name DECOVALEX stands for **DE**velopment of **CO**upled models and their **VAL**idation against **Ex**periments. The general goal of this project is to encourage multidisciplinary interactive and cooperative research on modeling coupled processes in fractured rocks and buffer materials, in support of the performance assessment for radioactive waste storage in geologic formations.

Three multi-year project stages of DECOVALEX have been completed in the past decade, mainly focusing on coupled thermal-hydrological-mechanical (THM) processes. The most recent project stage, DECOVALEX-III, included THM modeling work on two large-scale *in situ* heater experiments, the FEBEX experiment at Grimsel in Switzerland and the Drift Scale Test (DST) at Yucca Mountain in the USA. This modeling work has greatly enhanced our understanding of the coupled near-field processes in two different rock formations (crystalline rock versus volcanic tuff), hydrological settings (saturated versus unsaturated), and emplacement designs (backfilled drift versus open drift), and has added confidence in the predictions by comparison of measured data with the model results (e.g., Rutqvist et al., 2005a, 2005b).

Currently, a fourth multi-year project stage of DECOVALEX is under way, referred to as DECOVALEX-THMC. THMC stands for **T**hermal, **H**ydrological, **M**echanical, and **C**hemical processes. The project was initiated in January 2004 and will run through June 2007. Participating organizations are from USA, France, Japan, Sweden, Germany, China, and Canada. Five individual research tasks are defined within DECOVALEX-THMC, each of which is headed by a different participating organization. DOE leads Task D of the new DECOVALEX phase, entitled "Long-term Permeability/Porosity Changes in the EDZ and Near Field due to THC and THM Processes for Volcanic and Crystalline-Bentonite Systems." In its leadership role for Task D, DOE coordinates and organizes the cooperative research activities of the international research teams engaged in Task D (China, Germany, Japan, USA), and conducts its own modeling work for Task D. Scientists at Lawrence Berkeley National Laboratory (LBNL) support DOE in organizational matters and conduct the respective modeling studies.

The research program developed for Task D of DECOVALEX-THMC involves both geomechanical and geochemical research areas. The geomechanical project, referred to as D_THM, builds on the knowledge gained from modeling the short-term *in situ* heater experiments in DECOVALEX-III, and applies that knowledge to the evaluation of long-term THM processes in two generic geologic repositories for radioactive waste, where the regulatory compliance periods span over thousands to tens of-thousands of years. THM processes lead to changes in hydrological properties that can be very important for performance, because the flow processes in the vicinity of emplacement tunnels will be altered from their initial state. Some of these changes can be permanent (irreversible), in

6

which case they persist after the thermal conditions have returned to ambient; i.e., they will affect the entire regulatory compliance period. In general, THM changes are strongest close to the tunnels; i.e., they will be particularly relevant for the long-term flow behavior in the Excavation Disturbed Zone (EDZ) and the near-field environment. Research teams participating in Task D_THM model the THM processes in the fractured rock close to representative emplacement tunnels as a function of time, predict the mechanically induced changes in hydrological properties, and evaluate the impact on near-field flow processes. Currently, research teams from China, Germany, Japan, and the U.S. conduct modeling work on Task D_THM, each using different conceptual approaches and computer codes.

The new DECOVALEX-THMC project aims at expanding the traditional geomechanical scope of the previous DECOVALEX project stages by incorporating geochemical processes important for repository performance. As discussed in Section 2.2, chemical processes can permanently alter hydrological properties and flow paths in the near field by mineral precipitation and dissolution. They also affect the water and gas chemistry close to the waste packages, which are relevant for waste package corrosion, buffer stability, and radionuclide transport. Recognizing their increasing importance, Task D includes a geochemical research area, referred to as D_THC, that addresses long-term THC effects and their relevance in two generic repositories for radioactive waste. Research teams participating in Task D_THC model the THC processes in the fractured rock close to representative emplacement tunnels as a function of time, and predict the changes in water and gas chemistry, mineralogy, and hydrological properties. Currently, research teams from Germany, Japan, and the U.S. conduct modeling work on Task D_THC, each using different conceptual approaches and computer codes.

The generic waste repositories evaluated in Task D represent simplified versions of two possible repository sites and emplacement conditions considered by the participating organizations. The first repository is located in saturated crystalline rock; emplacement tunnels are backfilled with a bentonite buffer material. This repository is referred to as a *FEBEX* type, since many of its features are similar to the *FEBEX* field test setting. The second repository is a simplified model of the Yucca Mountain site, featuring a deep unsaturated volcanic rock formation with emplacement in open gas-filled tunnels (Yucca Mountain type). At first, each generic repository will be analyzed separately within the geomechanical and the geochemical research areas, respectively. (At later stages, the separate THM and THC model analyses may be integrated to a fully coupled geomechanical and geochemical analysis.) However, as D_THM and D_THC modeling studies are conducted assuming identical site and emplacement conditions, the results from the geomechanical and geochemical models can be easily compared.

The following activities were conducted during the first year of Task D research work: First, DOE and LBNL finalized the Task D description and produced a detailed report containing all necessary specifications for geomechanical and geochemical modeling analyses of the two generic repositories (see Appendix A). Then, four international research teams from China, Germany, Japan, and USA started their research work on D_THM and D_THC (see approaches and results in Sections 4 and 5 of this report). Three full DECOVALEX workshops were held to share research ideas and compare

modeling results (Utrecht, Netherlands, June 15-16, 2004; Kunming, China, February 21-24, 2005; Ottawa, Canada, October 4-7, 2005). In addition, DOE organized three meetings just for Task D research participants to discuss organizational and modeling issues specific to this task (Kunming, China, February 20, 2005; Berkeley, USA, July 21-22, 2005; Ottawa, Canada, October 4, 2005; see meeting summaries in Appendix B). In between workshops and meetings, the international research teams collaborated closely via email and telephone.

The close collaboration among international top scientists and engineers is one of the major benefits from participation in DECOVALEX-THMC. First, interaction with top international scientists helps to further the understanding of geomechanical and geochemical processes related to geologic storage of radioactive waste. Second, the cooperative research work conducted in the field of THMC modeling provides valuable peer-review of the modeling analyses in this field. Since all research teams work on identical tasks (but use different conceptual approaches and computer codes), research results from the participating teams can be easily compared. Good agreement between the different teams provides an additional proof of confidence into predictive models for THM and THC processes, which are important feeds for assessing the performance of the geologic repositories studied in different countries.

The value of analyzing two different repository sites and emplacement conditions is twofold: One repository setting resembles the geologic repository at Yucca Mountain, the designated site in the DOE program. Another repository setting (*FEBEX* type) is representative of the possible emplacement conditions considered in many European countries and Japan. Since the geomechanical and geochemical processes expected in such settings are different from each other, the demands and requirements on THM and THC simulation models are different. It is important to show that all models, proven to be capable of simulating one repository type, are equally valuable for the simulation of an alternative repository setting with different THM and THC processes.

2.   TASK D SUMMARY DESCRIPTION

The following section gives a brief summary of the problem definition for the simulation analyses to be conducted in Task D. A document containing a more comprehensive task description with all necessary specifications for modeling work was distributed to the individual research teams in May 2004 (Barr et al., 2004a). A first revision was issued in December 2004 (Barr et al., 2004b). The latest revision of this document is attached in Appendix A (Barr et al., 2005).

The nomenclature used for the different simulation problems defined in Task D is as follows. Simulation tasks with focus on geomechanical processes are referred to as D_THM, while simulation tasks with focus on geochemical processes are referred to as D_THC. Since two different generic repository settings are considered (*FEBEX* type and *Yucca Mountain* type), there are two subtasks each for D_THM and D_THC:

- Task D_THM1: Geomechanical simulations for a generic repository located in saturated crystalline rock, where emplacement tunnels are backfilled with buffer material (*FEBEX* type).
- Task D_THM2: Geomechanical simulations for a generic repository located in unsaturated volcanic rock, with emplacement in open gas-filled tunnels (*Yucca Mountain* type).
- Task D_THC1: Thermal-hydrological-chemical simulations for a generic repository located in saturated crystalline rock, where emplacement tunnels are backfilled with buffer material (*FEBEX* type).
- Task D_THC2: Thermal-hydrological-chemical simulations for a generic repository located in unsaturated volcanic rock, with emplacement in open gas-filled tunnels (*Yucca Mountain* type).

2.1   BASIC CONCEPTS OF GENERIC REPOSITORIES

Figure 2.1 presents the basic functions of the two repository types analyzed in Task D of DECOVALEX-THMC (*FEBEX* type and *Yucca Mountain* type). Both repository types depend on a multibarrier system relying on an engineered system (e.g., waste, canister, buffer, and excavation) and a natural system (rock mass). In the *FEBEX* case, the tunnels hosting waste canisters are backfilled with a low-permeability buffer material such as bentonite. Since the crystalline rock formation surrounding the repository is saturated with water, the tight (low-permeability) bentonite is necessary to prevent water flow and solutes from coming into contact with the waste canister. On the other hand, for an open-drift repository in an unsaturated tuff formation similar to *Yucca Mountain*, there is no protective bentonite buffer, but the open drift itself provides a natural capillary barrier that can limit liquid water from entering the drift. There is also a difference in the amount of heat and temperature rise. In a bentonite-backfilled repository, considered in most European countries and Japan, the temperature is generally kept below 100°C to prevent chemical alterations of the bentonite material. For the open-drift alternative (considered for the *Yucca Mountain* repository), the current design results in above-boiling temperatures within the tunnels and in the near field rock.

Emplacement Drift
located at about 500 to 1000 meters depths in saturated rock

Bentonite Buffer:
- Provides mechanical stability of the canister
- Retards the arrival of water (and corrosive solutes) to the canister
- Retains/retards migration of radio-nuclides if released from the canister

Copper/steel
Waste Canister
isolates waste

Bedrock: Provides a stable chemical and mechanical environment and retards radio-nuclides if released

a.

Emplacement Drift
located at about 300 meters depth in unsaturated rock

Capillary Barrier:
- Diverts water flow around drift
- Prevents water (and corrosive solutes) from seeping into the drift

Stainless steel and Alloy 22
Waste Package
isolates waste

Bedrock: Provides a stable chemical and mechanical environment and retards radio-nuclides if released

b.

Figure 2.1.   Schematic showing the two repository types evaluated in tasks D_THM and D_THC: (a) bentonite-back-filled repository in saturated rock (*FEBEX type*), and (b) open-drift repository in unsaturated rock (*Yucca Mountain type*)

2.2. GEOMECHANICAL AND GEOCHEMICAL PROCESSES AFFECTING HYDROLOGICAL PROPERTIES

The ultimate research topic in Task D is to evaluate and predict long-term changes in near-field hydrological properties as a result of heat-driven geomechanical and geochemical alterations. Such changes in hydrological properties (mostly with respect to fracture porosity and permeability) affect the flow and transport processes in the vicinity of emplacement tunnels and can thus be very important for performance assessment. The

following section gives a brief description of the coupled processes expected to occur in the two repository types.

Geomechanical Processes and Related Research Work

Significant geomechanical alterations are expected to occur in response to the heat output of the decaying radioactive waste. The strongest effects typically coincide with the period of the highest temperatures; i.e., depending on the repository type, during the first decades or centuries after emplacement (Figure 2.2). For example, in the case of a bentonite-backfilled repository, the drying and wetting of the bentonite induces shrinkage and swelling in various part of the buffer, with resaturation expected to occur within tens of years. In the case of an open-drift repository, the boiling of water creates a dryout zone in the near-field rock that will prevent liquid water from entering the drift for several hundred to more than one-thousand years.

At the same time, thermally induced stresses will act upon pre-existing fractures, which will open or close depending on the local stress. One of the important effects, i.e., thermal expansion of the rocks (with impact on fracture aperture), is generally recoverable as the temperature drops. However, increased thermal stress may also lead to irreversible or permanent impacts, which are most relevant for performance assessment (Figure 2.3). For example, if changes in the stress field during the heating period are sufficiently large, inelastic mechanical responses may be induced in the form of fracture shear slip or crushing of fracture asperities. These processes may change the fracture porosity and permeability permanently, since the rock loses its integrity. Furthermore, the elevated temperatures and stresses will be maintained for long time spans, which could give rise to increased microcracking and subcritical crack growth through stress corrosion or other related phenomena. Such inelastic mechanical responses in the fracture system would induce irreversible (permanent) changes in the hydrological properties of the rock mass.

Figures 2.1 and 2.2 suggest that for long-term THM processes, there are differences but also many similarities between the two repository cases, indicating that modelers face similar challenges and issues. Working together on both cases will help in evaluating similarities and differences, in comparing approaches and results, and in gaining a better overall understanding.
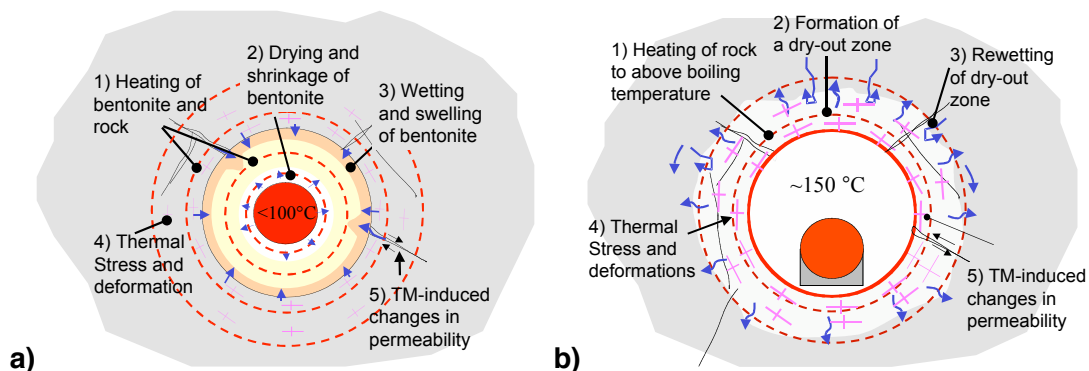
Figure 2.2.   Short-term coupled THM processes at (a) a bentonite-backfilled repository in
saturated rock and (b) an open-drift repository in unsaturated rock
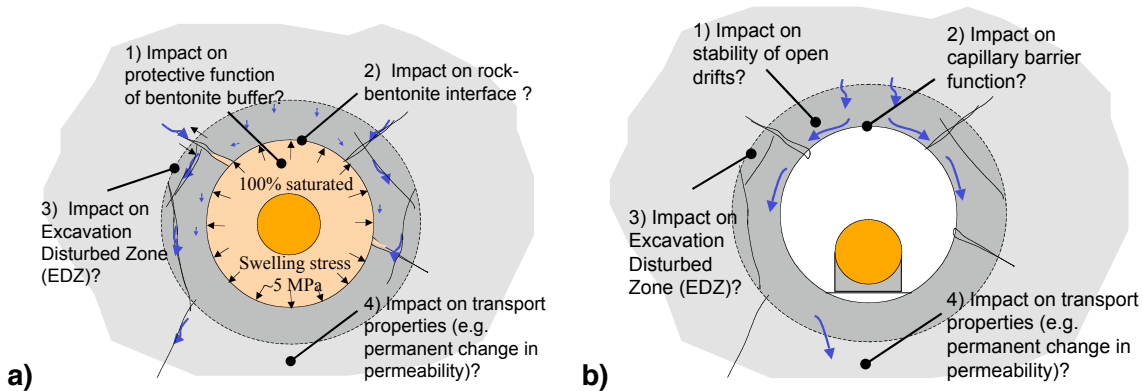
Figure 2.3.   Potential long-term impact of coupled THM processes at (a) a bentonite-back-filled
repository in saturated rocks and (b) an open-drift repository in unsaturated rock

Geochemical Processes and Related Research Work

The heat output of the decaying radioactive waste will induce important geochemical
reactions in the host-rock formations, owing to the changes in stabilities of minerals with
increasing temperature and changing water chemistry and also to greatly increased
reaction rates. Geochemical alteration include changes in water and gas chemistry in the
near field and within the tunnels, which affects the waste package environment and may
also jeopardize the integrity of buffer materials. In turn, buffer materials will interact with
formation water and minerals in the adjacent host rock, thus altering the buffer mineral
assemblage, pore water chemistry, physical, and hydrological properties.

In both formation rocks and buffer materials, mineral precipitation and dissolution will
give rise to long-term, possibly permanent changes in hydrological properties. Increased
temperature results in mineral-water disequilibrium and increases the reaction rates of
minerals with water, leading to enhanced mineral dissolution and precipitation. Effects of
mineral precipitation on fracture porosity and permeability are particularly strong when
temperatures are above boiling. In this case, vapor is driven away by the heat in all
directions and cools as it moves farther from the heat source, eventually condensing into
the liquid phase. Above the heat source, condensate flows back down by gravity and
capillary suction, only to boil again as it gets closer to the heat source. This cycle of
vaporization, condensation, and reflux can result in strong mineral alteration processes
where dissolution is dominant in the condensation zone and precipitation takes place at
the boiling front.

Figures 2.4 and 2.5 give a schematic illustration of the main long-term THC processes
expected in the two repository types.

Figure 2.4.   Possible THC processes with impact on hydrological properties near emplacement tunnels in unsaturated volcanic rock
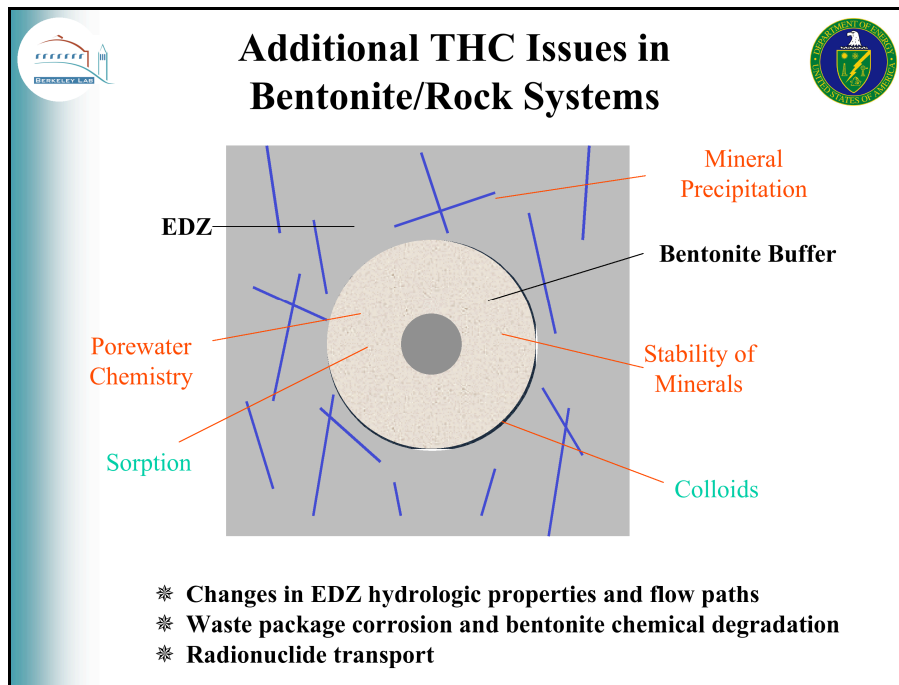
Figure 2.5.   Additional THC processes and their impact on hydrological properties in and near emplacement tunnels with bentonite backfill

2.3. BRIEF DESCRIPTION OF SIMULATION TASKS D_THM AND D_THC

The task description for D_THM and D_THC is designed such that the expected physical processes in future repositories are incorporated in a realistic manner, yet allow for somewhat simplified modeling as the geometries and boundary conditions have been simplified. Definitions are given such that model concepts as well as relevant property and parameter choices will have to be developed by the individual research teams (based on reports, data, and other sources), rather than being imposed in the task description. The idea is to encourage model comparison, not just code comparison.

Each task includes two different repository scenarios with similar geometry (depicted in Figure 2.6). Both analyze 2-D vertical cross sections perpendicular to the tunnel axis. The emplacement tunnels are assumed to be parallel, with a given distance between them. Symmetry considerations allow limiting the model to one representative emplacement tunnel, with the lateral boundaries at the centerlines of neighboring tunnels. Upper and lower boundaries are such that they remain unaffected by the heat. Waste packages are placed into the center of the tunnels. Heat emitted from the waste packages is provided as a time-dependent line load. Undisturbed flow is from top to bottom, either driven by hydraulic head gradients (saturated flow) or by gravity (unsaturated flow).
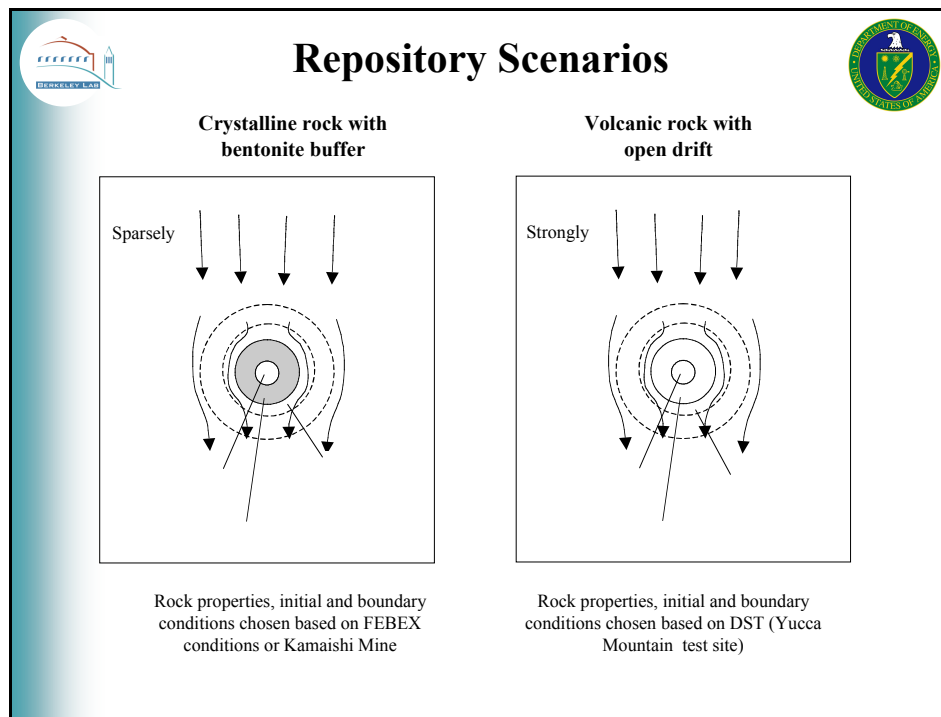
Figure 2.6.   Schematic showing the two repository scenarios chosen for D_THM and D_THC
(vertical cross sections perpendicular to drift axis)

Tasks D_THM and D_THC are conducted simultaneously, since the researchers working on THM processes are mostly different from those working on THC processes. In each task, participating teams are encouraged to work on both repository scenarios, either

simultaneously or sequentially, to enhance process understanding, and to ensure close cooperation. Both tasks may include an analysis and/or simulation component, using measured data to identify relevant processes and to allow for model comparison with experimental results. At later stages of Task D, i.e., after finalizing D_THM and D_THC, results from THM and THC analyses will be compared, and the need for a fully coupled thermal-hydrological-mechanical-chemical (THMC) simulation study will be evaluated. This latter subtask will require close interaction between THM and THC research teams.

2.3.1   Task D_THM: Workscope, Research Topics, and Modeling Phases

In this task, research teams conduct geomechanical modeling analysis of the long-term coupled processes in two generic repositories with simplified conditions and dimensions. Participating research teams model the THM processes in the fractured rock close to a representative emplacement tunnel as a function of time, predict the mechanically induced changes in hydrological properties, and evaluate the impact on near-field flow processes. Geochemical processes are neglected in Task D_THM. Two subtasks analyze the coupled THM processes in two generic repositories as follows:

- Task D_THM1: Generic repository located in saturated crystalline rock, where emplacement tunnels are backfilled with buffer material (*FEBEX* type).

- Task D_THM2: Generic repository located in unsaturated volcanic rock, with emplacement in open gas-filled tunnels (*Yucca Mountain* type).

Figure 2.7 gives a summary of the problem setup and the main challenges for D_THM.

Sub-Task D_THM

❑   Objective: Estimate Long-term THM changes in hydrological properties (reversible and irreversible) and analyze impact on flow

❑   Two repositories: D_THM1 (FEBEX type) and D_THM2 (YMP type)

❑   Problem Setup:
   ⊙   Detailed THM initial and boundary conditions are provided
   ⊙   Phase 1: All TH properties for rock and buffer material are directly provided
   ⊙   Later Phases: Relevant THM properties for rock, fractures, and buffer material will need to be derived based on given data or literature
   ⊙   Selected properties associated with uncertainty ranges

❑   Main Challenges:
   ⊙   Model conceptualization (discrete, continuum, hybrid,…)
   ⊙   Derivation of representative in-situ properties from available data
   ⊙   Conceptual model describing mechanically-induced changes in properties
   ⊙   Model uncertainty (parameter uncertainty and conceptual model uncertainty)

Figure 2.7.   Problem setup and main challenges for D_THM

The main processes considered in Task D_THM are heat transfer, fluid flow, stress and deformation, and geomechanical alterations in hydrologic properties (e.g., porosity and permeability). Specific THM research interests addressed in Task D_THM include, but are not limited to:

- Relative importance of thermal-mechanical changes to near-field hydrological properties and flow fields

- Relative importance of irreversible mechanical changes versus reversible mechanical changes

- Comparative analysis of THM effects in different host rock types and repository designs

- Evaluation of stress-permeability and stress-porosity relationships

- Importance of THM processes for performance assessment

- Assessment of fully coupled THMC processes (necessity, approaches)

- Assessment of uncertainties in the predictions resulting from uncertain parameters, alternative conceptual models, heterogeneities, and other factors

The predictive THM simulations may be conducted using various modeling techniques, for example discrete fracture models or continuum models. Model predictions should include the most likely results on THM-induced property changes as well as an evaluation of the uncertainties related to these predictions. This could involve stochastic modeling, resulting in a probability distribution of possible results or, at a minimum, estimation of upper and lower limits of results. In addition to the data and background information provided by the task leads, the research teams should utilize any available literature data to build their case, to ensure providing the best possible prediction of potential permanent changes based on the current state of knowledge.

The description of Task D_THM1 is based on data from the Grimsel Test Site (GTS) and the FEBEX *in situ* experiment, which were used in DECOVALEX III, Task 1. The design and material properties of the engineered system (canister, bentonite, and drift) are taken from the FEBEX *in situ* experiment. The rock properties and *in situ* conditions are also taken from the GTS/FEBEX site. However, in a few instances, data from the Kamaishi Mine in Japan (from DECOVALEX II) and the Laxemar site in Sweden are utilized to complement the GTS/FEBEX data set. The crystalline host rock in D_THM1 is sparsely fractured, which would suggest that the fractures might be modeled using discrete approaches, if necessary. The data set for Task D_THM2 is entirely derived from the Yucca Mountain site in Nevada and the lithographic rock units surrounding the Yucca Mountain Drift Scale Test. Here, the porous tuff rock is densely fractured, which would suggest that the fractures could be treated as a continuum. For both repository settings, a complete set of rock properties and *in situ* conditions with uncertainty ranges is given to the research teams, upon which to build their models for Task D_THM2 (see specifics on task definition in Appendix A).

The simulation work in Task D_THM is being conducted in three modeling phases that tackle increasing degrees of difficulty. After each phase, the results of the different research teams are compared to ensure that there are no systematic differences before

moving into the next, more complex model phase. The three phases for D_THM are defined as follows (Figure 2.8):

Phase 1. Model Inception
Phase 2. Preliminary Prediction and Sensitivity Study
Phase 3. Final Prediction and Uncertainty Analysis.

The purpose of the Model Inception Phase (Phase 1) is for the research teams to familiarize themselves with the problem by performing simulations in which all the properties are provided with explicit values while permanent changes are neglected. The results of the research teams are compared at the end of this phase to assure that all teams are starting the problem from a common basis. The comparison shall focus on the evolution of temperature and stress, because these are the driving forces behind mechanical and hydrological changes in the fractured rock mass. When research teams are satisfied with their analysis and their results agree with other research teams, they should go on to the next phase.

In Phase 2, the research teams start to develop their model with the goal of predicting mechanically induced permanent changes. This phase may include development of continuum models for representing the hydromechanical couplings at the two sites. It may also include generation of fracture networks based on available statistical data if a discrete model approach is used. Using the available site data and developed data (e.g., stress-permeability relationships), the research teams should conduct an initial parameter study. The purpose of this study is twofold, as follows:

- To demonstrate how the model is able to predict permanent changes in mechanical and hydrological properties

- To find conditions (e.g. strength properties, initial stress state) at which permanent changes are likely

The research teams should then predict coupled THM responses and potential permanent changes (if any). This should be conducted with whatever modeling approach the respective research team has developed. It may be a continuum model using homogenous properties or a heterogeneous stochastic continuum model. It may also be a discrete fracture model using fracture sets with regular fracture spacing or even stochastically generated fracture networks. At the end of this phase, the output results from the different research teams are compared. In particular, the evolution of permeability changes and their impact on the flow field needs to be studied. When research teams are satisfied with their preliminary model prediction, they should go on to the next phase to obtain the final prediction results.

In Phase 3, the research teams are asked to make their final prediction, including estimation of the resulting uncertainties. Examples of uncertainties includes:

- Uncertainties associated with parameters

- Uncertainties associated with model concepts (i.e., representation of discrete structures such as fractures and faults, constitutive relationships)

Parameter uncertainties could be related, for example, to uncertainties in input properties, such as permeability, *in situ* stress, or thermal expansion. Model uncertainties could be related to representation of the *in situ* fracturing. They may also be related to the constitutive models of the mechanical behavior of fractures or the constitutive models developed for continuum approaches. In part, estimation of these uncertainties will be based on scientific judgment. The end result of the uncertainty analysis can be a statistical distribution of the simulation outputs or, at a minimum, upper and lower bounds of possible results.

THM Modeling Phases

❑   Model Phase 1: Model Inception

⊙   Research teams conduct initial THM simulation with focus on temperatures and stresses, flow fields, saturations (not THM induced property changes)
⊙   All properties and initial conditions are explicitly provided to the teams, for a homogeneous isotropic setting
❋   *Comparison with other teams ensures common basis for next steps*

❑   Model Phase 2: Preliminary Prediction and Sensitivity Study

⊙   Instead of providing explicit parameter values, research teams will develop data based on raw data, reports, additional literature sources
⊙   Prediction of THM induced property changes
⊙   Sensitivity analysis with respect to THM property changes
❋   *Comparison with other teams to ensure that chosen model concepts work*

❑   Model Phase 3: Final Prediction and Uncertainty Analysis

⊙   Estimate model uncertainty associated with parameters (uncertainty ranges are provided)
⊙   Estimate model uncertainty associated with model concepts (representation of fracturing, constitutive relationships for stress-permeability relation, etc)

Figure 2.8.   Definition of Three Modeling Phases of Task D_THM

2.3.2   Task D_THC Workscope, Research Topics, and Modeling Phases

In this task, research teams conduct geochemical modeling analyses of the long-term coupled THC processes in two generic repositories, similar to those described for Task D_THM. Participating research teams model the THC processes in the fractured rock close to a representative emplacement tunnel as a function of time, and predict the changes in water and gas chemistry, mineralogy, and hydrological properties. The impact of geomechanical processes is neglected in this task. Two subtasks analyze the coupled THC processes in two generic repositories as follows:

• Task D_THC1: Generic repository is located in saturated crystalline rock, where emplacement tunnels are backfilled with buffer material (*FEBEX* type).

• Task D_THC2: Generic repository located in unsaturated volcanic rock, with emplacement in open gas-filled tunnels (*Yucca Mountain* type).

Figure 2.8 gives a summary of the problem setup and the main challenges for D_THC.

Sub-Task D_THC

❑ Objective: Estimate long-term changes in water/gas chemistry as well as mineralogical changes, analyze impact on flow

❑ Two repositories: D_THC1 (FEBEX type) and D_THC2 (YMP type)

❑ Problem Setup:

  ⊙ Detailed THC initial and boundary conditions are provided
  ⊙ Phase 1: All THC properties for rock and buffer material are directly provided
  ⊙ Later Phases: Relevant THC properties for rock, fractures, and buffer material will need to be derived based on given data or literature (e.g., mineral abundances and compositions, thermodynamic and kinetic data)
  ⊙ Selected properties associated with uncertainty ranges

❑ Main Challenge:

  ⊙ Develop appropriate conceptual model for complex heat-driven reactive transport including several species and phases
  ⊙ Conceptual model describing precipitation-dissolution-induced changes in properties
  ⊙ Assess model uncertainty stemming from both parameter uncertainty and conceptual model uncertainty

Figure 2.9.   Problem setup and main challenges for D_THC

The main processes considered in Task D_THC are heat transfer, fluid flow, reactive transport, and alterations in hydrologic properties. Specific THC research interests addressed in Task D_THC include, but are not limited to:

• Relative importance of thermal-chemical changes on the near-field hydrological properties and flow field

• Evolution of water and gas chemistry close to waste package

• Mineral precipitation/dissolution in the near-field and in bentonite

• Comparative analysis of THC effects in different repository designs/rock types

• Evaluation of the relation between mineral alteration, and hydrological properties

• Importance of THC processes for performance assessment

• Assessment of fully coupled THMC processes (necessity, approaches)

• Assessment of uncertainties in the predictions resulting from uncertain parameters, alternative conceptual models, heterogeneities, and other factors

The predictive THC simulations can be conducted using various modeling techniques—for example, discrete fracture models or continuum models. Model predictions should include the results of THC-induced changes to water and gas chemistry, mineralogy, hydrological properties, flow fields, and an evaluation of the uncertainties related to these predictions. This could involve systematic sensitivity studies, resulting in a distribution of possible results or, at a minimum, estimation of upper and lower limits of results.

The description of Task D_THC1 is based on various sources. The thermal-hydrological properties and their origin are identical to those defined in D_THM1, featuring a bentonite-backfilled emplacement tunnels hosted by a sparsely fractured crystalline formation. Properties of the bentonite buffer material are based on a sample investigated by the Japanese program. The chemical properties of the bentonite buffer and the host rock are taken from the Aspö site in Sweden and from the Japanese program. The input data for Task D_THC2 are entirely derived from the Yucca Mountain site in Nevada and the rock units surrounding the Yucca Mountain Drift Scale Test (densely fractured porous tuff formation). A complete set of geochemical data, rock properties, and *in situ* conditions with uncertainty ranges is provided to the research teams, upon which to build their models for Task D_THC (see Appendix A).

The simulation work in Task D_THC is conducted in three modeling phases that tackle increasing degrees of difficulty. After each phase, the results of the research teams are compared to ensure that there are no systematic differences before moving into the next, more complex model phase. The three phases are defined as follows (see Figure 2.10):

    Phase 1. Model Inception
    Phase 2. Preliminary Prediction and Sensitivity Study
    Phase 3. Final Prediction and Uncertainty Analysis

The purpose of the Model Inception Phase (Phase 1) is for the research teams to familiarize themselves with the conceptual model and problem setup by performing one simulation in which all the properties are provided for a limited set of mineral, aqueous, and gaseous species. The results of the research teams are compared at the end of this phase to assure that all teams are starting the problem from a common basis. The comparison focuses on the evolution of temperature, gas and water composition, and mineral precipitation/dissolution (in fractures, matrix, and the bentonite) for a simplified geochemical system. When research teams are satisfied with their analysis and their results agree with other research teams, they should go on to the next phase.

In Phase 2, a more complete geochemical system is considered. Also, the research teams focus on predicting permanent changes caused by mineral dissolution/precipitation concomitant with the evolution of water and gas chemistry. Using the available site data and various developed data (e.g., mineral dissolution/precipitation-porosity-permeability relationships), the research teams should conduct an initial parameter study. The purpose of this study is twofold, as follows:

- To demonstrate how the model is able to predict permanent changes in chemical (gas, water, and mineral) and hydrological properties
- To find conditions (e.g., initial mineralogy, fracture aperture, water chemistry, flow rates) at which permanent changes are possible

The research teams should then predict coupled THC responses and potential permanent changes (if any) for one realistic realization. This should be conducted with whatever modeling approach the respective research team has developed. It may be a continuum model using homogenous properties or a heterogeneous stochastic continuum model. It may also be a discrete fracture model using fracture sets with regular fracture spacing or

even stochastically generated fracture networks. At the end of this phase, the output results from the different research teams needs to be compared. In particular, the evolution of chemistry and permeability changes and their impact on the flow field will be studied. When research teams are satisfied with their preliminary model prediction, they should go on to the next phase to obtain the final prediction results.

In Phase 3, the research teams are asked to make their final prediction, including estimation of the resulting uncertainties. Examples of uncertainties include:

- Uncertainties associated with parameters (e.g., thermodynamic and kinetic data, reactive surface areas)
- Uncertainties associated with model concepts (mineral representations—ideal endmembers vs. solid solutions, mineral textures, equilibrium vs. kinetic reactions, distributions of mineral precipitates, etc.)

THC Modeling Phases

❑   Model Phase 1: Model Inception

⊙   Research teams conduct initial THC simulation with limited set of mineral, aqueous, and gaseous species (no property changes)
⊙   All properties and initial conditions are explicitly provided to the teams, for a homogeneous setting
⊙   Conceptual choices for reactive transport should follow suggested methodology
✳   *Comparison with other teams ensures common basis for next steps*

❑   Model Phase 2: Preliminary Prediction and Sensitivity Study

⊙   More complex geochemical system (additional species)
⊙   Conceptual choices for reactive transport based on raw data, reports, additional literature sources
⊙   Prediction of THC induced property changes
⊙   Sensitivity analysis
✳   *Comparison with other teams to ensure that chosen model concepts work*

❑   Model Phase 3: Final Prediction and "Focused" Uncertainty Analysis

⊙   Estimate model uncertainty associated with parameters (uncertainty ranges to be provided)
⊙   Estimate model uncertainty associated with model concepts (equilibrium vs. kinetic, reactive surface area calculation, permeability-precipitation relation)

Figure 2.10. Definition of three modeling phases of Task D_THC

2.3.3   Details of Task Description

Much more detail on all task specifications is given in the task description report (Barr et al., 2005) in Appendix A, including specifics on model geometry, boundary and initial conditions, modeling sequence (simulating initial state, excavation state, emplacement state), input data, supporting data, references, suggestions for potential model simplifications (in case certain model features are not available for research teams), proposed schedule, and output specifications.

3.   PARTICIPATING COUNTRIES AND TEAM MEMBERS

Japan, Germany, and the U.S. participate in both D_THM and D_THM. China participates in D_THM only. The following list gives names and addresses of all team members from the participating countries. Team members may either be representatives of the funding organizations or may be working for research institutes that support these funding organizations in conducting the scientific analyses.

United States: DOE Team

1	**Deborah Barr** U.S.Department of Energy (DOE), Office of Repository Development (ORD), Office of License Application & Strategy (OLA & S) deborah_barr@ymp.gov Tel: 1+702-794-5534; Fax: 1+702-794-1350
2	**Jens Birkholzer** Lawrence Berkeley National Laboratory (LBNL) Earth Sciences Division, MS 90-1116 Berkeley, CA 94720, USA jtbirkholzer@lbl.gov Tel: +1-510- 486-7134; Fax: +1-510-486-5686
3	**Jonny Rutqvist** Lawrence Berkeley National Laboratory Earth Sciences Division, MS 90-1116 Berkeley, CA 94720, USA Jrutqvist@lbl.gov Tel: +1-510-486-5432; Fax: +1-510-486-5686
4	**Eric Sonnenthal** Lawrence Berkeley National Laboratory Earth Sciences Division, MS 90-1116 Berkeley, CA 94720, USA ELSonnenthal@lbl.gov Tel: +1-510-486-5866; Fax: +1-510-486-5686

China: CAS TEAM

1	**Quansheng Liu** Institute of Rock and Soil Mechanics Chinese Academy of Sciences Wuhan, 430071, People's Republic of China liuqs@whrsm.edu.cn Tel.: +86-2787-198856; Fax: +86-2787-197386
2	**Chengyuan Zhang** Institute of Rock and Soil Mechanics Chinese Academy of Sciences Wuhan, 430071, People's Republic of China Zhangcy999whrsm@21cn.com
3	**Xiaoyan Liu** Institute of Rock and Soil Mechanics Chinese Academy of Sciences Wuhan, 430071, People's Republic of China

Germany: BGR Team

1	**Hua Shao** Federal Institute for Geosciences and Natural Resources Stilleweg 2, 30655 Hannover shao@bgr.de Tel: +49 511 643 2427; Fax: +49 511 643 3694
2	**Thomas Nowak** Federal Institute for Geosciences and Natural Resources Stilleweg 2, D-30655 Hannover thomas.nowak@bgr.de Tel.: +49 511 643 2437; Fax : +49 511 643 3694
3	**Mingliang Xie** Center for Applied Geoscience, University Tuebingen, Germany ZAG, Sigwartstr. 10, D-72076 Tuebingen, GERMANY mingliang.xie@uni-tuebingen.de Tel: +49-7071-29 73173; Fax: +49-7071-5059
4	**Wenqing Wang** Center for Applied Geoscience, University Tuebingen, Germany ZAG, Sigwartstr. 10, D-72076 Tuebingen, GERMANY Wenqing.wang@uni-tubbingen.de Tel:+49-7071-29-73176; Fax:+49-7071-5059
5	**Olaf Kolditz** Center for Applied Geoscience, University Tuebingen, Germany ZAG, Sigwartstr. 10, D-72076 Tuebingen, GERMANY kolditz@uni-tubbingen.de Tel:+49-7071-29-73176; Fax:+49-7071-5059

Japan: JNC Team

1	**Yoshihiro Oda** Japan Nuclear Cycle Development Institute (JNC) Muramatu 4-33, Tokai-mura, Ibaraki-ken, Japan oda@tokai.jnc.go.jp Tel: 81-29-287-0928 ; Fax: 81-29-282-9295
2	**Masakazu Chijimatsu** Hazama Corporation, 2-5-8, Kita-Aoyama, Minato-ku, Tokyo 107-8658 ,Japan mchiji@hazama.co.jp Tel:+ 81-3-3405-1124; Fax:+ 81-3-3405-1814

DECOVALEX Expert/Peer Reviewer for Task D:

1	**Ivars Neretnieks** Royal Institute of Technology, KTH Department of Chemical Engineering and Technology SE 100 44 Stokholm, Sweden niquel@ket.kth.se Tel. +46-8-790-8229, Fax. +46-8-790-6416

4.   TASK D_THM: GEOMECHANICAL ANALYSIS

The research teams involved in modeling Task D_THM (from China, Germany, Japan, and the U.S.) have made significant progress during the first year of task D work. Section 4.1 gives a brief summary on the current status of the geomechanical modeling work. Each team has provided a status report, which describes the conceptual model approaches and discusses modeling results. With some minor editing for format consistency, these status reports have been added as Appendices C through F of this letter report (see attached CD). To bring out similarities and discrepancies between different research approaches, the LBNL research team has conducted a comparative evaluation of all status reports with regards to the conceptual models used and the simulation results. This comparative evaluation is summarized in Section 4.2 for D_THM1 and Section 4.3 for D_THM2.

4.1.   SUMMARY STATUS OF D_THM RESEARCH WORK

All teams involved in modeling of D_THM have finalized model development work and have conducted simulation runs for at least one of the two repository scenarios (Table 4.1). Altogether, five different numerical codes were applied to simulate the test cases. DOE uses two alternative codes, TOUGH-FLAC (which is widely used within the Yucca Mountain Project) and ROCMAS. JNC uses a code named THAMES, BGR uses the GeoSys/Rockflow family of codes, and CAS works with a FEMLAB application referred to in the text as FRT-THM (FRT = Fluid-Rock Simulator). All these codes have been developed by the respective organizations or their supporting research institutions; i.e., no off-the-shelf software is used.

Table 4.1.   Research teams and numerical models applied within the Task D_THM of DECOVALEX-THMC

Team	Affiliation	Computer Code	Test Case Simulated
DOE-Team	Lawrence Berkeley National Laboratory (LBNL) for DOE	TOUGH-FLAC and ROCMAS	D_THM1 and D_THM2
JNC-Team	Japan Nuclear Cycle Development Institute (JNC)	THAMES	D_THM1 and D_THM2
BGR-Team	Center for Applied Geosciences Tuebingen, for BGR	GeoSys/Rockflow	D_THM1 and D_THM2
CAS-Team	Chinese Academy of Sciences	FRT-THM (FEMLAB application, combined with Mathlab)	D_THM1 and D_THM2

All teams started with the Model Inception Phase, where the problem is well defined, with most of the material properties and conditions specified in the task description report (Barr et al., 2005). The Task D meetings in Kunming, China, and in Berkeley, USA, and various email/telephone exchanges were utilized to conduct in-depth comparison of approaches and results between the different research teams. Various discrepancies were

24

evaluated in a team effort by going through some of the key plots of THM results. It was found that often these discrepancies were caused by differences in rock properties and boundary conditions, because some teams had misinterpreted the task description. These teams made adjustments in their model setup to be consistent with the other teams and conducted revised simulation runs. Eventually, all teams submitted Phase 1 simulation results together with a status report.

Our comparison of the individual status report results indicates that the overall agreement between the research teams is fairly good (see Sections 4.2.2 and 4.3.2 below). In a few cases, model revisions (mostly properties) are still necessary to improve the THM predictions of individual teams. These necessary revisions have been identified and will be conducted in the near future. Otherwise, the discrepancies between teams are rather small and can be explained by subtle differences in conceptual approaches (model simplifications). The good agreement provides a valuable basis for moving into Phase 2 of D_THM. Phase 2 modeling includes prediction of THM property changes with conceptual models chosen by the different research teams, sensitivity analysis with respect to THM property changes, application of alternative conceptual models for fractured rock (i.e., discrete, vs. continuum), and development of model data based on various reports and site data instead of using pre-defined values.

4.2. REPOSITORY CASE D_THM1 (FEBEX TYPE)

4.2.1   Comparison of Model Approaches

The basic modeling approaches employed by the four international teams (DOE, BGR, CAS, JNC) modeling D_THM1 are summarized in Table 4.2. All codes are capable of modeling thermal-hydrological-mechanical (THM) coupling. However, since TOUGH-FLAC currently does not account for the swelling pressure changes in a bentonite buffer material, it was run in a TH-only mode. In all other cases, simple elastic models are used for simulation of the rock-mechanical behavior, consistent with the simplified task definition for Phase 1 work. However, all models are generally capable of simulating elasto-plastic behavior, which can become necessary when stress-induced changes in hydrologic properties are to be considered in the next phases of D_THM1.

While the mechanical models for the rock-mechanical behavior are identical, the treatment of the evolution of swelling pressure in the bentonite is not consistent between the teams. All teams consider some sort of a saturation-dependent swelling impact, but use different functional relationships. For the scope of D_THM1, one is mostly concerned about the correct magnitude of the fully developed swelling stress, because this value defines the impact of bentonite swelling on the near-field rock during most of the postclosure time period (swelling is roughly expected fore the first 10 years after bentonite emplacement).

At this point, all teams use a single-continuum representation of the crystalline rock mass. This may change in later project phases, when the effect of sparsely distributed fractures may be considered in a more rigorous manner.

TOUGH-FLAC simulates complex multi-phase flow behavior, solving flow equations for both liquid and gas phases. In contrast, all other codes solve for variably saturated flow according to Richard's equation (assuming constant gas pressure), but do not explicitly account for gas flow along a gas pressure gradient. However, recognizing the impact of vapor movement in a thermally perturbed setting with evaporation processes, these codes account for transport of water vapor in a simplified manner, by solving a diffusion problem with diffusivity dependent on pressure and temperature gradients (e.g., see Appendix C, Equations 3.9 through 3.13).

Table 4.2.   Comparison of basic modeling approaches used for D_THM1

Team	Numerical simulator	Couplings considered	Mechanical model	Treatment of Buffer Swelling	Hydraulic model
DOE	TOUGH-FLAC	TH	NA	NA	Single continuum; multiphase liquid and gas flow
DOE	ROCMAS	THM	Elastic	Linear swelling strain model as a function of water saturation (targeted to give 5 Mpa at full saturation*)	Single continuum; unsaturated liquid flow, no gas flow; thermal vapor diffusion
BGR	GeoSys/ Rockflow	THM	Elastic	Alternative swelling model as a function of water saturation (possibly not targeted for 5 Mpa)	Single continuum, unsaturated liquid flow, no gas flow; thermal vapor diffusion
CAS	FRT-THM	THM	Elastic	Linear swelling strain model as a function of water saturation (targeted to give 5 Mpa at full saturation)	Single continuum, unsaturated liquid flow, no gas flow; thermal vapor diffusion
JNC	THAMES	THM	Elastic	Alternative swelling model as a function of water saturation (possibly not targeted for 5 Mpa)	Single continuum, unsaturated liquid flow, no gas flow; thermal vapor diffusion

* The target pressure of 5 MPa was specified in the task description (Barr et al., 2005).

4.2.2   Comparison of Model Results

In this section the calculated THM responses for Case D_THM1 (FEBEX type) are compared following output specification given in Barr et al. (2005, Section 6.5). The results of five different model analyses are compared. Those results were developed by

DOE, using TOUGH-FLAC and ROCMAS, by CAS using FRT-THM, by BGR using GeoSys/Rockflow, and by JNC using THAMES.

Temperature Evolution

Figures 4.1 and 4.2 show that the general trends and magnitudes of temperature are in agreement for the five different model analyses. Some of the differences that can be observed in Figures 4.1 and 4.2 are related to differences in the interpolation of the tabulated inputs of the heat decay function. The heat power function for D_THM1 was given in a graphical form, and each team extracted tabular values from this graph as input to the model. In addition, each numerical analysis evaluates the heat power at the current time step by interpolating between the tabulated input values. It is apparent from the comparison of the temperature evolution that a small difference in the heat input over a longer period of time can have a quite significant effect on the calculated temperature evolution. Figure 4.2 shows that the difference in temperature near the drift also results in a corresponding difference in the vertical temperature profiles at 1,000 and 10,000 years.

Four out of the five models predict a peak temperature of about 90°C to occur at about 20 years after emplacement, given at Point V1, located at the canister-buffer interface (see definition of points in Appendix A, Figure 6.1). The temperature evolution for the JNC model shows a much higher temperature in V1. These differences in the early temperature evolution are likely related to differences in the evolution of the liquid saturation in the bentonite buffer. The evolution of saturation in the buffer affects its thermal conductivity, which in turn impacts the temperature evolution at the canister-buffer interface (Point V1). However, with the exception of early JNC results in V1, Figure 4.1 shows that the overall agreement between the different models is quite good, especially in Point V6, located about 10 m from the drift.

Evolution of Water Saturation and Fluid Pressure

Figure 4.3 shows a general agreement in the evolution of liquid water saturation in the buffer for a point located in the buffer near the canister surface. In the first few years the initially 65% water-saturated bentonite dries to about 45 to 50%, followed by gradual resaturation. Three out of five models predict a time to full resaturation of about 25 years, whereas the BGR and JNC analyses indicate 70 and 250 years of resaturation time, respectively. Two main processes determine the resaturation time. First, there is a continuous capillary-driven liquid water flux from the fully saturated rock mass into the unsaturated bentonite. Initially, the capillary pressure in the buffer is about –70 MPa (at 65% saturation), leading to a steep capillary pressure gradient. The capillary-driven liquid flux is initially more than offset by thermally driven vapor diffusion, which tends to transport evaporated moisture from the inner hot regions of the buffer, along the thermal gradient, toward outer cooler regions. In the first few years, when the thermal gradient is steep, evaporation and thermal diffusion are sufficiently strong to cause a certain degree of drying near the canister surface. After a few years, as the thermal gradient becomes smaller, the vapor diffusion rate decreases, the inward capillary-driven liquid flux becomes dominant, and finally the entire buffer becomes fully saturated. Differences in the modeling approach and properties for unsaturated fluid flow and thermal diffusion in the bentonite could cause the observed differences in resaturation time.

27

Figures 4.4 and 4.5 present comparisons of the evolution of fluid pressure in the model domain. During the steady state analysis of the excavation sequence, the open drift tends to drain water from the surrounding rock mass, thereby reducing the pressure. The drainage is shown in Figure 4.5a as the pressure at t = 0 (after excavation) is reduced to be close to zero near and above the drift. After emplacement of the canister and buffer, the water inflow from the formation into the backfilled tunnel decreases and the fluid pressure in the surrounding rock mass increases slowly toward ambient hydrostatic conditions. The results in Figure 4.4 indicate that the ambient hydrostatic fluid pressure is fully restored after about 100 to 1,000 years. The time to restore the ambient fluid pressure depends mainly on the hydraulic properties of the rock mass, and may also be affected by the resaturation of the buffer. The time evolution of the fluid pressure is important for calculation of THM responses, since it affects the time evolution of effective stresses in the rock mass.

Evolution of Stress

Figure 4.6 compares the evolution of stress in the bentonite buffer. The results show that the calculated stress evolution is very different for different teams. The stress evolution is quite consistent between DOE and CAS results, though the final stress magnitude is different. The evolution of total stress in the buffer is mainly affected by the two sources:

1) Moisture swelling of bentonite as the buffer becomes fully saturated

2) Restoration of fluid pressure from an initially drained condition to fully restored hydrostatic pressure.

In addition, thermal expansion of the bentonite has some effect on the total stress evolution in the buffer. The differences in the stress evolution in Figure 4.6 are most likely related to differences in the model approaches and input parameters for moisture swelling. Because the evolution of swelling stress is important for the stability of the drift walls, a more consistent result of the evolution of stress in the buffer is desirable: The final magnitude of the swelling stress after resaturation and the approximate time at which it is achieved should at least be consistent between the different models. Further work is needed to resolve this inconsistency.

Figures 4.7 and 4.8 compare the evolution of horizontal stress in the rock mass. The first figure shows an apparent input error in the initial stresses in the JNC simulation results. Moreover, the initial stress is slightly lower in the DOE (ROCMAS) and CAS simulation results compared to those of BGR. The lower initial stress in the DOE and CAS simulation is an effect of the drainage of formation water into the excavated opening, leading to fluid pressure decrease (See further explanation in Appendix C, Section 4.3.2.) In the BGR results, water drainage is considered, but does apparently not affect the stress field. This needs to be checked in the BGR model.

Figure 4.8 shows that the profiles of horizontal stresses look similar to those of the vertical temperature profiles. The horizontal stresses increase strongest near the drift, where the temperature changes are most prominent. Also, the differences in stress profiles in Figure 4.8 are consistent with differences in temperature profiles in Figure 4.2.

Apart from the differences in the initial stress field, it seems that the thermally induced stress changes are quite consistent between the different models. (Note that the thermally induced stress is the difference between the initial stress and the peak stress.) The calculated stress in Point V3, which is located close to the drift wall, may be somewhat affected by the discretization differences between the four models. Because the stress gradient is very large near the drift wall, any interpolation between model grid points will lead to some inaccuracies.

Evolution of Displacement

Figures 4.9 and 4.10 present the evolution of vertical displacement. In the DOE (ROCMAS) and CAS analyses, the entire column settles initially about 0.05 m, caused by the drainage of water into the open excavation (V7 in Figure 4.9). The BGR model results do not indicate any initial settlement. The vertical profiles in Figure 4.10 show that the general shapes of the displacement profiles are consistent between the different models, except for the excavation phase.

All four models agree that the vertical displacement peaks at about 2,000 years after emplacement of waste. The magnitude of the peak displacement is controlled by the temperature change and the thermal expansion coefficient. (There is no impact of fluid pressure on the peak displacement because the fluid pressure has already been restored to the ambient hydrostatic fluid pressure at 2,000 years.) The peak displacement calculated by DOE (ROCMAS), CAS (FRT-THM) and JNC (THAMES) is about 0.25 m, whereas the peak value calculated by BGR is about 70% that of the three other teams. This difference in peak displacement should be resolved; the peak displacement depends exclusively on the correct temperature distribution and the value of the thermal expansion coefficient.

Evolution of Vertical Water Flux

Figure 4.11 presents a horizontal profile of the vertical percolation flux calculated by the DOE (ROCMAS) and CAS (FRT-THM) teams. So far, results for vertical percolation flux have not been provided by other teams. The numerical value of an initial vertical water flux of about 0.3 mm/yr was confirmed by analytical solution in Appendix C, Section. 4.3.5. The vertical flux is a result of the vertical hydraulic head gradient since the fluid pressure at the lower boundary was fixed at a pressure slightly less than hydrostatic. After long time (over 100 years) the water flux stabilizes somewhat with a diversion around the bentonite filled drift. The results of water flux are dependent on the temperature dependent hydraulic properties, in particular the fluid viscosity. The vertical percolation flux is important since it forms the basis for studying the impact of THM couplings on fluid flow.

Summary of Comparison of Model Results for THM1 Case

In summary, the overall trends and the magnitude of THM evolution are quite consistent between the different models. However, there is room for improvement regarding several

aspects that have an impact on the evolution of stress. The current differences in calculated THM responses are related to:

(1) Differences in the interpolation of the tabulated heat decay function

(2) Differences in the treatment of fluid pressure effects on the stress and displacement evolution

(3) Differences in the modeling approaches and input data for bentonite swelling.

These differences could be resolved as follows:

(1) The heat decay function could be more accurately defined by providing closely spaced tabular values for each team to use.

(2) The water drainage during the excavation phase and its effect on stress and strain should be considered in all models, choosing a finite excavation time of 30 years.

(3) The properties for the bentonite swelling need to be strictly defined, perhaps using a target swelling pressure.

Nevertheless, a reasonably good agreement has been achieved regarding the temperature and thermal stress in the rock mass. Therefore, research teams could begin the analysis of the next phase of Task D_THM, while continuing to resolve the remaining differences for Phase 1 results.
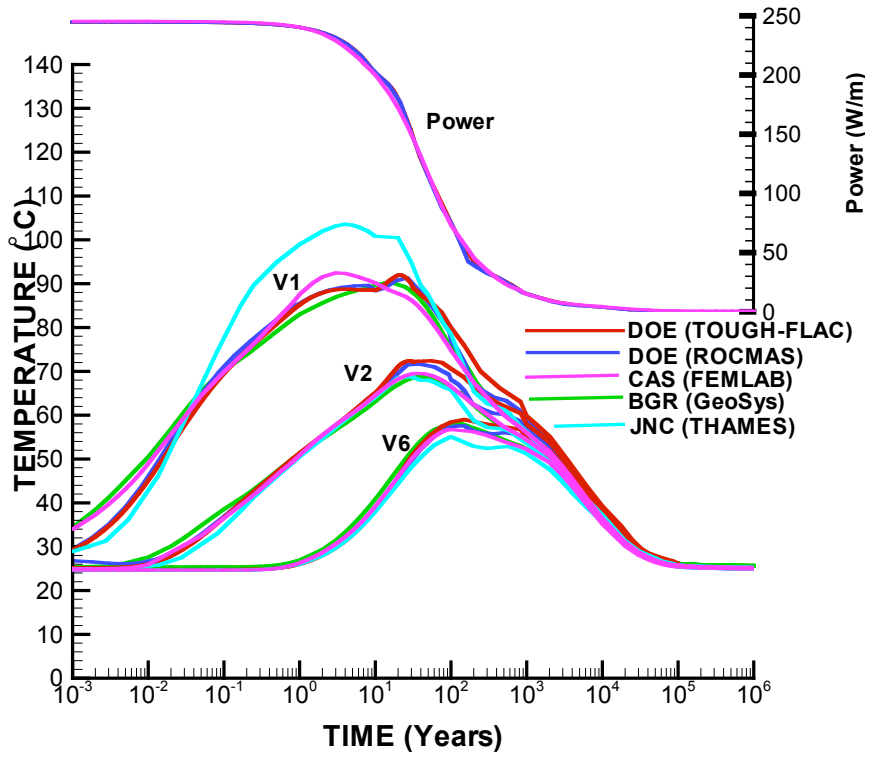
Figure 4.1.　Comparison of input power and temperature evolution at selected output points
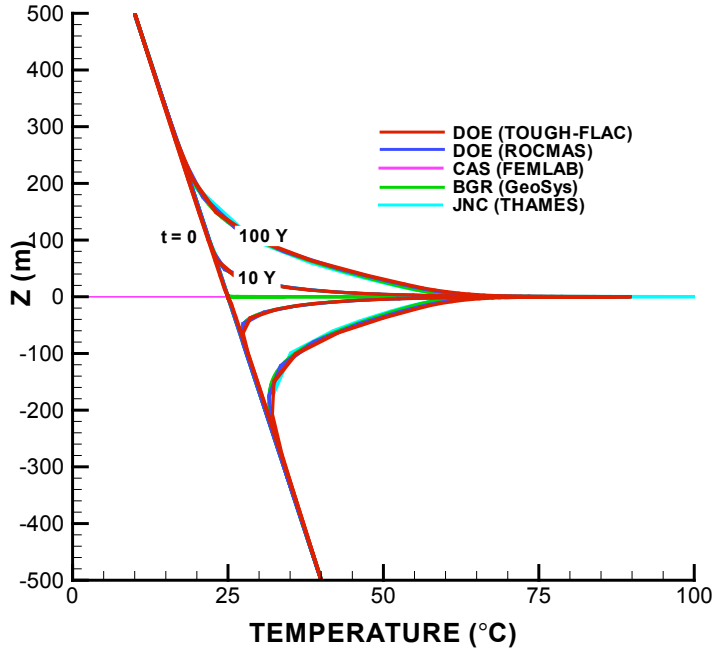
(a) Profiles for t ≤ 100 years
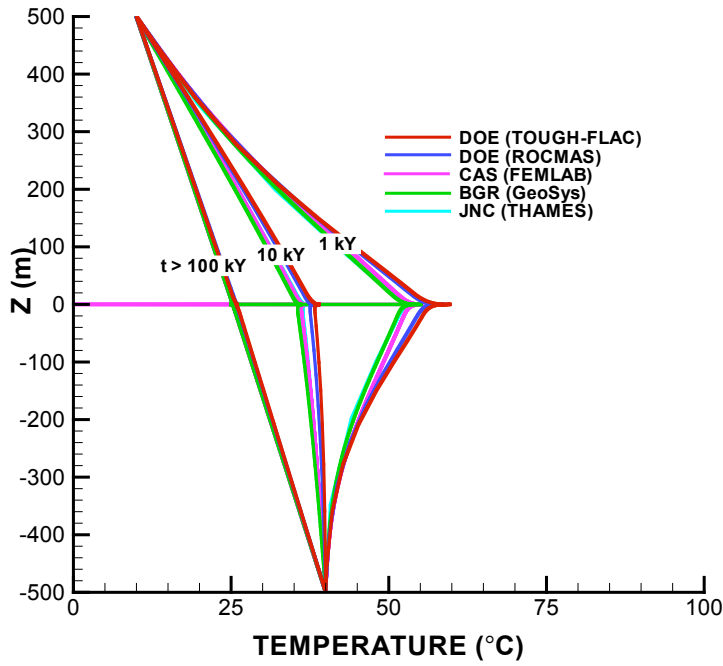
(b) Profiles for t ≥ 1000 years

Figure 4.2. Comparison of vertical temperature profiles
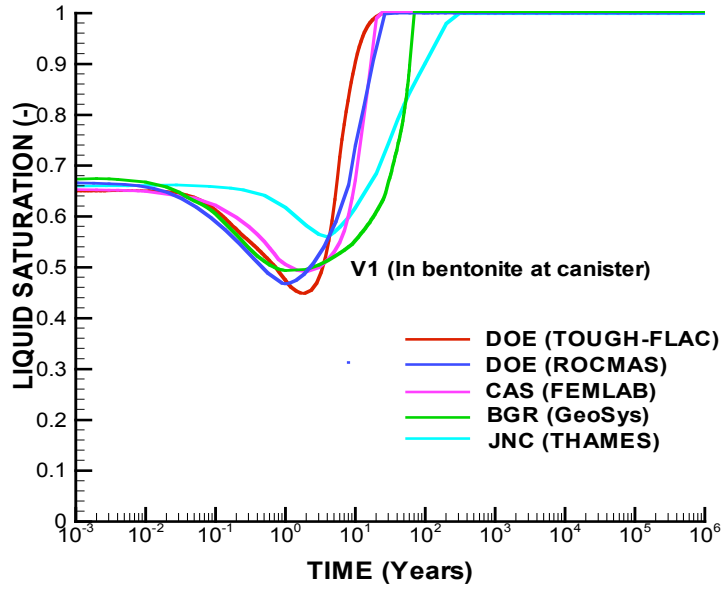
Figure 4.3.   Comparison of simulation results for the evolution of degree of saturation in bentonite (Point V1).
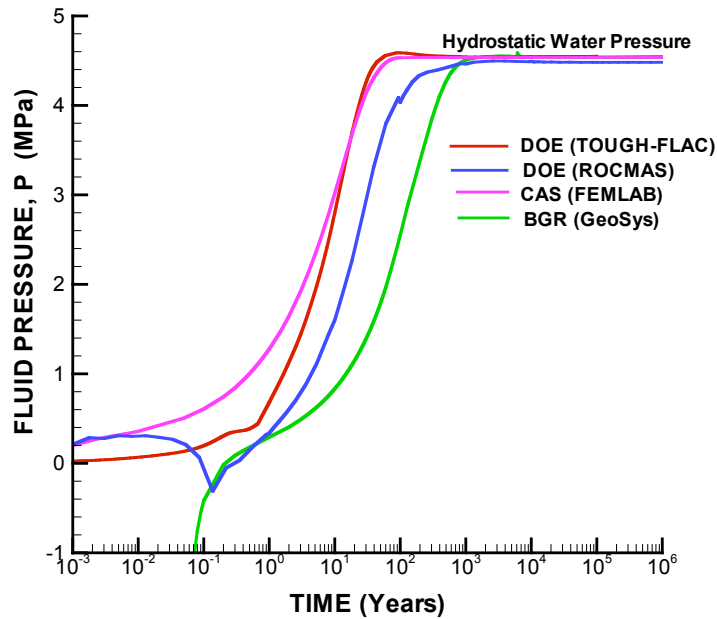
Figure 4.4.   Comparison of evolution of water pressure at Point V3 located at the drift wall.
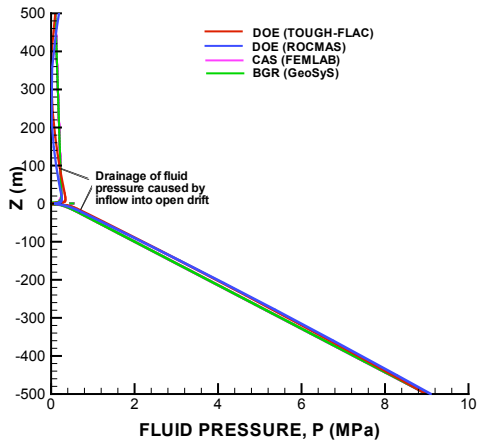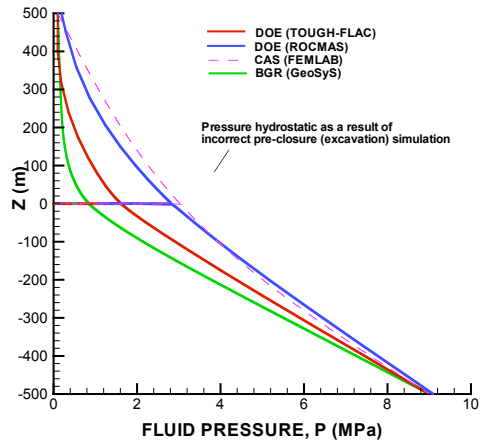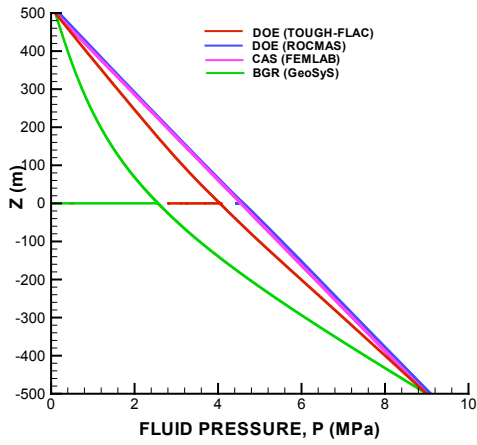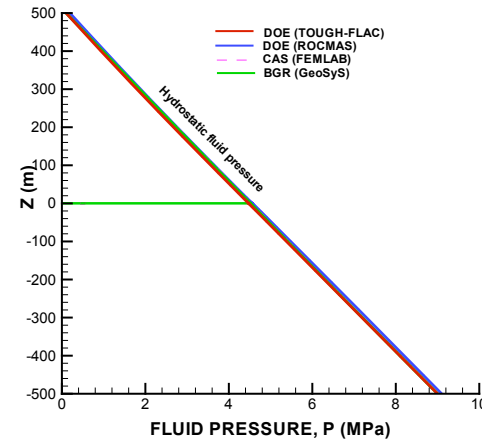
Figure 4.5. Comparison of simulation results of vertical pressure profiles
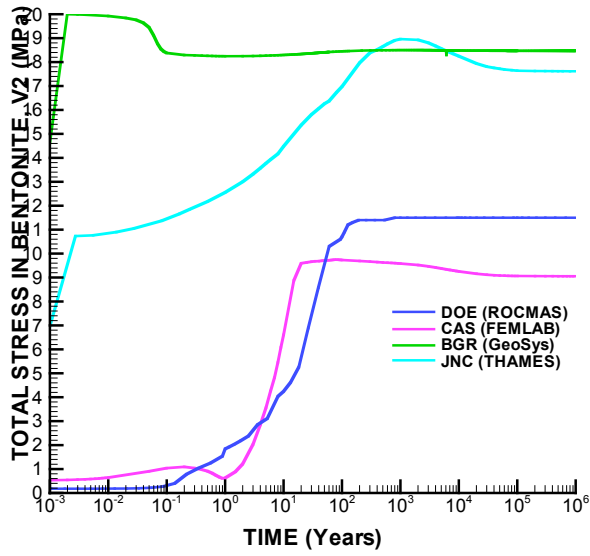
Figure 4.6. Comparison of evolution stress normal to the rock wall at point V1 located at the rock/bentonite interface
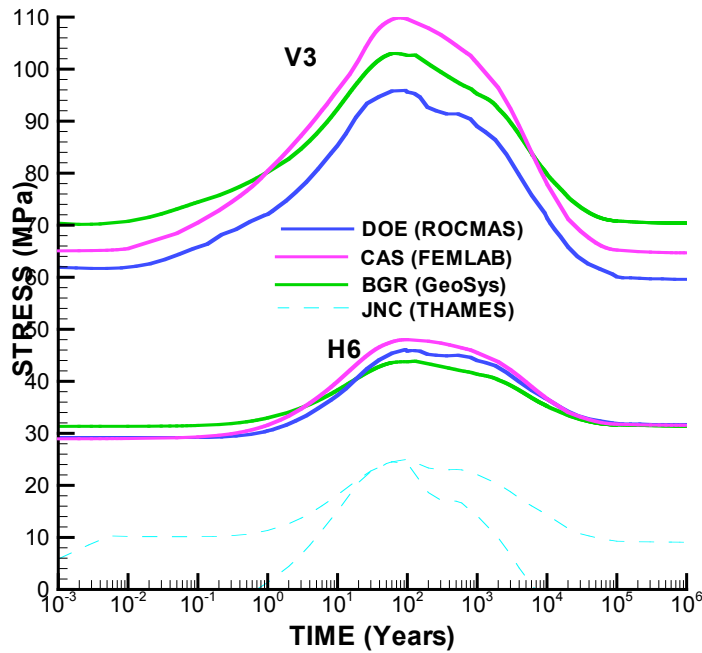
Figure 4.7. Comparison of evolution of horizontal stress in points V3 and H6
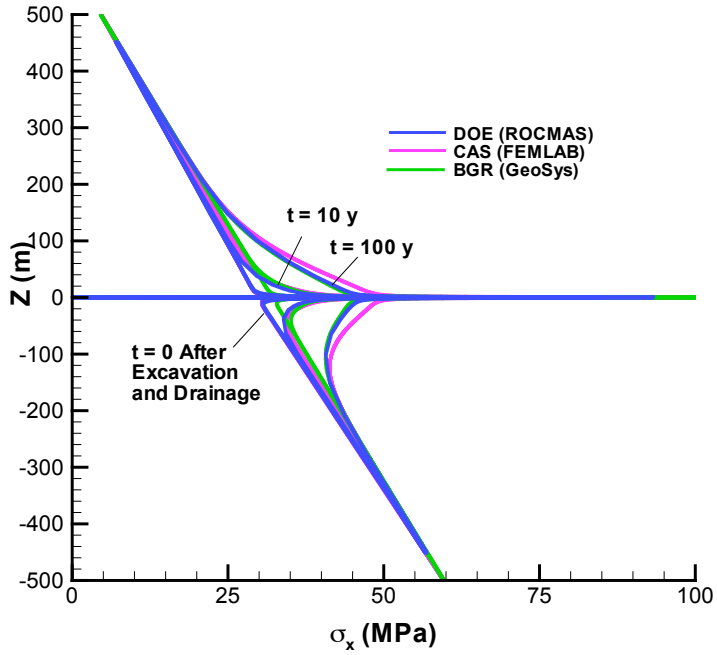
(a) Profiles for t ≤ 100 years
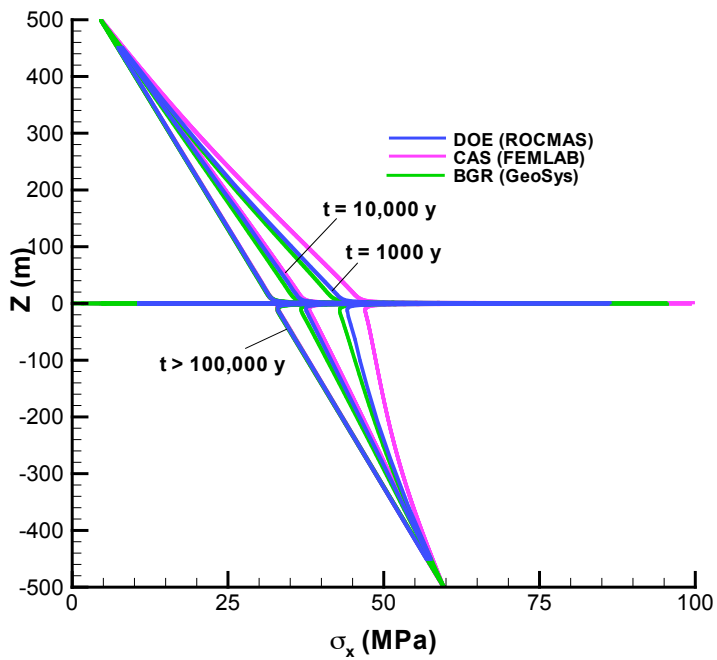
(b) Profiles for t ≥ 1000 years

Figure 4.8. Comparison of vertical profiles of horizontal stress
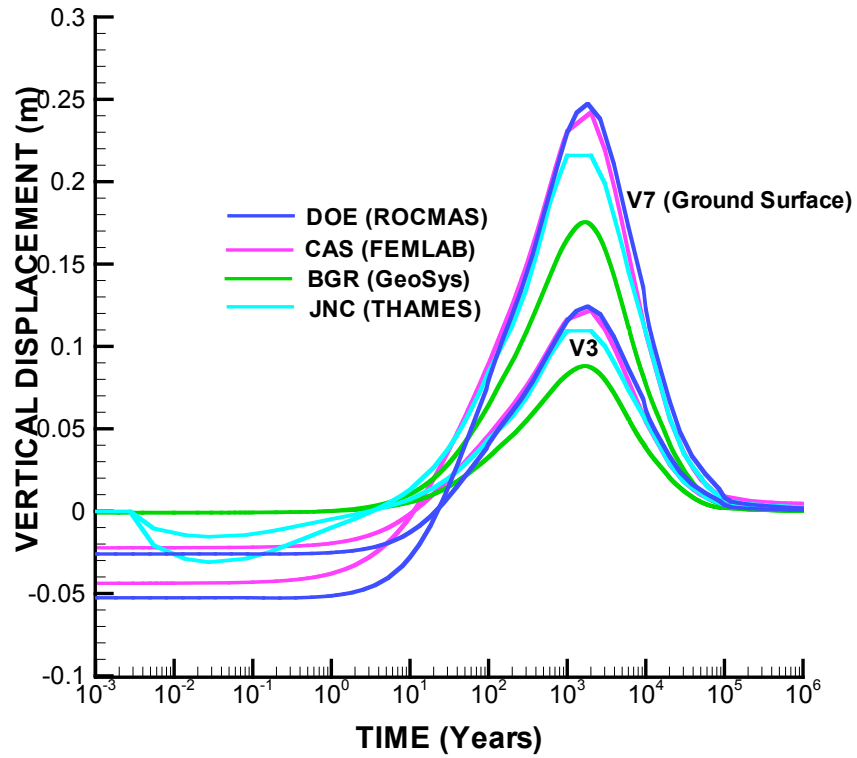
Figure 4.9.   Comparison of evolution of vertical displacement at the ground surface (V7) and at the drift (V3)
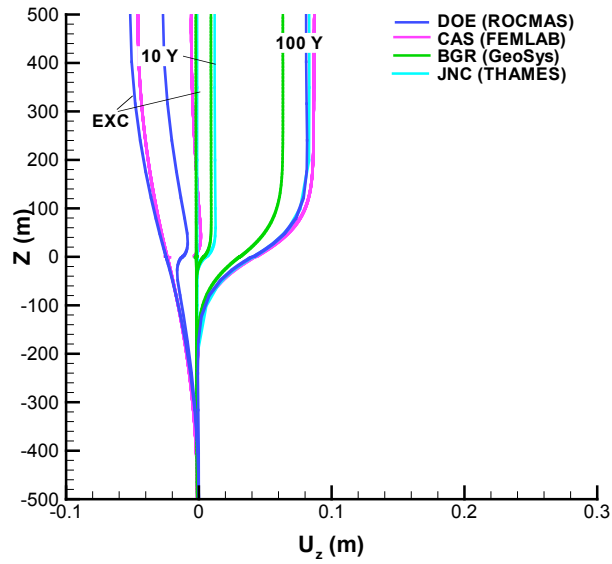
(a) Profiles for t ≤ 100 years
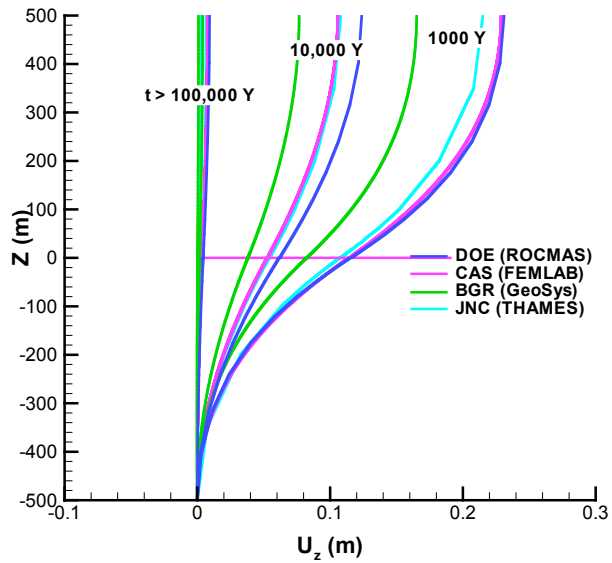
(b) Profiles for t ≥ 1,000 years

Figure 4.10. ROCMAS simulation results of vertical displacement profiles
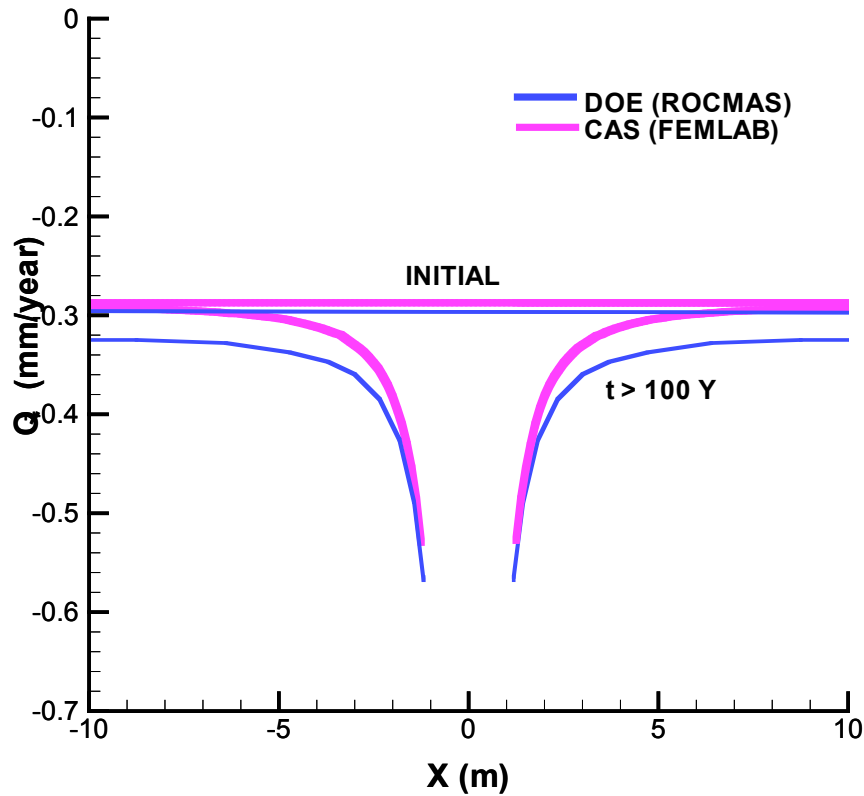
Figure 4.11.   Comparison of DOE (ROCMAS) and CAS simulation results of vertical flux through the repository horizon

4.3.   REPOSITORY CASE D_THM2 (YUCCA MOUNTAIN TYPE)

4.3.1   Comparison of Model Approaches

The basic modeling approaches employed by the four international teams (DOE, BGR, JNC, CAS) modeling D_THM2 are summarized in Table 4.3. All codes are capable of handling fully coupled thermal-hydrological-mechanical (THM) processes; however, the simulations with ROCMAS have been conducted in a TM-only mode for the sake of comparison with more complex models. Simple elastic approaches are used for simulation of the rock-mechanical behavior, consistent with the simplified task definition for Phase 1 work. However, all models are generally capable of simulating elasto-plastic behavior, which may become necessary when stress-induced changes in hydrologic properties are to be considered in the next phases of D_THM2.

The Yucca Mountain type of repository simulated in case D_THM2 involves complex two-phase flow (gas and liquid phases with components of air and water) interactions between fractures and matrix rock at high (above boiling) temperatures. Because of the higher peak temperatures, the thermal-mechanical effects are likely stronger than in the

FEBEX case (D_THM1). Boiling and subsequent condensation of pore water triggers moisture redistribution processes in the rock surrounding the repository drift that last for hundreds of years. The thermally induced liquid and gas flow processes are strongly affected by the vastly different hydrological properties of the fractures and the rock matrix, respectively. The matrix holds significant amounts of water even at ambient conditions, but has a very small permeability, so that overall matrix fluxes are small. The fracture network, on the other hand, is highly permeable, but has a small capillarity, and thus is typically dry under ambient conditions. However, as the near-drift rock is heated up and significant flux perturbation occurs, the fractures become important flow conduits for vapor and liquid. A proper analysis of near-field TH processes in the fractured porous rock would ideally require multi-phase flow and heat transport capabilities employed in a model that can account for the specific hydrologic properties and conditions of fractures and matrix, with their vastly differing permeabilities and moisture retention characteristics.

TOUGH-FLAC, which has been extensively applied in the modeling of coupled THM processes for the unsaturated zone at Yucca Mountain, has all the necessary modeling capabilities listed above. The code accounts for multi-phase flow in liquid and gas phases and deals with phase transition from boiling and condensation in a rigorous manner. Fracture and matrix conditions can be distinguished using the dual continuum model (DKM). A dual continuum model is based on the continuum concept, but uses two separate, overlapping continua for fractures and matrix. At each location, there are two nodes (or volumes) representing the fractures and the matrix, respectively, each having a pressure, saturation, temperature, or stress value. Thus, local disequilibrium between fractures and matrix can be modeled without explicitly accounting for all individual fractures and matrix blocks. This allows considering the hydrologic properties and conditions of fractures and matrix with their vastly different hydrologic properties. Dual continuum models are a good choice for D_THM2 (except for using discrete fracture-matrix continuum models or hybrid models), but require significant code development.

At this point, none of the other codes used for D_THM2 has the full multi-phase capability that is incorporated into TOUGH-FLAC, and certain simplifications become necessary. For example, as mentioned above, ROCMAS solves for thermal-mechanical processes only. Since saturation is unknown, the changes in thermal properties (as the formation dries out at above-boiling temperatures) are accounted for by a simplified temperature-dependent approach described in Barr et al. (2005, Section 6.4.2). The other codes solve Richard's equation for liquid flow, but neglect gas flow. Instead, they account for transport of water vapor in a simplified manner, by solving a diffusion problem with diffusivity dependent on pressure and temperature gradients.

Also, only TOUGH-FLAC is capable of representing the fractured rock mass as a dual continuum; single continuum models are used in all other simulations. It is clear from previous modeling exercises that the flow processes predicted with single continuum models are not adequate when the near-drift rock is heated up and significant flux perturbation occurs (with the fractures becoming important flow conduits for vapor and liquid). For future project phases, when understanding of flow processes becomes more important, teams that strive for a better hydrological response but want to avoid dual

continuum modeling may consider the so-called effective continuum model (ECM) (after Pruess et al. [1990]). An effective continuum model captures the different hydraulic characteristics of fractures and matrix, but assumes a local THM equilibrium between fractures and matrix at all times. For systems that are not too dynamic in nature, the ECM model gives quite adequate flow results.

Table 4.3.   Comparison of basic modeling approaches used for D_THM2

Team	Numerical simulator	Couplings considered	Mechanical model	Hydraulic model	Thermal Model for Boiling
DOE	TOUGH-FLAC	THM	Elastic	Dual continuum; multiphase liquid and gas flow	Full phase-change model for boiling
DOE	ROCMAS	TM	Elastic	NA	Temperature-dependent thermal properties adopted from (Barr et al., 2005, Section 6.4.2)
BGR	GeoSys/ Rockflow	THM	Elastic	Single continuum, unsaturated liquid flow, no gas flow; thermal vapor diffusion	Temperature-dependent thermal properties adopted from (Barr et al., 2005, Section 6.4.2)
JNC	THAMES	THM	Elastic	Single continuum, unsaturated liquid flow, no gas flow; thermal vapor diffusion	Unknown, probably simple conduction model without boiling
CAS	FRT-THM	THM	Elastic	Single continuum, unsaturated liquid flow, no gas flow; thermal vapor diffusion	Temperature-dependent thermal properties (Barr et al., 2005, Section 6.4.2)

4.3.2   Comparison of Model Results

In this section, the calculated THM responses for Case D_THM2 (Yucca Mountain type) are compared following output specification given in Barr et al. (2005, Section 6.5). The results of four different analyses are compared. These were developed by DOE, using TOUGH-FLAC and ROCMAS, by CAS using FRT-THM, by BGR using GeoSys/Rockflow, and by JNC using THAMES..

Temperature Evolution

Figures 4.12 and 4.13 compare the temperature evolution calculated from the five alternative models. The agreement between the different models is good. Similarly to the THM_1 case (*FEBEX* type), the temperature evolution in the THM_2 case (*Yucca*

Mountain type) depends somewhat on the interpolation of the tabulated input heat decay function. However, in the case of THM_2, the heat decay function is better defined through closely spaced tabular values.

In the THM_2 case, the temperature evolution is significantly affected by drying (through boiling of pore water) and rewetting of the near-field rock mass. A peak temperature of 120 to 125°C is calculated by the different models, with the CAS analysis yielding the highest value. It is likely that the slightly higher peak temperature obtained by the CAS is a result of a simplified analysis of the boiling-zone effect on heat transfer (simplified treatment of changes in thermal conductivity as the rock mass dries, simplified treatment of latent heat of vaporization as water boils; see Barr et al., 2005). A similarly high peak temperature was obtained by the DOE team when using the same kind of simplified boiling effect model (see Appendix C). The DOE team found that the simplified boiling model tends to overestimate the effect of boiling on the heat transfer. A pure conduction model yielded a temperature evolution that better matched that of a fully described two-phase fluid flow and heat transport model.

Evolution of Water Saturation

Figure 4.14 compares the initial saturation values in the entire domain for DOE (TOUGH-FLAC) and CAS (FRT-THM). The DOE (TOUGH-FLAC) model, featuring a dual continuum representation of the fractured rock, predicts matrix saturation values between 80 to 92%, whereas fracture saturation varies between 2 to 2.5%, with the highest values occurring at large depth. The CAS (FRT-THM) model uses a single continuum approach with retention properties equal to those of the matrix. Consequently, the CAS single continuum saturation distribution is close to that of the matrix results from the DOE (TOUGH-FLAC) model.

Figure 4.15 compares the evolution of liquid saturation at the drift wall for four models. The figure shows that rock at the top of the drift begins to dry at about 50 years, when boiling occurs at the drift wall. In the DOE (TOUGH-FLAC) analysis, the fractures dry quickly, whereas the matrix has not completely dried until about 100 years. Rewetting of fractures occurs after about 400 years, and the matrix is resaturated to original conditions at about 700 years. In contrast, the CAS and BGR models do not predict a full dryout to zero saturation. This is probably a result of neglecting fracture gas flow in the model. As a result, vapor produced from boiling cannot as easily migrate away from the boiling location as in a dual continuum model, where the fractures offer highly efficient conduits for vapor flow. The total dryout time till rewetting calculated by CAS (FRT-THM), DOE (TOUGH-FLAC) and BGR (GeoSys) models is similar, while the time evolution of saturation is somewhat different. The JNC (THAMES) results indicate limitations in solving the above boiling TH effects using the simplified single continuum approach. Better agreement is expected in future project phases, when more rigorous models (not just single continuum) will be used by the other teams to simulate flow in fractures and matrix rock.

Evolution of Stress

Figures 4.16 and 4.17 present the evolution the horizontal stress. The calculated results for four of the five model calculations are very consistent, both in trends and magnitudes. In contrast, the model results submitted by JNC (shown as a dashed line in Figure 4.16) suffer from some error in the input data. Based on the initial stress results, it appears that the JNC analysis does not properly account for the excavation of the drift. In the analyses by DOE,CAS and BGR, the initial stress is higher at Point V3 as a result of stress concentrations near the drift wall. In the JNC results, on the other hand, the initial horizontal stresses in V3 and H6 are the same, indicating no stress redistribution around the excavated drift. For the DOE, CAS and BGR simulations, the peak stress at V3 varies between 33 to 35 MPa, whereas the peak stress at H6 is almost identical at about 14 MPa. The slight variation in peak stress at V3 is likely caused by interpolation inaccuracies, stemming from different mesh discretizations in a region of steep stress gradients, as well as from differences in the exact location of the point representation in the numerical mesh. However, overall a good agreement in the calculated stress evolution has been achieved. More work is needed by the JNC team to improve the current prediction.

Evolution of Displacement

Figures 4.18 and 4.19 present the evolution of vertical displacements. The peak displacement at the ground surface is about 0.23 m and occurs after about 1,000 years. The agreement between the calculated displacements among three out of four models (DOE models, CAS model and JNC model) is very good. The result by BGR shows similar trend and magnitude but displays an unexplained kink at about 100 to 200 years.

Evolution of Vertical Water Flux

Figure 4.20 presents a horizontal profile of the vertical percolation flux calculated by the DOE (TOUGH-FLAC) and CAS (FRT-THM) models. The vertical flux has not been provided by other modeling teams at this time and the comparison in Figure 4.20 is made only for flux at t = 0 (after excavation). Figure 4.20 shows that the vertical flux away from the drift is 6 mm/year, which is dictated by the water flux supplied as infiltration at the top boundary of the model. The effect of the excavated drift and dryout zone around the drift on vertical flux is evident. At t = 0, the vertical flux is diverted around the drift (due to capillary barrier effects) leading to a water flux of about 15 to 20 mm/year near the drift wall. The DOE (TOUGH-FLAC) results also shows that at 100 years, the water is diverted around the dryout zone, which extends to a few meters from the drift wall (not shown in this figure). Within that dryout zone, water saturation is either zero (fractures) or very small (matrix) and liquid fluxes are practically zero.

Summary of Comparison of Model Results for THM2 Case

Overall, a good agreement in the evolution of temperature and stress was achieved. A small difference in peak temperature is caused by the simulation approach for TH coupling, but this has a minor impact on the mechanical responses. The thermal-mechanical effects can be accurately calculated using a simple thermal-elastic heat conduction model. The analysis of fluid flow, which involves complex interaction between matrix and fractures, has only been fully analyzed with DOE's TOUGH-FLAC model, featuring a dual continuum model. All other teams have used simple single continuum approaches, which are not capable of simulating the complex interaction

between fractures and matrix in a thermally perturbed system. Improved single continuum models, such as the effective continuum model approach (ECM), should be used by these teams in case they want to avoid the complexity of a full dual continuum representation. This should provide more consistent and comparable results in vertical flux and liquid saturation. This is important for a proper comparison of the impact of THM processes on the vertical percolation flux. However, the comparison of stress evolution by three models is good and sufficient for moving on to the next phase of Task D_THM2. Some revision is needed for the JNC model, which currently has difficulty predicting the stress conditions.
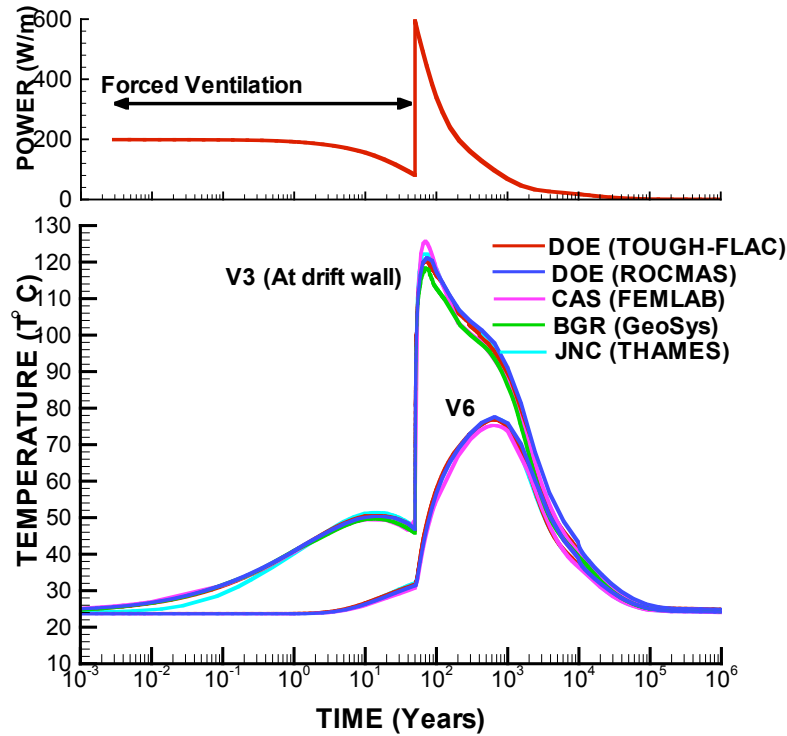
Figure 4.12.   Power and comparison of temperature evolution at two selected points
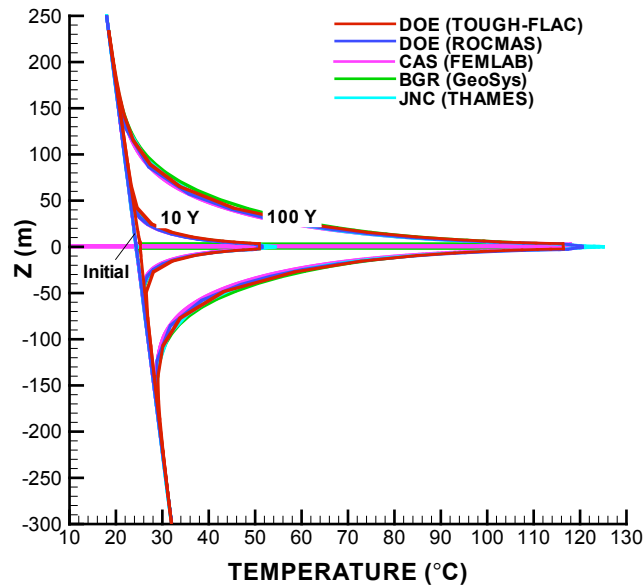
(a) Profiles for t ≤ 100 years
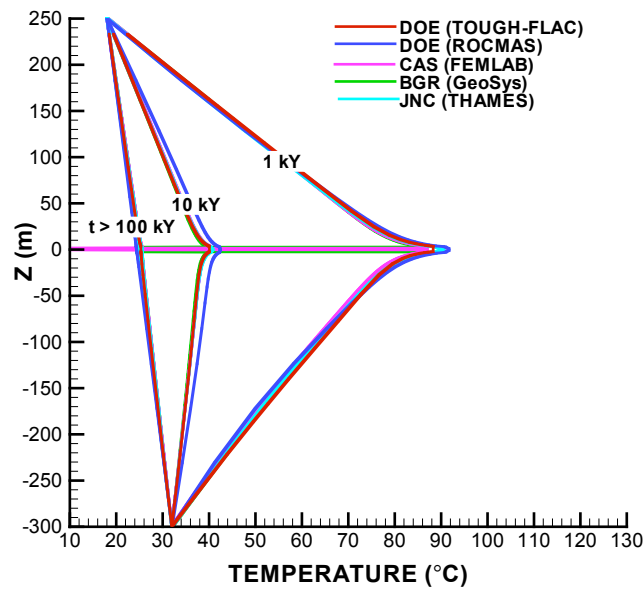
(b) Profiles for t ≥ 1000 years

Figure 4.13.   Comparison of vertical temperature profiles
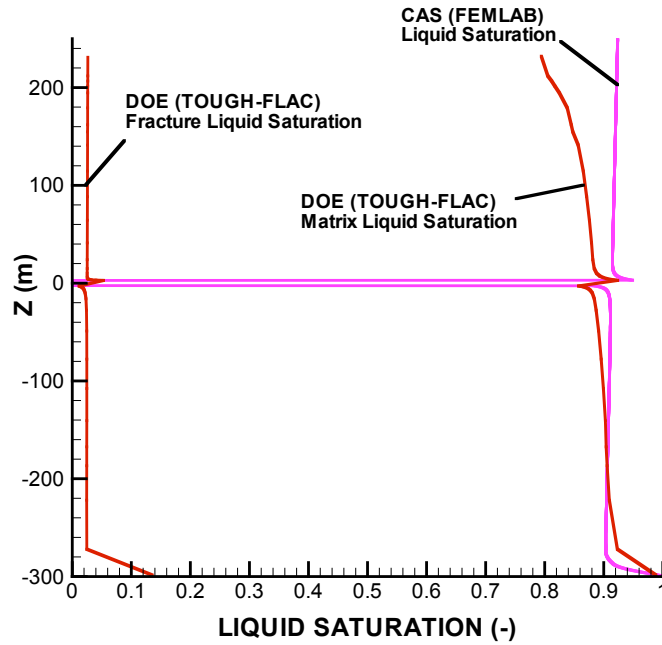
Figure 4.14. Simulation results of vertical profiles of initial saturation for a dual permeability model (DOE, TOUGH-FLAC) and a single continuum model (CAS, FEMLAB)
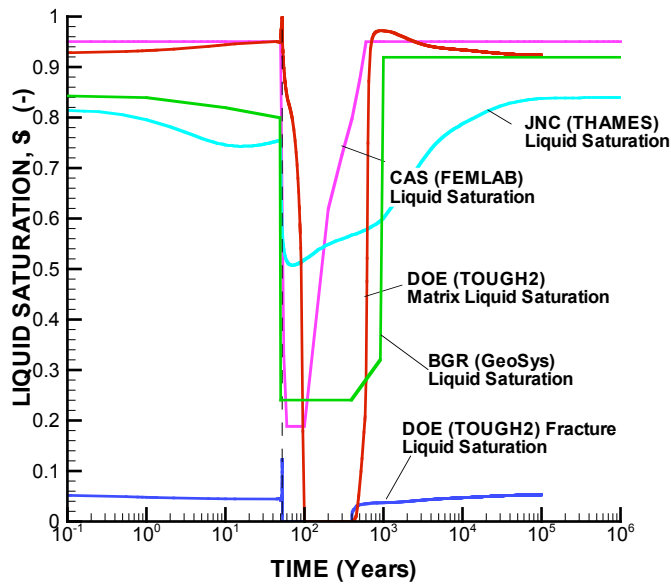
Figure 4.15. Evolution of liquid saturation in fracture and matrix continua at Point V3 located at the drift wall on top of the drift for a dual permeability model (DOE, TOUGH-FLAC) and single continuum models (CAS-FEMLAB, BGR-GeoSys, and JNC-THAMES)
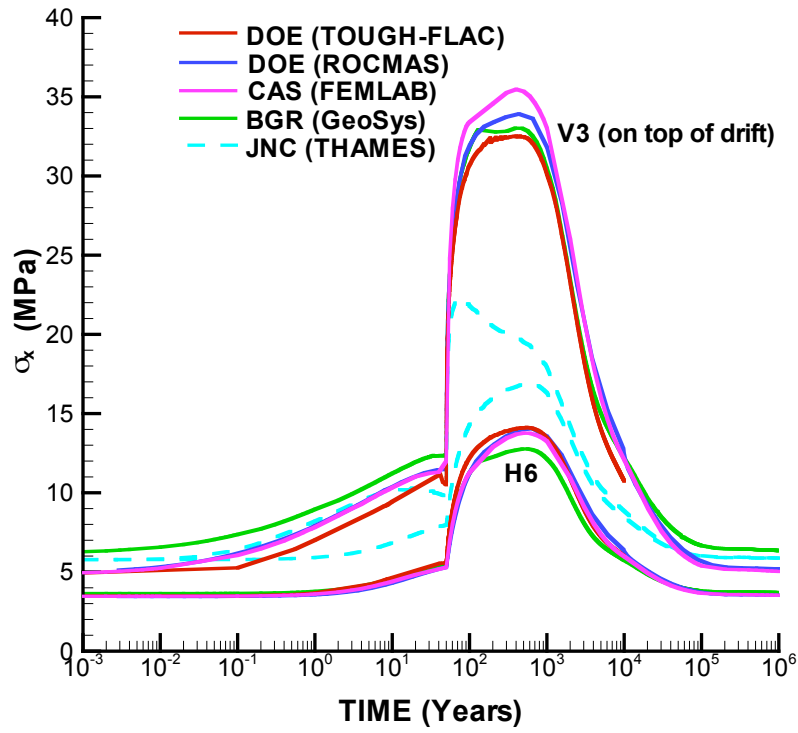
Figure 4.16. Comparison of simulation results of evolution of horizontal stresses in monitoring points V3 (near drift) and H6 (away from drift)
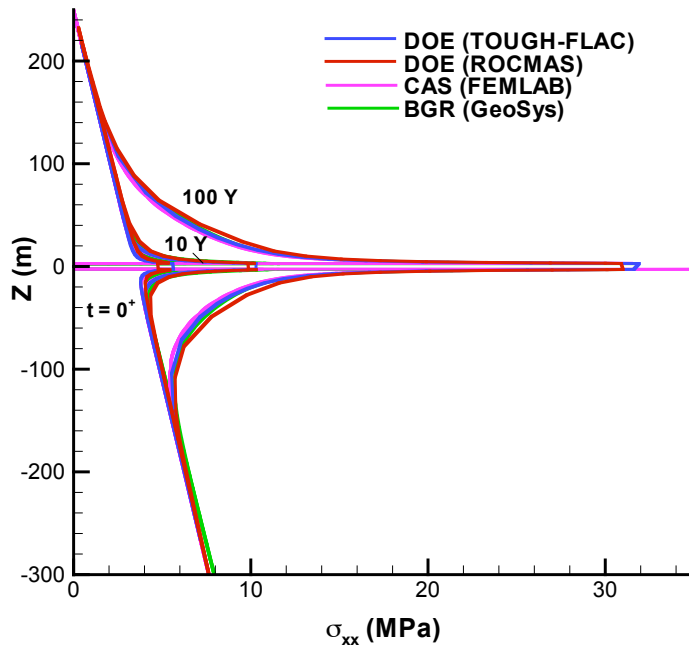
(a) Profiles for t ≤ 100 years
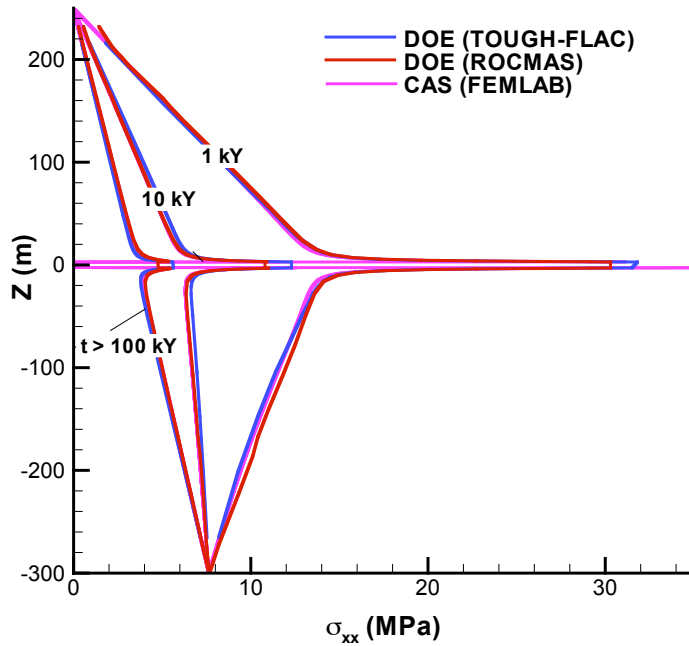
(b) Profiles for t ≥ 1000 years

Figure 4.17. Comparison of vertical profiles of horizontal stress
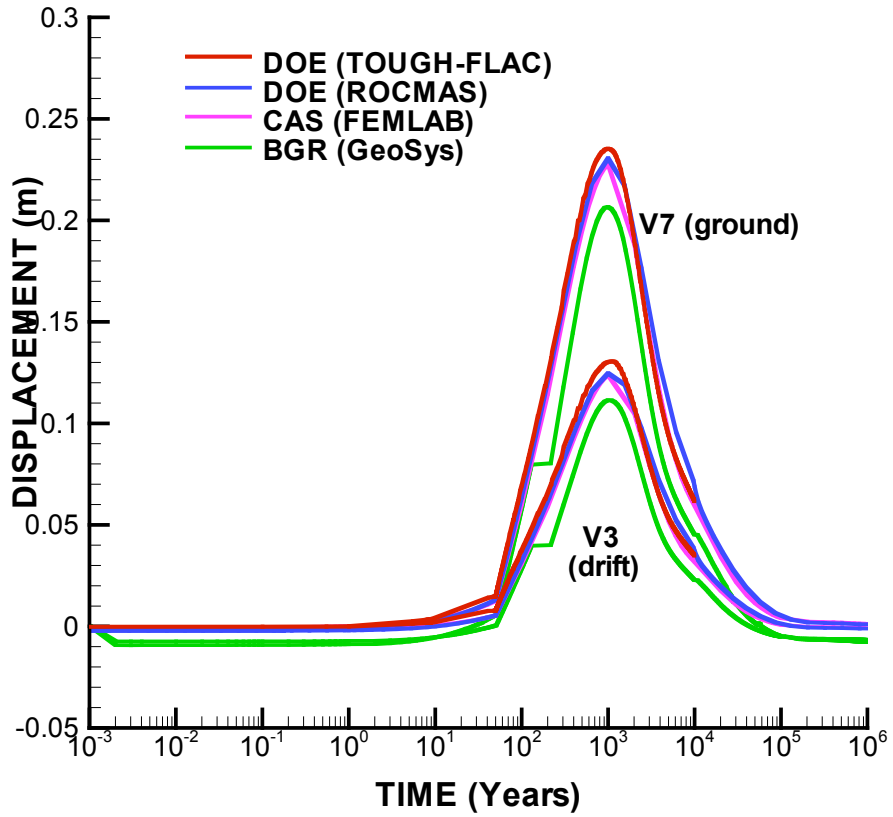
Figure 4.18. Comparison of simulated evolution of vertical displacement
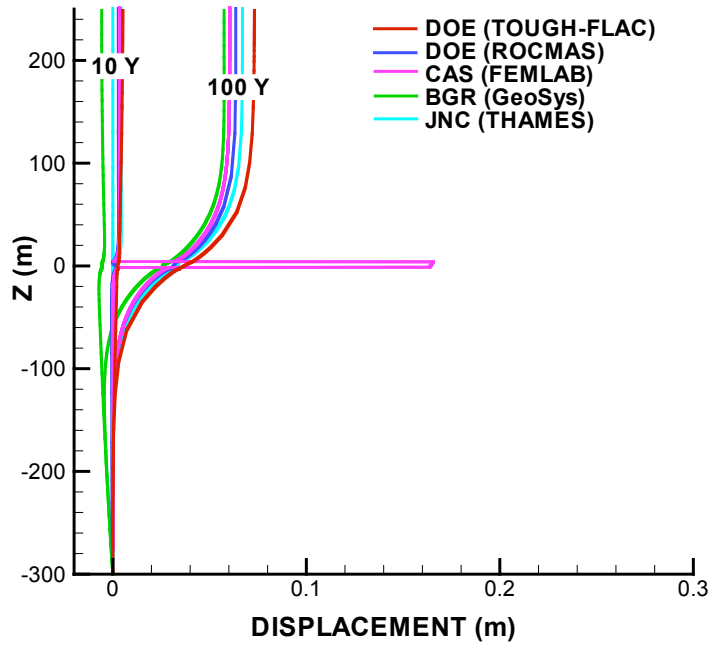
(a) Profiles for t ≤ 100 years
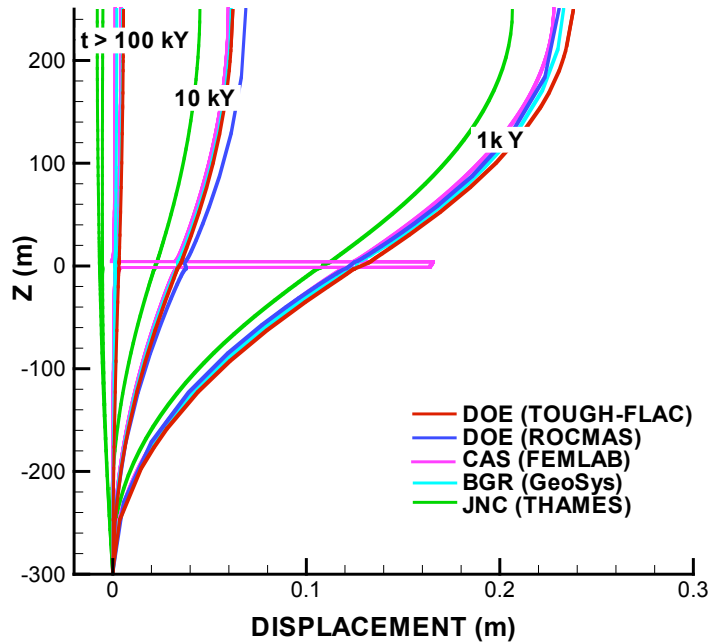
(b) Profiles for t ≥ 1000 years

Figure 4.19. Comparison of simulation results of vertical displacement profiles
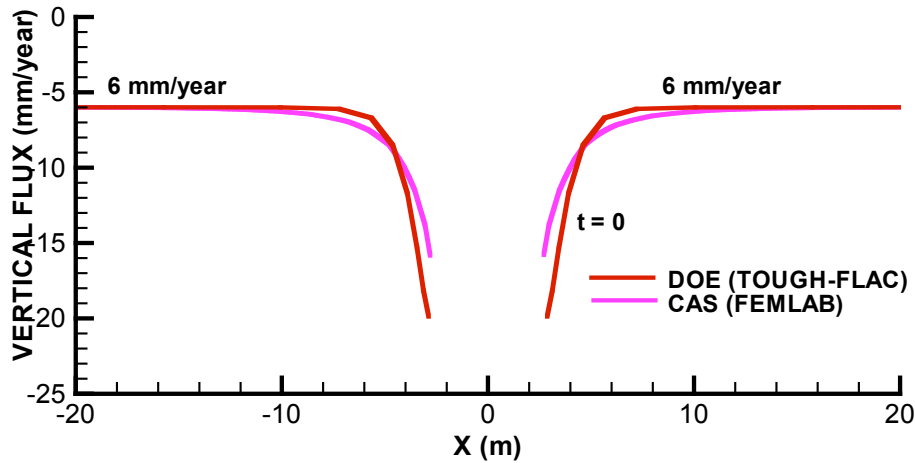
Figure 4.20. Comparison of TOUGH-FLAC and CAS simulation results of vertical flux across a horizontal profile

4.4.   FUTURE THM WORKSCOPE

As discussed in previous sections, the Phase 1 (Model Inception Phase) activities have largely been finalized, with good agreement among all teams for thermal and mechanical processes. A few remaining model discrepancies have been identified, and a few revised simulations will have to be conducted by individual teams for full completion of Phase 1. Thus, the next step for all team is to move forward into Phase 2 modeling. As summarized in Section 2.4.1, Phase 2 modeling involves more focus on hydrological processes, including prediction of THM property changes with conceptual models chosen by the different research teams, sensitivity analysis with respect to THM property changes plus uncertainty analysis, application of alternative conceptual models for fractured rock (i.e., discrete vs. continuum), and development of model data based on various reports and site data, instead of using pre-defined values (see Appendix A). Reports that may be used for D_THM1 are listed below, together with web sites from where they can be retrieved.

Table 4.4.   Supporting information for Phase 2 of D_THM1

Reference	Comment
Keusen H.R., Ganguin J., Shuler P. and Buletti M. (1989). Grimsel Test Site: Geology NAGRA NTB 87-14E, FEb 1989.	Download from LBNL web site: http://esd.lbl.gov/people/kavina/DECOVALEX/THM1_Phase2_Docs/
Amiguet J.-L. (1985). Grimsel Test Site. Felskennwerte von intaktem Granit. Zusammenstellung felsmechanisher Laborresultate diverse granitische Gesteine. NAGRA, NIB 85-05, Sep. 1985.	Download from LBNL web site: http://esd.lbl.gov/people/kavina/DECOVALEX/THM1_Phase2_Docs/
Pardillo J., Campos R. and Guimera J. (1997). Caracterizacion geologica de la zone de ensayo FEBEX (Grimsel – Suiza). CIEMAT, 70-IMA-M-2-01, May 1997.	Download from LBNL web site: http://esd.lbl.gov/people/kavina/DECOVALEX/THM1_Phase2_Docs/
Pardillo J. and Campos R. (1996). FEBEX-Grimsel Test Site (Switzerland). Considerations with respect to the fracture distribution. CIEMAT, 70-IMA-L-2l05, Mar. 1996.	Download from LBNL web site: http://esd.lbl.gov/people/kavina/DECOVALEX/THM1_Phase2_Docs/
Guimera J., Carrera J., Marinez L., Vazquez E., Ortuno F., Fierz T., Bulher C., Vives L., Meier P., Median A., Saaltink M., Ruiz B. and Pardillo J. (1998). FEBEX Hydrogeological characterization and modelling. UPC, 70-UPC-M-0-1001, Jan 1998.	Download from LBNL web site: http://esd.lbl.gov/people/kavina/DECOVALEX/THM1_Phase2_Docs/
Fujita T., Sugita Y., Chijimatsu M. and Ishikawa (1996). Mechanical properties of fracture. Power Reactor and Nuclear Fuel Development Corporation (PNC), Technical note 06-95-06.	Download from LBNL web site: http://esd.lbl.gov/people/kavina/DECOVALEX/THM1_Phase2_Docs/
DECOVALEX III (2000). Task 1. Modeling of FEBEX in situ test. Part A: Hydromechanical modeling of the rock.	Download from LBNL web site: http://esd.lbl.gov/people/kavina/DECOVALEX/THM1_Phase2_Docs/
DECOVALEX III (2001). Task 1. Modeling of FEBEX in situ test. Part B: Thermo-hydro-mechanical analysis of the bentonite behaviour.	Download from LBNL web site: http://esd.lbl.gov/people/kavina/DECOVALEX/THM1_Phase2_Docs/
Alonso et al. (2004). Final report of DECOVALEX III, Task1: FEBEX in situ test. SKI report expected during 2004.	Download from Decovalex website: Login and go to Documents / Reports from DECOVALEX III and BENCHPAR / Final reports / **Task 1** /

Reports that may be used for D_THM2 are listed below, together with web sites where they can be retrieved.

Table 4.5.   Supporting information for Phase 2 of D_THM2

Reference	Comment
BSC (Bechtel SAIC Company) 2003a. *Drift Degradation Analysis*. ANL-EBS-MD-000027 REV 02. Las Vegas, Nevada: Bechtel SAIC Company.	Download from: http://ocrwm.doe.gov/documents/amr/36086/index.htm
BSC (Bechtel SAIC Company) 2003b. *Calibrated Properties Model*. MDL-NBS-HS-000003 REV 01. Las Vegas, Nevada: Bechtel SAIC Company. ACC: DOC.20030219.0001.	Download from: http://ocrwm.doe.gov/documents/amr/41503/index.htm
CRWMS M&O (Civilian Radioactive Waste Management System Management and Operating Contractor) 2000. *Statistical Analysis of Empirical Rock Properties by Lithographic Units*. CAL-GCS-GE-000001 Revc 00. Las Vegas.	Download from LBNL web site: http://esd.lbl.gov/people/kavina/DECOVALEX/THM2_Phase2_Docs/
CRWMS M&O (Civilian Radioactive Waste Management System Management and Operating Contractor) 1997. *Yucca Mountain Site Geotechnical Report*. B00000000-01717-5705-00043 REV 01. Two volumes. Las Vegas, Nevada.	Download from LBNL web site: http://esd.lbl.gov/people/kavina/DECOVALEX/THM2_Phase2_Docs/
CRWMS M&O (2000). Fracture Geometry Analysis for the Stratigraphic Units of the Repository Host Horizon. ANL-EBS-GE-000006 REV 00. Las Vegas, Nevada.	Download from LBNL web site: http://esd.lbl.gov/people/kavina/DECOVALEX/THM2_Phase2_Docs/
Datta et al. (2004). DECOVALEX III, Task 2, Final Report. (SKI report expected during 2004).	Download from LBNL web site: http://esd.lbl.gov/people/kavina/DECOVALEX/THM2_Phase2_Docs/
Hoek E., Carranza-Torres C. and Corkum B., (2002). Hoek-Brown Failure Criterion – 2002 Edition 5th North American Rock Mechanics Symposium and 17th Tunnelling Association of Canada Conference: NARMS-TAC 2002, July 7-10 University of Toronto, Toronto, Ontario, Canada.	Download from LBNL web site: http://esd.lbl.gov/people/kavina/DECOVALEX/THM2_Phase2_Docs/
Mongano G.S., Singleton W.L., Moyer T.C., Beason S.C., Eatman G.L.W. Albin A.L. and Lung R.C. (1999) Geology of the ECRB Cross Drift – Exploratory Studies Facility, Yucca Mountain Project, Yucca Mountain, Nevada. Denver Colorado U.S. Geological Survey.	Download from LBNL web site: http://esd.lbl.gov/people/kavina/DECOVALEX/THM2_Phase2_Docs/
CRWMS M&O (1998). G*eology of the Exploratory Studies Facility Topopah Spring Loop*. BAB000000-01717-0200-00002 REV 01. Las Vegas, Nevada	Download from LBNL web site: http://esd.lbl.gov/people/kavina/DECOVALEX/THM2_Phase2_Docs/
Olsson W.A. and Brown S. (1995). *Mechanical properties of fractures from drill holes UE25-NRG-4, USW-NRG-6, USW-NRG-7, and USW-SD-9 at Yucca Mountain, Nevada*. Sandia National Laboratories Technical Report, Sand 95-1736. Albuquerque New Mexico. Sandia	Download from LBNL web site: http://esd.lbl.gov/people/kavina/DECOVALEX/THM2_Phase2_Docs/
Brown S.R. (1985) Simple mathematical model of a rough fracture. J. Geophys. Res. 100, 5941–5952.	Download from LBNL web site: http://esd.lbl.gov/people/kavina/DECOVALEX/THM2_Phase2_Docs/

5.   TASK D_THC: GEOCHEMICAL ANALYSIS

Three research teams are involved in modeling Task D_THC, from Germany, Japan, and the U.S. The CAS team from China has decided to primarily focus on geomechanical issues; however, it was indicated that they might join at a later stage. Overall, the progress made by the research teams has been good, considering that geochemical processes are new to the DECOVALEX project. While the DOE team has conducted geochemical modeling of the Yucca Mountain site for over 10 years, other teams have less experience with THC models. Section 5.1 below gives a brief summary on the current status of the geochemical modeling work. Each team has provided a status report, which describes the conceptual model approaches and discusses modeling results, if available. With some minor editing for format consistency, these status reports have been added as Appendices G through I of this letter report (see attached CD). To bring out similarities and discrepancies between different research approaches, the LBNL research team has conducted a comparative evaluation of the status reports with regards to the conceptual models used and the simulation results. This comparative evaluation is summarized in Section 5.2.1 (Conceptual Models) and Section 5.2.2 (Simulation Results). Note that the comparison was only conducted for Task D_THC1, since modeling results were not available yet for the Yucca Mountain task.

5.1. SUMMARY STATUS OF D_THC RESEARCH WORK

For the teams from Japan and Germany, most of the initial project stages were devoted to code development and model testing. The JNC team from Japan started development of a code that can be used for a fully coupled thermal-hydrological-mechanical-chemical analysis (Table 5.1). The code uses a coupling system (COUPLYS) that links individual process codes for geomechanical analysis (THAMES), mass transport (Dtransu-3D-EL), and reactive geochemistry (PHREEQC). The code is currently in its testing stage and has not yet been applied to the D_THC test cases. JNC is also conducting a series of laboratory experiments (COUPLE-experiment) to better understand the geochemical evolution in a heated bentonite-rock system (see status report in Appendix H). The experiment, when finalized in March 2006, may provide valuable input data for the geochemical modeling of D_THC1.

Germany's BGR team has also been heavily involved in code development and testing. A THM code (GeoSys Rockflow) was combined with the reactive geochemistry code PHREEQC. Initial model simulations have been conducted for D_THC1, featuring the simplified FEBEX case as defined in the Model Inception Phase (see status report in Appendix I). As a next step, the BGR team will move into modeling of D_THC2.

DOE's team has conducted preliminary simulation work on D_THC1. Modeling of the Yucca Mountain case in D_THC2 would involve moderate revisions of the predictive simulations that have already been conducted for the Yucca Mountain Program (to adapt to the simplified setting and geometry). This task has not been completed, but will be finished during the next year as other teams also move into modeling of D_THC2.

The FEBEX case in D_THC1 required development of a completely new geochemical model by the DOE team. Prior to this modeling work, a significant amount of work was needed to construct the D_THC1 problem description, e.g., defining the bentonite and rock mineralogy, as well as the water chemistry. This model definition work for D_THC1 was conducted in close collaboration with the research teams in Japan and Germany. It should be noted that some definitions for D_THC1 are still somewhat preliminary and may need further refinement.

Table 5.1.   Research teams involved in and numerical models applied within Task D_THC of DECOVALEX-THMC

Team	Affiliation	Computer Code	Test Case Simulated
DOE-Team	Lawrence Berkeley National Laboratory (LBNL) for DOE	TOUGHREACT	D_THC1
JNC-Team	Japan Nuclear Cycle Development Institute (JNC)	COUPLYS with THAMES, Dtransu-3D-EL and PHREEQC	NA
BGR-Team	Center for Applied Geosciences Tuebingen, for BGR	GeoSys/Rockflow with PHEEQC	D_THC1

All teams submitted reports on the current work status . These status reports suggest (a) that sophisticated THC codes have been developed by JNC and BGR that should soon be capable of simulating both D_THC1 and D_THC2, and (2) that the preliminary simulation results for D_THC1 (by DOE 's team and BGR's team) are in reasonable agreement. However, more detailed comparison and further model revisions will be necessary in the future.

5.2.   REPOSITORY CASE D_THC1 (FEBEX TYPE)

5.2.1   Comparison of Model Approaches

The basic modeling approaches employed by the two international teams (DOE and BGR) modeling D_THC1 are summarized in Table 5.2. Both codes are capable of modeling thermal-hydrological-chemical (THC) coupling. At this point, both teams use a single continuum representation of the crystalline rock mass. This may change in later project phases, when the effect of sparsely distributed fractures may be considered in a more rigorous manner.

Note that TOUGHREACT simulates complex multiphase flow behavior, solving flow equations for both liquid and gas phases. In contrast, Geosys/Rockflow solves for variably saturated flow according to Richard's equation (assuming constant gas pressure), but does not explicitly account for gas flow along a gas pressure gradient. However, recognizing the impact of vapor movement in a thermally perturbed setting with evaporation processes, the code accounts for transport of water vapor in a simplified

manner, by solving a diffusion problem with diffusivity dependent on pressure and temperature gradients (e.g., see Appendix C, Equations 3.9 through 3.13).

Table 5.2.   Comparison of basic modeling approaches used for D_THC1

Team	Numerical simulator	Couplings considered	Hydraulic model	Geochemical Model	Transport
DOE	TOUGHREACT	THC Sequential noniterative	Single continuum; multiphase liquid and gas flow	Equilibrium mineral-water reactions, using HKF activity model	Advection/ diffusion of total concentrations (sequential)
BGR	GeoSys/Rockflow with PHREEQC	THC Sequential noniterative	Single continuum, unsaturated liquid flow, no gas flow; thermal vapor diffusion	PHREEQC	Advection/ diffusion of total concentrations (sequential)

5.2.2   Comparison of Model Results

Some preliminary comparisons of the BGR and DOE results for THC1 are presented in this section. Two cases were run by each group; one assuming the bentonite and granite are fully water-saturated and another with the bentonite partly saturated.

5.2.2.1 Temperature History

Temperatures at point V1 in the bentonite adjacent to the canister are shown for the DOE (TOUGHREACT-TR) and BGR (GeoSys/RockFlow-GSRF) simulations. Temperatures for the BGR model quickly rise to higher values than that for the DOE simulation, with a peak value of 92.1 using GSRF and 85.4 with TR. Because TOUGH-FLAC and GSRF simulations show comparable temperatures (Figure 4.1), and TR uses the same modules for solving heat and fluid flow as TOUGH-FLAC, it is likely that there are set-up or gridding issues that give rise to the temperature discrepancies. The differences will have to be reconciled prior to the start of Phase 2. These temperature differences, though, are unlikely to result in significantly different geochemical behavior, because the system is below boiling and the differences become a few degrees or less after about 20 years.
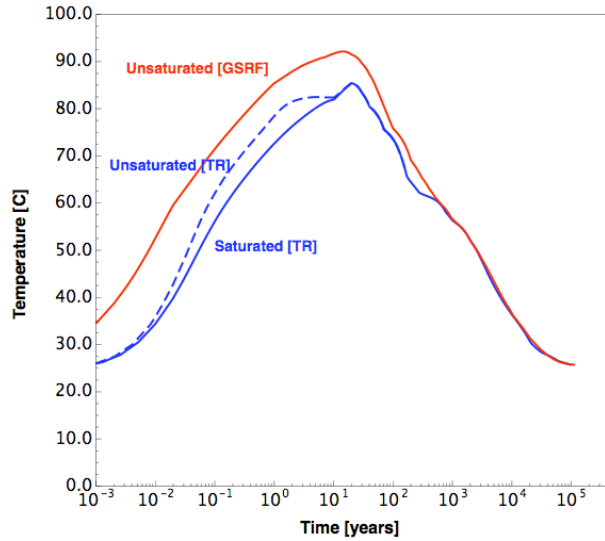
Figure 5.1.   Temperature history at point V1 using TOUGHREACT (TR) and GeoSys/RockFlow (GSRF).

5.2.2.2 Drying/Rewetting History of Bentonite

The evolution of liquid saturation at point V1 using GSRF and TR is shown in Figure 5.2. The minimum liquid saturation is somewhat lower in the TR simulation, dries out later, and fully rewets much more rapidly. These differences are likely a result of slightly different capillary pressure-saturation relations (alternative formulations given in the task description), and the different treatments of vapor transport, since the temperatures are consistently higher in the GSRF simulation, and therefore it would be expected to result in a lower minimum liquid saturation.
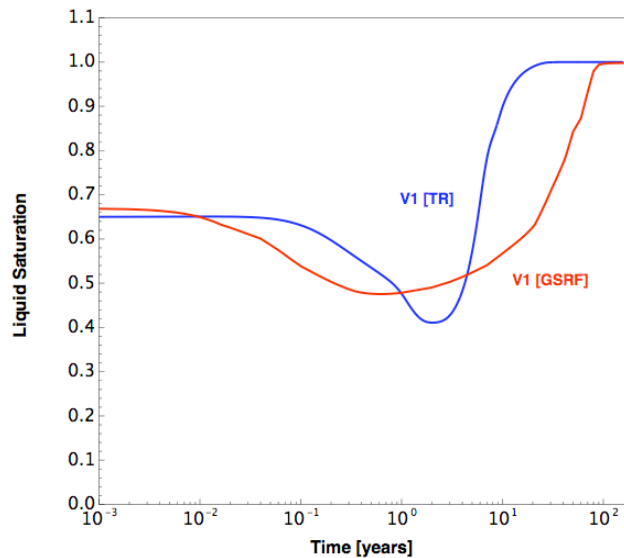
Figure 5.2.   Saturation history at point V1 using TOUGHREACT (TR) and GeoSys/RockFlow (GSRF).

57

5.2.2.3 Water Chemistry Evolution

Aqueous species concentration changes in the unsaturated case are dominated by diffusion and the influx of seawater during the rewetting phase, and modified by mineral-water reactions. Chloride (Cl) is controlled solely by molecular diffusion and flow, and therefore these aspects of the model can be compared without added uncertainties from the thermodynamics of mineral-water-reactions. Figure 5.3 shows a comparison of Cl and Na concentrations after 100 years. The TOUGHREACT chloride profile (solid green line) shows slightly greater diffusive exchange with the granite, probably owing to a larger tortuosity and porosity used in the DOE simulation. A small peak in the Cl concentration in the granite below the drift in the BGR results is not seen in the DOE simulation results. Otherwise, the profiles are very close. The Na profiles are also very similar with slightly lower concentrations in the bentonite for the BGR simulation. This may be due to a slightly less dissolution of albite in the granite with diffusion into the bentonite.
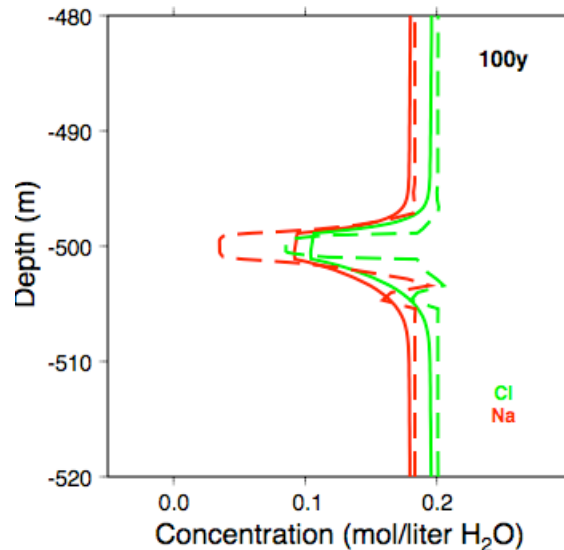
Figure 5.3.   Na and Cl concentrations for the unsaturated case after 100 years. TOUGHREACT results are shown as solid lines, and GeoSys/RockFlow results as dashed lines.

5.2.2.4 Mineral Evolution

Changes in mineral abundances can be compared qualitatively in Figure 5.4. The main effects in the granite are albite dissolution and quartz precipitation in both GSRF and TR simulations. Once a factor of 10 is applied to the GSRF results for unit equivalency, the amount of albite dissolved is about three times that seen in the TR results. Precipitation of K-feldspar in the bentonite adjacent to the granite is also seen in both simulations. In addition both simulations show calcite precipitation adjacent to the canister; however it extends through the entire bentonite in GSRF results, but not in TR results. It appears that the models are giving similar results for the major phases, but further comparisons will be necessary to compare the differences more systematically.
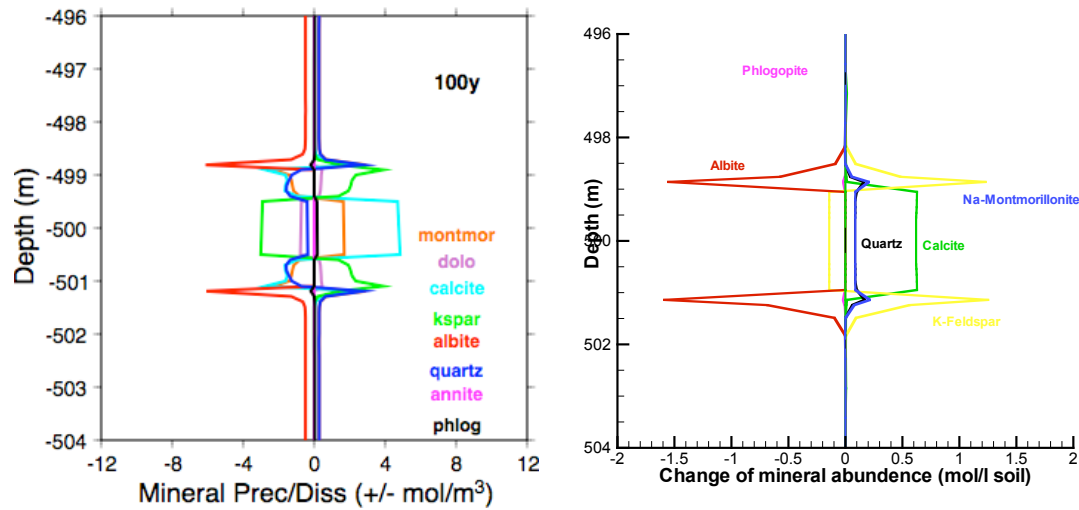
Figure 5.4.   TOUGHREACT (left) and GeoSys/RockFlow (right) simulations of mineral abundances after 100 years for the unsaturated case. TR results show changes in moles per m^3 volume of rock, whereas GSRF results show moles per liter rock (0.1 m^3). A factor of 10 must therefore be applied to the GSRF results for direct comparison to TR results.

5.2.2.5 Summary

The preliminary comparisons of THC1 simulation results from DOE and BGR show similar profiles in aqueous species concentrations, given some minor inconsistencies in input parameters and temperature evolution. The mineralogical changes are similar in general, and future comparisons should look closely at the time evolution of each phase. Very strong changes over distances of a few cm at the contact of the bentonite with the granite indicate the necessity of highly resolved grids and small time steps to minimize numerical errors and oscillations in concentrations and mineral abundances. Yet, the cross diffusion of heat and mass can lead to zoning in mineral alteration that may be difficult to discern from numerical errors. Therefore, the comparison of results using different discretizations and numerical approaches will allow for better scrutiny of the results.

5.3.   FUTURE THC WORKSCOPE

Phase 1 (Model Inception Phase) activities will be ongoing during the next year of Task D research work. As pointed out before, the task description of D_THC1 may need some further revision or clarification in response to issues that came up in the initial simulations conducted for this task. We also expect that model simulations for D_THC1 will have to be adjusted in response to comparative evaluation between the research teams, as discrepancies may need to be resolved.

We also expect all research teams to shift their focus towards the modeling of Task D_THC2, which is the Yucca Mountain case. One of the major conceptual difficulties

with this task is the internal heterogeneity of the fractured porous rock, with vastly differing permeabilities, moisture retention characteristics, and geochemical parameters in the fractures and the matrix, respectively. While dual continuum models are the best choice for D_THC2 (as discrete fracture-matrix continuum models or hybrid models are not feasible for the densely fractured formation), they require significant code development. Therefore, it is to be expected that some of the international research teams working on the Yucca Mountain case will *not* be using a dual continuum model. This raises the question of possible simplifications to the problem to avoid dual continuum modeling. In contrast to THM cases, however, a single continuum model of the fractured rock is not likely to produce reasonable geochemical results, because correct descriptions of liquid and gas chemistry require correct flux estimates of liquid and gas in fractures and matrix blocks. Even an effective continuum model (suggested for THM simulations) may not be sufficient. Thus one of the goals of future research within D_THC2 will be the joint development of simplified, yet realistic models for fracture-matrix representation.

6. SUMMARY AND CONCLUSIONS

In the international DECOVALEX-THMC project, DOE leads the modeling task entitled "Permanent Permeability/Porosity Changes in the EDZ and Near Field due to THC and THM Processes for Volcanic and Crystalline Rocks." In its leadership role for this task (referred to as Task D), DOE has defined the research program and model scenarios, has coordinated and organized the cooperative research activities of international research teams engaged in Task D, and has conducted its own modeling work. Scientists at Lawrence Berkeley National Laboratory (LBNL) support DOE in organizational matters and conduct the respective modeling studies. The current report describes the activities conducted during the first year of the DECOVALEX-THMC project.

The research program developed for Task D of DECOVALEX-THMC involves both geomechanical and geochemical research areas. Coupled THM and THC modeling is conducted to evaluate long-term THM and THC processes in two generic geologic repositories for radioactive waste, with the ultimate goal of evaluating the impact of geomechanical and geochemical processes on hydrologic properties and flow patterns. The two repositories represent simplified versions of possible repository sites and emplacement conditions considered by the participating organizations. The first repository is located in saturated crystalline rock; emplacement tunnels are backfilled with a bentonite buffer material. The second repository is a simplified model of the Yucca Mountain site, featuring a deep unsaturated volcanic rock formation with emplacement in open gas-filled tunnels (Yucca Mountain type). DOE and LBNL produced a detailed report containing all necessary specifications for the geomechanical and geochemical modeling analyses of the two generic repositories (see Appendix A).

Four international research teams from China, Germany, Japan, and USA have started research activities for the geomechanical and geochemical scenarios of Task D. Work was performed in a collaborative manner with close interaction during meetings, visits, via email, and per telephone. This close collaboration among international top scientists and engineers is really one of the major benefits from DOE's participation in DECOVALEX-THMC. Each team provided individual status reports on the progress of THM and THC modeling, included in Appendices C through I.

The research teams involved in modeling the geomechanical task have made significant progress during the first year of DECOVALEX-THMC. All teams finalized the model development work and presented results of the first modeling phase for both repository types. Comparison of these results indicates a good overall agreement between the research teams. Thus, DOE's models, proven to be capable of simulating the Yucca Mountain repository, are equally valuable for the simulation of an alternative repository setting with different THM processes, at least for the problem considered in the first modeling phase.

Based on the good model agreement for the THM task, teams will move into the next, more complex modeling phase during the next project year. This second phase includes prediction of THM-related property changes with conceptual models chosen by the

different research teams, sensitivity analysis with respect to THM property changes, application of alternative conceptual models for fractured rock (i.e., discrete, vs. continuum), and development of model data based on various reports and site data instead of using pre-defined values.

The two international research teams (Germany and Japan) participating in the geochemical tasks have mostly been working on code and model development during the last year. The BGR and DOE teams both conducted preliminary simulations for the first modeling phase of the FEBEX type repository task (D_THC1). Results from these simulations give great confidence in the transition to the more challenging Phase 2 and 3 analyses. Once the groups are satisfied with the magnitude and patterns of the geochemical changes, then the evaluation of changes to hydrological properties, i.e., porosity and permeability, will be a major goal of the simulations. In addition, more realistic treatment of bentonite-water reactions, including ion exchange, sorption, swelling and shrinkage, as well as kinetic rates of reaction, will be required.

D_THC1 was an ideal starting comparison for the groups because it allowed an excellent comparison of geochemical changes without the added effects of boiling and condensation, adding another layer of complexity and uncertainty. Now that the coupling of transport and water-rock reaction has been shown to give comparable results, then the transition to the Yucca Mountain type repository (D_THC2) can be made more smoothly in which alternate conceptual models of flow in unsaturated fractured rock must be evaluated (i.e., effective continuum, dual porosity, or dual permeability).

7. REFERENCES

Barr D., Birkholzer J., Rutqvist J., and Sonnenthal E., 2004a. Draft Description for DECOVALEX-THMC Task D: Long-Term Permeability/Porosity Changes in EDZ and Near Field, due to THM and THC Processes in Volcanic and Crystalline-Bentonite Systems. REV01, June 2004.

Barr D., Birkholzer J., Rutqvist J., and Sonnenthal E., 2004b. Draft Description for DECOVALEX-THMC Task D: Long-Term Permeability/Porosity Changes in EDZ and Near Field, due to THM and THC Processes in Volcanic and Crystalline-Bentonite Systems. REV01, December 2004.

Barr D., Birkholzer J., Rutqvist J., and Sonnenthal E., 2005. Draft Description for DECOVALEX-THMC Task D: Long-Term Permeability/Porosity Changes in EDZ and Near Field, due to THM and THC Processes in Volcanic and Crystalline-Bentonite Systems. REV01, August 2005 (see also in Appendix A).

Pruess, K.,1990. On thermohydrologic conditions near high-level nuclear wastes emplaced in partially saturated fractured tuff – 2. effective continuum approximation. Water Resources Research. 26(6), 1249-1261.

Rutqvist, J., D. Barr, R. Datta, A. Gens, M. Millard, S. Olivella, C.F. Tsang , and Y. Tsang., 2005a. Coupled thermal-hydrological-mechanical analysis of the Yucca Mountain Drift Scale Test – comparison of field results to predictions of four different models. *Int. J. Rock Mech. & Min. Sci* (in press).

Rutqvist J, Tsang CF, and Tsang Y., 2005b. Analysis of Coupled Multiphase Fluid Flow, Heat Transfer and Mechanical Deformation at the Yucca Mountain Drift Scale Test. Proceedings of the 40th U.S. Rock Mechanics Symposium, Anchorage, Alaska, USA, 25-29 June, 2005: American Rock Mechanics Association ARMA, Paper No. 893.

Appendix A

Draft Description for DECOVALEX THMC Task D

(Status August 2005)

Draft Description for DECOVALEX-THMC

TASK D:

Long-Term Permeability/Porosity Changes

in the EDZ and Near Field, Due to THM and THC Processes

in Volcanic and Crystalline-Bentonite Systems

Deborah Barr, Office of Repository Development, U.S. Dept. of Energy, and Jens Birkholzer (Contact), Jonny Rutqvist, Eric Sonnenthal, Earth Sciences Division, LBNL, USA

REV02, December 2004

SUMMARY

Task D explores various aspects of long-term/permanent changes in hydrological properties of the rock near waste emplacement drifts. These changes, caused by coupled thermal-hydrological-mechanical (THM) and thermal-hydrological-chemical (THC) processes, can significantly impact the flow paths in the near-field rock surrounding the emplacement tunnels, and thus need to be addressed in performance assessment. The main processes considered in Task D are heat transfer, fluid flow, stress/deformation, and reactive transport. The coupled THM and THC processes capable of causing long-term/permanent hydrological property changes in the near field include opening and closure of fractures caused by stress changes, shear movement/dilation along fractures, micro-cracking and fracture propagation (THM), and mineral precipitation and dissolution (THC). The relative importance of these processes may differ between the rock types and repository designs currently investigated in different countries.

The main workscope of Task D includes predictive analysis of the long-term coupled processes in generic repositories with simplified conditions and geometry. Participating research teams will model the THM and THC processes in the fractured rock close to a representative emplacement tunnel as a function of time, will predict the changes in hydrological properties, and will evaluate the impact on near-field flow processes. The impact of uncertainties in parameters and concepts will be evaluated. Two generic repositories situated in different host rock types will be analyzed for comparison. The first generic repository is located in saturated crystalline rock, where emplacement tunnels are backfilled with buffer material (*FEBEX type*). The second generic repository is located in unsaturated volcanic rock, with emplacement in open gas-filled tunnels (*Yucca Mountain type*). The geometry chosen for the two repository scenarios is similar. Participating teams are encouraged to work on both scenarios, either simultaneously or sequentially, to enhance process understanding and to ensure close cooperation. Initially, modeling of these tasks will be conducted separately for THM processes (D_THM) and THC processes (D_THC). At later stages, results from THM and THC analyses will be compared, and

the need for a fully coupled thermal-hydrological-mechanical-chemical (THMC) simulation study will be evaluated. This latter subtask will require close interaction between THM and THC research teams.

Modeling of Tasks D_THM and D_THC is complimented by analysis and/or simulation studies using measured data on THMC property changes from the *in situ* Drift Scale Test (DST) at Yucca Mountain, USA, and from the COUPLE laboratory experiment conducted at JNC in Japan. (If they become available during the project lifetime, new data from the FEBEX experiment may also be used.) This subtask is intended to help identify relevant processes and to allow for model validation.

TABLE OF CONTENTS

TABLE OF CONTENTS (Continued)

LIST OF FIGURES

LIST OF FIGURES

LIST OF TABLES

INTENTIONALLY LEFT BLANK

1. BACKGROUND AND MOTIVATION FOR TASK D

The DECOVALEX project is an international cooperative project initiated by SKI, the Swedish Nuclear Power Inspectorate, with participation of several international organizations. The general goal is to encourage multidisciplinary interactive and cooperative research on modeling coupled processes in fractured rocks and buffer materials, in support of the performance assessment for radioactive waste storage. Three multiyear project stages of DECOVALEX have been completed in the past decade, mainly focusing on coupled THM processes. The most recent project stage, DECOVALEX-III, included THM modeling work on two large-scale *in situ* heater experiments, the FEBEX experiment at Grimsel in Switzerland and the DST at Yucca Mountain in the USA. These two tasks on modeling field data have greatly enhanced our understanding of the coupled near-field processes in two different rock classes (crystalline rock versus volcanic tuff), hydrological settings (saturated versus unsaturated) and emplacement designs (backfilled versus open drift), and have added confidence in the predictions by comparison of measured data with the model results.

Task D in the new DECOVALEX-THMC project applies the knowledge gained from modeling the short-term *in situ* tests (test period between one and eight years) to the evaluation of long-term THM processes in two generic repositories (*FEBEX type* and *Yucca Mountain type*), where the regulatory compliance periods span over thousands to ten-thousands of years (D_THM). THM processes lead to changes in hydrological properties that can be very important for performance, because the flow processes in the vicinity of emplacement tunnels will be altered from their initial state. Note that some of these changes can be permanent (irreversible). In that case, they persist even after the thermal conditions are back to ambient; i.e., they will affect the entire regulatory compliance period. However, even if fully or partially reversible, the changes in hydrological properties can be relevant for most of the compliance period, because the heat produced by the radioactive waste decays very slowly. In general, these changes are strongest close to the tunnels; i.e., they will be particularly relevant for the long-term flow behavior in the Excavation Disturbed Zone (EDZ) and the near-field environment.

The new DECOVALEX-THMC project expands on the scope of the previous project phases by more fully incorporating chemical processes that are important for repository performance. As discussed in Section 2, chemical processes can permanently alter hydrological properties and flow paths in the near field; they also affect the water and gas chemistry close to the waste packages, which are relevant for waste package corrosion, buffer stability, and radionuclide transport. Recognizing their importance, Task D_THC addresses long-term THC effects and their relevance in the two generic repositories (*FEBEX type* and *Yucca Mountain type*).

The generic repository layouts analyzed in Task D_THM and Task D_THC are similar, so that comparison of results between the scenarios and expansion of models to a full THMC analysis will be straightforward. Figure 1.1 presents the basic functions of the two repository types. Both repository types depend on a multibarrier system including an engineered system (e.g., waste, canister, buffer and excavation) and a natural system (rock mass). A bentonite-backfilled repository in a mostly saturated system uses a tight (low-permeability) bentonite to prevent water flow and solutes from coming into contact with the waste canister. On the other hand, for an open-drift repository in an unsaturated system, there is no protective bentonite buffer, but the

open drift itself provides a natural capillary barrier that can limit liquid water from entering the drift. For the current concepts of the two repository types, there is also a difference in the amount of heat and temperature rise. In a bentonite-backfilled repository, considered in most European countries and Japan, the temperature is generally kept below 100 °C to prevent chemical changes in the bentonite material. For the open-drift alternative (considered by the United States), the current design results in above-boiling temperatures in the near field.

Emplacement Drift
located at about 500 to 1000 meters depths in saturated rock

Bentonite Buffer:
• Provides mechanical stability of the canister
• Retards the arrival of water (and corrosive solutes) to the canister
• Retains/retards migration of radio-nuclides if released from the canister

Copper/steel **Waste Canister** isolates waste

Bedrock: Provides a stable chemical and mechanical environment and retards radio-nuclides if released

a.

Emplacement Drift
located at about 300 meters depth in unsaturated rock

Capillary Barrier:
• Diverts water flow around drift
• Prevents water (and corrosive solutes) from seeping into the drift

Stainless steel and Alloy 22 **Waste Package** isolates waste

Bedrock: Provides a stable chemical and mechanical environment and retards radio-nuclides if released

b.

Figure 1.1.   Schematic showing the two repository types evaluated in tasks D_THM and D_THC: (a) bentonite-back-filled repository in saturated rocks (*FEBEX type*), and (b) open-drift repository in unsaturated rock (*Yucca Mountain type*)

2.   THM AND THC PROCESSES AFFECTING HYDROLOGICAL PROPERTIES

The cause for changes in hydrological properties (mostly fracture permeability and porosity) owing to heat-driven coupled processes can be mechanical or chemical in nature. The following subsections give a brief description of the coupled processes expected to occur in the two repositories.

2.1   COUPLED THM PROCESSES CONSIDERED

Thermally driven coupled THM processes occur in response to the heat output of the decaying radioactive waste. The strongest effects typically coincide with the period of the highest temperatures; i.e., depending on the repository type, during the first decades or centuries after emplacement (Figure 2.1). For example, in the case of a bentonite-backfilled repository, the drying and wetting of the bentonite induces shrinkage and swelling in various part of the buffer, with resaturation expected to occur within tens of years. In the case of an open-drift repository, the boiling of water creates a dryout zone in the near-field rock that will prevent liquid water from entering the drift for several hundred to more than a thousand years. At the same time, thermally induced stresses will act upon pre-existing fractures, which will open or close depending on the local stress. One of the important effects, i.e., thermal expansion of the rocks with impact on fracture aperture, is generally recoverable as the temperature drops. However, increased thermal stress may also lead to irreversible or permanent impacts, which are most relevant for performance assessment (Figure 2.2). For example, if changes in the stress field during the heating period are sufficiently large, inelastic mechanical responses may be induced in the form of fracture shear slip or crushing of fracture asperities. This process changes the fracture permeability permanently, since the rock loses its integrity. Furthermore, the elevated temperatures and stresses will be maintained for long time spans, which could give rise to increased micro-cracking and subcritical crack growth through stress corrosion or other related phenomena. Such inelastic mechanical responses in the fracture system would induce irreversible (permanent) changes in the hydrological properties of the rock mass.
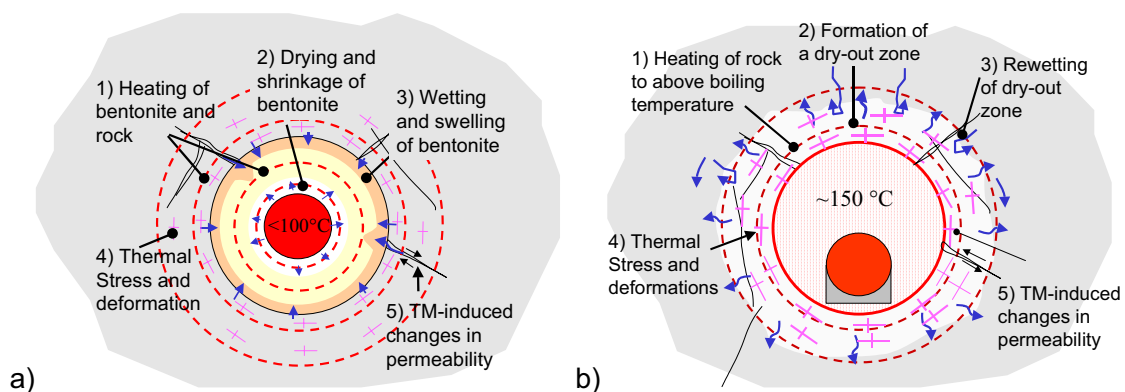
Figure 2.1.   Short term coupled THM processes at (a) a bentonite-backfilled repository in saturated rocks and (b) an open-drift repository in unsaturated rock
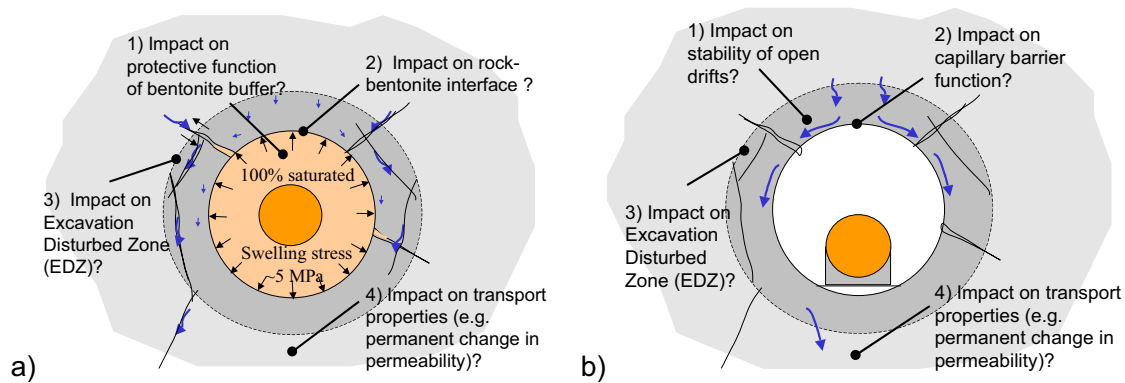
Figure 2.2.   Potential long-term impact of coupled THM processes at (a) a bentonite-back-filled repository in saturated rocks and (b) an open-drift repository in unsaturated rock

Figures 2.1 and 2.2 suggest that for long-term THM processes, there are differences but also many similarities between the two repository cases, indicating that modelers will face similar challenges and issues. Working together on both cases will help in evaluating similarities and differences, in comparing approaches and results, and in gaining an overall better understanding.

2.2   COUPLED THC PROCESSES CONSIDERED

Thermally driven coupled THC processes occur in response to the heat output of the decaying radioactive waste. These processes include changes in water and gas chemistry in the near field and within the drifts, which affect the waste package environment. They also include processes of mineral precipitation and dissolution, which give rise to long-term changes in hydrological properties. Increased temperature results in mineral-water disequilibrium and increases the reaction rates of minerals with water, leading to enhanced mineral dissolution and precipitation. Effects of mineral precipitation on fracture porosity and permeability are particularly strong when temperatures are above boiling. In this case, vapor is driven away by the heat in all directions and cools as it moves farther from the heat source, eventually condensing into the liquid phase. Above the heat source, condensate flows back down by gravity and capillary suction, only to boil again as it gets closer to the heat source. This cycle of vaporization, condensation, and reflux can result in strong dissolution/precipitation processes where dissolution is dominant in the condensation zone and precipitation must take place where concentrations may increase exponentially at the boiling front. Figures 2.3 and 2.4 give a schematic illustration of the main long-term THC processes expected in the two repository cases.
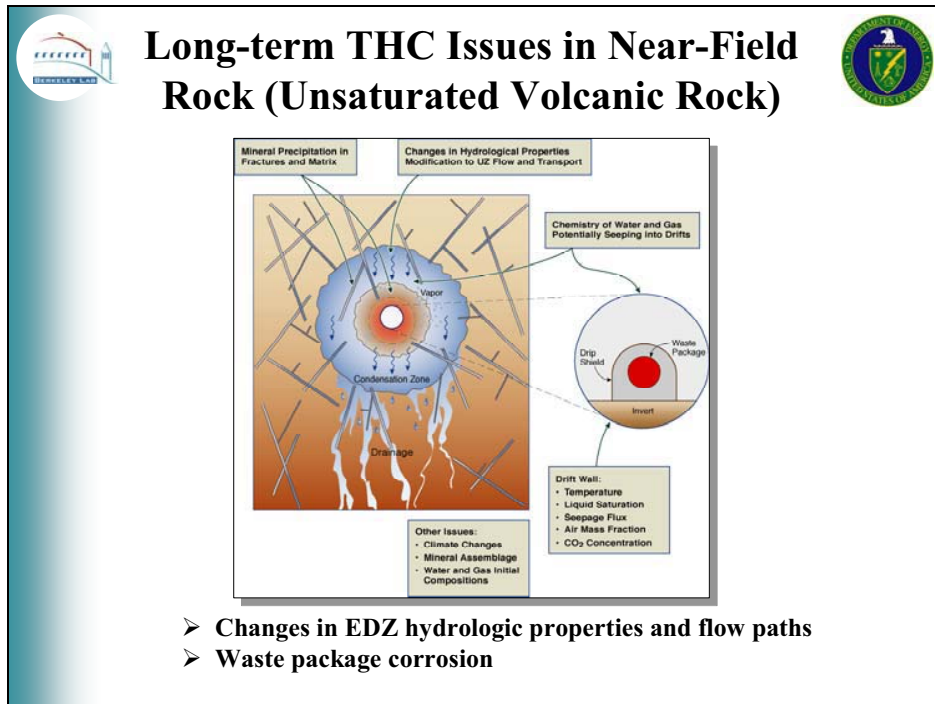
Figure 2.3.   Possible THC processes with impact on hydrological properties near emplacement tunnels in unsaturated volcanic rock
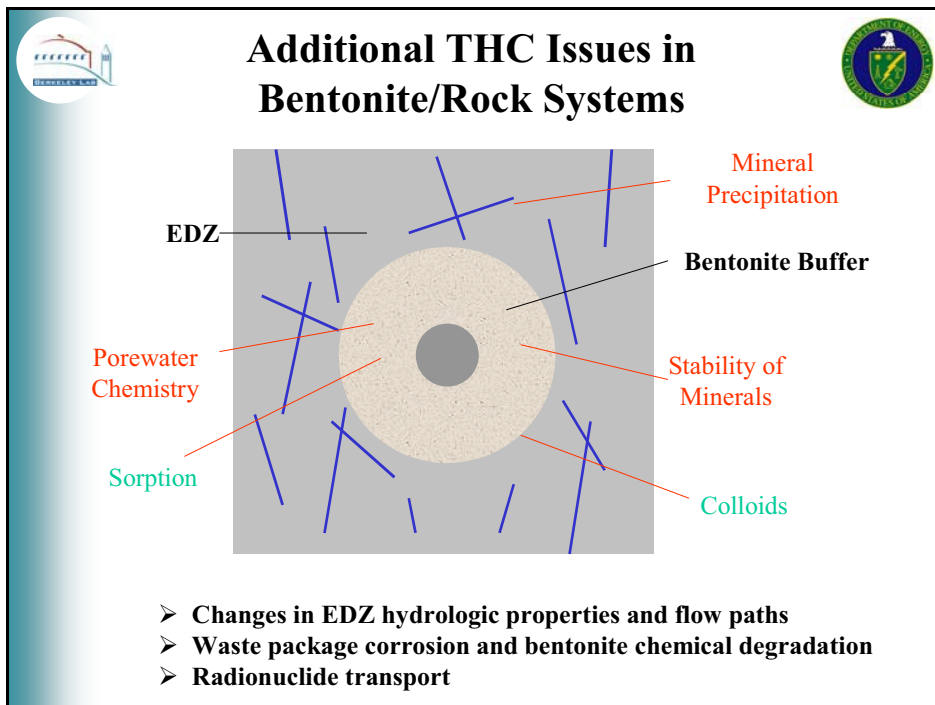
Figure 2.4.   Additional THC processes and their impact on hydrological properties in and near emplacement tunnels with bentonite backfill

INTENTIONALLY LEFT BLANK

3.   OVERALL WORKSCOPE AND SCHEDULE

3.1   RESEARCH TOPICS

Task D explores various aspects of long-term/permanent changes in hydrological properties of the rock near waste emplacement drifts. These changes, caused by coupled thermal-hydrological-mechanical (THM) and thermal-hydrological-chemical (THC) processes, can significantly impact the flow paths in near-field rock surrounding the emplacement tunnels (including the excavation-disturbed zone, EDZ), and thus need to be addressed in performance assessment. The main processes considered in Task D are heat transfer, fluid flow, stress/deformation, and reactive transport. Specific THM research interests addressed in Task D_THM include, but are not limited to:

- Relative importance of thermal-mechanical changes to near-field hydrological properties and flow fields

- Relative importance of irreversible mechanical changes versus reversible mechanical changes

- Comparative analysis of THM effects in different host rock types and repository designs

- Evaluation of stress-permeability and stress-porosity relationships

- Importance of THM processes for performance assessment

Specific THC topics addressed in Task D_THC include, but are not limited to:

- Relative importance of thermal-chemical changes on the near-field hydrological properties and flow field

- Evolution of water and gas chemistry close to waste package

- Mineral precipitation/dissolution in the near-field and in bentonite

- Comparative analysis of THC effects in different host-rock types and repository designs

- Evaluation of the relation between porosity changes, mineral alteration and hydrological properties

- Importance of THC processes for performance assessment

Additional research topics include both THM and THC processes:

- Relative importance of THM versus THC-related changes in hydrological properties

- Assessment of fully coupled THMC processes (necessity, approaches)

- Assessment of uncertainties in the predictions resulting from uncertain parameters, alternative conceptual models, heterogeneities, and other factors

3.2   WORKSCOPE OF TASKS

Task D of DECOVALEX-THMC includes the following main activities:

Task D_THM

THM modeling analysis of the long-term coupled processes in two generic repositories with simplified conditions and geometries. Participating research teams will model the THM processes in the fractured rock close to a representative emplacement tunnel as a function of time, will predict the changes in hydrological properties, and will evaluate the impact on the near-field flow processes (see details in Section 6 below). The impact of uncertainties in parameters and concepts will be evaluated. Two subtasks analyze the coupled THM processes in two generic repositories as follows:

- *Task D_THM1: Generic repository is located in saturated crystalline rock, where emplacement tunnels are backfilled with buffer material (FEBEX type).*

- *Task D_THM2: Generic repository located in unsaturated volcanic rock, with emplacement in open gas-filled tunnels (Yucca Mountain type).*

Task D_THC

THC modeling analysis of the long-term coupled processes in two generic repositories with simplified conditions and dimensions. Participating research teams will model the THC processes in the fractured rock close to a representative emplacement tunnel as a function of time, will predict the changes in hydrological properties, and will evaluate the impact on the near-field flow processes (see details in Section 7). The impact of uncertainties in parameters and concepts will be evaluated. Two subtasks analyze the coupled THM processes in two generic repositories identical to those analyzed in the D_THM task:

- *Task D_THC1: Generic repository is located in saturated crystalline rock, where emplacement tunnels are backfilled with buffer material (FEBEX type).*

- *Task D_THC2: Generic repository located in unsaturated volcanic rock, with emplacement in open gas-filled tunnels (Yucca Mountain type).*

The D_THM and D_THC tasks will be conducted simultaneously, since the researchers working on THM processes are most likely different from those working on THC processes. In each task, participating teams are encouraged to work on both repository scenarios, either simultaneously or sequentially, to enhance process understanding and to ensure close cooperation. Both tasks will include an analysis and/or simulation component using measured data to identify relevant processes and to allow for model comparison with experimental results. The experiments chosen for this task are the *in situ* Drift Scale Test (DST) at Yucca Mountain, USA, (Task D_THC2) and the COUPLE laboratory experiment conducted at JNC in Japan (Task D_THC1). Valuable data on THMC property changes are expected to be available in the second or third year of

DECOVALEX-THMC. (We may also try to utilize new data from the FEBEX experiment, if available.) Experimental data are not included in this draft description for Task D.

Prior to working on the modeling tasks, each research team is encouraged to conduct a preliminary assessment of the relative importance of THMC property changes for the different rock types and THMC conditions, using past DECOVALEX experience, available data from participating organizations, and from the open literature. At later stages, i.e., after finalizing D_THM and D_THC, results from THM and THC analyses will be compared, and the need for a fully coupled thermal-hydrological-mechanical-chemical (THMC) simulation study will be evaluated. This latter subtask requires close interaction between THM and THC research teams.

3.3   PROPOSED SCHEDULE

The following overall schedule is envisioned for Task D of DECOVALEX-THMC. Further details on the schedule in Phase 2 will be developed during the start-up phase.

Phase 1: Start-up Phase (0–6 months)

- Preliminary assessment of relative importance of THMC processes for different rock types and THMC conditions, using available data from participating organizations and open literature

- Discussion of BMT objectives and inputs

- Adjustments to reflect desires of different programs

- Preliminary scoping simulations for TH conditions to ensure comparability between project teams

Phase 2: Task D_THM (6–36 months; see details in Section 6)

- Predictive modeling of long-term THM processes for two generic repository settings D_THM1 and D_THM2, focusing on near-field conditions

- Three modeling phases: (1) model inception, (2) preliminary predictions with sensitivity analysis, and (3) final predictions with uncertainty ranges

- Analysis and/or modeling of the *in situ* DST (DOE) and the COUPLE experiment (JNC) for identification of relevant processes and model calibration/validation

- Comparison of THM results from different participants

- Comparison of different rock types and repository settings

Phase 2: Task D_THC (6–36 months, see details in Section 7)

- Predictive modeling of long-term THC processes for two generic repository settings D_THC1 and D_THC2, focusing on near-field conditions

- Three modeling phases: (1) model inception, (2) preliminary predictions with sensitivity analysis, and (3) final predictions with uncertainty ranges

- Analysis and/or modeling of the *in situ* DST (DOE) and the COUPLE experiment (JNC) for identification of relevant processes and model calibration/validation

- Comparison of THC results from different participants
- Comparison of different rock types and repository settings

Phase 3: THMC Evaluation Phase (36–42 months)

- Assessment of need for fully coupled THMC simulations (development of appropriate conceptual models for handling fully coupled processes)
- Assessment of overall importance of THMC effects on flow processes and performance assessment
- Compilations of lessons learned list

4. GENERAL BACKGROUND ON TASKS D_THM AND D_THC

The task description for D_THM and D_THC is designed such that the expected physical processes in future repositories are incorporated in a realistic manner, yet allow for somewhat simplified modeling as the geometries and boundary conditions have been simplified. Definitions are given such that model concepts and relevant property/parameter choices will have to be developed rather than provided. The idea is to encourage model comparison, not just code comparison. Figure 4.1 gives a brief summary of the problem setup and the main challenges for D_THM. The input parameters and the expected modeling outputs for D_THM are depicted in Figure 4.2. Figures 4.3 and 4.4 provide similar summaries for D_THC.

Each task includes two different repository scenarios with similar geometry (schematically depicted in Figure 4.5). Both analyze 2D vertical cross sections perpendicular to the tunnel axis. The emplacement tunnels are assumed to be parallel with a given distance between them. Symmetry considerations allow limiting the model to one representative emplacement tunnel, with the lateral boundaries at the centerlines to the neighboring tunnels. Upper and lower boundaries are chosen such that they remain unaffected by the heat input. The waste packages are placed into the center of the circular tunnels. Heat emitted from the waste packages is given as a time-dependent line load, in W per meter emplacement tunnel. Undisturbed flow is from the top to the bottom, either driven by hydraulic head gradients (saturated flow) or by gravity (unsaturated flow). Specifics are given in Sections 6 and 7. Table 4.1 gives a brief summary of the similarities and differences between the two repository scenarios.

Sub-Task D_THM

❑ Objective: Estimate Long-term THM changes in hydrological properties (reversible and irreversible) and analyze impact on flow

❑ Two repositories: D_THM1 (FEBEX type) and D_THM2 (YMP type)

❑ Problem Setup:
- Detailed THM initial and boundary conditions are provided
- Phase 1: All TH properties for rock and buffer material are directly provided
- Later Phases: Relevant THM properties for rock, fractures, and buffer material will need to be derived based on given data or literature
- Selected properties associated with uncertainty ranges

❑ Main Challenges:
- Model conceptualization (discrete, continuum, hybrid,…)
- Derivation of representative in-situ properties from available data
- Conceptual model describing mechanically-induced changes in properties
- Model uncertainty (parameter uncertainty and conceptual model uncertainty)

Figure 4.1.   Problem setup and main challenges for D_THM

D_THM:
Data Provided and Model Outputs

Inputs

- Geometry
- Initial and boundary conditions
- Thermal, hydraulic and mechanical properties
- Thermo-mechanical properties
- Hydro-mechanical properties
- Time-dependence of properties

Conceptual Models

Parameter Identification

THM Outputs

- Distributions and evolution of temperature, fluid pressure, stress, strain
- Long-term changes in hydrologic properties
- Safety factor for drift stability
- Long-term impact on flow field
- Uncertainties

Figure 4.2.   Input data and expected model output for D_THM

Sub-Task D_THC

❑   Objective: Estimate long-term changes in water/gas chemistry as well as mineralogical changes, analyze impact on flow

❑   Two repositories: D_THC1 (FEBEX type) and D_THC2 (YMP type)

❑   Problem Setup:

▪   Detailed THC initial and boundary conditions are provided
▪   Phase 1: All THC properties for rock and buffer material are directly provided
▪   Later Phases: Relevant (TH)C properties for rock, fractures, and buffer material will need to be derived based on given data or literature (e.g., mineral abundances and compositions, thermodynamic and kinetic data)
▪   Selected properties associated with uncertainty ranges

❑   Main Challenge:

▪   Develop appropriate conceptual model for complex heat-driven reactive transport including several species and phases
▪   Conceptual model describing precipitation-dissolution-induced changes in properties
▪   Assess model uncertainty stemming from both parameter uncertainty and conceptual model uncertainty

Figure 4.3.   Problem setup and main challenges for D_THC
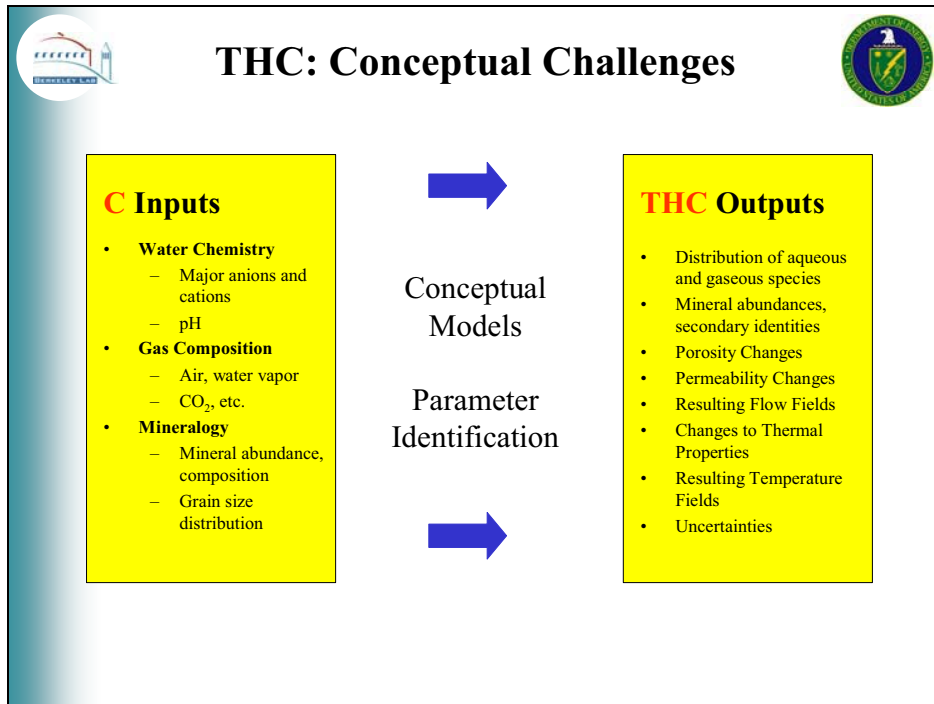
Figure 4.4.   Chemical input data and expected model output for D_THC
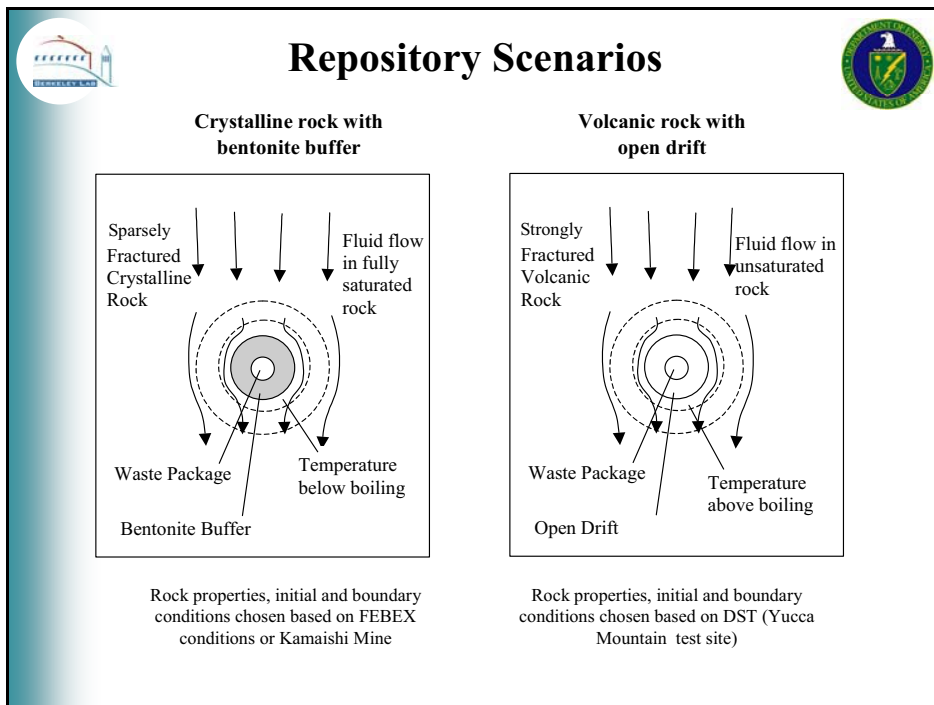
Figure 4.5.   Schematic showing the two repository scenarios chosen for D_THM and D_THC (vertical cross sections perpendicular to drift axis)

Table 4.1.   Summary of similarities and differences between repository scenarios

	Repository Scenario: FEBEX Type	Repository Scenario: Yucca Mountain Type
Compl. Period	To be defined	10,000 years
Geometry	Similar	Similar
Initial Heat Load	290 W/m	1,450 W/m (ventilation effects reduce this load during 50-year period)
Tunnel	Bentonite-filled	Open, no buffer
Flow in Tunnel	Initially unsaturated; swelling effects. Two-phase flow under thermal gradient.	Gas flow
Rock	Sparsely fractured crystalline rock	Densely fractured volcanic rock
Flow in Rock	Saturated in far-field rock. Initially unsaturated in near-field rock.	Unsaturated. Two-phase flow under thermal gradient

5. PREDICTIVE MODELING AND RELATION TO EXPERIMENTAL DATA

Both the D_THM and the D_THC tasks include a subtask that involves analysis and/or modeling using experiments providing measured data on THMC processes and their impact on hydrological properties. We suggest that research teams involved in modeling the generic repository scenarios decide at some later project stage if and to what extent they will participate in analyzing/modeling the experiments. Involvement in the experimental part is desirable, but not necessary for participation in D_THM or D_THC.

For the second repository scenario, i.e., the open-drift emplacement in unsaturated volcanic rock, the DST at Yucca Mountain provides valuable measurements of THM- and THC-related hydrological property changes. The DST is a large-scale, long-term heater test conducted in the unsaturated rock at Yucca Mountain (over 4 years of heating phase; about 50 m length of heated drift), with numerous measurements of thermal, hydrological, mechanical and chemical data (Figure 5.1). The heating phase of the DST (from December 1997 through January 2002) was already analyzed as a test case in one of the past DECOVALEX-III tasks. Currently, measurements are ongoing through a natural cooling phase of the test block, such that relevant data for the post-heating period are being generated. These ongoing cooling-phase measurements provide an excellent data base for assessing the possibility of permanent THM or THC property changes. THM-related property changes become evident, for example, in slow or sudden displacements, irreversible displacements after cool-down, or irreversible permeability changes after cool-down. THC-related property changes become evident in postmortem analysis of core samples and irreversible permeability changes after cool-down. Thus, the DST data will be quite valuable for validation of the THM and THC models.
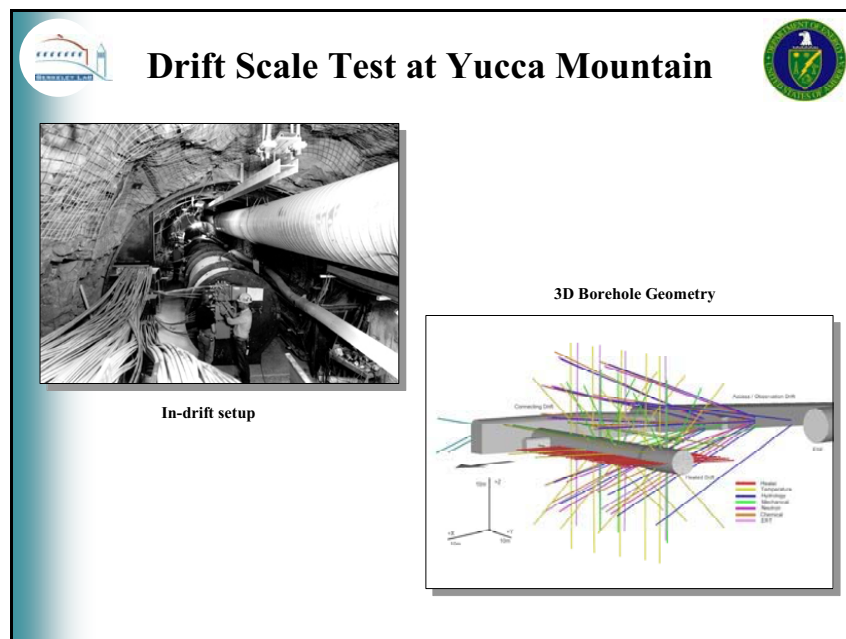
Figure 5.1. Schematic of the 3D borehole geometry for various sampling instruments and photo of in-drift setup with canister heaters in the DST

A comparably well-suited experiment is not available for the first repository scenario, i.e., the backfilled emplacement in saturated crystalline rock. Unfortunately, the recent and ongoing measurements from the large-scale, long-term FEBEX experiment cannot be used in the DECOVALEX-THMC project, because these data are not available to us As an alternative, participants may use data from the so-called COUPLE experiment conducted in later 2003 at JNC in Japan. This experiment analyzes the coupled THMC processes in a heated buffer-rock system at partially saturated conditions. In addition to some thermal and mechanical data, COUPLE is expected to provide information on the chemical evolution of porewater and minerals in the bentonite during/after resaturation and, hopefully, the potential for chemically induced property changes in the buffer material. The geometry and test conditions of COUPLE are depicted in Figure 5.2. Because of its limited scope and dimension, COUPLE will not provide measurements that can be used for model validation. It will, however, give valuable insight into the relevant THC processes in a bentonite-filled emplacement drift.
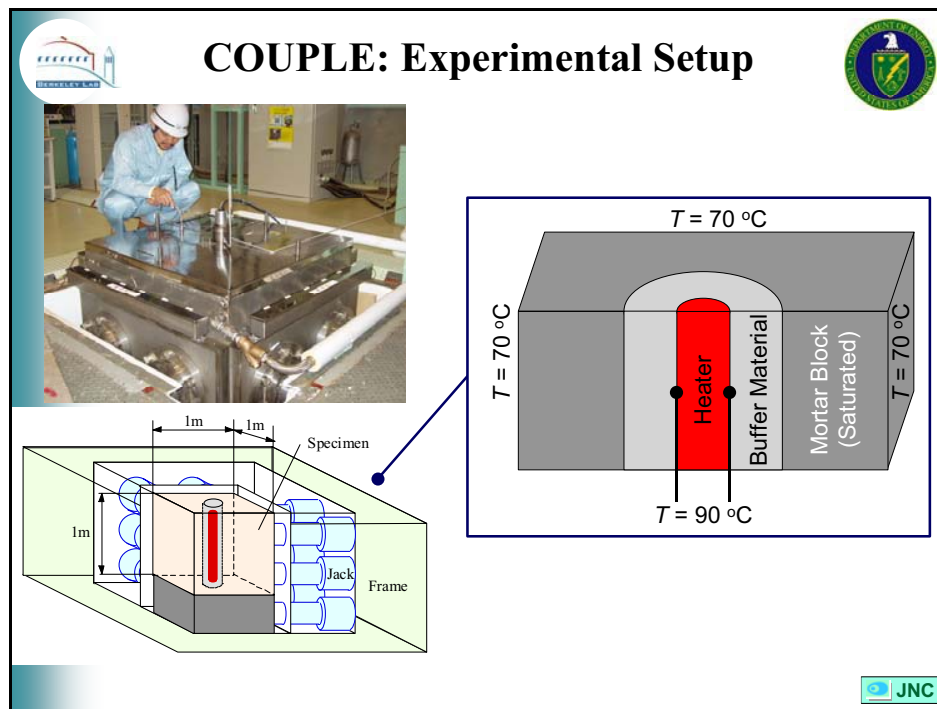
Figure 5.2.   Schematic of the COUPLE experiment and photo of the test block

The measured data from the DST and the COUPLE experiment, respectively, will be made available to participants at a later project stage, as soon as final reports become available.

6.   DETAILED DESCRIPTION OF TASK D_THM

In this task, research teams will conduct THM modeling analysis of the long-term coupled processes in two generic repositories with simplified conditions and dimensions. Participating research teams will model the THM processes in the fractured rock close to a representative emplacement tunnel as a function of time, will predict the mechanically induced changes in hydrological properties, and will evaluate the impact on near-field flow processes (see details in Section 6). THC processes will be neglected in Task D_THM. Two subtasks analyze the coupled THM processes in two generic repositories as follows:

- Task D_THM1: Generic repository located in saturated crystalline rock, where emplacement tunnels are backfilled with buffer material (FEBEX type).

- Task D_THM2: Generic repository located in unsaturated volcanic rock, with emplacement in open gas-filled tunnels (Yucca Mountain type).

The predictive THM simulations can be conducted using various modeling techniques, for example discrete fracture models or continuum models. Model predictions should include the most likely results on THM-induced property changes as well as an evaluation of the uncertainties related to these predictions. This could involve stochastic modeling, resulting in a probability distribution of possible results or, at a minimum, estimation of upper and lower limits of results. In addition to the data and background information provided by the task leads, the research teams should utilize any available literature data to build their case, to ensure providing the best possible prediction of potential permanent changes based on the current state of knowledge.

The description of Task D_THM1 is based on data from the Grimsel Test Site (GTS) and the FEBEX *in situ* experiment, which were used in DECOVALEX III, Task 1. The design and material properties of the engineered system (canister, bentonite, and drift) are taken from the FEBEX *in situ* experiment. The rock properties and *in situ* conditions are also taken from the GTS/FEBEX site. However, in a few instances, data from the Kamaishi Mine in Japan (from DECOVALEX II) and the Laxemar site in Sweden are utilized to complement the GTS/FEBEX data set. The data set for Task D_THM2 is entirely derived from the Yucca Mountain site in Nevada and the lithographic rock units surrounding the Yucca Mountain DST, which were used in DECOVALEX III, Task 2. A complete set of rock properties and *in situ* conditions with uncertainty ranges will be presented to the research teams, upon which to build their models for Task D_THM. In addition, the research teams should consider new results from the ongoing *in situ* THM experiments at FEBEX and DST for confidence building in their model predictions. These will be provided at a later project stage.

6.1   SCHEMATIC OF MODEL GEOMETRY

The model geometry for the two subtasks (Task D_THM1 and Task D_THM2) is fairly similar. Figure 6.1 presents a schematic description of the model geometry, the boundary conditions, specific areas of focus, and profiles/locations for which simulation outputs should be derived by the research teams. The specific values of the dimensions and boundary conditions for Task

D_THM1 and Task D_THM2 are given in Sections 6.3.1 and 6.4.1, respectively. The models are two-dimensional, representing one drift in the interior of a repository. Because of repetitive lateral symmetry, the models extend horizontally to the mid-distance between two drifts. Vertically, the models extend several hundred meters above and below the drift.

The lateral boundaries (vertical sides of the model) permit no cross-flow of fluid or heat. A zero-displacement restriction is applied for the displacement normal to the boundary surface (roller boundaries). The top boundary represents the ground surface and is free to move at a fixed temperature and pressure. The bottom boundary has a zero-displacement restriction for displacement normal to the boundary at a fixed temperature and pressure.

The output results from the different research teams will be collected for defined locations, profiles, and areas. The exact outputs to be delivered by the research teams to the task lead are given in Section 6.5. As illustrated in Figure 6.2, a refined model discretization is probably needed for the region close to the drifts. Below and above this region, the model discretization can be much coarser with homogeneous properties. It is up to the respective research teams how to discretize the problem within the given geometry and boundary conditions. Figure 6.2 shows four examples of possible modeling approaches for the fractured rock mass. Ideally, different research teams would use different modeling approaches, so that the differences and uncertainties related to chosen modeling techniques could be studied. No matter which modeling approach or model simplification is used, the research teams should assess the uncertainties and potential inaccuracies in their modeling predictions.
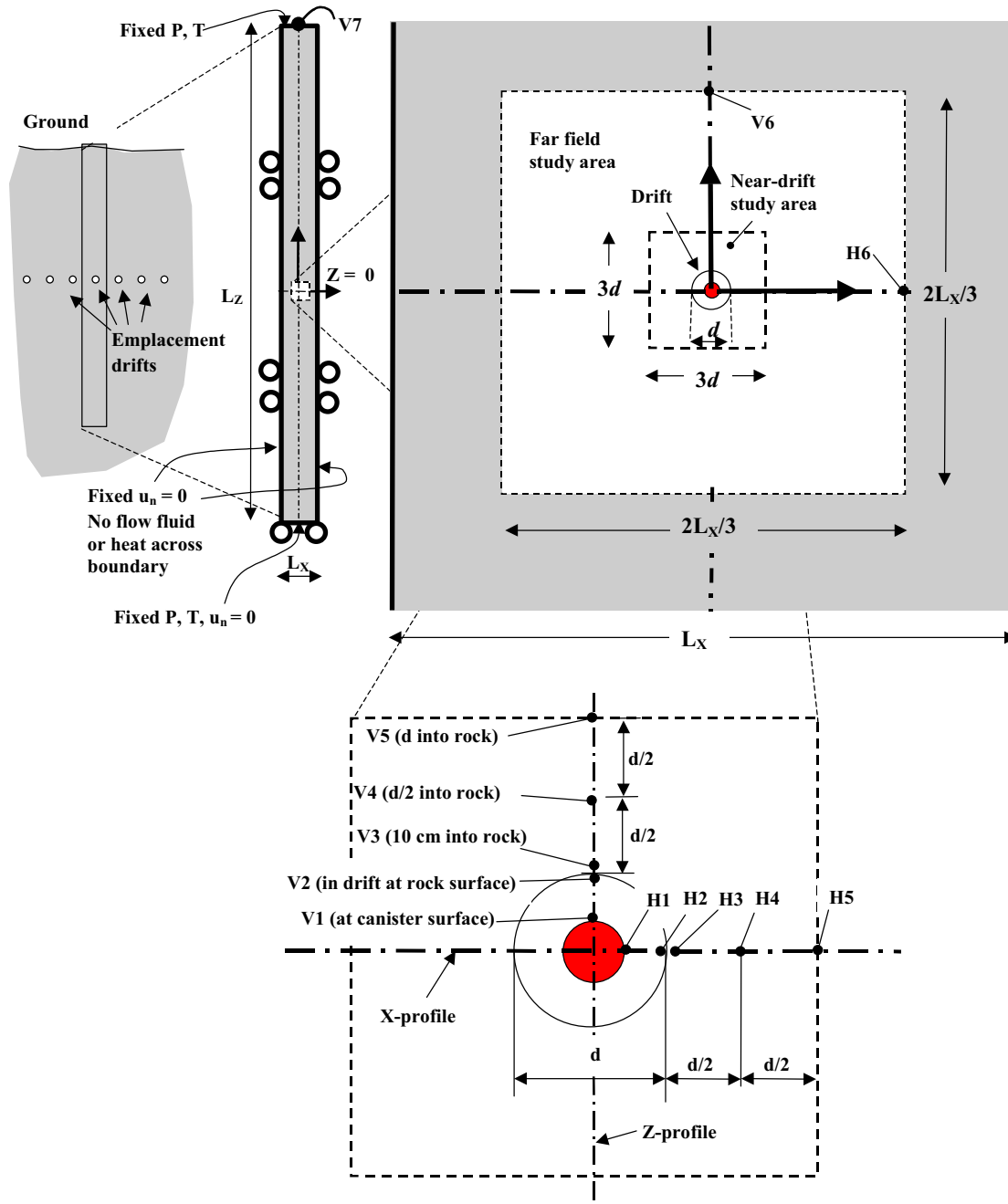
Figure 6.1.   General model geometry, boundary conditions, and locations of points, lines and areas for model output

a) Homogeneous discontinuum   b) Homogenous continuum

c) Stochastic discontinuum   d) Stochastic continuum
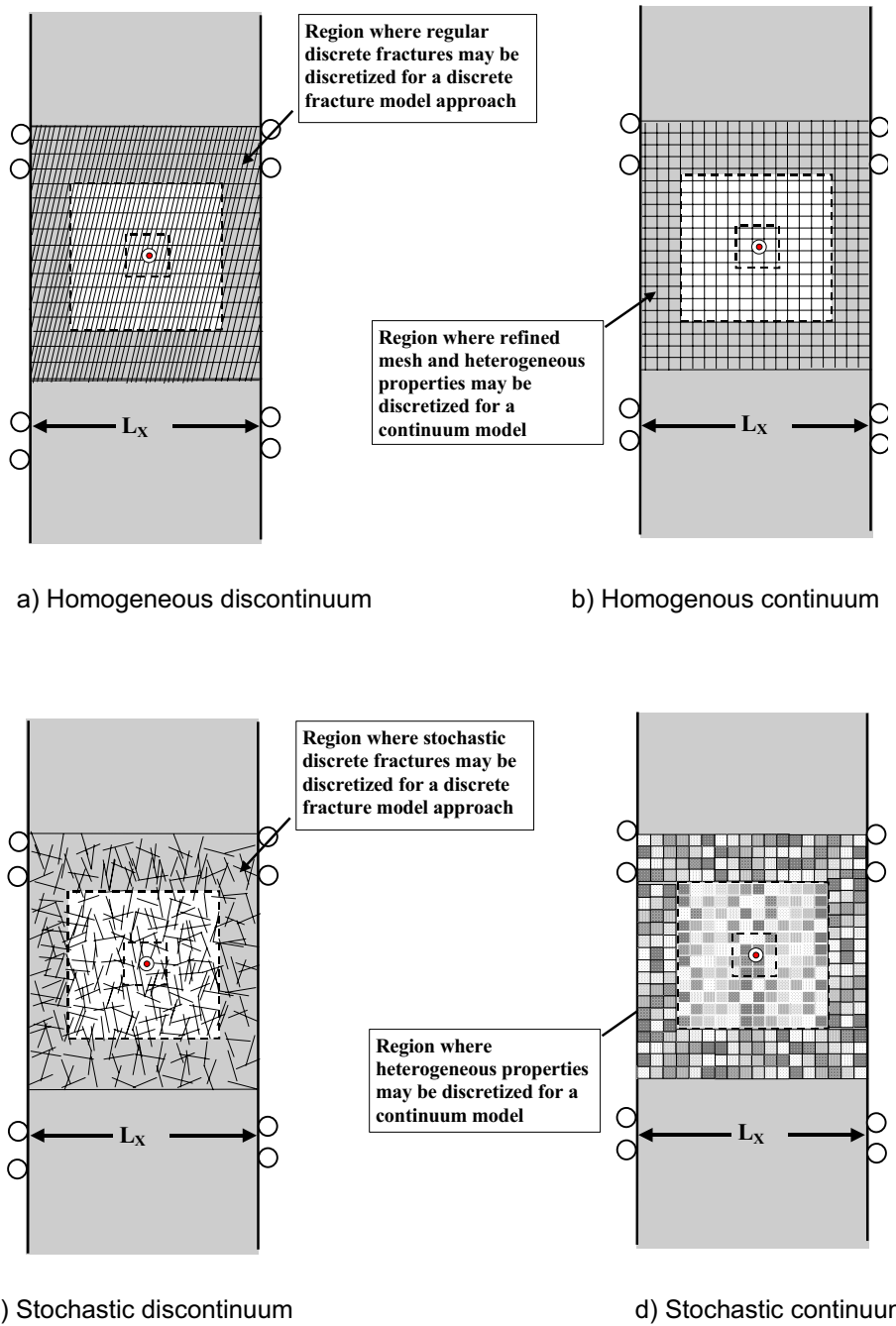
Figure 6.2.   Region of refined model discretization for four different types of models: (a) discrete fracture
               model with regular fracture sets, (b) continuum model with homogeneous properties, (c)
               discrete fracture model with stochastic generation for fractures, and (d) stochastic continuum
               model. (It is recommended that refined discretization goes beyond "far-field study area" to
               avoid possible boundary effects on calculated permeability changes.)

6.2   TASK D_THM MODELING PHASES

The simulation work in Task D_THM is conducted in three modeling phases:

Phase 1. Model Inception
Phase 2. Preliminary Prediction and Sensitivity Study
Phase 3. Final Prediction and Uncertainty Analysis.

Figure 6.3 specifies the work conducted in each phase. The purpose of the model inception phase (Phase 1) is for the research teams to familiarize themselves with the problem by performing one simulation in which all the properties are provided with explicit values while permanent changes are neglected. The results of the research teams will be compared at the end of this phase to assure that all teams are starting the problem from a common basis. The comparison will focus on the evolution of temperature and stress, because these are the driving forces behind mechanical and hydrological changes in the fractured rock mass. When research teams are satisfied with their analysis and their results agree with other research teams, they should go on to the next phase.

In Phase 2, the research teams start to develop their model with the goal of predicting mechanically induced permanent changes. This phase may include development of continuum models for representing the hydromechanical couplings at the two sites. It may include generation of fracture networks based on available statistical data if a discrete model approach is used. Using the available site data and developed data (e.g., stress-permeability relationships), the research teams should conduct an initial parameter study. The purpose of this study is twofold, as follows:

(1) To demonstrate how the model is able to predict permanent changes in mechanical and hydrological properties
(2) To find conditions (e.g. strength properties, initial stress state) at which permanent changes are possible

The research teams should then predict coupled THM responses and potential permanent changes (if any) for one realistic realization. This should be conducted with whatever modeling approach the respective research team has developed. It may be a continuum model using homogenous properties or a heterogeneous stochastic continuum model (Figure 6.2b and 6.2d). It may also be a discrete fracture model using fracture sets with regular fracture spacing or even stochastically generated fracture networks (Figure 6.2a and 6.2c). At the end of this phase, the output results from the different research teams will be compared. In particular, the evolution of permeability changes and their impact on the flow field will be studied. When research teams are satisfied with their preliminary model prediction, they should go on to the next phase to obtain the final prediction results, including uncertainty analysis.

In Phase 3, the research teams are asked to make their final prediction, including estimation of the resulting uncertainties. Examples of uncertainties includes:

(1) Uncertainties associated with parameters
(2) Uncertainties associated with model concepts (i.e., representation of discrete structures, constitutive relationships)

Parameter uncertainties could be related, for example, to uncertainties in the input properties, such as permeability, *in situ* stress, or thermal expansion measurements. Model uncertainties could be related to representation of the *in situ* fracturing. They may also be related to the constitutive models of the mechanical behavior of fractures or the constitutive models developed for continuum approaches. In part, estimation of these uncertainties will be based on scientific judgment. The end result of the uncertainty analysis can be statistical distribution of the simulation outputs or, at a minimum, upper and lower bounds of possible results.

Phase 1: Model Inception (about 6 months duration)

Input   **Modeling**   **Output**

Geometry

Known initial and boundary conditions

Known homogeneous, isotropic, linear material properties: E, ν, k, ϕ, λ etc.

Modeling assuming no data or model uncertainties and no permanent (inelastic) changes

Comparison of THM output: Mainly distribution and evolution of temperature, pressure, displacement and stress in the rock, and vertical flow through the repository horizon. Drying and wetting of bentonite and rock will also be compared.

When the research team is satisfied with their calculated evolution and distribution of stress in the rock mass—the driving force behind mechanically induced permanent changes—and their results are in agreement with others, the research team should go on to the next phase. The model inception will make sure that all research teams have correctly implemented boundary conditions and correctly modeled the basic THM behavior (assuming no permanent changes).

Phase 2: Preliminary Model Prediction and Parameter Study (about 12 months)

Input   **Modeling**   **Output**

Same geometry, initial and boundary conditions as in Step 1

Material properties have to be taken from available site data or developed by each research team using available site data. If there are no site data for certain parameters, literature data from similar rocks and sites could be used.

Preliminary model prediction of mechanically induced permanent changes:

a) Develop model for evaluation permanent changes (discrete or continuum?)

b) Parameter study (to identify key parameters and to find the conditions at which permanent changes are likely and not likely)

c) Predictions of coupled THM and permanent changes for one realistic realization (homogeneous or heterogeneous rock)

Comparison of THM output: Distribution and evolution of temperature, pressure, displacement, stress and permeability in rock. Vertical flow through the repository horizon should also be evaluated with and without mechanically induced permeability changes.

When the research team is satisfied with their preliminary model prediction of coupled THM processes, considering results of other research teams and new results from ongoing field experiments (FEBEX and DST), they should go on to the next phase and make the final prediction, including evaluation of uncertainties.

Phase 3: Final Prediction with Uncertainty Range (about 12 months)

Input   **Modeling**   **Output**

Same geometry, initial and boundary conditions as in Phase 1 and 2 (uncertainty range in the initial stress field may be introduced)

Same basic data sources as in Phase 2 should be used for model input and to derive model input data.

Final prediction with uncertainty analysis:

a) If necessary, revise/improve model for evaluation of permanent changes

b) Final prediction with evaluation of uncertainties (at least upper and lower bounds of predicted changes)

Final comparison of THM output: Same types of comparison as for the preliminary prediction above, but this time with uncertainty ranges for each parameter.

Synthesize results from all research teams and all modeling approaches, with emphasis on predictions of mechanically induced permanent changes and their uncertainties.

Figure 6.3.   Work scope of the three modeling phases of Task D_THM

6.3 DEFINITION OF D_THM1

This section gives specific definitions of Task D_THM1, representing a bentonite-filled repository in a saturated, sparsely fractured, granitic rock mass.

6.3.1 Specific Geometry and Modeling Sequence

Table 6.1 presents specifications of values for the model dimensions shown in Figure 6.1. The dimensions of the engineered barrier (drift, bentonite buffer, and waste canister) are taken from the FEBEX *in situ* test (see Task 1B definition from the DECOVALEX III project for more details about the engineered barrier system). The drift is located at a depth of 500 m, and the total vertical extension of the model is 1,000 m, with the top boundary located at the ground surface. The individual drifts are located at a distance of 35 m. (This distance was specified by the constraint of a maximum temperature of 100ºC at the contact between the canister and the bentonite.) The thermal power decay function for a reference fuel PWR element is given in Figure 6.4. In the reference design, four fuel elements are encapsulated into one canister and 87 canisters are placed into a 500 m long disposal drift. The canisters are 4.54 m long (equivalent to a heater in the FEBEX experiment) and are placed 2 m apart along the disposal drift. Assuming the waste is 30 years old at emplacement time, the average thermal power per meter drift is 4 × 400/5.54 ≈ 245 W/m at emplacement. (4 PWR elements per canister, 400 w per PWR element at 30 years [from Figure 6.4] along 4.54 m canister + 2 m separation results in 245 W/m). The entire thermal power decay function for the two-dimensional model can be calculated accordingly from Figure 6.4.

Figure 6.5 presents the modeling sequence, boundaries, and initial conditions for the coupled THM simulation to be performed for Task D_THM1. The initial conditions for the rock mass are defined at the pre-excavation stage (Figure 6.5a). The initial stress is given as $\sigma_h = 0.020 \cdot D + 0.6$ MPa (minimum principal horizontal stress), $\sigma_H = 0.055 \cdot D + 4.6$ MPa (maximum principal horizontal stress) and $\sigma_v = 2700 \cdot 9.81 \cdot D$ Pa (vertical stress), where D is elevation relative to ground surface (D = z − 500 and tensile stress is positive). The vertical thermal gradient is 30°C/km, with a fixed average temperature of 10°C at the ground surface and a fixed average temperature of 40°C at the bottom. The groundwater table is at the ground surface where the pressure is fixed to 0.1 MPa (atmospheric). At the bottom of the model, the fluid pressure is set to 9 MPa, slightly less than hydrostatic. This creates a small vertical head gradient and causes a vertical flow through the repository drift area, by which the impact of permeability changes on the fluid flow through the repository area can be studied. The excavation sequence can be simulated in a one-step steady-state calculation, with the elements in the drift removed, a constant temperature of 25°C, and a constant pressure of 0.1 MPa imposed at the drift boundary (Figure 6.5b). Alternatively, one may run a transient simulation using a finite excavation time before the bentonite and the heat-producing waste are emplaced. A finite excavation time is more realistic. We suggest using a finite excavation time of 30 years prior to waste emplacement. After the excavation simulation is completed (either steady-state or transient for 30 years), the waste canister, bentonite buffer, and backfill are installed instantaneously, and the postclosure simulation can start (Figures 6.5c and 6.5d).

Table 6.1.   Numerical values of model dimensions in Figure 6.1 for Task D_THM1

Dimension	Value
Vertical length, L_z	1,000 m
Horizontal length, L_x	35 m
Drift diameter, d	2.28 m
Diameter of waste canister	0.9 m
Dimensions of the near drift study area, (3d x 3d)	7 x 7 m
Dimensions of the far field study area, ($2L_x$/3 x $2L_x$/3)	25 m
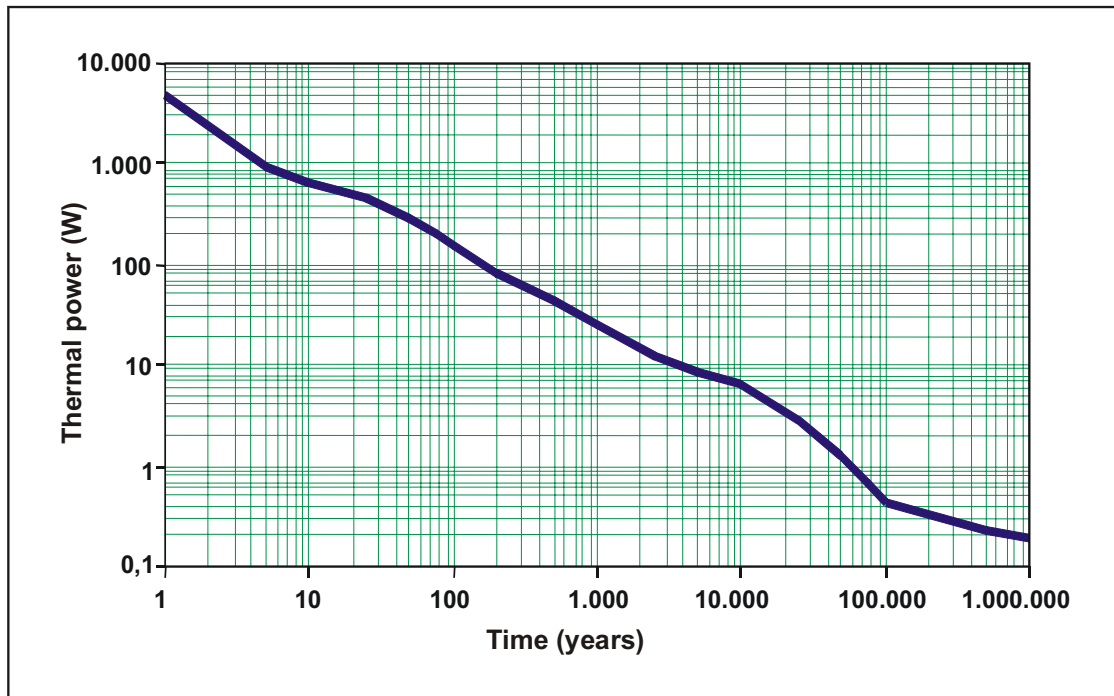
Figure 6.4.   Thermal power decay function of a reference fuel PWR element

a) Pre-excavation Conditions

b) Simulation of Excavation

c) Installation of Bentonite Buffer

d) Transient Simulation of Post-closure THM
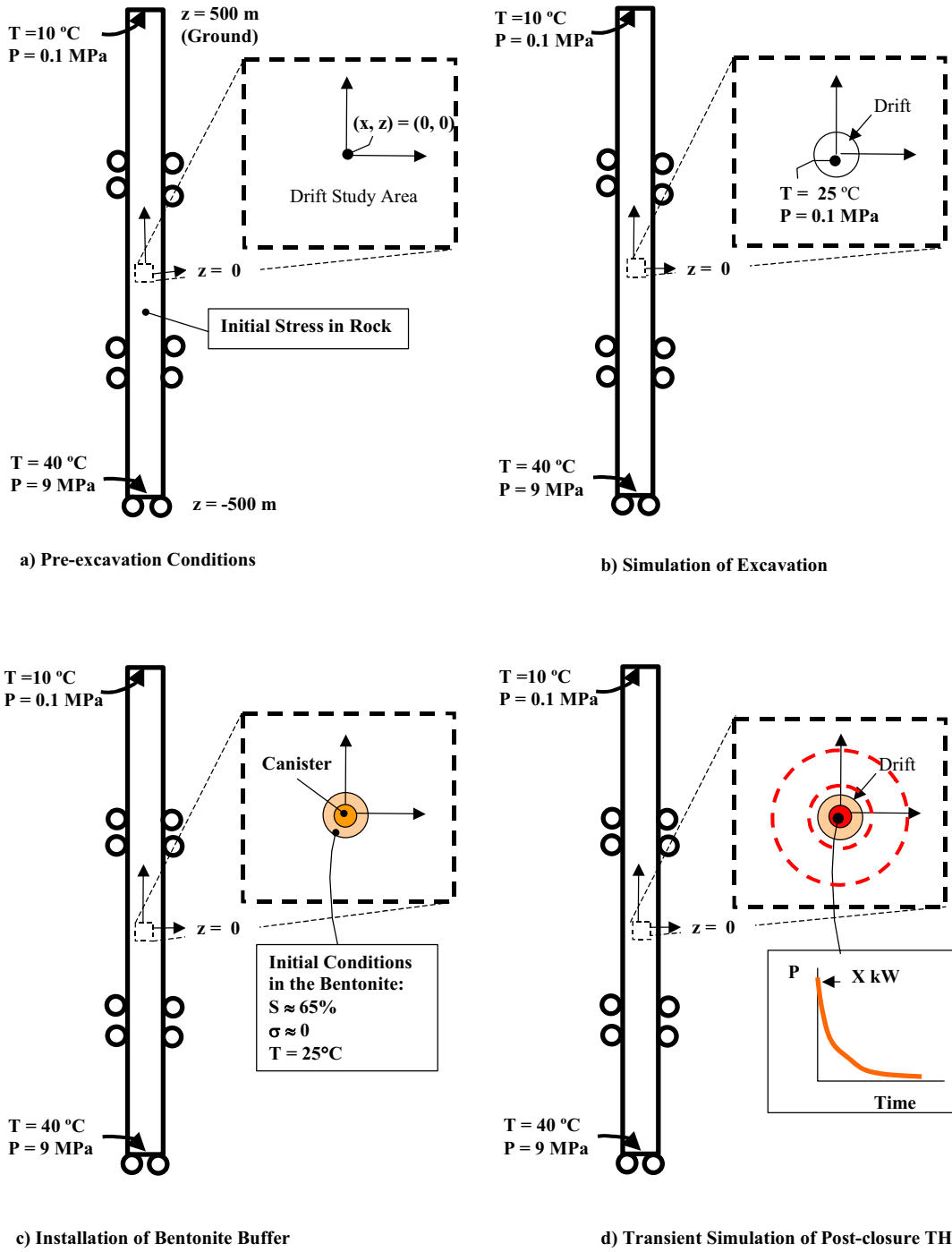
Figure 6.5.   Specific modeling sequence, boundaries, and initial conditions for Task D_THM1

6.3.2   Suggestions for Potential Model Simplifications

This section suggests simplifications for models that do not have the capabilities to simulate specific bentonite behavior during the initial resaturation phase. In this case, one can assume the bentonite to be fully saturated from the start, with a fully developed swelling pressure. Because the buffer will have reached full saturation within about 10 years, this simplification would only impact a very early period after emplacement, when the THM changes are rather small. Using this simplification, the temperature field should be calculated using pure heat conduction, with thermal conductivity of the bentonite taken at its fully saturation value ($\lambda = 1.3$ W/mK). The impact of the swelling stress on the surrounding rock should be simulated by applying a fully developed normal stress on the rock walls (Figure 6.6a). The applied total stress normal to the rock wall is equal to the fully developed swelling stress, which is an effective stress, plus a fully restored hydrostatic fluid pressure in the bentonite. In this case, the fully restored swelling stress is about 5 Mpa, and a fully restored fluid pressure is about 5 MPa (hydrostatic fluid pressure at a depth of 500 m). A refinement can be made by considering a gradual increase of the thermal conductivity and swelling stress in the bentonite during the first 10 years. Using a linear function of time would probably be sufficiently accurate (Figure 6.6b). This kind of simplification might be useful for a distinct element model, which may have limited capability for explicit simulation of the bentonite resaturation process. Comparison of modeling results from different teams and modeling approaches during the model inception phase (Phase 1) will reveal whether the specific simplifications applied by a research team are acceptable.

| (a) | (b) |
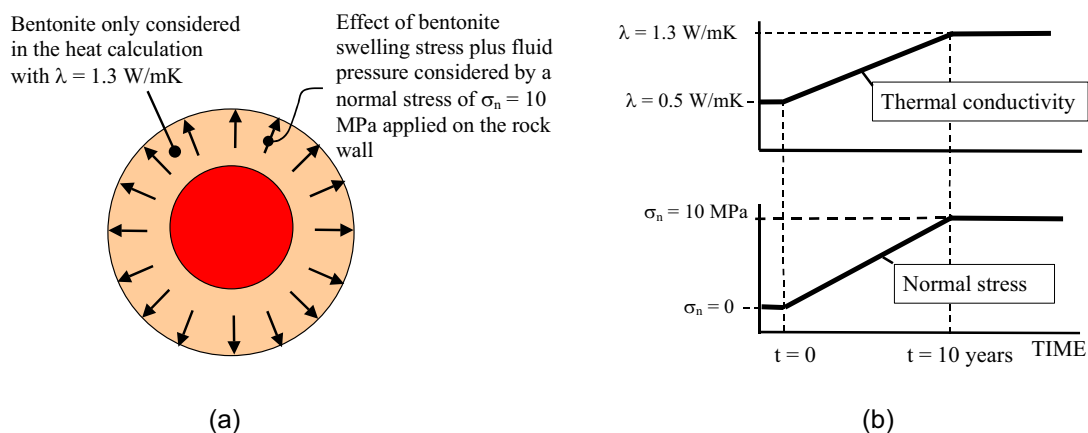
Figure 6.6.   Suggested model simplification for models that may not have the capability for explicit modeling of the bentonite resaturation process. (a) Saturated thermal conductivity of the bentonite and a normal stress applied to the drift wall, simulating the fully saturated conditions. (b) A linear change in thermal conductivity and swelling stress may be assumed the during expected resaturation time.

6.3.3   Input Data for Phase 1 (Model Inception)

The model inception simulation is conducted using specified input parameters, without data or model uncertainties, and without the need for developing parameters from measured data and other sources. In the model inception simulation, the rock is assumed to be homogeneous,

isotropic, and linear elastic. A homogeneous, isotropic rock mass implies that mechanical and hydrological properties are independent of stress (or depth) and will remain constant in time and space throughout the simulation. The material properties for the model inception phase are given in Table 6.2a. These mean properties are taken from the GTS/FEEBEX data set; they are fairly typical for any granitic rock. The Young's modulus of the rock mass has been reduced by about 70% compared to the intact rock values, to account for the effect of deformable fractures.

Table 6.2a.   Rock properties for Phase 1 (model inception)

Parameter	Value
Density, [kg/m^3]	2700
Porosity, [-]	0.01
Biot's constant, α [-]	1.0
Young's Modulus, [GPa]	35
Poissons ratio, [-]	0.3
Specific heat, [J/kg·°C]	900
Thermal conductivity, [W/m·°C]	3.0
Thermal expansion coefficient [1/°C]	$1 \cdot 10^{-5}$
Permeability, [m^2]	1×10^{-17}

The specified bentonite THM properties are mostly taken from the FEBEX experiment. They were presented in Task 1B definition of DECOVALEX III (DECOVALEX III, 2000). Table 6.2a summarizes the bentonite properties to be used in Task D_THM1. Alternatively, research teams may also use the simplification scheme suggested in Section 6.3.2.

Table 6.2b. Bentonite properties for Phase 1 (model inception).

Parameter	Value
Dry density, [kg/m^3]	$1.6 \cdot 10^3$
Porosity, [-]	0.41
Saturated permeability, [m^2]	$2.0 \cdot 10^{-21}$
Relative permeability, k_{rl}	$k_{rl} = S^3$
Moisture swelling coefficient [-]	0.238
Poisson ratio, [-]	0.35
Thermal expan. coeff., [1/°C]	$1.0 \cdot 10^{-5}$
Dry specific heat, [J/kg·°C]	$c_s = 1.38T + 732.5$
Thermal cond., [W/m·°C]	$\lambda_m = 1.28 - \dfrac{0.71}{1 + e^{(S-0.65)/0.1}}$ (with s liquid saturation)
Tortuosity factor for vapor diffusion (accounts for tortuous diffusion paths)	0.8

Research team that model the unsaturated behavior in the bentonite and the rock during the initial resaturation phase need characteristic curves for moisture retention and relative permeability. We suggest using the following characteristic curves for the FEBEX bentonite and the granite rock.

In the FEBEX project, experimental data of saturation, S_l versus suction, s for FEBEX bentonite have been fitted by means of the van Genuchten expression:

$$S_l = S_{l_0} + (S_{l_{max}} - S_{l_0})\left[1 + (s/P_0)^{\frac{1}{1-\lambda}}\right]^{-\lambda} \tag{6.1}$$

or to a modification of this expression that is more suitable for higher values of suction:

$$S_l = S_{l_0} + (S_{l_{max}} - S_{l_0})\left[1 + (s/P_0)^{1/(1-\lambda)}\right]^{-\lambda}\left[1 - s/P_s\right]^{\lambda_s} \tag{6.2}$$

where $S_{l\,0}$ and $S_{l\,max}$ are the residual and maximum degree of saturation and P_0 (Mpa; Mpa is Mega-Pascal), P_s (MPa), λ and λ_s are material parameters.

For the FEBEX bentonite, the water retention curve described by the following equation closely match experimental data:

$$S = 0.01 + (0.99)\left[1 + (s/35)^{1.43}\right]^{-0.30}\left[1 - s/4000\right]^{1.5} \tag{6.3}$$

The curve is plotted in Figure 6.7, green line.

A good match to experimental data at saturation values above about 40% is obtained with the following standard van Genuchten function:

$$S_r = 0.01 + (0.99)\left[1 + (s/30)^{1.43}\right]^{-0.30} \tag{6.4}$$

This is plotted in Figure 6.7, purple line. In DECOVALEX-THMC Task D THM_1, the retention curve defined in Equation (6.3) (green line in Figure 6.7) should be used if possible. If a research team can only use a standard van Genuchten function, the function defined in Equation (6.4) may be used.

The saturated permeability for the bentonite should be set to $2 \cdot 10^{-21}$ m^2. Relative permeability of the bentonite should be defined by the following expression:

$$k_{rl} = S_l^3 \tag{6.5}$$

The rock mass should have a water retention curve represented by van Genuchten parameters, P_0 = 1.47 MPa and λ = 0.6 (β = 2.5). That is:

$$S_l = \left[1 + (s/1.47)^{2.5}\right]^{-0.60} \tag{6.6}$$

where residual saturation is set to 0.0. This function is blue line in Figure 6.7. The relative permeability for the rock mass is defined by the function(blue line in Figure 6.7):

$$k_{rl} = \sqrt{S_l}\left\{1 - (1 - S_l^{1/0.6})^{0.6}\right\}^2 \tag{6.7}$$
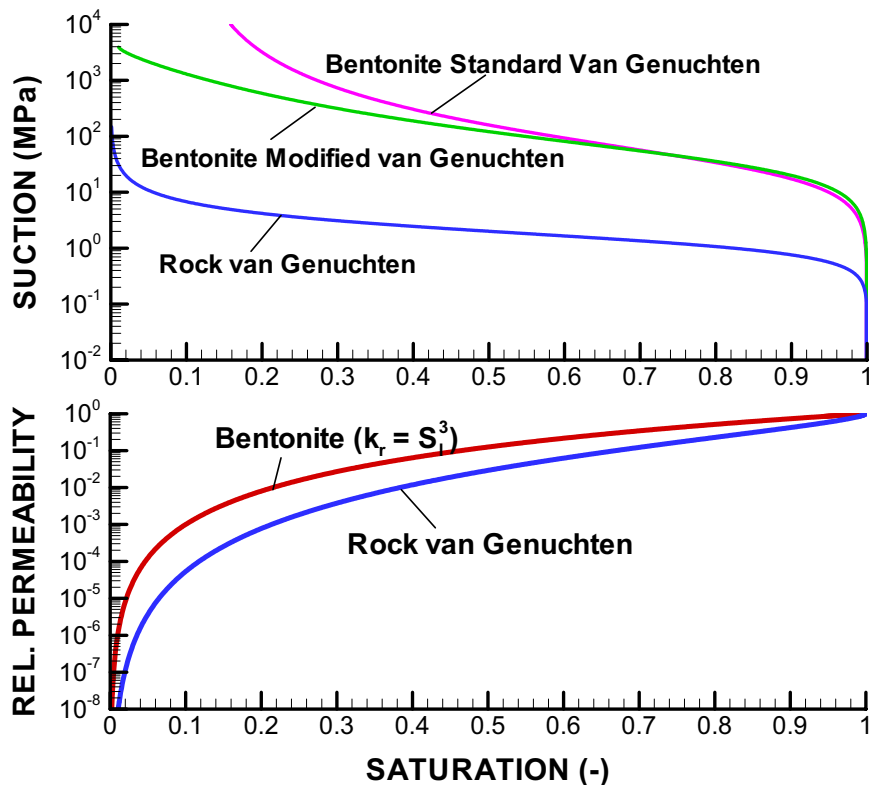
Figure 6.7. Characteristic Curves for D_THM1 bentonite and granite rock

6.3.4   Input Data for Phases 2 and 3 (Preliminary and Final Predictions with Uncertainties)

The input data for Phases 2 and 3 represent a typical site in fractured granitic rock, with most properties extracted from the GTS/FEBEX data set. The subsections below give a summary of the geological characterization, based on the DECOVALEX III, Task 1a definition with some additions of data from the Kamaishi Mine, Japan, and the Laxemar site, Sweden. The research teams may also use the original cited sources to extract and develop input data for their models (see Section 6.3.4.8). Rock properties are given with their uncertainty ranges, such as the standard deviations, as provided in the original sources. The individual research teams should decide how to use and propagate these uncertainties in their model predictions.

6.3.4.1   Intact Rock Properties

Intact rock properties of granitic rocks were provided in the DECOVALEX III, Task 1a definition. A literature review by Amiguest (1985) was cited, as well as a study by Keusen et al. (1989). Table 6.3 presents these data and includes additional data from the Kamaishi Mine heater test for reference. In this subtask, the properties for the Grimsel granodiorite should preferably be used since this is the rock type surrounding the FEBEX drift. For missing values, properties from

other sites may be used. The bentonite properties given in Table 6.2b shall not be changed in Phases 2 and 3.

<p style="text-align:center">Table 6.3.   Intact rock properties</p>

Parameter	Granodiorite (Grimsel) mean±std	Granite (Grimsel) mean±std	Granite (various sites 1985) mean (range)	Granodiorite (Kamaishi) mean (range)
Density [kg/m^3]	2706±13.6	2660±23.8	2640 (2600-2680)	2746 (2731-2755)
Porosity [%]		0.4-1.0	1.6 (0.5-2.5)	0.25-0.66
Un. Comp. Strength [MPa]	116.9±47.9	169.1±37.1	185 (150-220)	122.8 (119-125)
Young's Modulus [GPa]	47.3±15.4	53.3±11.0	60 (45-75)	61 (55-65)
Poisson's ratio [-]	0.33±0.15	0.37±0.12 0.33±0.03	0.25 (0.20-0.30)	0.3 (0.28-0.33)
Tensile strength [MPa]	9.54±2.17	9.06±1.48	10 (5-15)	11.0 (10.8-11.2)
Triaxial Comp. Strength (σ_3; σ_1) [MPa]	5.0; 230.0±70.7 10.0; 287.0±24.7 20.0; 355.0±28.3	5.0; 263.0±29.9 10.0; 333.0±20.6 20.0; 410.0±63.3		10.0; 219.6 15.0; 252.7 30.0; 330.3
Cohesion [MPa]				21.9
Internal frict. Angle				51.8
Coeff. Of Lin. Thermal Expan. [K^{-1}]			$8.0\cdot10^{-6}$ (5-$12\cdot10^{-6}$)	$8.21\cdot10^{-6}$
Thermal conductivity [W/mK]	2.66±0.19 (dry) 3.22±0.19 (wet)	2.58±0.19 (dry) 3.34±0.35 (wet)	3.3 (2.7-3.8)	2.71 (at 20ºC) 2.61 (at 60ºC) 2.54 (at 90ºC)
Specific heat [J/kgK]			920 (800-1250)	833
Hydraulic conductivity [m/s]		$5\cdot10^{-12}$ (10 MPa) 3.5-$4.5\cdot10^{-12}$ (5-15 MPa) $5\cdot10^{-12}$ (10 MPa)	10^{-12} (0.1-5 $\cdot10^{-12}$)	$1.0\cdot10^{-13}$ (10 MPa) 6.610^{-14} (20 MPa)

6.3.4.2   Fracturing

Most of the rock at the GTS is granite and granodiorite. Both have been affected by several episodes of fracturing. Keusen et al. (1989) found twelve possible discontinuity systems (see Figure 6.7), from which the systems shown in Table 6.4 were selected as those clearly existing. Figures 6.8 and 6.9 present examples of pole diagrams for orientation data and discontinuity spacing, respectively, for the different sets (Keusen et al. (1989).

Based on Keusen et al. (1989), and on direct observation, Pardillo and Campos (1996) and Pardillo et al. (1997) suggest the following geological features as relevant for regional groundwater flow:

- Shear zone S_1 and S_2 of azimut 140–150/80-90
- Fracture zones and Lamprophyre dikes, of azimuth 205–220/80

Shear zones have considerable thickness in the area of concern (5 to 20 m). At the intersection with tunnels, they display major water flows, indicating their relevance as preferential flow paths. There is considerable uncertainty about the distribution of hydraulic parameters in the shear zone, or whether the hydraulic conductivity tensor displays preferential directions. Lamprophyre dikes also have considerable dimensions (thickness up to several meters), but they are less important as preferential flow paths than the shear zones (DECOVALEX III, Task 1a definition, p. 16).

Keusen et al. (1989) provide the complete fracture mapping and statistics of the structural geology at the GTS area. This includes discontinuity orientation, extent, spacing, connectivity, mineralization, number of open versus closed fractures, and number of water-bearing fractures. The fracture data presented in Keusen et al. (1989) should be consulted by the research teams in developing their coupled THM model.
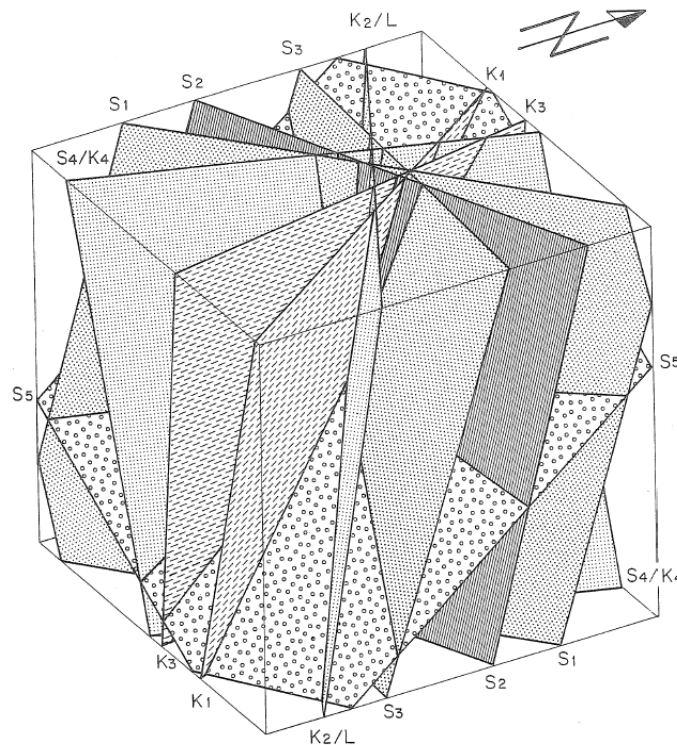
Figure 6.8. Block diagram fracture systems at the GTS (S: schistosity-related systems; K: joints systems; L: Lamprophyre). For a better overview, the subhorizontal system ZK and the hypothetical system S_6 were left out (Keusen et al., 1989).

Table 6.4.   Discontinuity systems shown to exist at the GTS (Keusen et al., 1989)

System	Comments
S_2	Main schistosity (azimut strongly overlapping with S_1; the two systems cannot be separated on the basis of orientation)
S_1 and S_3	Equivalent system pair (conjugates)
S_4/K_4 and K_2/L_2	Equivalent system pair (+ orthogonal)
K_1 and K_3	Equivalent system pair (conjugates)
ZK	Tension joints
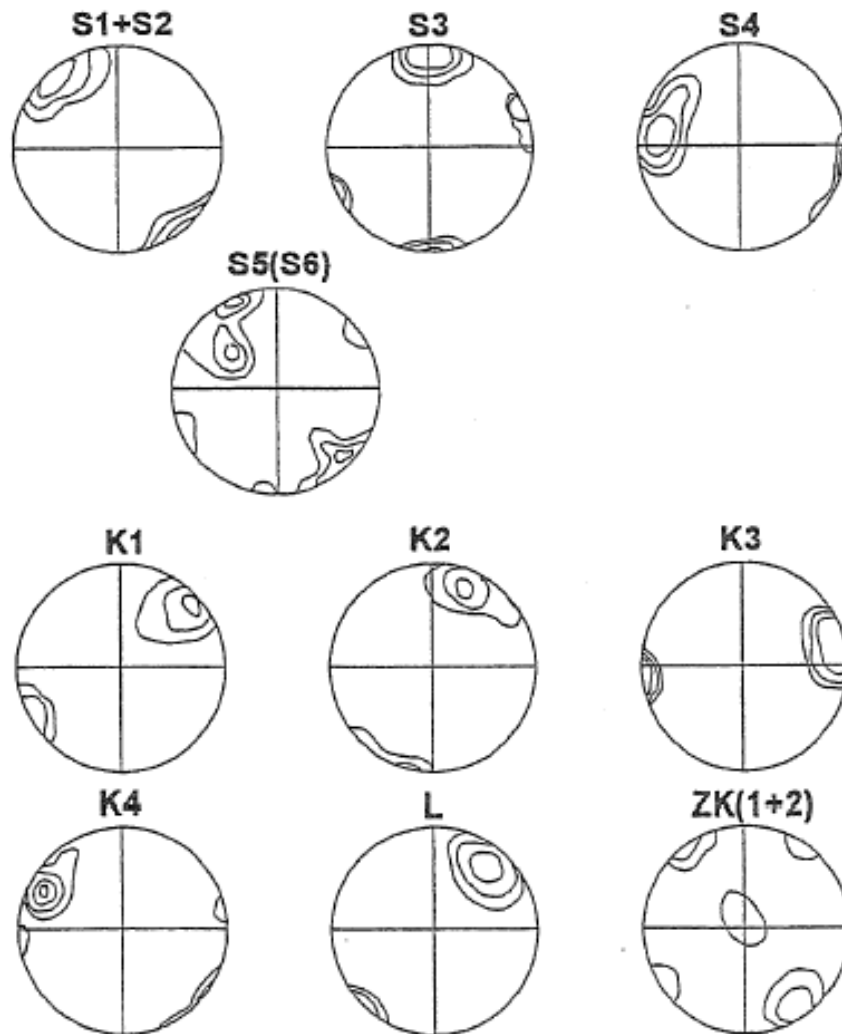
Figure 6.9.   Pool diagrams of orientation data for the different fracture systems (from Pardillo and Campos, 1996)
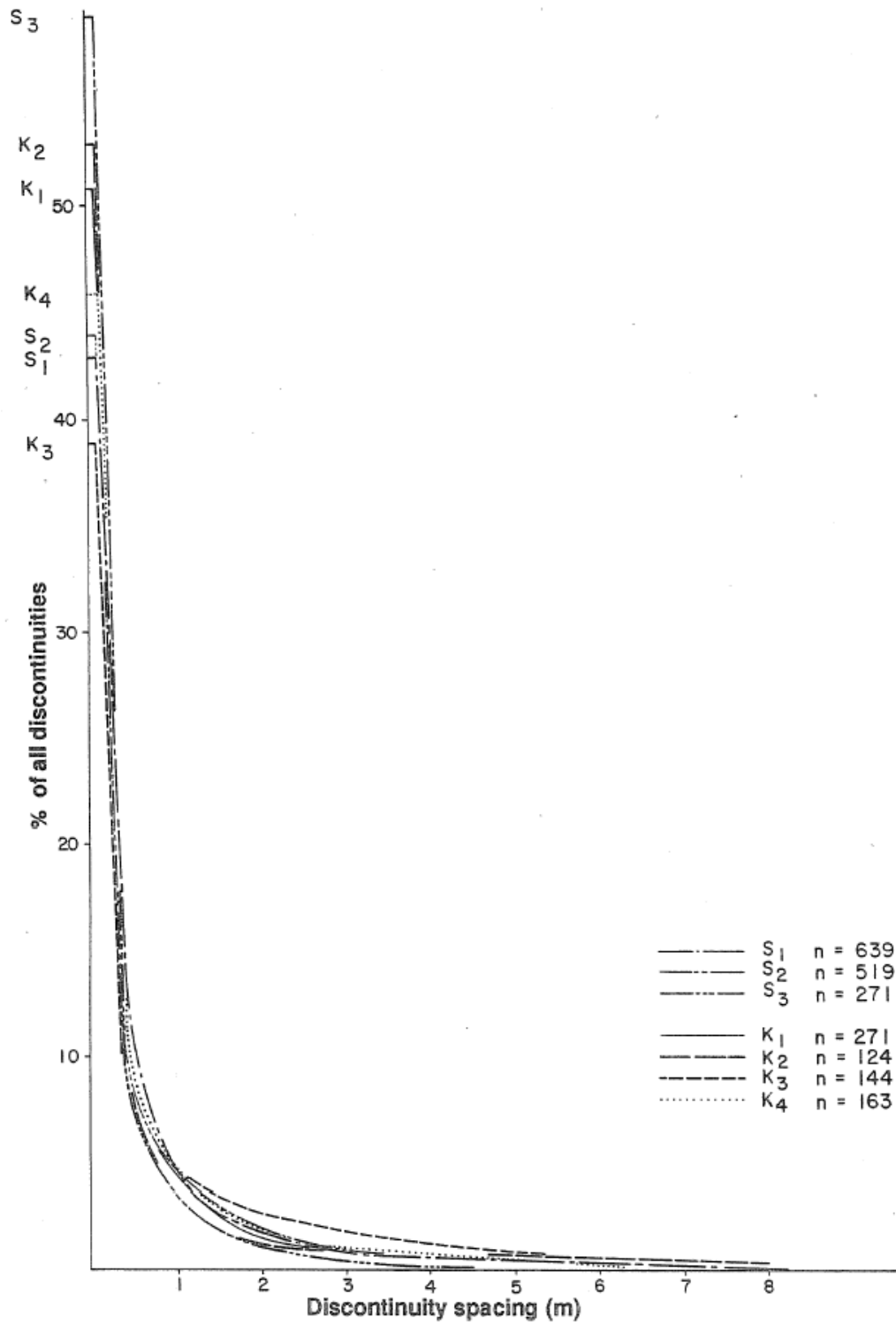
Figure 6.10. Mean values of discontinuity spacing for the whole GTS (Keusen et al., 1989)

6.3.4.3   Fracture Properties

Only a few data are available on rock-mechanical properties of fractures at the GTS area. No experiments have been performed to evaluate changes in permeability with normal stress or shear displacement. Because of the lack of site-specific data, the research teams will generally have to resort to the rock-mechanics literature for estimating fracture properties for crystalline rocks.

The Kamaishi Mine experiment, which was part of DECOVALEX II, is one example of a crystalline rock site where mechanical properties of single fractures were evaluated (Fujita et al., 1996). The experimental work included laboratory tests for both shear and normal loading. In addition, the basic fracture parameters for the Barton-Bandis joint model were evaluated from 22 samples, including the joint-wall compressive strength (JCS), the joint roughness coefficient (JRC), and the residual friction angle ϕ_r. Table 6.5 presents the values determined from the 22 samples (fracture length is about 6 cm on average).

Table 6.5.   Basic fracture parameters collected at Kamaishi Mine

Parameter	Average value	Range
JCS (MPa)	105	77.8-140.3
JRC	8.83	1.25-16.35
ϕ_r (degrees)	30.3	26.06-32.86

The average values and ranges of the Kamaishi data are similar to literature data for the 130 rock joints shown in Figure 6.11. Experimental values of shear and normal compression tests at the Kamaishi Mine heater test were also compared to literature data. It was shown that the Kamaishi data spanned almost the entire range of literature data, but are applicable to the Barton-Bandis joint model.
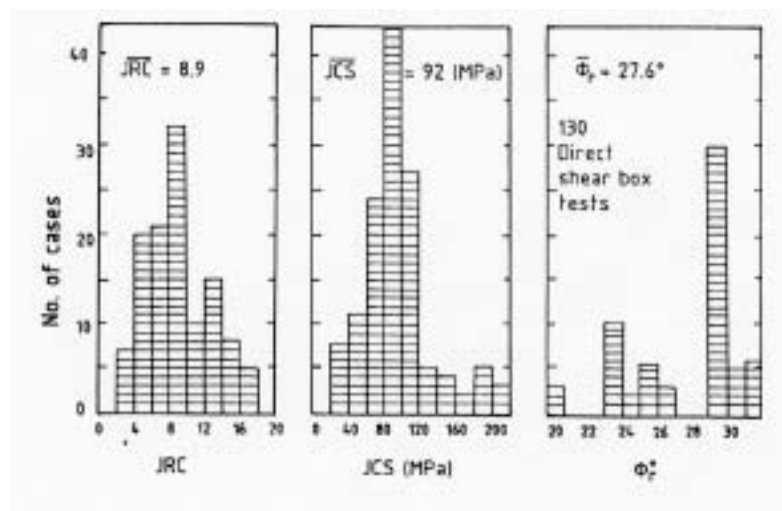
Figure 6.11. JRC, JCS, and ϕ_r statistics from 130 joints (Fujita et al., 1996)

The research teams may use the basic rock-joint parameters given in Table 6.5 to derive the constitutive relationships for mechanical and coupled hydromechanical behavior of rock joints. For example, the relationship linking normal stress and shear displacement to fracture permeability can be derived from the Barton-Bandis joint model. Because the fracture data at the Kamaishi Mine are widely distributed, such distribution should be propagated in the modeling to estimate uncertainty ranges of the predicted THM behavior. The research teams are not limited to using the Kamaishi Mine data set and the basic Barton-Bandis parameters in Table 6.5. Some research teams may want to use models other than the Barton-Bandis model, or may want to use completely different approaches to derive constitutive models for their coupled THM model. Other literature data on the mechanical and hydromechanical behavior of rock fractures in crystalline rock may be used for support. In any case, for the final model prediction, uncertainties associated with each approach and data used should be evaluated and propagated through the simulation results.

6.3.4.4   Rock Mass Hydrogeologic Properties

The hydrological properties at the GTS and around the FEBEX *in situ* test were reviewed in the DECOVALEX III, Task 1a definition. Experimental data stem from extensive testing in the rock mass surrounding the FEBEX drift, as summarized in Guimera et al. (1998). Figure 6.12 presents the results of single borehole packer tests conducted at the site. The results of these tests, which were performed with packer intervals varying from 0.8 to 6.94 m, show transmissivity varying over 6 orders of magnitude, with most of the values falling in the range between 10^{-11} and 10^{-10} m^2/s. Transmissivity values of $1 \cdot 10^{-9}$ to $1 \cdot 10^{-7}$ m^2/s typical represents shear zones or other highly conductive flow features. For the rock-mass away from highly conductive flow features, an anisotropic bulk rock-mass permeability was estimated as $k_x = 4.6 \cdot 10^{-12}$ m/s, $k_y = 9.2 \cdot 10^{-12}$ m/s and $k_z = 6.9 \cdot 10^{-11}$ m/s, where k_x and k_y are horizontal and k_z is vertical permeability. This would include the effect of small-scale fracturing. The intact rock permeability may be on the order of 10^{-12} m/s.
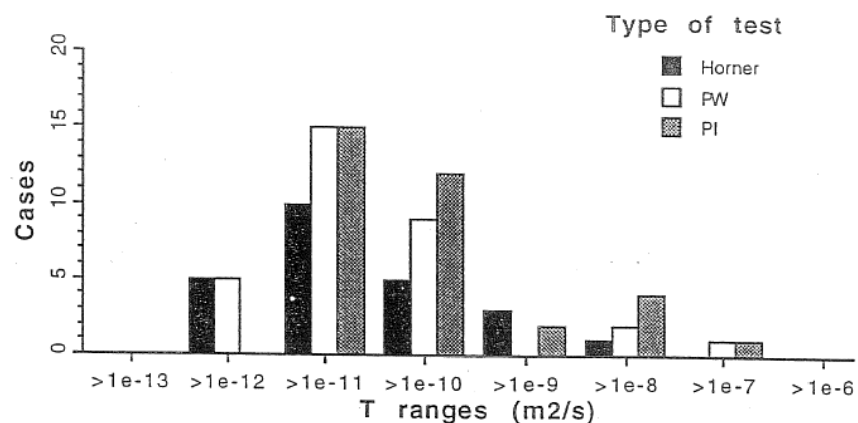
Figure 6.12. Summary of the results of packer tests conducted in boreholes surrounding the FEBEX drift (Guimera et al., 1998)

6.3.4.5   Rock Mass Mechanical and Hydromechanical Properties

Equivalent continuum properties for the fractured rock mass may have to be developed regardless of whether a continuum or a discrete fracture approach is used. Even when the discrete fracture approach is utilized for the near-drift focus areas, other regions further away from the drift will have to be modeled as an equivalent continuum, due to computational limitations. Thus, equivalent continuum properties (and possibly stochastic distributions) need to be derived for different scales. There are several empirical and theoretical approaches in the literature for deriving such continuum rock-mass properties, e.g., the rock mass deformation modulus and the rock-mass strength properties. This derivation should be based on the intact rock properties, the degree of fracturing, and the fracture properties. It is up to the individual research teams to derive appropriate properties for their modeling approach. The most difficult and important task is to derive a constitutive relationship for mechanically induced permeability changes in the fractured rock mass. The uncertainties associated with the derived properties need to be evaluated and propagated in the model simulations for the final predictions.

6.3.4.6   In Situ Stress Field

Estimates for the *in situ* stress field at the GTS are given in the DECOVALEX III, Task 1a definition, based on information found in Keusen et al. (1989). In general, the maximum horizontal stress lies between 18 and 45 MPa oriented towards the SE, i.e., perpendicular to the main alpine schistosity S2. However, the GTS is located in a mountain accessed from a horizontal tunnel and may not be representative of the model geometry assumed in Figure 6.1. Therefore, the measured *in situ* stress field from the Laxemar site in Sweden is utilized instead. At Laxemar, the maximum and minimum horizontal stress magnitudes are defined as (in MPa):

$$\sigma_h = 0.020 \cdot D + 0.6 \ (\pm 25\%)$$
$$\sigma_H = 0.055 \cdot D + 4.6 \ (\pm 25\%),$$

where D is the elevation relative to the ground surface (D = z − 500), and ± values in parentheses are uncertainty spans. At 500 m depth, the maximum horizontal stresses are between 20 to 45 MPa, which is almost identical to the GTS. On the other hand, the minimum horizontal stress is between 7 and 14 MPa, which is substantially lower than at the GTS. For the present task, the emplacement drift is assumed to be oriented perpendicular to the S2 discontinuity, and hence, the maximum compressive stress is oriented perpendicular to the axis of the drift (Section 6.3.4.7). The vertical stress can be estimated from the weight of the overlying rock mass.

6.3.4.7   Orientation of Emplacement Drift Relative to Discontinuity System

The emplacement drift is oriented along the strike of the S2 discontinuity system, which implies that σ_H is oriented perpendicular to the axis of the emplacement drift.

6.3.4.8   References for Task D_THM1

Table 6.6 lists several references that might be useful for the research teams when developing their model for Task_D_THM1. These reports were distributed to research teams that worked on Task 1 during DECOVALEX III. Most of these reports can be provided to the individual research teams upon request.

Table 6.6.   List of references cited for Task_D_THM1

Reference	Comment
Keusen H.R., Ganguin J., Shuler P. and Buletti M. (1989). Grimsel Test Site: Geology NAGRA NTB 87-14E, FEb 1989.	The main source of geology, material properties, fracturing, and information about hydrogeology at the GTS area.
Amiguet J.-L. (1985). Grimsel Test Site. Felskennwerte von intaktem Granit. Zusammenstellung felsmechanisher Laborresultate diverse granitische Gesteine. NAGRA, NIB 85-05, Sep. 1985.	A review of mechanical and thermal mechanical properties in granitic rock including the GTS.
Pardillo J., Campos R. and Guimera J. (1997). Caracterizacion geologica de la zone de ensayo FEBEX (Grimsel – Suiza). CIEMAT, 70-IMA-M-2-01, May 1997.	Summarizes geology including fracturing in the rock mass surrounding the FEBEX *in situ* test (in Spanish).
Pardillo J. and Campos R. (1996). FEBEX-Grimsel Test Site (Switzerland). Considerations with respect to the fracture distribution. CIEMAT, 70-IMA-L-2l05, Mar. 1996.	Provides a summary of Pardillo et al (1997) in English.
Guimera J., Carrera J., Marinez L., Vazquez E., Ortuno F., Fierz T., Bulher C., Vives L., Meier P., Median A., Saaltink M., Ruiz B. and Pardillo J. (1998). FEBEX Hydrogeological characterization and modelling. UPC, 70-UPC-M-0-1001, Jan 1998.	Synthesis of hydrogeology around the FEBEX drift including summary of hydraulic testing.
Fujita T., Sugita Y., Chijimatsu M. and Ishikawa (1996). Mechanical properties of fracture. Power Reactor and Nuclear Fuel Development Corporation (PNC), Technical note 06-95-06.	Laboratory and field measurement of mechanical properties of fractures at the Kamaishi Mine site to be used in Task_D_THM1.
DECOVALEX III (2000). Task 1. Modeling of FEBEX in situ test. Part A: Hydromechanical modeling of the rock.	DECOVALEX III Task 1A definition that includes a summary of rock-mass data around the FEBEX *in situ* test, from which much information has been extracted to this document.
DECOVALEX III (2001). Task 1. Modeling of FEBEX in situ test. Part B: Thermo-hydro-mechanical analysis of the bentonite behaviour.	DECOVALEX III Task 1B definition that includes a summary of bentonite properties for FEBEX *in situ* test from which the buffer properties should be extracted for Task_D_THM1
Alonso et al. (2004). Final report of DECOVALEX III, Task1: FEBEX in situ test. SKI report expected during 2004.	Provides information about modeling approached used and modeling results for the FEBEX *in situ* test during DECOVALEX III.

6.4 DEFINITION OF D_THM2

This section gives specific definitions of Task D_THM2, representing a repository drift in unsaturated, densely fractured volcanic rock. The definition is based on the current concept for a nuclear waste repository at Yucca Mountain, Nevada.

6.4.1 Specific Geometry and Modeling Sequence

Table 6.7 presents value specifications for the model dimensions shown in Figure 6.1. The dimensions of the engineered barrier (drifts and waste canisters) are taken from the Yucca Mountain repository design. The drift is located at a depth of 250 m, and the total vertical extension of the model is 550 m with the top boundary located at the ground surface. The heat power released from the waste canister as a function of time is shown in Figure 6.13, with numerical values given in Table 6.8. These values are for a thermal line load of 1450 W/m drift length and can be used directly in the two-dimensional model simulation. They include a 50-year period of forced ventilation, during which 86% of the decay heat is removed by air flow.

Table 6.7.   Numerical values of model dimensions in Figure 6.1 for Task D_THM2

Dimension	Value
Vertical length, L_z	550 m
Horizontal length, L_x	81 m
Drift diameter, d	5.5 m
Diameter of waste canister	1.7 m
Dimensions of the near drift study area, (3d x 3d)	16.5 x 16.5 m
Dimensions of the far field study area, ($2L_x/3$ x $2L_x/3$)	54 x 54 m
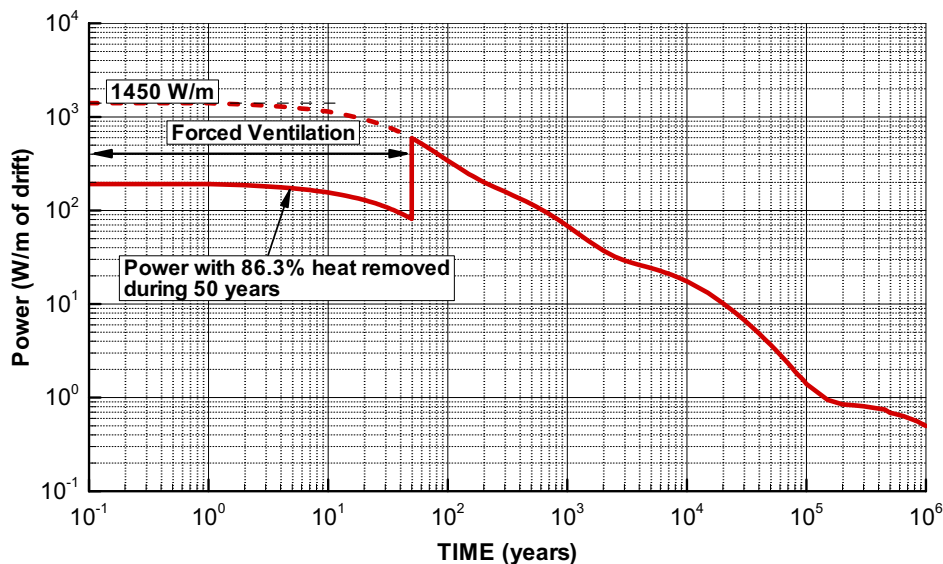
Figure 6.13. Thermal power decay function (values given in Table 6.8)

Table 6.8. Thermal power per meter drift for 1,450 W/m initial thermal line load reduced by 86.3% for 50 years as a result of drift ventilation

Time (years)	Power (W/m)	Time (years)	Power (W/m)	Time (years)	Power (W/m)	Time (years)	Power (W/m)	Time (years)	Power (W/m)
0.00E+00	1.99E+02	4.00E+01	9.38E+01	7.91E+01	4.16E+02	7.00E+02	9.21E+01	9.01E+04	1.64E+00
1.00E+00	1.92E+02	4.10E+01	9.25E+01	8.01E+01	4.12E+02	7.51E+02	8.72E+01	9.51E+04	1.52E+00
2.00E+00	1.86E+02	4.20E+01	9.11E+01	8.11E+01	4.07E+02	8.01E+02	8.28E+01	1.00E+05	1.40E+00
3.00E+00	1.81E+02	4.30E+01	8.97E+01	8.21E+01	4.03E+02	8.51E+02	7.88E+01	1.50E+05	9.44E-01
4.00E+00	1.77E+02	4.40E+01	8.85E+01	8.31E+01	3.99E+02	9.01E+02	7.50E+01	2.00E+05	8.46E-01
5.00E+00	1.73E+02	4.50E+01	8.71E+01	8.41E+01	3.95E+02	9.51E+02	7.16E+01	2.50E+05	8.26E-01
6.00E+00	1.69E+02	4.60E+01	8.59E+01	8.51E+01	3.91E+02	1.00E+03	6.84E+01	3.00E+05	8.08E-01
7.00E+00	1.66E+02	4.70E+01	8.47E+01	8.61E+01	3.87E+02	1.50E+03	4.73E+01	3.50E+05	7.83E-01
8.01E+00	1.62E+02	4.80E+01	8.34E+01	8.71E+01	3.83E+02	2.00E+03	3.72E+01	4.00E+05	7.64E-01
9.01E+00	1.59E+02	4.90E+01	8.23E+01	8.81E+01	3.79E+02	2.50E+03	3.21E+01	4.50E+05	7.46E-01
1.00E+01	1.56E+02	5.00E+01	8.12E+01	8.91E+01	3.76E+02	3.00E+03	2.93E+01	5.00E+05	6.88E-01
1.10E+01	1.52E+02	5.00E+01	5.93E+02	9.01E+01	3.72E+02	3.50E+03	2.75E+01	5.50E+05	6.70E-01
1.20E+01	1.49E+02	5.10E+01	5.85E+02	9.11E+01	3.69E+02	4.00E+03	2.62E+01	6.00E+05	6.51E-01
1.30E+01	1.47E+02	5.20E+01	5.77E+02	9.21E+01	3.65E+02	4.50E+03	2.52E+01	6.50E+05	6.33E-01
1.40E+01	1.44E+02	5.30E+01	5.69E+02	9.31E+01	3.62E+02	5.00E+03	2.42E+01	7.00E+05	6.09E-01
1.50E+01	1.41E+02	5.40E+01	5.61E+02	9.41E+01	3.59E+02	5.50E+03	2.34E+01	7.51E+05	5.91E-01
1.60E+01	1.38E+02	5.50E+01	5.54E+02	9.51E+01	3.55E+02	6.00E+03	2.26E+01	8.01E+05	5.73E-01
1.70E+01	1.36E+02	5.60E+01	5.47E+02	9.61E+01	3.52E+02	6.50E+03	2.18E+01	8.51E+05	5.56E-01
1.80E+01	1.34E+02	5.70E+01	5.39E+02	9.71E+01	3.49E+02	7.00E+03	2.11E+01	9.01E+05	5.32E-01
1.90E+01	1.32E+02	5.80E+01	5.32E+02	9.81E+01	3.46E+02	7.51E+03	2.05E+01	9.51E+05	5.15E-01
2.00E+01	1.30E+02	5.90E+01	5.26E+02	9.91E+01	3.43E+02	8.01E+03	1.98E+01	1.00E+06	4.97E-01
2.10E+01	1.27E+02	6.00E+01	5.19E+02	1.00E+02	3.40E+02	8.51E+03	1.92E+01		
2.20E+01	1.25E+02	6.10E+01	5.12E+02	1.10E+02	3.15E+02	9.01E+03	1.86E+01		
2.30E+01	1.23E+02	6.20E+01	5.06E+02	1.20E+02	2.94E+02	9.51E+03	1.80E+01		
2.40E+01	1.21E+02	6.30E+01	5.00E+02	1.40E+02	2.59E+02	1.00E+04	1.75E+01		
2.50E+01	1.19E+02	6.40E+01	4.94E+02	1.50E+02	2.45E+02	1.50E+04	1.32E+01		
2.60E+01	1.17E+02	6.50E+01	4.88E+02	1.60E+02	2.35E+02	2.00E+04	1.02E+01		
2.70E+01	1.15E+02	6.60E+01	4.82E+02	1.70E+02	2.25E+02	2.50E+04	8.21E+00		
2.80E+01	1.13E+02	6.70E+01	4.76E+02	1.80E+02	2.16E+02	3.00E+04	6.76E+00		
2.90E+01	1.11E+02	6.80E+01	4.70E+02	1.90E+02	2.08E+02	3.50E+04	5.68E+00		
3.00E+01	1.10E+02	6.90E+01	4.65E+02	2.00E+02	2.01E+02	4.00E+04	4.85E+00		
3.10E+01	1.08E+02	7.00E+01	4.60E+02	2.50E+02	1.76E+02	4.50E+04	4.19E+00		
3.20E+01	1.06E+02	7.10E+01	4.54E+02	3.00E+02	1.59E+02	5.00E+04	3.68E+00		
3.30E+01	1.04E+02	7.20E+01	4.49E+02	3.50E+02	1.45E+02	5.50E+04	3.25E+00		
3.40E+01	1.03E+02	7.31E+01	4.44E+02	4.00E+02	1.34E+02	6.00E+04	2.88E+00		
3.50E+01	1.01E+02	7.41E+01	4.39E+02	4.50E+02	1.25E+02	6.50E+04	2.58E+00		
3.60E+01	9.97E+01	7.51E+01	4.34E+02	5.00E+02	1.17E+02	7.00E+04	2.33E+00		
3.70E+01	9.81E+01	7.61E+01	4.30E+02	5.50E+02	1.10E+02	7.51E+04	2.11E+00		
3.80E+01	9.67E+01	7.71E+01	4.25E+02	6.00E+02	1.03E+02	8.01E+04	1.91E+00		
3.90E+01	9.52E+01	7.81E+01	4.20E+02	6.50E+02	9.73E+01	8.51E+04	1.75E+00		

Figure 6.14 presents the modeling sequence, boundaries, and initial conditions for a coupled THM simulation to be performed in Task D_THM2. The initial conditions for the rock mass are defined at the pre-excavation stage (Figure 6.14a). Fixed average temperatures are used as temperature boundary conditions at the ground surface (18°C) and the water table (32°C), resulting in an average thermal gradient of 25°C/km. An average infiltration rate of 6 mm/year is imposed at the ground surface, at a fixed gas pressure of 0.1 MPa. A steady-state simulation is to be conducted, first to calculate a steady initial distribution of pressure, temperature, and liquid saturation. During this simulation, the temperature at the bottom of the model is fixed, but the gas pressure should be free to change. The simulation will result in steady vertical gravity-driven liquid flux from the ground surface down to the water table. After temperature and pressure have reached steady-state conditions, the gas pressure at the bottom of the model should be fixed at the steady-state value. If a dual-continuum model is used with both matrix and fracture continua present at any location in space, there will be different values of liquid saturation in the matrix and in the fractures, owing to strong differences in capillarity. An initial stress field should be given for the mechanical simulation before running the model to static equilibrium. The end of this simulation results in a steady THM state. The excavation sequence (Figures 6.14b and 6.14c) can be simulated in a one-step steady-state calculation, with the elements in the drift removed and a constant temperature and pressure assigned in the open drift. The capillary pressure in the drift should be set close to zero. Alternatively, one may run a transient simulation using a finite excavation time before the heat-producing waste is emplaced. A finite excavation time is more realistic. We suggest using a finite excavation time of 30 years prior to waste emplacement. After the excavation simulation is completed (either steady-state or transient for 30 years), another simulation should be started with the heat-decay function initiated and the heating of the rock included. It is a good approximation to assume a perfect heat transfer from the waste package to the walls of the drift, because of significant radiative heat transfer in the open drift.
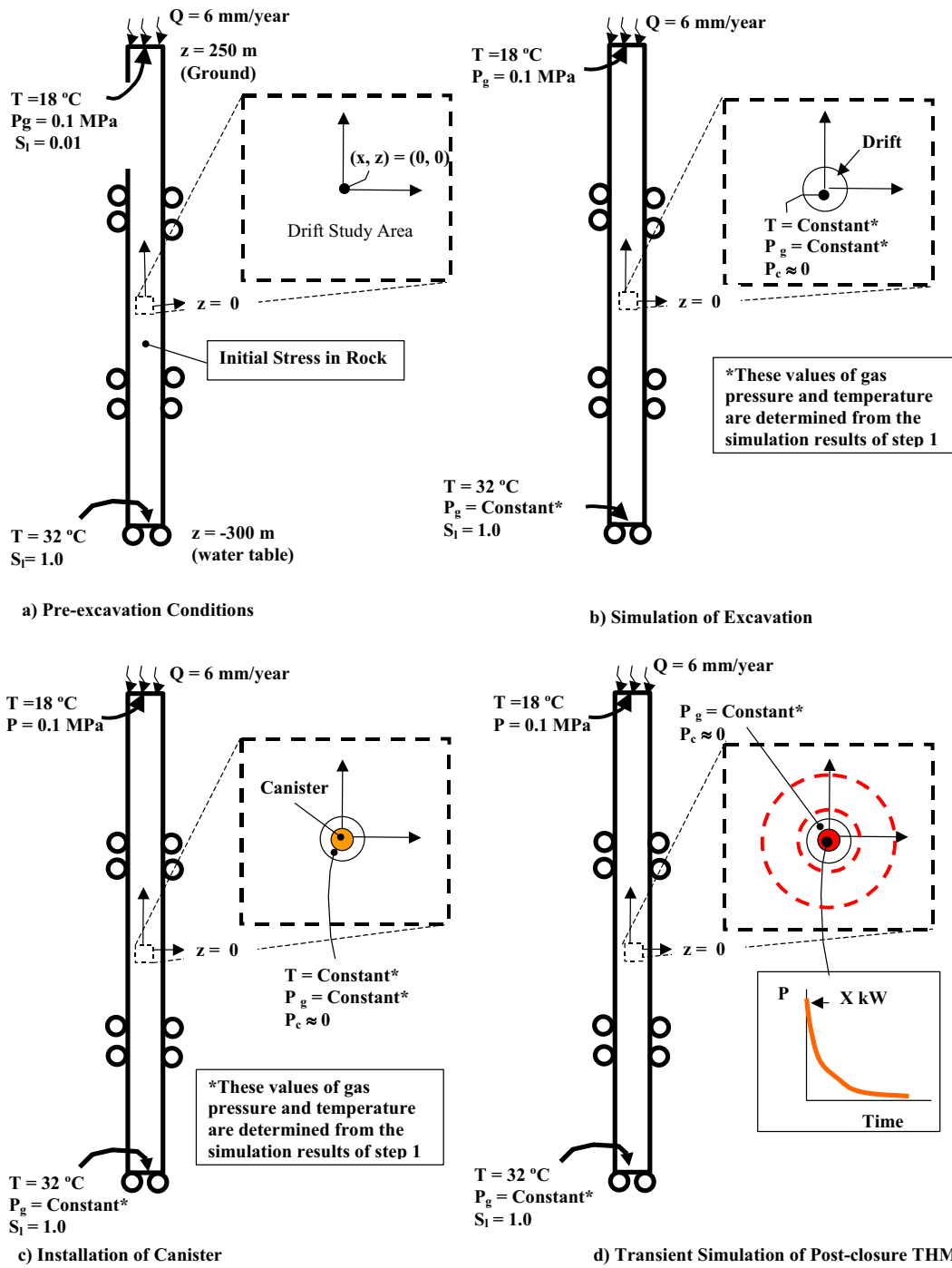
Figure 6.14. Specific modeling sequence, boundaries, and initial conditions for Task D_THM2

6.4.2   Suggestions for Potential Model Simplifications

The modeling of this case involves above-boiling temperatures that induce strong two-phase flow conditions (liquid and air with boiling and condensation) in the fractured rock near the drift wall. Furthermore, a dual-continuum model is recommended to accurately represent the hydrology of the system. Dual-continuum models are often applied to fractured porous rocks, where one component (the fractures) typically has large permeability, but small porosity, while the other component (the rock matrix) has a larger porosity, but small permeability. A dual continuum model is based on the continuum concept, but uses two separate, overlapping continua for fractures and matrix. At each location, there are two nodes (or volumes) representing the fractures and the matrix, respectively, each having a pressure, saturation, temperature, or stress value. Thus local disequilibrium between fractures and matrix can be modeled without explicitly accounting for all individual fractures and matrix blocks. This allows considering the hydrologic properties and conditions of fractures and matrix with their vastly differing permeabilities and moisture retention characteristics. While dual continuum models are the best choice for D_THM2 (except for using discrete fracture-matrix continuum models or hybrid models), they require significant code development.

Many models focusing on THM or TM processes may not have the capabilities to model thermally induced two-phase flow and may not have dual-continuum capabilities. If thermally induced two-phase flow cannot be simulated, a simplified approach can be used as outlined below, where the temperature field in the rock is simulated without a full two-phase flow simulation. If dual-continuum is not possible, a simpler single continuum approach may be used. For application of a single continuum approach, the research teams are encouraged to review the upcoming DECOVALEX III, Task 2 report (Datta et al., 2004), in which both single and dual-continuum models were applied to simulate coupled THM processes at the DST. The preferred choice for Task D_THM2, however, is a dual continuum model, because a single continuum representation misses some important hydraulics of the fracture-matrix system. An alternative model choice for those teams that want to avoid dual continuum complications is the "effective continuum representation" (ECM) after Pruess et al. (1990). An effective continuum model allows accounting for the different hydraulic characteristics of fractures and matrix, but assumes a local THM equilibrium between fractures and matrix at all times. For systems that are not too dynamic in nature, the ECM model gives adequate flow results, much better than those predicted by a single continuum model. Information about the ECM and its possible implementation into existing single continuum codes can be provided upon request.

Because the focus of this task is on potential TM-induced permanent changes in the fractured rock surrounding the drift, it is important to calculate the temperature field with sufficient accuracy. The temperature field is the driving force behind TM-induced changes. Therefore, if the temperature field can be accurately represented, the TM-induced changes can be calculated without significant loss of accuracy. The simplest approach is a pure thermal conduction model, with a thermal conductivity and heat capacity close to the initial saturation conditions. Although convective heat transfer processes are important near the drift during the first 1,000 years, heat conduction generally dominates heat transfer in the system.

The pure conduction approach can be refined by using a pore-water boiling model as described by Damjanac et al. (2000). In the pore-water boiling model illustrated in Figure 6.15, boiling is simulated by increasing the volumetric heat capacity of the rock mass over a temperature range T1 to T2. The increase in heat capacity is described by Equation (6.1), which dictates the amount of latent heat required to vaporize the pore water present in the rock.

$$\Delta(\rho C) = \frac{\rho_w \phi S_l h_v}{\Delta T} \tag{6.8}$$

where
ρ_w = density of water ($\approx$1,000 kg/m^3)
ϕ = porosity ($\approx$ 0.13)
S_l = liquid water saturation ($\approx$ 0.95)
h_v = latent heat of vaporization (2.2526×10^3 kJ/kg)
ΔT = boiling temperature range ($\approx$20°C)

Boiling is assumed to begin at 94°C (T1) and end at 114°C (T2). For temperatures below 94°C, the rock mass remains "wet" at its initial saturation level. For temperatures above 114°C, the rock mass becomes "dry." As seen in Figure 6.15, the thermal conductivity of the rock mass varies linearly over this temperature range, using the wet and dry values of thermal conductivity as given in Table 6.9. Also, the heat capacity varies linearly in the temperature interval T1 to T2. For increasing temperature, during pore-water boiling, the values of the heat capacity are determined by the path c-d. If pore-water boiling occurs without reaching temperature T2, the values of the heat capacity are determined by the path d-c upon decreasing temperatures. If the rock mass becomes dry (i.e., exceeds temperature T2), the values of the heat capacity are determined by path e-b when temperature decreases. It is assumed that the rock mass returns to its initial saturation when reaching temperature T$_1$. The heat of vaporization is not recovered at resaturation of the rock mass.

The above approach was used by Damjanac et al. (2000) for thermal-mechanical modeling and estimation of TM-induced permeability changes, using both continuum (FLAC) and distinct element (UDEC) approaches. Using this simplified approach, the boiling effect on the temperature distribution can be easily emulated, and the temperature field is likely to be sufficiently accurate for analysis of TM-induced changes and evaluation of potential permanent changes in the rock mass surrounding the drift. The accuracy of the simplification scheme can be checked at the end the model inception phase, by comparison of model results with more sophisticated modeling approaches by other research teams.

a)

b)
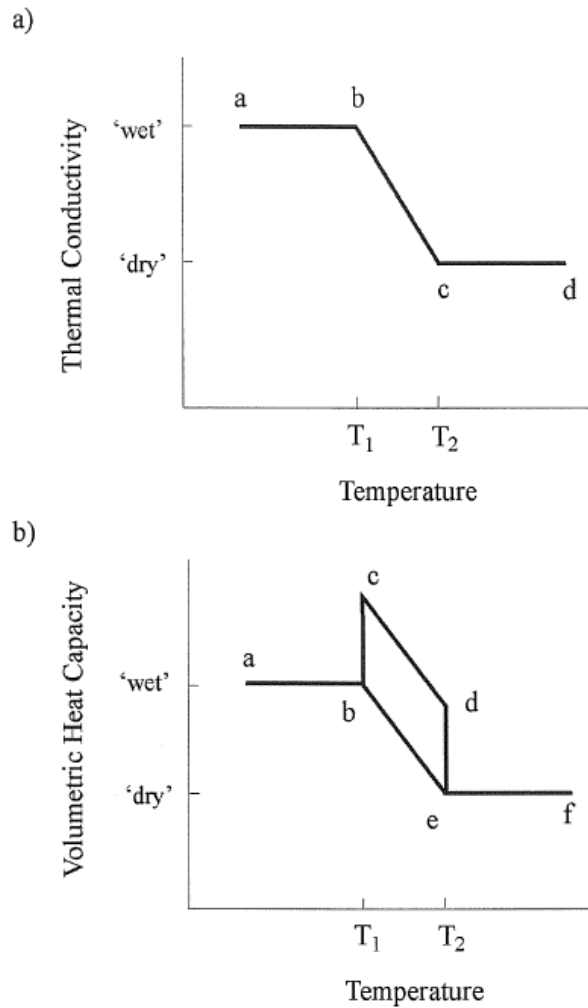
Figure 6.15. Illustration of pore-water boiling model that can be used for model simplification (from Damjanac et al., 2000).

6.4.3   Specific Input Data for Phase 1 (Model Inception)

The model inception simulation is conducted using specified input parameters, without data or model uncertainties and without the need for developing parameters from measured data and other sources. In the model inception simulation, the rock is assumed to be homogeneous, isotropic, and linear elastic. The mechanical and hydrological properties are independent of stress (or depth). Table 6.9a presents the material properties for the model inception phase. We have chosen the mean properties of one of the main stratigraphic units in which the emplacement drifts will be located at the Yucca Mountain (i.e., the middle nonlithophysal [Tptpmn] unit of Topopah Spring Tuff).

Hydrologic properties are given for both the fracture and the matrix continua, to support a dual-continuum model for simulation of the unsaturated fluid flow. The volume fraction V_F of the

fractures per total volume of rock is 0.0083; thus the volume fraction V_M of intact rock matrix is 0.9917. Note that the fracture permeability is defined as the Darcy permeability k_F of the fracture continuum; i.e., the given permeability value should not be multiplied by the volume fraction to give the continuum value. In contrast, the permeability value given for the matrix represents the intact rock. In theory, this value should be multiplied by the volume fraction V_M to arrive at the matrix continuum permeability. However, since V_M is almost equal to one, the given matrix permeability value is a good estimate for the continuum permeability.

A dual continuum model also requires information of the geometry of the fractures and the matrix block. The first parameter is the fracture-matrix interface area, which should be set to 13.5 m^2 per unit bulk volume of fractured rock. The second parameter is the representative distance between the fractures and the center of matrix blocks, which should be set to 3.9 cm. The larger the interface area, the more intense is the heat and mass exchange between the two continua. The smaller the distance, the larger is the gradient between fracture and matrix continua at given disequilibrium conditions.

Table 6.9a.   Thermal-hydrologic-mechanical properties used in simulations (hydraulic properties for dual-continuum model)

Type	Property	Value
Hydraulic properties of the fractured continuum	Permeability (m^2)	3.3×10^{-13}
	Volume fraction of interconnected fractures (-)	0.0083
	van Genuchten's air-entry pressure (kPa)	9.615
	van Genuchten's exponent, m (-)	0.633
	Residual saturation (-)	0.01
Hydraulic properties of the matrix continuum	Permeability (m^2)	1.77×10^{-19}
	Volume fraction of rock matrix (-)	0.9917
	Initial porosity (-)	0.13
	van Genuchten's air-entry pressure (kPa)	118.3
	van Genuchten's exponent, m (-)	0.317
	Residual saturation (-)	0.19
Thermal and Mechanical properties of the rock mass (equivalent continuum properties)	Wet thermal conductivity (W/m °K)	2.29
	Dry thermal conductivity (W/m °K)	1.49
	Grain Specific Heat, J/(kg °K)	985
	Grain Density (kg/m^3)	2550
	Bulk Density (saturated) (kg/m^3)	2360
	Young's modulus (GPa)	15
	Poisson's ratio (-)	0.21
	Thermal expansion coefficient (1/°C)	1.0×10^{-5}

The Young's modulus of the rock mass has been reduced to about 50% compared to intact rock, based on empirical estimates that take into account the effect of fractures. A representative value from measurements on intact rock samples has been selected for the coefficient of thermal expansion. For the model inception phase, the initial stress field should be defined using $\sigma_v =$

2360·9.81·D (in Pa), $\sigma_h = 0.50\cdot\sigma_v$), and $\sigma_H = 0.6\cdot\sigma_v$, where D is elevation relative to ground surface (D = z – 500 and tensile stress is positive). σ_H is oriented normal to the tunnel axis.

For those teams using single-continuum approaches, hydraulic properties of the single continuum shall be taken from Table 6.9b, representing the bulk fractured porous rock. The single continuum properties chosen are mostly similar to the matrix properties, acknowledging the fact that the hydrologic situation at Yucca Mountain at ambient state is mostly governed by the matrix properties. (Ambient percolation is very small, so that fractures are dry and non-conductive). For research teams that choose to model this case as a TM calculation using the suggested simplification in Section 6.4.2, hydraulic properties are not needed.

Table 6.9b.   Hydrologic properties of a single continuum

Type	Property	Value
Hydraulic properties of the fracture-matrix continuum	Permeability (m^2)	3.87×10^{-17}
	Porosity (-)	0.13
	van Genuchten's air-entry pressure (kPa)	118.3
	van Genuchten's exponent, m (-)	0.317
	Residual saturation (-)	0.19

6.4.4   Input Data for Phases 2 and 3 (Preliminary and Final Prediction with Uncertainty)

The input data for Phases 2 and 3 are extracted from the wealth of data available on the Yucca Mountain site. The subsections below give a summary of the geological characterization. The research teams may also use the original cited sources to extract and develop input data for their models (see Section 6.4.4.8). The rock properties are given with their uncertainty ranges, such as the standard deviations, as provided in the original sources. The individual research teams should decide how to use and propagate these uncertainties in their model predictions. Additional detailed data and reports can be provided upon request.

6.4.4.1   Intact Rock Thermal and Mechanical Properties

A large number of laboratory tests have been performed to determine intact rock properties of various geological units at Yucca Mountain. Tables 6.10 through 6.12 present thermal and mechanical properties for the Tptpmn unit (corresponding to the TSw2 thermal-mechanical unit). These data have been extracted from the 1997 Site Geotechnical Report (CWRMS M&O 1997).

Table 6.10.   Intact rock thermal and mechanical properties determined from core samples

Parameter	mean±std (range)	Source
Dry bulk density [kg/m^3]	2270±0.08 (1.84-2.42)	CRWMS M&O (1997)
Saturated bulk density [kg/m^3]	2370±0.03 (2.12-2.46)	CRWMS M&O (1997)
Grain Density [kg/m^3]	2550±0.03 (2.50-2.60)	CRWMS M&O (1997)
Thermal Conductivity [W/m-K]	2.29±0.42 (saturated) 1.49±0.44 (dry)	CRWMS M&O (1997)
Porosity [%]	10.99±2.85 (8.0-27.7)	CRWMS M&O (1997)
Un. Comp. Strength [MPa]	187.47±64.92	CRWMS M&O (1997)
Young's Modulus [GPa]	32.93±5.47	CRWMS M&O (1997)
Poisson's ratio [-]	0.21±0.04	CRWMS M&O (1997)
Tensile strength [MPa]	11.56±3.80	CRWMS M&O (1997)

Table 6.11.   Mean coefficient of thermal expansion during heat-up and cool-down measured on core samples (CRWMS M&O 1997)

Temperature range (ºC)	Mean coefficient of thermal expansion (10^{-6}/ºC)	
	Dry	Sat
25-50	6.67±1.20	7.14±0.65
50-75	8.31±0.42	7.47±1.51
75-100	8.87±0.40	7.46±1.21
100-125	9.37±0.55	9.07±2.41
125-150	10.10±0.88	9.98±0.77
150-175	10.96±1.16	11.74±1.28
175-200	12.22±1.50	13.09±1.40
200-225	14.52±2.57	15.47±1.75
225-250	20.79±1.20	19.03±3.09

Table 6.12.   Thermal capacitance measured on core samples (CRWMS M&O 1997)

Temperature (ºC)	Thermal capacitance (ρC) (J/cm^{3}K)
25	1.79±0.11
50	1.88±0.11
75	2.00±0.11
100	2.16±0.11
125	2.32±0.11
150	2.45±0.13
175	2.43±0.18
200	2.40±0.16
225	2.39±0.17
250	2.39±0.19

6.4.4.2   Fracturing

The fracturing in the crystal-poor middle nonlithophysal zone (Tptpmn) is described in the recent Drift Degradation Analysis (2003), based on surveys of exposures in underground research tunnels at Yucca Mountain (the ESF and ECRB tunnels, described in Mongano et al., 1999). Smooth high-angle fractures are typical of the zone, but low-angle, continuous shears and cooling joints are also present. Another feature characteristic of the Tptpmn is the presence of a concentration of vapor-phase partings, subparallel to the dip of the unit. Extensive geotechnical mapping of fracture has been performed in the entire ESF main loop and the ECRB Cross Drift (CRWMS M&O 1998; Mongano et al., 1999). The density of fractures with trace length greater than 1 m is approximately 2 to 4 per meter. Surveys included ull periphery geological mapping and detailed line surveys (consisting of a description of orientation, trace length, small and large scale roughness, and end termination for all fractures with trace length of greater or equal to one meter).

Data from the EFS main loop comprise 4.5 km of the Tptpmn unit. CRWMS M&O (1998) gives a good summary of data from fracture mappings for 500 m sections of the EFS. Also provided are results from fracture mappings in several excavated alcoves. In general, the average fracture spacing from the detailed line survey along the tunnel varies from 0.16 to 0.61 m (CRWMS M&O 1998). There are in general three to four fracture sets in the Tptpmn unit. The three main fracture sets are:

1.   One prominent vertical, southeast-trending
2.   One less prominent vertical, southwest-trending
3.   One less prominent subhorizontal

The dominating fracture set is clearly defined as a southeast-trending fracture set, which represents the preferred direction of almost 50% of all the fractures mapped in the Tptmn unit. Apart from these three fractures sets, another vertical fracture set is sometimes discernable. The highest intensity of fracturing along the detailed line survey is associated with the southeast trending fracture set, ranging from an average true fracture spacing of 0.23 to 1.65 m.   The

average true spacing for the southwest trending fracture set ranges from 0.57 to 2.30 m, whereas the spacing for the subhorizontal fracture set ranges from 0.19 to 1.75 m. In addition, there are randomly oriented fractures that account for about 30% of the mapped fractures in the Tptpmn unit. Figures 6.16 and 6.17 present examples of fracture data for one 500 m interval along the EFS. Four joint sets have been identified in this interval. Figure 6.17 shows that the true average spacing for fractures in the dominating southeast fracture set is 0.78 m in this case.
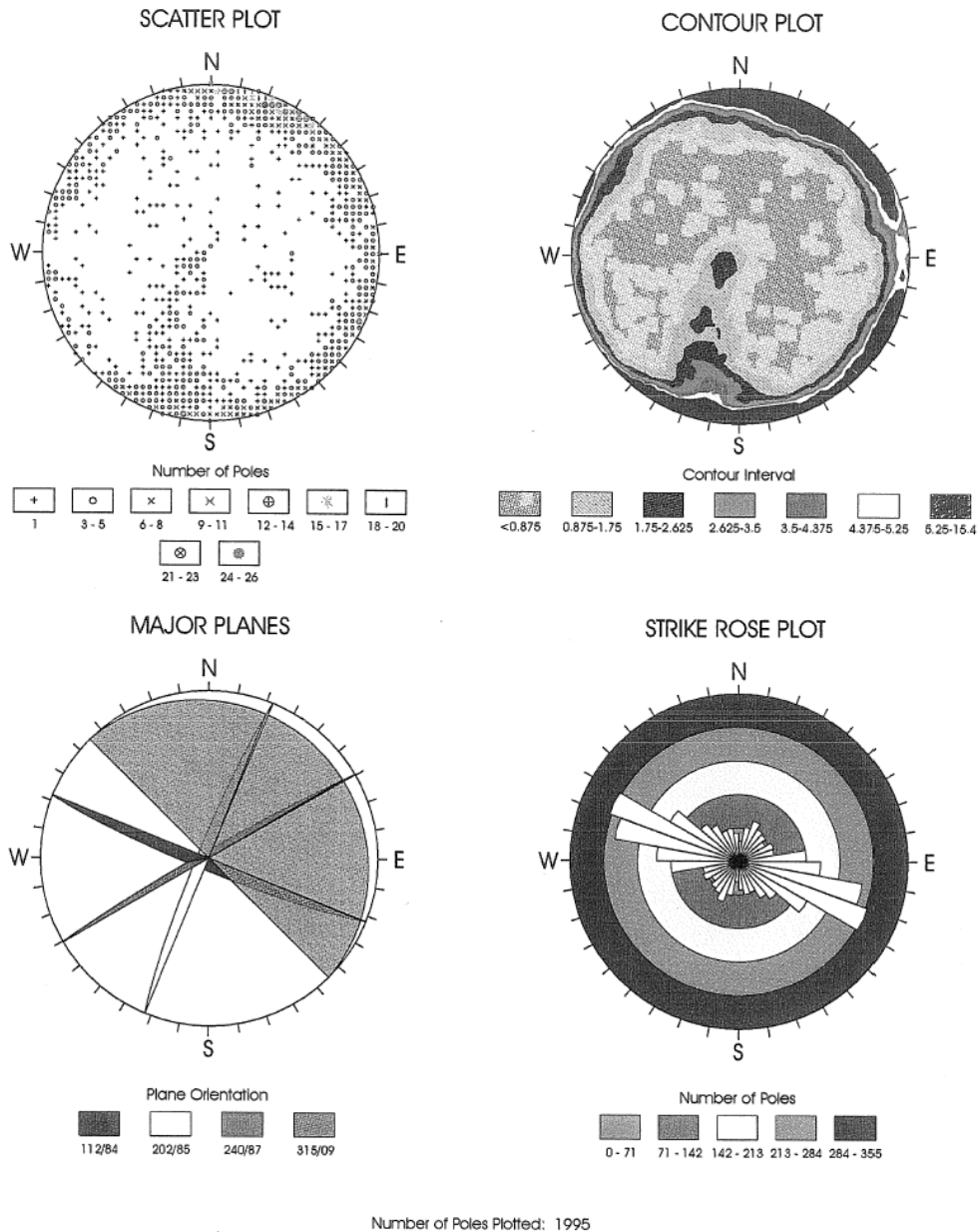
Figure 6.16. Identification of fracture sets in the Tptpmn unit along one 500 m long interval of the EFS (CRWMS M&O 1998)

Figure 6.17. Histogram and cumulative frequency distribution of fracture spacing data for Joint Set 1 of the data presented in Figure 6.16 (CRWMS M&O 1998)

In general, the fractures have relatively short continuous trace length, with ends often terminating either against other fractures or in solid rock, leaving a solid rock "bridge" between joint tracks. The subvertical fractures, in particular, often have curved surfaces with large-amplitude (dozens of centimeters) asperities and wavelengths of meters. These fractures often terminate in solid rock, with discontinuous interconnection to adjacent joint tracks or against other joints. The sub-horizontal vapor-phase partings are relatively continuous structures seen throughout the Tptpmn. These continuous, but anastamosing fractures are filled with a concentration of vapor-phase minerals (primarily tridymite and cristobalite). The surfaces are rough on a small scale and, as a result of the mineral filling, have cohesion (unlike the subvertical fractures).

In the Drift Degradation Analysis (BSC, 2003a) a representative FracMan simulation of the actual fracture network was constructed, based on the detailed line survey and full periphery geological data (for fractures with tracelength larger than 1 meter). This FracMan simulation was done for the purpose of calculating potential block-size for rock fall and its impact on the waste overpack. For the Tptpmn unit, four sets were identified and defined, based on orientation data (Figure 6.18). A good agreement with the actual fracture data and the full periphery geological maps was obtained for the statistical parameter given in Table 6.13. Research teams may use this distribution if they attempt to build a discrete fracture model. However, it should be pointed out that these data are generated with a cut-off length of 1 m, meaning that all fractures with a trace length shorter than 1 m have been neglected.

Figure 6.18. Pole plot of Tptpmn detailed line survey data from ESF main loop and ECRB Cross Drift

Table 6.13. FracMan input parameters for reproducing fracturing in the Tptpmn unit (for fractures with trace length larger than 1 meter)

Fracture set	Set 1	Set 2	Set 3	Random
Model type	Baecher	Baecher	Baecher	Baecher
Orientation (trend/plunge)	030/06	125/02	239/76	060/00
Distribution type	Fisher	Fisher	Fisher	Fisher
k dispersion	70	70	70	05
Size equivalent radius (m)	1.80	1.53	2.09	1.35
Distribution type	Power (3.1)	Power (3.1)	Power (3.1)	Power (3.1)
Termination %	10	5	0	5
Intensity	0.4	0.10	0.05	0.07

In addition to the detailed-line survey, small-scale fracture surveys have been conducted at a few selected locations in the ESF tunnel. Figure 6.19 presents fracture traces mapped in two 6 m panels in the Tptpmn unit. The fracture-trace-length distributions show the typical negative exponential nature, with a concentration in the range of 10 cm to 20 cm trace lengths. Fractures with trace lengths larger than 1 m only account for about 20% of all fractures mapped in these two locations. Thus, the fracture spacings shown in Table 6.13 may account for only 20% of all fractures in the field.
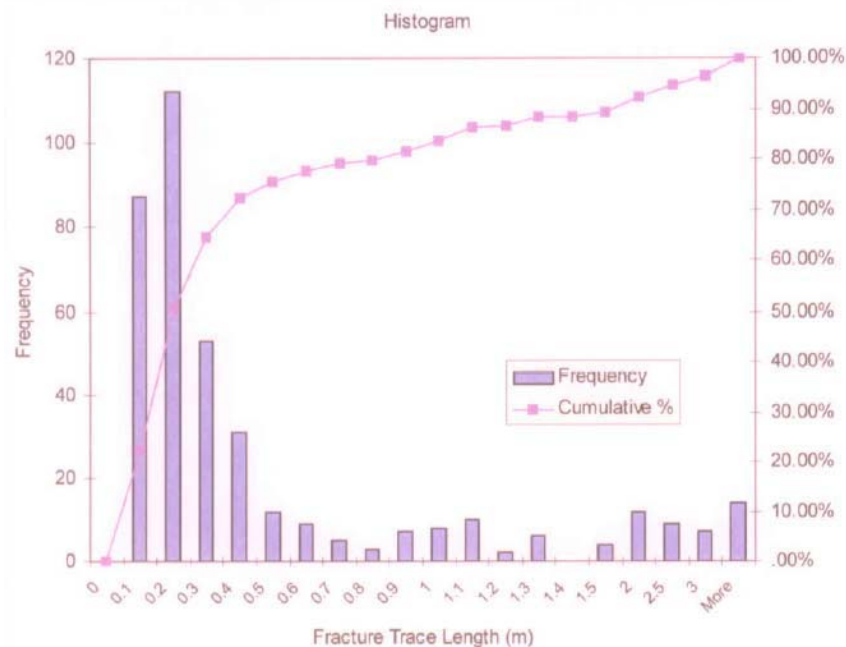
Figure 6.19. Fracture traces from small-scale fracture surveys in the Tptpmn unit

6.4.4.3   Fracture Mechanical Properties

Table 6.14 summarizes the mechanical properties of natural fractures determined by samples from boreholes at Yucca Mountain (Olsson and Brown 1995). In addition, surface topography measurements on fracture surfaces have been made, with measurement techniques and analysis described as described by Brown (1985). These measurements provide, for example, the power spectral-density function of surface profiles and the probability density function for the height of the composite topography. Details on how these functions are computed and their significance to surface roughness characterization are given by Brown (1985). The roughness characteristics of fracture surfaces, derived from the profiles for these rocks, agree qualitatively with the simple mathematical model of Brown (1985), derived from fracture data in many other rock types. Figures 6.20-6.22 show examples of output from one out of 22 fractures tested and reported in Olsson and Brown (1995). The entire report can be provided to the research teams upon request.

Table 6.14.   Fracture mechanical properties determined from laboratory tests

Normal stiffness at 2.5 MPa , (GPa/m)	73.5±38.2	CRWMS M&O (1997)
Cohesion (MPa)	0.86±0.81	CRWMS M&O (1997)
Coefficient of friction (tanϕ)	0.87±0.09	CRWMS M&O (1997)
Peak shear strength (MPa) (for three different tests at each normal stress level)	(1.9, 2.4 , 3.3) at σ_n = 2.5 MPa (5.5, 5.5, 6.6) at σ_n = 5.0 MPa (7.7, 9.0, 12.0) at σ_n = 10.0 MPa (11.9, 14.0, 15.5) at σ_n = 15.0 MPa	CRWMS M&O (1997)
Residual shear strength (MPa) (for three different tests at each normal stress level)	(1.8, 2.3, 2.7) at σ_n = 2.5 MPa (4.5, 4.8, 5.2) at σ_n = 5.0 MPa (7.1, 10.4, 8.6) at σ_n = 10.0 MPa (8.6, 14.0, 10.2) at σ_n = 15.0 MPa	CRWMS M&O (1997)
Dilation angle (degrees) (for three different tests at each normal stress level)	(1.1, 8.5, 13.7.) at σ_n = 2.5 MPa (1.2, 17.3, 15.1) at σ_n = 5.0 MPa (33.4, 18.4, 17.7) at σ_n = 10.0 MPa (10.2, 33.4, 18.4) at σ_n = 15.0 MPa	Olsson and Brown (1995)
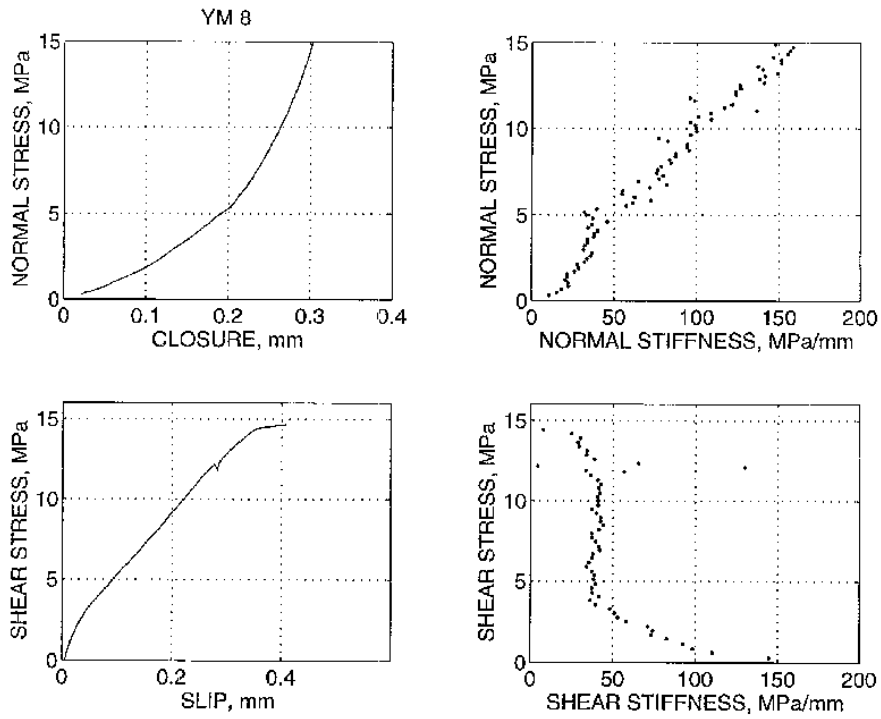
Figure 6.20. Example of shear and normal stiffness data for one sample (from Olsson and Brown, 1995)
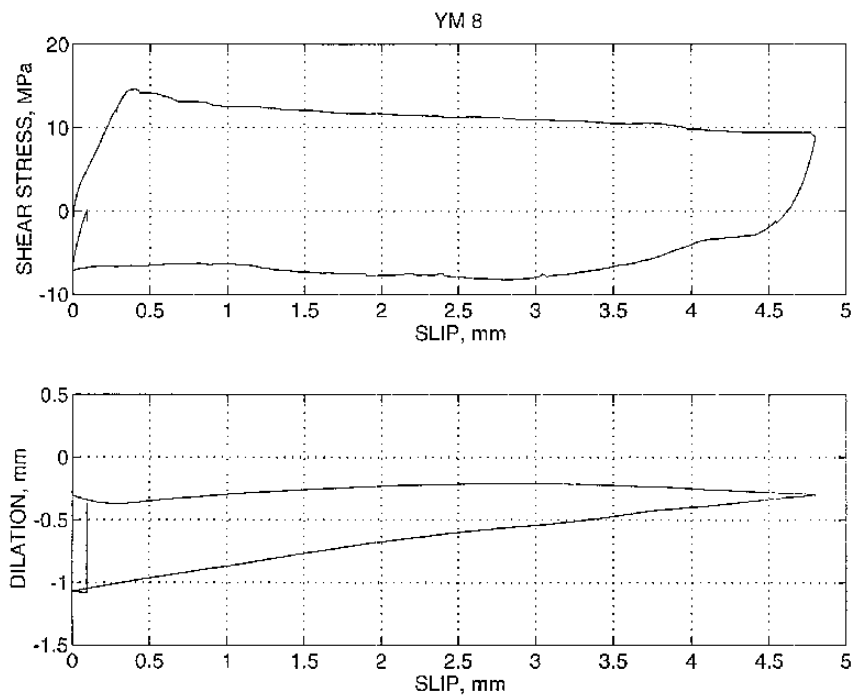
Figure 6.21. Example of shear strength and dilation data for one sample (Olsson and Brown, 1995)

YM8
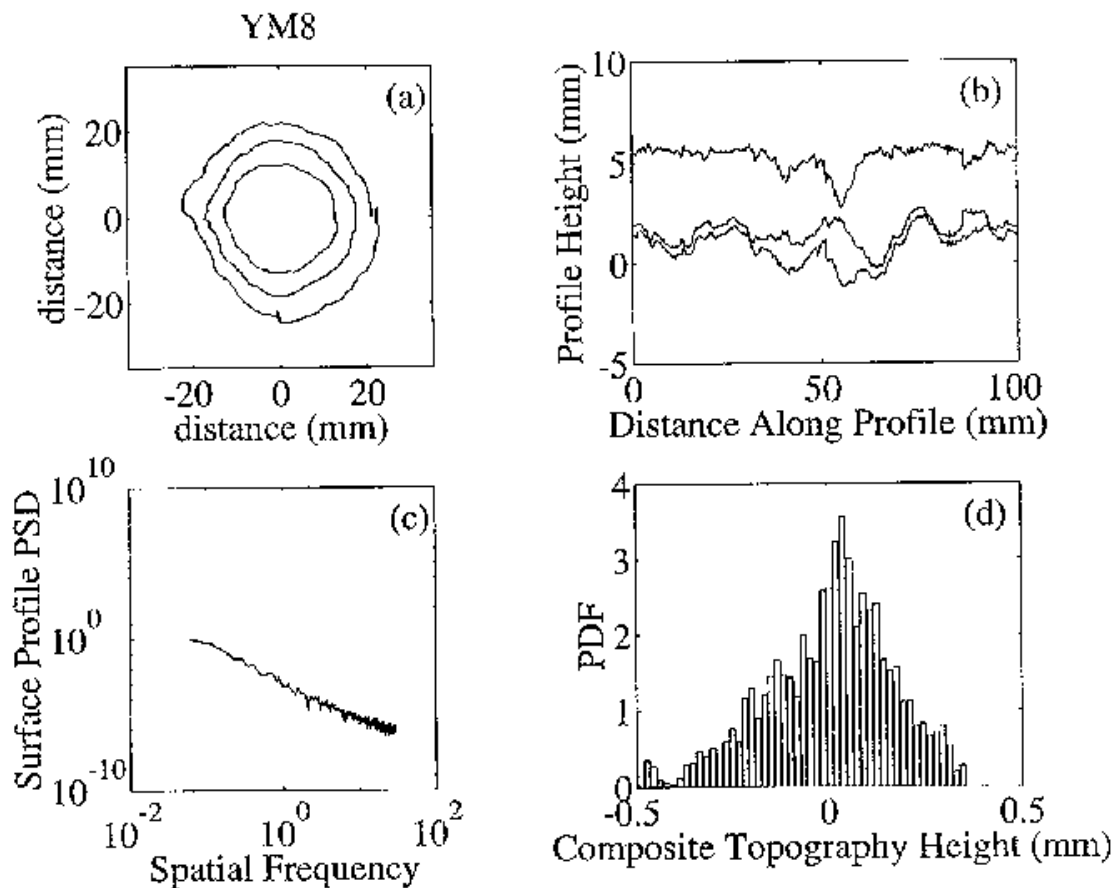
Figure 6.22. Example of profilometer data for one sample (Olsson and Brown, 1995)

6.4.4.4 Rock Mass Hydrogeologic Properties

A key issue for simulating fluid flow in the fractured porous rock at Yucca Mountain is the representation of fracture and matrix flow under multiphase, nonisothermal conditions. Dual-continuum approaches have been sucessfully applied for these purposes. To use dual-continuum models, hydrogeologic properties need to be provided for both fracture and matrix continua.

The hydrological properties for the matrix and fracture systems listed in Table 6.15 have been determined largely by model calibration, in addition to direct measurements. Direct measurements of fracture permeability have been conducted at various scales. Figure 6.23 shows measurements of fracture permeability in the Tptpmn unit through air-injection testing in packed-off borehole sections. The values labeled as NRG-6, NRG-7a, SD-12, and UZ#16 stem from injection tests conducted in vertical boreholes with a packer spacing of about 4 m. Values labeled as SHT&DST are the results of injection tests conducted with a packer spacing of about 5 to 8 m in horizontal boreholes. The four niche entries are results of air-injection tests conducted in small-scale packers with a packer spacing of 0.3 m. In these tests, the permeability at each 0.3 m interval of the boreholes is several orders larger than the matrix permeability. This demonstrates that at least one hydraulic conductive fracture intersects each interval and is connected to a network of hydraulically relevant fractures.
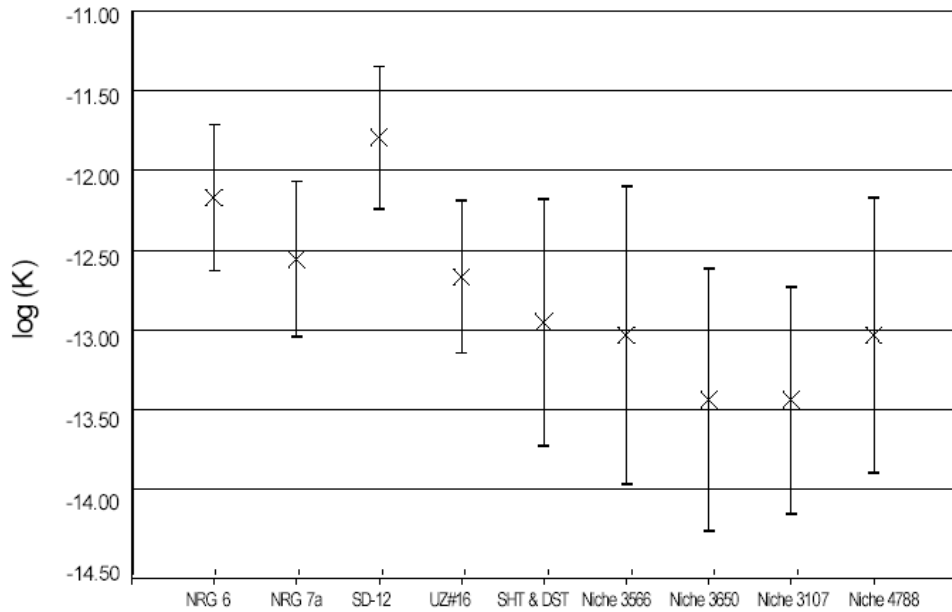
Figure 6.23. Fracture permeability for Tptpmn unit measured by air-injection tests in packed-off borehole sections (BSC 2003b)

Table 6.15.   Fracture and matrix hydrogeologic properties (BSC 2003b)

Type	Property	Value
Hydraulic properties of the fracture continuum	Permeability Log k (m2)	-12.48±0.47
	Porosity (-)	0.0085±0.0025
	van Genuchten's alpha Log α (Pa-1)	-3.89±0.24
	van Genuchten's exponent, m (-)	0.633
	Residual saturation (-)	0.01
	Fracture frequency (m-1)	4.32±3.42
Hydraulic properties of the matrix continuum	Permeability Log k (m2)	-18.75±0.97
	Initial porosity (-)	0.13
	van Genuchten's alpha Log α (Pa-1)	-5.07±0.49
	van Genuchten's exponent, m (-)	0.317
	Residual saturation (-)	0.19

6.4.4.5   Rock Mass Mechanical and Hydromechanical Properties

Equivalent continuum properties of the fractured rock mass at Yucca Mountain have been derived using various empirical methods. Values of each *in situ* generated parameter for the rock mass have been classified into five categories, according to the frequency of occurrence of that parameter. Rock-mass-quality categories one through five correspond to cumulative frequency occurrence of 5%, 20%, 40%, 70%, and 80%, respectively. The five rock-mass quality categories provide a basis for ground support design at different levels of confidence.

The rock-mass mechanical parameters have been characterized using both the Rock-Mass-Quality (Q) and Rock-Mass Rating (RMR) indices. These indices were determined using full peripheral mapping. The Q values determined over the range of rock-mass conditions were more sensitive to joint characteristics than the RMR values; therefore, Q values were used in the assessment of rock-mass parameters. The following rock-mass parameters were assessed: modulus of elasticity, Poisson's ratio, cohesion, friction angle and dilation angle, uniaxial compressive strengths, tensile strength, NGI's rock-mass quality index (Q), and the geological strength index (GSI).

Table 6.16.   Rock mass properties for Tptpmn unit (CRWMS M&O 2000)

Rock mass quality category	1	2	3	4	5
Cumulative frequency	5%	20%	40%	70%	90%
Rock quality, Q	0.47	1.1	1.8	4.3	9.4
GSI	48.5	53.6	57.0	61.2	65.8
Rock Mass Modulus (GPa)	9.16	12.33	14.98	19.08	24.81
Rock Mass UCS (MPa)	12.87	15.82	18.28	22.06	27.34
Cohesion (MPa)	1.94	2.33	2.66	3.17	3.90
Friction Angle (degree)	56.4	57.1	57.5	57.9	58.2
Dilation Angle (degree)	28.2	28.6	28.8	28.9	29.1
Tensile Strength (MPa)	1.17	1.38	1.55	1.83	2.22

Current simulation analyses of the DST (see Section 5) have demonstrated that the strength parameters developed in Table 6.16 result in too small a uniaxial compressive strength for the rock mass. An alternative assessment of the rock-mass properties was therefore conducted for the drift scale test in the Drift Degradation Analysis (BSC, 2003a). The rock-mass properties were calculated using the Hoek-Brown failure criterion (Hoek et al., 2002), which is expressed as:

$$\sigma_1 = \sigma_3 + \sigma_{ci} \left(m_b \frac{\sigma_3}{\sigma_{ci}} + s \right)^a \tag{6.9}$$

where σ_1 and σ_3 are the major and minor effective principal stresses at failure;
        σ_{ci} is the uniaxial compressive strength of the intact material;
        m_b, s, and a are material constants.

This approach uses the geological strength index (GSI) to characterize rock-mass strength (Hoek et al., 2002). To apply Q system data to this approach, the Q system parameters related to stress (i.e., J_w and SRF) should be equal to 1 (Hoek et al., 2002), such that

$$GSI = 9 \ln Q' + 44 \tag{6.10}$$

where

$$Q' = \left(\frac{RQD}{J_n} \right) \times \left(\frac{J_r}{J_a} \right) \tag{6.11}$$

RQD = rock quality designation
J_n = joint set number
J_r = joint roughness number
J_a = joint alteration number.

The material constants m_b, s, and a are given by

$$m_b = m_i \exp\left(\frac{GSI - 100}{28 - 14D}\right) \tag{6.12}$$

$$s = \exp\left(\frac{GSI - 100}{9 - 3D}\right) \tag{6.13}$$

$$a = \frac{1}{2} + \frac{1}{6}\left(e^{-GSI/15} - e^{-20/3}\right) \tag{6.14}$$

where m_i is the value of m_b for intact rock and is determined based on laboratory triaxial test data. D is a factor that depends on the degree of disturbance to which the rock mass has been subjected by blast damage and stress relaxation. D is 0 for mechanically excavated tunnels.

Following the Hoek-Brown approach, the rock mass modulus of deformation is given by

$$E_m = \left(1 - \frac{D}{2}\right) \cdot 10^{(GSI-10)/40} \quad \text{for } \sigma_{ci} > 100 \text{ MPa} \tag{6.15}$$

$$E_m = \left(1 - \frac{D}{2}\right)\sqrt{\frac{\sigma_{ci}}{100}} \cdot 10^{(GSI-10)/40} \quad \text{for } \sigma_{ci} < 100 \text{ MPa} \tag{6.16}$$

where E_m is the rock mass modulus of deformation in GPa. The global rock mass strength is determined as

$$\sigma_{cm} = \sigma_{ci} \cdot \frac{\left(m_b + 4s - a(m_b - 8s)\right)\left(m_b/4 + s\right)^{a-1}}{2(1 + a)(2 + a)} \tag{6.17}$$

A mean intact rock strength of 168 MPa was calculated from core sample tests. The value of m_i was calculated by fitting triaxial test data to Equation 6.2 expressed in terms of intact rock, so that the material constants are given by (Hoek et al., 2002):

$m_b = m_I$
$s = 1$
$a = 0.5$

Rock mass properties for the DST resulting from the Hoek-Brown approach are provided in Table 6.17. The rock-mass parameters were determined in eleven 5 m intervals along the heated

drift of the DST. The table shows average values and ranges of values obtained for the eleven 5-meter intervals. Note that the range of GSI values in Table 6.16, which represents results from the entire ESF, is similar to the range of GSI values in Table 6.17, representing the rock at the DST, and that the range of rock deformation modulus is similar in the two tables. However, the rock mass compressive strength is higher when using the Hoek-Brown approach (Table 6.17). These higher values appear more accurate, based on current THM simulations of the DST and recent observations of small-scale rock failure at the crown of the heated drift. Simulations of the DST indicate that a small-scale failure in the crown of the drift can occur when the maximum compressive stress reaches about 60 MPa (BSC 2003a).

The most difficult and important task might be to derive constitutive relationships for mechanically induced permeability changes in the fractured rock mass. Such a relationship was developed and used for simulations of the drift scale test during for DECOVALEX III, Task 2. Research team may consult the upcoming DECOVALEX III Task 2 report (Datta et al., 2004) when developing their models. The uncertainties associated with the derived properties needs to be evaluated and propagated in the model simulations for the final predictions.

Table 6.17.   Hoek-Brown rock mass parameters for the Tptpmn unit at the drift scale test (extracted from BSC 2003a).

Parameter	Value Average (range)
Mean intact uniaxial compressive strength, σ_{ci} (MPA)	168
Intact material constant, m_I	23.8
Q-index, Q'	7.9 (2.9-12.8)
Geological Strength Index, GSI	61.4 (53.5-67.0)
Rock mass material constant, m_b	6.1 (4.5-7.3)
Rock mass material constant, s	0.017 (0.01-0.03)
Rock mass material constant, a	0.5
Global Rock Mass Compressive Strength	56.5 (47.8-63.2)
Rock mass modulus of deformation, E_m	20.0 (12.2-26.6)

6.4.4.6   In Situ Stress Field

Reasonable estimates of the *in situ* stresses at the repository horizon are given in the 1997 Yucca Mountain Site Geotechnical Report (Table 6.18). The direction of the maximum principal stress is vertical, owing to the lithostatic load. Horizontal stresses vary between 3.5 MPa and 4.2 MPa, although the range may be as wide as 2.1 to 7 MPa. For Task D_THM2, a vertical stress according to the weight of the overburden rock should be assumed. Horizontal stresses and their uncertainty ranges should be calculated from the vertical stress information given in Table 6.18.

Table 6.18.   Summary of *in situ* stress at repository horizon (CRWMS M&O 1997)

Parameter	Average Value	Range of Values
Minimum Horizontal Stress/Vertical Stress Ratio	0.5	0.3-0.8
Maximum Horizontal Stress/Vertical Stress Ratio	0.6	0.3-1.0
Bearing of Minimum horizontal stress	N57°W	N57°W-N65°W
Bearing of Maximum Horizontal Stress	N32°E	N25°E-N40°E

6.4.4.7   Orientation of Emplacement Drift Relative to Discontinuity System

The emplacement drifts for the proposed Yucca Mountain repository are oriented at N72°E, which is approximately normal to the strike of the dominating fracture system.

6.4.4.8   References for Task D_THM2

Table 6.19 lists several references for Task D_THM2. Most of these references can be provided to the individual research teams upon request. For example, the report by Olson and Brown (1995) includes fracture data for all 22 samples, should a research team find this useful. Reports with more details on fracturing can also be provided to research teams that want to develop discrete fracture network models.

Table 6.19.   List of reference cited for Task_D_THM2

Reference	Comment
BSC (Bechtel SAIC Company) 2003a. *Drift Degradation Analysis*. ANL-EBS-MD-000027 REV 02. Las Vegas, Nevada: Bechtel SAIC Company.	Provides information on fracturing and rock mass properties including statistical model of fracturing.
BSC (Bechtel SAIC Company) 2003b. *Calibrated Properties Model*. MDL-NBS-HS-000003 REV 01. Las Vegas, Nevada: Bechtel SAIC Company. ACC: DOC.20030219.0001.	Provides hydrological properties of fractured and matrix continua.
CRWMS M&O (Civilian Radioactive Waste Management System Management and Operating Contractor) 2000. *Statistical Analysis of Empirical Rock Properties by Lithographic Units*. CAL-GCS-GE-000001 Revc 00. Las Vegas, Nevada.	Provides empirically developed rock mass properties with statistical distribution.
CRWMS M&O (Civilian Radioactive Waste Management System Management and Operating Contractor) 1997. *Yucca Mountain Site Geotechnical Report*. B00000000-01717-5705-00043 REV 01. Two volumes. Las Vegas, Nevada.	Provides most of the thermal mechanical data for Task_D_THM2.
Damjanac B., Brandshaug T.,Carranza-Torres C, Detournay C. and Perrochet P. (2000). An evaluation of local thermo-mechanical effects on seepage into waste disposal rooms at Yucca Mountain. Itasca Consulting Group Inc November 2000.	Report shows how to simplify model analysis for modeling of boiling when using a thermal conduction model.
Datta et al. (2004). DECOVALEX III, Task 2, Final Report. (SKI report expected during 2004).	Information on modeling approaches and model results for modeling of the drift scale test during DECOVALEX III.
Hoek E., Carranza-Torres C. and Corkum B., (2002). Hoek-Brown Failure Criterion – 2002 Edition 5th North American Rock Mechanics Symposium and 17th Tunnelling Association of Canada Conference: NARMS-TAC 2002, July 7-10 University of Toronto, Toronto, Ontario, Canada.	Reference for deriving rock mass properties using the Hoek-Brown failure criterion.
Mongano G.S., Singleton W.L., Moyer T.C., Beason S.C., Eatman G.L.W. Albin A.L. and Lung R.C. (1999) Geology of the ECRB Cross Drift – Exploratory Studies Facility, Yucca Mountain Project, Yucca Mountain, Nevada. Denver Colorado U.S. Geological Survey.	Provides information on fracturing at the Yucca Mountain to be considered in Task_D_THM2.
CRWMS M&O (1998). G*eology of the Exploratory Studies Facility Topopah Spring Loop*. BAB000000-01717-0200-00002 REV 01. Las Vegas, Nevada	Provides information on fracturing at the Yucca Mountain to be considered in Task_D_THM2.
Olsson W.A. and Brown S. (1995). *Mechanical properties of fractures from drill holes UE25-NRG-4, USW-NRG-6, USW-NRG-7, and USW-SD-9 at Yucca Mountain, Nevada*. Sandia National Laboratories Technical Report, Sand 95-1736. Albuquerque New Mexico, Sandia National Laboratories	Results of laboratory test on single fractures and surface roughness information.
Brown S.R. (1985) Simple mathematical model of a rough fracture. J. Geophys. Res. 100, 5941–5952.	Describes techniques for topography measurements on fracture surfaces and theoretical analysis of roughness data

6.5   OUTPUT SPECIFICATIONS

The research teams are requested to provide simulation outputs at the specified points, lines, and regions shown in Figure 6.1. These outputs have been specified to ensure easy comparison of model results between different research teams. It is important that all teams follow this guidance. Figure 6.1 displays more points than are currently used. However, output for these extra points may be requested during the course of Task D_THM, and more points and lines may be added based on suggestions at future DECOVALEX workshops or task force meetings.

A few points are assigned for monitoring the evolution of measurable parameters. These are parameters that can be monitored at a real site for performance confirmation. Outputs will be collected along two lines (profiles): x-profile (along z = 0) and z-profile (along x = 0). The advantage of collecting data along lines is that results from discrete and continuum models can be readily compared. In addition, two areas have been assigned for contouring and possible statistical evaluation of permanent changes. The Near Drift Study Area is designated for more detailed studies of permanent changes adjacent to the drift, including the excavation-disturbed zone. The Far Field Study Area is designated for studies of potential permanent changes of the fractured rock outside the excavation disturbed zone.

A detailed output definition is given in Tables 6.20 - 6.23 for Modeling Phases 1, 2, and 3. At this time, the outputs for Phase 1 (model inception) are completely defined. The output specification for Phases 2 and 3 is preliminary and may be changed in the future, based on the results of the model inception phase and depending on which modeling approaches are used by the different research teams. However, the preliminary output definition for Phases 2 and 3 should be a guide for the research teams in selecting and developing their models, such that the output requirements can be met.

Table 6.20.   Output specification for time evolution at points for Phases 1, 2, and 3

Parameter	Specification	Comment	Illustration of expected output
Temperature	T at Point V1, V2 and V6	Shows the evolution of temperature at canister, rock surface and in the rock mass at the level of the repository.	
Pressure	P at Points V3 and H6	Shows the evolution of fluid pressure in the rock mass.	
Stress in back-fill (only Task D_THM1)	σ_z (total stress) at Points V1 and V2	Total stress in the bentonite normal to the canister surface and rock surface. This total stress is the sum of the effective stress produced by the bentonite swelling pressure and the water pressure.	
Stress in rock	σ_x in points V3 and H6	The maximum compressive stress in the entire model is expected to be the horizontal stress in points V3 during the heating. The horizontal stress at H6 represents the general increase in horizontal thermal stress at the repository level.	
Displacement	u_z in points V3, V6 and V7	Vertical displacement at drift wall, in rock away from the drift and at the groundsurface. The relative displacement between V3 and V6 may be calculated from this output and the displacement on the groundsurface may be important for performance confirmation.	
Saturation in bentonite (Task D_THM1 only)	S_l at V1	Evolution of liquid saturation near the canister. This will show when the buffer gets fully saturated.	
Saturation in rock	S_l at V3	Evolution of liquid saturation just above the drift. This will show when the dry-out zone disappears (fully re-wetted conditions) at the drift wall.	
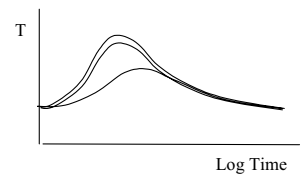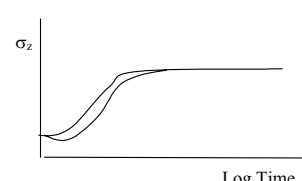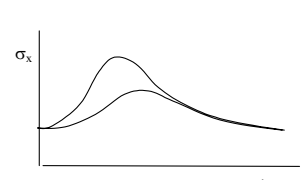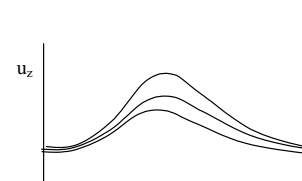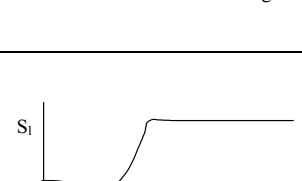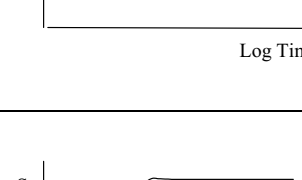
Table 6.21.   Output specification for output along lines for Phases 1, 2, and 3

Parameter	Specification	Comment	Illustration of expected output
Temperature	T along x-profile and z-profile (at selected times, e.g., 1, 10, 100, 1000, 10000, 100000 years)	Will shows temperature profile and potential boundary effects	
Stress	σ_x and σ_z along x-profile and z-profile (at selected times)	Shows horizontal and vertical distribution of stress changes	
Displacement	u_z along z-profile (at selected times)	Shows accumulated vertical displacement contributing to surface deformations	
Saturation	S_l along x-profile and z-profile (at selected times)	Shows drying/wetting profile in bentonite (Task D_THM1) and the extent of dry-out zone in the rock (Task D_THM2)	 (Illustration shows example of S_l along x-profile for Task D_THM2 illustrated)
Vertical water flux	Q_z (vertical flux) across x-profile (at selected times)	The total mass flux of liquid water (kg/second) across 0.5 meter long bins (intervals) along the x-profile. The total mass flux rather than velocity is chosen to be facilitate comparison of discrete fracture and continuum approach.	 (Illustration shows this output for a heterogeneous continuum)

Table 6.21.   Output of permeability changes along lines for Phases 2 and 3 (continued)

Parameter	Specification	Comment	Illustration of expected output
Transmissivity (Permeability)	Vertical transmissivity across x-profile (at selected times, e.g., 1, 10, 100, 1000, 10000, 100000 years)	Shows how vertical transmissivity changes during the entire heating cycle and may reveal permanent changes in transmissivity at 10,000 years. In a continuum model with several elements over a 0.5 meter bin the arithmetic mean of the should be calculated for the 0.5 meter bin. For a discrete fracture model, the arithmetic mean of fracture transmissitivities of fractures crossing the bin should be calculated. Discrete fracture model Continuum model 	 (Illustration shows how T_z may change as a results of increased thermal stress during the heating for a heterogeneous continuum or discrete fracture model)
	Vertical transmissivity along z-profile (at selected times)	Shows the changes of vertical transmissivity over the entire vertical length of the model. Mean transmissivity taken over L_x may be used in this case.	
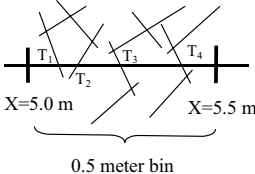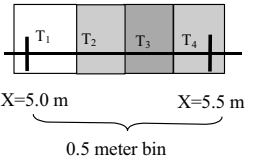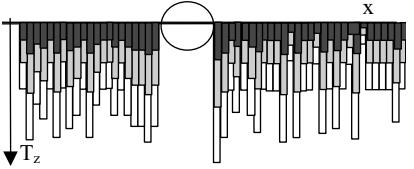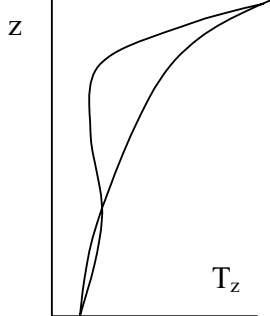
Table 6.22.   Output specification within near drift and far field study areas for Phases 2 and 3

Parameter	Specification	Comment	Illustration of expected output
Stress	σ_x, σ_x, σ_{max}, σ_{min} on the scale of the near drift study area and far field study area (at selected times, e.g., 1, 10, 100, 1000, 10000, 100000 years)	Contour will show the stress field and areas where with the highest potential for mechanically induced changes	Data should be supplied to the task force lead (x, z, σ_x, σ_x, σ_{max}, σ_{min}) who will make this plots for comparison between different teams Near drift study area Far field study area
Parameter showing inelastic response	Inelastic zone on the scale of the near drift study area and far field study area (at selected times)	Which parameter is plotted here depends on the modeling approach. A specific parameter for comparison between different approaches may be defined later.	 Near drift study area Far field study Inelastic zone
Permeability	Permeability changes on the scale of the near drift study area and far field study area (at selected times)	The plot should indicate how much permeability has changed compared with its initial value.	 Near drift study area Far field study k/k_i
Flux Vectors	Flux changes in the far-field (at selected times)	Flux vectors will show the changes in the flow field as a result of THM property changes.	X,Z, v
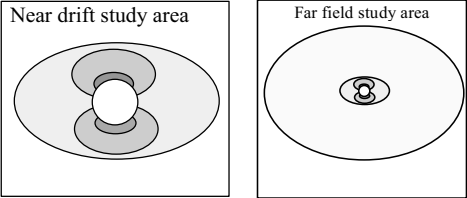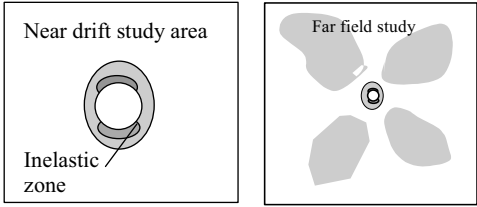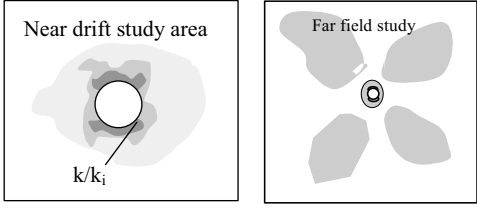
Table 6.23.   Outputs in points and along lines with uncertainty range for Phase 3

Parameter	Specification	Comment	Illustration of expected output
All parameters defined in Tables 6.20 through 6.22	Predictions at points and along lines with error bar (at selected times)	It is up to the research teams to decide how they will present uncertainties (e.g. standard deviation or upper and lower limit).	Illustration shows example of prediction of stress evolution in a point and transmissivity along z-profile. σ_x Upper Mean Lower Log Time z Mean T_z
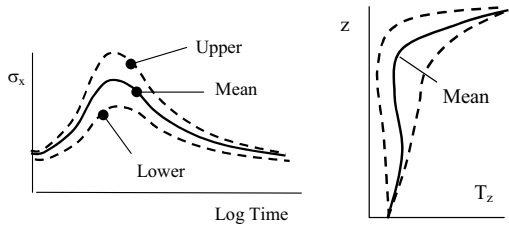
INTENTIONALLY LEFT BLANK

7.   DETAILED DESCRIPTION OF D_THC

In this task, research teams will conduct THC modeling analyses of the long-term coupled THC processes in two generic repositories, as presented in Section 6 for Task D_THM. Participating research teams will model the THC processes in the fractured rock close to a representative emplacement tunnel as a function of time, and will predict the changes in water and gas chemistry, mineralogy, and hydrological properties. The impact on near-field flow processes (see details in Section 6) owing to THM processes will be neglected in Task D_THC. Two subtasks analyze the coupled THC processes in two generic repositories as follows:

- Task D_THC1: Generic repository is located in saturated crystalline rock, where emplacement tunnels are backfilled with buffer material (FEBEX type).
- Task D_THC2: Generic repository located in unsaturated volcanic rock, with emplacement in open gas-filled tunnels (Yucca Mountain type).

The predictive THC simulations can be conducted using various modeling techniques, for example discrete fracture models or continuum models. Model predictions should include the results of THC-induced changes to water and gas chemistry, mineralogy, hydrological properties, flow fields, and an evaluation of the uncertainties related to these predictions. This could involve systematic sensitivity studies, resulting in a distribution of possible results or, at a minimum, estimation of potential upper and lower limits of results.

The description of Task D_THC1 is based on various sources. The thermal-hydrological properties and their origin are identical to those defined in D_THM1 in Section 6.3. The chemical properties of the bentonite buffer and the host rock are taken from Aspö and from the Japanese program. Properties of the bentonite buffer material are based on a sample investigated by the Japanese program. As discussed in Section 6 and further in this section, the input data for Task D_THC2 are entirely derived from the Yucca Mountain site in Nevada and the rock units surrounding the Yucca Mountain Drift Scale Test (DST), which were used in DECOVALEX III, Task 2. A complete set of geochemical data, rock properties, and *in situ* conditions with uncertainty ranges will be presented to the research teams, upon which to build their models for Task D_THC. In addition, the research teams should consider new results from the ongoing *in situ* experiments at FEBEX and DST for confidence building in their model predictions. These will be provided at later project stages once they become available.

7.1   MODEL GEOMETRY

The model geometries are identical to those discussed in Section 6.1 for the THM analyses.

7.2   TASK D_THC MODELING PHASES

The methodology for Task D_THC is conducted in three phases:

    Phase 1. Model Inception (conceptual model development, model set-up, model
                simulations for simplified conditions)
    Phase 2. Model predictions for more complex conditions and sensitivity analysis
    Phase 3. Final model predictions with evaluation of uncertainties.

The purpose of the Model Inception Phase (Phase 1) is for the research teams to familiarize themselves with the conceptual model and problem set-up by performing one simulation in which all the properties are provided for a limited set of mineral, aqueous, and gaseous species. The results of the research teams will be compared at the end of this phase to assure that all teams are starting the problem from a common basis. The comparison will focus on the evolution of temperature, gas composition, water composition, and mineral precipitation/dissolution (in fractures, matrix, and the bentonite) for a simplified geochemical system. When research teams are satisfied with their analysis and their results agree with other research teams, they should go on to the next phase.

In Phase 2, a more complete geochemical system will be considered. Also, the research teams focus on predicting permanent changes caused by mineral dissolution/precipitation concomitant with the evolution of water and gas chemistry. Using the available site data and developed data (e.g., mineral dissolution/precipitation-porosity-permeability relationships), the research teams should conduct an initial parameter study. The purpose of this study is twofold, as follows:

(1) To demonstrate how the model is able to predict permanent changes in chemical (gas, water, and mineral) and hydrological properties
(2) To find conditions (e.g., initial mineralogy, fracture aperture, water chemistry, flow rates) at which permanent changes are possible

The research teams should then predict coupled THC responses and potential permanent changes (if any) for one realistic realization. This should be conducted with whatever modeling approach the respective research team has developed. It may be a continuum model using homogenous properties or a heterogeneous stochastic continuum model (Figure 6.2b and 6.2d). It may also be a discrete fracture model using fracture sets with regular fracture spacing or even stochastically generated fracture networks (Figure 6.2a and 6.2c). At the end of this phase, the output results from the different research teams will be compared. In particular, the evolution of chemistry and permeability changes and their impact on the flow field will be studied. When research teams are satisfied with their preliminary model prediction, they should go on to the next phase to obtain the final prediction results, including uncertainty analysis.

In Phase 3, the research teams are asked to make their final prediction, including estimation of the resulting uncertainties. Examples of uncertainties include:

(1) Uncertainties associated with parameters (e.g., thermodynamic and kinetic data, reactive surface areas)
(2) Uncertainties associated with model conceptualizations (mineral representations – ideal endmembers vs. solid solutions, mineral textures, equilibrium vs. kinetic reactions, distributions of mineral precipitates, etc.)

7.3   TASK D_THC1

This section gives specific definitions for Task D_THC1, representing a bentonite-filled repository in a saturated, sparsely fractured, granitic rock mass. More specific aspects of the modeling phases introduced in Section 7.2 involved in this task are as follows:

1. **Phase 1:** THC model of bentonite enclosed on granite. Mineral-water reactions considered but no cation exchange and sorption. Simplified model of granite mineralogy, bentonite mineralogy treated. Water chemistry is initially of dilute meteoric origin. Initially run without thermal loading, followed by thermal loading. Investigators will choose the types of mineral-water reactions to consider (equilibrium and/or kinetic). No swelling of the bentonite is treated, and no permeability and flow field changes owing to mineral precipitation/dissolution are considered.

2. **Phase 2:** THC model of bentonite enclosed on granite. Mineral-water reactions treated, including cation exchange and sorption, if deemed necessary by the investigators. Because the purpose is to evaluate major chemical changes that can lead to hydrological property changes, a more complete mineral assemblage for the granitic host rock and the bentonite can be assessed in this phase. Investigators will choose the mineral assemblage, the necessary reaction-transport processes, in addition to the choices made for the physical model description (e.g, continuum vs. discrete fracture model). Water chemistry of dilute meteoric origin and a comparison of results using the deep brine composition. Thermal loading considered with swelling/contraction of bentonite buffer. Porosity and permeability changes that result from precipitation/dissolution are considered.

3. **Phase 3:** Uncertainties will be addressed through evaluation of various potential processes, such as mixing of brine and dilute meteoric water, changes to parameter values, potential effects of mechanical effects on THC processes.

Details and references regarding the initial geochemical conditions are discussed below.

7.3.1   Specific Model Geometry and Modeling Sequence

The geometry for Task D_THC1 is the same as that presented in Table 6.1, Section 6.3.1 for D_THM1. Thermal power inputs are provided in Figure 6.4. Hydrological and thermal initial and boundary conditions are the same as those for D_THM1, Figure 6.5. Hydrological and thermal rock properties are identical to those chosen for D_THM1, Tables 6.2a, 6.2b, an d the description in Section 6.3.3. The modeling sequence for D_THC1 is similar to that described in Section 6.3.1, Figure 6.5. The specific THC modeling sequence is as follows:

1. Obtain steady-state flow and temperature conditions   (i.e., ambient geothermal gradient/boundary temperatures) for rock mass (excluding bentonite).

2. Use output of steady-state simulation as input to transport simulation, to obtain steady-state aqueous and gaseous species distributions for the rock mass. Use this distribution as input to ambient temperature THC simulation (excluding thermal loading), and excluding bentonite. This reference case that can be used as a chemical steady-state initial condition to thermal loading case.

3. TH simulation, including thermal loading in bentonite-drift, without swelling effects. THC simulation, including thermal loading in bentonite-filled drift, without swelling effects, and without hydrological property changes. THC simulation, including thermal loading in bentonite-filled drift, without swelling effects, and including hydrological property changes. THC simulation, including thermal loading in bentonite-filled drift, swelling effects, and hydrological property changes.

Sequence (2) and (3) should be repeated for different levels of complexity of chemical input parameters and processes. Results can then be directly compared, and used as part of the evaluation of uncertainties in Phase 3.

7.3.2   Suggestions for Potential Model Simplifications

The model simplifications suggested in 6.3.2 are also appropriate for D_THC1 simulations. Assumption of a fully saturated bentonite buffer, and a fully developed swelling pressure, with a prescribed fluid chemistry would simplify the initial transient phase that may be more difficult to predict, both from the consideration of transport and reaction.

7.3.3   Input Data for Phase 1 (Model Inception)

7.3.3.1 Initial Mineralogical Data for Granitic Host Rock

Mineralogical abundances for the granitic host rock are based on data from the Smaland granite (Rhen et al. 1997) and listed in Table 7.1. Minor phases will be neglected in Phase 1, and mineralogical data should be renormalized to 100%. For Phase 2 and 3, minor phases should be included, with abundances based on published data, which are important to specific aspects of the chemistry of the water or mineral reactions specific to fractures versus those in the rock matrix.

Table 7.1   Mineralogical Abundances in the Smaland Granite (Rhen et al., 1997)

Mineral	Abundance (weight fraction)
Quartz	0.2756
K-Feldspar	0.2724
Plagioclase	0.3964
Annite	0.0489
Phlogopite	0.0067

Reactive surfaces areas for the minerals specific to this rock will require some assumptions and testing using more simple reactive models (1-D steady-state flow) to obtain chemical characteristics consistent with the measured ambient water chemistry.

7.3.3.2 Initial Mineralogical Data for the Bentonite

Bentonite mineralogical compositions can differ greatly, thus affecting their chemical and physical properties. For this problem, the Kunigel VI Na-bentonite will be used, with specifics given below in Table 7.2 (Table 1, Ochs et al., 2004). In order to simplify the problem in Phase

1, minor abundances of pyrite and zeolites can be neglected. Both cation exchange and mineral-water reactions must be considered for the bentonite-water reactions. However, for Phase 1, only mineral-water dissolution/precipitation reactions should be considered. Because of the presence of carbonate minerals and feldspars, in addition to quartz, this bentonite should show stronger effects of mineral dissolution/precipitation. In Phases 2 and 3, the effects of ion exchange and sorption will be added. Volume changes, and subsequent permeability/flow field changes, owing to clay swelling and mineral dissolution/precipitation are neglected in Phase 1, but should be included in Phase 2 and 3.

Table 7.2   Mineralogical Abundances in the Kunigel-VI Bentonite (Ochs et al., 2004)

Mineral	Abundance (weight %)
Na-montmorillonite	47.5
Quartz	33.5
K-Feldspar	4.1
Calcite	2.35
Dolomite	2.9
Pyrite	0.6

7.3.3.3 Initial Water Chemistry

Initial water chemistry for Phase 1 will be based on water from the Litorina Sea in Sweden. Laaksoharju (2002) described three cases in which water of different origins (shallow, deep, mixed) flowing toward the tunnel resulted in either calcite precipitation (shallow and mixed) in fractures or none (deep). For Phase 1, we consider a shallow water as an initial composition in the granite. The initial water chemistry in the granite is summarized in Table 7.3.

Table 7.3   Initial Water Chemistry in Granite

Litorina Sea	pH=7.7	
	Mg/liter	Mol/kg H2O
Cl	6500	1.833E-01
Na	3674	1.598E-01
K	134	3.427E-03
Ca	151	3.767E-03
Mg	448	1.843E-02
HCO3	93	1.524E-03
SO4	890	9.265E-03
	Total	4.110E-01
	Charge Balance (%)	1.032E+00

The initial water chemistry of the bentonite is summarized in Table 7.4.

Table 7.4   Initial Water Chemistry in Bentonite

Bentonite	pH=8.4
	Mol/kg H2O
Cl	1.500E-05
Na	3.600E-03
K	6.200E-05
Ca	1.100E-04
Mg	5.500E-05
HCO3	3.500E-03
SO4	1.100E-04
SiO2	3.400E-04
Total	7.727E-03
Charge Balance (%)	3.326E+00

7.3.3.4 Transport Properties

Flow of fluid through the fractured granite will be treated as part of the THM model development. To consider tranport through the bentonite, chemical diffusion must be considered. Various papers have been dedicated to this (e.g., Ichikawa et al. 2004). For Phase 1, a simple Fickian tracer diffusion model will be employed using a single diffusion coefficient. For Phases 2 and 3, more complex chemical diffusion models should be employed with a comparison of results.

7.3.4   Input Data for Phase 2 and 3 (Preliminary and Final Predictions with Uncertainties)

Initial mineral abundances, water chemistry, and equilibrium and kinetic for the bentonite and surrounding granitic rock will utilize data described in Phase 1 and references described in Table 7.5. Phases 2 and 3 will consider several more complex geochemical processes, including ion exchange, sorption, and redox processes involving pyrite in the bentonite. In these phases, the water composition will also include a deep brine (Phase 2) in addition to the dilute water of meteoric origin, and in Phase 3, mixing of the two waters. Under the thermal regime, including chemical reactions with bentonite, transport between the fractured granite, and mixing of different water compositions, a much more complex spatial and temporal pattern of water-rock reactions can be generated.

A main focus in Phases 2 and 3 is to assess the potential for THC related permeability changes in the host rock (primarily in the fractures) and their effect on the flow field. These can be modeled using various methods, as discussed in Section 7.4.4.3. Various porous media models may be employed for treating permeability changes in the bentonite, as discussed widely in the literature. It will be up to the investigators to choose the models to describe coupling between mineralogical/porosity changes and permeability changes.

Table 7.5   List of references cited for Task D_THC1

Reference	Comment
Ichikawa Y., Kawamura K., Fujii N., and Kitayama K., 2004., *Microstructure and micro/macrodiffusion behavior of tritium in bentonite.* Applied Clay Science, Volume 26, 75-90.	Model for diffusion in bentonite
Laaksoharju, M., Aspö Hard Rock Laboratory. *Update of the hydrogeochemical model 2002.* GeoMod GW Report. October 2003.	Water chemistry at Aspö
Ochs M., Lothenbach B., Shibata M., and Yui M., *Thermodynamic modeling and sensitivity analysis of porewater chemistry in compacted bentonite,* Physics and Chemistry of the Earth, Parts A/B/C, Volume 29, Issue 1, 2004, Pages 129-136.	Kunigel VI Na-bentonite mineralogical composition
Rhen I., Backborn G., Gustafson G., Stanfors R., and Wikberg P., ASPÖ HRL – Geoscientific evaluation 1997/2. *Results from pre-investigations and detailed site characterization. Summary report. SKB Technical Report 97-03.* Swedish Nuclear Fuel and Waste Management Company, Stockholm, Sweden.	Mineralogical data for granitic rocks at Aspö

7.3.5   Uncertainty Analysis For Phase 3

Many conceptual model choices are available in Phase 2 (e.g., equilibrium versus kinetic mineral-water reactions, calculation of reactive surface areas in unsaturated systems, permeability-mineral precipitation relations, etc.). The analysis of uncertainties in the results could potentially become limitless given the huge number of input data and the many choices available to describe THC processes in unsaturated fractured rock. Therefore, it is important for the research groups to focus on uncertainties that are important for a more limited set of outcomes (e.g., permeability and flow modification and a subset of the more important chemical species), rather than concentrations of each individual species. These focus uncertainties shall be defined in future workshops.

7.4   TASK D_THC2

This section gives specific definitions of Task D_THC2, representing a repository drift in unsaturated, densely fractured volcanic rock. The definition is based on the current concept for a nuclear waste repository at Yucca Mountain, Nevada. Specific data are derived from the Yucca Mountain site or specifically from the area of the DST. As pointed out in Section 7.2, the work should be conducted in three phases with increasing levels of uncertainty, as follows:

1. **Phase 1:** Simplified geochemical system with basic species. No consideration of the effect of precipitation/dissolution on permeability and flow field.

2. **Phase 2:** More complete geochemical system. Coupling of mineral precipitation/dissolution to permeability and flow field.

3. **Phase 3:** Uncertainty evaluation, caused by parameter uncertainty and conceptual model uncertainty.

7.4.1   Specific Model Geometry and Modeling Sequence

The geometry for Task D_THC2 is the same as that presented in Table 6.7, Section 6.4.1 for D_THM2. Thermal power inputs are provided in Table 6.8. Hydrological and thermal initial and boundary conditions are the same as those for D_THM2, Figure 6.14. Hydrological and thermal rock properties are identical to those chosen for D_THM2, Tables 6.9a and 6.9b. The modeling sequence for D_THC2 is similar to that described in Figure 6.14; however, excavation effects are not included in D_THC2. The modeling sequence is as follows:

1. Obtain steady-state flow and temperature conditions for rock mass (not including air-filled drift)

2. Use output of steady-state simulation as input to THC simulation, not including thermal loading and excluding the air-filled drift (reference case that could potentially be used as a chemical steady-state initial condition to thermal loading case)

3. THC simulation, including thermal loading in air-filled drift. This phase should also include a reference TH simulation to compare effects on flow to THC simulation. Permeability changes and coupling to flow are neglected in Phase 1

Sequence (2) and (3) should be repeated for different levels of complexity of chemical input parameters and processes. Results can then be directly compared, and used as part of the evaluation of uncertainties in Phase 3.

7.4.2   Suggestions for Potential Modeling Simplifications

Some simplifications presented in Section 6.4.2 can be made, while others are not suitable for modeling THC processes under boiling conditions in fractured rock. First, the use of effective continuum or single continuum models will capture neither the chemical effects of boiling in the rock matrix, nor the gas-phase transport to fractures, nor the condensation plus reaction in fractures. Therefore, dual-continuum, multiple-continuum, or discrete fracture (with an active

rock matrix) approaches are required. It is recognized, however, that most of the research teams working on D_THC2 will *not* be using a dual-continuum model or a multi-continuum because significant code development is involved. Discrete fracture approaches may not be feasible for the intensely fractured rock mass at Yucca Mountain. Thus, one of the primary goals of future research within D_THC2 will be the joint development of simplified, yet realistic model for the fractured porous rock mass at Yucca Mountain. On the other hand, the pure conduction approach presented in Section 6.4.2 for modeling the temperature evolution would be a suitable simplification for THC processes.

7.4.3   Specific Input Data for Phase 1 (Model Inception)

This initial simulation is based on a simplified geochemical system, done to test the effect of TH processes on aqueous and gaseous species transport, gas-water equilibration, and mineral precipitation. Input data for Phase 1 are part of the complete set described in Section 7.4.4, as follows:

Aqueous Species: H_2O, H^+, Na^+, Cl^-, HCO_3^-, SiO_2 (aq)

Gaseous species: H_2O, air, CO_2

Minerals (primary and secondary): cristobalite (primary), amorphous silica (secondary), calcite (primary and secondary), halite (secondary)

Mineral abundances and reactive surface areas for all minerals described in Phase 1 and in Phase 2 are listed in Table 7.6. These data correspond to the Tptpmn unit, which is a devitrified welded high-silica rhyolitic tuff. Thermodynamic data are listed in Appendix 1. Kinetic data are listed in Appendix 2.

7.4.4   Input Data For Phase 2 and 3 (Preliminary and Final Prediction with Uncertainties)

Phases 2 and 3 consider a more complete geochemical system, with all the major mineral phases, aqueous, and gaseous species, plus some minor components. Coupling of mineral dissolution/precipitation to permeability and unsaturated flow is an important additional process that allows for many more choices of conceptual and mathematical models. The following data are given as a starting point for the analysis. Many of the parameter data, and their mathematical representation in a reactive-transport model required choices that other researchers may follow (recommended for Phase 1) or alternatively may decide to use other formulations and/or data (recommended for Phases 2 and 3). Some data, such as the initial mineral abundances and the initial water chemistry are specific to the Yucca Mountain site, while the kinetic and thermodynamic data are derived from open literature sources, or estimated.

7.4.4.1 Initial and Boundary Geochemical Conditions

The model for Phases 2 and 3 includes the major aqueous species, minerals, and gaseous components in the Tptpmn unit, plus others that could potentially precipitate. The geochemical model consists of the following primary aqueous species: H^+, Na^+, K^+, Ca^{2+}, Mg^{2+}, AlO_2^-, NO_3^-, SO_4^{2-}, F^-, Cl^-, HCO_3^-, SiO_2(aq), and $HFeO_2$(aq). Gaseous components include air, H_2O, and CO_2. minor species, such as F^-, are included for their relevance to waste package corrosion. The initial

mineralogy of the tuff matrix and fracture coatings is represented by the following assemblage (some as endmembers of an ideal solid-solution phase): α-cristobalite, opal, tridymite, quartz, K-feldspar, albite, anorthite, Ca-smectite, Na-smectite, Mg-smectite, illite, calcite, fluorite, gypsum, hematite, stellerite, clinoptilolite, mordenite, and heulandite. Several other secondary phases should also be considered (e.g., amorphous silica, kaolinite, and sepiolite), as well as a set of potential salt phases that can precipitate during the complete dry-out of the rock.

Initial mineral volume fractions and reactive surfaces areas (for mineral-water reactions described by kinetic rates of dissolution/precipitation) are given in Table 7.6. The reactive surface areas have been calculated based on various considerations of rock and mineral texture (matrix minerals) and fracture spacing and area (fracture minerals). More detailed discussion of the calculations is given in BSC (2003c).

The initial water chemistry was derived from matrix pore water extracted from the Topopah Spring middle nonlithophysal unit (Tptpmn) in Alcove 5, near the DST ("HD-PERM" water; BSC 2003c, Table 6.2-1). The initial water and gas chemistry for D_THC2 is listed in Table 7.7.

Table 7.6   Mineral Volume Fractions and Reactive Surface Areas for the Tptpmn Unit For Task D_THC2

	Volume Fraction		Reactive Surface Area	
	Matrix	Fracture	Matrix (cm^2/g)	Fracture (m^2/m^3)
K-Feldspar	0.32265	0.19520	90.7	2126.9
Albite	0.23826	0.14415	90.7	2126.9
Anorthite	0.00802	0.00485	90.7	2126.9
Ca-Smectite	0.00517	0.01872	1086.6	2126.9
Na-Smectite	0.00221	0.00802	1086.6	2126.9
Mg-Smectite	0.00517	0.01872	1086.6	2126.9
Illite	0.00385	0.01396	1086.6	2126.9
Tridymite	0.02310	0.01397	90.7	2126.9
Cristobalite	0.35588	0.21530	90.7	2126.9
Quartz	0.02526	0.01529	90.7	2126.9
Hematite	0.00036	0.00022	92.3	2126.9
Calcite	0.00007	0.01984	92.3	2126.9
Stellerite	0.00000	0.32175	92.3	2126.9
Heulandite	0.00000	0.00000	92.3	2126.9
Mordenite	0.00000	0.00000	92.3	2126.9
Clinoptilolite	0.00000	0.00000	92.3	2126.9
Kaolinite	0.00000	0.00000	1086.6	2126.9
Am. Silica	0.00000	0.00000	1086.6	2126.9
Opal	0.00990	0.00990	1086.6	2126.9
Fluorite	0.00010	0.00010	92.3	2126.9

NOTE: Minerals with initially zero volume fraction in matrix and fractures are important as secondary minerals (such as heulandite, mordenite, etc.)

Table 7.7.   Initial pore-water and gas compositions[1]

Sample ID:		HD-PERM[4] (Alcove 5)
Water		
	Units	
Temperature	°C	25
pH (measured)	pH	8.31
Na^+	mg/L	61.5
K^+	mg/L	8
Ca^{2+}	mg/L	101
Mg^{2+}	mg/L	17
$SiO_{2(aq)}$	mg/L	70.5
Cl^-	mg/L	117
SO_4^{2-}	mg/L	116
HCO_3^- (calc)[2]	mg/L	200
NO_3^-	mg/L	6.5
F^-	mg/L	0.86
Al^{3+} (calc)[2]	Molal	6.173E-10
Fe^{3+} (calc)[2]	Molal	1.155E-12
Gas		
$log(PCO_2)$[2]	Bar	-3.1
CO_2 (approx)[3]	ppmv	~900

NOTES: (1) Source: Table 6.2-1 in BSC 2003c
(2) Calculated (see Table 6.2-1 in BSC 2003c)
(3) Converted to ppmv using total pressure equal to one bar
(4) Average of Tptpmn porewater analyses ESF-HD-PERM-2 (30.1'-30.5')ESF HD-PERM-3 (34.8'-35.1').

At the initial state, aqueous and gaseous species concentrations in the rock should be set uniformly, based on the measured pore water composition and calculated equilibrium values for CO_2 and some aqueous species (Table 7.6). The air-filled drift CO_2 concentration should be fixed to approximately that of the atmosphere (~ 380 ppmv). Both the top and bottom boundary conditions should be open to gas and aqueous species transport. The top and bottom boundaries should also be set so that no mineral reactions take place (and therefore no changes in aqueous species concentrations occur as a result of mineral-water reactions). The side boundaries should be set as no-flux for gas and aqueous-species transport (to simulate adjacent equally-spaced waste emplacement tunnels).

7.4.4.2   Kinetic Rate Laws

The text below explains choices of kinetic rate laws that have been used in BSC (2003c). Other researchers may follow these choices (recommended for Phase 1) or alternatively may decide to use other formulations and/or data (recommended for Phases 2 and 3).

Rates of mineral dissolution and precipitation close to equilibrium can be described via a relationship of the rate to the saturation index (Q/K), as follows (Steefel and Lasaga 1994):

$$Rate(mol\ s^{-1}kg_{water}^{-1}) = sgn\left[\log\left(\frac{Q}{K}\right)\right]kA\prod_i a_i^p\left[\left(\frac{Q}{K}\right)^m - 1\right]^n \qquad \text{(Eq. 7-1)}$$

where a_i is the activity of each inhibiting or catalyzing species, and p is an empirically determined exponent and the variable A is the reactive surface area expressed in units of $m_{mineral}^2 / kg_{water}$. The rate constant k (in mol m^{-2} s^{-1}) is given as (Steefel and Lasaga 1994):

$$k = k_0 \exp\left[\frac{-E_a}{R}\left(\frac{1}{T} - \frac{1}{298.15}\right)\right] \qquad \text{(Eq. 7-2)}$$

where the temperature dependence of reaction rate is related to the activation energy (E_a) in units of kJ/mol and T is the temperature in Kelvin units. Following Steefel and Lasaga (1994), by neglecting the effect of pH or other aqueous species activities on reaction rates, we set $p=0$ for each species so that the product $\prod_i a_i^p = 1$ can be eliminated from Equation 7-1. The ratio of the species activity product (Q) and the equilibrium constant (K) describes the extent to which a mineral is in disequilibrium with a given solution composition. For Q/K equal to one, the mineral is at equilibrium, and thus the net rate of reaction becomes zero. For Q/K greater than one, the mineral is oversaturated and thus the rate becomes negative. The expression "*sgn [log(Q/K)]*" ensures that the correct sign is enforced when the exponents m and n are not equal to one. The variable A is the reactive surface area expressed in units of $m_{mineral}^2 / kg_{water}$. In the case of ideal solutions, the saturation index of the solid solution is calculated as the sum of the saturation indices of the individual end members, and the reaction rate of the solid solution is calculated.

Carroll et al. (1998) noted that the calculated rates of amorphous silica precipitation, based on Rimstidt and Barnes (1980), are about three orders of magnitude lower than those observed in geothermal systems. Carroll et al. (1998) presented experimental data on amorphous silica precipitation for more complex geothermal fluids at higher degrees of supersaturation, and also for a near-saturation simple fluid chemistry. Under far from equilibrium conditions, the rate law for amorphous silica precipitation has been expressed as (Carroll et al. 1998):

$$Rate(mol\ s^{-1}kg_{water}^{-1}) = kA\left(\frac{Q}{K}\right)^m \qquad \text{(Eq. 7-3)}$$

7.4.4.3   Fracture Permeability Changes

The text below explains choices of constitutive relationships that have been made in BSC (2003c). Other researchers may follow these choices (recommended for Phase 1) or alternatively may decide to use other formulations and/or data (recommended for Phases 2 and 3).

In many experimental and natural systems, permeability reductions to values near zero occur at porosities significantly greater than zero. This generally is the result of mineral precipitation preferentially closing the narrower interconnecting apertures. The hydraulic aperture, as calculated from the fracture spacing and permeability (as determined through air-permeability measurements) using a cubic law relation, is a closer measure of the smaller apertures in the flow system. The initial hydraulic aperture $b_{0,h}$ (m) is calculated using the following cubic law relation:

$$b_{0,h} = \left[12 k_0 s\right]^{1/3} \qquad \text{(Eq. 7-4)}$$

where k_0 is the initial fracture permeability (m^2) and s is the fracture spacing (m) for a single fracture set. The permeability (k') resulting from a change in the hydraulic aperture is given by

$$k' = \frac{\left(b_{0,h} + \Delta b\right)^3}{12 s} \qquad \text{(Eq. 7-5)}$$

where Δb is the aperture change resulting from mineral precipitation/dissolution. The aperture change resulting from a calculated volume change can be approximated by assuming precipitation of a uniform layer over the entire geometric surface area of the fracture, assuming also that this area (as well as the fracture spacing) remains constant. The initial aperture available for precipitation (b_g, the geometric, rather than the hydraulic, aperture) can be calculated from the ratio of the initial fracture porosity ($\phi_{f,0}$) to the fracture surface area (A_f), as follows:

$$b_g = \phi_{f,0} \Big/ A_f \qquad \text{(Eq. 7-6)}$$

For a dual-permeability model, changes in the fracture porosity are calculated based on the porosity of the fracture medium, so that Δb can be approximated by

$$\Delta b = \frac{\left(\phi'_{fm} - \phi_{fm,0}\right)}{\phi_{fm,0}} b_g \qquad \text{(Eq. 7-7)}$$

The parameters b_g and s for the Tptpmn unit are 6.278×10^{-4} m, and 0.2315 m, respectively (BSC 2003c).

7.4.5   Uncertainty Analysis For Phase 3

Many conceptual model choices are available in Phase 2 (e.g., equilibrium versus kinetic mineral-water reactions, calculation of reactive surface areas in unsaturated systems, permeability-mineral precipitation relations, etc.). The analysis of uncertainties in the results could potentially become limitless given the huge number of input data and the many choices available to describe THC processes in unsaturated fractured rock. Therefore, it is important for the research groups to focus on uncertainties that are important for a more limited set of outcomes (e.g., permeability and flow modification and a subset of the more important chemical species), rather than concentrations of each individual species. These focus uncertainties shall be defined in future workshops.

7.5   OUTPUT SPECIFICATIONS

The research teams are requested to provide simulation outputs at the specified points, lines, and regions (see Figure 6.1). These outputs have been specified to ensure easy comparison of model results between different research teams. The output regions for D_THC are based on those described in D_THM; however, an excavation-disturbed zone is not considered in D_THC. It is important that all teams follow this guidance. As discussed in Section 6.5, Figure 6.1 displays more points than are currently used. However, output for these extra points may be requested during the course of Task D_THC, and more points and lines may be added based on suggestions at future DECOVALEX workshops or task force meetings.

A few points are assigned for monitoring the evolution of measurable parameters. These are parameters that can be monitored at a real site for performance confirmation. Outputs will be collected along two lines (profiles): x-profile (along z = 0) and z-profile (along x = 0). The advantage of collecting data along lines is that results from discrete and continuum models can be readily compared. In addition, two areas have been assigned for contouring and possible statistical evaluation of permanent changes. The Far Field Study Area is designated for studies of potential permanent changes of the fractured rock away from the drift wall (and outside the area of excavation effects examined in D_THM).

A detailed output definition is given in Tables 7.8 through 7.10 for Simulation Phases 1, 2, and 3. At this time, the outputs for Phase 1 (model inception) are completely defined. The output specification for Phases 2 and 3 is preliminary and may be changed in the future, based on the results of the model inception phase and depending on which modeling approaches are used by the different research teams. However, the preliminary output definition for Phase 2 and 3 should be a guide for the research teams in selecting and developing their models, such that the output requirements can be met.

Table 7.8.   Output specification for time evolution at points for Phases 1, 2, and 3

Parameter	Specification	Comment	Illustration of possible output
Temperature	T along x-profile and z-profile (at selected times, e.g., 1, 10, 100, 1000, 10000, 100000 years)	Will shows temperature profile and potential boundary effects	
Aqueous species concentrations	Concentrations (mg/L) along x-profile and z-profile (at selected times)	Shows effects of boiling, transport, and mineral-water reactions on water chemistry	Varies according to reactivity of species,
Gaseous species concentrations	Concentrations (ppmv) along x-profile and z-profile (at selected times)	Shows effects of boiling, transport, and mineral-water reactions on gas chemistry	Varies according to gas solubility and transport properties
Mineral Abundances	Abundances (volume fraction changes) along x-profile and z-profile (at selected times)	Shows effects of boiling, transport, and mineral-water reactions on mineral abundances	Varies according to solubilities and reaction rates of minerals
Vertical water flux	Q_z (vertical flux) across x-profile (at selected times)	The total mass flux of liquid water (kg/second) across 0.5 meter long bins (intervals) along the x-profile.	 (Illustration shows this output for a heterogeneous continuum)
Permeability	Vertical permeability across x-profile (at selected times)	Shows how vertical permeability changes during the entire heating cycle and may reveal permanent changes in permeability at 10,000 years. In a continuum model with several elements over a 0.5 meter bin, the arithmetic mean should be calculated for the 0.5 meter bin.	 (Illustration shows how *k* may change as a results of mineral precipitation during the heating phase for a heterogeneous continuum)

Table 7.9.   Output specification within far field study areas for Phases 2 and 3

Parameter	Specification	Comment	Illustration of expected output
Aqueous chemistry (m/L) and pH	Aqueous chemistry on the scale of the far field study area (at selected times, e.g., 1, 10, 100, 1000, 10000, 100000 years)	Contours will show the distribution of water chemistry in the far field study area	Data should be supplied to the task force lead (x, z, pH, Na, Cl, SiO2, etc) who will make this plots for comparison between different teams Patterns will vary depending on the species
Gas chemistry (ppmv)	Gaseous chemistry on the scale of the far field study area (at selected times)	Contours will show the distribution of gas chemistry in the far field study area	Data should be supplied to the task force lead (x, z, CO2) who will make this plots for comparison between different teams
Mineral abundances (volume fraction changes)	Mineral abundances on the scale of the far field study area (at selected times)	Contours will show the distribution of mineral abundance changes in the far field study area	Data should be supplied to the task force lead (x, z, quartz, calcite, etc) who will make this plots for comparison between different teams Patterns will vary depending on the mineral
Permeability	Permeability changes on the scale of the far field study area (at selected times)	The plot should indicate how much permeability have changes compared with its initial value.	X, Z, k
Flux Vectors	Flux changes in the far-field (at selected times)	Flux vectors will show the changes in the flow field as a result of mineral precitation/dissolu-tion	X,Z, v

Table 7.10.   Outputs in points and along lines with uncertainty range for Phase 3

Parameter	Specification	Comment	Illustration of expected output
All parameters defined in Tables 7.8 through 7.9	Predictions at points and along lines with error bar (at selected times)	It is up to the research teams to decide how they will present uncertainties (e.g. standard deviation or upper and lower limit).	Depends on parameter chosen

8.   SUMMARY AND OUTLOOK FOR TASK D

Task D of DECOVALEX-THMC can be summarized as follows:

- Task D focuses on long-term THC and THM processes with impact on near-field flow processes

- Task D_THM addresses THM processes, D_THC addresses THC processes

- Both tasks include two different repository scenarios (rock types, emplacement concepts), i.e., D_THM1 and D_THM2 as well as D_THC1 and D_THC2

- Similarity in geometry and setup allows for comparison of processes and scenarios

- At this early project stage, task definitions are flexible to accommodate interest of different participants

- Experimental data analysis/modeling supports task definition and model validation

- Sub-tasks participation is possible (e.g., THC only, THM only); however, each group should ideally look at both repository scenarios

Research teams that are interested in participating in Task D of DECOVALEX-THMC are encouraged to provide suggestions and improvements for this draft description. We hope for plenty of interest in Task D and expect fruitful cooperation and interaction.

INTENTIONALLY LEFT BLANK

9. REFERENCES

Alonso et al., 2000. *Final report of DECOVALEX III, Task1: FEBEX in situ test*. SKI report expected during 2004.

Amiguet J.-L. 1985. *Grimsel Test Site*. Felskennwerte von intaktem Granit. Zusammenstellung felsmechanisher Laborresultate diverse granitische Gesteine. NAGRA, NIB 85-05, Sep. 1985.

Brown, S.R. (1985). Simple mathematical model of a rough fracture. J. Geophys. Res. 100, 5941–5952.

BSC (Bechtel SAIC Company) 2003a. *Drift Degradation Analysis*. ANL-EBS-MD-000027 REV 02. Las Vegas, Nevada: Bechtel SAIC Company.

BSC (Bechtel SAIC Company) 2003b. *Calibrated Properties Model*. MDL-NBS-HS-000003 REV 01. Las Vegas, Nevada: Bechtel SAIC Company. ACC: DOC.20030219.0001.

BSC (Bechtel SAIC Company) 2003c. *Drift-Scale Coupled Processes (DST and THC Seepage) Models*. MDL-NBS-HS-000001 REV 02. Las Vegas, Nevada: Bechtel SAIC Company.

Carroll, S.; Mroczek, E.; Alai, M.; and Ebert, M. 1998. *Amorphous Silica Precipitation (60 to 120°C): Comparison of Laboratory and Field Rates*. Geochimica et Cosmochimica Acta, 62, (8), 1379-1396.

CRWMS M&O (Civilian Radioactive Waste Management System Management and Operating Contractor) 2000. *Statistical Analysis of Empirical Rock Properties by Lithographic Units*. CAL-GCS-GE-000001 Revc 00. Las Vegas, Nevada.

CRWMS M&O (Civilian Radioactive Waste Management System Management and Operating Contractor) 1997. *Yucca Mountain Site Geotechnical Report*. B00000000-01717-5705-00043 REV 01. Two volumes. Las Vegas, Nevada.

CRWMS M&O (1998). Ge*ology of the Exploratory Studies Facility Topopah Spring Loop*. BAB000000-01717-0200-00002 REV 01. Las Vegas, Nevada

Damjanac B., Brandshaug T.,Carranza-Torres C, Detournay C. and Perrochet P 2000. *An evaluation of local thermo-mechanical effects on seepage into waste disposal rooms at Yucca Mountain*. Itasca Consulting Group Inc November 2000.

Datta et al. 2004. *DECOVALEX III, Task 2, Final Report*. (SKI report expected during 2004).

DECOVALEX III 2001. Task 1. *Modeling of FEBEX in situ test. Part B: Thermo-hydro-mechanical analysis of the bentonite behaviour.*

DECOVALEX III 2000. Task 1. *Modeling of FEBEX in situ test. Part A: Hydromechanical modeling of the rock.*

Fujita T., Sugita Y., Chijimatsu M. and Ishikawa 1996. *Mechanical properties of fracture.* Power Reactor and Nuclear Fuel Development Corporation (PNC), Technical note 06-95-06.

Guimera J., Carrera J., Marinez L., Vazquez E., Ortuno F., Fierz T., Bulher C., Vives L., Meier P., Median A., Saaltink M., Ruiz B. and Pardillo J. 1998. *FEBEX Hydrogeological characterization and modelling.* UPC, 70-UPC-M-0-1001, Jan 1998.

Hoek E., Carranza-Torres C. and Corkum B. 2002. *Hoek-Brown Failure Criterion – 2002 Edition* 5th North American Rock Mechanics Symposium and 17th Tunnelling Association of Canada Conference: NARMS-TAC 2002, July 7-10 University of Toronto, Toronto, Ontario, Canada.

Ichikawa Y., Kawamura K., Fujii N. and Kitayama K., 2004. *Microstructure and micro/ macrodiffusion behavior of tritium in bentonite.* Applied Clay Science, Volume 26, pp. 75-90.

Keusen H.R., Ganguin J., Shuler P. and Buletti M. 1989. *Grimsel Test Site: Geology NAGRA* NTB 87-14E, FEb 1989.

Laaksoharju, M. 2003, *Update of the hydrogeochemical model 2002.* GeoMod GW Report, Aspö Hard Rock Laboratory, October 2003.

Mongano G.S., Singleton W.L., Moyer T.C., Beason S.C., Eatman G.L.W. Albin A.L. and Lung R.C. 1999. *Geology of the ECRB Cross Drift – Exploratory Studies Facility, Yucca Mountain Project, Yucca Mountain, Nevada.* Denver Colorado U.S. Geological Survey.

Ochs M., Lothenbach B., Shibata M. and Yui M. 2004, *Thermodynamic modeling and sensitivity analysis of porewater chemistry in compacted bentonite,* Physics and Chemistry of the Earth, Parts A/B/C, Volume 29, Issue 1, pp. 129-136.

Olsson W.A. and Brown S 1995. *Mechanical properties of fractures from drill holes UE25-NRG-4, USW-NRG-6, USW-NRG-7, and USW-SD-9 at Yucca Mountain, Nevada.* Sandia National Laboratories Technical Report, Sand 95-1736. Albuquerque New Mexico, Sandia National Laboratories

Pardillo J., Campos R. and Guimera J. 1997. *Caracterizacion geologica de la zone de ensayo FEBEX (Grimsel – Suiza).* CIEMAT, 70-IMA-M-2-01, May 1997.

Pardillo J. and Campos R. 1996. *FEBEX-Grimsel Test Site (Switzerland). Considerations with respect to the fracture distribution.* CIEMAT, 70-IMA-L-2l05, Mar. 1996.

Pruess, K. (1990). On thermohydrologic conditions near high-level nuclear wastes emplaced in partially saturated fractured tuff – 2. effective continuum approximation. Water Resources Research. 26(6), 1249-1261.

Rimstidt, J.D. and Barnes, H.L. 1980. *The Kinetics of Silica–Water Reactions.* Geochimica et Cosmochimica Acta, 44, 1683-1699.

Rhen I., Backborn G., Gustafson G., Stanfors R., and Wikberg P. 1997, *Results from pre-investigations and detailed site characterization. Summary report. SKB Technical Report 97-03.* ASPÖ HRL – Geoscientific evaluation 1997/2. Swedish Nuclear Fuel and Waste Management Company, Stockholm, Sweden.

Steefel, C.I. and Lasaga, A.C. 1994. *A Coupled Model for Transport of Multiple Chemical Species and Kinetic Precipitation/Dissolution Reactions with Application to Reactive Flow in Single Phase Hydrothermal Systems.* American Journal of Science, 294, (5), 529-592.

INTENTIONALLY LEFT BLANK

APPENDIX I – THERMODYNAMIC DATABASE (BSC 2003C)[1]

Mineral	Molecular Weight (g/mol)	Molar Volume (cm³/mol)	Reaction Stoichiometry[1]	0 (°C)	25 (°C)	60 (°C)	100 (°C)	150 (°C)	200 (°C)	250 (°C)	300 (°C)
							log (K)				
albite-low	262.223	100.070	(1)alo2-, (1)na+, (3)sio2(aq)	-21.697	-20.179	-18.365	-16.686	-15.096	-13.987	-13.293	-12.963
anorthite	278.207	100.790	(2)alo2-, (1)ca+2, (2)sio2(aq)	-21.229	-20.484	-19.640	-18.960	-18.514	-18.485	-18.839	-19.547
calcite	100.087	36.934	(1)ca+2, (-1)h+, (1)hco3-	2.226	1.849	1.333	0.774	0.100	-0.584	-1.326	-2.215
clinopt/10	277.660	126.410	(2.6)h2o, (0.68)alo2-, (0.28)ca+2, (0.08)k+, (0.04)na+,(2.92)sio2(aq)	-20.216	-18.475	-16.703	-15.136	-13.577	-12.339	-11.395	-10.816
clpt/10-r02	277.660	126.410	(2.6)h2o, (0.68)alo2-, (0.28)ca+2, (0.08)k+, (0.04)na+,(2.92)sio2(aq)	-17.760	-16.020	-14.250	-12.680	-11.120	-9.880	-8.940	-8.360
cristoba-a	60.084	25.740	(1)sio2(aq)	-3.542	-3.192	-2.867	-2.589	-2.306	-2.071	-1.877	-1.742
fluorite	78.075	24.542	(1)ca+2, (2)f-	-10.310	-10.037	-9.907	-9.967	-10.265	-10.784	-11.555	-12.703
gypsum	172.172	74.690	(2)h2o, (1)ca+2, (1)so4-2	-4.533	-4.482	-4.609	-4.904	-5.410	-6.058	-6.874	-7.971
halite	58.442	27.015	(1)na+, (1)cl-	1.492	1.586	1.618	1.578	1.450	1.242	0.936	0.468
hematite	159.688	30.274	(-1)h2o, (2)hfeo2(aq)	-26.438	-23.927	-21.486	-19.661	-18.293	-17.573	-17.272	-17.248
heuland/10	279.347	126.640	(2.6)h2o, (0.8)alo2-, (0.33)ca+2, (0.04)k+, (0.1)na+, (2.8)sio2(aq)	-21.097	-19.348	-17.565	-15.992	-14.437	-13.217	-12.306	-11.779
heul/10-r02	279.347	126.640	(2.6)h2o, (0.8)alo2-, (0.33)ca+2, (0.04)k+, (0.1)na+, (2.8)sio2(aq)	-18.620	-16.870	-15.090	-13.510	-11.960	-10.740	-9.830	-9.300
illite	378.963	135.080	(0.44)h2o, (2.06)alo2-, (1.12)h+, (0.5)k+, (0.22)mg+2, (3.72)sio2(aq)	-45.566	-42.016	-38.333	-35.129	-32.064	-29.760	-28.120	-27.254
kaolinite	258.160	99.520	(1)h2o, (2)alo2-, (2)h+, (2)sio2(aq)	-43.234	-39.917	-36.348	-33.216	-30.252	-28.074	-26.558	-25.754
microcline-b	278.332	108.741	(1)alo2-, (1)k+, (3)sio2(aq)	-23.770	-21.820	-19.530	-17.440	-15.470	-14.080	-13.170	-12.670
morden/10	269.631	127.350	(2.2)h2o, (0.6)alo2-, (0.15)ca+2, (0.09)k+, (0.21)na+, (3)sio2(aq)	-19.244	-17.542	-15.820	-14.298	-12.776	-11.558	-10.617	-10.021
mord/10-r02	269.631	127.350	(2.2)h2o, (0.6)alo2-, (0.15)ca+2, (0.09)k+, (0.21)na+, (3)sio2(aq)	-16.950	-15.250	-13.530	-12.010	-10.480	-9.270	-8.330	-7.730
opal-proxy	60.084	29.000	(1)sio2(aq)	-3.501	-3.005	-2.627	-2.358	-2.118	-1.926	-1.765	-1.632
quartz	60.084	22.688	(1)sio2(aq)	-4.153	-3.743	-3.348	-3.006	-2.661	-2.376	-2.142	-1.976
sepiolite	323.913	142.830	(-4)h+, (5.5)h2o, (2)mg+2, (3)sio2(aq)	17.631	15.992	13.961	12.164	10.536	9.352	8.397	7.457
sio2(amor.)	60.084	29.000	(1)sio2(aq)	-2.954	-2.670	-2.422	-2.213	-1.998	-1.815	-1.663	-1.562
smect-ca-cal	365.394	132.510	(0.52)h2o, (1.77)alo2-, (0.145)ca+2, (0.96)h+, (0.26)mg+2, (3.97)sio2(aq)	-40.190	-36.970	-33.660	-30.790	-28.010	-25.900	-24.370	-23.550
smect-na-cal	366.250	132.510	(0.52)h2o, (1.77)alo2-, (0.96)h+, (0.26)mg+2, (0.29)na+, (3.97)sio2(aq)	-40.290	-36.980	-33.560	-30.560	-27.660	-25.440	-23.820	-22.900
smect-mg-cal	363.107	132.510	(0.52)h2o, (1.77)alo2-, (0.96)h+, (0.405)mg+2, (3.97)sio2(aq)	-40.240	-37.060	-33.790	-30.950	-28.200	-26.110	-24.600	-23.790

[1] Note: References and supporting information can be supplied as an electronic file.

Mineral	Molecular Weight (g/mol)	Molar Volume (cm³/mol)	Reaction Stoichiometry[1]	log (K)							
				0 (°C)	25 (°C)	60 (°C)	100 (°C)	150 (°C)	200 (°C)	250 (°C)	300 (°C)
steller/10	281.733	133.1	(2.8)h2o, (0.79)alo2-, (0.39)ca+2,(0.01)na+, (2.81)sio2(aq)	-21.144	-19.432	-17.691	-16.156	-14.636	-13.444	-12.553	-12.041
stell/10-r02	281.733	133.1	(2.8)h2o, (0.79)alo2-, (0.39)ca+2,(0.01)na+, (2.81)sio2(aq)	-18.37	-16.88	-15.4	-14.12	-12.86	-11.89	-11.2	-10.87
sylvite	74.551	37.524	(1)k+, (1)cl-	0.525	0.846	1.122	1.285	1.330	1.238	1.013	0.604
tridymite	60.084	26.586	(1)sio2(aq)	-3.946	-3.572	-3.193	-2.834	-2.413	-1.995	-1.587	-1.203
hydglassfe3	48.466	20.536	(-0.0006)h+, (0.5981)sio2(aq), (0.1180)alo2-, (0.0556)na+, (0.0594)k+, (0.016)ca+2, (0.0002)mg+2, (0.0055)hfeo2(aq), (0.0783)h2o	1.646	1.462	1.209	0.978	0.759	0.584	0.415	0.211
mgso4	120.369	45.250	(1)mg+2, (1)so4-2	6.237	4.882	3.1	1.263	-0.811	-2.748	-4.677	-6.787
nano3	84.995	50.000	(1)na+, (1)no3-	-0.811	-0.206	0.403	0.88	1.275	1.518	1.651	1.665
k2so4 (arcanite)	174.260	65.500	(2)k, (1)so4-2	-2.273	-1.801	-1.469	-1.365	-1.488	-1.826	-2.365	-3.19
na2so4 (thenardite)	142.043	53.330	(2)na+, (1)so4-2	-0.35	-0.309	-0.438	-0.705	-1.15	-1.716	-2.473	-3.548

Gaseous Species	Molecular Weight (g/mol)	Molecular Diameter (m)	Reaction Stoichiometry	0 (°C)	25 (°C)	60 (°C)	100 (°C)	150 (°C)	200 (°C)	250 (°C)	300 (°C)
co2(g)	44.01	2.50E-10	(-1)h2o, (1)h+, (1)hco3-	-7.677	-7.814	-8.053	-8.357	-8.769	-9.217	-9.720	-10.339

NOTES: [1] Negative number in parenthesis indicate the species is on the left side of equation.

Minerals names or abbreviations above are those used in the database and may not exactly match names used in the text of the report. Names ending by /10 indicate the stoichiometry, molecular weight, molar volume, and log(K) values for those minerals were divided by 10 compared to original data. Glass phases glass1 and glass were used with the extended-case and base-case geochemical systems, respectively.

Aqueous Species	Molecular Weight (g/mol)	r_{ej}	Charge	Reaction Stoichiometry[1]	0 (°C)	25 (°C)	60 (°C)	100 (°C)	150 (°C)	200 (°C)	250 (°C)	300 (°C)
Al+3	26.982	3.33	3	(-2)h2o, (1)alo2-, (4)h+	-25.795	-22.883	-19.571	-16.582	-13.676	-11.409	-9.598	-8.167
Al(OH)2+	60.996	2.31	1	(1)alo2-, (2)h+	-13.655	-12.289	-10.825	-9.600	-8.530	-7.823	-7.396	-7.238
AlOH+2	43.989	2.8	2	(-1)h2o, (1)alo2-, (3)h+	-20.068	-17.926	-15.567	-13.519	-11.625	-10.242	-9.232	-8.547
CO2(aq)	44.010	0	0	(-1)h2o, (1)h+, (1)hco3-	-6.580	-6.345	-6.268	-6.388	-6.724	-7.197	-7.787	-8.528
CO3-2	60.009	2.81	-2	(-1)h+, (1)hco3-	10.624	10.329	10.130	10.084	10.200	10.465	10.871	11.464
CaCO3(aq)	100.087	0	0	(1)ca+2, (-1)h+, (1)hco3-	7.505	7.002	6.455	5.975	5.492	5.057	4.589	3.978
CaCl+	75.531	2.31	1	(1)ca+2, (1)cl-	0.356	0.293	0.094	-0.215	-0.682	-1.227	-1.870	-2.677
CaCl2(aq)	110.983	0	0	(1)ca+2, (2)cl-	0.456	0.644	0.634	0.400	-0.118	-0.844	-1.802	-3.116
CaF+	59.076	2.31	1	(1)ca+2, (1)f-	-0.655	-0.682	-0.862	-1.171	-1.650	-2.217	-2.888	-3.728
CaHCO3+	101.095	2.31	1	(1)ca+2, (1)hco3-	-1.094	-1.047	-1.158	-1.413	-1.848	-2.383	-3.027	-3.840
CaHSiO3+	117.170	2.31	1	(-1)h+, (1)ca+2, (1)h2o, (1)sio2(aq)	8.778	8.575	8.115	7.596	7.043	6.588	6.200	5.837
CaOH+	57.085	2.31	1	(-1)h+, (1)ca+2, (1)h2o	14.085	12.833	11.416	10.142	8.903	7.928	7.126	6.434
CaSO4(aq)	136.142	0	0	(1)ca+2, (1)so4-2	-2.071	-2.111	-2.265	-2.511	-2.910	-3.433	-4.144	-5.188
Fe+3	55.845	3.46	3	(3)h+, (1)hfeo2(aq), (-2)h2o	-14.305	-12.018	-9.602	-7.594	-5.807	-4.521	-3.530	-2.696
FeCl+2	91.298	2.8	2	(1)cl-, (3)h+, (-2)h2o, (1)hfeo2	-15.770	-13.498	-11.217	-9.449	-8.047	-7.230	-6.813	-6.721
FeF+2	74.843	2.8	2	(1)f-, (3)h+, (-2)h2o, (1)hfeo2(aq)	-20.032	-18.018	-16.038	-14.546	-13.418	-12.827	-12.608	-12.697
FeF2+	93.842	2.31	2	(2)f-, (3)h+, (-2)h2o, (1)hfeo2(aq)	-22.323	-20.368	-18.459	-17.037	-16.011	-15.569	-15.590	-16.086
FeO+	71.844	2.31	1	(1)h+, (-1)h2o, (1)hfeo2(aq)	-7.324	-6.368	-5.372	-4.561	-3.865	-3.393	-3.060	-2.807
FeO2-	87.844	1.81	-1	(-1)h+, (1)hfeo2(aq)	10.231	9.602	8.839	8.111	7.381	6.822	6.430	6.249
FeOH+2	72.852	2.8	2	(2)h+, (-1)h2o, (1)hfeo2(aq)	-11.409	-9.813	-8.174	-6.853	-5.727	-4.964	-4.415	-3.979
FeSO4+	151.909	2.31	1	(1)so4-2, (3)h+, (-2)h2o, (1)hfeo2(aq)	-15.846	-13.946	-12.089	-10.700	-9.681	-9.213	-9.179	-9.602
HAlO2	59.988	0	0	(1)alo2-, (1)h+	-7.080	-6.450	-5.846	-5.409	-5.119	-5.035	-5.120	-5.384
HF	20.006	0	0	(1)f-, (1)h+	-2.985	-3.168	-3.474	-3.848	-4.338	-4.859	-5.437	-6.135
HF2-	39.005	1.81	-1	(1)h+, (2)f-	-2.238	-2.551	-2.960	-3.385	-3.880	-4.374	-4.915	-5.578
HNO3(aq)	63.013	0	0	(1)h+, (1)no3-	1.540	1.303	0.952	0.556	0.074	-0.412	-0.936	-1.579
HSiO3-	77.092	1.81	-1	(-1)h+, (1)h2o, (1)sio2(aq)	9.811	9.585	9.241	8.960	8.802	8.833	9.035	9.433
KCl(aq)	74.551	0	0	(1)cl-, (1)k+	2.840	2.536	2.141	1.731	1.255	0.785	0.278	-0.344
KHSO4(aq)	136.170	0	0	(1)h+, (1)k+, (1)so4-2	2.039	1.495	0.595	-0.476	-1.817	-3.172	-4.601	-6.242
KOH(aq)	56.106	0	0	(-1)h+, (1)h2o, (1)k+	15.498	14.439	13.314	12.378	11.552	10.978	10.570	10.267
KSO4-	135.162	1.81	-1	(1)k+, (1)so4-2	-0.886	-0.880	-0.991	-1.195	-1.521	-1.921	-2.419	-3.090
MgCO3(aq)	84.314	0	0	(-1)h+, (1)hco3-, (1)mg+2	7.742	7.350	6.929	6.574	6.228	5.911	5.543	5.019
MgCl+	59.758	2.31	1	(1)cl-, (1)mg+2	0.097	0.135	0.041	-0.173	-0.537	-0.992	-1.550	-2.276
MgF+	43.303	2.31	1	(1)f-, (1)mg+2	-1.387	-1.352	-1.478	-1.739	-2.169	-2.691	-3.321	-4.125
MgHCO3+	85.322	2.31	1	(1)hco3-, (1)mg+2	-1.077	-1.036	-1.160	-1.423	-1.852	-2.369	-2.984	-3.758
MgHSiO3+	101.397	2.31	1	(-1)h+, (1)h2o, (1)mg+2, (1)sio2(aq)	8.454	8.325	7.943	7.501	7.036	6.666	6.358	6.072
MgOH+	41.312	2.31	1	(1)mg+2, (1)h2o	9.725	9.815	9.917	10.012	10.104	10.177	10.236	10.285
MgSO4(aq)	120.369	0	0	(1)mg+2, (1)so4-2	-2.184	-2.230	-2.393	-2.641	-3.031	-3.539	-4.236	-5.271
NaCO3-	82.999	1.81	-1	(-1)h+, (1)hco3-, (1)na+	9.725	9.815	9.917	10.012	10.104	10.177	10.236	10.285
NaCl(aq)	58.442	0	0	(1)cl-, (1)na+	0.829	0.777	0.651	0.473	0.214	-0.093	-0.478	-1.013
NaF(aq)	41.988	0	0	(1)f-, (1)na+	1.082	0.998	0.833	0.623	0.338	0.010	-0.397	-0.957

Aqueous Species	Molecular Weight (g/mol)	r_{ej}	Charge	Reaction Stoichiometry[1]	0 (°C)	25 (°C)	60 (°C)	100 (°C)	150 (°C)	200 (°C)	250 (°C)	300 (°C)
NaHCO3(aq)	84.007	0	0	(1)hco3-, (1)na+	-0.398	-0.154	0.075	0.244	0.358	0.374	0.277	0.004
NaHSiO3(aq)	100.081	0	0	(-1)h+, (1)h2o, (1)na+, (1)sio2(aq)	7.603	7.754	7.780	7.795	7.873	8.014	8.190	8.365
NaOH(aq)	39.997	0	0	(-1)h+, (1)h2o, (1)na+	15.132	14.205	13.210	12.377	11.642	11.130	10.762	10.480
NaSO4-	119.053	1.81	-1	(1)na+, (1)so4-2	-0.677	-0.700	-0.842	-1.063	-1.389	-1.772	-2.242	-2.873
OH-	17.007	1.4	-1	(-1)h+, (1)h2o	14.940	13.995	13.027	12.255	11.631	11.284	11.168	11.300
SiF6-2	142.076	3	-2	(-2)h2o, (1)sio2(aq), (4)h+, (6)f-	-27.654	-26.275	-25.220	-24.654	-24.534	-24.919	-25.819	-27.436

Primary Aqueous Species	Molecular Weight (g/mol)	r_{ej}	Charge
H2O	18.015	0.00	0
AlO2-	58.980	1.81	-1
Ca+2	40.078	2.87	2
Cl-	35.453	1.81	-1
F-	18.998	1.33	-1
H+	1.008	3.08	1
HCO3-	61.017	2.10	-1
HFeO2(aq)	88.852	0.00	0
K+	39.098	2.27	1
Mg+2	24.305	2.54	2
Na+	22.990	1.91	1
NO3-	62.005	2.81	-1
SiO2(aq)	60.084	0.00	0
SO4-2	96.064	3.15	-2

APPENDIX II – KINETIC DATA (BSC 2003C)[2]

MINERAL	$k_{+/-}$ (mol m^{-2} s^{-1})[1] at 298.15 K	E_a (kJ/mol)[2]	m[3]	n[3]	Comment [4]
α-Cristobalite SiO_2	3.45×10^{-13}	68.9	1	1	dissolution only
Quartz SiO_2	4.52×10^{-14}	90.1	1	1	dissolution only
Tridymite SiO_2	3.45×10^{-13}	68.9	1	1	dissolution only
Amorphous silica SiO_2	7.32×10^{-13}	60.9	1	1	dissolution
	1.0×10^{-10}	50	4.4	1	precipitation
Opal-proxy SiO_2	7.32×10^{-13}	60.9	1	1	dissolution only
Microcline = K-spar $KAlSi_3O_8$	1.78×10^{-13}	36	1	1	reversible
Albite-low $NaAlSi_3O_8$	7.08×10^{-13}	67.7	1	1	reversible
Anorthite $CaAl_2Si_2O_8$	3.16×10^{-12}	67.7	1	1	dissolution only
Illite $K_{0.5}(Mg_{0.22}Al_{1.78})(Si_{3.72}Al_{0.28})O_{10}(OH)_2$	2.0×10^{-14}	58.6	1	1	reversible
Smectite-Ca $Ca_{0.145}(Mg_{0.26}Al_{1.74})(Si_{3.97}Al_{0.03})O_{10}(OH)_2$	2.0×10^{-14}	58.6	1	1	reversible
Smectite-Mg $(Mg_{0.405}Al_{1.74})(Si_{3.97}Al_{0.03})O_{10}(OH)_2$	2.0×10^{-14}	58.6	1	1	reversible
Smectite-Na $Na_{0.29}(Mg_{0.26}Al_{1.74})(Si_{3.97}Al_{0.03})O_{10}(OH)_2$	2.0×10^{-14}	58.6	1	1	reversible
Sepiolite $Mg_2Si_3O_{7.5}OH \cdot 3H_2O$	2.67×10^{-14}	58.6	1	1	reversible

---

[2] Note: References and supporting information can be supplied as an electronic file.

Kinetic Data (continued)

MINERAL	$k_{+/-}$ (mol m^{-2} s^{-1})[1] at 298.15 K	E_a (kJ/mol)[2]	m[3]	n[3]	Comment [4]
Kaolinite $Al_2Si_2O_5(OH)_4$	1.0×10^{-13}	7.1 ($\pm$ 2.5)	1	1	reversible
Heulandite $Ca_{0.33}K_{0.04}Na_{0.1}$ $(Al_{0.8}Si_{2.8}O_{7.2}) \cdot 2.6H_2O$	5.66×10^{-13}	58.0	1	1	dissolution
Clinoptilolite $Ca_{0.28}K_{0.08}Na_{0.04}$ $(Al_{0.68}Si_{2.92}O_{7.2}) \cdot 2.6H_2O$	2.37×10^{-13}	58.0	1	1	reversible
Stellerite $Ca_{0.39}Na_{0.01}(Al_{0.79}Si_{2.81}O_{7.2})$ $\cdot 2.8H_2O$	5.66×10^{-13}	58.0	1	1	reversible
Mordenite $Ca_{0.15}Na_{0.21}K_{0.09}(Al_{0.6}Si_3O_{7.2})$ $\cdot 2.2H_2O$	5.66×10^{-13}	58.0	1	1	reversible
Calcite	1.60×10^{-6}	48.1	1	1	reversible
$CaCO_3$	equilibrium	NA	NA	NA	local equilibrium
Gypsum $CaSO_4 \cdot 2H_2O$	equilibrium	NA	NA	NA	local equilibrium
Fluorite CaF_2	1.22×10^{-7}	0.0	1	2	reversible
Hematite Fe_2O_3	equilibrium	NA	NA	NA	local equilibrium
Goethite FeOOH	equilibrium	NA	NA	NA	local equilibrium
Glass (vitrophyre)	7.72×10^{-15}	91.0	1	1	dissolution only

NOTES: (1) $k_{+/-}$: dissolution/precipitation rate constants at 298.15 K.
(2) E_a: Activation energy.
(3) Exponents m and n in Equations 7-1 and 7-3.
(4) "dissolution only" means precipitation of this mineral is not allowed, "reversible" indicates the same precipitation and dissolution rate apply.

Appendix B

**Meeting Summaries for Task Force Meetings in
Kunming, China, February 20, 2005
Berkeley, CA, July 21-22, 2005
Ottawa, Canada, October 4, 2005**
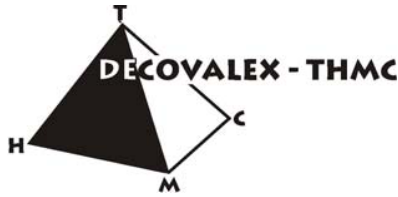
DECOVALEX-THMC
TASK D Meeting Summary

Harbour Plaza Hotel, Kunming, China
Sunday, February 20, 8:45 am – 4 pm

Participants

Task Force Lead:

DOE: Deborah Barr, deborah_barr@ymp.gov
Jens Birkholzer, jtbirkholzer@lbl.gov

Research Teams:

BGR: Mingliang Xie, mingliang.xie@uni-tuebingen.de
Wenqing Wang, wenqing.wang@uni-tuebingen.de

JNC: Yoshihiro Oda, oda@tokai.jnc.go.jp
Masakazu Chijimatsu, mchiji@hazama.co.jp

CAS: Quansheng Liu, liuqs@whrsm.ac.cn
Chengyuan Zhang, zhangcy999whrsm@21cn.com
Xiaoyan Liu, liuxy_whrsm@hotmail.com

DOE: Jonny Rutqvist, jrutqvist@lbl.gov
Eric Sonnenthal, elsonnenthal@lbl.gov

Funding Organization, DECOVALEX Representatives, and Others:

BGR: Hua Shao, shao@bgr.de
Thomas Nowak, thomas.nowak@bgr.de

KTH: Lanru Jing, lanru@kth.se
Ove Stephansson, ove@gfz-potsdam.de
Ivars Neretnieks, niquel@ket.kth.se

LBNL: Chin-Fu Tsang, cftsang@lbl.gov

BRIUG: Ju Wang, wangju98@163.net
Honggang Zhao, hgz72@sohu.com
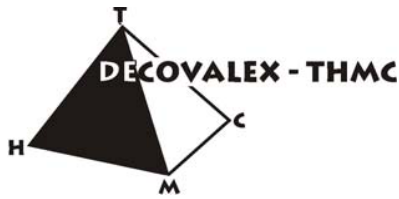
Meeting Summary

The Task Force Meeting on Task D started with a general presentation of Jens Birkholzer on Task D and the expectations on the meeting, followed by technical presentations by various research teams in THM and THC modeling, and finalized with a discussion on technical and organizational issues. The various presentations are provided on the DECOVALEX web site.

Presentations on THM Modeling

Presentation by Wenqing Wang, BGR, "D_THM1 Analysis"

Dr. Wang presented work conducted by the BGR team on modeling the Sub-Task THM1 (bentonite-filled drift in saturated crystalline rock). He explained the conceptual model, the code development (Geosys/Rockflow), model simplifications, and provided results for the postclosure case (bentonite swelling is not explicitly modeled, but simplified with boundary condition). Model results were not provided to other research teams prior to meeting so that comparison was not immediately possible.

Summary Status:
Model development finalized for D_THM1 problem
Preliminary D_THM1 simulation results available

Technical Discussion Points:
Heat power boundary condition not consistent with task definition
Horizontal and vertical model extent not consistent with task definition (i.e., same heat input will lead to higher temperatures and different stress conditions compared to other teams)

Next Work Steps Suggested by Wenqing Wang:
Rerun THM1 simulation with adjusted heater power boundary condition
Move into modeling of D_THM2

Further Recommendations by Task Force Lead:
Adjust model extent in D_THM1 to allow comparison with other teams
Send results from revised model to all other teams for comparison as soon as they are available

Presentation by Chengyuan Zhang, CAS, "THM Simulation on FEBEX and YMP DST Conception Model"

Dr. Zhang presented work conducted by the CAS team on modeling the Sub-Tasks THM1 (bentonite-filled drift in saturated crystalline rock) and THM2 (open drift in unsaturated volcanic rock). He explained the conceptual model with governing equations, the code development (using a combination of Matlab and FEMLAB), and presented
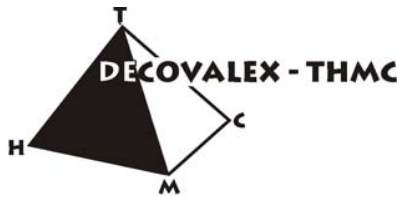
model results for both Sub-Tasks. All model stages such as initial conditions prior to excavation, excavation, buffer installation, and post-closure were considered. For D_THM1, preliminary comparison with LBNL results indicated good overall agreement, but some differences in peak temperature and pre-closure drying. Task D_THM2 was simulated with a multi-phase flow representation so that unsaturated flow could be considered. The fractured porous rock was simplified using a single continuum model. Again, comparison with LBNL indicated good overall agreement with minor differences in peak temperature and peak stress near the drift.

Summary Status:
Model development finalized for D_THM1 problem
D_THM1 simulation results available
D_THM2 simulation results for single continuum model available

Technical Discussion Points:
In the D_THM1 case, there was no bentonite drying in the model results. This indicates that the evaporative potential of the increased temperatures is not taken into account in the model (evaporation by vapor diffusion in the direction of smaller temperatures leads to drying even though the temperatures remain below boiling).
That the bentonite is not drying may also cause a difference in the peak temperature between CAS and LBNL. As the bentonite dries, the thermal conductivity decreases which may explain the higher peak temperature in the LBNL results.

Next Work Steps Suggested by Chengyuan Zhang:
Finalize comparison with other teams and resolve discrepancies by possibly adjusting modeling runs
More benchmark testing
Develop dual-continuum modeling for D_THM2
Move forward to more complex conceptual models including fracture network reconstruction with fracture-index kriging and multiple-point geostatistics (Modeling Phase 2)

Further Recommendations by Task Force Lead:
Check for vapor diffusion in the model
Send results from revised model to all other teams for comparison as soon as they are available

Presentation by Yoshihiro Oda, JNC, "THMC Model Developments"

Dr. Oda presented work conducted by the JNC team on the development of a fully coupled THMC model that can be used to study the Sub-Tasks THM1 (bentonite-filled drift in saturated crystalline rock) and THM2 (open drift in unsaturated volcanic rock). He showed a matrix with all the various coupling between T-H-M- and C, explained the necessary features of the code, and introduced the method of coupling the code THAMES for THM with PHREEQC for C, and Dtransu-EL for separate gas and liquid transport.
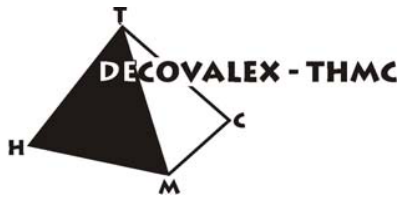
Example results were presented, but are not final as the JNC team found model bugs that need fixing.

Summary Status:
Model development in testing and bug fixing stage
No simulation results on D_THM1 or D_THM2

Technical Discussion Points:
None.

Next Work Steps Suggested by Yoshihiro Oda:
Finalize code development and testing
Conduct simulation runs for D_THM1 and D_THM2

Further Recommendations by Task Force Lead:
Send results from final model to all other teams for comparison as soon as they are available.
Consider possibility of modeling the THM tasks with a previous version on THAMES (not coupled to C) if problems with fully coupled code persist

Presentation by Jonny Rutqvist, DOE, "Modeling of Task D THM Part by DOE/LBNL Research Team, THM1 FEBEX Case and THM2 YMP Case, Step 1 Model Inception"

Dr. Rutqvist presented work conducted by the DOE team on modeling the Sub-Tasks THM1 (bentonite-filled drift in saturated crystalline rock) and THM2 (open drift in unsaturated volcanic rock). He used two separate models with different degrees of complexity, one is TOUGH2-FLAC, the other is ROCMAS. TOUGH2-FLAC has a more complex treatment of multiphase flow, above-boiling temperatures, dual-continuum modeling compared to ROCMAS. Model results were provided for both TOUGH2-FLAC and ROCMAS simulations, and selected results were also compared to the CAS simulations. The different codes gave reasonably accurate results, indicating that simplified model is sufficient in the Model Inception Phase. Some discrepancies between CAS and LBNL results need resolution; saturations have not been compared in detail yet.

Summary Status:
Model development finalized
D_THM1 simulation results available
D_THM2 simulation results available
ROCMAS runs with some boundary problems

Technical Discussion Points:
Simulation results for D_THM1 gave peak temperature of about 108°C, which is not consistent with design criteria. A revised heater power curve with a maximum power of 245 W/m (instead of about 290 W/m) was tested and found to be reasonable. This should be used by all other teams that are working on D_THM1 or D_THC1.
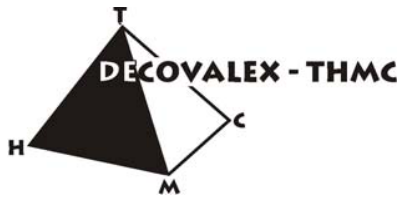
Next Work Steps Suggested by Jonny Rutqvist:
Additional alternative modeling for code-to-code comparison
Move into more complex conceptual models (Modeling Phase 2)

Further Recommendations by Task Force Lead:
Conduct comparison of results from other teams as soon as they are available

Presentations on THC Modeling

Presentation by Mingliang Xie, BGR, "Task D_THC1"

Dr. Xie presented work conducted by the BGR team on modeling the Sub-Task THC1 (bentonite-filled drift in saturated crystalline rock). He explained the conceptual model, the code development which when final is a fully coupled THMC code (Geosys/Rock-flow coupled with PHREEQC), explained a specific method for modeling the swelling of bentonites, and provided results 1-D and 2-D modeling of bentonite chemistry and near-field chemistry. Only the BGR team presented preliminary results for D_THC1 so that comparison with other teams was not possible.

Summary Status:
Model development finalized for D_THC1 problem
Preliminary D_THM1 simulation results available

Technical Discussion Points:
Heat power boundary condition not consistent with task definition (fixed temperature instead of fixed energy). This seems to give rise to numerical problems because the ambient system is instantaneously converted into a "hot" system, with related drastic changes in chemistry.
Horizontal and vertical model extent not consistent with task definition (i.e., same heat input will lead to higher temperatures and different stress conditions compared to other teams).
Simulations were run to about 100 days only, because of above-mentioned numerical problems. Therefore, long-term changes in chemistry could not be observed yet.
The permeability of the near-field rock was increased compared to the task definition by about one order of magnitude (from 10^{-17} m^2 to 8×10^{-17} m^2), to provide for more efficient gas-pressure release. This may be a problem related to the simplified model setup in Phase 1 (Model Inception Phase), where the presence of fractures is ignored.

Next Work Steps Suggested by Mingliang Xie:
Revised modeling of D_THC1
Move focus on heat effect on geochemical system in fractured rock
Add capability of modeling high-temperature chemistry and two-phase flow for D_THC2

Further Recommendations by Task Force Lead:
Send results from revised model to all other teams for comparison as soon as they are available
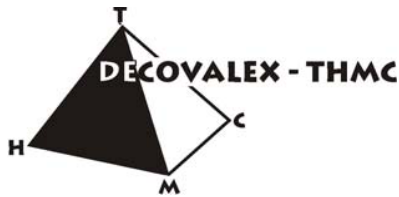
Presentation by Eric Sonnenthal, DOE, "Task D THC1 and THC2"

Dr. Sonnenthal presented the status of work conducted by the DOE team on the Sub-Tasks THC1 (bentonite-filled drift in saturated crystalline rock) and THC2 (open drift in unsaturated volcanic rock). For D_THC1, he explained the primary objectives of the task, listed the important processes to capture, and spent some time on giving the rationale for the task definition parameter choices. He also pointed out that there is more interaction needed between the research teams to define some conceptual model choices for the first phase of D_THC1 modeling. For D_THC2, he also gave an introduction into objectives, processes, task definition, and model setup, and then presented results from the current Yucca Mountain THC prediction model. The model setup is more complex in terms of geometry and geologic layering, but otherwise fairly representative for the D_THC2 task.

Summary Status:
No model results yet for D_THC1
Model result for problem setup similar to Task D_THC2 available (not identical, though)

Technical Discussion Points:
Consistent thermodynamic and kinetic data sets and modeling approaches need to be worked out for Phase 1 in D_THC1 (Model Inception Work). Unsaturated hydrologic properties for the Kunigel V1 bentonite must be added to the task definition.
Task D_THC2 is better defined, but consistent approaches needed to capture the dual-permeability aspects of the system and the two-phase behavior.

Next Work Steps Suggested by Eric Sonnenthal:
Start modeling of D_THC1
Revised modeling of D_THC2 to reproduce exactly the task specifications

Further Recommendations by Task Force Lead:
Send results from revised model to all other teams for comparison as soon as they are available

Presentation by Yoshihiro Oda, JNC, "In-room THMC COUPLE Experiment"

Dr. Oda presented the status of experimental and modeling analysis conducted for the in-room COUPLE experiment. Modeling was conducted to compare observed temperatures and water contents. Data from various techniques to understand chemical changes in the buffer were presented (e.g., x-ray diffraction, scanning electron microscope, etc.). In general, the experimental time was too short to observe significant changes in the bentonite composition. Therefore, a new longer experiment is planned at JNC. How the COUPLE data can be used in support of Task D is not defined yet. With respect to modeling the Sub-Tasks D_THC1 and D_THC2, a coupled THMC code is currently being developed and tested (see Dr. Oda's first talk).

Summary Status regarding Task D_THC:
No simulation results yet for THC modeling (work in progress on debugging code)
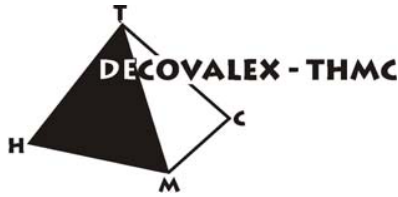
Technical Discussion Points:
None.

Next Work Steps Suggested by Yoshihiro Oda:
Start modeling of D_THC1 and D_THC2 after finalizing code development

Further Recommendations by Task Force Lead:
Send results from revised model to all other teams for comparison as soon as they are available

Summary and Discussion Items

A.   Technical Issues

1. Progress of Work

Since the last workshop in Utrecht, there was good progress by all research teams participating in Task D. All teams are in the model inception phases.

Regarding THM: Three teams presented results for D_THM1, two teams for D_THM2. Initial comparison revealed some need for model setup changes (i.e., boundary conditions, model domain, etc.), but generally reasonable agreement.

Regarding THC: One team presented preliminary results for D_THC1, one team for D_THC2. No comparison between teams yet. More code development needed by most research teams.

2. Changes and Additions to Task Definition: Heater Power

The heater power in Task D_THM1 and D_THM2 should be set to a maximum power of 245 W/m, because otherwise the maximum temperature may end up above the boiling point of water. The time-dependent curve given in the Task Definition (Section 6.3.1) should thus be adjusted by assuming a waste package gap of 1.5 m instead of 1 m.

3. Changes and Additions to Task Definition: Processes

Ivars Neretnieks suggests analyzing the impact of local water flow from the formation into the bentonite from flowing fractures, and the mechanical/chemical response to that (D_THM1 and D_THC1). This interesting question will be addressed in Modeling Phase 2, when the presence of fractures is to be considered by the research teams. He also suggests evaluating the importance of diffusive transport of air in the liquid phase, as a possible mechanism to release the trapped air in the bentonite buffer (D_THM1 and D_THC1). Nitrogen may be required to be added to the list of species evaluated in D_THC1.
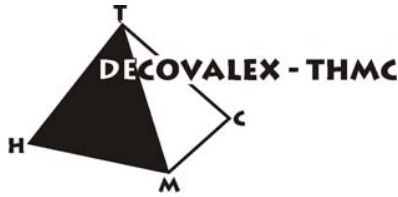
4. Changes and Additions to Task Definition: Conceptual Model for Task D_THC1

After some discussion, the groups confirmed the original choice of the Kunigel V1 bentonite. Addition of unsaturated hydrologic properties for Kunigel V1 to the task definition is still required. Some agreement will still need to be made regarding a consistent set of thermodynamic and kinetic data.

5. Changes and Additions to Task Definition: Revised Task Definition Report

The report describing the task definition (current status December 2004) will be revised by the Task Lead to reflect the changes/additions discussed in the workshop. This will be done till end of April 2005. Main points are (1) revising the heater output for Task D_THM1 and D_THC1, (2) adding the unsaturated hydrologic properties of the Kunigel V1 bentonite, (3) correcting typos.

B. Participation/Status/Organization/Reporting

1. Sub-Task Participation

All teams, except for CAS, committed to participate in all Sub-Tasks D_THM1, D_THM2, D_THC1, and D_THC2. Currently, CAS focuses on the THM tasks only.

2. General Schedule till next Workshop (probably early October in Canada)

THM tasks: Finalize Phase 1 (Model Inception Phase) and move into Phase 2 till the next workshop. Task Lead will provide necessary data, reports, and other information for Phase 2 on the DECOVALEX website till end of April 2005.

THC tasks: Finalize major fraction of Phase 1 work

It is expected that the ongoing research work during the next 6 to 7 months will be shared regularly and interactively with all other research teams via email, to facilitate continuous interaction/comparison of ideas and results. For example, research results that need to be revised in response to the Task Force Meeting in Kunming should be sent out during the next few weeks.

Progress reports will be provided by all research teams till the end of August 2005 at the latest, about 1 month before the next workshop. These should include description of the model and modeling results. The reports serve two purposes: (1) to enable comparison of research results prior to the workshop and preparation of comparative graphs, (2) to enable the Task Lead to write an Interim Summary Report for Task D that is due shortly after the next workshop.
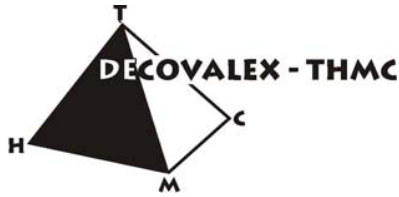
3. Interactive Exchange of Ideas

The Task Lead brings up the concept of a "Chat-Room"-Mentality between the research teams, which is to be understood as exchanging questions, ideas, suggestions, and results between the entire Task D group per email address list, as a means to promote in-depth interaction not just at biannual workshops, but continuously. Research team members are

strongly encouraged to use this interaction vehicle without hesitation. The Task Lead will send out regular reminders as to promote such interaction.

4. Comparison of Results

Research teams that send simulation results out for comparison are encouraged to not just deliver plots and viewgraphs, but also the data behind them. For example, for a pressure evolution plot, please also provide the underlying time versus pressure data so that comparative plots can be made.

All such plots should follow the output specifications defined in the Task D Definition, Section 6.5 and 7.5.
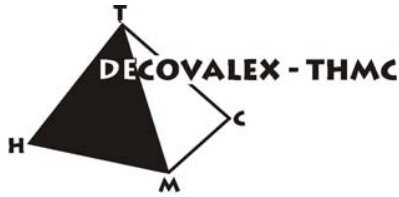
DECOVALEX-THMC
TASK D Meeting Summary

Lawrence Berkeley National Laboratory, Berkeley, CA, USA
July 21 and 22, 2005, 9:30 to 5 pm

Participants

Task Force Lead:

DOE: Deborah Barr, deborah_barr@ymp.gov
            Jens Birkholzer, jtbirkholzer@lbl.gov

Research Teams:

BGR: Mingliang Xie, mingliang.xie@uni-tuebingen.de

JNC: Masakazu Chijimatsu, mchiji@hazama.co.jp

CAS: Could not attend, but sent presentation on status of THM work

DOE: Jonny Rutqvist, jrutqvist@lbl.gov
            Eric Sonnenthal, elsonnenthal@lbl.gov

Funding Organization, DECOVALEX Representatives, and Others:

BGR: Hua Shao, shao@bgr.de

KTH: Robert Zimmermann, r.w.zimmerman@imperial.ac.uk

LBNL: Chin-Fu Tsang, cftsang@lbl.gov

CNSC: Son Nguyen, Nguyens@cnsc-ccsn.gc.ca

Meeting Summary

The Task Force Meeting on Task D started with welcome notes by Chin-Fu Tsang and Jens Birkholzer, followed by presentations and discussions on technical and organizational issues regarding THM (Thursday, July 21, 2005) and THC (Friday, July 22, 2005) modeling. The various presentations are provided on a LBNL web site at
http://esd.lbl.gov/people/kavina/DECOVALEX/Presentations/
and will soon be uploaded on the usual DECOVALEX web site as well.

1
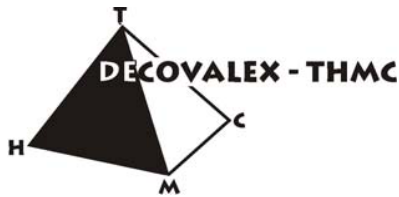
Day 1: Presentations and Discussions on THM Modeling

Introduction to THM Presentations by Jens Birkholzer

Jens Birkholzer introduced different points of discussion and stated the expectations for the meeting regarding THM modeling:

- Status of work of different teams and comparative evaluation with the goal of finalizing Phase 1 (Model Inception Phase) of D_THM

- Start-up discussion for Phase 2 (prediction of THM induced property changes; various conceptual models) of D_THM and presentation of background information/material

- Reporting schedule with the goal of having status reports of each individual team by August 15

- Possible abstracts for GeoProc 2005

- Next task force meeting

Presentation by Jonny Rutqvist, DOE, "Modeling of Task D THM Part by DOE/LBNL Research Team, THM1 FEBEX Case and THM2 YMP Case, Step 1 Model Inception"

Summary Status:
Model development finalized
Two codes used for code-to-code comparison (TOUGH2 = multiphase plus geomechanical code; ROCMAS = single phase + geomechanical code)
D_THM1 simulation results available for both codes (multi-phase simulation of liquid and gas with TOUGH2; single phase liquid with ROCMAS)
D_THM2 simulation results available for both codes (multi-phase dual-continuum with TOUGH2; single continuum with ROCMAS)
Reasonable agreement between two codes; some differences in temperature evolution

Technical Discussion Points:
Introduced bentonite TH properties that should be used by all teams modeling D_THM1, in particular characteristic curves (see Appendix).
Ran excavation step till steady-state (zero-pressure assumption in drift), which leads to significant drainage of the rock. Better assume a 30-year excavation period (see Appendix).

Next Work Steps Suggested by Jonny Rutqvist:
Make final changes and report adjustments till August 15, 2005
Move into more complex conceptual models (Modeling Phase 2)
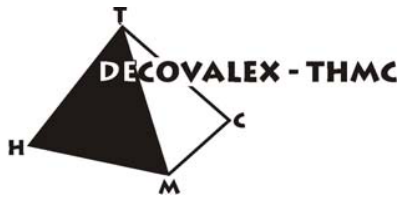
Presentation by Mingliang Xie, BGR, "Progress on D_THM Analysis"

Summary Status:
Model development finalized for D_THM1 problem
Code GeoSys/Rockflow is a single phase geomechanical code
D_THM1 simulation results available

Technical Discussion Points:
Characteristic curves for D_THM1 are different from Jonny's curves (very slow resaturation of bentonite)
Heat curve different from suggested heat curve (all time-dependent values need to be scaled down instead of deleting the first value)
Horizontal initial stress too small (due to typo in task description)
Vapor diffusion not included in code (because of single phase representation, diffusion must be accounted for as temperature-dependent process)
Pressure-induced change in pore space is possibly accounted for twice (by solving for THM changes as well as by assigning a storativity term)

Next Work Steps Suggested by Mingliang Xie:
Rerun D_THM1 simulation with suggested modifications and report till August 15, 2005
Move into modeling of D_THM2, including extension of code to multi-phase flow

Presentation by Masakazu Chijimatsu, JNC, "Progress of Task D (THM) by JNC Team" (together with Yoshihiro Oda)

Summary Status:
THM modeling conducted with code THAMES, a single phase geomechanical code
D_THM1 results are not finished yet, but may be available till August 15, 2005
D_THM2 results were presented, using a single phase single-continuum representation (with single-continuum parameters similar to previous DECOVALEX DST test case)

Technical Discussion Points:
Horizontal stresses for D_THM2 are much smaller than those by Jonny Rutqvist
Hydrological behavior in D_THM2—with boiling of rock water, vapor transport, and subsequent resaturation—is different from TOUGH2 results, because of single continuum approach (comparison should therefore focus on thermal and mechanical changes)
Choice of single continuum properties should be adjusted according to new specifications (see Appendix)

Next Work Steps Suggested by Masakazu Chijimatsu:
Rerun D_THM2 simulation and report till August 15, 2005
Possibly run D_THM1 simulation till August 15, 2005
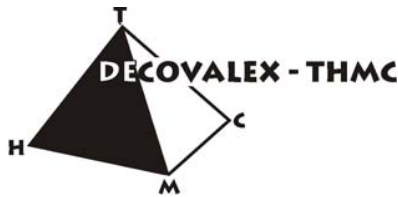
Presentation by Chengyuan Zhang, CAS, "THM Simulation based on FEBEX and YMP Inception Model"
(presentation was given by Jonny Rutqvist, since Chengyuan Zhang could not attend)

Summary Status:
Model development finalized for D_THM1 and D_THM2
D_THM1 simulation results were presented, using single phase + geomechanical code
D_THM2 simulation results were presented, using single phase, single continuum + geomechanical code
Some plots included direct comparison with Jonny Rutqvist's results, making comparative evaluation easy

Technical Discussion Points:
Bentonite properties used in D_THM1 are different from those used by other teams
Bentonite drying and resaturation has similar general behavior compared to Jonny Rutqvist's result, but is much slower (indicates that vapor diffusion is correctly accounted for, but bentonite properties are different)
Probably due to slow resaturation, stress evolution in bentonite is much slower too
Single continuum properties chosen for D_THM2 should be adjusted (see Appendix)
Latent heat of vaporization used for thermal capacity curve is too small (caused by typo in task description)

Next Work Steps Suggested by Chengyuan Zhang:
NA

General Discussion THM: Modeling Discrepancies

Discrepancies between the different teams modeling D_THM were evaluated in a team effort by going through some of the key plots of THM results. It was found that often these discrepancies were caused by differences in rock properties and boundary conditions. A list of necessary clarifications and revisions to the DECOVALEX THM Task D description was generated and sent out via email immediately after the workshop. For completeness, this list of THM clarifications and revisions is given in the Appendix. The modifications will soon be incorporated into a revised version of the task description document. The following items are covered:

- Definition of bentonite properties in D_THM1
- Characteristic curves for D_THM1
- Initial horizontal stress for D_THM1
- Finite excavation time in D_THM1
- Heat generation in D_THM1
- Definition of continuum properties in D_THM2
- Latent heat of vaporization in D_THM2
- Bulk density of rock mass in D_THM2
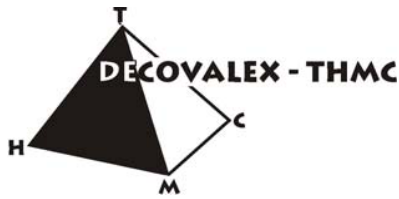
General Discussion THM: Dual Continuum Modeling of D_THM2

It is recognized that most of the research teams working on D_THM2 (Yucca Mountain case) will *not* be using a dual-continuum model for representing the flow processes in the unsaturated fractured porous rock. A dual continuum model is based on the continuum concept, but uses two separate, overlapping continua for fractures and matrix. At each location, there are two nodes (or volumes) representing the fractures and the matrix, respectively, each having a pressure, saturation, temperature, or stress value. Thus local disequilibrium between fractures and matrix can be modeled without explicitly accounting for all individual fractures and matrix blocks. This allows considering the hydrologic properties and conditions of fractures and matrix with their vastly differing permeabilities and moisture retention characteristics. While dual continuum models are the best choice for D_THM2 (except for using discrete fracture-matrix continuum models or hybrid models), they require significant code development.

Alternatively, as pointed out in the task description document, research teams may use single continuum models. This requires definition of single continuum properties (in order to represent the bulk fractured porous rock), as given in the Appendix. The single continuum properties chosen in the Appendix are mostly similar to the matrix properties, acknowledging the fact that the hydrologic situation at Yucca Mountain at ambient state is mostly governed by the matrix properties. (Ambient percolation is very small, so that fractures are dry and non-conductive). However, as the near-drift rock is heated up and significant flux perturbation occurs (with the fractures becoming important flow conduits for vapor and liquid), the single continuum properties are not very good. Thus, a simple single continuum model for Yucca Mountain will not give adequate flow results for the heated situation, while the thermal and the mechanical response are reasonably well captured.

For teams that strive for a better hydrological response but want to avoid dual continuum modeling, we recommend the so-called effective continuum model (ECM) after Pruess et al. (Water Resources Research, 1990, Vol 26, No. 6, pp. 1249-1261). An effective continuum model allows accounting for the different hydraulic characteristics of fractures and matrix, but assumes a local THM equilibrium between fractures and matrix at all times. For systems that are not too dynamic in nature, the ECM model gives quite adequate flow results. We will send out information about the ECM and its possible implementation into existing single continuum codes in separate documents.

General Discussion THM: Start of Phase 2 Modeling

Research teams are encouraged to move forward into Phase 2 modeling after finalizing Phase 1 of the D_THM studies with a good agreement with other the teams. Goals and materials for Phase 2 modeling were presented by Jens Birkholzer. Phase 2 modeling includes prediction of THM property changes with conceptual models chosen by the
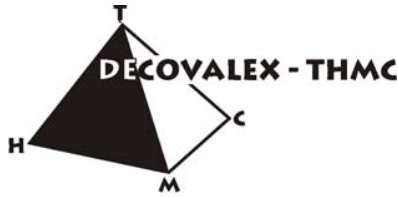
different research teams, sensitivity analysis with respect to THM property changes plus uncertainty analysis, application of alternative conceptual models for fractured rock (i.e., discrete, vs. continuum), and development of model data based on various reports and site data instead of using pre-defined values. Reports that may be used for D_THM1 are listed below, together with web sites where they can be retrieved.

Reference	Comment
Keusen H.R., Ganguin J., Shuler P. and Buletti M. (1989). Grimsel Test Site: Geology NAGRA NTB 87-14E, FEb 1989.	Download from LBNL web site: http://esd.lbl.gov/people/kavina/DECOVALEX/THM1_Phase2_Docs/
Amiguet J.-L. (1985). Grimsel Test Site. Felskennwerte von intaktem Granit. Zusammenstellung felsmechanisher Laborresultate diverse granitische Gesteine. NAGRA, NIB 85-05, Sep. 1985.	Download from LBNL web site: http://esd.lbl.gov/people/kavina/DECOVALEX/THM1_Phase2_Docs/
Pardillo J., Campos R. and Guimera J. (1997). Caracterizacion geologica de la zone de ensayo FEBEX (Grimsel – Suiza). CIEMAT, 70-IMA-M-2-01, May 1997.	Download from LBNL web site: http://esd.lbl.gov/people/kavina/DECOVALEX/THM1_Phase2_Docs/
Pardillo J. and Campos R. (1996). FEBEX-Grimsel Test Site (Switzerland). Considerations with respect to the fracture distribution. CIEMAT, 70-IMA-L-2l05, Mar. 1996.	Download from LBNL web site: http://esd.lbl.gov/people/kavina/DECOVALEX/THM1_Phase2_Docs/
Guimera J., Carrera J., Marinez L., Vazquez E., Ortuno F., Fierz T., Bulher C., Vives L., Meier P., Median A., Saaltink M., Ruiz B. and Pardillo J. (1998). FEBEX Hydrogeological characterization and modelling. UPC, 70-UPC-M-0-1001, Jan 1998.	Download from LBNL web site: http://esd.lbl.gov/people/kavina/DECOVALEX/THM1_Phase2_Docs/
Fujita T., Sugita Y., Chijimatsu M. and Ishikawa (1996). Mechanical properties of fracture. Power Reactor and Nuclear Fuel Development Corporation (PNC), Technical note 06-95-06.	Download from LBNL web site: http://esd.lbl.gov/people/kavina/DECOVALEX/THM1_Phase2_Docs/
DECOVALEX III (2000). Task 1. Modeling of FEBEX in situ test. Part A: Hydromechanical modeling of the rock.	Download from LBNL web site: http://esd.lbl.gov/people/kavina/DECOVALEX/THM1_Phase2_Docs/
DECOVALEX III (2001). Task 1. Modeling of FEBEX in situ test. Part B: Thermo-hydro-mechanical analysis of the bentonite behaviour.	Download from LBNL web site: http://esd.lbl.gov/people/kavina/DECOVALEX/THM1_Phase2_Docs/
Alonso et al. (2004). Final report of DECOVALEX III, Task1: FEBEX in situ test. SKI report expected during 2004.	Download from Decovalex website: Login and go to Documents / Reports from DECOVALEX III and BENCHPAR / Final reports / **Task 1** /

Reports that may be used for D_THM2 are listed below, together with web sites where they can be retrieved.

Reference	Comment
BSC (Bechtel SAIC Company) 2003a. *Drift Degradation Analysis*. ANL-EBS-MD-000027 REV 02. Las Vegas, Nevada: Bechtel SAIC Company.	Download from: http://ocrwm.doe.gov/documents/amr/36086/index.htm
BSC (Bechtel SAIC Company) 2003b. *Calibrated Properties Model*. MDL-NBS-HS-000003 REV 01. Las Vegas, Nevada: Bechtel SAIC Company. ACC: DOC.20030219.0001.	Download from: http://ocrwm.doe.gov/documents/amr/41503/index.htm
CRWMS M&O (Civilian Radioactive Waste Management System Management and Operating Contractor) 2000. *Statistical Analysis of Empirical Rock Properties by Lithographic Units*. CAL-GCS-GE-000001 Revc 00. Las Vegas.	Download from LBNL web site: http://esd.lbl.gov/people/kavina/DECOVALEX/THM2_Phase2_Docs/
CRWMS M&O (Civilian Radioactive Waste Management System Management and Operating Contractor) 1997. *Yucca Mountain Site Geotechnical Report*. B00000000-01717-5705-00043 REV 01. Two volumes. Las Vegas, Nevada.	Download from LBNL web site: http://esd.lbl.gov/people/kavina/DECOVALEX/THM2_Phase2_Docs/
CRWMS M&O (2000). Fracture Geometry Analysis for the Stratigraphic Units of the Repository Host Horizon. ANL-EBS-GE-000006 REV 00. Las Vegas, Nevada.	Download from LBNL web site: http://esd.lbl.gov/people/kavina/DECOVALEX/THM2_Phase2_Docs/
Datta et al. (2004). DECOVALEX III, Task 2, Final Report. (SKI report expected during 2004).	Download from LBNL web site: http://esd.lbl.gov/people/kavina/DECOVALEX/THM2_Phase2_Docs/
Hoek E., Carranza-Torres C. and Corkum B., (2002). Hoek-Brown Failure Criterion – 2002 Edition 5th North American Rock Mechanics Symposium and 17th Tunnelling Association of Canada Conference: NARMS-TAC 2002, July 7-10 University of Toronto, Toronto, Ontario, Canada.	Download from LBNL web site: http://esd.lbl.gov/people/kavina/DECOVALEX/THM2_Phase2_Docs/
Mongano G.S., Singleton W.L., Moyer T.C., Beason S.C., Eatman G.L.W. Albin A.L. and Lung R.C. (1999) Geology of the ECRB Cross Drift – Exploratory Studies Facility, Yucca Mountain Project, Yucca Mountain, Nevada. Denver Colorado U.S. Geological Survey.	Download from LBNL web site: http://esd.lbl.gov/people/kavina/DECOVALEX/THM2_Phase2_Docs/
CRWMS M&O (1998). G*eology of the Exploratory Studies Facility Topopah Spring Loop*. BAB000000-01717-0200-00002 REV 01. Las Vegas, Nevada	Download from LBNL web site: http://esd.lbl.gov/people/kavina/DECOVALEX/THM2_Phase2_Docs/
Olsson W.A. and Brown S. (1995). *Mechanical properties of fractures from drill holes UE25-NRG-4, USW-NRG-6, USW-NRG-7, and USW-SD-9 at Yucca Mountain, Nevada*. Sandia National Laboratories Technical Report, Sand 95-1736. Albuquerque New Mexico, Sandia	Download from LBNL web site: http://esd.lbl.gov/people/kavina/DECOVALEX/THM2_Phase2_Docs/
Brown S.R. (1985) Simple mathematical model of a rough fracture. J. Geophys. Res. 100, 5941–5952.	Download from LBNL web site: http://esd.lbl.gov/people/kavina/DECOVALEX/THM2_Phase2_Docs/

General Discussion THM: Reporting Schedules

Revised simulation results from the Phase 1 modeling work are expected from each team **at the latest by August 15**, summarized in a status report that also includes specifics on the chosen codes and conceptual models. We will use the August 15 reports as the basis for a summary status report for Task D, with detailed comparison between teams, to be completed by September 15. For conducting such comparison, we will need your selected **simulation results in tabular form (Ascii or Excel)**. It is very important to stick to the proposed schedule so that we have time to conduct a meaningful comparison.

General Discussion THM: GeoProc 2006

Abstracts for GeoProc 2006 in Nanjing, China, are due by November 30, 2005. Research teams are encouraged to start planning their presentations and papers for this workshop, which will have a specific section on DECOVALEX. There will one DOE presentation on the definition and goal of task D_THM, and there will be joint papers summarizing the comparative evaluation of D_THM1 and D_THM2, respectively, by all research teams and led by the LBNL/DOE team. In addition, each research team should think about individual papers with interesting research topics related to the DECOVALEX effort. GeoProc abstract planning to be concluded at the Ottawa workshop.

General Discussion THM: Next Task Force Meetings

The next Task D meeting will be held in conjunction with the DECOVALEX workshop in Ottawa, Canada. The task force meeting will be on October 3, 2005, one day prior to the first day of the DECOVALEX workshop.

Between the Ottawa and the Nanjing workshops, there will probably be another task force meeting for Task D, most likely in February 2006. Location to be decided in Ottawa.
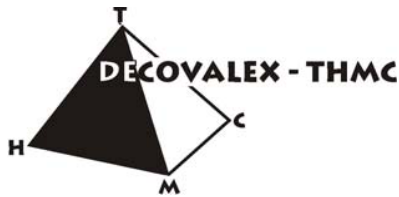
Day 2: Presentations on THC Modeling

Introduction to THC Presentations by Jens Birkholzer

Jens Birkholzer introduced different points of discussion and stated the expectations for the meeting regarding THC modeling:

- Status of work of different teams (model development and simulation results)
- Discussion of task description with the goal of finalizing all decisions on inputs and data bases for both D_THC1 and D_THC2
- Clarifications and revisions from D_THM discussions relevant for D_THC
- Reporting schedule with the goal of having status reports of each individual team by August 15
- Possible abstracts for GeoProc 2005
- Next task force meeting

Presentation by Eric Sonnenthal, DOE, "Task D THC1 and THC2"

Summary Status:
No model results yet for D_THC1
Model result for problem setup similar to D_THC2 presented, using the reactive transport code TOUGHREACT with a multiphase dual-continuum concept
Comparison with other teams not possible, since so far only team modeling D_THC2

Technical Discussion Points:
Brings up various conceptual model choices that are relevant for THC modeling of the fractured porous rock in the D_THC2 example (many of these specific choices are related to the different THC behavior of fractures versus porous matrix)
Raises question of possible simplifications to the problem to avoid dual continuum modeling (there is consensus, however, that representing the dual continuum behavior is more important in THC than in THM, because correct descriptions of liquid and gas chemistry require correct flux estimates of liquid and gas)
More work needed on dual continuum versus alternative conceptual models

Next Work Steps Suggested by Eric Sonnenthal:
Finalize all task descriptions together with Mingliang Xie from the BGR team in a joint effort immediately after the task force meeting
Start modeling of D_THC1
Revised modeling of D_THC2
Explore possibility of avoiding dual continuum models for D_THC2

9
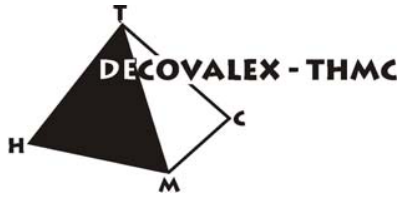
Presentation by Mingliang Xie, BGR, "Task D_THC1"

Summary Status:
Model development finalized for D_THC1 problem
D_THC1 simulation results presented, for up to 100,000 years, using a fully coupled
THMC code (Geosys/Rockflow coupled with PHREEQC) (single phase flow)
Comparison with other teams not possible, since so far only team modeling D_THC1

Technical Discussion Points:
Equilibrium model used for chemical reactions
Bentonite hydrological properties need to be adjusted (see Appendix)

Next Work Steps Suggested by Mingliang Xie:
Finalize all task descriptions together with Eric Sonnenthal of LBNL team in a joint
effort immediately after the task force meeting
Revised modeling of D_THC1
Add capability of modeling high-temperature chemistry and two-phase flow for D_THC2

**Presentation by Masakazu Chijimatsu, JNC, "Progress for Task D (THC) by JNC
Team" (together with Yoshihiro Oda)**

Summary Status regarding Task D_THC:
Development of fully coupled THMC code finalized (single phase flow, PHREEQC for
chemistry)
Results from first test runs presented (problem setup different from D_THC1 or
D_THC2)
Provides measured data of bentonite permeability vs. change in mineral composition
Provides update on ongoing COUPLE experiment (second experiment); experiment will
be finalized end of March in 2006

Technical Discussion Points:
Bentonite permeability correlation with chemical composition can be useful for other
teams

Next Work Steps Suggested by Yoshihiro Oda:
Start modeling of D_THC1 and D_THC2 after code testing finalized
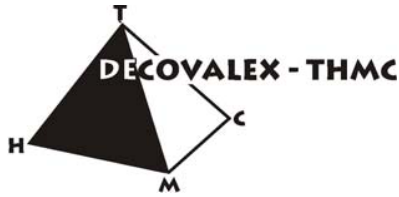
General Discussion THC: Modeling Discrepancies

Modeling discrepancies between THC results could not be evaluated since BGR results were obtained for D_THC1, while LBNL results were obtained for D_THC2.

General Discussion THC: Clarifications and Revisions for THC

After the task force meeting, Eric Sonnenthal of LBNL team and Mingliang Xie of BGR team worked for several days in a joint effort to finalize all task descriptions for D_THC1 and D_THC2. Various clarifications and revisions to D_THC1 and D_THC2 were made. The modifications will soon be incorporated into a revised version of the task description document. The following main items were covered:

D_THC1

- Mineralogy of granite and bentonite (Kunigel V1) revised in D_THC1
- For the Smaland Granite in D_THC1, biotite was split into the annite and phlogopite endmembers, with thermodynamic data from EQ3/6 chosen
- Water chemistry in granite (Litorina Sea) and in bentonite chosen

Mineralogical Abundances in the Smaland Granite (modified from Rhen et al., 1997)

Mineral	Abundance (weight fraction)
Quartz	0.2756
K-Feldspar	0.2724
Plagioclase	0.3964
Annite	0.0489
Phlogopite	0.0067

Mineralogy of the Kunigel-V1 Bentonite (modified from Ochs et al., 2004)

Mineral	Abundance (weight %)
Na-montmorillonite	47.5
Quartz	33.5
K-Feldspar	4.1
Calcite	2.35
Dolomite	2.9
Pyrite	0.6
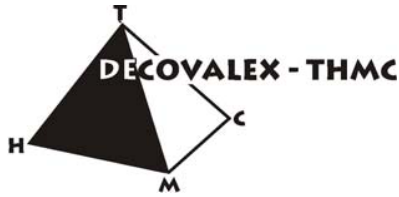
Initial water chemistry in granite and bentonite

Litorina Sea	pH=7.7	
	Mg/liter	Mol/kg H2O
Cl	6500	1.833E-01
Na	3674	1.598E-01
K	134	3.427E-03
Ca	151	3.767E-03
Mg	448	1.843E-02
HCO3	93	1.524E-03
SO4	890	9.265E-03
	Total	4.110E-01
	Charge Balance (%)	1.032E+00
Bentonite	pH=8.4	
	Mol/kg H2O	
Cl	1.500E-05	
Na	3.600E-03	
K	6.200E-05	
Ca	1.100E-04	
Mg	5.500E-05	
HCO3	3.500E-03	
SO4	1.100E-04	
SiO2	3.400E-04	
Total	7.727E-03	
Charge Balance (%)	3.326E+00	

D_THC2

- The full mineral assemblage given in the Task Description was decided to be used in stage 1 because BGR and LBNL can handle this complexity
- Questions still remain on how to handle dual-permeability in BGR code
- Some questions still on use of kinetic mineral-water reactions in PHREEQC

General Discussion THC: Clarifications and Revisions for THM

The clarifications and revisions concerning THM properties, as documented in the Appendix, also apply to D_THC1 and D_THC2.
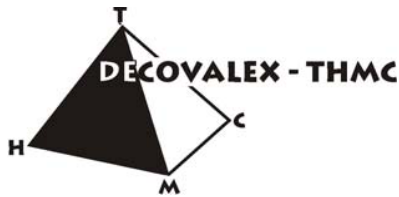
General Discussion THC: Dual Continuum Modeling of D_THC2

It is recognized that most of the research teams working on D_THC2 (Yucca Mountain case) will *not* be using a dual-continuum model for representing the flow processes in the unsaturated fractured porous rock. A dual continuum model is based on the continuum concept, but uses two separate, overlapping continua for fractures and matrix. At each location, there are two nodes (or volumes) representing the fractures and the matrix, respectively, each having a pressure, saturation, temperature, or concentration value. Thus local disequilibrium between fractures and matrix can be modeled without explicitly accounting for all individual fractures and matrix blocks. This allows considering the hydrologic properties and conditions of fractures and matrix with their vastly differing permeabilities, moisture retention characteristics, and geochemical parameters. While dual continuum models are the best choice for D_THC2 (except for using discrete fracture-matrix continuum models or hybrid models), they require significant code development. This raises the question of possible simplifications to the problem to possibly avoid dual continuum modeling. In contrast to THM cases, however, a single continuum model of the fractured rock is not likely to produce reasonable geochemical results, because correct descriptions of liquid and gas chemistry require correct flux estimates of liquid and gas in fractures and matrix blocks. Even an effective continuum model (suggested for THM simulations) may not be sufficient. Thus one of the goals of future research within D_THC2 will be the joint development of simplified, yet realistic models for fracture-matrix representation.

General Discussion THM: Reporting Schedules

A status report on THC modeling progress is expected from each team **at the latest by August 15**, which should include specifics on the chosen codes and conceptual models as well as simulation results. We will use the August 15 reports as the basis for a summary status report for Task D, due by September 15.

General Discussion THM: GeoProc 2006

Abstracts for GeoProc 2006 in Nanjing, China, are due by November 30, 2005. Research teams are encouraged to start planning their presentations and papers for this workshop, which will have a specific section on DECOVALEX. There will one DOE presentation on the definition and goal of task D_THC, and there will be joint papers summarizing the comparative evaluation of D_THC1 and D_THC2, respectively, by all research teams and led by the LBNL/DOE team. In addition, each research team should think about individual papers with interesting research topics related to the DECOVALEX effort. GeoProc abstract planning to be concluded at the Ottawa workshop.

General Discussion THM: Next Task Force Meetings

See THM General Discussion.
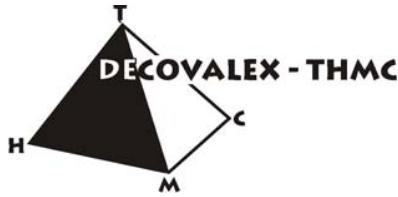
Appendix: Clarifications and Revisions to Task D Description (THM)

Status July 25, 2005; Jens Birkholzer, Deborah Barr, Jonny Rutqvist, Eric Sonnenthal

The 2nd task force meeting for DECOVALEX Task D was held in Berkeley on July 21, and 22, 2005. Comparison of results from the different research teams suggested some clarifications and revisions to the DECOVALEX THMC Task D description (December 2004 Status). Below is a short list of these modifications. The modifications will soon be incorporated into a revised version of the task description document.

1.   Definition of Bentonite Properties in D_THM1 (D_THC1)

Various discrepancies between research teams were a result of using different bentonite properties. In order to have a common basis for bentonite properties, we suggest to use the following properties.

Table 1. Properties of bentonite.

Parameter	Value
Dry density, [kg/m^3]	$1.6 \cdot 10^3$
Porosity, [-]	0.41
Saturated permeability, [m^2]	$2.0 \cdot 10^{-21}$
Relative permeability, k_{rl}	$k_{rl} = S^3$
Moisture swelling coefficient [-]	0.238
Poisson ratio, [-]	0.35
Thermal expan. coeff., [1/°C]	$1.0 \cdot 10^{-5}$
Dry specific heat, [J/kg·°C]	$c_s = 1.38T + 732.5$
Thermal cond., [W/m·°C]	$\lambda_m = 1.28 - \dfrac{0.71}{1 + e^{(S-0.65)/0.1}}$ (with s liquid saturation)
Tortuosity factor for vapor diffusion (accounts for tortuous diffusion paths)	0.8

2.   Characteristic Curves for D_THM1 (D_THC1)

No characteristic curves (moisture retention, relative permeability) were provided in the DECOVALEX THMC Task D description (December 2004 Status). This resulted in
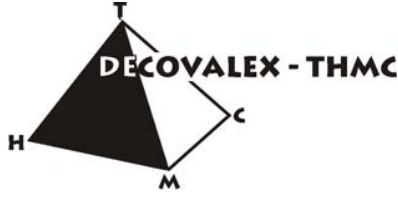
significant differences among research teams (resaturation times). We suggest using the following characteristic curves for the FEBEX bentonite and for the granite rock.

In the FEBEX prject, experimental data of saturation, S_l versus suction, s for FEBEX bentonite have been fitted by means of the van Genuchten expression:

$$S_l = S_{l_0} + (S_{l_{max}} - S_{l_0})\left[1 + \left(s/P_0\right)^{\frac{1}{1-\lambda}}\right]^{-\lambda} \tag{1}$$

or to a modification of this expression that is more suitable for higher values of suction:

$$S_l = S_{l_0} + (S_{l_{max}} - S_{l_0})\left[1 + \left(s/P_0\right)^{1/(1-\lambda)}\right]^{-\lambda}\left[1 - s/P_s\right]^{\lambda_s} \tag{2}$$

where $S_{l\,0}$ and $S_{l\,max}$ are the residual and maximum degree of saturation and P_0 (MPa), P_s (MPa), λ and λ_s are material parameters.

For the FEBEX bentonite, the water retention curve described by the following equation closely match experimental data:

$$S = 0.01 + \left(0.99\right)\left[1 + \left(s/35\right)^{1.43}\right]^{-0.30}\left[1 - s/4000\right]^{1.5} \tag{3}$$

The curve is plotted in Figure 1, green line.

A good match to experimental data at saturation values above about 40% is obtained with the following standard van Genuchten function:

$$S_r = 0.01 + \left(0.99\right)\left[1 + \left(s/30\right)^{1.43}\right]^{-0.30} \tag{4}$$

This is plotted in Figure 1, purple line. In DECOVALEX-THMC Task D THM_1, the retention curve defined in Equation (3) (green line in Figure 1) should be used if possible. If a research team can only use a standard van Genuchten function, the function defined in Equation (4) may be used.

The saturated permeability for the bentonite should be set to $2 \cdot 10^{-21}$ m^2. Relative permeability of the bentonite should be defined by the following expression:

$$k_{rl} = S_l^3 \tag{5}$$

The rock mass should have a water retention curve represented by van Genuchten parameters, $P_0 = 1.47$ MPa and $\lambda = 0.6$ ($\beta = 2.5$). That is:
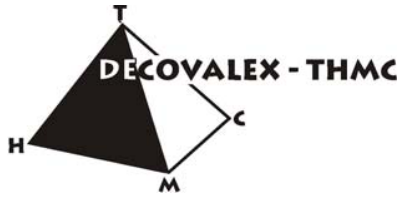
$$S_l = \left[1 + (s/1.47)^{2.5} \right]^{-0.60} \tag{6}$$

where residual saturation is set to 0.0. This function is blue line in Figure 1. The relative permeability for the rock mass is defined by the function:

$$k_{rl} = \sqrt{S_l} \left\{ 1 - (1 - S_l^{1/0.6})^{0.6} \right\}^2 \tag{7}$$

This function is the blue line in Figure 1.
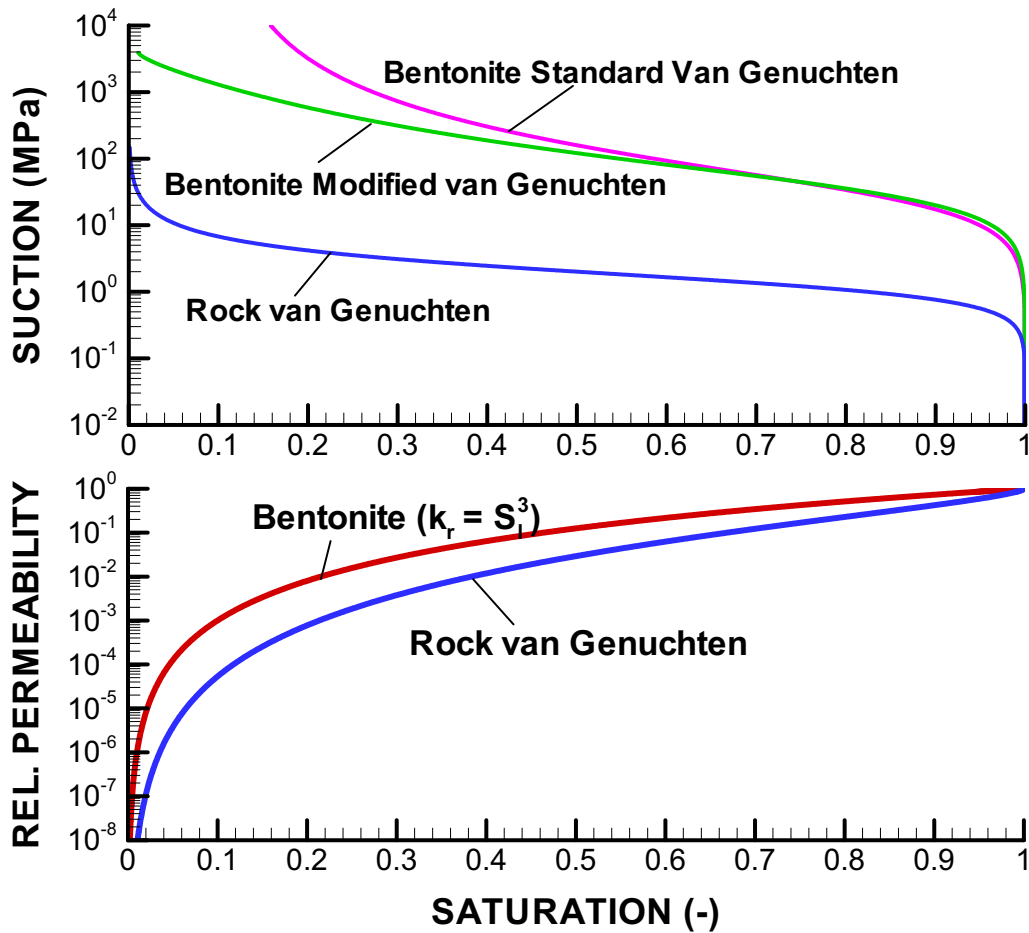
Figure 1. Characteristic Curves for D_THM1 bentonite and granite rock
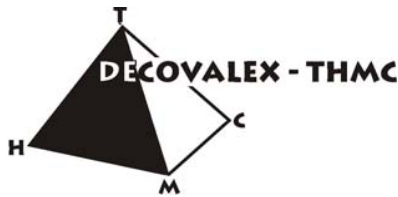
3. Initial Horizontal Stress for D_THM1

The initial horizontal stress in D_THM1, as given on page of the DECOVALEX THMC Task D description (December 2004 Status), is not correct. The text reads as:

"The initial stress is given as σ_h = 0.020·D+0.6 Pa (minimum principal horizontal stress), σ_H = 0.055·D+4.6 Pa (maximum principal horizontal stress)"

While the equations are correct, the unit needs to be MPa (i.e., Mega-Pascal = 1e6 Pa) instead of Pa. Thus the corrected text reads:

"The initial stress is given as σ_h = 0.020·D+0.6 MPa (minimum principal horizontal stress), σ_H = 0.055·D+4.6 MPa (maximum principal horizontal stress)"

The vertical stress given in the task description is correct (given in Pa).

4. Finite Time for Excavation State in D_THM1

The DECOVALEX THMC Task D description (December 2004 Status) suggests simulating the excavation conditions until a steady-state flow field has been achieved (see Section 6.3.1 and Figure 6.5b). It is more realistic to assume a finite excavation time before the bentonite and the heat-generating radioactive waste are emplaced. We suggest using a finite excavation time of 30 years prior to waste emplacement.

5. Heat Generation in D_THM1

In previous meetings, the heat generation rate was adjusted from an initial value of 290 W/m to an initial value of 245 W/m This means that the original heat power generation table (heat given as a function of time) needs to be consistently scaled down by the factor of 245/290.

6. Definition of Continuum Properties in D_THM2

At this stage, JNC, BGR, and CAS are using a single continuum model to describe the fractured rock mass at Yucca Mountain. This requires that single continuum properties need to be used instead of the fracture and matrix properties given in Table 6.9 of the task description. Discrepancies between research teams were a result of using different continuum properties. In order to have a common basis for single continuum modeling, we suggest using the following single continuum properties.

Type	Property	Value
Hydraulic properties of the fracture-matrix continuum	Permeability (m^2)	3.87×10^{-17}
	Porosity (-)	0.13
	van Genuchten's air-entry pressure (kPa)	118.3
	van Genuchten's exponent, m (-)	0.317
	Residual saturation (-)	0.19

The preferred choice, however, is a dual continuum model, because a single continuum representation misses some important hydraulics of the fracture-matrix system. An alternative model choice for those teams that want to avoid dual continuum complications is the "effective continuum representation" (ECM) after Pruess et al. (Water Resources Research, 1990, Vol 26, No. 6, pp. 1249-1261). An effective continuum model allows accounting for the different hydraulic characteristics of fractures and matrix, while avoiding a full dual continuum solution. We will send out information about the ECM in separate documents.

7. Latent Heat of Vaporization in D_THM2

The DECOVALEX THMC Task D description (December 2004 Status) gives a wrong value for the latent heat of vaporization to be used in Equation 6.1. The latent heat of vaporization is 2.2526×10^3 kJ/kg instead of 2.2526×10^{-3} kJ/kg.

8. Bulk Density of Rock Mass in D_THM2

The DECOVALEX THMC Task D description (December 2004 Status) gives a slightly inconsistent value for the bulk density of the rock mass in Table 6.9. The bulk density of the rock mass in Table 6.9 should be 2360 kg/m^3 instead of 2370 kg/m^3. The value of 2360 kg/m^3 is consistent with the value used to define the initial vertical stresses on page 51 of the task description.

Appendix C

Status Report for D_THM

DOE Team

Coupled Thermal-Hydrological-Mechanical Analysis within the Framework of DECOVALEX-THMC Task D_THM

Step 1: Model Inception

The US Department of Energy (DOE) Research Team

Report to DECOVALEX Task D Coordinator

Aug 25, 2005

Jonny Rutqvist

Lawrence Berkeley National Laboratory
Earth Sciences Division, MS 90-1116
Berkeley, CA 947 20
USA

TABLE OF CONTENTS

1 INTRODUCTION

This report presents coupled thermal-hydrological-mechanical (THM) simulation results for DECOVALEX-THMC, Task D, conducted by the Lawrence Berkeley National Laboratory (LBNL) on the behalf of the U.S. Department of Energy (DOE). The DECOVALEX-THMC, Task D, is described by Barr et al. (2004), which defines detailed tasks to be conducted by participating research teams. DECOVALEX-THMC, Task D, explores various aspects of long-term, permanent changes in hydrological properties of rock near waste emplacement drifts. These changes, caused by THM and THC processes can significantly impact the flow path in the near-field rock surrounding the emplacement tunnels, and thus need to be addressed in performance assessment.

The DECOVALEX-THMC, Task D_THM, includes two subtasks to analyze coupled THM processes in two generic repositories, as follows (Barr et al., 2004):

- Task D_THM1: Generic repository is located in saturated crystalline rock, where emplacement tunnels are backfilled with buffer material (FEBEX type).

- Task D_THM2: Generic repository is located in unsaturated volcanic rock, with emplacement in open gas-filled tunnels (Yucca Mountain type).

The model geometry for the two subtasks is schematically presented in Figure 1.1 The specific dimensions for Task D_THM1 and Task D_THM2 are given in Table 1.1 and 1.2. The models are two dimensional, representing one drift in the interior of a repository. Because of repetitive lateral symmetry, the models extend horizontally to the mid-distance between two drifts. Vertically, the models extend several hundred meters above and below the drift.

This report presents results for Task D_THM, Step 1. It is a model inception step in which the problem is well defined, with all the material properties and conditions given explicit values. The results of the model inception step presented in this report will be compared to results derived by other research teams within the DECOVALEX-THMC group.

The approach taken by the DOE research team is to use two independent numerical simulators to perform two comparative coupled THM analyses. The two numerical simulators used are:

- TOUGH-FLAC

- ROCMAS

The TOUGH-FLAC simulator will be the primary analysis tool, because this simulator has been developed, qualified, and applied within DOE's Yucca Mountain Project. It has been extensively used to simulate coupled THM processes around repositories of the Yucca Mountain type (similar to Task D_THM2). It is important to the DOE to test the TOUGH-FLAC code against independent coupled THM codes, such as those developed by other research teams within the DECOVALEX-THMC. The ROCMAS code has also been developed at LBNL and has been mostly applied for analysis of coupled THM processes around repositories in saturated crystalline rocks, where the emplacement drifts are backfilled with buffer material (similar to Task

D_THM1). In this report, we intend to analyze both Task D_THM1 and D_THM2 with both TOUGH-FLAC and ROCMAS.

Figure 1.1 General model geometry, boundary conditions, and locations of points, lines, and areas for model output (Barr et al., 2004)

Table 1.1. Numerical values of model dimensions in Figure 1.1 for Task D_THM1 (Barr et al., 2004)

Dimension	Value
Vertical length, L_z	1,000 m
Horizontal length, L_x	35 m
Drift diameter, d	2.28 m
Diameter of waste canister	0.9 m
Dimensions of the near drift study area, (3d × 3d)	7 × 7 m
Dimensions of the far field study area, ($2L_x/3 \times 2L_x/3$)	25 m

Table 1.2. Numerical values of model dimensions in Figure 1.1 for Task D_THM2 (Barr et al., 2004).

Dimension	Value
Vertical length, L_z	550 m
Horizontal length, L_x	81 m
Drift diameter, d	5.5 m
Diameter of waste canister	1.7 m
Dimensions of the near drift study area, (3d × 3d)	16.5 × 16.5 m
Dimensions of the far field study area, ($2L_x/3 \times 2L_x/3$)	54 × 54 m

2 TOUGH-FLAC

TOUGH-FLAC is a numerical simulator for analysis of coupled THM processes under multi-phase fluid-flow conditions, and is based on the linking of the two established codes TOUGH2 and FLAC3D. The TOUGH-FLAC simulator was applied within the preceding DECOVALEX III project for coupled THM analysis of the Yucca Mountain Drift Scale Test (Rutqvist et al., 2005a and b).

2.1 BASIC APPROACH

The two computer codes TOUGH2 (Pruess et al., 1999) and FLAC3D (Itasca Consulting Group 1997) have been coupled for the analysis of coupled multiphase flow, heat transport, and rock deformations in fractured porous media (Rutqvist et al., 2002). The TOUGH2 code is designed for hydrological analysis of multi-phase, multicomponent fluid and heat transport, while FLAC3D is designed for rock and soil mechanics. FLAC3D has the capability to analyze coupled HM and TM responses of soil, rock, or other types of materials that may undergo plastic flow when their yield limit is reached. The codes are coupled through external modules: one that calculates changes in effective stress as a function of multi-phase pore pressure and thermal expansion; and one that corrects porosity, permeability, and capillary pressure as a function of stress (Figure 2.1). In the following, the governing equations and numerical procedures for TOUGH2 and FLAC3D are first described separately. Thereafter, the coupling of the two codes is explained, including approach, coupling functions, and numerical procedure.

2.2 GOVERNING EQUATIONS AND NUMERICAL PROCEDURE IN TOUGH2

In the formulation for TOUGH2, the total mass balance of each fluid component is accumulated from relevant contributions in each phase ($\psi = g$ for gas and $\psi = l$ for liquid). For a component (e.g. $\kappa = a$ for air, $\kappa = w$ for water), we obtain

$$\frac{\partial}{\partial t} M^{\kappa} - Q^{\kappa} = -\nabla \cdot \left(\mathbf{q}_l^{\kappa} + \mathbf{q}_g^{\kappa} \right) \tag{2.1}$$

where M^{κ} is the mass per unit volume of component κ computed as

$$M^{\kappa} = \phi S_l \rho_l X_l^{\kappa} + \phi S_g \rho_g X_g^{\kappa} \tag{2.2}$$

where ϕ is porosity, S_{ψ} and ρ_{ψ} are saturation and density of phase ψ, and X_{ψ}^{κ} is the mass fraction of component κ in fluid phase ψ.

The mass flux of each component, κ, within each fluid phase, ψ, can be written as the sum of the advective (Darcy) and nonadvective (diffusive) fluxes as:

$$\mathbf{q}_{\psi}^{\kappa} = -\rho_{\psi} X_{\psi}^{\kappa} \frac{\mathbf{k} k_{r\psi}}{\mu_{\psi}} \left(\nabla P_{\psi} - \rho_{\psi} \mathbf{g} \nabla z \right) + \mathbf{i}_{\psi}^{\kappa} \tag{2.3}$$

where the diffusive flux is computed (using Fick's law) as

4

$$\mathbf{i}_\psi^\kappa = -\rho_\psi D_v \mathbf{I} \nabla X_\psi^\kappa \tag{2.4}$$

with D_v as an effective molecular-diffusion coefficient in a porous media that depends on temperature, gas pressure, medium tortuosity, and gas saturation (Pruess et al., 1999).

Considering all contributions to the heat storage and flux over all phases, the energy conservation equation is assembled as:

$$\frac{\partial}{\partial t}\left(\phi S_l \rho_l e_l + \phi S_g \rho_g e_g + (1-\phi)\rho_s C_s T\right) - Q^h = -\nabla \cdot (\mathbf{q}^h) \tag{2.5}$$

where e_ψ are internal energies of each phase, C_s is specific heat of solid, $\mathbf{q}^h$ is energy flux density (including advective and diffusive fluxes) , and Q^h is the heat source term.

The total heat flux is given by the sum of the advective flux contributions over the fluid phases, and the diffusive flux as

$$\mathbf{q}^h = \sum_\psi \sum h_\psi^\kappa \mathbf{q}_\psi^\kappa + \mathbf{i}_m^h \tag{2.6}$$

where h_ψ^κ is enthalpy (energy per unit mass) of component κ in phase ψ, and the diffusive or conductive heat conduction is governed by Fourier's law:

$$\mathbf{i}_m^h = -\lambda_m \mathbf{I} \nabla T \tag{2.7}$$

where λ_m is the apparent macroscopic (over all phases) thermal conductivity.

In TOUGH2, the continuum equations are discretized in space using the integral finite-difference method (Pruess et al., 1999). Time is discretized as first-order finite-difference, and a fully implicit scheme is adopted in which the fluxes are expressed in terms of the unknown thermodynamic parameters at time level $t^{k+1} = t^k + \Delta t$, leading to the following nonlinear algebraic equations:

$$R_n^{(\kappa)k+1} \equiv M_n^{(\kappa)k+1} - M_n^{(\kappa)k} - \frac{\Delta t}{V_n}\left\{\sum_m A_{nm} q_{nm}^{(\kappa)k+1} + V_n Q_n^{(\kappa)k+1}\right\} \tag{2.8}$$

where subscripts n and m label element and element face, R is the residual, M is mass or energy per unit volume (Equation 2.2), V is element volume, A is area of element face, q is flux (Equation 2.3 and 2.6) and Q is the source term. The TOUGH2 code performs a complete simultaneous solution of the discretized mass- and energy-balance equations. To handle nonlinearity, a Newton-Raphson iteration scheme is adopted, in which the Jacobian is numerically evaluated for selected primary variables and the solution is achieved when the residual R becomes small.

2.3   GOVERNING EQUATIONS AND NUMERICAL PROCEDURE IN FLAC3D

When running the FLAC3D code in its mechanical or thermomechanical configuration mode, it solves the equation of motion,

$$\nabla \cdot \boldsymbol{\sigma} + \rho_m \mathbf{g} = \rho_m \frac{d\mathbf{v}}{dt} \tag{2.9}$$

in an iterative manner with a stress-strain law. The incremental stress and strain during a time step is governed by various elastic or elasto-plastic constitutive laws, which can be written in a general form as

$$\Delta \boldsymbol{\sigma}' = \mathbf{H}(\boldsymbol{\sigma}', \dot{\boldsymbol{\varepsilon}}\Delta t) \tag{2.10}$$

in which $\mathbf{H}$ contains given material functions, $\dot{\boldsymbol{\varepsilon}}$ is the infinitesimal strain-rate tensor, and Δt is a time increment. Equation (2.10) is valid for small strain, but in the FLAC3D code a large strain formulation can be invoked, in which the stress tensor is corrected for rotational strains.

The infinitesimal strain rate, $\dot{\boldsymbol{\varepsilon}}$, and infinitesimal strain, $\boldsymbol{\varepsilon}$, is governed by the restrictions

$$\dot{\boldsymbol{\varepsilon}} = \frac{1}{2}\left(\nabla \mathbf{v} + (\nabla \mathbf{v})^{tr}\right) \qquad \boldsymbol{\varepsilon} = \frac{1}{2}\left(\nabla \mathbf{u} + (\nabla \mathbf{u})^{tr}\right) \tag{2.11}$$

where tr denotes the transpose of a tensor. As usual, the total strain increment can be decomposed into elastic, plastic, and thermal expansion parts, according to:

$$\Delta \boldsymbol{\varepsilon} = \Delta \boldsymbol{\varepsilon}^e + \Delta \boldsymbol{\varepsilon}^P + \Delta \boldsymbol{\varepsilon}^T \tag{2.12}$$

where the thermal strain is given by

$$\Delta \boldsymbol{\varepsilon}^T = \mathbf{I}\beta_T \Delta T \tag{2.13}$$

and where β_T is the linear thermal expansion coefficient, $\mathbf{I}$ is the unit tensor, and T is temperature.

The constitutive laws in Equation (2.10) work on the effective stress, which can be calculated (by invoking the FLAC3D groundwater configuration) as:

$$\boldsymbol{\sigma}' = \boldsymbol{\sigma} + \mathbf{I}\alpha P \tag{2.14}$$

where α is Biot's effective stress parameter (Biot, 1941) and P is pore pressure.

In FLAC3D, the continuum equations are discretized in space using a first-order finite difference technique and special mixed discretization approach. In this approach, the finite difference equations are derived using constant strain-rate elements of tetrahedral shapes, which are then overlain to form final zone elements. The overlaying technique is necessary to provide more modes of deformations during plastic flow. Time derivatives are discretized using an explicit finite difference formulation, leading to the following form of the motion equation:

$$\mathbf{v}_i^{(t+\Delta t/2)} = \mathbf{v}_i^{(t-\Delta t/2)} + \frac{\Delta t}{m}\sum_i \mathbf{F}_i^t \tag{2.15}$$

where $\mathbf{v}$ indicates nodal velocities, m is the lumped nodal mass, and $\mathbf{F}$ is nodal force. In FLAC3D, the basic explicit dynamic calculation iterates between solving the equation of motion and the stress-strain constitutive equation using a sufficiently small time step to assure numerical stability. In one time step, the equation of motion is first invoked to calculate new velocities based on previous velocities and forces. The nodal velocities are then used to derive new strain rates and stress, which in turn are used to update the force vector of Equation (2.15). The final

solution is reached (using a damped solution) when the body is in equilibrium or in steady-state flow (plastic flow), and the out-of-balance force goes to zero.

2.4 COUPLING OF TOUGH2 AND FLAC3D

When linking two codes, the coupled equations cannot be solved simultaneously; they should be solved sequentially, with coupling parameters passed to each equation at specific intervals. Therefore, in this study, the TOUGH2 and FLAC3D codes are executed sequentially on compatible numerical grids and linked through external coupling modules, which serve to pass relevant information between the field equations that are solved in the respective codes (Figure 2.1).

2.4.1 Hydromechanical Coupling Approach

The approach taken here is to couple TOUGH2 and FLAC3D through the concept of effective stress or modified effective stress and nonlinear empirical expressions for changes in hydraulic properties as a function of effective stress. These empirical functions could be estimated from laboratory data and should if possible be determined by model calibration against field experiments at a relevant scale. The coupling functions take into account the most essential couplings including the effects of rock deformation on porosity, permeability, and capillary pressure, as well as the effects of fluid pressure and temperature on rock deformation. Using this approach, the governing equations presented for each code in Section 3 and 4 are essentially unchanged and solved sequentially within respective code. However, for the case of a rapidly changing effective stress (relative to fluid mobility), the mass-balance Equation (2.1) can be corrected with an additional term as:

$$\frac{\partial}{\partial t} M^\kappa + M^\kappa \alpha \frac{\partial \varepsilon_v}{\partial t} - Q^\kappa = -\nabla \cdot \left(\mathbf{q}_{rl}^\kappa + \mathbf{q}_{rg}^\kappa \right) \tag{2.16}$$

where ε_v is volumetric strain and subscript r on the flux terms indicates mass flux relative to the solid phase. Equation (2.16) takes into account the movement of fluid relative to the rock and the movement of the rock relative to a fixed control volume. The expression is approximate in the sense that some smaller terms for the effect of grain compressibility have been neglected and small strain is assumed.

2.4.2 TOUGH-FLAC Coupling Modules

A TH to M link takes multi-phase pressures, saturation, and temperature from the TOUGH2 simulation and provides updated temperature, and pore pressure to FLAC3D (Figure 2.1). Because a TOUGH2 mesh uses one gridpoint within each element, and FLAC3D nodes are located in element corners, data have to be interpolated from mid-element (TOUGH2) to corner locations (FLAC3D). After data transfer, FLAC3D internally calculates thermal expansion and effective stress according to Equations (2.13) and (2.14), with the thermal expansion and effective-stress coefficients given in the FLAC3D input deck. A coupling module for this link essentially performs the interpolation from TOUGH2 to FLAC3D nodes and calculates an average pore pressure in FLAC3D nodes, based on a material-specific effective stress law.

An M to TH link takes element stress or deformation from FLA3D and corrects element porosity, permeability, and capillary pressure for TOUGH2. In TOUGH2, the newly updated hydraulic properties for each element are entered into the fluid and heat-flow calculation through Equation (2.8). In addition, the effects of volumetric stain in Equation (2.16) can be entered into Equation (2.8) as an extra contribution to the source term. No interpolation in space is required for this data transfer because stress and strain are defined in FLAC3D elements, which are identical to TOUGH2 elements. A TOUGH-FLAC coupling module for this link should calculate the hydraulic property changes, based on material-specific theoretical or empirical functions.

2.4.3   TOUGH-FLAC Numerical Procedure

A separate batch program can control the coupling and execution of TOUGH2 and FLAC3D for the linked TOUGH-FLAC simulator. In this case, it was done within the FLAC3D input file using the FLAC-FISH programming language (Itasca Consulting Group Inc., 1997). The calculation is stepped forward in time with the transient TH analysis in TOUGH2, and at each time step or at the TOUGH2 Newton iteration level, a quasi-static mechanical analysis is conducted with FLAC3D to calculate stress-induced changes in porosity and intrinsic permeability. The resulting THM analysis may be explicit sequential, meaning that the porosity and permeability is evaluated only at the beginning of each time step, or implicit sequential, with permeability and porosity updated on the Newton iteration level towards the end of the time step using an iterative process.

The explicit sequential scheme requires less computation effort because each code is executed only once in each time step, which also implies that data is only transferred once in each time step. The explicit sequential solution should be accurate if the porosity and permeability varies slowly with time or if the time step size is relatively small. For example, when modeling coupled THM processes around a nuclear waste repository, it is expected that slowly evolving thermal strains cause the most changes in porosity and permeability.
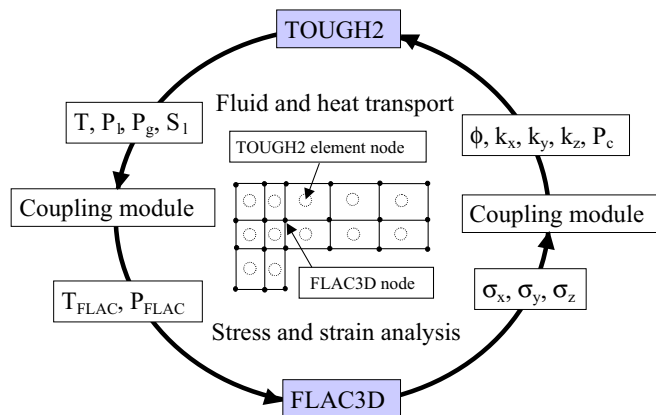
8

Figure 2.1. Schematic of coupling between TOUGH2 and FLAC3D

3 ROCMAS

ROCMAS is a finite element program developed at LBNL for analysis of coupled thermohydromechanical (THM) processes in partially saturated geological media (Noorishad and Tsang, 1996; Rutqvist et al., 2001a). In the previous DECOVALEX II project, the code was applied for analysis of the Kamaishi Mine Heater Test (Rutqvist el al., 2001b). Moreover, in DECOVALEX III, the code was applied for analysis of the FEBEX *in situ* test, using a state surface model for describing the hydromechanical behavior of bentonite.

3.1 BASIC APPROACH AND ASSUMPTIONS

In ROCMAS, the formulation of coupled thermohydroelasticity in terms of Biot's theory of consolidation (Biot, 1941) is extended to partially saturated media through Philip and de Vries' (1957) theory for heat and moisture flow in soil. In this theory, three phases, solid, liquid, and gas, are present. However, it is assumed that the gas pressure P_g is constant and equal to atmospheric pressure throughout the porous medium. As a consequence, vapor transport occurs only through molecular diffusion driven by a gradient in vapor concentration (density), while advection of vapor with bulk gas flow is neglected. The vapor density in the medium is governed by Kelvin's relation, assuming thermodynamic equilibrium for pore liquid in contact with its vapor, and phase transitions occur as evaporation-condensation processes. During heat transfer, coexisting fluid and solid components are assumed to be in local thermal equilibrium (i.e., locally they are at the same temperature). The mechanical behavior of the porous media consists of the gas, liquid, and solid-matter responses to local pressure and the overall material (skeleton) response to effective stresses. With this approach and these assumptions, three balance equations—water mass balance, energy conservation, and linear momentum balance—and a number of constitutive relations are required for a full description of the THM state. These equations are derived and presented in detail below.

3.2 GENERAL BALANCE EQUATIONS

Three mass balance equations are derived based on the general assumptions and hypotheses about the porous media described in Section 3.1 above. The water mass-balance equation for the coupled hydraulic and mechanical system is obtained by combining the water mass-balance equations (for water vapor and liquid water) with the solid mass-balance equation. Considering the grain compressibility, but neglecting a few small terms related to the grain density changes caused by internal fluid pressure and temperature, the following coupled water mass-balance equation is derived (Rutqvist et al., 2001a):

$$\phi \frac{\partial}{\partial t}\left(S_l \rho_l + S_g \rho_v\right) + \left(S_l \rho_l + S_g \rho_v\right)\alpha \frac{\partial \varepsilon_v}{\partial t} = -\nabla \cdot \left(\mathbf{q}_{rl} + \mathbf{q}_{rv}\right) \tag{3.1}$$

where ϕ is porosity, S_l and S_g are liquid and gas saturation, ρ_l and ρ_v are liquid water and vapor densities, α is Biot's effective stress parameter, ε_v is volumetric strain, and $\mathbf{q}_{rl}$ and $\mathbf{q}_{rv}$ are flux densities for liquid and vapor flow.

Assembling the contributions to energy storage and heat flow over all phases results in the following form of the energy conservation equation (Rutqvist et al., 2001a)

$$\frac{\partial}{\partial t}\left[(1-\phi)\rho_s h_s + \phi\left(h_l S_l \rho_l + h_v S_g \rho_v\right)\right] = -\nabla \cdot \left(\mathbf{i}_m^h + h_l \mathbf{q}_{rl} + h_v \mathbf{q}_{rv}\right) \quad (3.2)$$

where the storage content in the gas phase is dominated by the vapor, and mechanical energy conversion is neglected. In Equation (3.2) h_s, h_l, and h_v are specific enthalpies (per unit mass of the phase), and $\mathbf{i}_m^h$ is the apparent heat conduction over all phases.

The final balance equation is the law of conservation of linear momentum, which in the absence of an inertia term reduces to the static stress equilibrium for macroscopic total stresses:

$$\nabla \cdot \boldsymbol{\sigma} + \rho_m \mathbf{g} = 0 \quad (3.3)$$

where σ is the total stress tensor, $\mathbf{g}$ is a vector for the acceleration resulting from gravity, and ρ_m is the average density of the mixture:

$$\rho_m = (1-\phi)\rho_s + \phi S_l \rho_l + \phi S_g \rho_g \quad (3.4)$$

Hence, neglecting the air mass balance, Equations (3.1) to (3.3) are the basic balance equations in ROCMAS.

3.3 CONSTITUTIVE EQUATIONS AND CONSTRAINTS

Neglecting the effects of osmotic suction and adsorbed liquid water, the liquid saturation S_l is assumed to be a function of capillary pressure P_c and temperature, and the following relations apply:

$$S_l = S_l(P_c, T) \quad (3.5)$$
$$P_c = P_g - P_l \quad (3.6)$$
$$S_g = 1 - S_l \quad (3.7)$$

where P_l is liquid water pressure, P_g is total gas pressure, and S_g is gas saturation. With the assumption of atmospheric gas pressure (and thus $P_l \approx -P_c$), the liquid water and vapor flux is obtained as:

$$\mathbf{q}_{rl} = -\rho_l \frac{\mathbf{k}k_{rl}}{\mu_l}\left(\nabla P_l - \rho_l g \nabla z\right) \quad (3.8)$$

and

$$\mathbf{q}_{rv} = -D_v \mathbf{I} \nabla \rho_v \quad (3.9)$$

which has been derived assuming that ρ_g is constant. Assuming a local thermodynamic equilibrium between liquid water and its vapor, the vapor density can be obtained through Kelvin's relationship for relative humidity, r_H, of the moist air in a porous media as

$$\rho_v = \rho_{vS}(T)RH = \rho_{vS} \exp\left(\frac{P_l}{\rho_l R_v T}\right) \quad (3.10)$$

11

where ρ_{vS} is the temperature-dependent saturated vapor density and R_v is the specific gas constant for water vapor. The vapor gradient in Equation (3.9) is further expanded using Equation (3.10), leading to the following expression for the vapor flux:

$$\mathbf{q}_{rv} = -\rho_l \left(D_{Pv} \mathbf{I} \nabla P_l + D_{Tv} \mathbf{I} \nabla T \right) \tag{3.11}$$

where

$$D_{Pv} = \frac{D_v \rho_v}{\rho_l^2 R_v T} \tag{3.12}$$

is the isothermal vapor diffusivity, and

$$D_{Tv} = f_{Tv} D_v \left(\frac{RH}{\rho_l} \frac{\partial \rho_{vS}}{\partial t} - \frac{\rho_v P_l}{\rho_l^2 R_v T^2} \right) \tag{3.13}$$

is the thermal vapor diffusivity.

All the parameters in Equations (3.12) and (3.13) are known from other constitutive relations except for f_{Tv}, a thermal diffusion enhancement factor (Philip and de Vries, 1957), and the effective molecular diffusion coefficient, D_v, which should be experimentally determined. The effective molecular diffusion coefficient is calculated using an empirical relation for molecular diffusion of water vapor and reduction factors, taking into account the porous media properties, using the following expression:

$$D_v = \tau S_g \phi 2.16 \times 10^{-5} \left(T_{abs} / 273.15 \right)^{1.8} \tag{3.14}$$

where τ is a tortuosity factor.

The permeability of a porous soil depends on its porosity and an empirical relative permeability function as

$$\mathbf{k} = \mathbf{k}(\phi) \cdot k_r(S_l) \tag{3.15}$$

where $\mathbf{k}(\phi)$ is the hydraulic permeability tensor of the porous media (in soil literature denoted as *intrinsic permeability*) and k_r is the relative permeability function for liquid and flow. For fractured rock, the hydraulic permeability may be dominated by flow in the fracture system and related to stress or strain, rather than porosity, thus:

$$\mathbf{k}(\phi) = \mathbf{k}(\sigma', \varepsilon) \tag{3.16}$$

Heat conduction is governed by Fourier's law, which is written as

$$\mathbf{i}_m^h = -\lambda_m \mathbf{I} \nabla T \tag{3.17}$$

where λ_m is the apparent macroscopic thermal conductivity over all phases. If porosity is high, λ_m may be strongly dependent on the medium's liquid water content.

The specific enthalpies in Equation (3.2) are expressed in terms of specific heat and temperature as:

$$h_s + h_l = C_S(T - T_0) + C_l(T - T_0) \tag{3.18}$$

$$h_v = h_{Pv} + h_{L0} = C_{Pv}(T - T_0) + L_0(T_0) = C_{Pl}(T - T_0) + L(T) \tag{3.19}$$

where L_0 is the latent heat of vaporization of liquid water at T_0.

The total energy flux in Equation (3.2) is then written as:

$$\mathbf{q}_h = -\lambda\mathbf{I}\nabla T + C_{Pl}(T - T_0)\mathbf{q}_{rl} + [C_{Pl}(T - T_0) + L(T)]\mathbf{q}_{rv} \tag{3.20}$$

where the first term represents pure conduction, and second and third terms are enthalpy transport by liquid and vapor flow, respectively. Following de Vries (1958), we substitute Equation (3.11) into Equation (3.19) to derive the following expression:

$$\mathbf{q}_h = -(\lambda + \rho_l LD_{Tv})\mathbf{I}\nabla T - \rho_l LD_{Pv}\mathbf{I}\nabla P + C_{pl}(\mathbf{q}_{rl} + \mathbf{q}_{rv})(T - T_0) \tag{3.21}$$

In practice, the conductivity of the porous media may be experimentally determined as a function of saturation, including the effects of pure conduction and latent heat transport under thermal gradient:

$$\lambda + \rho_l LD_{Tv} = \lambda_m(S_l) \tag{3.22}$$

With the basic assumption of small strain, the total strain tensor, $\boldsymbol{\varepsilon}$, and volumetric strain, ε_V, is defined as usual:

$$\boldsymbol{\varepsilon} = \frac{1}{2}\left(\nabla\mathbf{u} + (\nabla\mathbf{u})^{\mathbf{tr}}\right) \qquad \text{and} \qquad \varepsilon_v = \nabla\cdot\mathbf{u} \tag{3.23}$$

where $\mathbf{u}$ is the displacement vector and tr denotes the transpose of the tensor.

A modified effective stress law effective stress law can be derived in terms of Biot's parameters as:

$$\boldsymbol{\sigma} = \boldsymbol{\sigma}' - \alpha\mathbf{I}S_l P \tag{3.24}$$

where the average pore pressure is calculated using the volume average of each phase and assuming a negligible gas pressure.

Alternatively, a state surface model using a logarithmic relationship proposed by Lloret and Alonso (1985) defined as:

$$e = a + b\log\sigma_m'' + c\log s + d\log\sigma_m''\log s \tag{3.25}$$

can be used. In Equation (3.24) the void ratio is a function of two independent stress variables: A net mean stress defined as:

$$\sigma_m'' = \sigma_m - P_g \tag{3.26}$$

and suction

$$s = P_g - P_l \tag{3.27}$$

σ_m in Equation (3.26) is the mean stress is defined as:

$$\sigma_m = \frac{1}{3}\left(\sigma_x + \sigma_y + \sigma_z\right) \tag{3.28}$$

Finally, the stress-strain constitutive equation is written as

$$d\boldsymbol{\sigma}' = \mathbf{D} : \left(d\boldsymbol{\varepsilon} - d\boldsymbol{\varepsilon}_T - d\boldsymbol{\varepsilon}_{sw}\right) = \mathbf{D} : \left(d\boldsymbol{\varepsilon} - \mathbf{I}\beta_{TD}dT - \mathbf{I}\beta_{sw}dS_l\right) \tag{3.29}$$

if a conventional effective stress law is used, or as

$$d\boldsymbol{\sigma}'' = \mathbf{D} : \left(d\boldsymbol{\varepsilon} - d\boldsymbol{\varepsilon}_T - d\boldsymbol{\varepsilon}_s\right) = \mathbf{D} : \left(d\boldsymbol{\varepsilon} - \mathbf{I}\beta_{TD}dT - \mathbf{I}\beta_s dS_l\right) \tag{3.30}$$

if the state surface approach is used. $\mathbf{D}$ is the tangential stiffness matrix, $\boldsymbol{\varepsilon}$ is total solid skeletal strain, $\boldsymbol{\varepsilon}_T$ is thermal strain caused by temperature increases, and $\boldsymbol{\varepsilon}_{sw}$ is swelling strain caused by saturation changes and $\boldsymbol{\varepsilon}_s$ is strain caused by changes in suction pressure.

3.4   FIELD EQUATIONS AND SOLUTION APPROACH

The final field equations are derived by substituting flux and stress terms in Equations (3.8), (3.11), (3.20), (3.23), and (3.24) into the basic balance equations [Equations (3.1), (3.2) and (3.3)], and expanding the equations in terms of primary variables. The three following governing equations—expressed in terms of strain, ε, fluid pressure, P, and temperature, T—are obtained:

$$C_{Pe}\frac{\partial \varepsilon_V}{\partial t} + C_{PP}\frac{\partial P}{\partial t} + C_{PT}\frac{\partial T}{\partial t} + \nabla \cdot \left(\mathbf{K_{PP}}\nabla P\right) + \nabla \cdot \left(\mathbf{K_{PT}}\nabla T\right) = J_P \tag{3.31}$$

$$C_{TP}\frac{\partial P_l}{\partial t} + C_{TT}\frac{\partial T}{\partial t} + \nabla \cdot \left(\mathbf{K_{Tp}}\nabla P\right) + \nabla \cdot \left(\mathbf{K_{TT}}\nabla T\right) + \mathbf{V_{TT}} \cdot \nabla T + J_T \tag{3.32}$$

$$\nabla \cdot \left(\mathbf{C_{ee}}\frac{\partial \boldsymbol{\varepsilon}}{\partial t}\right) + \nabla \cdot \left(\mathbf{C_{eP}}\frac{\partial P}{\partial t}\right) + \nabla \cdot \left(\mathbf{C_{eT}}\frac{\partial T}{\partial t}\right) = J_e \tag{3.33}$$

which are the fluid flow, heat transfer, and force balance equations, respectively.

The final governing equations [Equations (3.31), (3.32), and (3.33)] are discretized using a standard Galerkin finite-element-solution approach to obtain a set of matrix equations as

$$\begin{bmatrix} \mathbf{0} & \mathbf{0} & \mathbf{0} \\ \mathbf{0} & \overline{\mathbf{K}}_{\mathbf{PP}} & \overline{\mathbf{K}}_{\mathbf{PT}} \\ \mathbf{0} & \overline{\mathbf{K}}_{\mathbf{TP}} & \overline{\mathbf{K}}_{\mathbf{TT}} \end{bmatrix} \begin{Bmatrix} \overline{\mathbf{u}} \\ \overline{\mathbf{P}} \\ \overline{\mathbf{T}} \end{Bmatrix} + \begin{bmatrix} \overline{\mathbf{C}}_{\mathbf{uu}} & \overline{\mathbf{C}}_{\mathbf{uP}} & \overline{\mathbf{C}}_{\mathbf{uT}} \\ \overline{\mathbf{C}}_{\mathbf{Pu}} & \overline{\mathbf{C}}_{\mathbf{PP}} & \overline{\mathbf{C}}_{\mathbf{PT}} \\ \mathbf{0} & \overline{\mathbf{C}}_{\mathbf{TP}} & \overline{\mathbf{C}}_{\mathbf{TT}} \end{bmatrix} \frac{\partial}{\partial t} \begin{Bmatrix} \overline{\mathbf{u}} \\ \overline{\mathbf{P}} \\ \overline{\mathbf{T}} \end{Bmatrix} = \begin{Bmatrix} \overline{\mathbf{J}}_{\mathbf{u}} \\ \overline{\mathbf{J}}_{\mathbf{P}} \\ \overline{\mathbf{J}}_{\mathbf{T}} \end{Bmatrix} \tag{3.34}$$

where coefficient matrices, $\overline{\mathbf{K}}_{\mathbf{PP}}$ etc, contain appropriate finite-element shape functions and transformation matrices (see Noorishad and Tsang (1996)), and $\overline{\mathbf{u}}$, $\overline{\mathbf{P}}$, and $\overline{\mathbf{T}}$ are nodal parameters. The discrete equations are integrated in time from t to t + Δt using a finite difference scheme. However, because many practical problems have a large time-constant difference between the fluid-flow equation and the heat equation, we use an interlaced solution approach. In this method, the hydromechanical equations are solved directly first, and thereafter, the heat equation is solved for an appropriate time step. After time integration, the Jacobian is derived in a Newton-Raphson or modified Newton-Raphson formulation, and the linearized equations are solved with a direct solver.

4   MODELING OF TASK D_THM1 (FEBEX TYPE REPOSITORY)

Modeling of the Task D_THM1 was conducted according to the steps shown in Figure 4.1. This case was analyzed using both ROCMAS and TOUGH2 codes. A fully coupled THM ROCMAS simulation was conducted, and in this section comparisons are made to a coupled TH simulation with the TOUGH2 code. A coupled THM analysis with the TOUGH-FLAC code has not yet been conducted, since TOUGH-FLAC currently does not have the capability of modeling the moisture swelling and development of swelling stress in the bentonite buffer. Such capabilities might be implemented in the future.

4.1   GENERAL CONSIDERATIONS

For a FEBEX type of repository, it is important to capture the THM evolution within the bentonite buffer and its interaction with the surrounding rock mass. This includes thermally driven drying and shrinkage of the bentonite in the first few years, followed by a bentonite resaturation and swelling in the next tens of years. Thermally induced stresses in the surrounding rock, which takes places over hundreds of years, is expected to be potentially the most important mechanisms for creating THM induced permanent changes in the hydrological properties. The heat source developed for the present ROCMAS and TOUGH2 analyses were extracted from Figure 6.4 in the Task D description (Barr et al., 2004). Accordingly, Barr et al., (2004), Section 6.3.1, the initial thermal power at emplacement was set to 290 W/m. However, the initial test simulation indicated that the maximum temperature in the bentonite would exceed 100°C, which is not in agreement with the design of this type of repository. The initial thermal power was therefore reduced to 245 W/m, by increasing the assumed axial separation of adjacent waste canisters from 1 to 2 m.

Rock properties for modeling of the FEBEX type repository were given in the Task D definition (Barr et al., 2004) and are listed in Table 4.1. The bentonite properties are those used for modeling of the FEBEX *in situ* experiment during DECOVALEX III and are listed in Table 4.2. It should be noted that the permeability of the rock is much larger than that of the bentonite. Therefore, the surrounding rock is not expected to be desaturated by suction from the bentonite, and the buffer resaturation time will be controlled by the hydraulic properties of the bentonite itself.

4.2   ROCMAS AND TOUGH2 MODELS OF TASK D_THM1

The ROCMAS code was applied in DECOVALEX III for analysis of the FEBEX *in situ* experiment. In DECOVALEX III, material properties for the bentonite was determined and tested using the results of coupled THM laboratory experiments on bentonite. Furthermore, the model was tested by comparison of simulated and observed THM responses at the FEBEX *in situ* experiment. Thus, the ROCMAS simulation of Task D_THM1 is expected to provide a very good reference for comparison to the results of TOUGH-FLAC.

One main difference between ROCMAS and TOUGH2 modeling approaches is the handling of the gas phase. In ROCMAS, the gas phase is assumed to be static at a constant atmospheric gas pressure. There is no movement of air, because there is no gradient in gas pressure. The model

considers storage and transport of water vapor within the static gas phase in the form of molecular diffusion. The rate of vapor transport, as expressed by Equation (3.9), depends on the gradient of vapor density. In ROCMAS, the molecular diffusion is cast into its dependency on pressure and thermal gradients (Equation 3.11). In TOUGH2, on the other hand, the multiphase fluid flow capabilities of the TOUGH2 code implies that changes in gas pressure and movement of gas can take place along the gas pressure gradient. Thus, two-phase fluid flow effects on the resaturation process can be studied. In TOUGH2, the vapor diffusion is modeled using Fick's law and depends on the gradient of mass fraction of water in the gas phase according to Equation (2.4). With consistent input parameters, the handling of the vapor diffusion should be equivalent in ROCMAS and TOUGH2.

In both ROCMAS and TOUGH2, a simplified approach for modeling of the mechanical behavior of the bentonite is adopted for this case. The buffer is assumed to be elastic with a volumetric swelling and a swelling stress that depends on the changes in water saturation, ΔS_l, according to:

$$\Delta\sigma' = 3K_D\Delta\varepsilon_{sw} = K_D\Delta S_l\beta_{sw} \tag{4.1}$$

where $\Delta\sigma'$ is the induced swelling stress (an effective stress), K_D is the bulk modulus, and β_{sw} is the moisture swelling coefficient.

The swelling strain model is designed to produce a swelling stress of 5 MPa at full saturation. An average bulk modulus of about 20 MPa is assumed for the bentonite. The initial saturation is 65%, and therefore ΔS_l to full saturation is 0.35 (1–0.65). Using this information, we calculate the appropriate moisture swelling coefficient, using Equation (4.1), as:

$$\beta_{sw} = \frac{\Delta\sigma'}{3K_D\Delta S_l} = \frac{5\cdot 10^6}{3\cdot 20\cdot 10^6\cdot 0.35} = 0.238 \tag{4.2}$$

The approach for modeling swelling can be considered a rational engineering approach to simulate the evolution of swelling stress and strain during the resaturation of the buffer. It is sufficient in this case, because the DECOVALEX THMC Task D is focused on the THMC-induced permanent changes in the surrounding rock mass. Such simplified swelling model could also be readily implemented into a TOUGH-FLAC analysis.

At this stage, the problem has been solved with ROCMAS fully coupled THM analysis and with TOUGH2 TH analysis. The capabilities of modeling bentonite swelling have yet to be implemented for a TOUGH-FLAC coupled THM analysis.

For the TOUGH2 simulation we need to define a storage parameter (pore compressibility) for the water flow that reflects the effect of storage by rock deformation. With the standard TOUGH2 code, the porosity can change as a function of fluid pressure and temperature, according to:

$$d\phi = C_\phi dP + \beta_{T\phi}dT \tag{4.3}$$

where C_ϕ is pore compressibility and $\beta_{T\phi}$ pore thermal expansion. Pore compressibility is important for the fluid flow calculation in properly accounting for water storage in the porous

rock. Under drained conditions, the pore compressibility is related to the bulk elastic parameters of the rock, according to:

$$C_\phi = \frac{\alpha}{\phi K} \hspace{5cm} (4.4)$$

where α is Biot's effective stress parameter and K is the drained bulk modulus. Using the material properties given in Table 4.1, we arrive at a pore compressibility of 3.2×10^{-9} Pa^{-1}.

Figure 4.2 presents the numerical grid used for both ROCMAS and TOUGH2 simulations. The grid is rather coarse and consists of 360 elements. Using this coarse mesh, one simulation can be executed within a few minutes. The numerical grid will be refined for later stages of Task D.

4.3   ROCMAS AND TOUGH2 SIMULATION RESULTS

In the following subsections, the results of THM responses are presented according to the output specifications given in Barr et al., 2004, Section 6.5. Comparison of simulation results from ROCMAS and TOUGH2 are made whenever possible.

4.3.1   Temperature Evolution

Figure 4.3 and 4.4 compare ROCMAS and TOUGH2 simulation analyses for temperature evolution. Temperature evolution in the two analyses is almost identical for the first 50 years, and a peak temperature of 91°C is achieved after 23 years. After 50 years, temperatures becomes slightly higher in the TOUGH2. A close analysis of the heat-power-input function reveals that the higher temperature in the TOUGH2 simulation is related to the difference in the interpolation of the heat power input. The heat-power function was input as tabulate values at selected times. Each code interpolates the values of the tabulate values to the current time. In both codes, an average values of heat power over the current time step is determined based on a linear interpolation scheme. Slight differences in the interpolated values can occur because the interpolation schemes are slightly different and because the length of the time step can be different in the two codes.

4.3.2   Evolution of Water Saturation and Fluid Pressure

Figure 4.5 and 4.6 presents the evolution of water saturation in the bentonite. There is a general agreement in the evolution of saturation, withdrying near the canister to about 46% and a resaturation time of about 25 to 30 years. The slight disagreement in these results is expected, considering the differences in approach and ability to capture multi-phase fluid flow in the two numerical codes.

Figure 4.7 and 4.8 presents the evolution of water pressure in the model domain. This output was not requested in the current Task D definition. However, the evolution of the water pressure is important for the evolution of the effective stresses and should therefore be included for comparison between the results of different research teams. During the steady-state analysis of the excavation sequence, the drift will tend to drain the water pressure above the drift to zero or negative pressure. This drainage of water pressure above the drift created some numerical

difficulties in the TOUGH2 simulation, because the rock will tend to desaturate a few hundred meters below the ground. To prevent desaturation, the fluid pressure at the ground surface and in the drift was set slightly above the 0.1 MPa given in the Task D definition. Figures 4.8 and 4.9 indicate a slightly faster pressure recovery in the TOUGH2 analysis compared to the fully coupled THM analysis with ROCMAS. Also, the ROCMAS calculation yields a slight negative pressure (desaturation) at 0.1 to 0.3 years.

4.3.3   Evolution of Stress

Figure 4.9 presents the evolution of stress in the bentonite buffer. The figure shows that the total stress in the buffer becomes fully developed along with the fluid pressure at about 100 years. About 50% of the total stress in the buffer is a result of fluid pressure increase, whereas the rest is caused by moisture swelling as the saturation increases from an initial 65% to 100%. The final stress at Point V2 is 11.5 MPa (Figure 4.9).

Figure 4.10 through 4.14 presents the evolution of vertical and horizontal stress. The initial stress given in the task definition is (at 500 m depth) about 13.2 MPa in vertical stress and 32.1 MPa in horizontal stress. However, Figure 4.10 shows that at t = 0 (that is, after excavation) the horizontal stress at the depth of the drift (500 m) is about 29.2 MPa (see σ_x at point H6). Figure 4.12a also shows a general reduction in the horizontal stress after excavation of the drift. This general reduction in total stress is a result of drained fluid pressure near the excavation. Figure 4.11b compares simulation results with and without consideration of hydromechanical coupling in the rock mass (Biot's $\alpha = 0$ or 1). The figure shows that for an uncoupled solution, the general stress reduction in horizontal stress from about 32 MPa to 29 MPa will not occur. At Point V3, much higher horizontal stresses are achieved, caused by the stress redistribution around the drift.

The calculated stresses at V3 can be checked against Kirch solution for a circular opening in an infinite elastic medium. Using Kirsch solution, the tangential stress, σ_θ, can be calculated as:

$$\sigma_\theta = \frac{1}{2}(\sigma_x + \sigma_z)\left(1 + \frac{a^2}{r^2}\right) - \frac{1}{2}(\sigma_x - \sigma_z)\left(1 + 3\frac{a^4}{r^4}\right)\cos 2\theta - P\left(\frac{a^2}{r^2}\right) \qquad (4.5)$$

where σ_x and σ_z are stresses in the x and z direction, a is the radius of the opening, r is the radius, θ is the angle relative to the x-axis, and P is the internal pressure within the opening.

The numerical results in Figure 4.11a show that the horizontal stress at Point V3 is 61.8 MPa at t = 0 (after excavation but before heating). According to the Task D description, Point V3 is located at $\theta = 90°$ at a distance of 10 cm from the drift wall. However, in results presented in Figure 4.13, V3 is the vertical stress for the closest element of the mesh, which is centered about 9 cm from the drift wall, but at an angle of 78.8°. For $\sigma_x = 29.2$ MPa, $\sigma_z = 13.2$ MPa, a = 1.14, r = 1.23 (9 cm from drift wall), and $\theta = 78.8°$, the analytical tangential stress according to Equation (4.5) is $\sigma_\theta = 62.3$ MPa. Thus, the value of 61.8 MPa achieved from the numerical model is a reasonable correct. (A slight disagreement is expected due to numerical disrcetization error and the fact that σ_θ is not exactly horizontal at $\theta = 78.8°$.) Using Equation (4.5), we can also show that for the exact location of V3 ($\theta = 90°$ and 10 cm from the wall), $\sigma_\theta = 64.3$ MPa.

During the thermal peak, the horizontal stress at Point H6 increases from 29.1 MPa to about 46.0 MPa. At the same time, a peak stress of about 95.8 MPa is achieved at V3. Figure 4.15 shows that the vertical stress does not change significantly except very close to the drift. The analytical solution can be used to estimate the peak stress for a check of the numerical results. For $\sigma_x = 46.0$ MPa, $\sigma_z = 13.2$ MPa, a = 1.14, r = 1.23, $\theta = 78.8°$, and P = 10 MPa, the analytical tangential stress according to Equation (4.5) is $\sigma_\theta = 94.9$ MPa. In this analytical estimate the expected P is the expected swelling stress in the bentonite buffer which is about 10 MPa. The numerical result (95.8 MPa) is within 1% of the analytical estimate (94.9 MPa). For the exact location of V3 ($\theta = 90°$ and 10 cm from the wall), Equation (4.5) yields $\sigma_\theta = 97.7$ MPa.

At 100,000 years, the temperature has declined to ambient and the fluid pressure is fully restored. The horizontal stress at Point H6 have declined to 31.7 MPa, which close to the initial stress. At V3, the calculated horizontal stress is about 59.1 MPa. The analytical solution for $\sigma_x = 31.7$ MPa, $\sigma_z = 13.2$ MPa, and P = 10 MPa, yields a tangential stress of about 59.6 MPa.

In summary, the calculated stress field in Figures 4.11 through 4.15 is reasonable and the stress concentration in point V3 is accurately calculated. The horizontal stress for Point V3 shown in Figure 5.9a is for the numerical element closest to V3, and is expected to be about 97% of the horizontal stress at the exact location of V3.

4.3.4 Evolution of Displacement

Figures 4.16 and 4.17 present the evolution of vertical displacement. The entire column first settles at 0.052 m (about 5 cm), caused by the drainage of the water into the open excavation. Figure 4.9 shows an average pressure decline of 2.45 MPa [5.0-0.1)/2]. The compaction can be estimated analytically for a laterally constrained medium as:

$$\Delta z = L_z \frac{1 - v - v^2}{(1 - v^2)E} \Delta P \tag{4.6}$$

For $L_z = 1,000$ m, $v = 0.3$, E = 35 MPa, and $\Delta P = 2.45$ MPa, Equation (4.4) yields $\Delta z = 0.052$ m, which is exactly the value achieved in the numerical analysis.

The peak displacement at the ground surface is 0.25 m and occurs after about 2,000 years.

4.3.5 Evolution of Vertical Water Flux

Figure 4.18 presents a horizontal profile of the vertical percolation flux. Only the results for the initial 10,000 and 100,000 years are shown. The vertical flux during the excavation and the early time after emplacement is not included, because the flow tends to be directed towards the open or recently filled drift rather than being vertical.

The numerical analysis indicates a vertical percolation flux of about 0.3 mm/year. The vertical steady state percolation flux in the model can be estimated from the following analytical expression:

$$q_z = -\frac{k\rho g}{\mu} + \frac{k}{\mu}\frac{dp}{dz}$$
(4.7)

For $k = 1.0 \times 10^{-17}$ m^2, $\rho = 1{,}000$ kg/m^3, g = 9.81 m/s^2, $\mu = 1 \times 10^{-3}$ Ns/m^2, and $dp/dz = 8{,}900$, equation x yields a vertical percolation flux of -9.1×10^{-11} m/s (-0.29 mm/year). However, in the numerical modeling, both viscosity and density are temperature dependent. The viscosity at the average temperature of 25°C is about 0.9×10^{-3} Ns/m^2 which would yield a percolation flux of -1.0×10^{-11} m/s (-0.32 mm/year). A higher flow rate at 10,000 years compared to that at 100,000 years can be explained by the temperature dependency of viscosity.

Table 4.1. Rock properties for modeling of Task D_THM1 Step 1

Parameter	Value
Density, [kg/m^3]	2700
Porosity, [-]	0.01
Biot's constant, α [-]	1.0
Young's Modulus, [GPa]	35
Poissons ratio, [-]	0.3
Specific heat, [J/kg·°C]	900
Thermal conductivity, [W/m·°C]	3.0
Thermal expan, coefficient [1/°C]	$1 \cdot 10^{-5}$
Permeability, [m^2]	1×10^{-17}

Table 4.2. Properties of bentonite

Parameter	Value
Dry density, [kg/m^3]	$1.6 \cdot 10^3$
Porosity, [-]	0.41
Saturated permeability, [m^2]	$2.0 \cdot 10^{-21}$
Relative permeability, k_{rl}	$k_{rl} = S^3$
Water retention (Modified Van-Genuchten Function [Rutqvist et al., 2004])	$S = 0.01 + (0.99)\left[1 + (s/35)^{1.43}\right]^{-0.30}\left[1 - s/4000\right]^{1.5}$
Moisture swelling coefficient [-]	0.238
Poisson ratio, [-]	0.35
Thermal expan. coeff., [1/°C]	$1.0 \cdot 10^{-5}$
Dry specific heat, [J/kg·°C]	$c_s = 1.38T + 732.5$
Thermal cond., [W/m·°C]	$\lambda_m = 1.28 - \dfrac{0.71}{1 + e^{(S-0.65)/0.1}}$
Flow times tortousity factor	0.8
Thermal diffusion factor	1.0
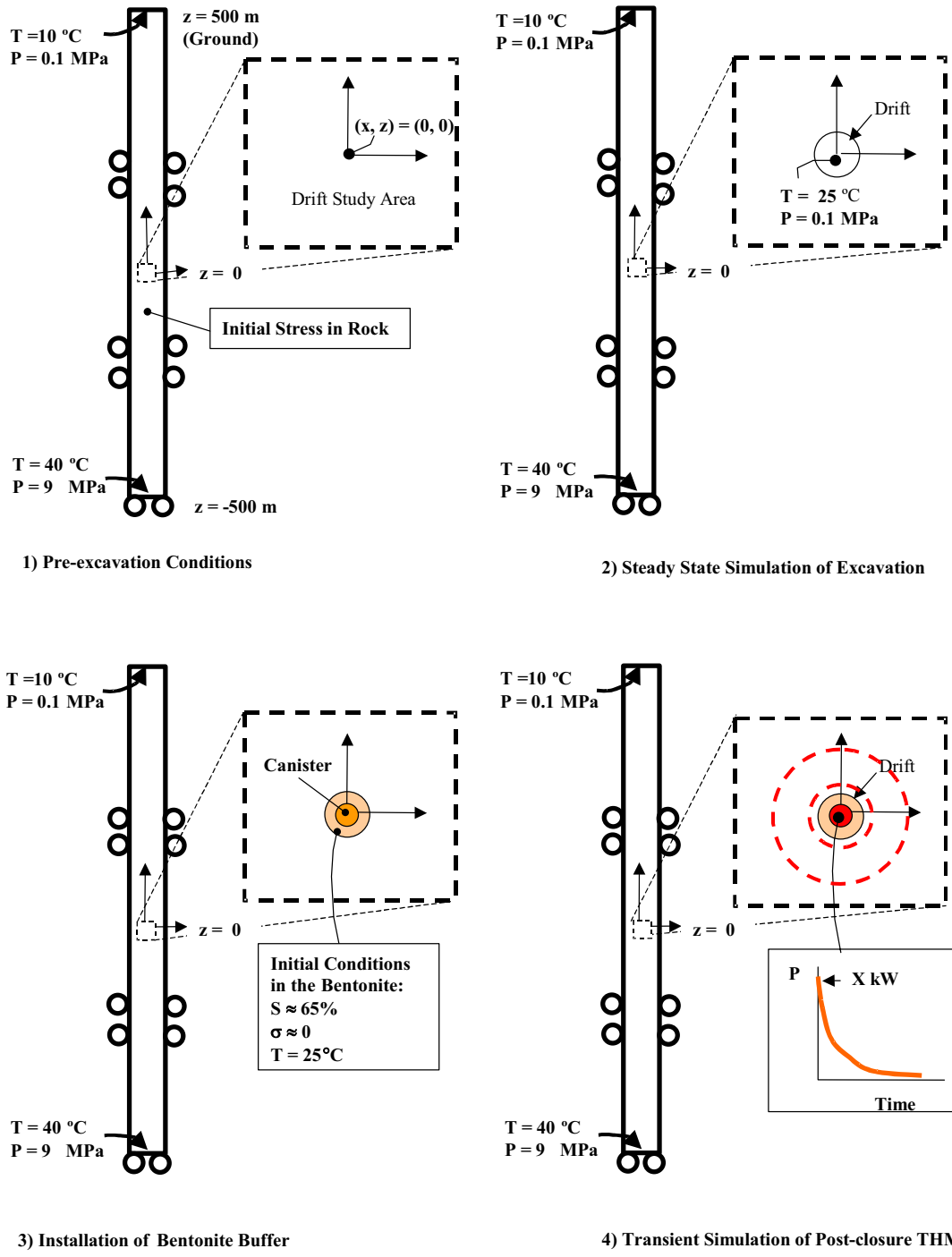
Figure 4.1. Specific modeling sequence, boundary and initial conditions for Task D_THM1 (Barr et al., 2004)
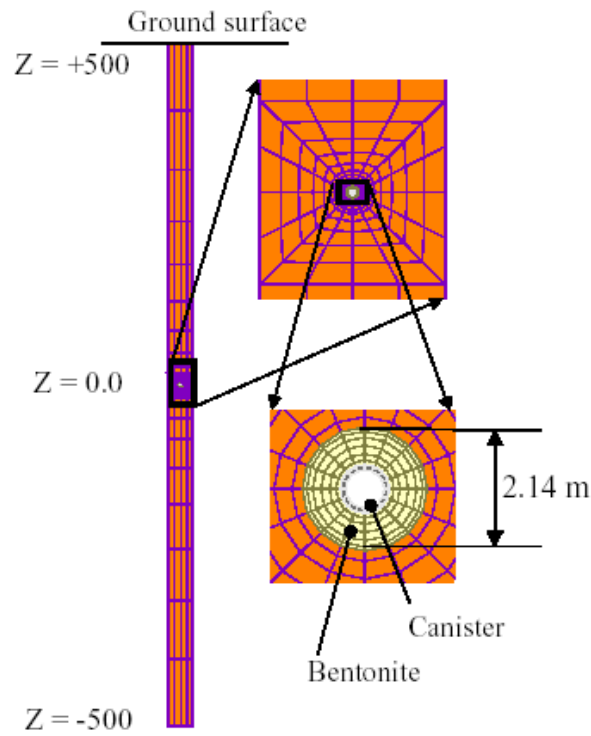
Figure 4.2. Numerical grid used for both ROCMAS and TOUGH2 simulations
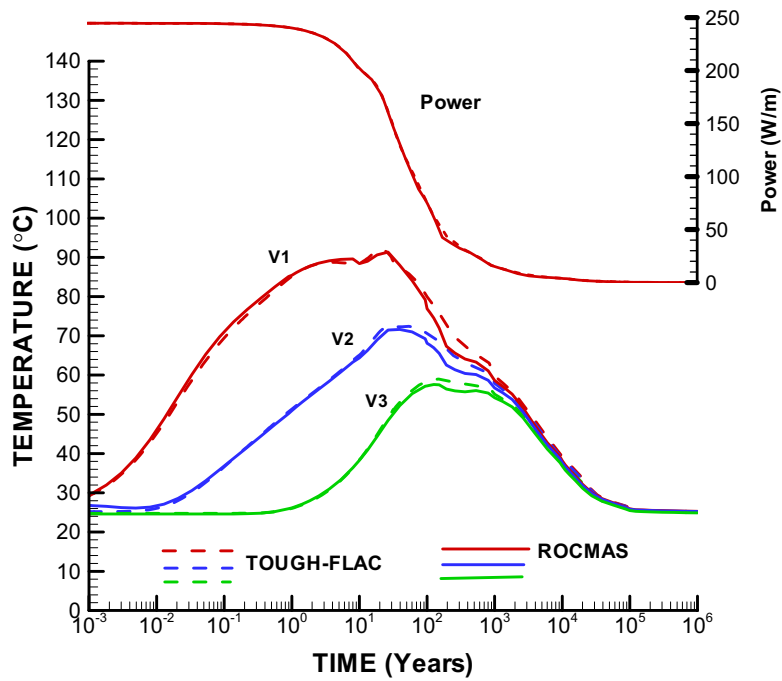
Figure 4.3. Power and comparison of temperature evolution for TOUGH-FLAC and ROCMAS simulation results
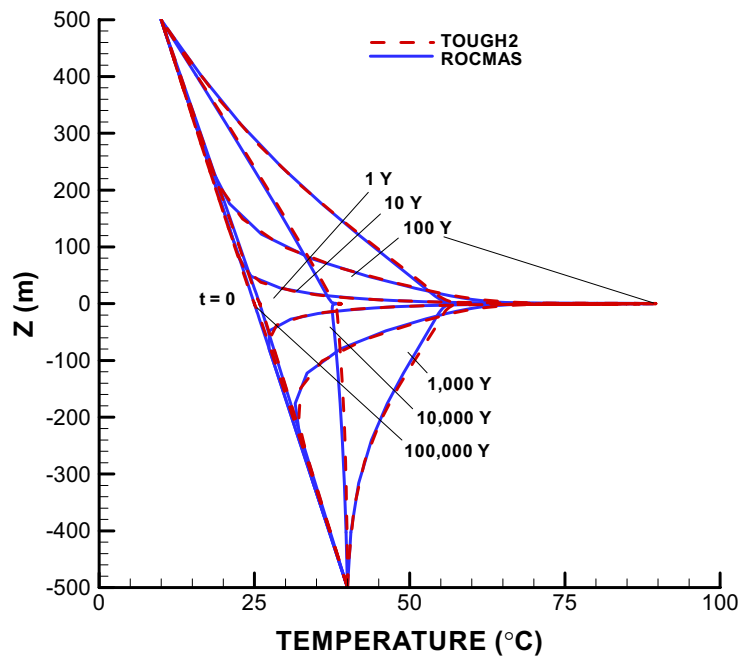
Figure 4.4. Comparison of vertical temperature profiles for ROCMAS and TOUGH-FLAC (TOUGH2) simulations
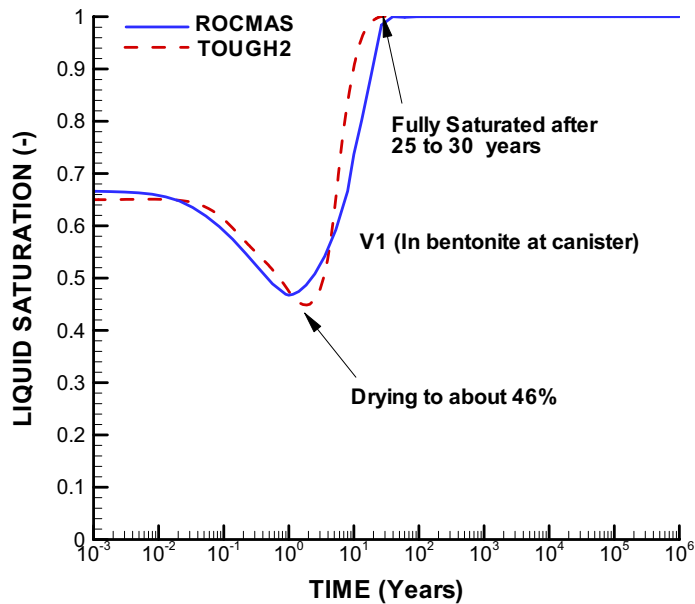
Figure 4.5. Comparison of TOUGH-FLAC (TOUGH2) and ROCMAS simulation results for the evolution of degree of saturation in bentonite (Point V1)

23
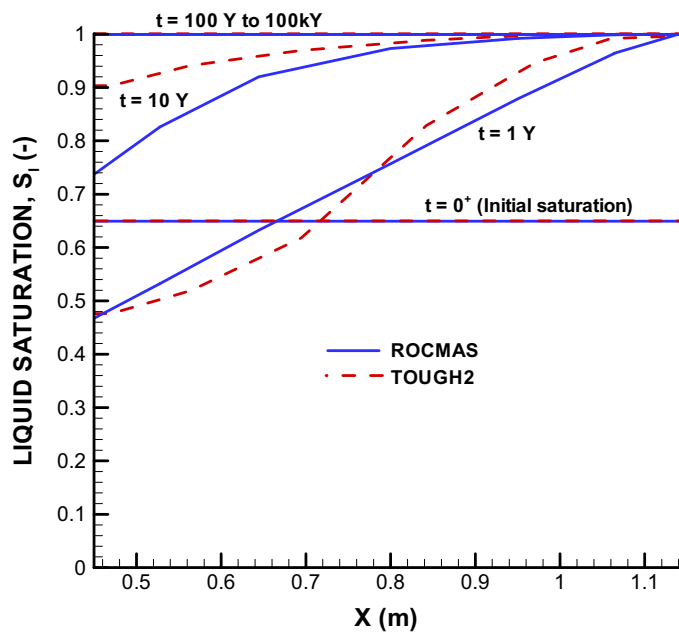
Figure 4.6. Comparison ROCMAS and TOUGH2 simulation results of horizontal saturation profile in the bentonite buffer
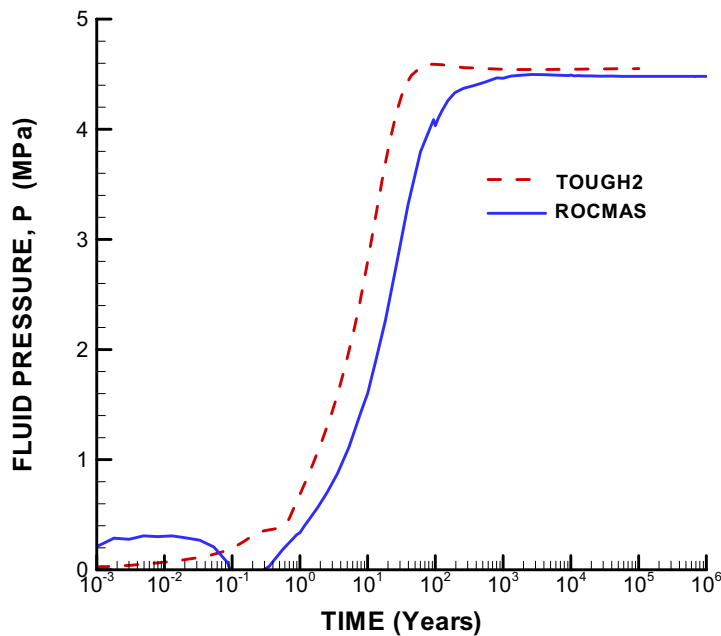
Figure 4.7. Comparison of ROCMAS and TOUGH2 simulation result of the evolution of fluid pressure at Point V3
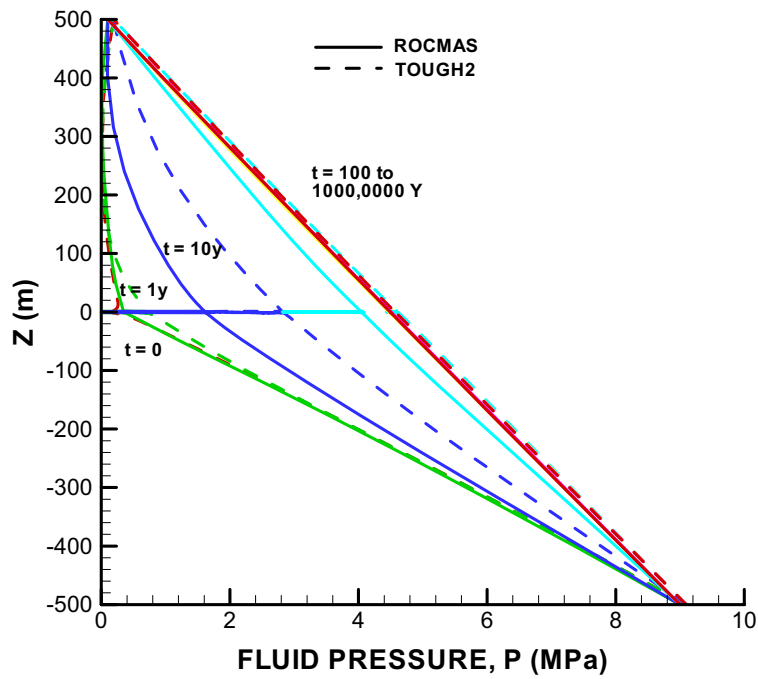
Figure 4.8. Comparison of TOUGH2 and ROCMAS simulation results of vertical pressure profiles

Figure 4.9. ROCMAS simulation results of the evolution of stress in buffer (Point V2)
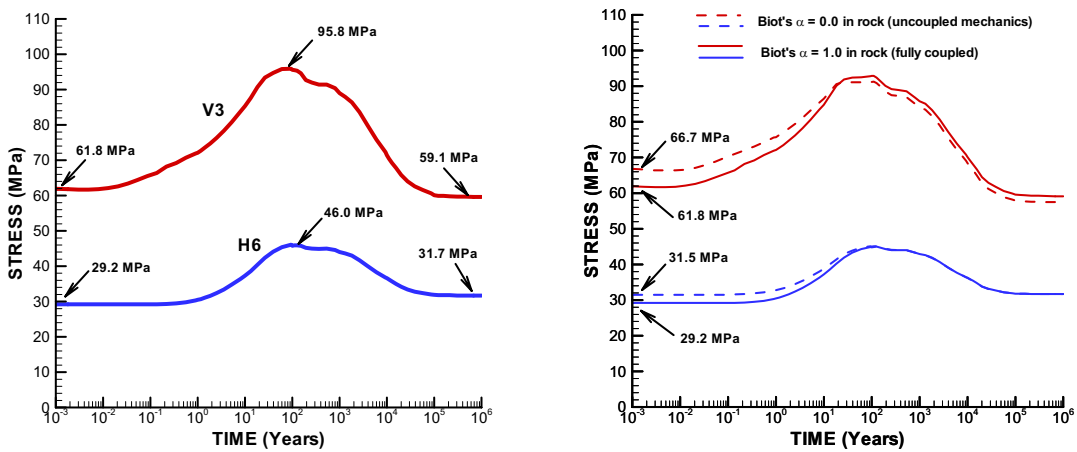
Figure 4.10. ROCMAS simulation results of evolution of horizontal stress at Points V3 and H6
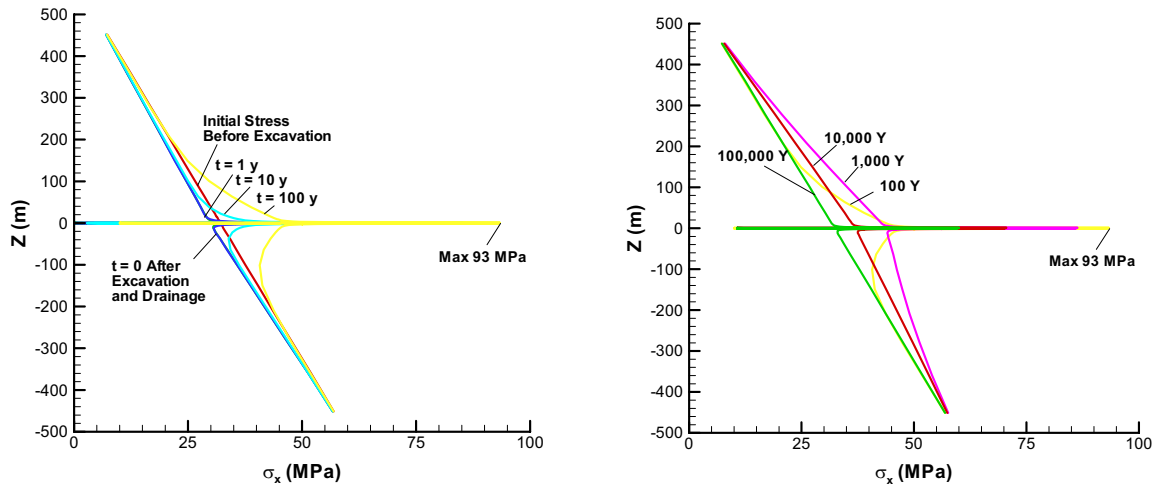
Figure 4.11. ROCMAS simulation results of vertical profiles of horizontal stress
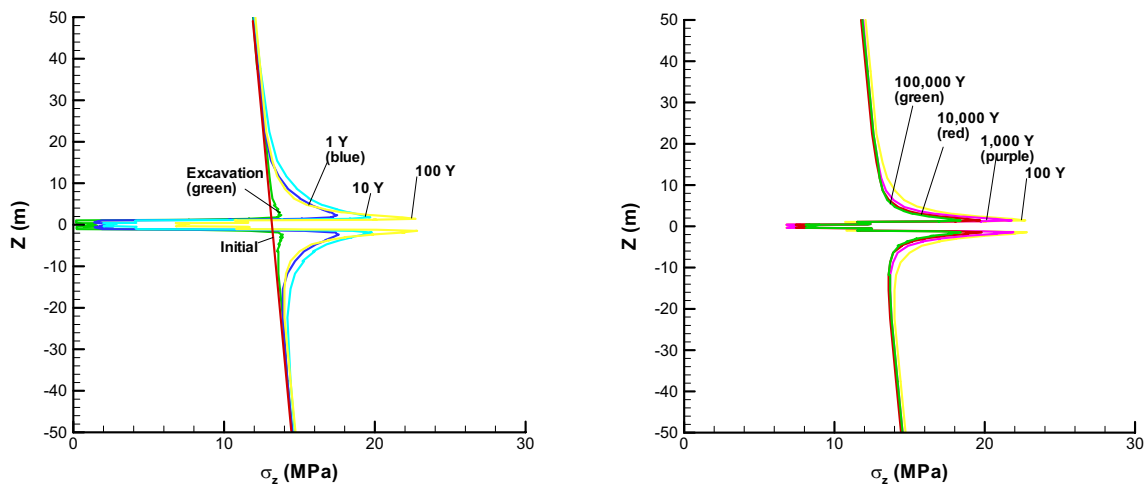
Figure 4.12. ROCMAS simulation results of vertical profiles of vertical stress

26
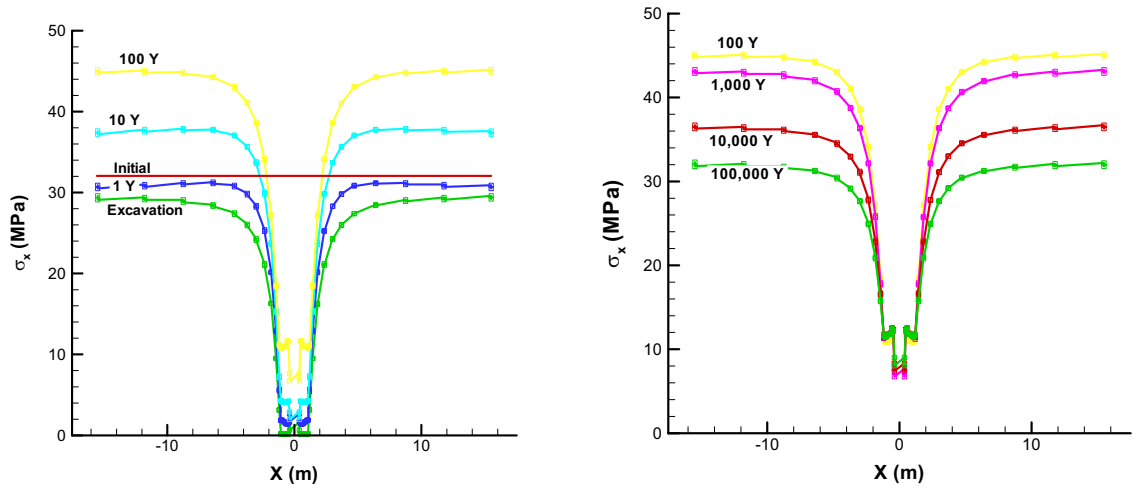
Figure 4.13. ROCMAS simulation results of horizontal profiles of horizontal stress
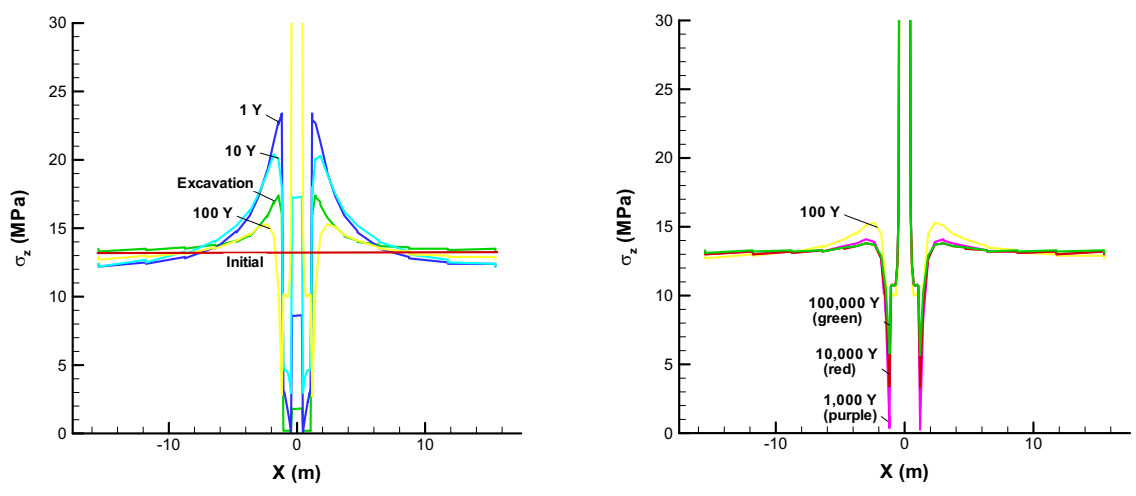
Figure 4.14. ROCMAS simulation results of horizontal profiles of vertical stress
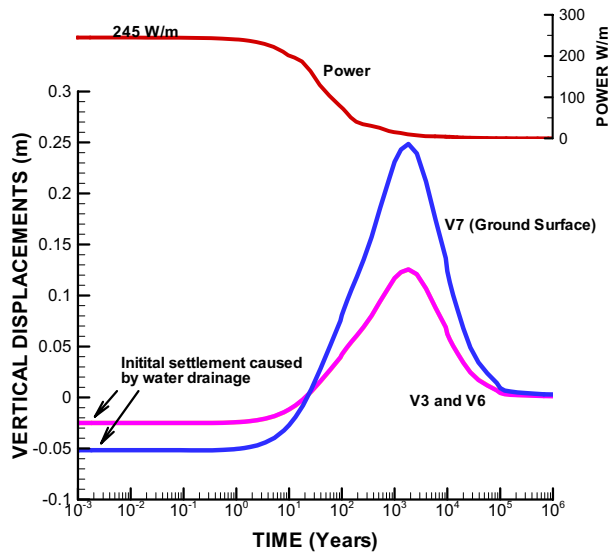
Figure 4.15. ROCMAS simulation results of the evolution of vertical displacements
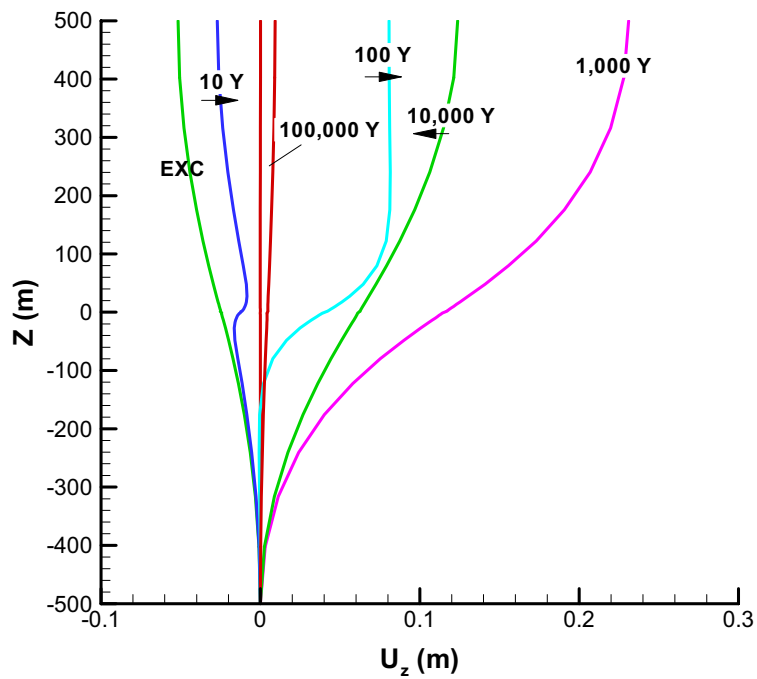
Figure 4.16. ROCMAS simulation results of vertical displacement profiles

28
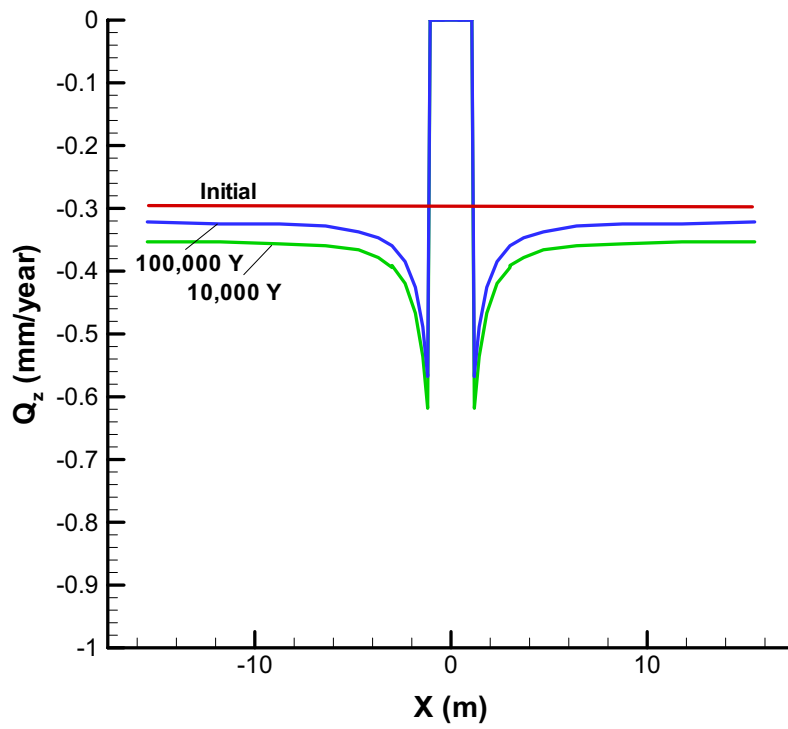
Figure 4.17. ROCMAS simulation results of vertical flux through the repository horizon

5   MODELING OF TASK D_THM2 (YUCCA MOUNTAIN TYPE REPOSITORY)

Modeling of the Task D_THM2 was conducted according to the steps shown in Figure 5.1. The case was analyzed using both ROCMAS and TOUGH-FLAC codes. The analysis with the TOUGH-FLAC code is a complete, fully coupled THM simulation, with multi-phase flow in both fractures and matrix rock. The ROCMAS analysis is applied for a simplified TM simulation, in which the effects of boiling on the thermal calculation are considered through a simplified modeling approach. The two analyses are compared regarding TM responses.

5.1   GENERAL CONSIDERATIONS

For a Yucca Mountain type of repository, the early time coupled THM behavior includes complex two-phase flow (gas and liquid phases with components of air and water) interactions between fractures and matrix rock at high (above boiling) temperatures. The heat driven drying in the rock surrounding the repository drift will last for hundreds of years, affecting the thermal conduction through saturation dependent rock thermal conductivity and rock specific heat. Similar to the FEBEX case, thermally induced stresses in the surrounding rock, which takes places over hundreds of years, are expected to be the most important mechanisms for creating THM induced permanent changes in the hydrological properties. Because of high temperature, the thermal-mechanical effects can be expected to be stronger in this case than in the FEBEX case. A proper analysis of near-field TH processes would require multi-phase flow and heat transport capabilities. However, simplified analysis models might be employed for the analysis of TM effects.

Rock properties for modeling of the Yucca Mountain type repository were given in the Task D definition and are listed in Table 5.1.

5.2   TOUGH-FLAC AND ROCMAS MODELS OF TASK D_THM2

TOUGH-FLAC has been extensively applied in the modeling of coupled THM processes for the unsaturated zone at Yucca Mountain. Therefore, the first approach to modeling Task D_THM2 would be to modify an existing model of a repository in the unsaturated zone. The model is modified in terms of material properties and distances to the upper and lower boundaries. Using an existing model would provide a good benchmark for comparison to other research teams and to develop additional models for next steps of Task D_THM2. The multi-phase flow capabilities of the TOUGH2 code are suitable for modeling of Task D_THM2.

In the TOUGH-FLAC analysis of this case, the dual permeability method (DKM) is applied to evaluate fluid, heat flow, and transport in fractured rock. The dual permeability method accounts for these differences by assuming two separate, but interacting continua that overlap each other in space, one describing flow and transport in the fractures, the other describing flow and transport in the matrix. Each continuum is simulated with a separate numerical grid, separate TH properties, and separate variables (pressure, saturation, and temperature). Thus, at each location in space, there is a fracture gridblock and an overlapping matrix gridblock. The two gridblocks at each location are connected to model the interaction between the two continua. Global flow and transport occur within the fracture continuum and the matrix continuum, while local interflow occurs between the two continua as a result of the local pressure and temperature differences.

The interflow between fractures and matrix is handled using a quasi-steady transfer, estimating the exchange of fluid, gas, and heat between the two components by a linear gradient approximation.

The ROCMAS does not include the full two-phase flow, but the gas phase is assumed to be static at an atmospheric pressure. In this case, the ROCMAS code is be used to model the problem in a simplified way basically simulating the thermal-mechanical behavior (i.e., temperature, thermal stress and thermal displacement). Some of the two-phase flow effects near the drift are modeled using a simplified approach that was described in the Task D description (Barr et al., 2004).

Because the system is unsaturated and the capillary pressure in the fracture system is relatively small, hydraulic processes may not affect mechanical processes significantly. Therefore, in the TOUGH-FLAC analysis, only temperature needs to be transferred from TOUGH2 to FLAC3D (see Figure 2.1).

Figure 5.1 shows the numerical grids used. The ROCMAS grid is rather coarse and consists of 268 elements. The open drift between the waste package and the rock wall is simulated as a material with a very high thermal conductivity, and porosity equal to 1. The TOUGH-FLAC grid is denser and consists of about 1,600 elements. Only one half of the total model domain is simulated using symmetry conditions at the left vertical boundary crossing the repository drift (Figure 5.1b). In the TOUGH-FLAC simulation, the open drift is modeled as a material with very high thermal conductivity, high hydraulic permeability, porosity 1.0, and zero capillary pressure.

5.3   ROCMAS AND TOUGH-FLAC SIMULATION RESULTS

In the following subsections the results of THM responses are presented according to the outputs specification given in Barr et al. (2004), Section 6.5. Comparisons of simulation results from ROCMAS and TOUGH2 are made whenever possible. Comparisons are also made to estimates using simplified analytical solutions.

5.3.1   Temperature Evolution

Figure 5.3 through 5.5 present the temperature evolutionfor ROCMAS and TOUGH-FLAC simulations. In Figure 5.3, a comparison of two ROCMAS simulations is made. In one simulation case, the effect of boiling on the temperature evolution is simulated using the simplified boiling model that accounts for changes in thermal conductivity and heat capacity due to drying, wetting, and release of latent heat. In the other case, a pure thermal conduction model is used. Figure 5.3 shows that the simulated boiling model produces a higher peak temperature (126°C for simulated boiling and 121°C for no simulated boiling). The main reason for a higher peak temperature is that in the simulated boiling zone—a zone near the drift with a temperature above 94°C where drying takes place—the thermal conductivity is lowered. Figure 5.4 shows that the best match between TOUGH-FLAC and ROCMAS is achieved when comparing the TOUGH-FLAC multi-

phase flow simulation results with the ROCMAS results for pure conduction. A detailed analysis of the simulation results indicates that the simulated boiling model for ROCMAS would overestimate the effects of boiling on thermal properties. Drying of the matrix rock takes place slowly and does not extend as far as the 94°C isotherm. Therefore, the pure conduction model provides a better match to the temperature evolution calculated with the more rigorous two-phase flow and heat transport formulation in TOUGH2. Figure 5.4 and 5.5 show that the agreement between ROCMAS and TOUGH2 calculated temperature evolution is very good. A slight difference in temperature between 1,000 and 10,000 years is caused by slightly different interpolations of the tabulated heat power function.

5.3.2   Evolution of Water Saturation

Figure 5.6 presents the evolution of water saturation at the drift wall and Figures 5.7 and 5.8 present vertical and horizontal profiles of water saturation. Figure 5.6 shows that the fracture and matrix at the top of the drift begins to dry out at about 50 years, when boiling occurs at the drift wall. The fractures dry quickly, whereas the matrix is not completely dried until about 100 years. Rewetting of fractures occurs after about 400 years, and the matrix is resaturated to original conditions at about 700 years. Away from the drift, the liquid saturation in fractures and matrix rock is approximately constant in time. The matrix saturation varies between 80 to 92%, whereas fracture saturation varies between 2 to 2.5%, with the highest values occurring at greatest depth (Figure 5.7). Figure 5.8b shows that at 100 years, fractures dry completely to a distance of almost 2 m from the drift wall.

5.3.3   Evolution of Stress

Figure 5.9 and 5.10 present the evolution of horizontal stress. The initial stress given in the task definition is 5.78 MPa in vertical stress and 3.47 MPa in horizontal stress at a depth of 250 m. Figure 5.9 shows that at t = 0 (after excavation) and at t = 100,000 years (after heat decay), the horizontal stress is 3.47 MPa at Point H6, whereas the horizontal stress at V3 is about 5 MPa. As in the FEBEX case, the calculated stresses at V3 can be checked against Kirch's solution for a circular opening in an infinite elastic medium.

The results, presented in Figure 5.9, show that V3 is the vertical stress for the closest element of the mesh. For the ROCMAS simulation, this element is centered about 22 cm from the drift wall, at an angle of 78.8°, whereas the closest TOUGH-FLAC element centers 12.5 cm from the drift wall at about 90°. For σ_x = 5.78 MPa, σ_z = 3.47 MPa, the analytical solution (Equation 4.5) yields σ_θ = 5.2 and 4.8 MPa at the element closest to Point V3 in the ROCMAS and TOUGH2 mesh respectively. This is almost identical to the numerical results in Figure 6.6 at t = 0 and t = 100,000 years.

During the thermal peak, the horizontal stress at Point H6 increases to 14 MPa. At the same time, a peak stress of about 33 to 34 MPa is achieved in V3, for ROCMAS and TOUGH-FLAC respectively. Again, the analytical solution can be used to estimate the peak stress for a check of the numerical results. For σ_x = 14 MPa, and σ_z = 5.78 MPa, the analytical tangential stress according to Equation (4.5) is σ_θ = 32 and 35 MPa for closest elements in ROCMAS and TOUGH-FLAC, respectively. Thus, the numerical results are slightly lower than the ones estimated with the analytical solution, but are reasonable close.

32

5.3.4 Evolution of Displacement

Figures 5.11 and 12 present the evolution of vertical displacement. The peak displacement at the ground surface is about 0.23 m and occurs after about 1,000 years. The agreement between calculated displacements by ROCMAS and TOUGH-FLAC is very good.

5.3.5 Evolution of Vertical Water Flux

Figure 5.13 presents a horizontal profile of the vertical percolation flux. The vertical flux away from the drift is 6 mm/year, which is dictated by the water flux supplied as infiltration on the top of the model. The effect of the drift and dryout zone on vertical flux is evident. At t = 0, the vertical flux is diverted around the drift (due to the capillary barrier effect), leading to a water flux of up to 20 mm/year near the drift wall. At 100 years, the water is diverted around the dryout zone.

Table 5.1. Thermal-hydrologic-mechanical properties used in simulations (Barr et al., 2004)

Type	Property	Value
Hydraulic properties of the fractured continuum	Permeability (m^2)	3.3×10^{-13}
	Porosity (-)	0.0083
	van Genuchten's air-entry pressure (kPa)	9.615
	van Genuchten's exponent, m (-)	0.633
	Residual saturation (-)	0.01
Hydraulic properties of the matrix continuum	Permeability (m^2)	1.77×10^{-19}
	Initial porosity (-)	0.13
	van Genuchten's air-entry pressure (kPa)	118.3
	van Genuchten's exponent, m (-)	0.317
	Residual saturation (-)	0.19
Thermal and Mechanical properties of the rock mass (equivalent continuum properties)	Wet thermal conductivity (W/m °K)	2.29
	Dry thermal conductivity (W/m °K)	1.49
	Grain Specific Heat, J/(kg °K)	985
	Grain Density (kg/m^3)	2550
	Bulk Density (saturated) (kg/m^3)	2370
	Young's modulus (GPa)	15
	Poisson's ratio (-)	0.21
	Thermal expansion coefficient (1/°C)	1.0×10^{-5}
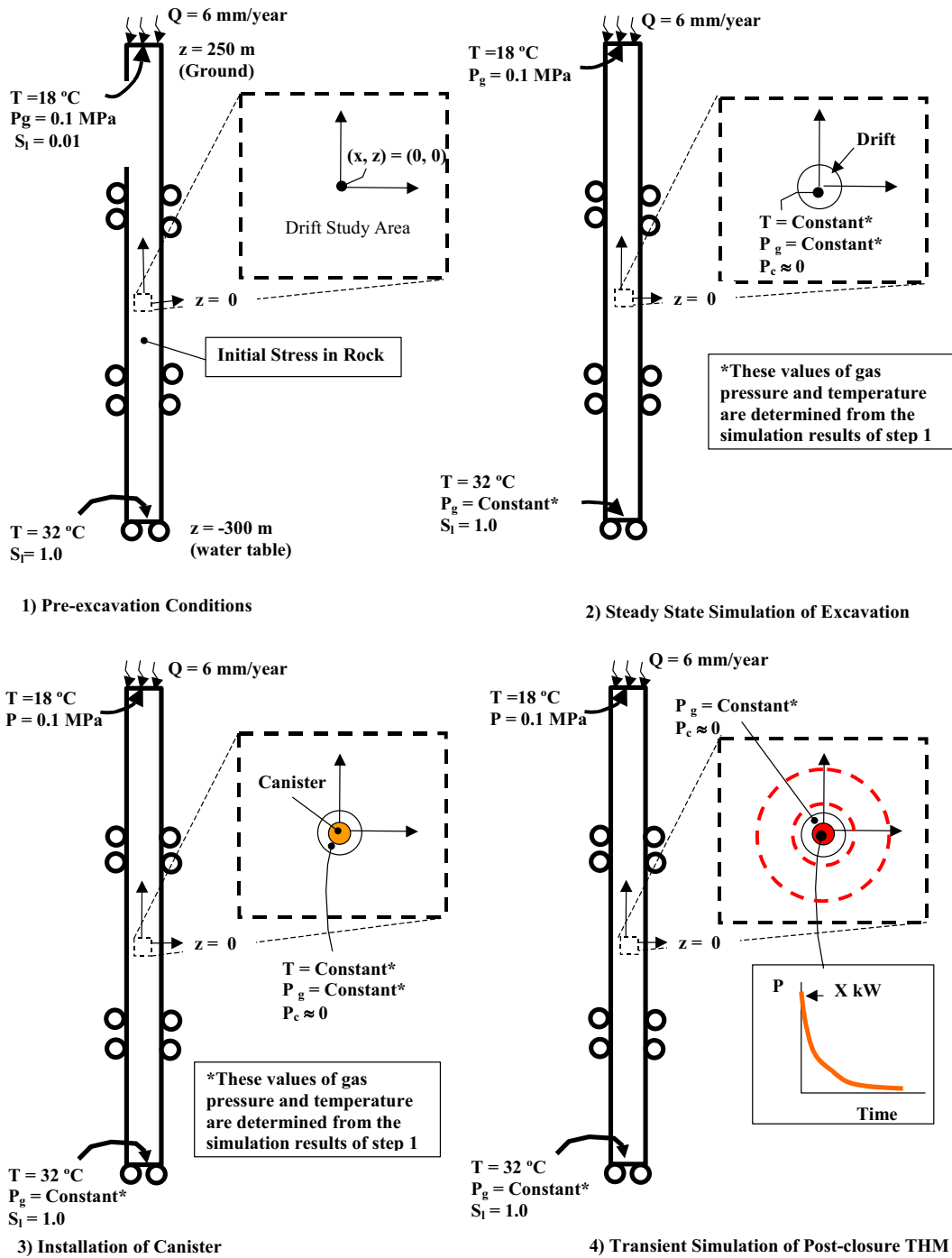
Figure 5.1. Specific modeling sequence, boundary, and initial conditions for Task D_THM2 (Barr et al., 2004)

Ground surface

Z = + 250

Z = 0.0

Z = - 300

Ground Water Table

5.5 m
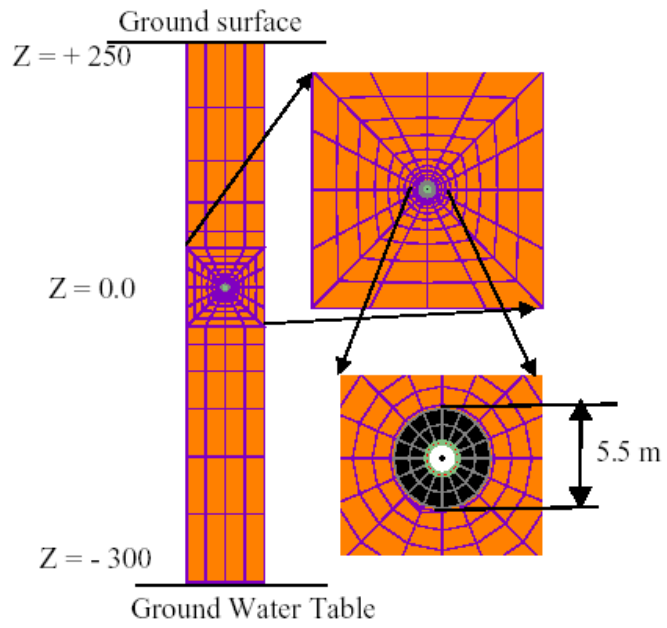
(a) ROCMAS mesh
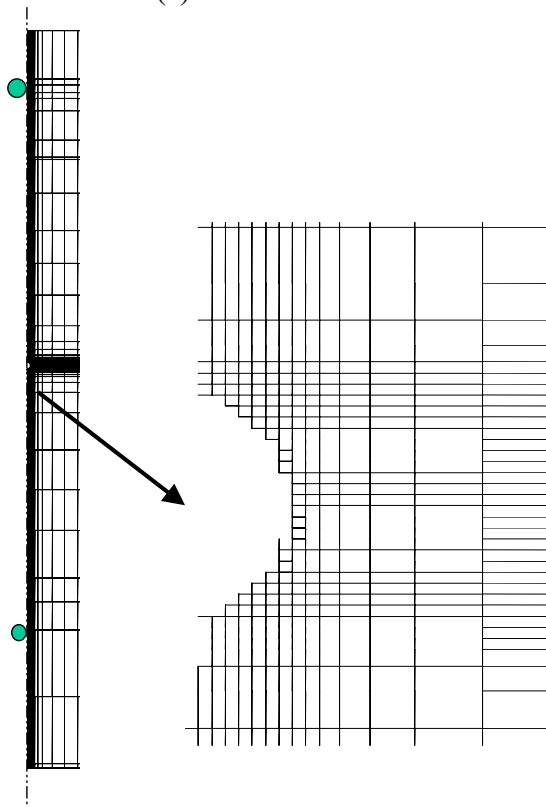
(b) TOUGH-FLAC mesh

Figure 5.2. Numerical grids for simulation of YMP case
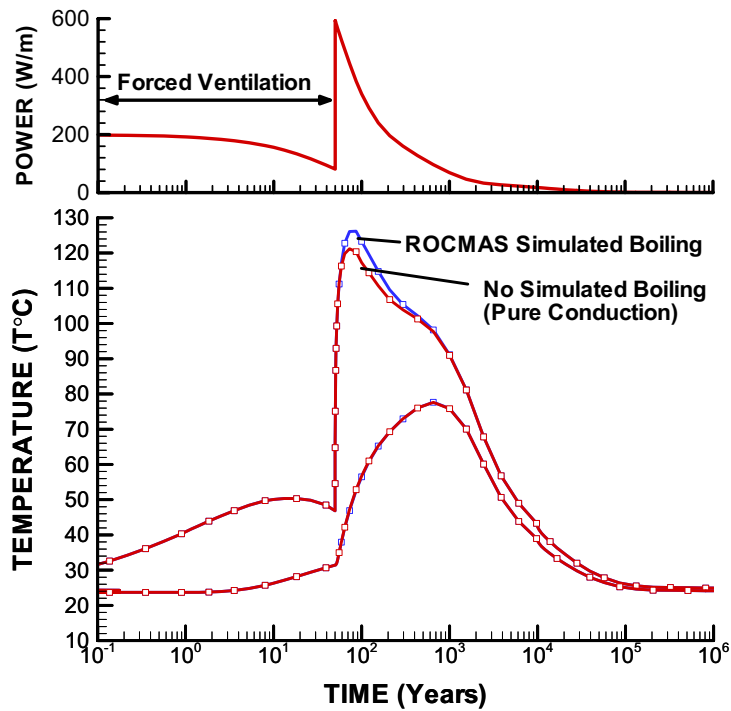
Figure 5.3. Power and comparison of temperature evolution for ROCMAS results with and without simulated boiling effects
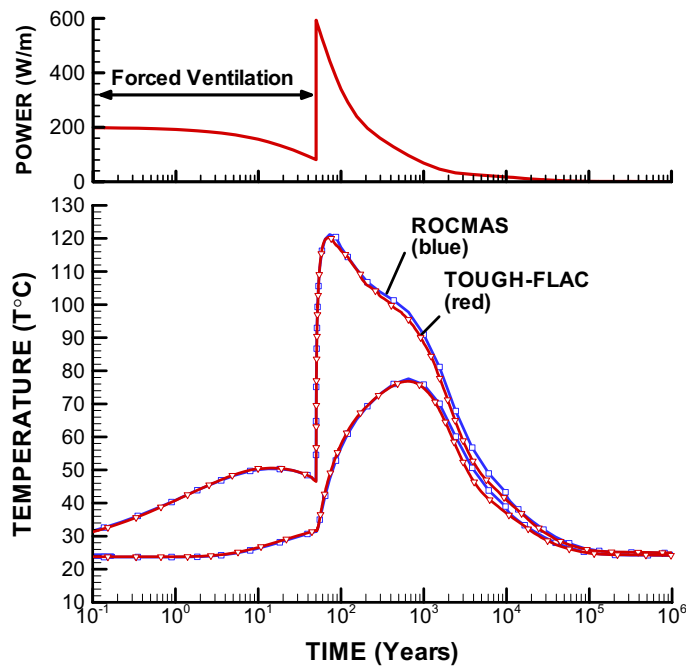
Figure 5.4. Power and comparison of temperature evolution for TOUGH-FLAC and ROCMAS simulation results

36
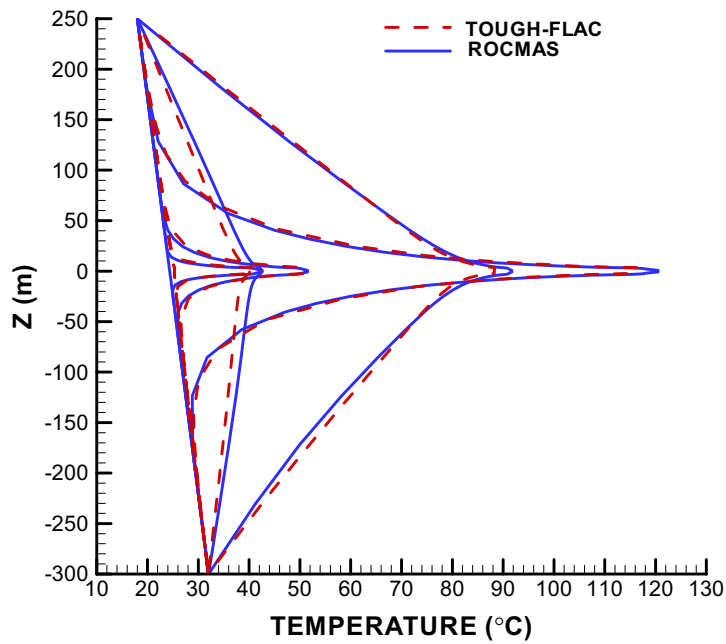
Figure 5.5. Comparison of vertical temperature profiles for ROCMAS and TOUGH-FLAC simulations
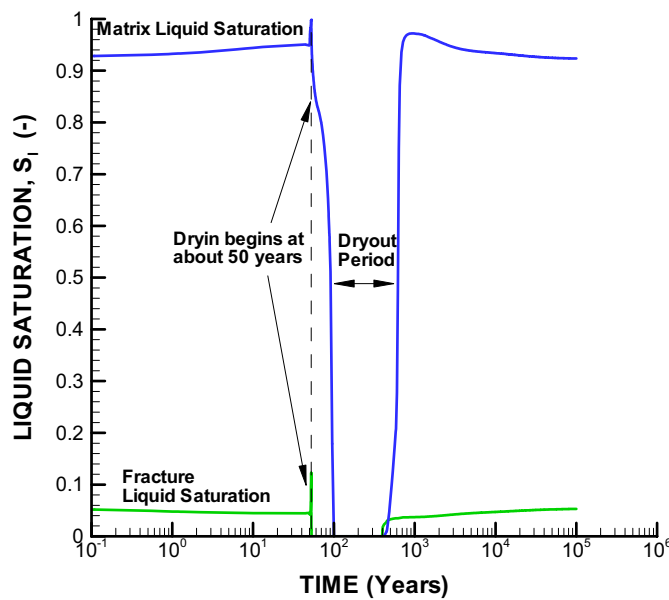
Figure 5.6. TOUGH-FLAC results of evolution of liquid saturation in fracture and matrix continua at Point V3 located at the drift wall on top of the drift

37
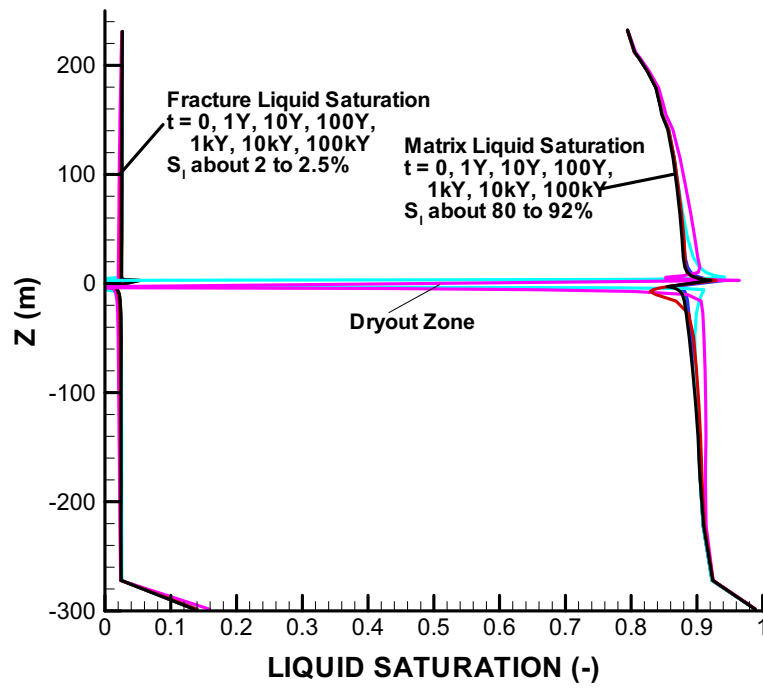
Figure 5.7. TOUGH-FLAC simulation results of vertical saturation profiles for fracture and matrix continua
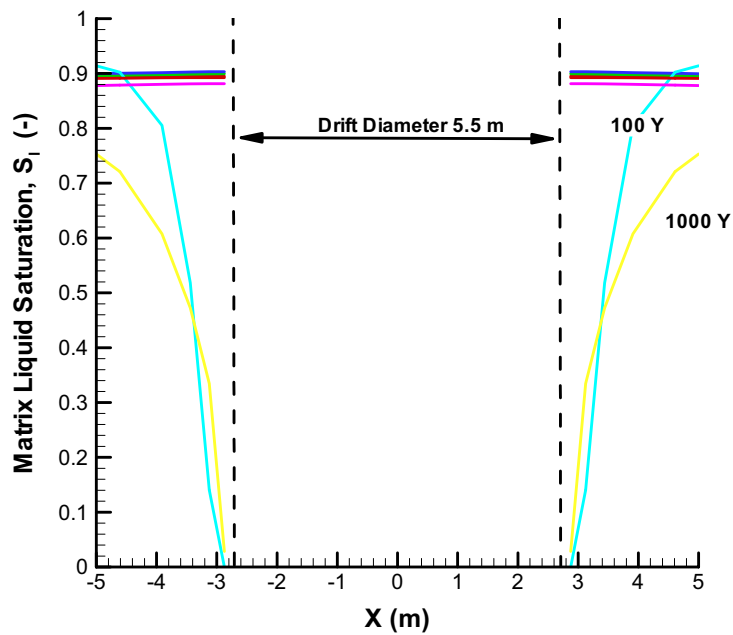
(a) Matrix saturation
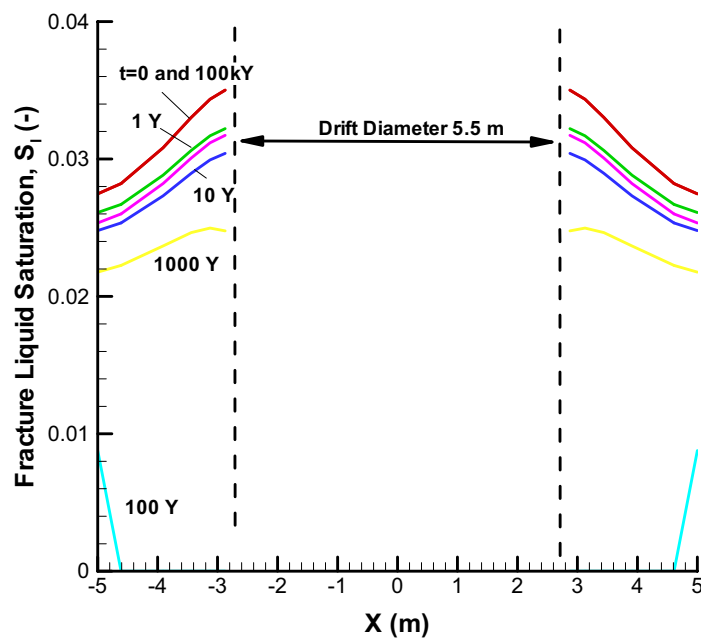
(b) Fracture saturation

Figure 5.8. TOUGH-FLAC simulation results of horizontal profiles of liquid saturation in matrix and fracture continua
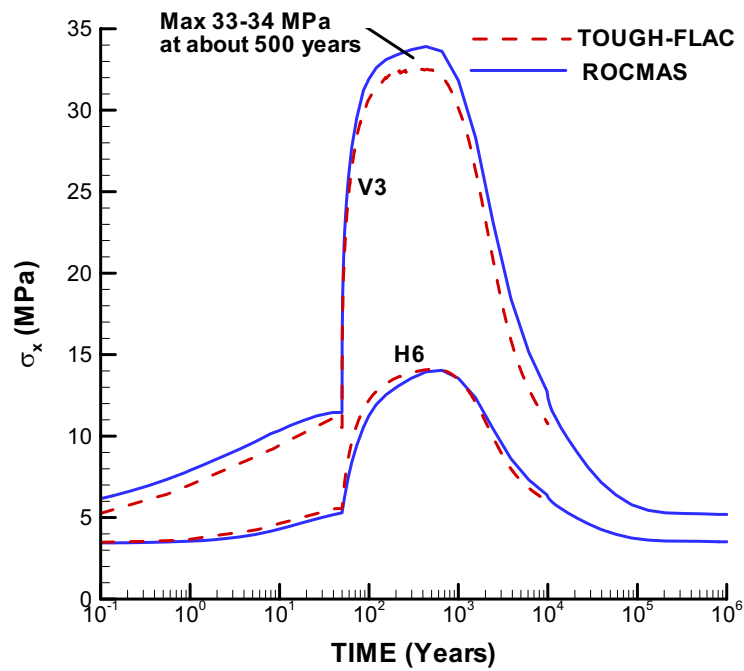
5.9. Comparison of ROCMAS and TOUGH-FLAC simulation results of evolution of horizontal stresses at monitoring points V3 and H6
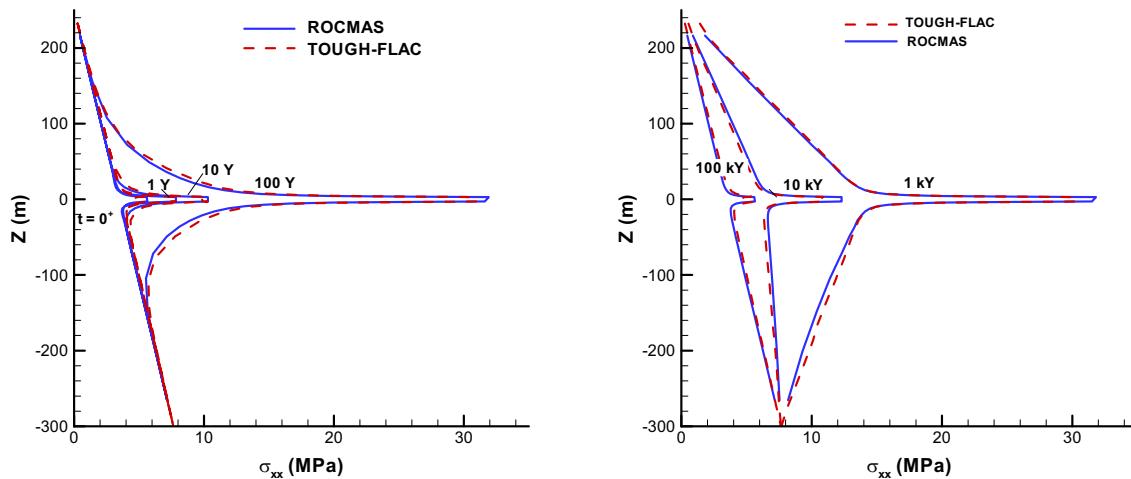
Figure 5.10. Comparison of ROCMAS and TOUGH-FLAC simulation results of horizontal stress

40
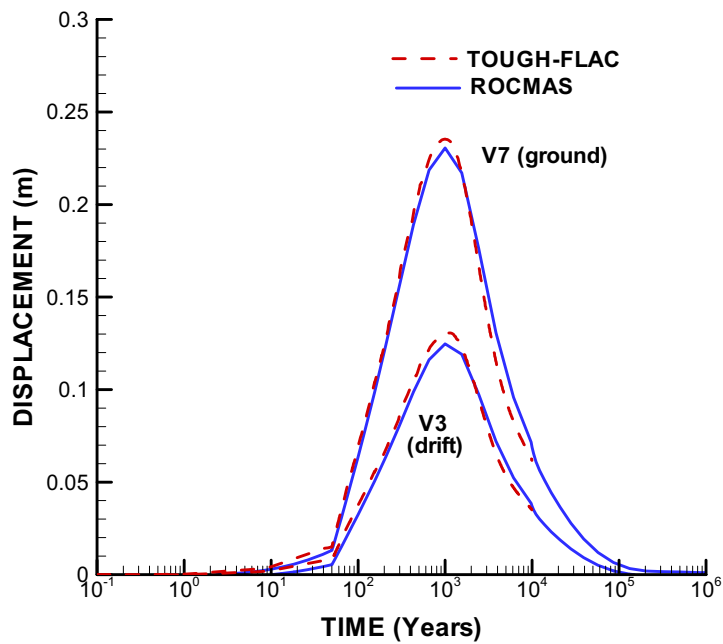
Figure 5.11. Comparison of ROCMAS and TOUGH-FLAC simulation results of time evolution of vertical displacement
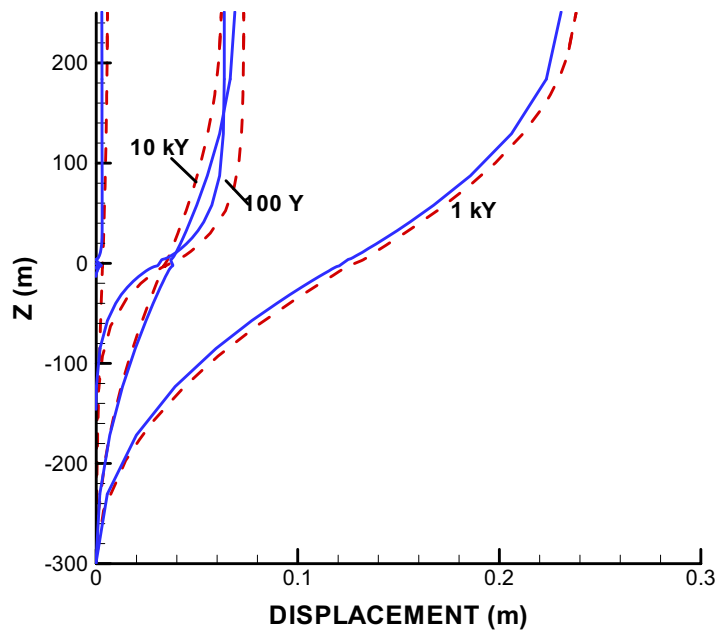
Figure 5.12. Comparison of ROCMAS and TOUGH-FLAC simulation results of vertical displacement profiles
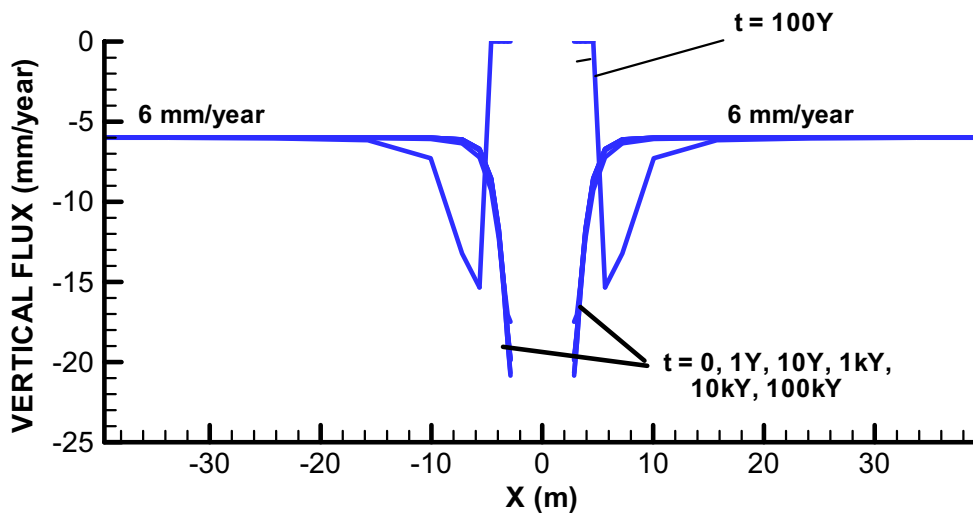
Figure 5.13. TOUGH-FLAC simulation results of vertical flux across a horizontal profile

6 SUMMARY AND DISCUSSION

The modeling of DECOVALEX-THMC, Task D_THM1 and 2, Step 1 was conducted with two different simulators what use different model approaches. The analysis of the two cases with the two simulators yielded a very good agreement in trends and magnitude of coupled THM responses. Slight disagreement between ROCMAS and TOUGH2 simulation results, in temperature evolution during the decay of the heat power functions, is caused by differences in the interpolation of the tabulated heat power input. The slight differences in temperature also slightly impact the calculated thermal-mechanical stresses and displacements. However, the very good agreement in trends and magnitude of thermal, hydraulic, and mechanical responses using ROCMAS and TOUGH-FLAC provides confidence in both models. Moreover, the calculated thermal-mechanical stresses are approximately the same for the two different analyses, and therefore we are sufficiently confident in the results of this model inception step, and we will now continue on to the analysis of the next step of DECOVALEX-THMC Task D.

7 REFERENCES

Biot, M.A., 1941. General theory of three dimensional consolidation. *J. Applied Physics*, 1941, 12, 155–164.

Barr D., Birkholzer J., Rutqvist J., and Sonnenthal E., 2004. Draft Description for DECOVALEX-THMC TaskD: Long-Term Permeability/Porosity Changes in EDZ and Near Field, due to THM and THC Processes in Volcanic and Crystalline-Bentonite Systems. REV01, June 2004.

van Genuchten, M. T., 1980. A closed-form equation for predicting the hydraulic conductivity of unsaturated soils. *Soil Sci Soc Am J 44*: pp. 892-898.

Itasca Consulting Group Inc., 1997. *FLAC-3D Manual: Fast Lagrangian Analysis of Continua in 3 Dimensions–Version 2.0.* Itasca Consulting Group Inc., Minnesota, USA.

Lloret A. and Alonso E.E., 1985. State surfaces for partially saturated soils. *Proc 11th Int Conf Soil Mech Fdn Engng, San Francisco, Vol. 2*, pp. 557-562.

Noorishad, J. and Tsang, C.-F., 1996. Coupled thermohydroelasticity phenomena in variable saturated fractured porous rocks—Formulation and numerical solution. In Stephansson, O., Jing, L., and Tsang, C.-F. editors. *Coupled Thermo-Hydro-Mechanical Processes of Fractured Media*. Developments in Geotechnical Engineering, Elsevier, 79, pp. 93–134.

Philip, J.R. & de Vries, D.A., 1957. *Moisture movement in porous material under temperature gradients.* EOS Trans., *AGU*. 38: 222-232.

Pruess, K., Oldenburg, C., and Moridis., G., 1999. *TOUGH2 User's Guide, Version 2.0*, Report LBNL-43134, Lawrence Berkeley National Laboratory, Berkeley, California.

Rutqvist, J., Borgesson, L., Chijimatsu, M., Kobayashi, A., Nguyen, T.S., Jing, L., Noorishad, J. & Tsang, C.-F., 2001a. Thermohydromechanics of partially saturated geological media: governing equations and formulation of four finite element models. *Int. J. Rock. Mech*. Min. Sci. 38(1): 105-127.

Rutqvist, J.; Borgesson, L.; Chijimatsu, M.; Nguyen, T.S.; Jing, L.; Noorishad, J.; and Tsang, C.-F., 2001b. Coupled thermo-hydro-mechanical analysis of a heater test in fractured rock and bentonite at Kamaishi Mine--Comparison of field results to predictions of four finite element codes. *International Journal of Rock Mechanics and Mining Sciences, 38,* 129-142.

Rutqvist, J., Wu, Y.-S., Tsang, C.-F. & Bodvarsson, G., 2002. A modeling approach for analysis of coupled multiphase fluid flow, heat transfer, and deformation in fractured porous rock. *Int. J. Rock Mech. Min*. Sci. 39: pp. 429-442.

Rutqvist, J., D. Barr, R. Datta, A. Gens, M. Millard, S. Olivella, C.F. Tsang , and Y. Tsang., 2005a. Coupled thermal-hydrological-mechanical analysis of the Yucca Mountain Drift Scale Test – comparison of field results to predictions of four different models. *Int. J. Rock Mech. & Min. Sci* (in press).

Rutqvist J, Tsang CF, and Tsang Y., 2005b. Analysis of coupled multiphase fluid flow, Heat Transfer and Mechanical Deformation at the Yucca Mountain Drift Scale Test. *Proceedings of the 40th U.S. Rock Mechanics Symposium*, Anchorage, Alaska, USA, 25-29 June, 2005: American Rock Mechanics Association ARMA, Paper No. 893.

de Vries, D.A, 1958. Simultaneous transfer of heat and moisture in porous media. *Trans. Am. Geophys. Un*., 39, 909–916.

Appendix D

Status Report for D_THM

JNC Team (Japan)

PROGRESS ON DECOVALEX-THMC TASK-D THM

Japan Atomic Energy Research and Development Agency (JAEA) Team
Yoshihiro Oda, Tomoo Fujita (JAEA), Masakazu Chijimatsu (HZM)
e-mail address: Oda.yoshihiro@jaea.go.jp

1. INTRODUCTION

During and after DECOVALEX-III, Japan Nuclear Cycle Development Institute (JNC) tries to develop the models and code for evaluating coupled thermo-hydro-mechanical phenomena in engineered barrier system. In Task D we try to verify our models and code by comparing them with others through THM1 (FEBEX type repository) and THM2 (Yucca Mountain type repository).

2. CONSTITUTIVE EQUATIONS AND GOVERNING EQUATIONS IN THAMES

THMC calculation code "THAMES" (Chijimatsu et al., 2000) was an extension of the coupled thermo-hydro-mechanical code developed by Ohnishi et al. (1985). This model can account for water diffusion in unsaturated clay (Philip and de Vries, 1957), water movement caused by thermal gradient (de Vries, 1974), and swelling pressure as a result of buffer wetting. In this chapter, the full governing equations are explained below.

2.1 Mass balance of groundwater equation

Fluid mass conservation equation is written as follows.

$$\frac{\partial(\theta\rho_l)}{\partial t} + \left(q_i^l + q_i^v\right)_{,i} + Q_l = 0 , \qquad (1)$$

where $\theta\,(=nS_r)$ is the volumetric water content, n [-] is the porosity, S_r [-] is the degree of liquid saturation, ρ_l is the density of liquid, q [kg/m^{2}s] is the fluid flux, and Q [kg/m^{3}s] is the sink(+) or source(-) of fluid. The superscript l of q signifies liquid and v signifies vapor. The flux of the liquid and vapor are written as follows.

$$q_i^l + q_i^v = -\rho_l\left(r_k k_{ij} h_{,j} + D_T T_{,i}\right), \qquad (2)$$

where r_k [-] is the relative permeability, k [m/s] is the saturated hydraulic conductivity, h [m] is the hydraulic head, D_T [m^2/s/°C] is the thermal water diffusivity, and T [°C] is the temperature. Determining D_T, requires calibration. The relationship between

volumetric water content and suction (the water retention curve) obeys the van Genuchten model.

$$\theta = \theta_{\min} + \left(\theta_{\max} - \theta_{\min}\right)\left[1 + \left(\alpha_{VG}\psi\right)^{n_{VG}}\right]^{-m_{VG}},\tag{3}$$
$$m_{VG} = 1 - 1/n_{VG},$$
$$\psi = -\left(h - z\right),$$

where ψ [m] is the suction, and α_{VG} [1/m] and n_{VG} [-] are van Genuchten parameters.

2.2 Balance of momentum equation

The balance-of-momentum increment is expressed by

$$\Delta\sigma_{ij,j} = 0,\tag{4}$$

where σ [Pa] is the total stress and Δ is the increment. The relationship between the total stress and the effective stress in saturated media is given by:

$$\sigma_{ij} = \sigma'_{ij} + p\delta_{ij}\tag{5}$$

where σ' [Pa] is the effective stress, δ [-] is the Kronecker's delta, and p [Pa] is the pore-water pressure

$$p = \rho^l g\left(h - z\right),\tag{6}$$

where g [m/s^2] is the gravity acceleration.

On the other hand, the effective stress in the unsaturated area is

$$\sigma_{ij} = \sigma'_{ij} + pS_r\delta_{ij}.\tag{7}$$

In the case of swelling materials such as bentonite, however, the second term is neglected. The effect of swelling pressure is included in effective stress, which consists of the stress due to strain, swelling pressure, and thermal stress; its increment is expressed by

$$\Delta\sigma'_{ij} = \frac{1}{2}C_{ijkl}\left(\Delta u_{k,l} + \Delta u_{l,k}\right) - \Delta\sigma_{sw}\delta_{ij} - \beta\Delta T\delta_{ij}\tag{8}$$

where C [Pa] is the elastic matrix tensor, u is the displacement, σ_{sw} [Pa] is the swelling pressure, and β [Pa/°C] is the coefficient used to determine the stress induced from the temperature change, expressed below for the case of an isotropic elastic body:

$$\beta = (3\lambda + 2\mu)\alpha_s \tag{9}$$

where, λ [Pa] and μ [Pa] are Lame's coefficients, defined as follows.:

$$\lambda = \frac{\nu E}{(1+\nu)(1-2\nu)}, \tag{10}$$

$$\mu = \frac{E}{2(1+\nu)}, \tag{11}$$

where E [Pa] is the Young's modulus, ν [-] is the Poisson's ratio, and α_s [1/°C] is the thermal expansion coefficient of porous medium.

σ_{sw} is expressed as follows.

$$\Delta\sigma_{sw} = -F\rho_{w0}g\Delta\psi, \tag{12}$$

where ψ is the water potential head [m], ρ_{w0} is the density of water in reference state [kg/m^3], and g is the gravity acceleration [m/s^2]. F is the function of the degree of saturation, defined as follows.

2.3 Balance of Energy Equation

The balance of energy equation is expressed as follows:

$$\frac{\partial\left[(\rho C_v)_m T\right]}{\partial t} + q_{i,i}^h + Q^h = 0, \tag{13}$$

where q^h [kJ/m^2/sec] is the heat flux and Q^h [kJ/m^3/sec] is the heat source. The term $(\rho C_v)_m$ [kJ/kg/°C] is the specific heat of the field, consisting of water and structured particles (i.e., porous rock mass, buffer), defined by:

$$(\rho C_v)_m = nS_r\rho_l C_{vl} + (1-n)\rho_s C_{vs}, \tag{14}$$

where C_{vl} [kJ/m^3/°C] is the specific heat of water, and C_{vs} [kJ/m^3/°C] is the specific heat of structured particles. The contribution from the gas phase is neglected.

3

Heat flux consists of flux caused by advection, dispersion, and latent heat.

$$q_i^h = q_i^{ad.} + q_i^{dis.} + q_i^{lh.},$$ (15)

where

$$q_i^{ad.} = nS_r\rho_l v_i T,$$ (16)

$$q_i^{dis.} = -\lambda_m T_{,i},$$ (17)

$$q_i^{lh.} = LD_{\theta v}\theta_{,i},$$ (18)

Here, v [m/s] is the velocity, L is , $D_{\theta v}$ is, and λ_m [W/m/°C] is the field's thermal conductivity consisting of water and structured particles, defined by:

$$\lambda_m = nS_r\lambda_l + (1-n)\lambda_s$$ (19)

where λ_l is the thermal conductivity of water and λ_s is the thermal conductivity of structured particles. The contribution from the gas phase is neglected.

3. TASK D THM1 (FEBEX-TYPE REPOSITORY)

The basic models and parameters were determined and described in the report of DECOVALEX-III Task 1. Here the models with those concepts and some developments are described.

3.1 Parameter Setting for Buffer Material

3.1.1 Thermal properties

(1) Specific Heat

The specific heat is taken from the laboratory experiments on bentonite S-2. The specific heat capacity is given as

$$(\rho C)_m = (1-n)\rho_s C_s + nS_r\rho_w C_w,$$ (20)

where C_s is the specific heat of solid particle [J/kg°C], C_w is the specific heat of water [J/kg°C], n is the porosity [-], S_r is the degree of saturation, ρ_s is the density of solid particle [kg/m^3], and ρ_w is the density of water [kg/m^3]. The specific heat of solid particle C_s is a function of temperature as follows.

$$C_s = 1.38T + 732.5.$$ (21)

(2) Thermal Conductivity

Thermal conductivity is a function of the degree of saturation, as follows.

$$\lambda = 1.28 - \frac{0.71}{1 - \exp\left[(S_r - 0.65)/0.10\right]} . \tag{22}$$

Figure 1 shows the relationship between degree of saturation and thermal conductivity.
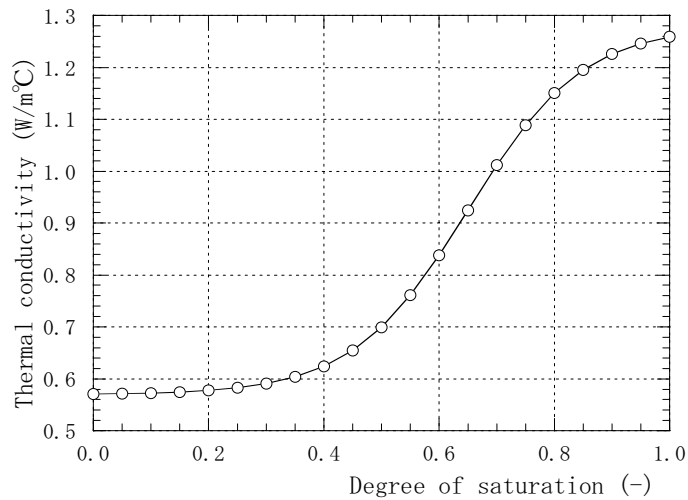
Figure 1 Dependence of thermal conductivity on degree of saturation

(3) Thermal Expansion of the Porous Medium

The linear thermal expansion coefficient is 1.0×10^{-4} [1/°C], as taken from the laboratory experiments.

3.1.2 Hydraulic properties

(1) Saturated Hydraulic Conductivity

Saturated hydraulic conductivity, k [m/s] of FEBEX bentonite is the function of the dry density, ρ_d [g/cm^3] as follows.

$$\log(k) = -6.00\rho_d - 4.09 \quad (\rho_d = 1.30 \sim 1.47),$$

$$\log(k) = -2.96\rho_d - 8.57 \quad (\rho_d = 1.47 \sim 1.84). \tag{23}$$

Assume that these values were obtained at 25°C. They can be converted into intrinsic permeability K [m^2] by the following equation.

$$K = \frac{\mu k}{\rho_w g} \tag{24}$$

where μ is the viscosity of water [Pa s], ρ_w is the density of water [kg/m^3], and g is the gravity acceleration [m/s^2]. Viscosity and density of water at 25°C are

$$\mu \ (25°C) = 0.893 \times 10^{-3} \text{ [Pa s]}, \tag{25}$$

$$\rho_w \ (25°C) = 997.04 \text{ [kg/m}^3\text{]}. \tag{26}$$

From Equations (25), (26), (27), intrinsic permeability was estimated as follows:

$$\log(K) = -6.00\rho_d - 11.13 \ \left(\rho_d = 1.30 \sim 1.47\right),$$

$$\log(K) = -2.96\rho_d - 15.61 \ \left(\rho_d = 1.47 \sim 1.84\right). \tag{27}$$

Figure 2 shows the relationship between intrinsic permeability and dry density.
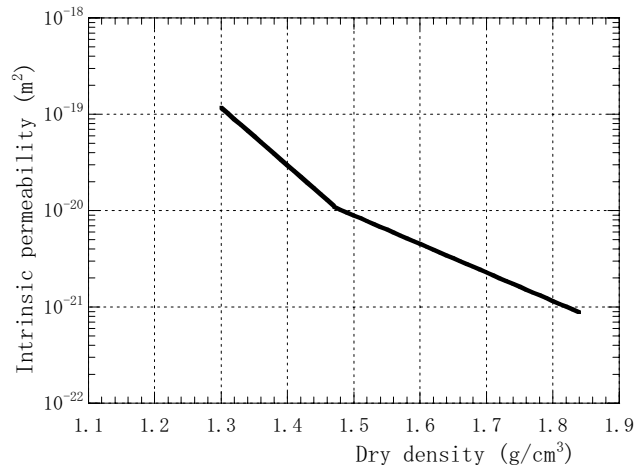
Figure 2 Relationship between intrinsic permeability and dry density

(2) RelativePermeability

Unsaturated hydraulic conductivity k_{uns} is greatly dependent on the degree of saturation. It can be given as the product of relative permeability, k_r by saturated permeability, k_{sat}. Relative permeability for FEBEX bentonite is given as follows:

$$k_r = S_r^m. \tag{28}$$

The value of m was identified by back analysis from laboratory tests. Table 1 shows the result of it. Various m values were obtained by different laboratory tests. For the simulation, the m value 3.0 is used.

Table 1 Exponent for relative permeability law obtained from different types of tests

Application		Value of m
Test	Infiltration Test(CIEMAT)	4.64
	Infiltration Test(UPC-DIT)	3.50
	Heat and water flow test 1	3.06
	Heat and water flow test 2	1.10
	Heat and water flow test 3	1.68
Analysis		3.0

(3) Water Retention Curve

The water retention curve is the relationship between suction, ψ [MPa], and degree of saturation, S_r [-], and is given as

$$\frac{S_r - S_{r\min}}{S_{rmaz} - S_{r\min}} = \left[1 + \left(\frac{\psi}{P_0}\right)^{n_{VG}}\right]^{1-\frac{1}{n_{VG}}}, \tag{29}$$

where $S_{r\min}$ and $S_{r\max}$ are minimum and maximum saturation, and P_0 and ψ are material parameters. The values of these properties are specified in Table 2. The values for the analysis of the in situ test correspond to those of dry density , 1.60 to 1.65g/cm^3 during wetting. The van Genuchten model as shown in Equation (31) is used for the simulation, with the parameters for Equation (31) determined as Equations (32) and (33).

$$\frac{S_r - S_{r\min}}{S_{rmaz} - S_{r\min}} = \left[\frac{1}{1 + \left(\alpha_{VG}\psi\right)^{n_{VG}}}\right]^{1-\frac{1}{n_{VG}}}, \tag{30}$$

$$\alpha_{VG} = 0.033 \ [1/\text{MPa}], \tag{31}$$

$$n_{VG} = 2.125 \ [\text{-}]. \tag{32}$$

The retention curve for simulation is shown in Figure 3.

7

Table 2 Parameters of the retention curves

Process	Dry density ρ_d [g/cm^3]	P_0 [MPa]	$\dfrac{1}{n_{VG}} - 1$	$S_{r\,min}$	$S_{r\,max}$
Wetting path	1.70-1.75	90.0	0.45	0.00	1.00
	1.60-1.65	30.0	0.32	0.10	1.00
	1.58-1.59	4.5	0.17	0.00	1.00
Drying path	1.70-1.75	180.0	0.62	0.00	1.00
	1.58-1.59	30.0	0.15	0.00	1.00
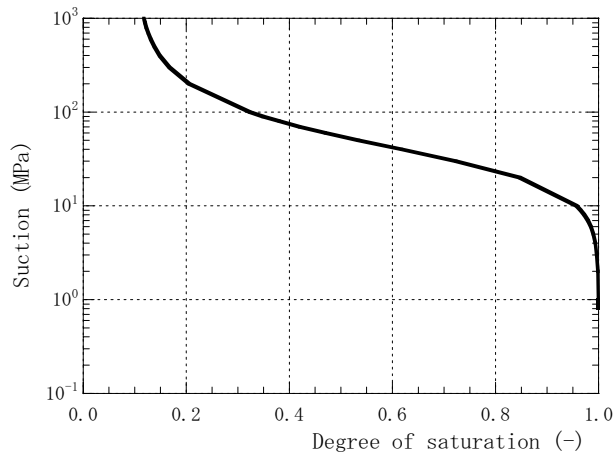
Figure 3 Water retention curve in analysis

(4) Thermal Water Diffusivity

Moisture movement resulting from thermal gradient in an unsaturated area is expressed by using the coefficient of thermal water diffusivity, D_T. The value of D_T is determined by back analysis using data from the laboratory tests by UPC. Intrinsic permeability, relative permeability, and water retention curve are those specified above. Analytical conditions are as follows:

Size of specimen :   diameter 38 mm, height 76 mm

Initial dry density :   1,680 kg/m^3

Thermal boundary conditions :   2.6 W at one end and fixed at the other

Initial water content :   15.3, 16.9, 17.1%

Thermal water diffusivity obtained from the back analysis of the laboratory test is as follows:

$$D_T = 2.0 \times 10^{-12} \ [\text{m}^2/\text{s}/°\text{C}], \tag{33}$$

3.1.3 Mechanical properties

(1) Elastic Modulus

Figure 4 shows the relationship between the shear modulus and the dry density, and Figure 5 shows the relationship between the shear modulus and the degree of saturation obtained by laboratory tests. These figures show that the shear modulus increases with the increase of the dry density and degree of saturation. Therefore, we assume that shear modulus G [MPa] is expressed by using dry density ρ_d [g/cm^3] and degree of saturation S_r [%], as in the following linear equation:

$$G = c_1 + c_2\rho_d + c_3 S_r. \tag{34}$$

The following equation shows the result of regression analysis using the test result in S3=0.01 MPa.

$$G = -234.7 + 0.176\rho_d + 2.1S_r. \tag{35}$$

Figure 6 shows the comparison of the relationship concerning shear modulus between the value from Equation (36) and the measured value. For our simulation, the elastic modulus is needed. Elastic modulus E is calculated as follows:

$$G = \frac{E}{2(1+\nu)}. \tag{36}$$

where ν is the Poisson's ratio.
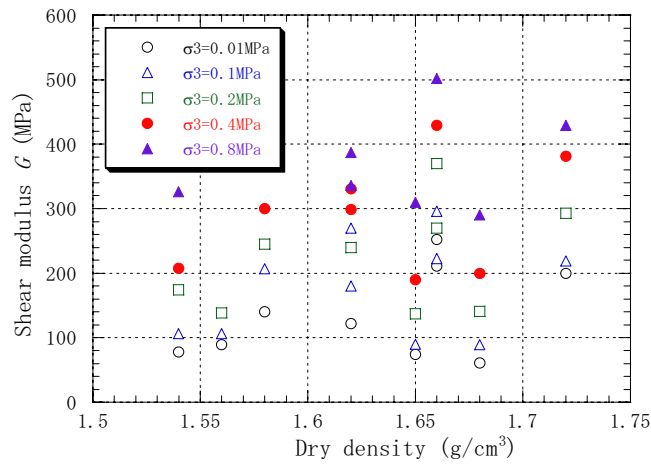
Figure 4. The relationship between shear modulus and dry density
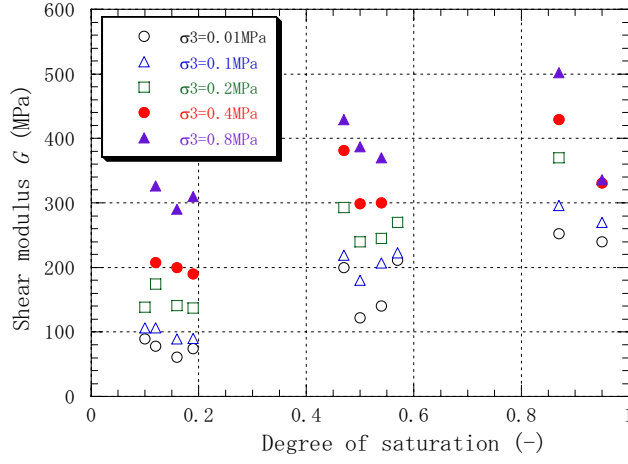
Figure 5. The relationship between shearing modulus and degree of saturation
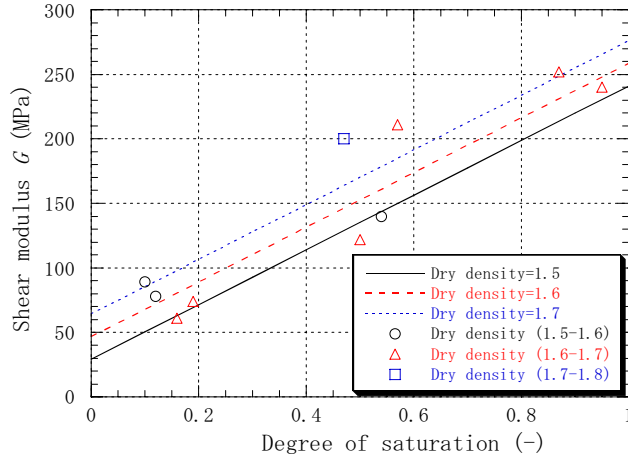
Figure 6. Comparison of the relationship concerning shear modulus

(2) Swelling Pressure

The maximum swelling pressure of FEBEX bentonite is defined as a function of dry density,

$$\sigma_{sw\max} = \exp\!\left(6.77 \times 10^{-3}\rho_d - 9.07\right), \tag{37}$$

where $\sigma_{sw\max}$ [MPa] is maximum swelling pressure, and ρ_d [kg/m^3] is dry density.

During the resaturation process of the buffer, the swelling pressure under unsaturated conditions is important, although the above equation is limited to saturated conditions.

Free energy change is asumed to be equal to potential swelling pressure (Nakano et al.1984) and is approximately equal to the suction in the case of the buffer material. Because gravity potential of the buffer is negligible compared with the osmotic, the matric potential is the main contribution to the suction. Therefore, it can be said that the swelling pressure is expressed by suction. The suction, however, is consumed during the resaturation process, not only by swelling but also by soil structure changes. We define the function F that illustrates the ratio of suction contributing to swelling pressure, as follows:

$$\Delta \sigma_{sw} = -F \Delta \psi .$$ (38)

F F is defined as a function of saturation.

$$F = \frac{1}{2} \sigma_{sw\max} S_r^{\frac{1}{2}} \frac{\partial S_r}{\partial \psi} .$$ (39)

3.2. Parameters of Other Materials

The parameters of other materials are shown in Table 3.

Table 3 Parameters for FEBEX

		Rock	Bentonite	Canister
Density [kg/m^3]		2,640	1,600	7,000
Young's modulus [MPa]		3,200	function	Rigid
Poisson's ratio [-]		0.30	0.40	
Initial porosity [-]		10^{-4}	0.46	
Intrinsic permeability [m^2]		1.0×10^{-17}	2.0×10^{-21}	
VG parameter	θ_s [-]	0.01	Eq(31)-(33)	Impermeable
	θ_r [-]	0.0		
	α_{VG} [1/m]	5.2×10^{-4}		
	n_{VG} [-]	1.6		
Relative permeability [-]		Mualem model (1976)	$k_r = S_r^{3.0}$	
Thermal water diffusivity		Not considered		
Thermal conductivity [W/m/K]		3.0	Eq(23)	53.0
Specific heat [kJ/kg/K]		0.90	Eq(22)	0.46
Thermal expansion [1/K]		1.0×10^{-5}	1.0×10^{-5}	1.0×10^{-5}

Mualem model: $r_k = \sqrt{S_e}\left[1-\left(1-S_e^{1/m}\right)^m\right]^2, S_e = \dfrac{\theta - \theta_r}{n(\theta_s - \theta_r)}$

3.3 Numerical Simulation

Based on the description, the mesh for Task D THM1 (FEBEX Type Repository) was made as shown in Figure 7. It has 7,110 nodes and 3,440 elements. Temperature and water pressure at the top surface and bottom line are fixed at their initial value. Some

displacements are constrained: The vertical displacements at the bottom line, the horizontal displacements normal to the tunnel axis at both sides, and the horizontal displacements parallel to the tunnel axis. Calculations were done under the thermal power decay function of a reference fuel PWR element (245 W/m case) (Table 4).
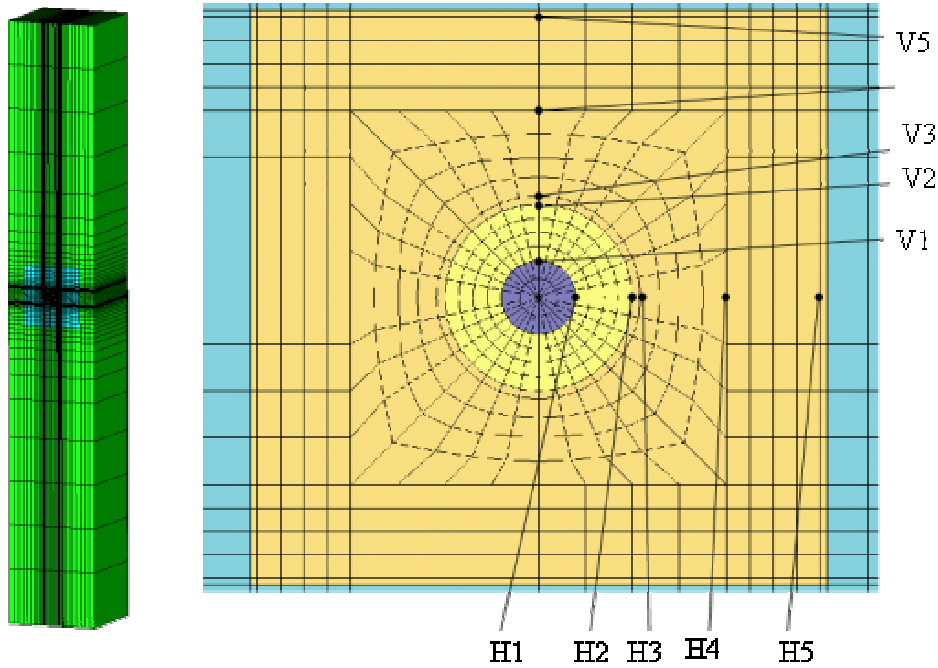
Figure 7 Mesh for Task D THM1 (FEBEX Type Repository)

Table 4. Thermal Power Decay Function (245W/m case)

Time [years]	Power [W/m^3]	Time [years]	Power [W/m^3]	Time [years]	Power [W/m^3]
0.00E+0	3.84563E+2	5.70E+2	3.84563E+1	1.9970E+4	3.07650E+0
1.00E+1	3.17264E+2	7.70E+2	2.88422E+1	2.9970E+4	2.11510E+0
2.00E+1	2.88422E+2	9.70E+2	2.40352E+1	5.9970E+4	9.61407E-1
3.00E+1	2.40352E+2	1.47E+3	1.92281E+1	9.9970E+4	4.32633E-1
4.00E+1	2.01895E+2	1.97E+3	1.44211E+1	1.9997E+5	3.07650E-1
7.00E+1	1.44211E+2	2.97E+3	1.05755E+1	2.9997E+5	2.78808E-1
1.30E+2	9.61407E+1	3.97E+3	8.65266E+0	3.9997E+5	2.30738E-1
1.70E+2	6.72985E+1	5.97E+3	7.69126E+0	7.9997E+5	1.92281E-1
2.70E+2	5.28774E+1	9.97E+3	6.24915E+0	9.9997E+5	1.73053E-1
3.70E+2	4.80704E+1				

3.4 Results

Figure 8 shows the temperature evolutions at the points shown in Figure 7. Maximum temperature is 104°C, achieved after 5 years. Figure 9 shows the vertical profile of

12

temperature; Figure 10 shows the water saturation evolution in the bentonite near the canister. Water saturation near the canister is about 56% up to 5 years, and resaturation time is about 200 years. Figure 11 shows the evolution of vertical displacement. Peak displacement at the ground surface is 0.21 m and occurs after 1,000 to 2,000years. Figure 12 shows the profile of vertical displacement; Figure 13 shows the evolution of stress in the bentonite. Stress increased to about 8 MPa and became constant after 1,000 years.
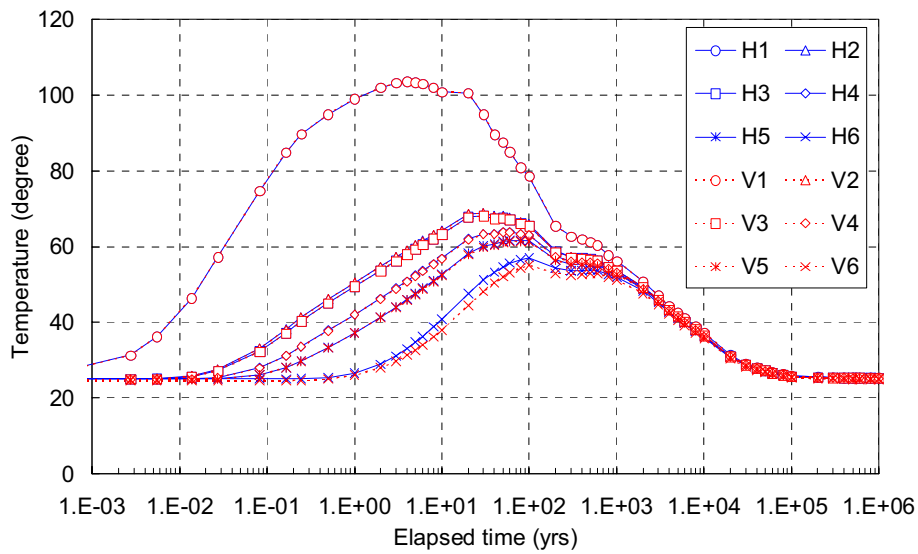
Figure 8. Evolution of temperature
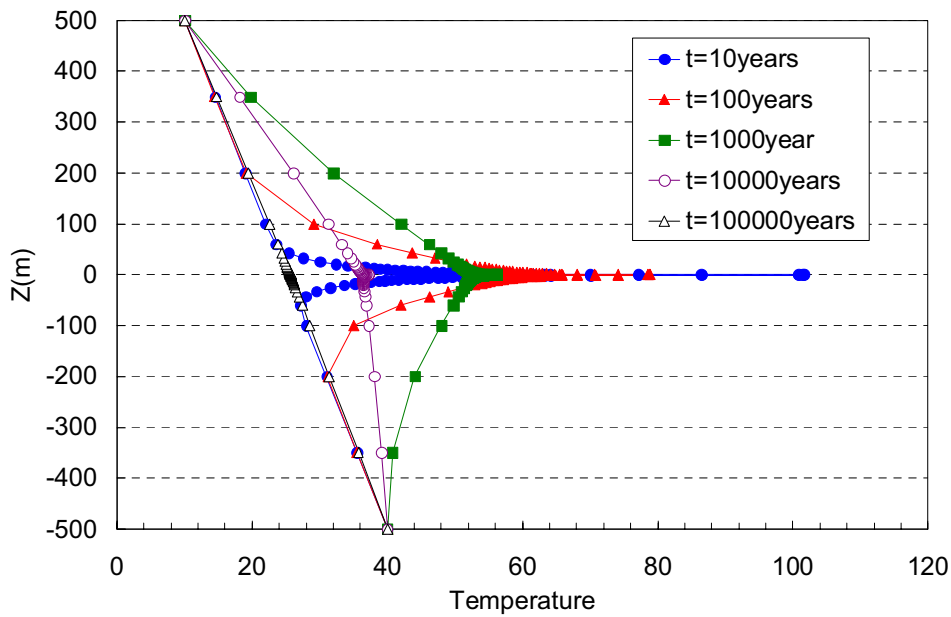
Figure 9. Vertical temperature profile
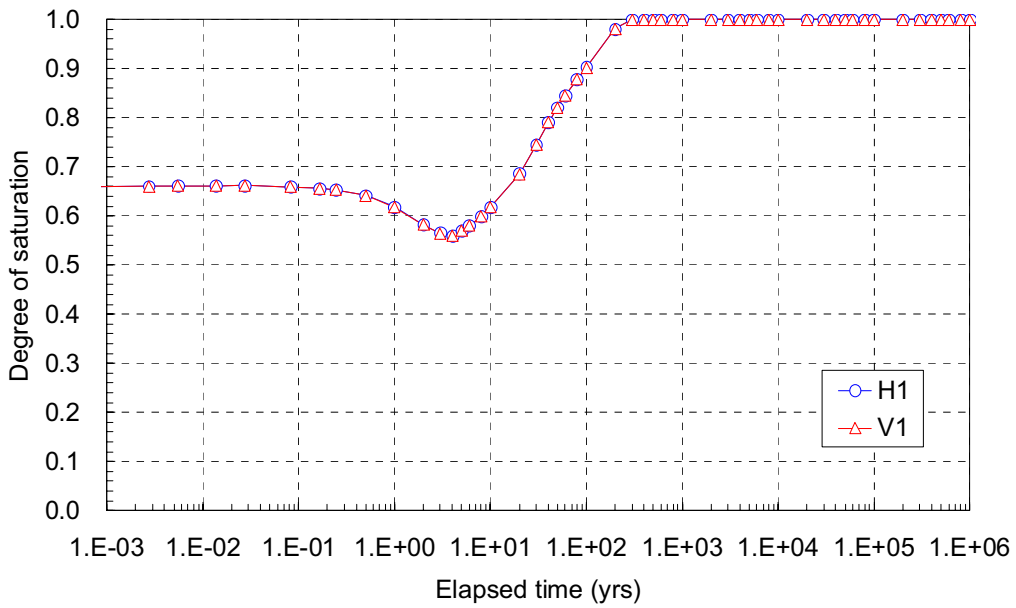
Figure 10. Evolution of degree of saturation

Figure 11. Evolution of vertical displacement

14
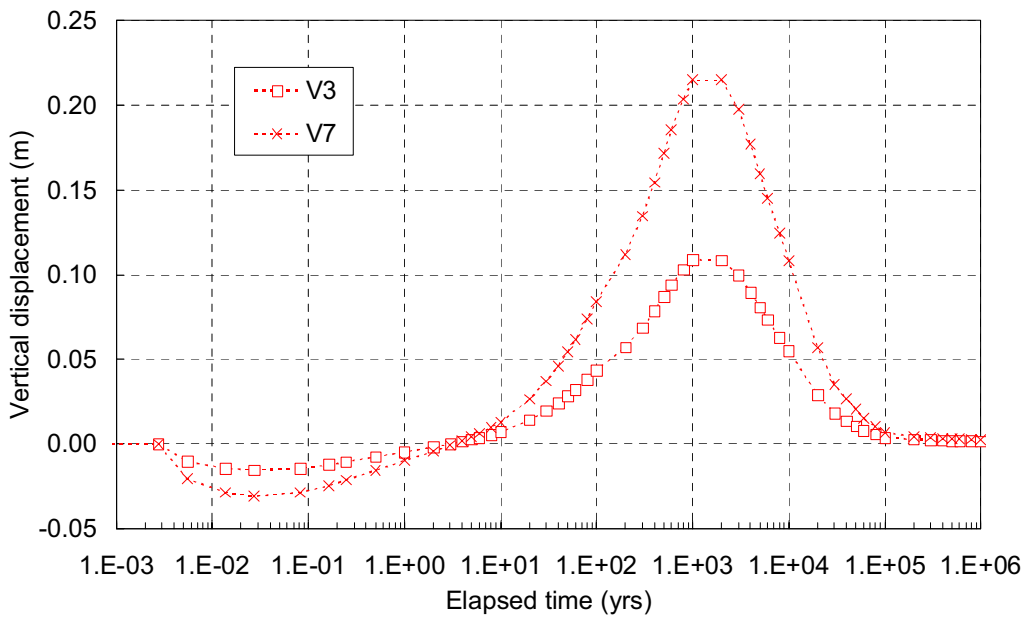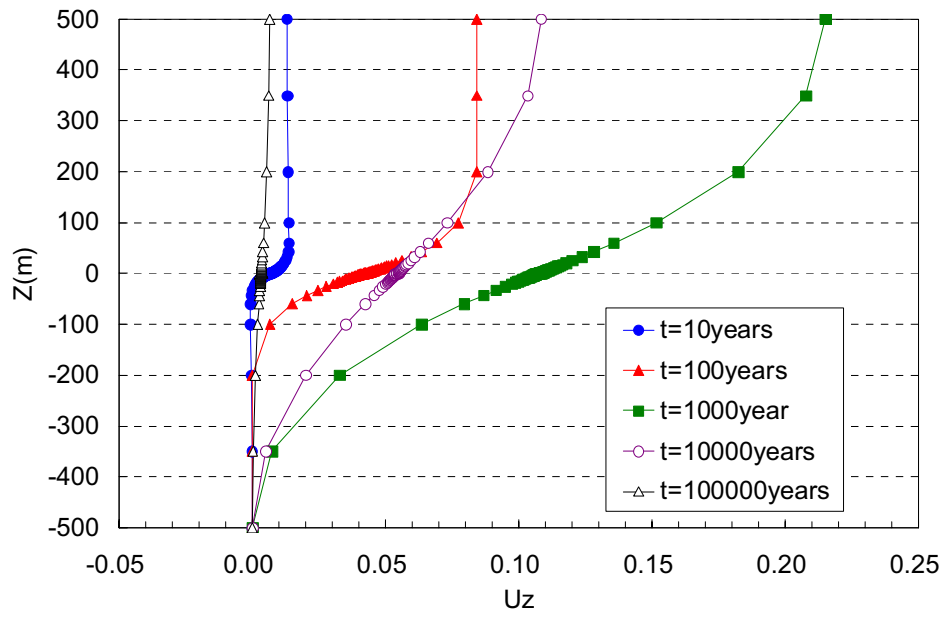
Figure 12. Vertical displacement profile
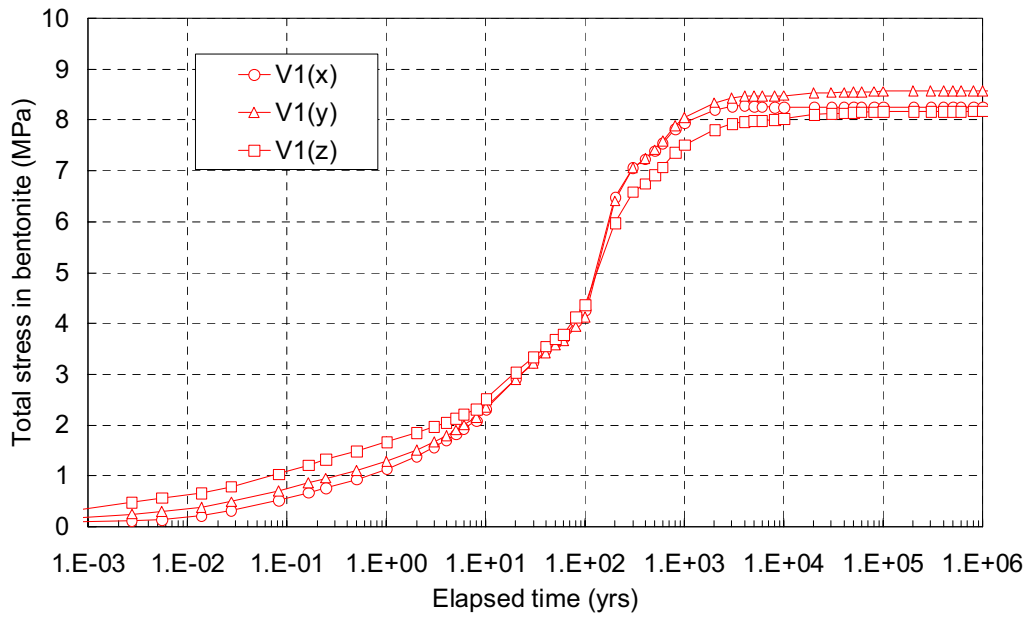
Figure 13. Evolution of total stress in bentonite

15

4. TASK D THM2 (YUCCA MOUNTAIN TYPE REPOSITORY)

4.1 Models

THM2 calculations are based on Ito's model (Sonnenthal et al., 2005). Thermal conductivity and the specific heat of medium are set up as follows:

$$\lambda_m = \lambda_m^{dry} + \left(\lambda_m^{sat.} - \lambda_m^{dry}\right)S_r, \tag{40}$$

$$C_m = C_m^0. \tag{41}$$

Intrinsic permeability and porosity for our simulation are estimated because our hydrological model is based on a single continuum model.

$$K = \left(1 - n^F\right)K^M + n^F K^F, \tag{42}$$

$$n = n^M + n^F, \tag{43}$$

where superscript F signifies Fracture and M Matrix.

In our hydrological modeling, we assume that the pressure heads of the matrix and fractures are always the same. Based on this assumption, we set degree of saturation and relative permeability as shown in Equations and estimate retention curve and relative permeability for our hydraulic model.

$$S = \frac{n^M S^M + n^F S^F}{n^M + n^F}, \tag{44}$$

$$Kk_r = \left(1 - n^F\right)K^M k_r^M + n^F K^F k_r^F. \tag{45}$$

Vapor movement, modeled as diffusion resulting from thermal gradient and thermal vapor diffusivity D_{Tv} is estimated through comparison with simulated liquid saturation by the TOUGH code (Datta (2002)).

$$D_{Tv} = D_{Tv}^0 \exp\left(a_3 T^3 + a_2 T^2 + a_1 T + T_0\right). \tag{46}$$

$$D_{Tv} = 1.0 \times 10^4 \exp\left(2.754 \times 10^{-7} T^3 - 2.041 \times 10^{-4} T^2 + 6.706 \times 10^{-2} T - 3.209 \times 10^1\right).$$

The parameters of other materials are shown in Table 5.

Table 5. Parameters for YMP

		Tptpmn Rock	Air, Canister
Density [kg/m³]		2,530	8,610
Young's modulus [MPa]		15,000	Rigid
Poisson's ratio [-]		0.21	
Initial porosity [-]		0.13	
Intrinsic permeability [m²]		2.739×10^{-15}	Impermeable
VG Parameter	θ_s [-]	0.11	
	θ_r [-]	0.0198	
	α_{VG} [1/m]	0.0225	
	m_{VG} [-]	1.328	
Relative permeability [-]		Mualem model (1976)	
Thermal water diffusivity		function (24)	
Thermal conductivity [W/m/K]		function (22)	8
Specific heat [kJ/kg/K]		985	200
Thermal expansion [1/K]		1.0×10^{-5}	0

Mualem model: $\sqrt{S_e}\left[1 - \left(1 - S_e^{1/m}\right)^m\right]^2$

4.2 Numerical Simulation

Based on the description, the mesh for Task D THM2 (Yucca Mountain Type Repository) was constructed as in Figure 13, with 5,232 nodes and 2,522 elements. The temperature at top surface and bottom line, and the saturation at bottom line, are constrained. Some displacements are constrained: the vertical displacements at the bottom line, the horizontal displacements normal to the tunnel axis at both sides, and the horizontal displacements that are parallel to the tunnel axis. Calculations were done under the thermal power per meter drift for a 1,450 W/m initial thermal line load, reduced by 86.3% for 50 years as a result of the drift ventilation case (Table 6).
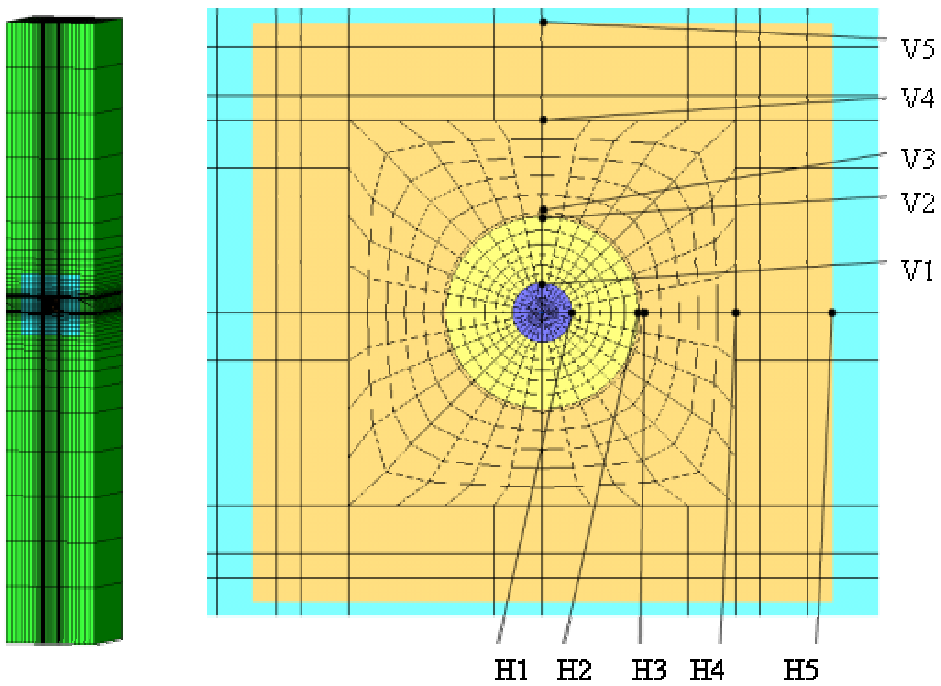
Figure 13. Numerical mesh for THM2 (Yucca Mountain type repository)

Table 6. Thermal power decay function

Time [years]	Power [W/m^3]	Time [years]	Power [W/m^3]	Time [years]	Power [W/m^3]
0.00E+0	8.76729E+1	6.00E+1	2.28655E+2	7.51E+2	3.84175E+1
1.00E+0	8.45890E+1	6.10E+1	2.25571E+2	8.01E+2	3.64790E+1
2.00E+0	8.19455E+1	6.20E+1	2.22927E+2	8.51E+2	3.47167E+1
3.00E+0	7.97427E+1	6.30E+1	2.20284E+2	9.01E+2	3.30426E+1
4.00E+0	7.79804E+1	6.40E+1	2.17640E+2	9.51E+2	3.15446E+1
5.00E+0	7.62182E+1	6.50E+1	2.14997E+2	1.00E+3	3.01348E+1
6.00E+0	7.44559E+1	6.60E+1	2.12354E+2	1.50E+3	2.08388E+1
7.00E+0	7.31342E+1	6.70E+1	2.09710E+2	2.00E+3	1.63891E+1
8.01E+0	7.13719E+1	6.80E+1	2.07067E+2	2.50E+3	1.41422E+1
9.01E+0	7.00502E+1	6.90E+1	2.04864E+2	3.00E+3	1.29086E+1
1.00E+1	6.87285E+1	7.00E+1	2.02661E+2	3.50E+3	1.21156E+1
1.10E+1	6.69663E+1	7.10E+1	2.00018E+2	4.00E+3	1.15429E+1
1.20E+1	6.56446E+1	7.20E+1	1.97815E+2	4.50E+3	1.11023E+1
1.30E+1	6.47634E+1	7.31E+1	1.95612E+2	5.00E+3	1.06617E+1
1.40E+1	6.34417E+1	7.41E+1	1.93409E+2	5.50E+3	1.03093E+1
1.50E+1	6.21200E+1	7.51E+1	1.91206E+2	6.00E+3	9.95682E+0
1.60E+1	6.07983E+1	7.61E+1	1.89444E+2	6.50E+3	9.60437E+0
1.70E+1	5.99172E+1	7.71E+1	1.87241E+2	7.00E+3	9.29597E+0
1.80E+1	5.90360E+1	7.81E+1	1.85038E+2	7.51E+3	9.03163E+0
1.90E+1	5.81549E+1	7.91E+1	1.83276E+2	8.01E+3	8.72324E+0

2.00E+1	5.72738E+1	8.01E+1	1.81514E+2	8.51E+3	8.45890E+0
2.10E+1	5.59521E+1	8.11E+1	1.79311E+2	9.01E+3	8.19455E+0
2.20E+1	5.50709E+1	8.21E+1	1.77549E+2	9.51E+3	7.93021E+0
2.30E+1	5.41898E+1	8.31E+1	1.75786E+2	1.00E+4	7.70993E+0
2.40E+1	5.33087E+1	8.41E+1	1.74024E+2	1.50E+4	5.81549E+0
2.50E+1	5.24275E+1	8.51E+1	1.72262E+2	2.00E+4	4.49379E+0
2.60E+1	5.15464E+1	8.61E+1	1.70500E+2	2.50E+4	3.61706E+0
2.70E+1	5.06653E+1	8.71E+1	1.68737E+2	3.00E+4	2.97824E+0
2.80E+1	4.97841E+1	8.81E+1	1.66975E+2	3.50E+4	2.50242E+0
2.90E+1	4.89030E+1	8.91E+1	1.65653E+2	4.00E+4	2.13675E+0
3.00E+1	4.84624E+1	9.01E+1	1.63891E+2	4.50E+4	1.84598E+0
3.10E+1	4.75813E+1	9.11E+1	1.62569E+2	5.00E+4	1.62129E+0
3.20E+1	4.67001E+1	9.21E+1	1.60807E+2	5.50E+4	1.43184E+0
3.30E+1	4.58190E+1	9.31E+1	1.59485E+2	6.00E+4	1.26883E+0
3.40E+1	4.53784E+1	9.41E+1	1.58164E+2	6.50E+4	1.13666E+0
3.50E+1	4.44973E+1	9.51E+1	1.56401E+2	7.00E+4	1.02652E+0
3.60E+1	4.39246E+1	9.61E+1	1.55080E+2	7.51E+4	9.29597E-1
3.70E+1	4.32197E+1	9.71E+1	1.53758E+2	8.01E+4	8.41484E-1
3.80E+1	4.26029E+1	9.81E+1	1.52436E+2	8.51E+4	7.70993E-1
3.90E+1	4.19420E+1	9.91E+1	1.51115E+2	9.01E+4	7.22531E-1
4.00E+1	4.13252E+1	1.00E+2	1.49793E+2	9.51E+4	6.69663E-1
4.10E+1	4.07525E+1	1.10E+2	1.38779E+2	1.00E+5	6.16794E-1
4.20E+1	4.01357E+1	1.20E+2	1.29527E+2	1.50E+5	4.15896E-1
4.30E+1	3.95189E+1	1.40E+2	1.14107E+2	2.00E+5	3.72720E-1
4.40E+1	3.89902E+1	1.50E+2	1.07939E+2	2.50E+5	3.63909E-1
4.50E+1	3.83734E+1	1.60E+2	1.03533E+2	3.00E+5	3.55979E-1
4.60E+1	3.78447E+1	1.70E+2	9.91277E+1	3.50E+5	3.44964E-1
4.70E+1	3.73161E+1	1.80E+2	9.51626E+1	4.00E+5	3.36594E-1
4.80E+1	3.67433E+1	1.90E+2	9.16380E+1	4.50E+5	3.28663E-1
4.90E+1	3.62587E+1	2.00E+2	8.85541E+1	5.00E+5	3.03110E-1
4.99999E+1	3.57741E+1	2.50E+2	7.75399E+1	5.50E+5	2.95180E-1
5.00E+1	2.61256E+2	3.00E+2	7.00502E+1	6.00E+5	2.86809E-1
5.10E+1	2.57732E+2	3.50E+2	6.38823E+1	6.50E+5	2.78879E-1
5.20E+1	2.54207E+2	4.00E+2	5.90360E+1	7.00E+5	2.68306E-1
5.30E+1	2.50683E+2	4.50E+2	5.50709E+1	7.51E+5	2.60375E-1
5.40E+1	2.47158E+2	5.00E+2	5.15464E+1	8.01E+5	2.52445E-1
5.50E+1	2.44074E+2	5.50E+2	4.84624E+1	8.51E+5	2.44956E-1
5.60E+1	2.40990E+2	6.00E+2	4.53784E+1	9.01E+5	2.34382E-1
5.70E+1	2.37466E+2	6.50E+2	4.28672E+1	9.51E+5	2.26892E-1
5.80E+1	2.34382E+2	7.00E+2	4.05763E+1	1.00E+6	2.18962E-1
5.90E+1	2.31738E+2				

4.3 Results

Figure 14 and 15 are temperature distributions. In this calculation, maximum temperature is 120.81°C after 71 years at V3, and 77.125°C after 650 years at V6. Figure 16 shows the vertical profile of temperature, which Figures 17 and 18 show the water saturation evolution. Water saturation near the canister dries to about 32.3% after 70 years, and resaturation is very slow. Figure 19 and 20 show the evolution of horizontal stress. Horizontal stress has peak at 22.2 MPa after 76.1 years (V3) and 15.6 MPa after 550 years, and that quickly became smaller after it peaks. Figure 21 shows the evolution of vertical displacement. The peak displacement at ground surface is 0.233 m and occurs after 1,000 to 2,000years.
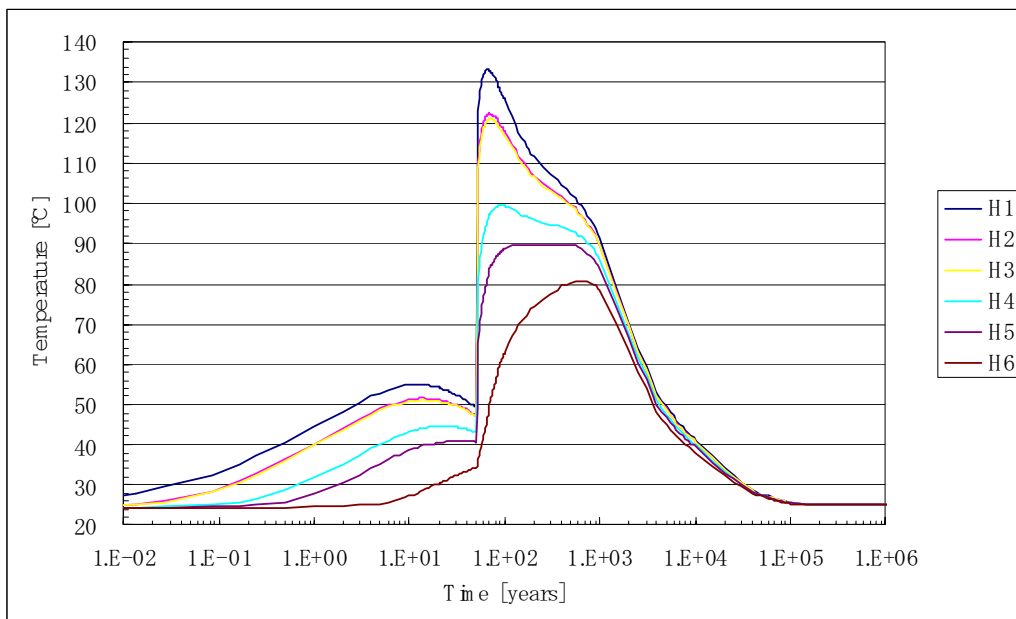
Figure 14. Temperature profiles at horizontal points
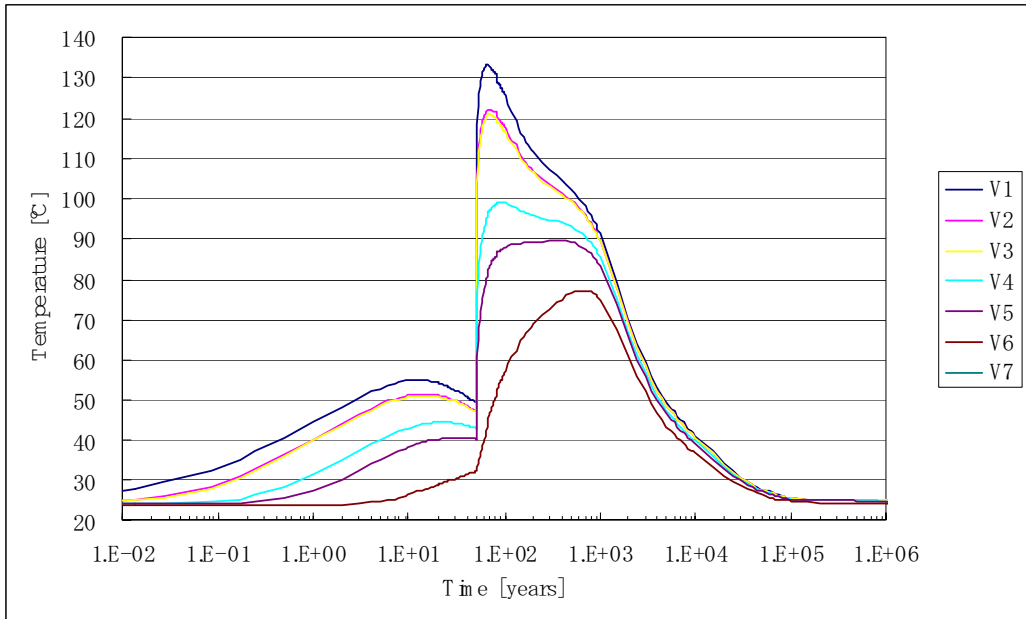
Figure 15. Temperature profiles at vertical points
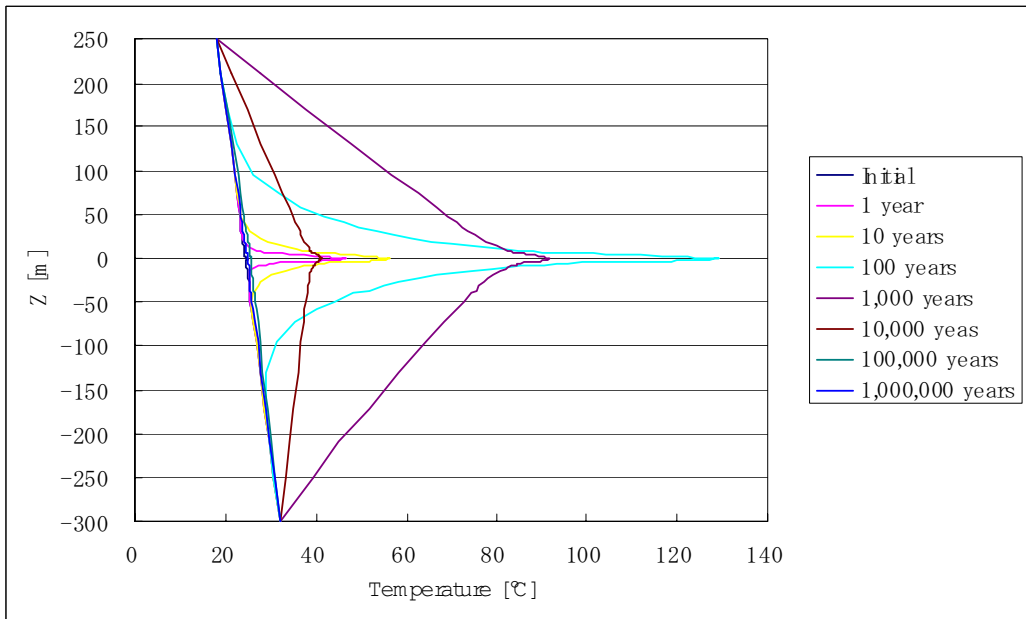
Figure 16. Temperature profiles on Z-axis

21
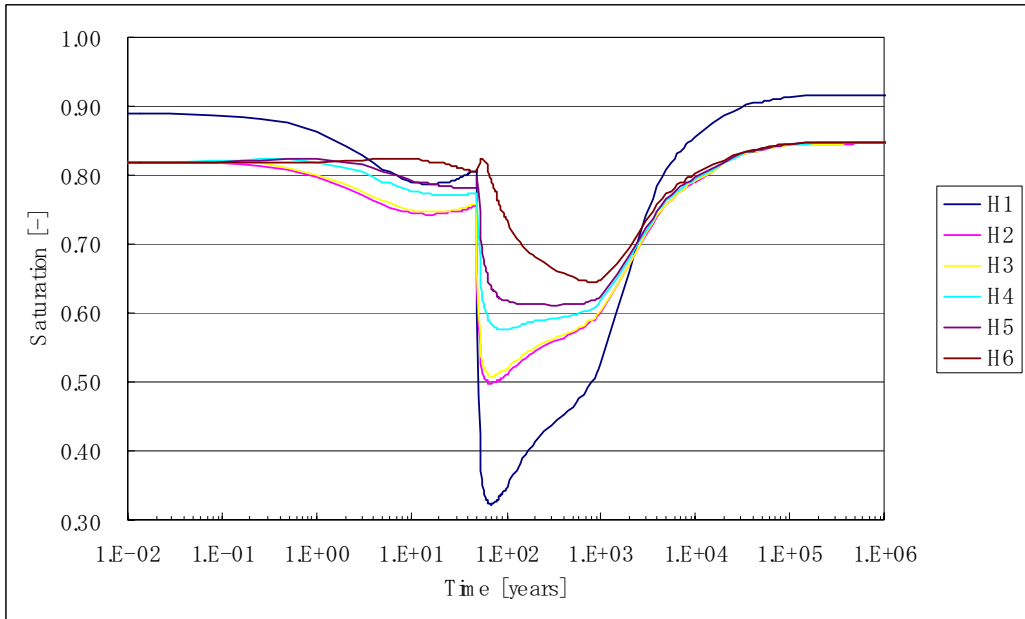
Figure 17. Saturation profiles at horizontal points
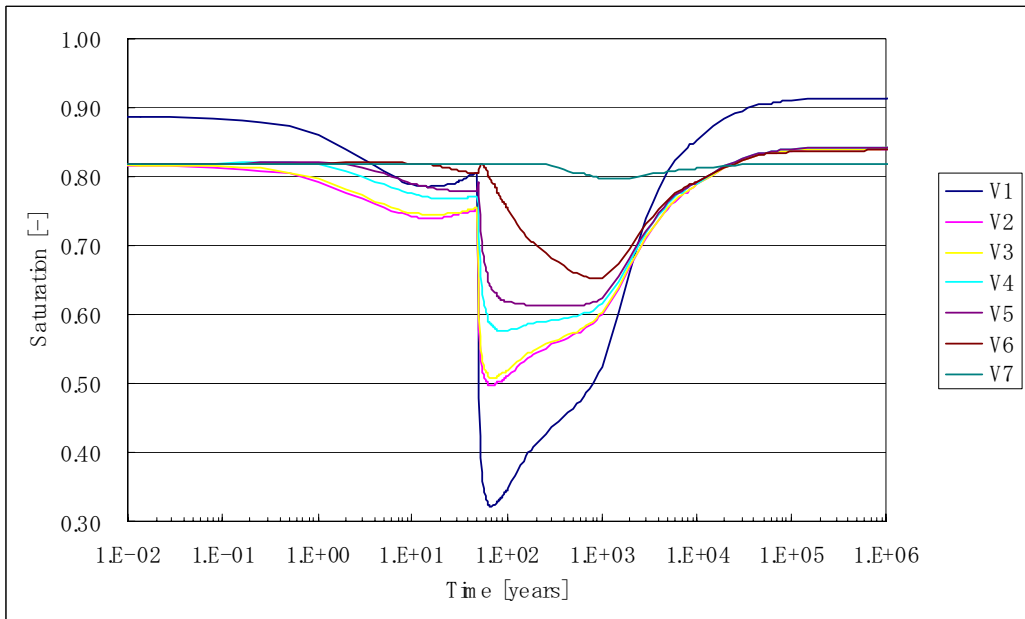
Figure 18. Saturation profiles at vertical points

22
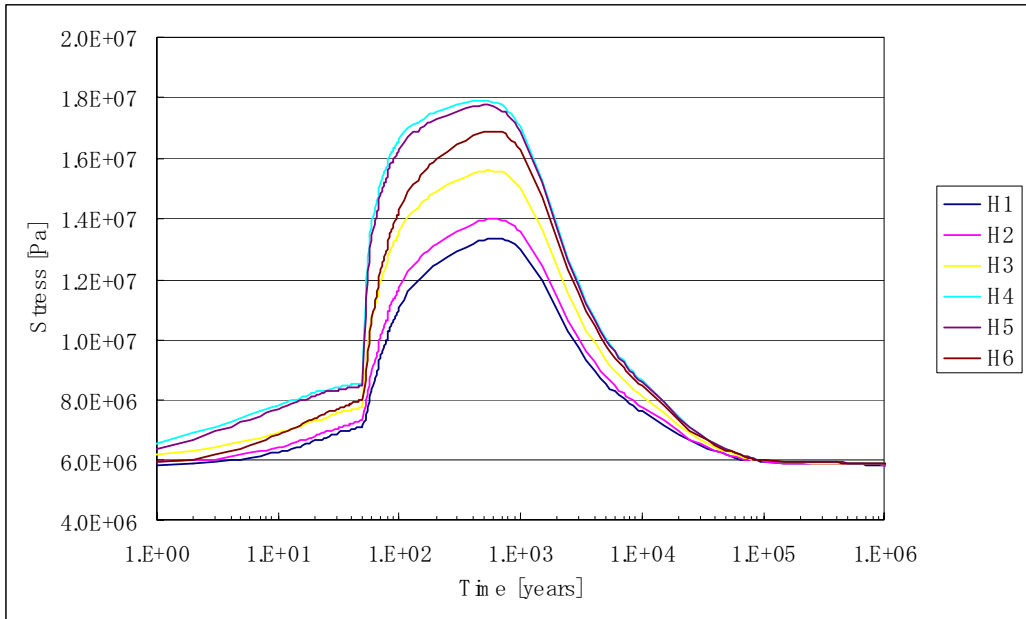
Figure 19. Horizontal stress profiles at horizontal points
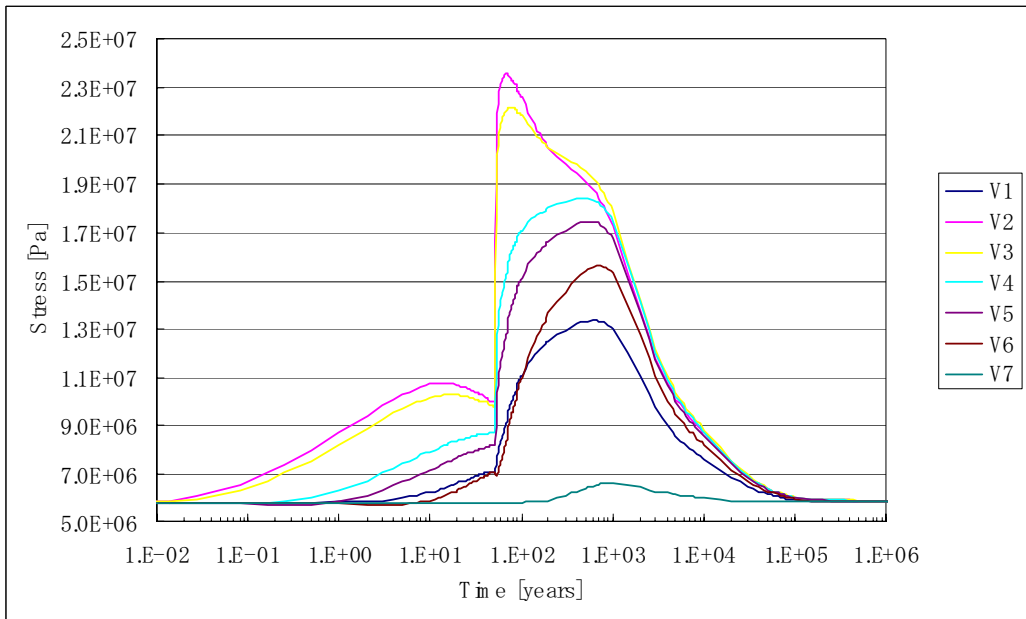
Figure 20. Horizontal stress profiles at vertical points

23
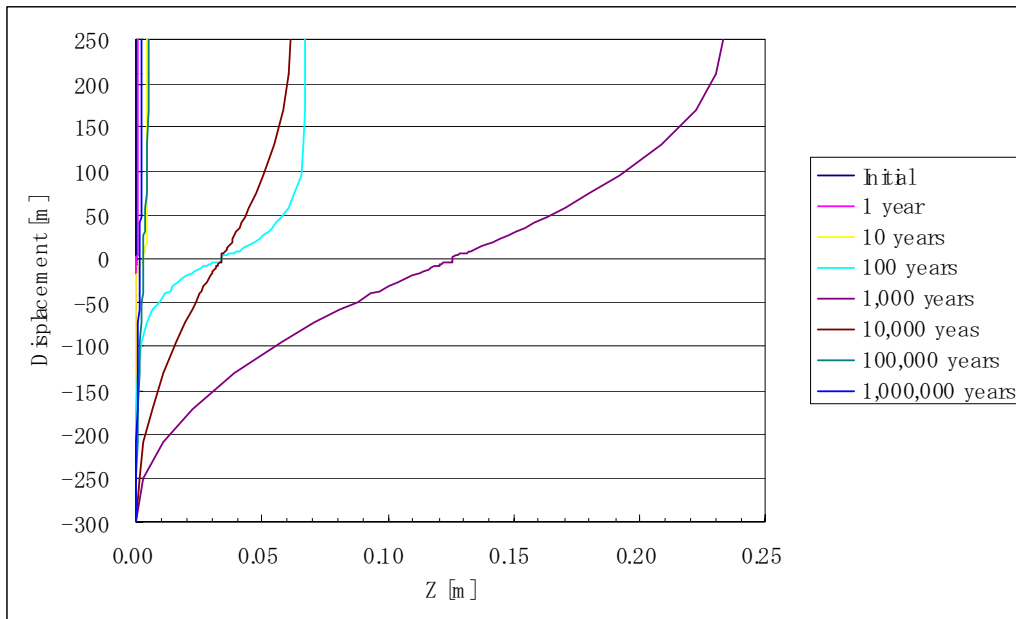
Figure 21. Vertical displacement on Z-axis

5. SUMMARY AND DISCUSSION

Japan's Team has calculated THM1 (FEBEX) and THM2 (Yucca Mountain) using the THAMES code. In these calculations, THAMES treated only the phase after canister is ruptured. These results show the difference for the saturation compared with others. It maybe mainly comes from the difference of the handling for thermal water diffusivity.

6. REFERENCES

Chijimatsu, M., Fujita, T., Kobayashi, A. and Nakano, M. 2000. Experiment and validation of numerical simulation of coupled thermal, hydraulic and mechanical behaviour in the engineered buffer materials, Int. J. Numer. Anal. Meth. Geomech., 24, 403-424.

ENRESA 1998. FEBEX Full-Scale Engineered Barriers Experiment in Crystalline Host Rock, Pre-Operational Stage, Summary Report

ENRESA 2000. FEBEX Project Final Report, Publicaciones tecnica 1/2000.

Fujita T., Kobayashi A. and Börgesson L. 1996. Experimental investigation and mathematical simulation on coupled T-H-M processes of the engineered buffer materials, the TC3 problem. In: Stephansson O, Jing L, Tsang C-F editors. Coupled thermo-hydro-mechanical processes of fractured media, Developments in Geotechnical Engineering, No. 79, Amsterdam: Elsevier, 369-392.

Komine H., Kurikami, H., Chijimatsu, M., Kobayashi, A., Sugita Y. and Ohnishi, Y. 2003. Coupled thermal, hydraulic and mechanical simulation with theoretical model for swelling characteristics, GeoProc 2003.

Mualem, Y. 1976, A conceptual model of hysteresis, Water Resour. Res., 10(3), 514-520.

Nakano, M., Amemiya, Y., Fujii, K. and Ishida, A. 1984. Water Penetration and Swelling Pressure of Restrained Unsaturated Clay(in Japanese). JSIDRE 112: pp. 55-66.

Ohnishi, Y., Shibata, H. and Kobayashi, A. 1985, Development of Finite Element Code for the Analysis of Coupled Thermo-Hydro-Mechanical Behaviors of a Saturated-Unsaturated Medium, Proc. of Int. Symp. on Coupled Process Affecting the Performance of a Nuclear Waste Repository, Berkeley, pp. 263-268.

Ohnishi, Y., Shibata, H. and Kobayashi, A. 1987. Development of finite element code for the analysis of coupled thermo-hydro-mechanical behavior of a saturated-unsaturated medium. In: Tsang, C.-F. Coupled Processes Associated with Nuclear Waste Repositories, Academic Press, Orlando, pp. 551-557.

Philip, J.R. and de Vries, D.A. 1957. Moisture movement in porous materials under temperature gradient, Transactions, Aemerican Geophysical Union, 38(2), 229-237.

Rutqvist J., Börgesson L., Chijimatsu M., Nguyen S., Jing L., Noorished J. and Tsang C-F. 2001. Coupled thermo-hydro-mechanical analysis of a heater test in fractured rock and bentontie at Kamaishi Mine – comparison of field results to predictions of four finite element codes, IJRMMS, 38(1) 129-142.

Sonnenthal E., Ito A., Spycher N., Yui M., Apps J., Sugita Y., Conrad M., and Kawakami S. 2005. International Journal of Rock Mechanics & Mining Sciences, 42(6), 698–719.

Sugita Y., Ito A., Chijimatsu M. and Kurikami H. 2002. Prediction analysis A for the PRP with numerical code THAMES, SKB IPR-02-24.

de Vries, D.A. 1974, Heat transfer in soils. In: Heat and Mass Transfer in the Biosphere:. 1. Transfer Processes in Plant Environment (D.A. De Vries and N. H.Afghan, eds.) New York, John Wiley & Sons Inc.

Appendix E

Status Report for D_THM

BGR Team (Germany)

Center of Applied Geosciences
University of Tübingen

Geozentrum Hannover
Bundesanstalt für Geowissenschaften und Rohstoffe

_____

DECOVALEX IV Task D, BGR Team

Progress on THM Analysis

W. Wang, M. Xie and O. Kolditz (UT)
T. Nowak, H. Kunz and H. Shao (BGR)

_____

Tübingen   August   2005

1. INTRODUCTION

In the past couple of months, the work of THM simulation has focused on code development for GeoSys/Rockflow. A universal finite element object, ELE_FEM, as well as topological element objects, ELE_GEO, for multi-physical problems has been developed. It has tested successfully for several problems such as liquid flow, Richard's flow, heat transport, elasto-plastic deformation and the various couplings among them [7]. We utilized the present version of GeoSys/Rockflow to analyze the DECOVALEX THMC THM1 problems, the details of which can be found in the definition of Task D [1]. The details of the analysis are described as follows.

2. CONCEPTUAL MODEL

We split the simulation into two phases. In the first phase, an initial state for stress, water pressure and temperature is established by excavation simulation. For the initial stress analysis, we first set up a stress profile using the assumption given in [1], then get the initial stress after excavation with the Mana's method. The operation simulation, i.e. THM simulation after installing canister and bentonite to cave, is done in the second phase. Figure 1 depicts the simulation procedure.
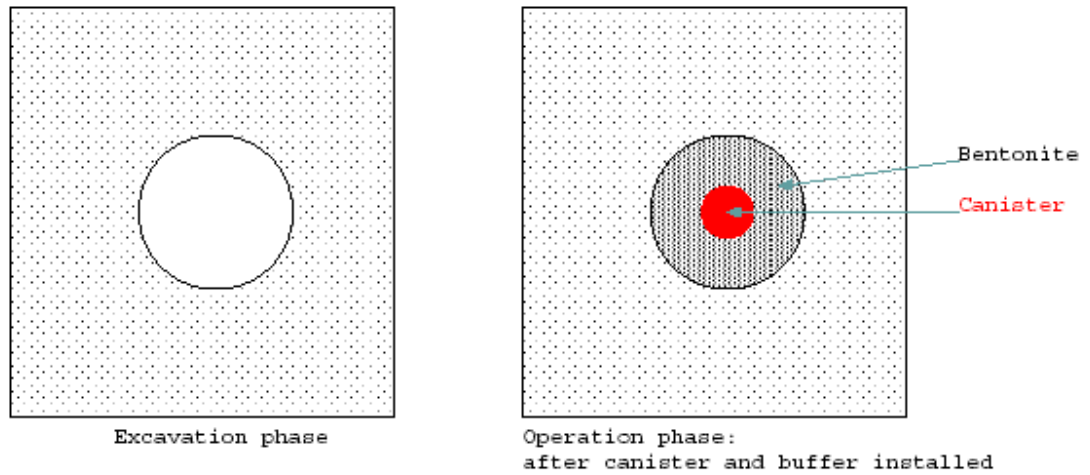
Figure 1: Phase of analysis

3. GOVERNING EQUATIONS

The governing equations, which are essential for the analysis, are detailed below.

1.1   NON ISOTHERMAL FLOW IN POROUS MEDIA

Consider the general case of a flow problem in deformable porous media under the Richard's approximation. With the classical Darcy's law, the large scale water flow $\mathbf{q}_w$ is defined as

$$\mathbf{q}_w = -nS\left(\rho_w \frac{k_{rel}\mathbf{k}}{\mu}(\nabla p - \rho\mathbf{g})\right) \tag{1}$$

where S is water saturation, p is the water pressure, ρ is density, n is the effective porosity of the media, μ is viscosity of flow, $\mathbf{k}_{\text{rel}}$ is the relative permeability, $\mathbf{g}$ is the gravity force by density and $\mathbf{k}$ denotes permeability tensor. Meanwhile, we consider vapor flow in the filled pores due to molecular diffusion, which is coupled with temperature. Similar to what is defined in [6], the vapor flow is given by

$$\mathbf{q}_v = -D_{pv}\nabla P - f_{Tv}D_{Tv}\nabla T \tag{2}$$

where f_{Tv} is a thermal diffusion enhancement factor that takes value of 1.0 in the present simulation, and D_{pv} and D_{Tv} are diffusion coefficients that take the form of the:

$$
\begin{aligned}
D_{pv} &= \frac{D_v \rho_v}{\rho_w R T_{abs}} \\
D_{Tv} &= D_v \left(h\frac{\partial \rho_{vS}}{\partial T} - \frac{\rho_v P}{\rho_w R T_{abs}^2} \right)
\end{aligned}
\tag{3}
$$

with h the relative humidity according to

$$h = e^{P/\rho_w R T_{abs}} \tag{4}$$

.

Here, R (= 461.6 J/kgK is the specific gas constant for water vapour, and ρ_{vS} is the saturated vapour density given by:

$$\rho_{vS} = 10^{-3}\, e^{19.891 - 4975/T_{abs}} \tag{5}$$

Vapour density is $\rho_v = h\rho_{vS}$.

The expressions of flow defined in Equations (1) and (2) lead to the governing equation of the flow field in the terms of the mass-balance equation given by

$$
\begin{aligned}
n &\left[\frac{\rho_w - \rho_c}{\rho_w}\frac{\partial S}{\partial p} + S\beta_p + (1-S)\frac{\rho_v}{\rho_w^2 R T_{abs}} \right]\frac{\partial S}{\partial t} \\
&+ \nabla \cdot (\mathbf{q}_w + \mathbf{q}_v)/\rho_w + S\frac{\partial}{\partial t}(\nabla \cdot \partial \mathbf{u}) \\
&n\frac{1-S}{\rho_w}\left(h\frac{\partial \rho_{vS}}{\partial T} + \frac{\rho_v P}{R T_{abs}^2} \right)\frac{\partial T}{\partial t} = 0
\end{aligned}
\tag{6}
$$

for any point $\mathbf{x} \in \Omega \in \mathrm{R}^n$ with n the dimension of the real space. In Equation (6), β_p is storativity. The unknowns of Equation (6) to be solved are saturation of the phase S, fluid pressure p, and the coupling term, i.e., temperature and displacement $\mathbf{u}$, deduced by solid deformation. The boundary conditions for this problem can be simplified for this Richard's flow model to:

$$\mathbf{q}_w \cdot \mathbf{n} = q_\Gamma, \forall x \in \partial\Omega \tag{7}$$

or to the Dirchlet type as

$$p = p_\Gamma, \quad S = S_\Gamma, \forall x \in \partial\Omega \tag{8}$$

This initial-boundary-value problem can be solved with the corresponding initial conditions of unknowns.

1.2   DEFORMATION

Assuming solid grains themselves are incompressible, i.e., $d^s\mathbf{u}/d^st = 0$, deformations in porous media can be described by the momentum balance equation in terms of stress, given the following equations for the bentonite material:

$$\nabla \cdot (\boldsymbol{\sigma} - Sp\,\mathbf{I} - \alpha\mathbf{I}\Delta T) + \rho\mathbf{g} = 0 \tag{9}$$

and for rock:

$$\nabla \cdot (\boldsymbol{\sigma} - \alpha\,\mathbf{I}\Delta T) + \rho\mathbf{g} = 0 \quad, \tag{10}$$

where σ is the effective stress of the porous medium, α is the thermal expansion coefficient, and $\mathbf{I}$ is the identity. Density of porous media consists of the portion contributed by liquid l and by the portion contributed of solid as $\rho = n\rho^l + (1+n)\,\rho^s$. The swelling pressure in bentonite is calculated by

$$\boldsymbol{\sigma}_{sw} = S^2 \sigma_{sw}^{max}\,\mathbf{I}$$

1.3   HEAT TRANSPORT

For the heat transport problem, we consider the convective transport, i.e., the transport of heat by flow. There are two recognized, basic kinds of convection, *forced convection* and *free convection*. In the former, the velocity of convective motion has no impact on the fluid temperatures, and heat energy transport is forced by the flow movement. In the latter, flow velocities are driven solely by buoyancy effects in the fluid, and these are related to temperature change through the coefficient of thermal expansion. In real groundwater systems, there is a mixture of both types of convection. The simple expression of heat flux in forced convection is given by

$$\mathbf{q}_T = -K_e \nabla T + n \sum_{\gamma}^{phase} (\rho^\gamma C_p^\gamma) T\mathbf{v} \tag{11}$$

for $x \in \Omega \in \mathrm{R}^n$, where K_e is the heat conductivity and $\sum_{\gamma}^{phase} (\rho^\gamma C_p^\gamma) T\mathbf{v}$ is the flux of heat

transported by velocity **v** per unit area. Across the entire rock face, this flux is reduced by the effective porosity *n*. Using the definition of heat flux in Equation (11), the governing equation of the convective heat transport can be derived for all points $x \in \Omega \in \mathrm{R}^n$ as

$$\sum_{\gamma}^{phase} (\rho^{\gamma} C_p^{\gamma}) \frac{\partial T}{\partial t} - \nabla \mathbf{q}_T + Q_T = 0 \tag{12}$$

with boundary condition

$$\mathbf{q}_T \cdot \mathbf{n} = q_T|_{\Gamma}, \text{ or } T = T_{\Gamma}, \forall x \in \partial\Omega \tag{13}$$

and initial condition

$$T(x) = T_0(x), \forall x \in \Omega \tag{14}$$

4. STAGGERED SCHEME

The staggered strategy is used for the coupling simulation. To avoid computing flow within the canister domain and to simulate the impact of gravity from canister to buffer, the strategy of activating/de-activating elements within the canister domain is employed. That is:

- During the deformation process, canister elements are used with steel material parameters.
- During the flow process, canister elements are devoided using the zero Neumann boundary condition on the canister surface.
- During the heating process, canister elements are devoided taking heating power as a Neumann boundary condition on the canister surface.

The staggered scheme, together with the Galerkin finite element approach, may damage mass conservation on the global scale. This is caused by the term in the vapour flux expression (Equation (2)) related to temperature. Applying an integration scheme to the flux term of Equation (6) with a test function *v*, we can integrate the second term of Equation (2) as

$$\int_{\Omega} D_{pv} v \nabla(\nabla \mathrm{P}) \mathrm{d}\Omega$$

$$\int_{\Omega} D_{Tv} v \nabla(\nabla \mathrm{T}) \mathrm{d}\Omega \tag{15}$$

Integrating Equation (15) part by part leads to

$$\int_{\Gamma} D_{pv} (v \nabla \mathrm{P}) \cdot \mathbf{n} \mathrm{d}\Gamma - \int_{\Omega} D_{pv} \nabla v \nabla \mathrm{P} \mathrm{d}\Omega \tag{16}$$

$$\int_\Gamma D_{Tv}(v\nabla \mathrm{T}) \cdot \mathbf{n} \mathrm{d}\Gamma - \int_\Omega D_{Tv}\nabla v\nabla \mathrm{T}\mathrm{d}\Omega \qquad (17)$$

Equations (16) and (17) imply the application of additional Neumann boundary conditions for pressure or temperature to the system equation, arising from the mass conservation equation (Equation (6)) to retain the mass conservation principle if a staggered scheme is applied.

5. SIMULATION

5.1. MODEL SETUP

For comparison with other teams, the model results are provided at the specified points given in the task definition by D. Barr, J. Birkholzer, J. Rutqvist, and E. Sonnenthal in [1], as shown in Figure 2.
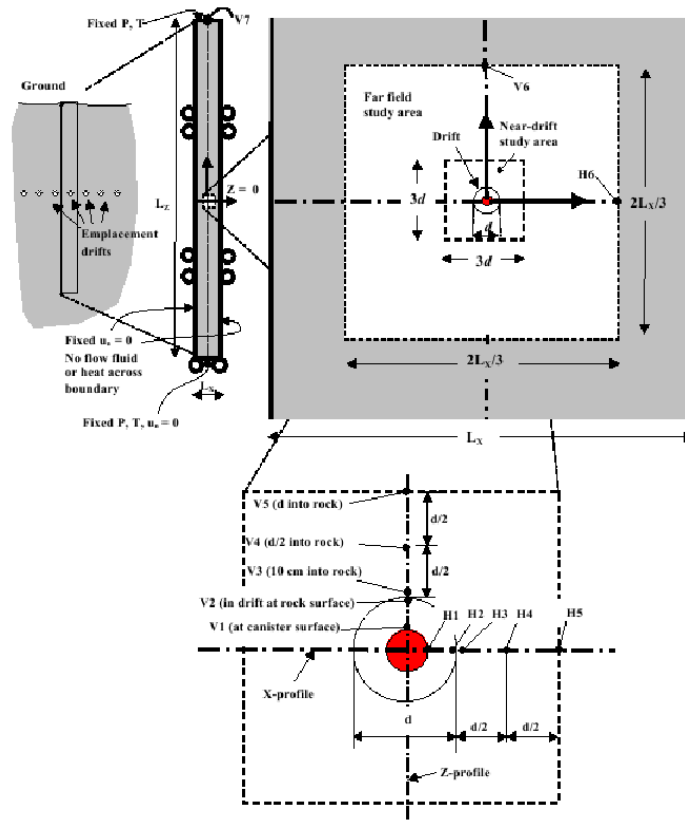
Figure 2: Model setup given in [1]

5.2. MATERIAL PARAMETERS

The material parameters for rock mass and buffer are given in Tables 1 and 2 , respectively. Vapour flux is only considered for bentonite.

Table 1: Rock mass		
Parameter	Unit	Value
Density	Kg/ m^3	2700
Young's modulus	GPa	35.0
Poisson ratio	-	0.3
Biot's constant	-	1
Thermal expansion coefficient	-	1.0e-5
Thermal conductivity	W/mK	3
Thermal capacity	J/kgK	900
Porosity	-	0.01
Storativity	1/Pa	4.4e-10
Saturated permeability	m^2	1.0e-17

Table 2: Bentonite		
Density	Kg/ m^3	1600
Young's modulus	MPa	317
Poisson ratio	-	0.35
Biot's constant	-	1
Tortuosity	-	0.67e-5
Thermal expansion coefficient	-	1.0e-5
Thermal conductivity	W/mK	1.3
Thermal capacity	J/kgK	900
Porosity	-	0.389
Saturated permeability	m^2	2.0e-21

The relationship between capillary pressure and saturation, for both rock and bentonite, is depicted in Figure 3.
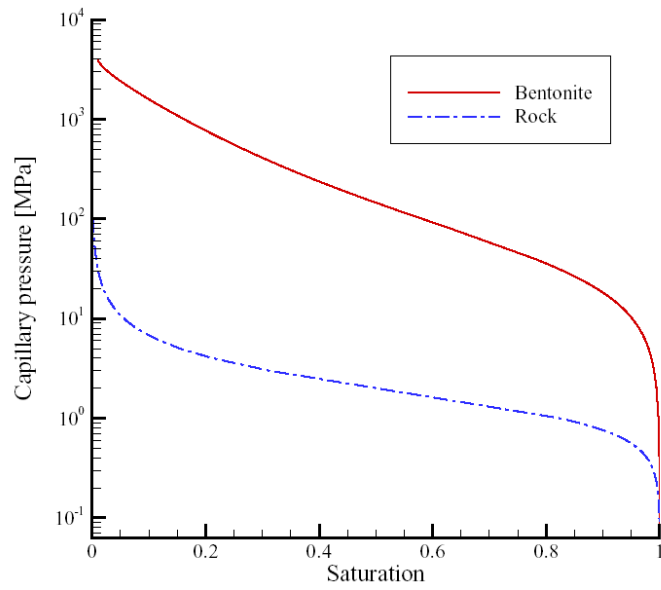
Figure 3: Capillary pressure vs. saturation

The relationship between relative permeability and saturation is depicted in Figure 4
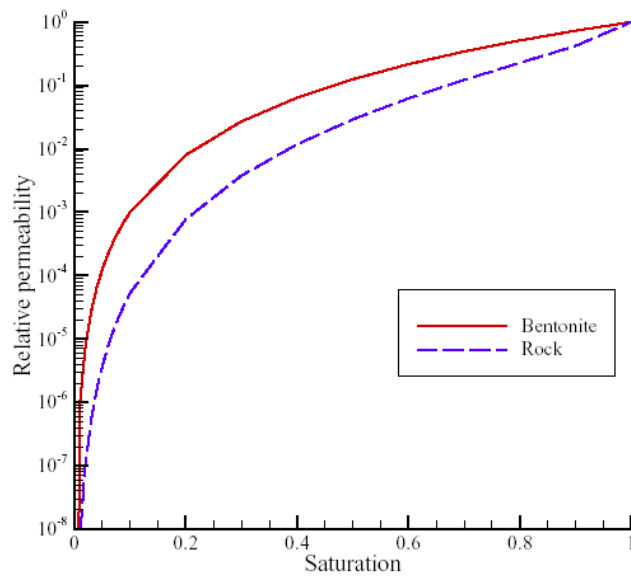
Figure 4: Relative permeability vs. saturation

5.3. SIMULATION OF EXCAVATION PHASE

For the deformation processes, we use Mana's method to establish the medium profile of stress for rock mass under the plane strain assumption. Discretizing the domain, including the patch to be excavated, the simulation takes four steps:

1. Compute stress of the entire domain deduced by gravity only, using the assumption given in the task definition, e.g., $\sigma_v = 2700 * 9.81 * D$ Pa, $\sigma_h = 0.02 * D + 4.6$ MPa and $\sigma_H = 0.55 * D + 4.6$ MPa, where D is the depth from ground surface.
2. Obtain the released force on the surface of cave.
3. Analyze the domain with cave, using the released force as a unique boundary condition.
4. Obtain stress after excavation by summarizing the stresses of Steps 1 and 3.

Such simulations are governed by the momentum balance equation:

$$\nabla \cdot \boldsymbol{\sigma} + \rho \mathbf{g} = 0 \tag{18}$$

where $\boldsymbol{\sigma}$ is the effective stress of the porous medium. Displacement $\mathbf{u}$ is the primary variable to be solved by substituting the constitutive law, which is

$$\boldsymbol{\sigma} = \mathbb{C}\,\epsilon$$
$$\epsilon = \frac{1}{2}(\nabla \mathbf{u} + (\nabla \mathbf{u})^{\mathrm{T}}) \tag{19}$$

,

with $\mathbb{C}$ a fourth-order material-related tensor and ε the strain. T signifies the transpose of a matrix. The deformation problem can be considered as a boundary-value problem, with boundary conditions given by

$$\boldsymbol{\sigma} : \mathbf{n} = t, \text{ or} \qquad \forall \boldsymbol{x} \in \partial\Omega \tag{20}$$
$$\mathbf{u} = \mathbf{u}_\Gamma$$

Assuming that the initial stress before excavation is σ_0, a schematic excavation simulation is demonstrated in Figure 5:
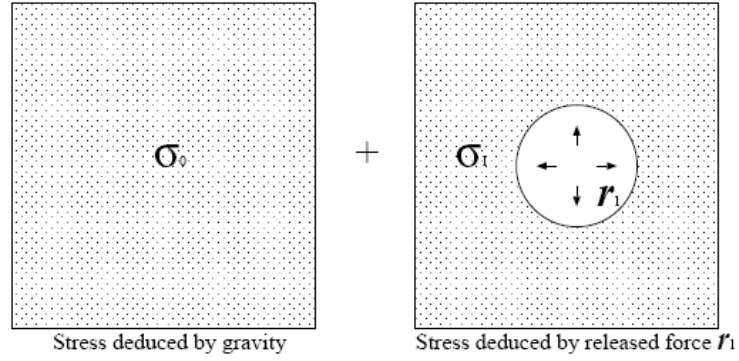
Figure 5: Domain to be excavated

where r_Γ is the node force of element nodes on the surface of the excavated domain, given by

$$r_\Gamma = \int_{\Omega_e} \mathbf{B}^\mathsf{T} \boldsymbol{\sigma}_0 \, \mathrm{d}\Omega$$

.

Here, **B** is the strain-displacement matrix and Ω_e is the excavated domain. Stress after excavation, $\boldsymbol{\sigma}_0$, is therefore given as $\boldsymbol{\sigma} = \boldsymbol{\sigma}_0 + \boldsymbol{\sigma}_1$.

The initial conditions of water pressure and temperature are obtained simply by running a one-step TH coupling process.

After the first step simulation, i.e., computing stresses produced exclusively by the gravity, the vertical stress is about 13.25 MPa and horizontal stress is 32.1 MPa. The horizontal stress at Point V3 after excavation that we obtained is 64.1 MPa, which is very close to the analytic solution of 64.3 MPa given in Rutqvist's report [6]. However, the horizontal stress decreases to 31.47 MPa, a change less than that given in [6], from 32.1M Pa to 29 MPa.

Figure 6 shows the calculated horizontal stress distribution of that portion of the domain close to the canister surface after excavation.
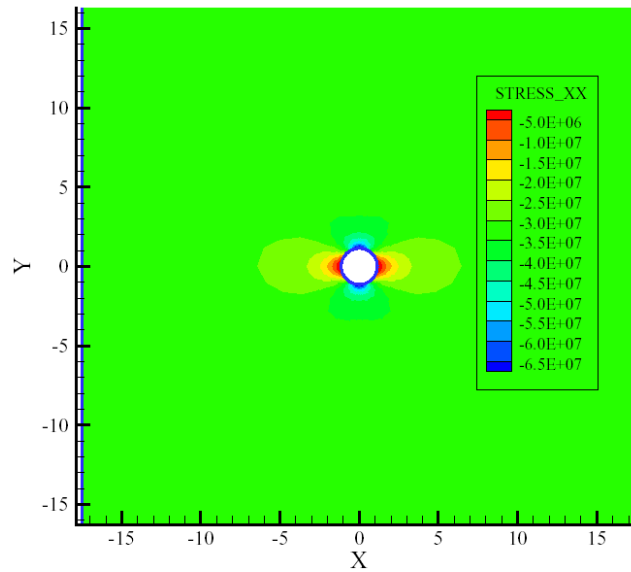
Figure 6: Vertical stress after excavation

5.4. SIMULATION OF OPERATION PHASE

The DECOVALEX THMC THM1 problem is simulated with the above initial-condition setup.

The grid of the problem domain, with a close-up view in the vicinity of the canister, is depicted in Figure 7 .
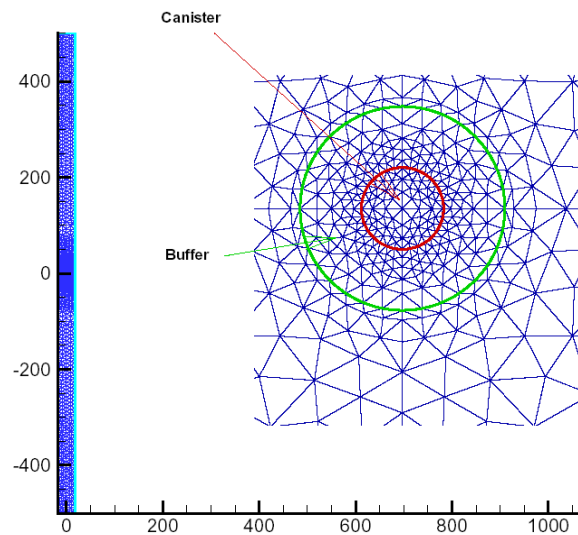
Figure 7. Grid of analyzed domain

The mesh is produced by GINA, a versatile mesh tool developed by H. Kunz at BGR. For the flow process, we have developed a two-phase model for isothermal flow processes tested only

for several limited problems. In the present stage, the Richard's model is employed to simulate the flow process. Strong coupling is taken account in computing flow and deformation. The heating process is assumed to be coupled with the flow process by means of advection and dispersion. The impact of heat-transport process to flow process is implicitly realized by the mean thermal stress.

Figure 8 shows the temperature evolution obtained in our study. The maximum temperature and the elapsed time this temperature is reached are similar to those obtained by LBNL.

Figure 11 show calculations for maximum vertical displacement and the time at which this value is reached. Again, these are very close to those obtained by the LBNL team. The water saturation at V1 dries to 0.49 at about 1 year and reaches 1.0 at about 70 years (Figure 9). Our initial settlement is smaller at a scale of 10^{-4} m because we assume that displacement is zero after the excavation process. The maximum displacement on the ground surface (V7) of about 0.175 m occurs after about 2,000 years. Vertical stress results obtained by the LBNL team and our team have a difference at Point V3 and V6. Such differences are deduced by the difference in the initial stresses we obtained at those points, as stated in Section 5.3. The storativity number of 4.4e-10 adopted for the rock mass insures the fully saturated condition, i.e., positive pressure, of the rock over most of the domain at the beginning of the time evolution (Figure 26).

5.5   EVOLUTION OF STATE VARIABLES: VERTICAL OBSERVATION POINTS

The evolution of temperature, saturation, water pressure, displacement and stresses are illustrated in Figures 8–13, respectively.
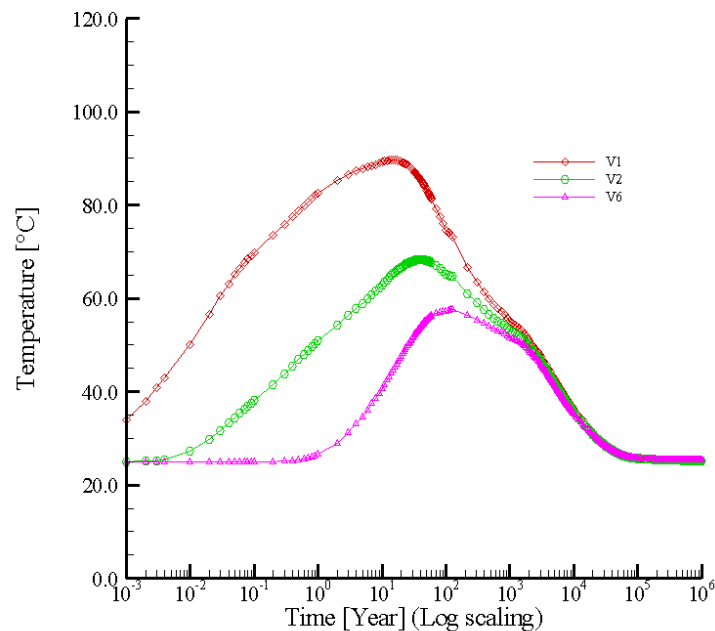
Figure 8: Evolution of temperature over time
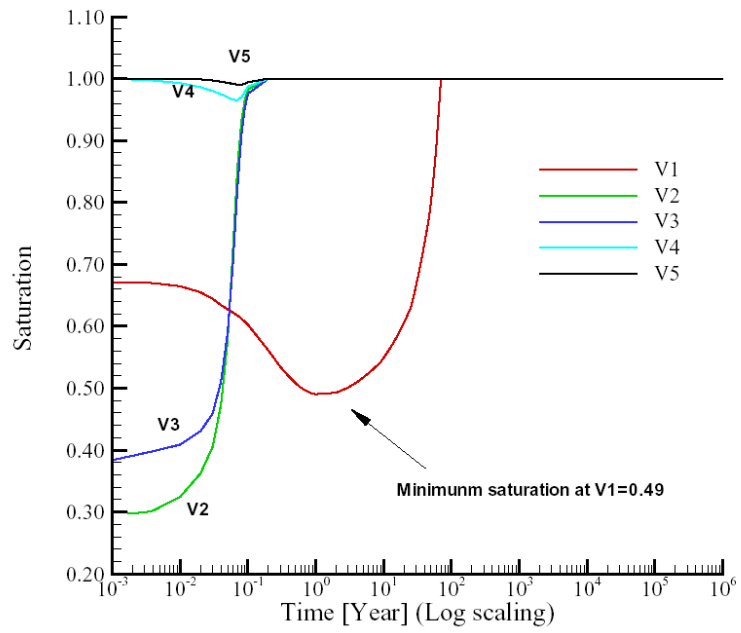
Figure 9: Evolution of saturation over time
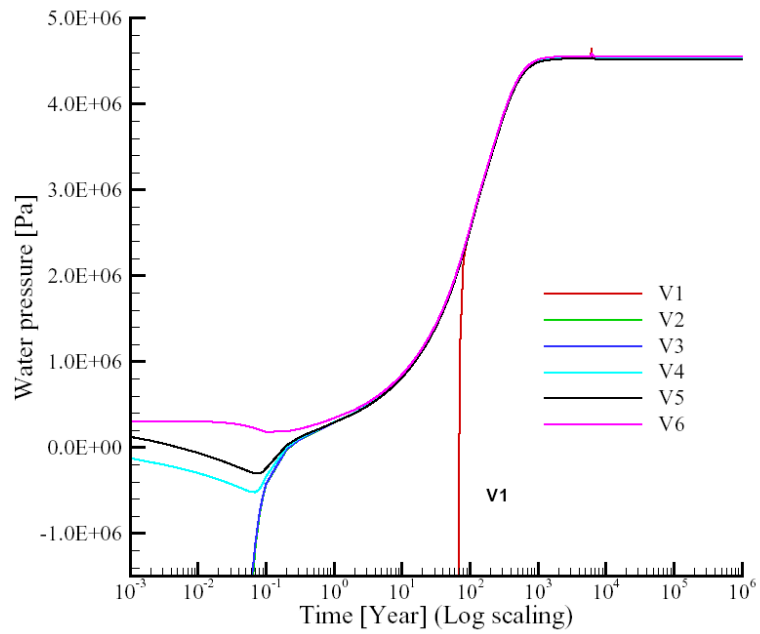
Figure 10: Evolution of pressure over time
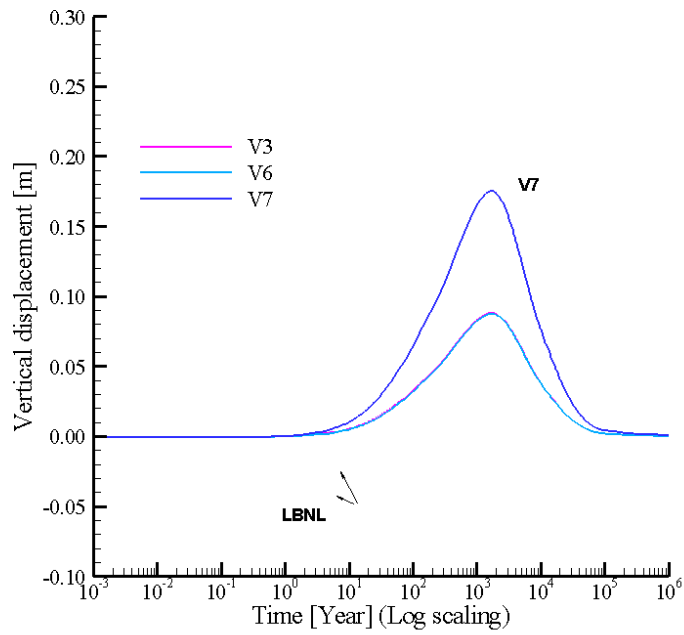
Figure 11: Evolution of vertical displacement over time
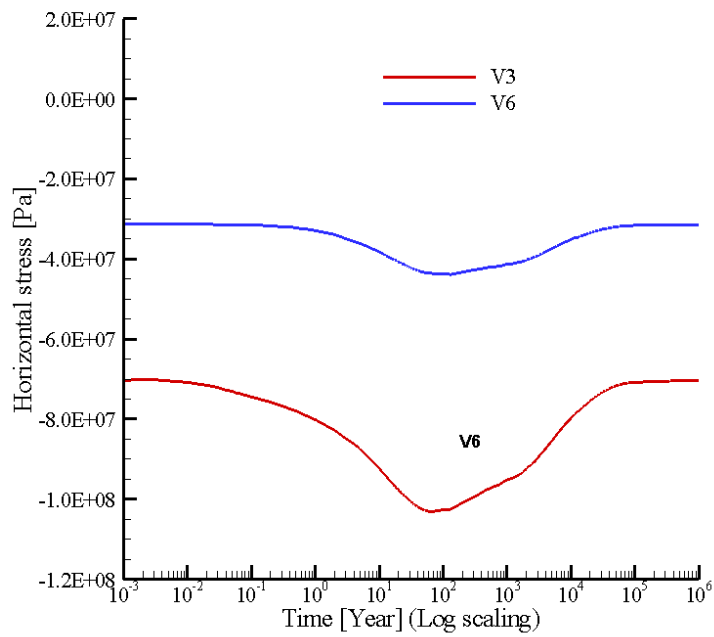
Figure 12: Evolution of horizontal stress over time
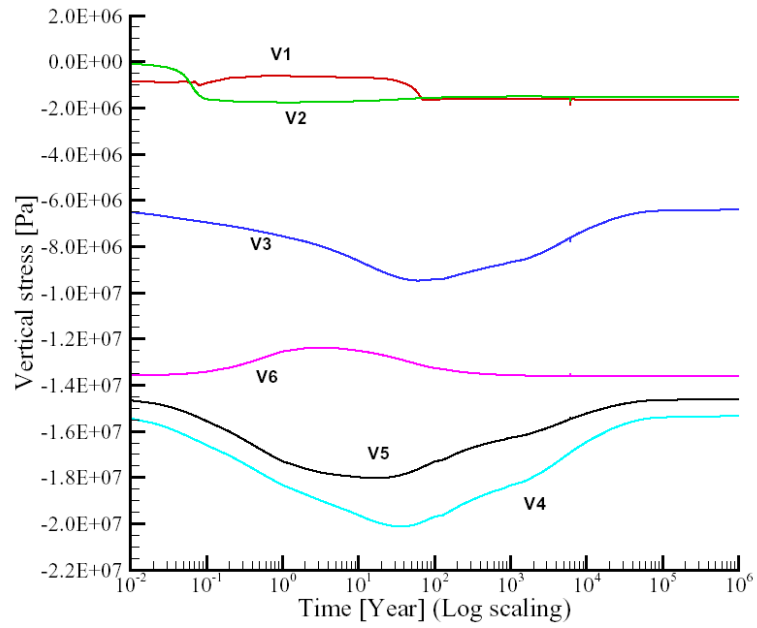
Figure 13: Evolution of vertical stress over time

5.6 EVOLUTION OF STATE VARIABLES: HORIZONTAL OBSERVATION POINTS

The evolution of variables at horizontal observation points is shown in Figures 14–19.
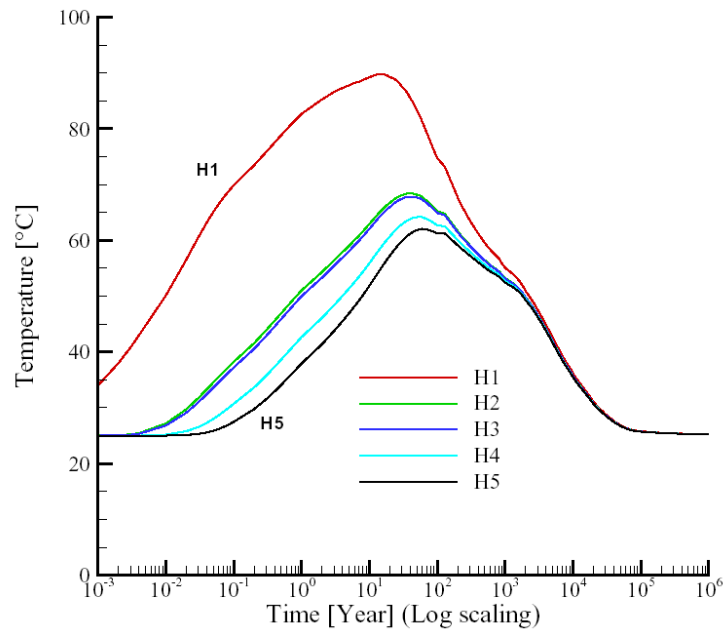
Figure 14: Evolution of temperature over time
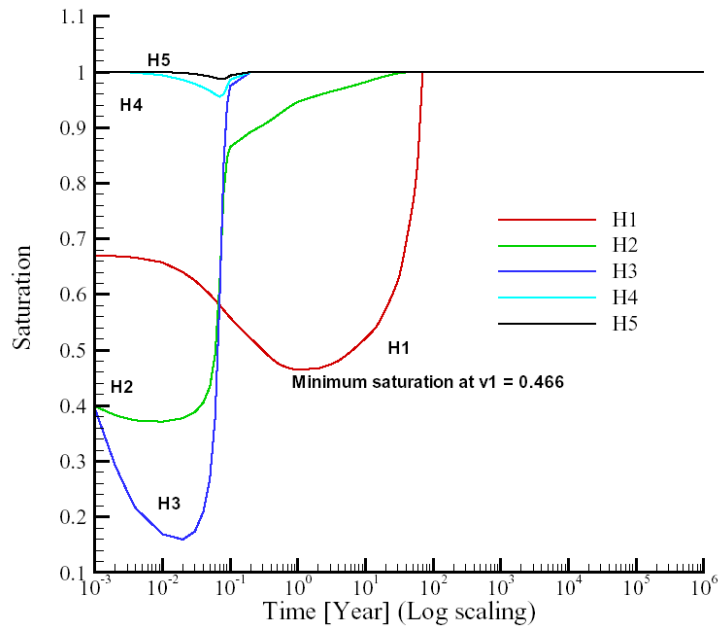
Figure 15: Evolution of saturation over time
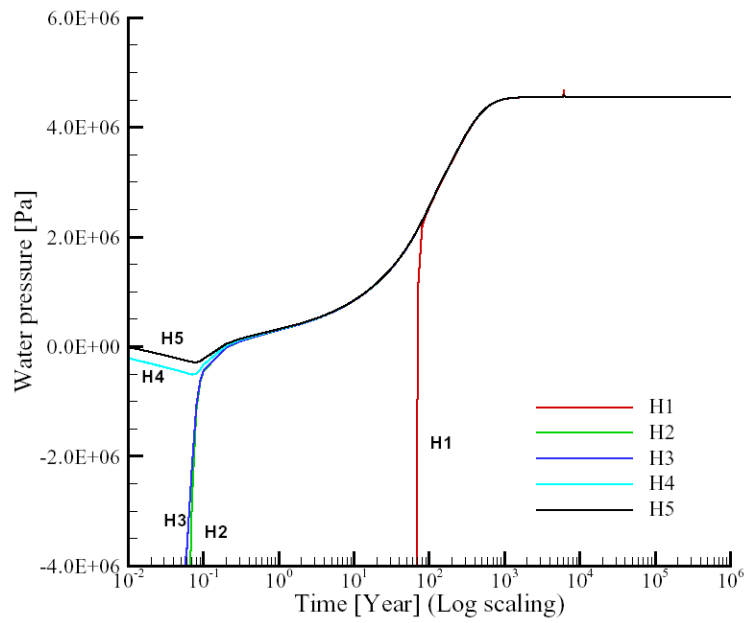
Figure 16: Evolution of pressure over time
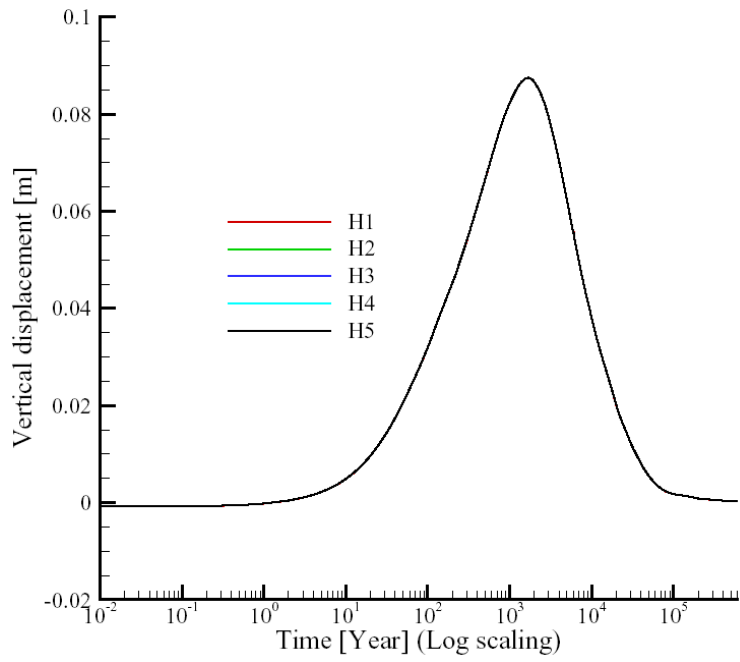
Figure 17: Evolution of vertical displacement over time
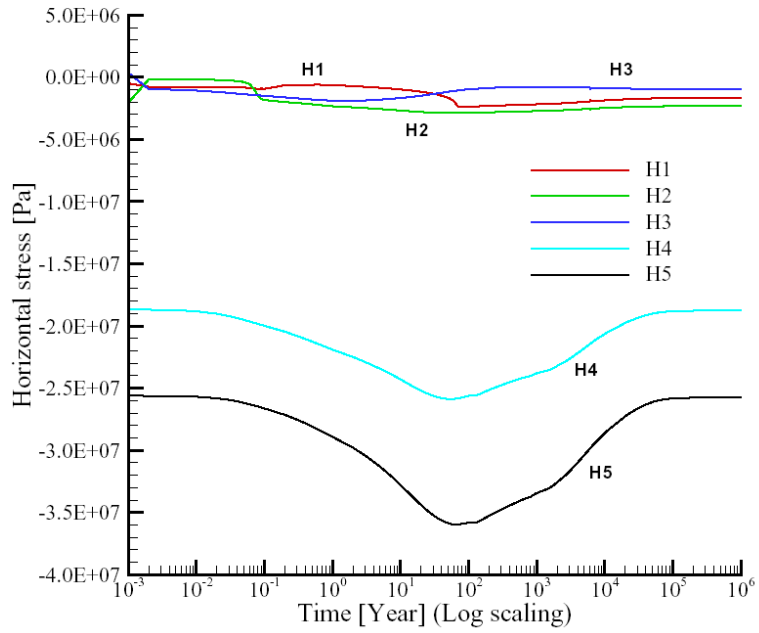
Figure 18: Evolution of horizontal stress over time
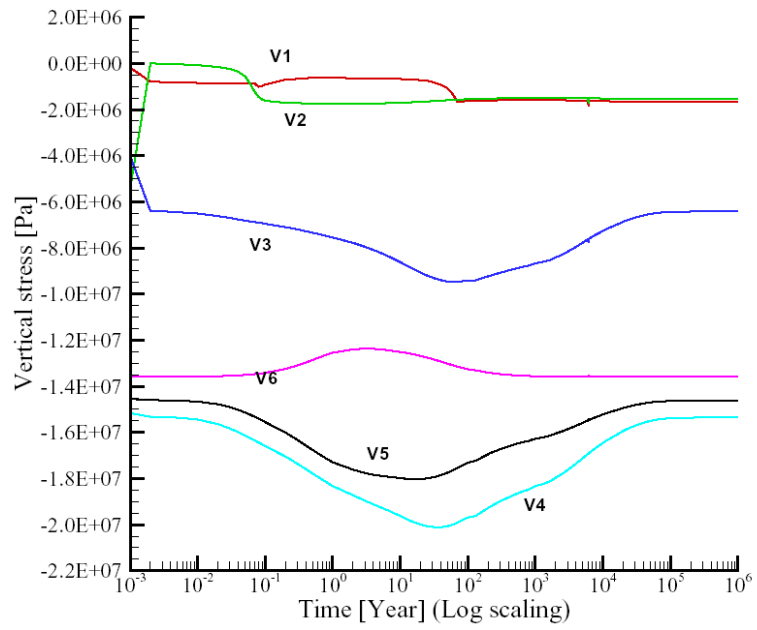
Figure 19: Evolution of vertical stress over time

5.7 PROFILE OUTPUT: HORIZONTAL LINE AT Z = 0 M

The output along horizontal profiles is given in Figures 20–24, respectively.
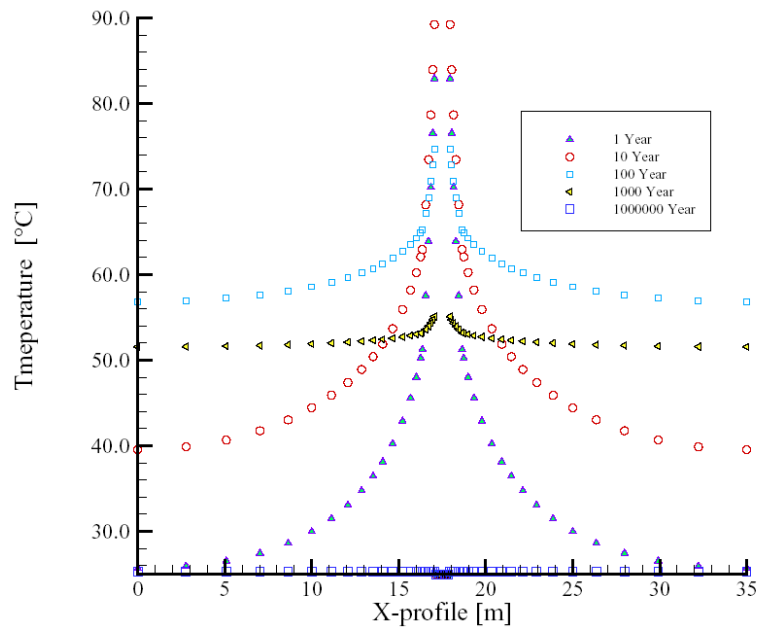
Figure 20: Horizontal profile: temperature
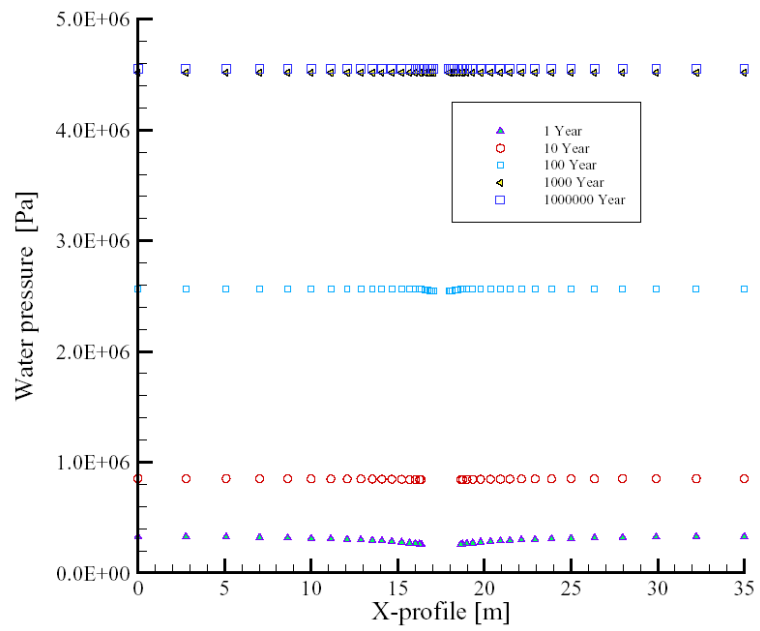
Figure 21: Horizontal profile: water pressure
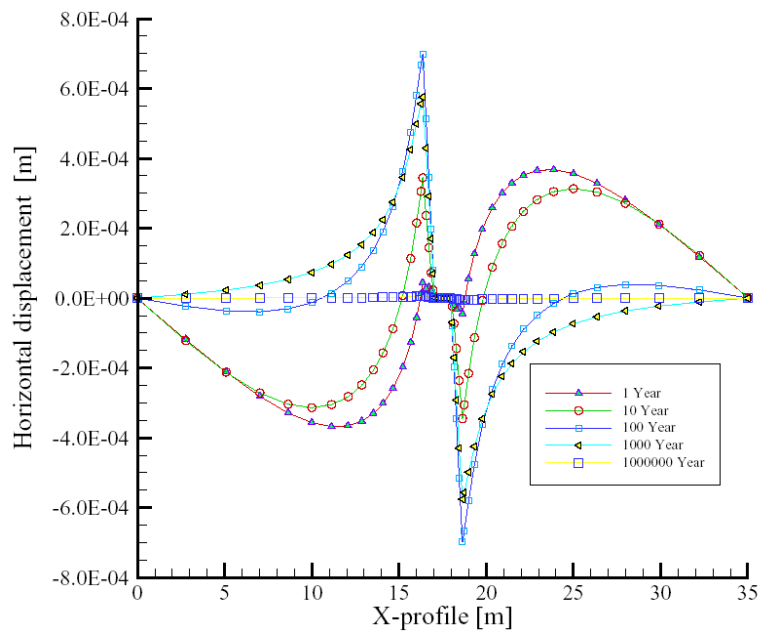
Figure 22: Horizontal profile: horizontal displacement
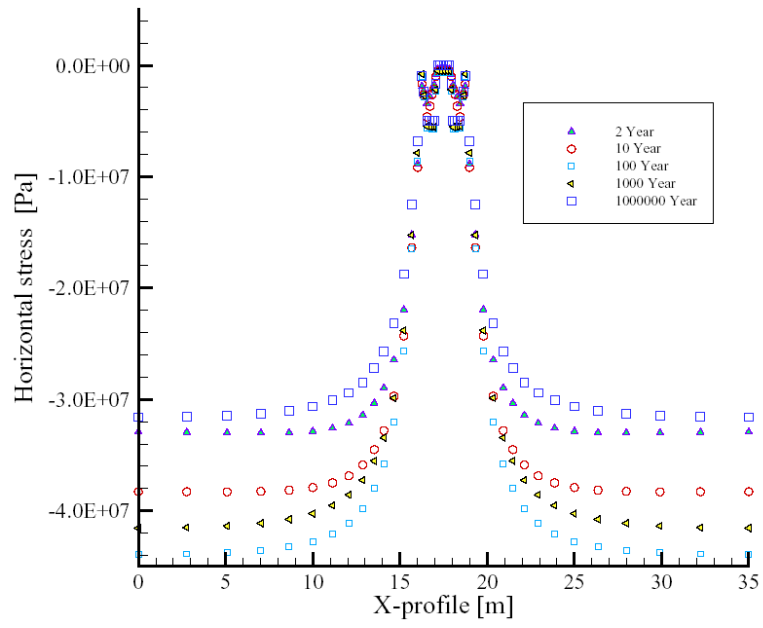
Figure 23: Horizontal profile: horizontal stress
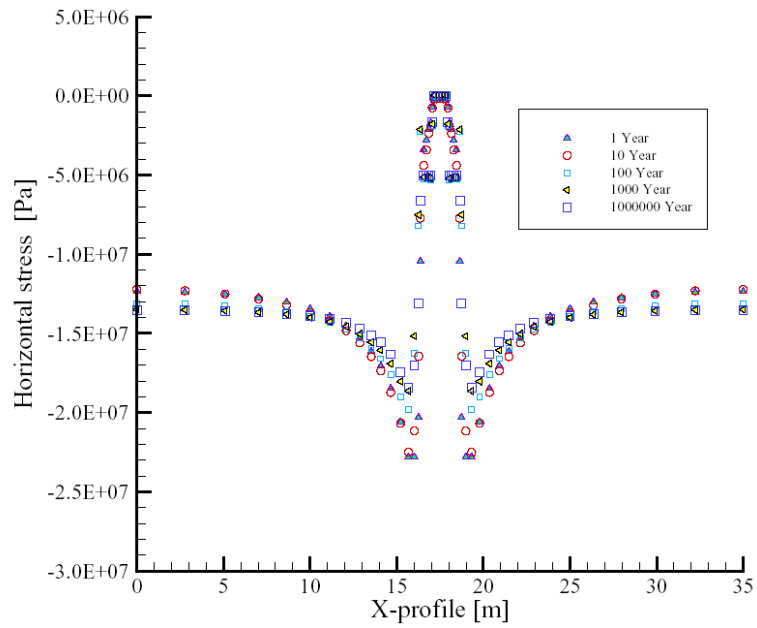
Figure 24: Horizontal profile: vertical stress

5.8 PROFILE OUTPUT: VERTICAL SYMMETRY AXIS AT X = 0 M

The output along vertical profiles is given in Figures 25–29, respectively.
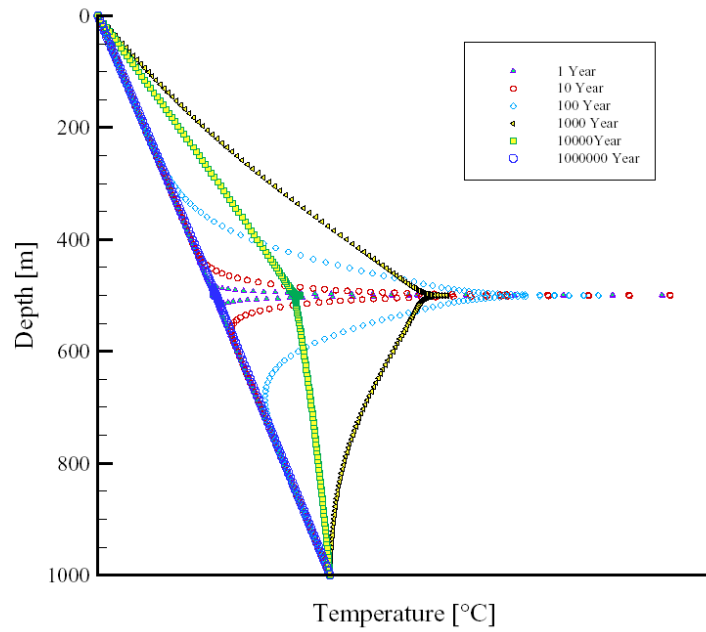
Figure 25: Vertical profile: temperature
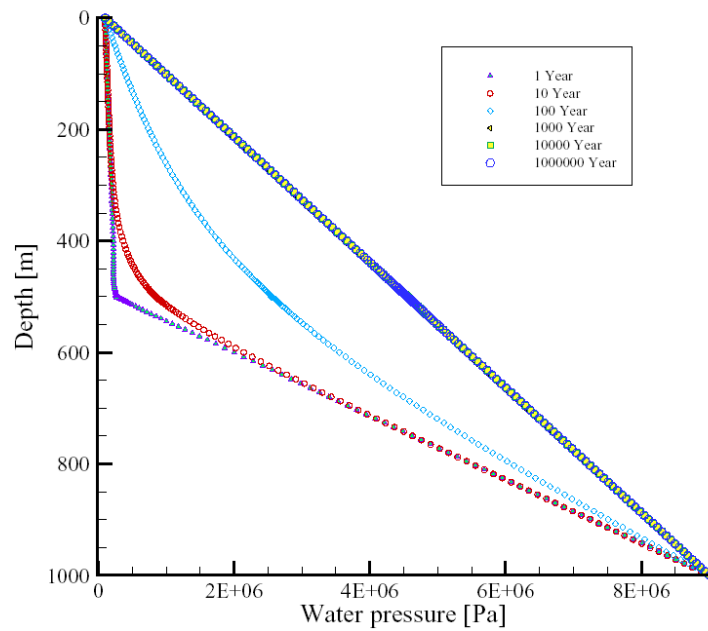
Figure 26: Vertical profile: water pressure
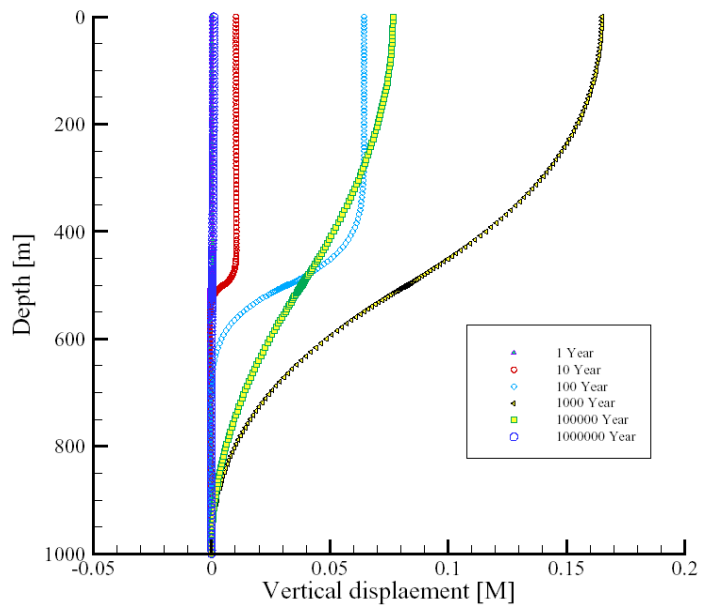
Figure 27: Vertical profile: vertical displacement
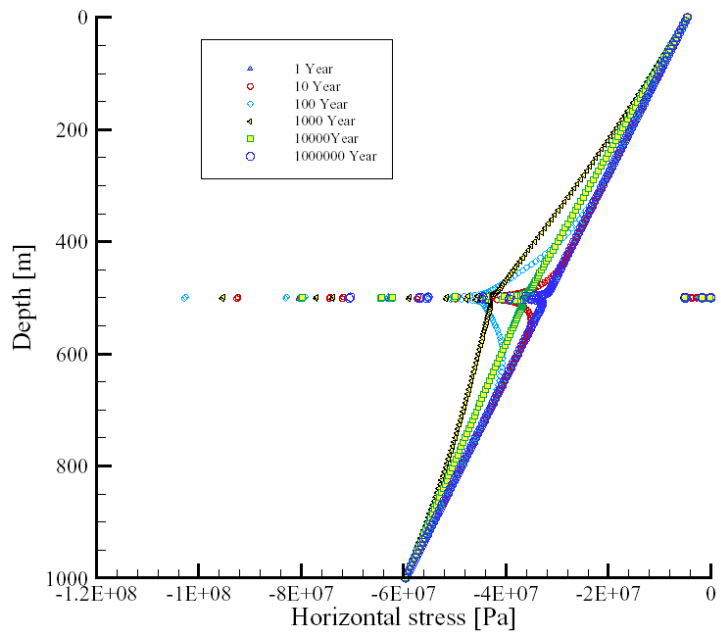
Figure 28: Vertical profile: horizontal stress
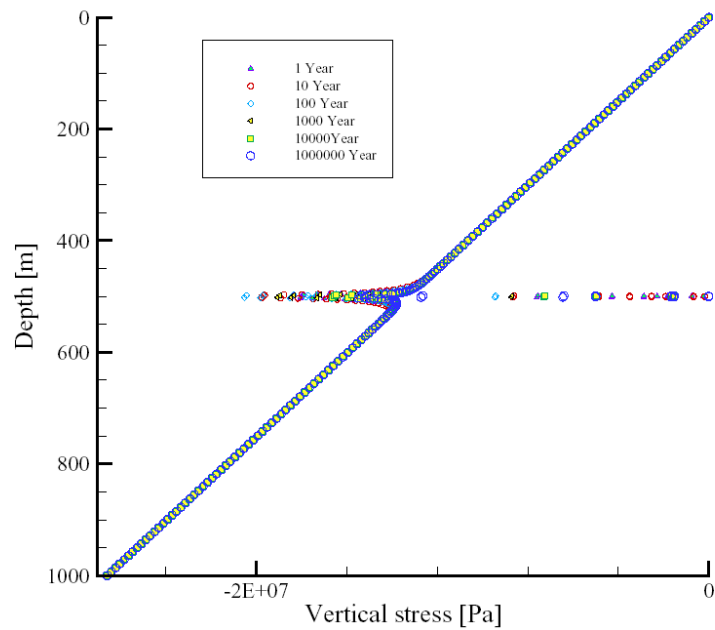
Figure 29: Vertical profile: vertical stress

6. CONCLUDING REMARKS AND OUTLOOK

In this report, the THM1 problem of DECOVALEX THMC is analyzed using the newly designed universal finite element class. The analysis of deformation assumes a plane strain condition. Mana's method is applied for excavation analysis of stress, and Richard's model is employed for unsaturated flow in buffer and rock. The impact of velocity on heat conductivity is taken into account by thermal analysis. A staggered strategy is utilized to deal with the THM coupling problem.

We compared the results obtained by LBNL and our team. The temperature evolution at all points and the stress evolution at V3 and H6 are close to that obtained by LBNL. Minimum de-saturation at point V1 and H1 is reached at about 1 year with values of 0.49 and 0.47. The first number is higher than the 0.47 obtained by LBNL team. However, the time of full saturation at Point V1 is 70 years, which is later than that obtained by LBNL. Our time for when variables reach the maximum values is the same as that obtained by LBNL. The swelling pressure effect in bentonite is not as significant in our simulation; we will improve this point in the future study.

At the present time, our work for this project involves developing a visco-elasto-plastic model for the buffer material, as well as a time step control strategy for the ordinary differential equations arising from the project. We will conduct the THM2 simulation using the revised code after the beforementioned model expansions have been completely finished.

2 ACKNOWLEDGMENTS

BIBLIOGRAPHY

[1] D. Barr, J. Birkholzer, J. Rutqvist, and E. Sonnenthal. Draft description for DECOVALEX-THMC task D: Long-term permaebility/porosity changes in edz and near field, due to THM and THC processes in volcanic and crystalline-bentonite systems. Technical report, Earth Sciences Division, Lawrence Berkeley National Laboratory, USA, 2004.

[2] O. Kolditz and J. de Jonge. Non-isothermal two-phase flow in low-permeable porous media. *Computational Mechanics*, 33 (5): 345-364, 2004.

[3] O. Kolditz, W. Wang, J. de Jonge, M. Xie, and S. Bauer. A process-oriented approach to compute thm problems in porous media - part 1: Theoretical and informatics background. In T. Schanz, editor, *Unsaturated Soils: Numerical and Theoretical Approaches*, pages 53-66. Springer, 2004a.

[4] O. Kolditz, W. Wang, J. de Jonge, M. Xie, and S. Bauer. A process-oriented approach to compute thm problems in porous media - part 2: Numerical applications. In T. Schanz, editor, *Unsaturated Soils: Numerical and Theoretical Approaches*, pages 231-250. Springer, 2004b.

[5] J. Korsawe, G. Starke, W. Wang, and O. Kolditz. Finite element analysis of poro-elastic consolidation in porous media: Standard and mixed approaches. *Computer Methods in Applied Mechanics and Engineering*, in print, 2005.

[6] J. Rutqvist. Coupling thermal-hydrological-mechanical analysis within the framework of DECPVALEX-THMC, Task D_THM, step 1: Model inception. Technical report, Earth Sciences Division, Lawrence Berkeley National Laboratory, USA, 2005.

[7] W. Wang and O. Kolditz. Object-oriented finite element analysis of thermo-hydro-mechanical (THM) problems in porous media. *To be submitted*, 2005.

[8] W. Wang, M. Datcheva, T. Schanz, and O. Kolditz. Computational aspects for elasto-plasticity with rotational hardening. *Computational Mechanics*, in print, 2005.

[9] M. Xie, S. Bauer, O. Kolditz, T. Nowak, and H. Shao. Non-isothermal multicomponent reactive transport in partially saturated porous media. *accepted by J. Contaminant Hydrology*.

[10] M. Xie, S.S. Agus, T. Schanz, and O. Kolditz. An upscaling method and numerical modelling of swelling/shrinking processes in compacted bentonite/sand mixtures. *International Journal for Numerical and Analytical Methods in Geomechanics*, 28: 1479-1502, 2004.

Center of Applied Geosciences
University of Tübingen

Geozentrum Hannover
Bundesanstalt für Geowissenschaften und Rohstoffe

_____

DECOVALEX IV Task D, BGR Team

Progress on THM Analysis

Part II: Modeling of Yucca mountain type repository

W. Wang, M. Xie and O. Kolditz (UT)
T. Nowak, H. Kunz and H. Shao (BGR)

_____

Tübingen   October   2005

1. MODEL SEP-UP

The model set-up for D_THM2 (Yucca Mountain type) is given in the task description in [1]. Figure 1 depicts the mesh of the analyzed domain with a close look at the canister.
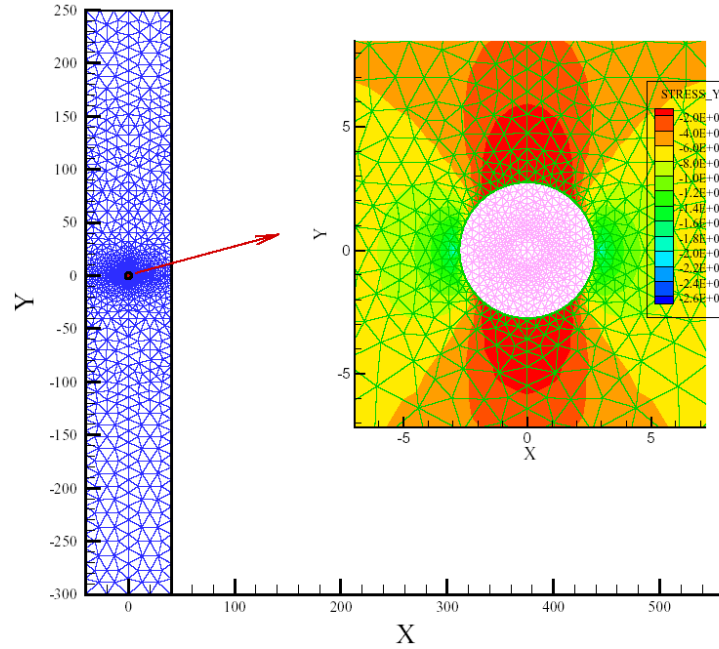
Figure 1: Mesh

2. MATERIAL PROPERTIES

As an inception analysis, we use the single continuum THM model. The material parameters for the rock mass are given in Tables 1 and 2.

Table 1: Hydraulic properties of the fracture-matrix continuum		
Parameter	Unit	Value
Porosity	-	0.13
Saturated permeability	m^2	3.87×10^{-17}
van Genuchten's air pressure	kPa	118.3
van Genuchten's exponent m	-	0.317
Residual saturation	-	0.19

Based on the residual saturation given in Table 1, the initial saturation on the top is assumed as 0.21.

Table 2: Thermal and mechanical properties (equivalent continuum)		
Parameter	Unit	Value
Bulk density	kg/m^3	2360
Young's modulus	GPa	15
Poisson ratio	-	0.21
Biot's constant	-	1
Thermal expansion coefficient	-	1.0×10^{-5}
Wet thermal conductivity	W/mK	2.29
Dry thermal conductivity	W/mK	1.49
Grain specific heat	J/kgK	985

A simplified boiling model is adopted in the heat transport simulation. The specific heat capacity during phase change is approximated by a time average method as follows

$$c_p = \frac{H_n - H_{n-1}}{T_n - T_{n-1}} \tag{1}$$

where H represents enthalpy and n is the time step.

3. SIMULATION OF EXCAVATION PHASE

The procedure of excavation simulation is similar to that used in the D_THM1 analysis. The initial stresses are given as

σ_z =2360*9.81*D (D, depth)
σ_h =0.5σ_z
σ_H =0.6σ_z

The values of stresses at the observation point V3 are

σz =-5.721MPa
σh =-2.861MPa
σH =-3.433MPa

before excavation and

σz =-0.308MPa
σh = 5.425MPa
σH =-6.071MPa

after excavation. The distribution of vertical stress around the cave is shown in Figure 1.

4. SIMULATION OF OPERATION PHASE

In this section, the results of the D_THM2 simulation using the object oriented designed software GeoSys/Rockflow(GS/RF) [3] are given and compared with simulation results from the LBNL team [2].

Figure 2 shows a comparison of the temperature evolution between ROCMAS, TOUGH-FLAC and GS/RF simulations. The maximum temperature we obtained is 118.1^{o}C at about 71 years after emplacement.

Drying at V3 begins at about 51.6 year (Figure 3) , which is close to that obtained by LBNL simulation. Note that drying is a result of the vaporization behavior of water. Since the single continuum model is used in the present analysis, the values of and the distribution of water saturation are different from that obtained by LBNL.

Figure 4 shows that the maximum vertical displacement and the time this value is reached is very similar for all simulations. The vertical displacement at the top (V7) reaches a maximum value of 0.21m at about 978 years. The peak horizontal stress at V3 is about 33.0 MPa from 130 to about 500 years (Figure 5).

4.1. EVOLUTION OF STATE VARIABLES: VERTICAL OBSERVATION POINTS

The evolution of temperature, saturation, water pressure, displacement, and stress are illustrated in Figures 2 through 6, respectively, for vertical observation points.
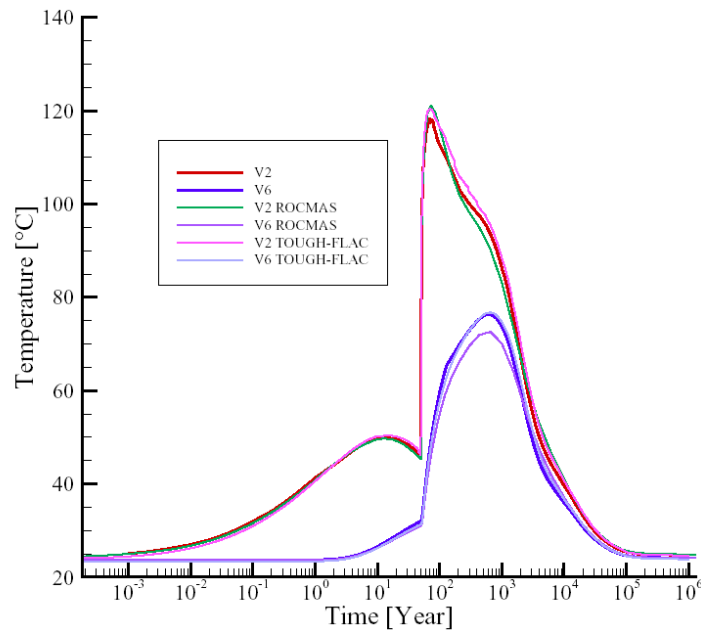
Figure 2: Evolution of temperature with time
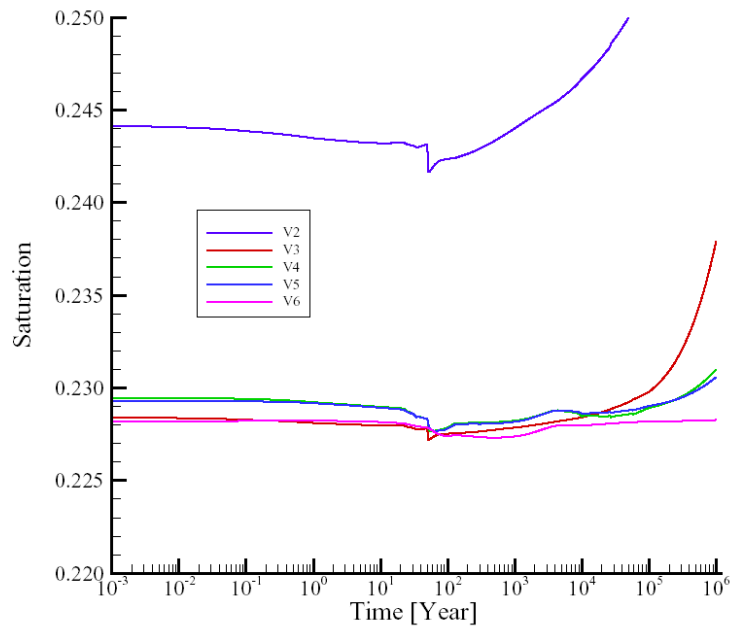
Figure 3: Evolution of saturation with time
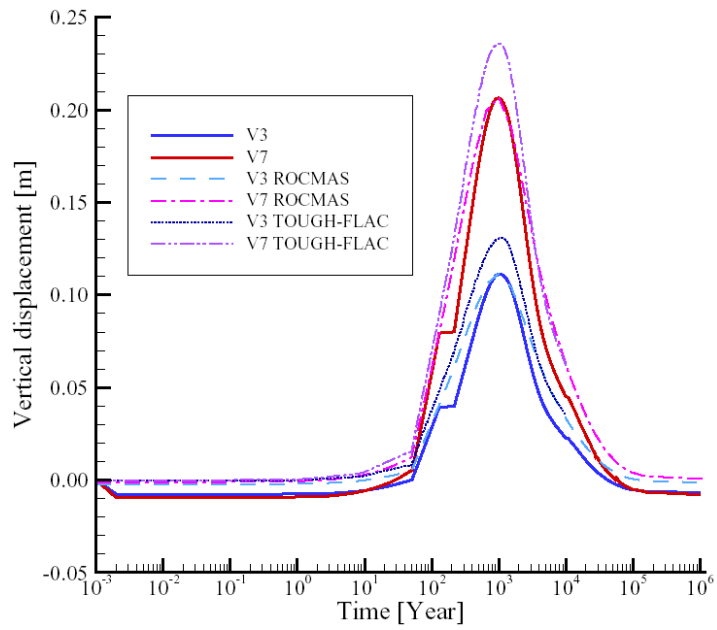
Figure 4: Evolution of vertical displacement with time
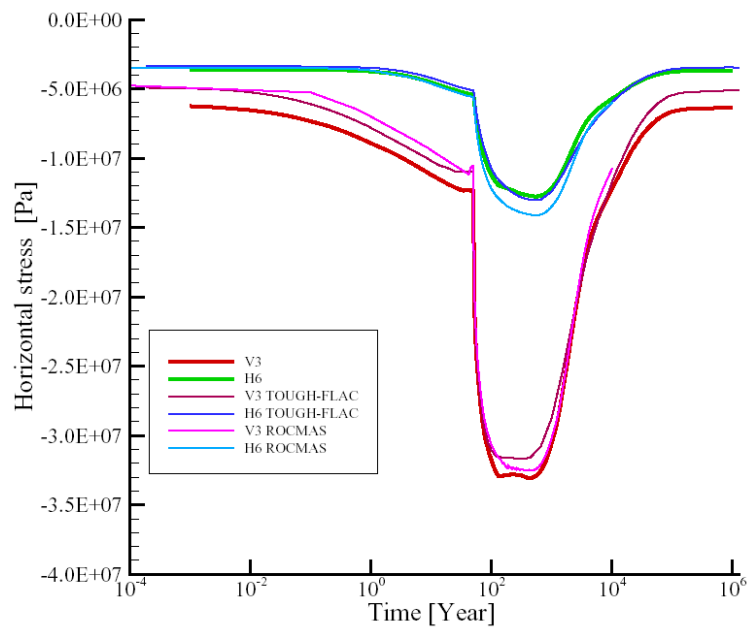
Figure 5: Evolution of horizontal stress with time
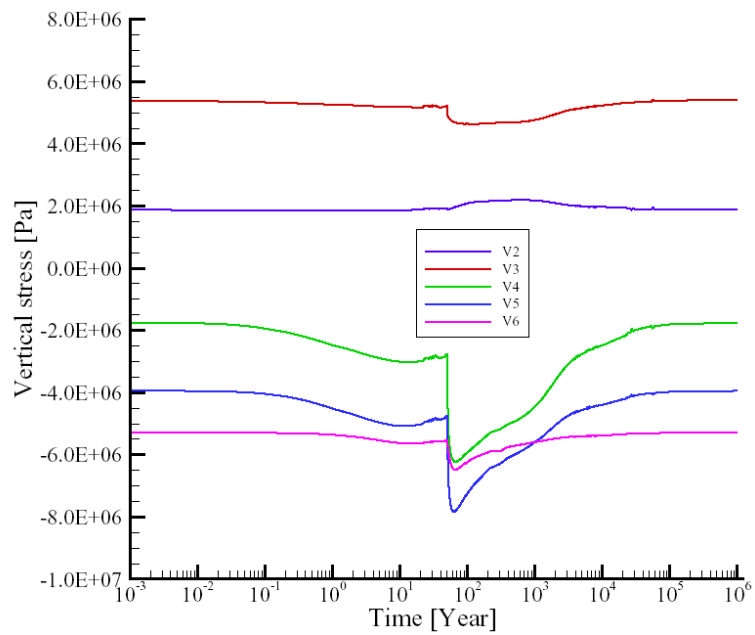
Figure 6: Evolution of vertical stress with time

4.2. EVOLUTION OF STATE VARIABLES: HORIZONTAL OBSERVATION POINTS

The evolutions of state variables for horizontal orientation points are shown in Figures 7 through 10, respectively.
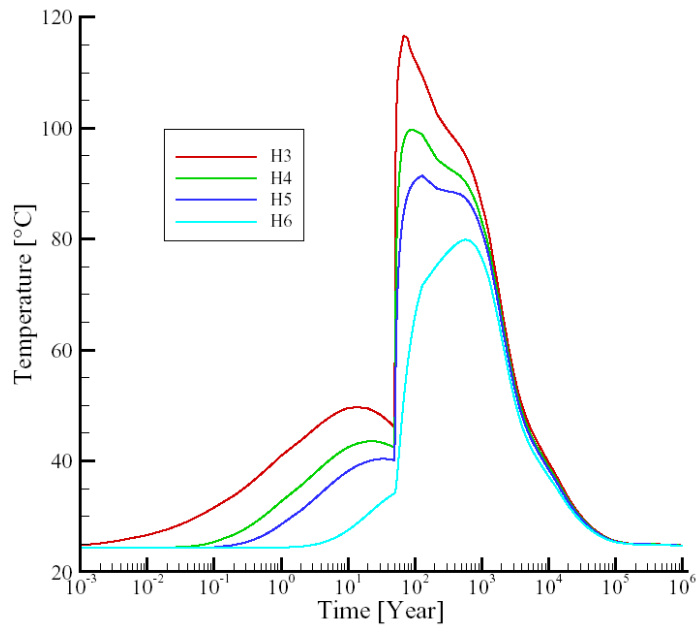
Figure 7: Evolution of temperature with time
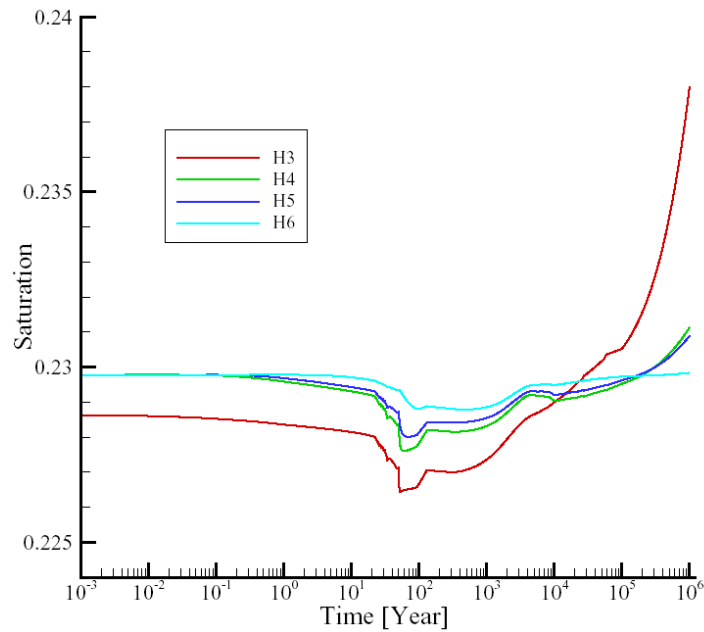
Figure 8: Evolution of saturation with time
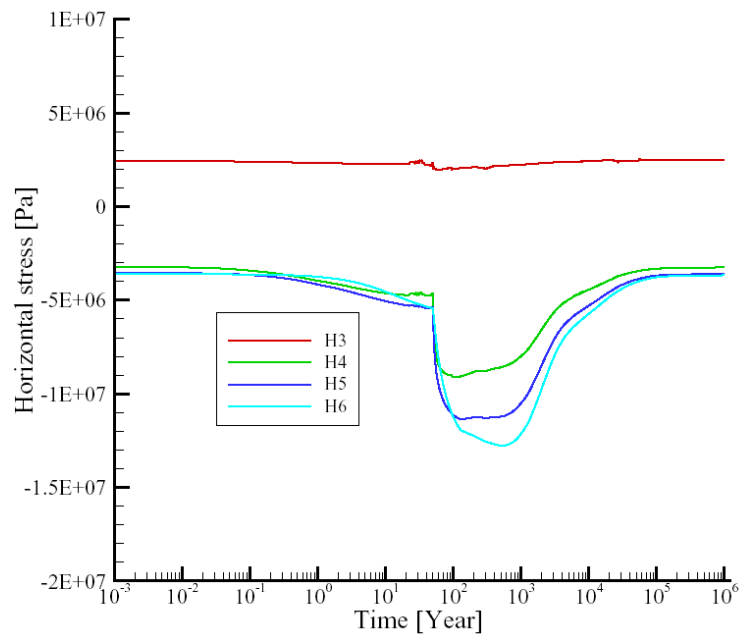
Figure 9: Evolution of horizontal stress with time
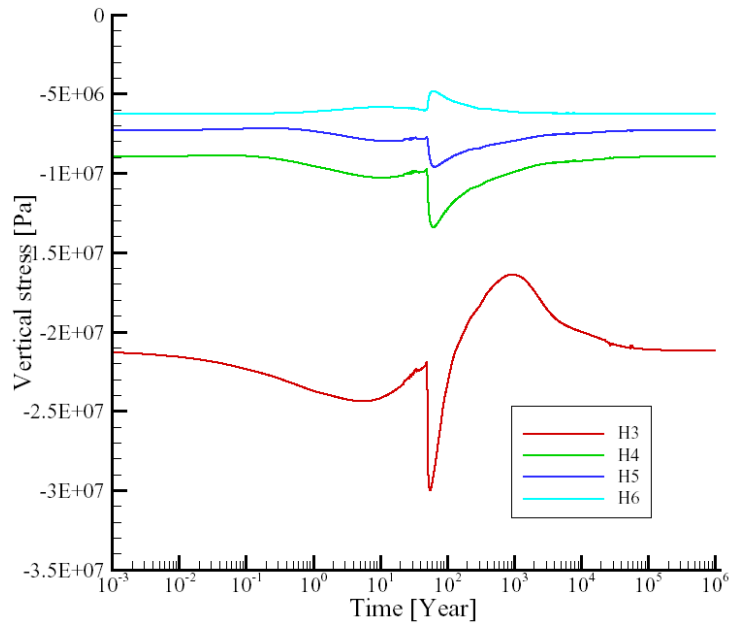
Figure 10: Evolution of vertical stress with time

4.3. PROFILE OUTPUT: HORIZONTAL LINE AT *Z*=0

Simulation results for a horizontal profile are given in Figures 11through 14, respectively.
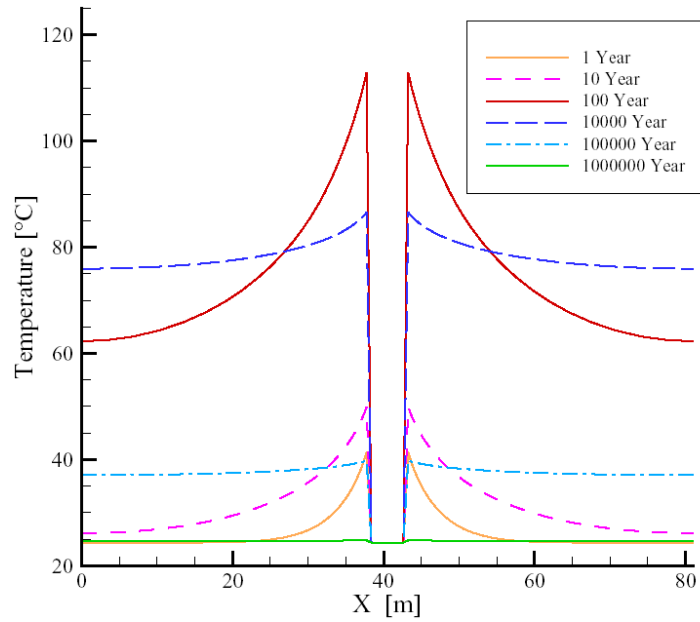
Figure 11: Horizontal profile: temperature
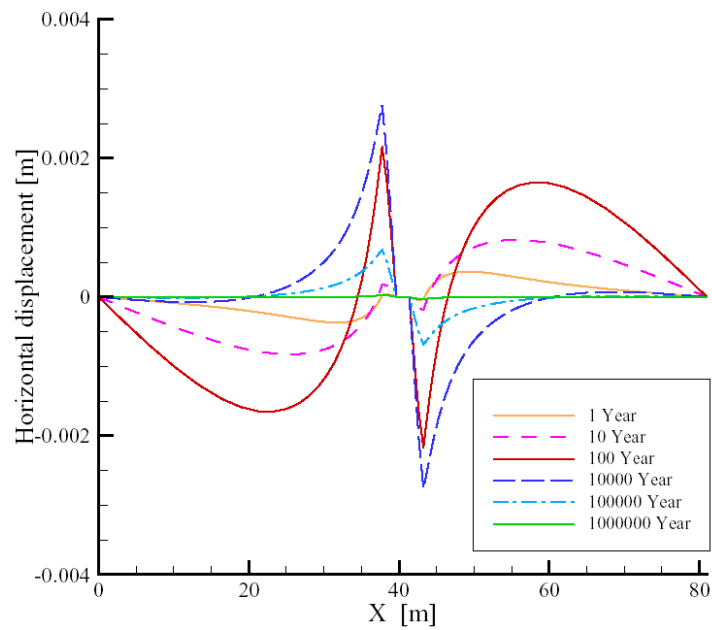
Figure 12: Horizontal profile: horizontal displacement
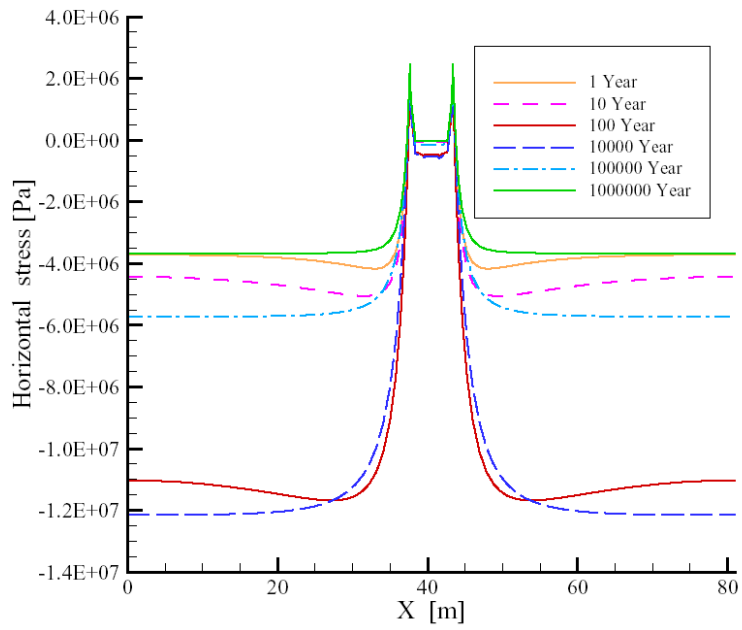
Figure 13: Horizontal profile: horizontal stress
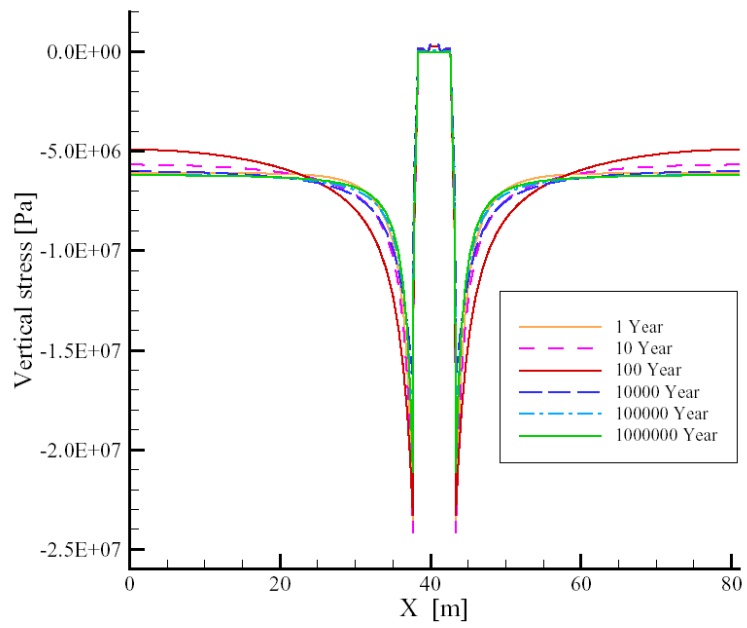
Figure 14: Horizontal profile: vertical stress

4.4. PROFILE OUTPUT: VERTICAL SYMMETRY AXIS

Simulation results for a vertical profile are given in Figures 15 through 18, respectively.
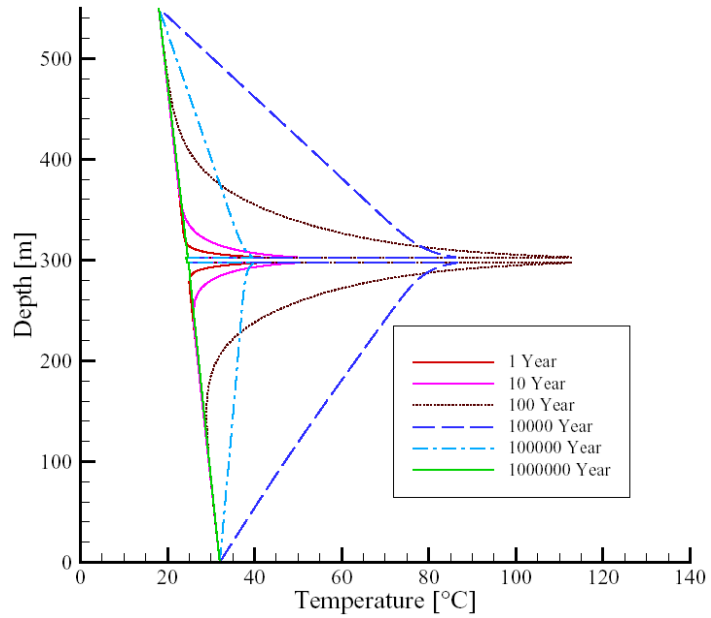
Figure 15: Vertical profile: temperature
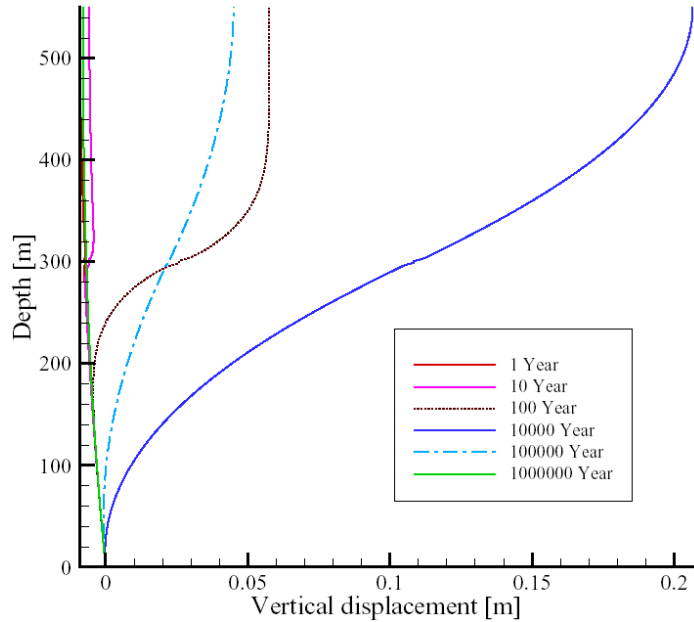
Figure 16: Vertical profile: vertical displacement
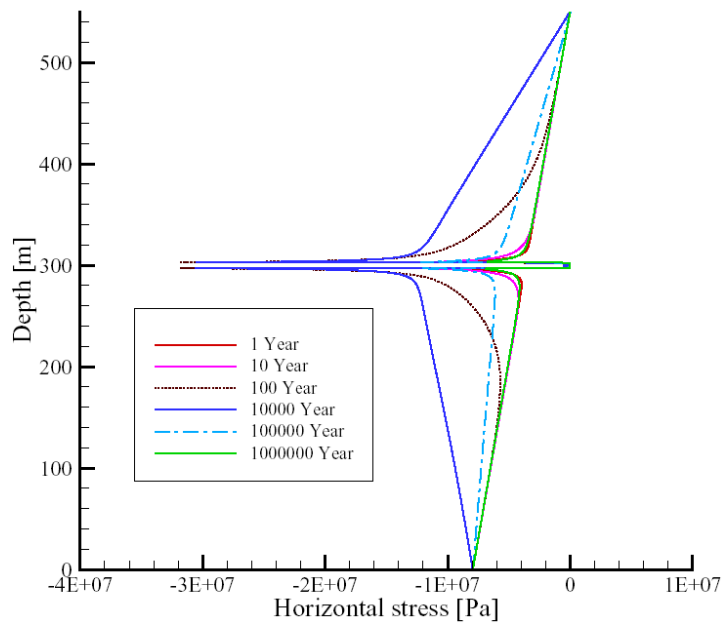
Figure 17: Vertical profile: horizontal stress
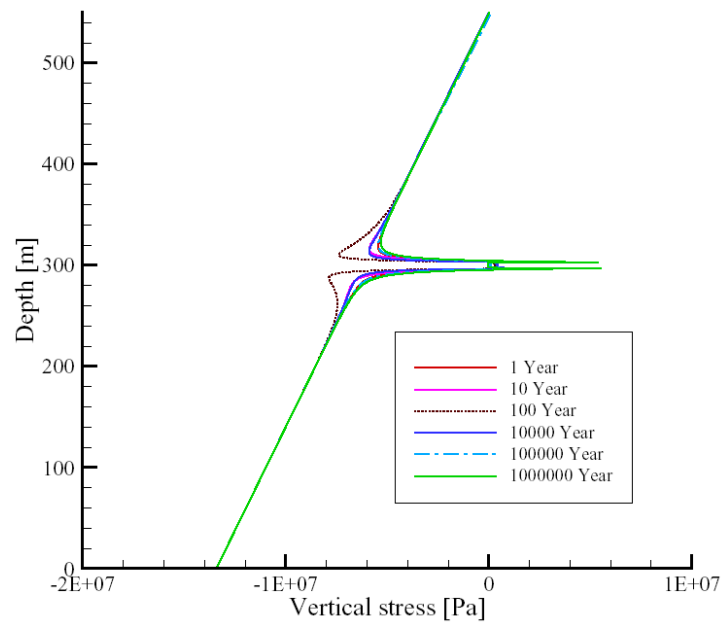
Figure 18: Vertical profile: vertical stress

5. REMARKS

The hydraulic behavior of the Yucca Mountain type repository is not well represented by the present simulation. A revised simulation is currently being conducted where the upper boundary condition of the model domain is adjusted. Instead of using a fixed saturation value of 0.21, we prescribe a fixed water infiltration flux of 6 mm/yr (see task description in [3]). Figures 19 and 20 show the preliminary results of saturation for this revised simulation.
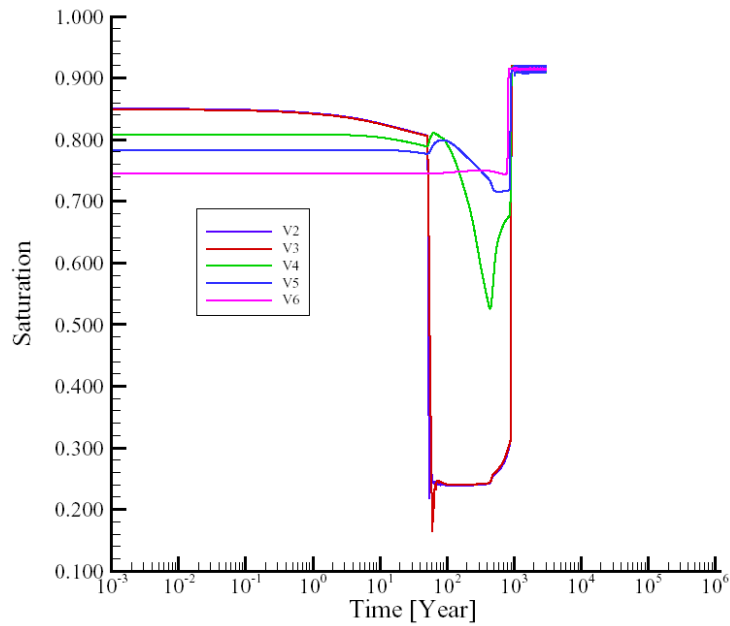
Figure 19: Improved evolution of saturation with time (V points)
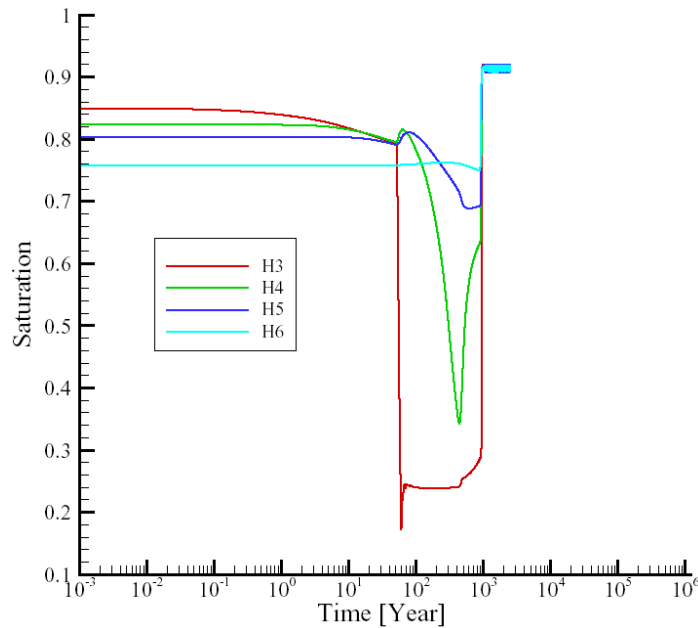
Figure 20: Improved evolution of saturation with time (H points)

BIBLIOGRAPHY

[1]   D. Barr, J. Birkholzer, J. Rutqvist, and E. Sonnenthal. Draft description for DECOVALEX-THMC Task D: Long-term permeability/porosity changes in the EDZ and near field, due to THM and THC processes in volcanic and crystalline-bentonite systems. Technical Report, Earth Sciences Division, Lawrence Berkeley National Laboratory, USA, 2004.

[2]   J. Rutqvist. Coupling thermal-hydrological-mechanical analysis within the framework of DECPVALEX-THMC, Task D_THM, Step 1: Model inception. Technical report, Earth Sciences Division, Lawrence Berkeley National Laboratory, USA, 2005.

[3]   W. Wang and O. Kolditz. Object-oriented finite element analysis of thermo-hydro-mechanical (THM) problems in porous media. *To be submitted*, 2005.

Appendix F

Status Report for D_THM

CAS Team (China)

Numerical Simulation of Coupled THM Processes in Phase I of Decovalex_IV_Task_D

Liu Quansheng, Zhang Chengyuan, and Liu Xiaoyan
Institute of Rock and Soil Mechanics, The Chinese Academy of Sciences
WuHan, 430071, HuBei, China

1 INTRODUCTION

This report presents coupled thermal-hydrological-mechanical (THM) modeling and simulation results for DECOVALEX-IV, Task D, conducted by the Wuhan Institute of Rock and Soil Mechanics, the Chinese Academy of Sciences (CAS). Task D_THM includes two subtasks that involve analysis of coupled THM processes in two generic repositories, as follows:

① Task_D THM1: A generic repository located in saturated crystalline rock, where emplacement tunnels are backfilled with buffer material (FEBEX type).
② Task_D THM2: A generic repository located in unsaturated volcanic rock, with emplacement in open gas-filled tunnels (*Yucca Mountain type*).
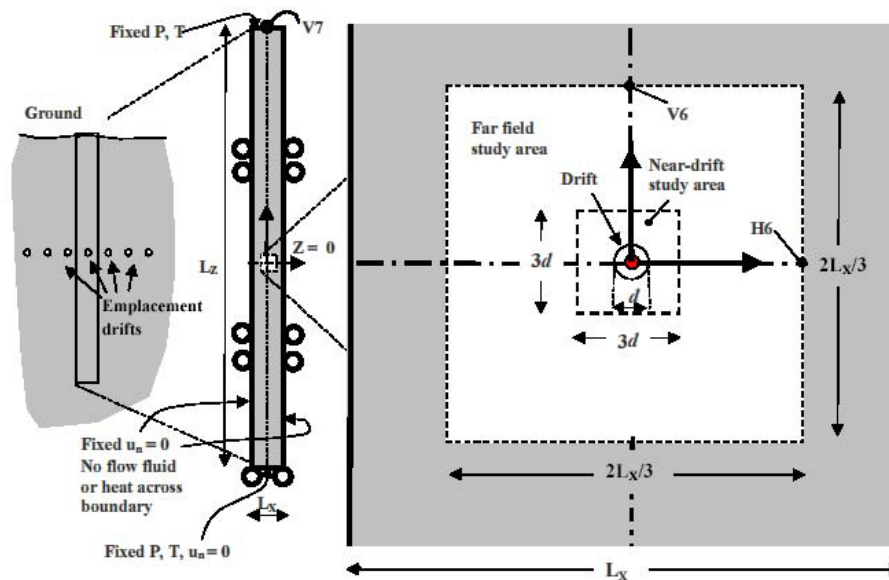
Figure 1. Schematic general model geometry, boundary conditions

The geometry chosen for the two repository scenarios is similar in the calibration phase (seen in Figure 1). We have developed a set of generic coupled THM governing equations, but in this phase, simplified equations are used for calibration according to Task D Phase 1 definitions. In the simulations, we use Matlab[TM] for coding and FEMLAB[TM] (tool box of Matlab[TM]) as FEM solver of our equations. Parameters and conditions are derived from the Task D definition (Barr et al., 2004) and the "Clarifications and Revision" file (LBNL, 2005; see also Appendix A for the latest revision of the task description). Relevant modeling and simulation results are presented as below (THM1 FEBEX case and THM2 Yucca Mountain case).

2 MODELING AND SIMULATION OF THM1 (FEBEX CASE)

2.1 MODELING

Coupled THM processes are solved for in our simulation. We adopt a set of simplified governing equations for the purpose of calibration in Task D Phase 1. The coupled THM model consists of a poro-elastic deformation model, an unsaturated flow model, and a heat transfer model, which are described below.

The simplified *deformation model* can be written as,

$$\frac{\partial}{\partial x_j}\left[D_{ijkl}\frac{\partial du_k}{\partial x_l}-(FdS+\gamma dT+p_l)\delta_{ij}\right]+dF_i=0 \tag{1}$$

where u_k denotes the displacement component of the solid skeleton, γdT denotes thermal expansion of the solid skeleton with change of solid temperature, and p_l denotes pressure of liquid. FdS denotes moisture swelling of bentonite. S is water saturation. Also this equation can be used in simulating the surrounding rock when the term FdS is ignored. In this way, a simplified swelling model could be readily introduced into our numerical code. F_i is the external force.

For the FEBEX bentonite, the water retention curve can be described as a function of suction s by the following equation, which closely matches experimental data:

$$S = 0.01 + (0.99)\left[1+(s/35)^{1.43}\right]^{-0.30}\left[1-s/4000\right]^{1.5} \tag{2}$$

The modified *unsaturated/saturated flow model* in porous media is given as

$$C_m\frac{\partial p_l}{\partial t}+\nabla\cdot\left[-\frac{k_l}{\eta}k_{rl}\nabla(p_l+\rho_f gD)\right]=Q_s \tag{3}$$

where p_l represents pressure of liquid phase, k_l is isotropic permeability, and relative permeability k_{rl} is a function of water saturation,

$$k_{rl}=S^3 \tag{4}$$

Specific capacity C_m is given as a function of porosity ϕ of the medium

$$C_m=-\phi\cdot\partial S\big/\partial s, \tag{5}$$

The source term Q_s includes j_{lg}, denoting the rate of moisture transfer between liquid phase and gas phase (positive for vaporisation and negative for condensation):

$$j_{lg}=\omega(p_{sv}-p_v) \tag{6}$$

where ω is the liquid phase transfer coefficient, p_{sv} is the saturated vapor pressure, and p_v is the vapor pressure. In the rock mass, Q_s is set to zero as water vaporization and condensation are neglected. In this phase, vapor diffusion in the rock mass is also neglected

The *heat transport model* can be simplified to

$$(\rho C)\frac{\partial T}{\partial t} + \nabla \cdot (-\lambda_m \nabla T) = Q_T \tag{7}$$

where T represents temperature of solid phase (saturated by water with same temperature at each time step). ρ is bulk density of the porous medium, C is heat capacity of the porous medium, and λ_m is thermal conductivity. The source term Q_T includes contributions of thermal power (in boundary regions of bentonite) and latent heat of vaporization (in the bentonite layer). During vaporization and condensation,

$$Q_T = \rho_{water} \cdot L \cdot j_{lg} \tag{8}$$

where L is latent heat of vaporization.

2.2 SIMULATION RESULTS

Basing on the detailed description and parameters from the Task D definition (Barr et al., 2004) and from the 'Clarifications and Revisions' file (Table 2), coupled THM simulation were conducted (see parameters in Tables 1 and 2). The simulations are performed in several sequential stages (seen in Figure 2, with detailed initial and boundary conditions).

Table 1. Properties of Rock Mass

Parameter	Value
Density, [kg/m^3]	2700
Porosity, [-]	0.01
Biot's constant, α [-]	1.0
Young's Modulus, [GPa]	35
Poissons ratio, [-]	0.3
Specific heat, [J/kg·°C]	900
Thermal conductivity, [W/m·°C]	3.0
Thermal expan, coefficient [1/°C]	$1 \cdot 10^{-5}$
Permeability, [m^2]	1×10^{-17}

Table 2. Properties of bentonite.

Parameter	Value
Dry density, [kg/m^3]	$1.6 \cdot 10^3$
Porosity, [-]	0.41
Saturated permeability, [m^2]	$2.0 \cdot 10^{-21}$
Relative permeability, k_{rl}	$k_{rl} = S^3$
Moisture swelling coefficient [-]	0.238
Poisson ratio, [-]	0.35
Thermal expan. coeff., [1/°C]	$1.0 \cdot 10^{-5}$
Dry specific heat, [J/kg·°C]	$c_s = 1.38T + 732.5$ (with T_{abs})
Thermal cond., [W/m·°C]	$\lambda_m = 1.28 - \dfrac{0.71}{1 + e^{(S-0.65)/0.1}}$ (with s liquid saturation)
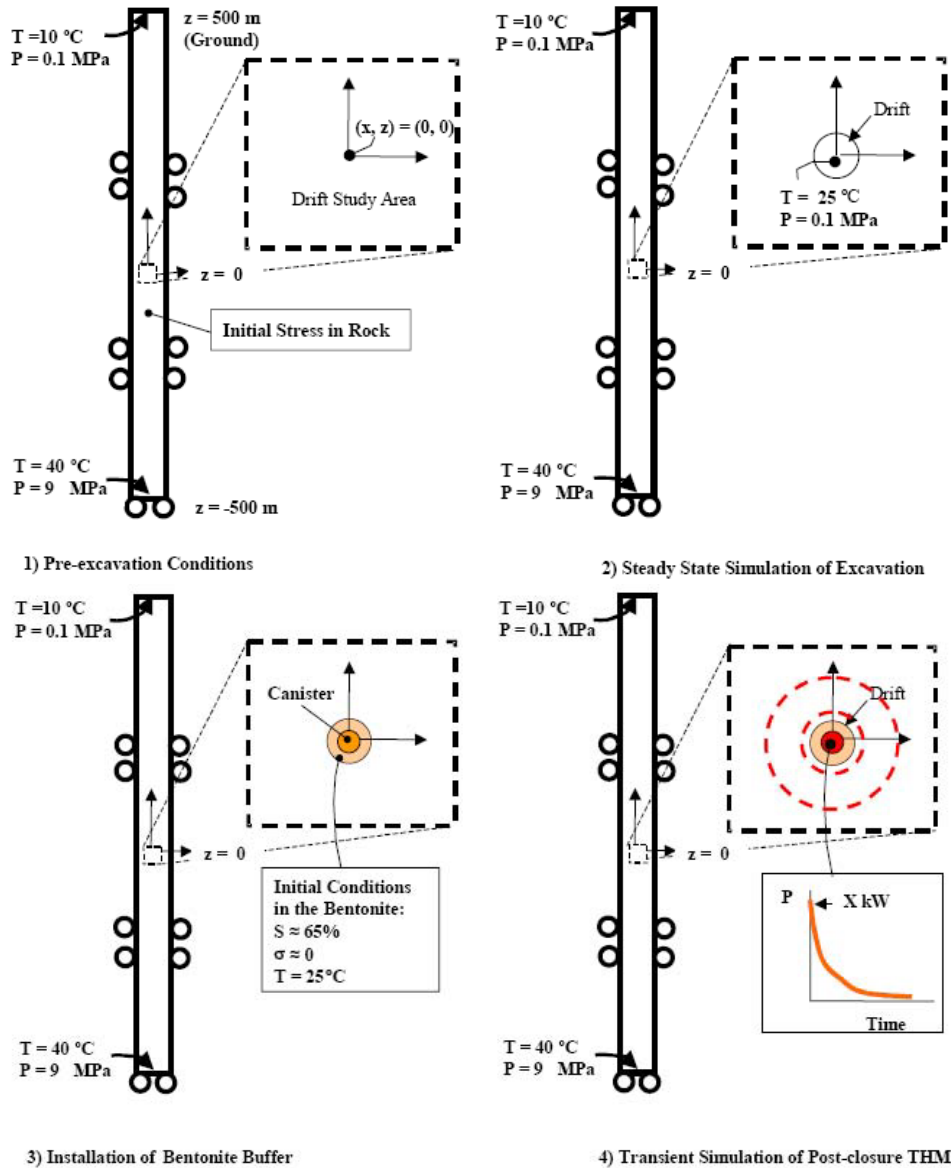
Figure 2. Specific modeling sequence, boundary and initial conditions
for Task D_THM1 simulation (Barr et al., 2004)

The initial total stresses are set to $\sigma_v = 2700 \cdot 9.81 \cdot D$ Pa and $\sigma_H = 0.055 \cdot D + 4.6$ MPa (maximum principal horizontal stress), where D is elevation relative to ground surface. Stresses include contributions of fluid pressure in the saturated rock mass before excavation.

Some parameters are defined as function of other parameters. In heat transport model, heat capacity is

$$C = (1600*(1.38*T+732.5)+1000*\phi*S*4162)/\rho_{ben} \qquad (9)$$

and bulk density ρ_{ben} is

$$\rho_{ben} = 1600 + \phi * S * 1000 \tag{10}$$

Figure 3 shows the relevant numerical grids used in our simulation. There are about 2300 elements. The red dashed lines represent vertical and horizontal profiles across the waste canister (named z-profile and x-profile respectively) for output of simulation results.
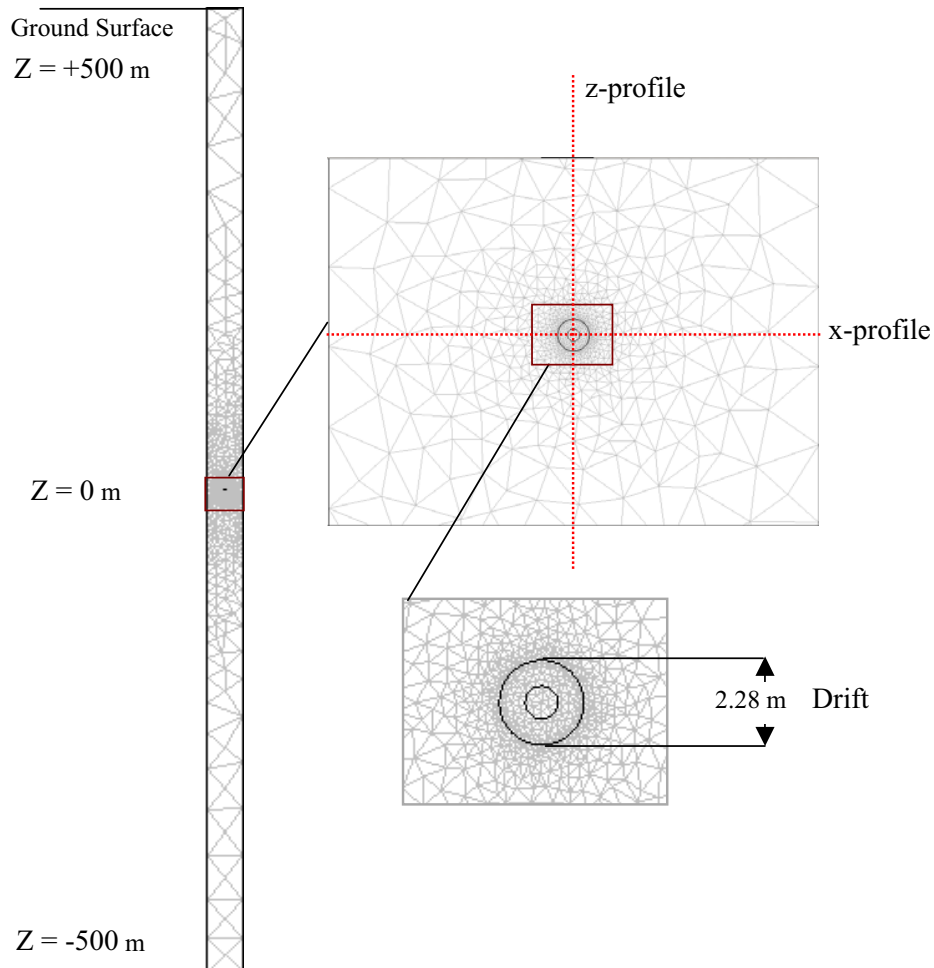
Figure 3. Numerical grid used for the THM1 FEBEX case simulations.

Simulation results are described below.

Evolution of temperature

First of all, evolution of temperature is basic driving force in coupled THM simulation. Figure 4 shows the evolution of temperature at points V1, V2 and V6. Canister surface temperature reaches its peak, 92°C, in ten years, which means saturation water will not boil at any time after closure of drift. The red line in Figure 4 denotes the thermal power of the waste canister in the FEBEX case (fitted as a curve with plotted data from the Task D definition (Barr et al., 2004)).
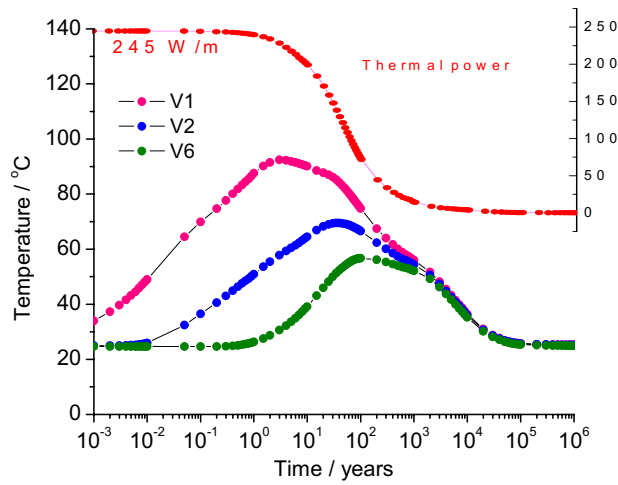
Figure 4. Temperature evolution at test points of THM1 FEBEX case simulation.

The evolution of temperature along vertical and horizontal profiles is not plotted here, but provided in complementary data files.

Evolution of Stress

Figure 5 shows the evolution of stress in the bentonite buffer at the drift surface. It can be seen that the total stress in the buffer becomes fully developed along with the fluid pressure at about 100 years. About half of the total stress in the buffer is a result of fluid pressure increase whereas the rest is caused by the moisture swelling as the saturation increases from an initial 65% to 100%. The peak stress in point V2 is about 9.7MPa at about hundred years, which then drops gradually to 9.1 MPa because of the decrease in the rock mass temperature.
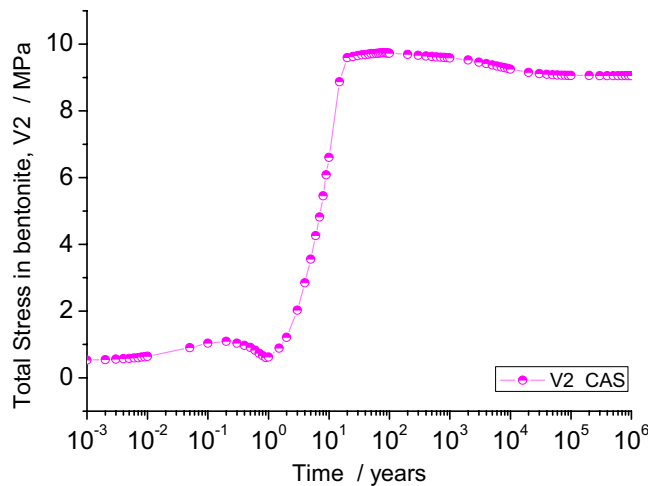
Figure 5. Total vertical stress evolution at test point V2 (at drift surface)

Figure 6 shows that horizontal stress at point H6 increases from 31 MPa to about 50 MPa with the thermal peak, and from 65 MPa to about 110 MPa in V3 at the same time.

Figure 7 shows the evolution of vertical displacement at points V3, V6 and V7. The vertical displacement at V7 (ground surface) is negative at the beginning of the simulation because the change of fluid pressure caused by drainage during excavation of the drift is taken into account in the simulation.
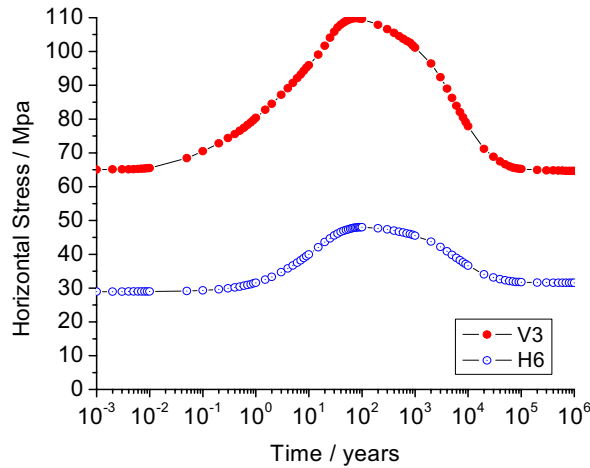
Figure 6. Horizontal stress evolution at test points V3 and H6
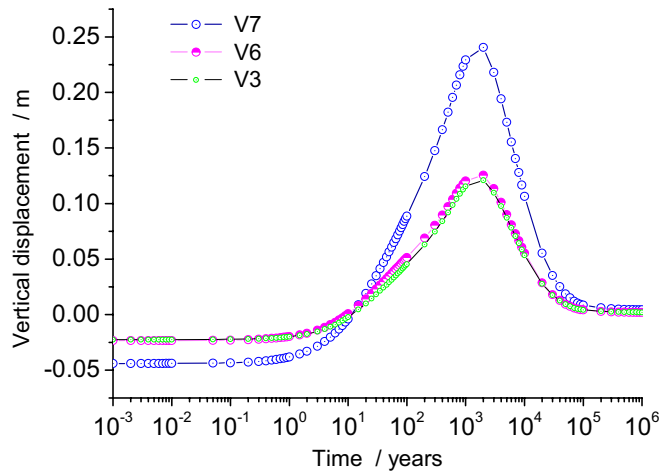
Figure 7. Vertical displacement evolution at test points V3, V6 and V7

Figure 8 shows the evolution of horizontal stress along the x-profile. Stresses are clearly affected by thermal expansion during temperature change over long periods of time. Figure 9 shows the evolution of vertical displacement along the z-profile. It can be seen that drainage causes considerable deformation.
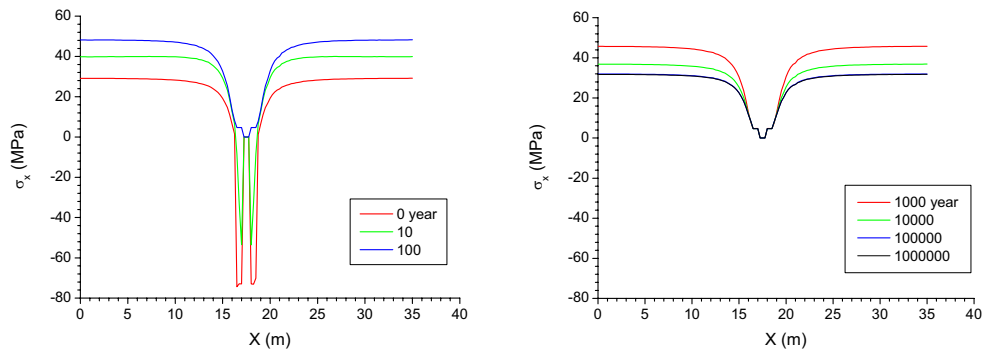
Figure 8. Horizontal stress evolution along x-profile
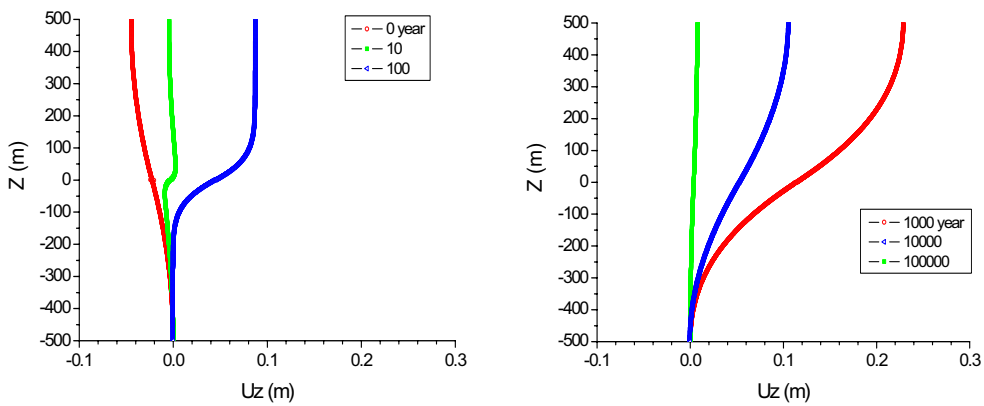
Figure 9. Vertical displacement evolution along z-profile

Evolution of Water Saturation and Fluid Pressure

Figure 10 represents the evolution of water saturation in the bentonite at the surface of the waste canister. Resaturation occurs after about 25~30 years. The drying near the canister is due to water vaporization, which makes water saturation drop to about 48% in 1~2 years.
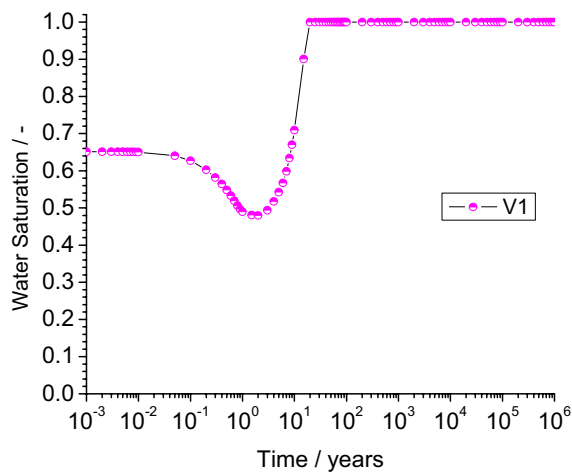
Figure 10. Water saturation evolution at test point V1 (surface of canister)

The fluid pressure at V3 (in the rock mass near the surface) is shown in Figure 11. It takes 100 years for the pressure at V3 to return to its initial hydraulic condition (~4.6MPa) before the excavation-related drainage. A clearer image of this process is shown in Figure 12. The red line represents the water pressure distribution in the entire vertical column at the beginning of simulation. About 100 years after excavation, the profile has returned to its initial static hydraulic condition and keeps unchanged from thereon.

Figure 13 shows the evolution of vertical downward water flux along the x-profile. The initial flux is about 0.29mm/year before excavation. Drainage and resaturation of bentonite make it increase sharply and then decrease slowly. After 100 years, fluxes will become steady as seen in Figure 13.
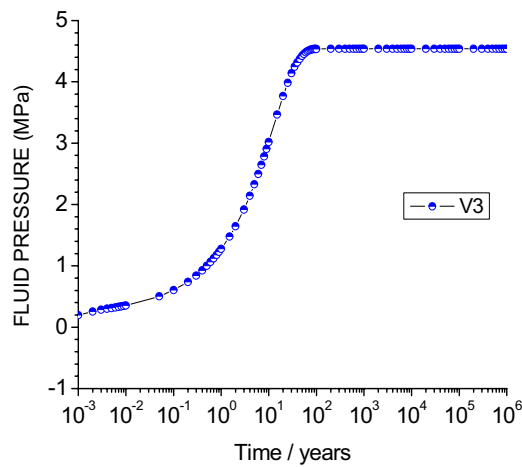
Figure 11. Fluid pressure evolution at at test point V3
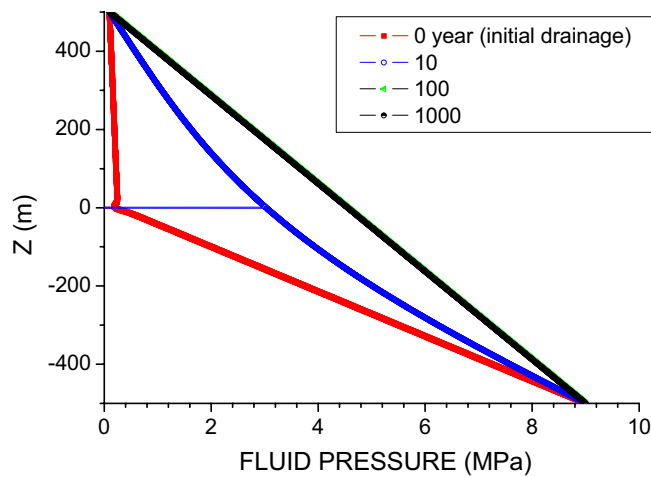
Figure 12. Fluid pressure evolution simulation results of vertical profiles
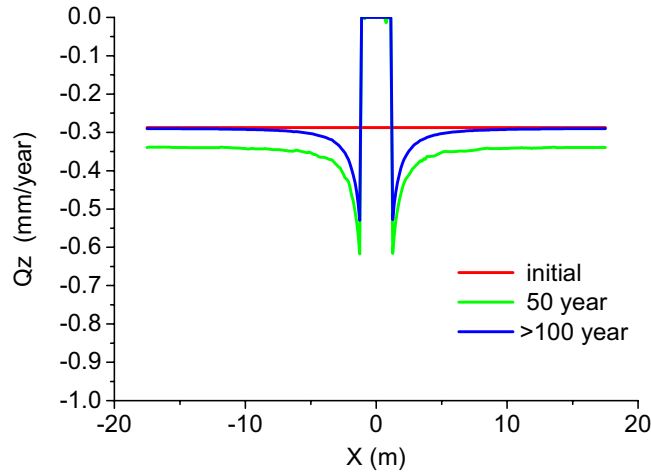
Figure 13. Simulation results of vertical flux through the repository horizon.

3 MODELING OF TASK D THM2 (YUCCA MOUNTAIN CASE)

3.1 MODELING

The governing equations used in Yucca Mountain case simulation are similar to those used in FEBEX case. Because there is higher heat release for the waste canister, pore water near the drift surface will boil for hundreds of years. Therefore it is important to simulate the boiling and drying evolution in the surrounding rock mass.

A practical boiling model is used in our simulation (derived from the Task D description given in Barr et al., 2004). Its evolution of thermal conductivity and heat capacity of rock mass are shown in Figure 14. Boiling is assumed to begin at 94 ^{o}C (T1) and end at 114 ^{o}C (T2). For temperatures below 94 ^{o}C, the rock mass remains wet at its initial saturation level. For temperatures above 114 ^{o}C, the rock mass becomes dry. As seen in Figure 14, the thermal conductivity varies linearly over this temperature range. Also, the heat capacity varies linearly in the temperature interval from T1 to T2. For increasing temperature during pore-water boiling, the values of the heat capacity are determined by the path c-d. If pore-water boiling occurs without reaching temperature T2, the values of the heat capacity are determined by the path d-c upon decreasing temperatures. If the rock mass becomes dry (i.e., temperature exceeds T2), the values of the heat capacity are determined by path e-b when temperature decreases. It is assumed that the rock mass returns to its initial saturation when reaching temperature T1. The heat of vaporization is not recovered at resaturation of the rock mass.
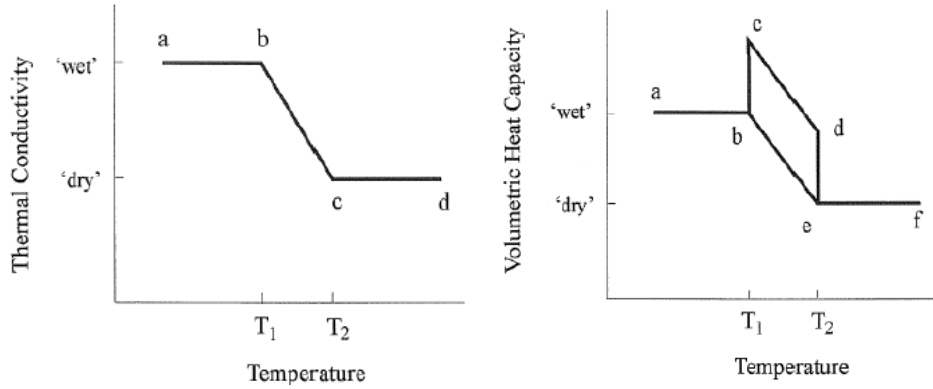
Figure 14. Illustration of pore-water boiling model used in simulation
for model simplification (from Damjanac et al., 2000)

In this boiling model, the change of heat capacity (path b-c) can be calculated by

$$\Delta C = \frac{\rho_{water} \cdot \phi \cdot S_{water} \cdot L}{\rho_{solid} \cdot (T2 - T1)} \tag{11}$$

where L is latent heat of vaporization, set to 2.2526×10^3 kJ/kg, S_{water} is water saturation, and ϕ is rock porosity.

3.2 SIMULATION RESULTS

The geometry and model conditions are from the detailed description and data from the Task D definition (Barr et al., 2004) and the 'Clarifications and Revisions' file (Table 3). The simulations consist of several sequential modeling stages (seen in Figure 15, with detailed initial and boundary conditions). The initial stress is set to $\sigma_v = 2360 \cdot 9.81 \cdot D$ Pa, and $\sigma_H = 0.6 \cdot \sigma_v$ (maximum principal horizontal stress), where D is elevation relative to ground surface. In the flow model, the drift surface is set to a no-flux boundary, which prevents water flowing into the dry drift (filled with air). Pressure of gas is constant everywhere, at 1.01e5 Pa.

Table 3. Properties of rock mass.

Type	Property	Value
Thermal and Mechanical properties of the rock mass (equivalent continuum properties)	Bulk Density (saturated) (kg/m3)	2360
	Young's modulus (GPa)	15
	Poisson's ratio (-)	0.21
	Thermal expansion coefficient (1/°C)	1.0×10^{-5}
	Wet thermal conductivity (W/m °K)	2.29
	Dry thermal conductivity (W/m °K)	1.49
Hydraulic properties of the fracture-matrix continuum	Permeability (m²)	3.87×10^{-17}
	Porosity (-)	0.13
	van Genuchten's air-entry pressure (kPa)	118.3
	van Genuchten's exponent, m (-)	0.317
	Residual saturation (-)	0.19

Figure 15. Specific modeling sequence, boundary and initial conditions
for Task D_THM2 (Barr et al., 2004).

Figure 16 shows the numerical grids used in the THM2 simulation. There are about 1700 elements. The red dashed lines represent vertical and horizontal profiles across the waste canister (named z-profile and x-profile respectively) for output of simulation results.
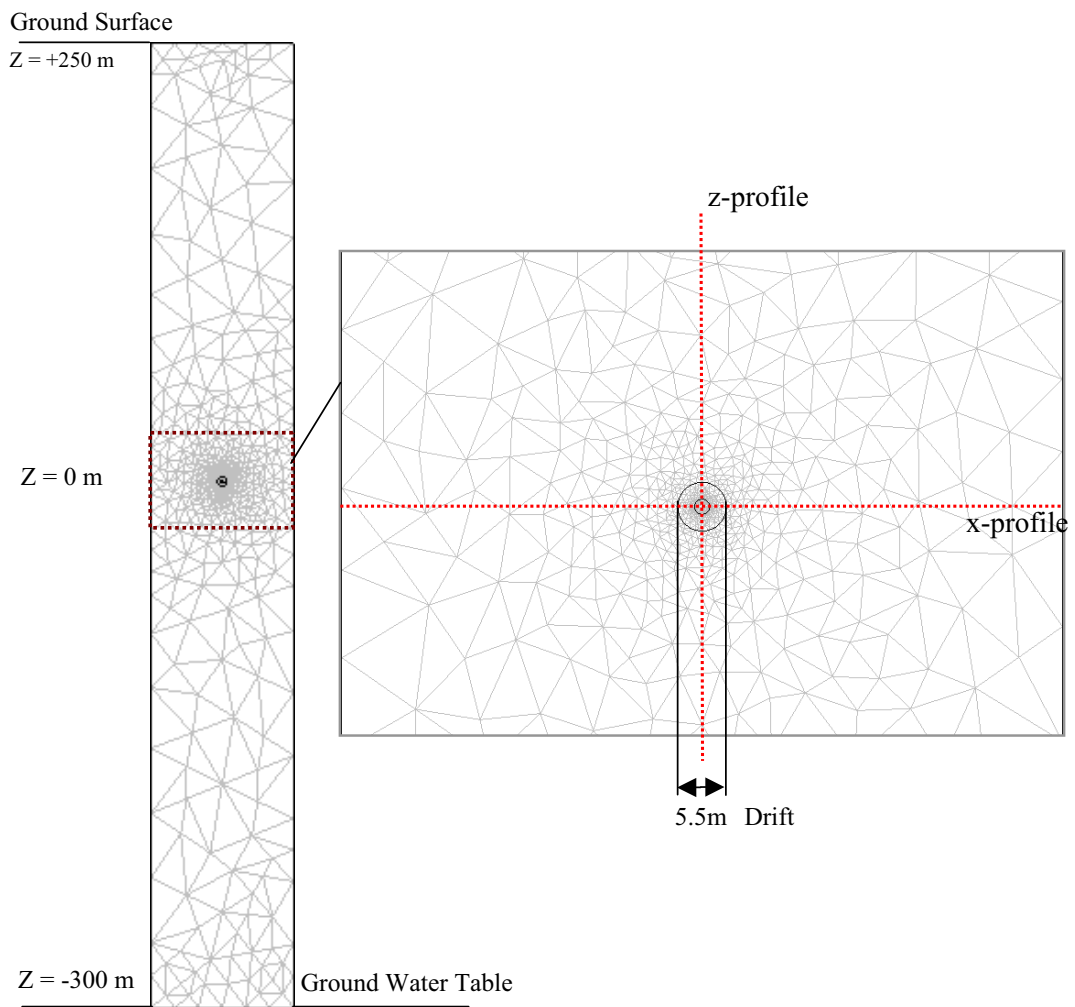
Figure 16. Numerical grid used in THM2 Yucca Mountain case simulations.

Simulation results are given in the figures below.

Evolution of Temperature

The evolution of temperature is shown in Figure 17. There is a low level of thermal power caused by the 50-year period of forced ventilation, during which 86% of the decay heat of from canister is removed by air flow. After that, the canister surface temperature increases very quickly, exceeds the boiling point and reaches its peak temperature of 125°C at about 70 years. The high temperature causes rock mass drying over hundreds of years.

It can be seen that the temperature evolution at V2 is nearly the same as that at V1. Because there is significant radiative heat transfer in the open drift, it is a good approximation to assume a perfect heat transfer from the waste package to the walls of the drift. The slight difference of temperature between V1 and V2 is due to very high (effective) heat conductivity of air in simulation (representing the very efficient radiative heat exchange in the open drift).
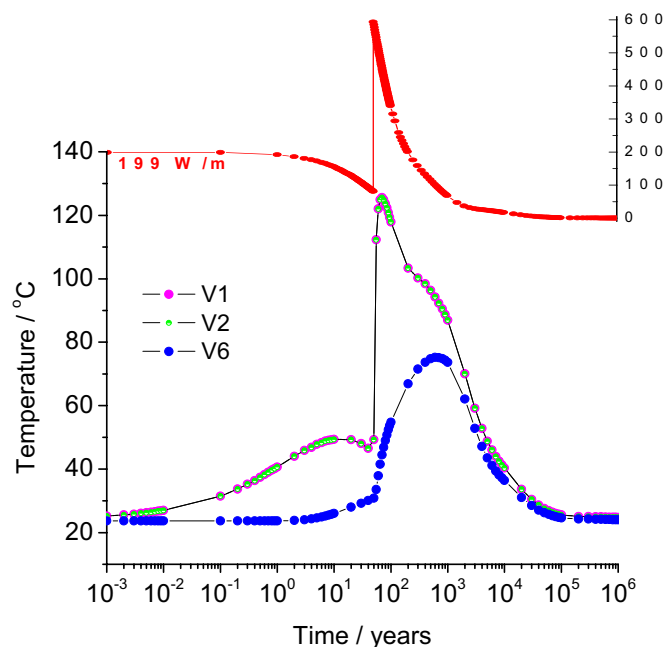
Figure 17. Temperature evolution at test points of THM2 Yucca Mountain case simulation.

The red line in Figure 17 denotes the thermal power of the waste canister in THM2 (fitted as a curve with data from the Task D definition; Barr et al., 2004). It is more accurate than that of THM1 case.

Figure 18 shows the temperature evolution along the z-profile. It can be seen that the entire rock column is affected by heating. The temperature field returns to its initial condition in 1e6 years.
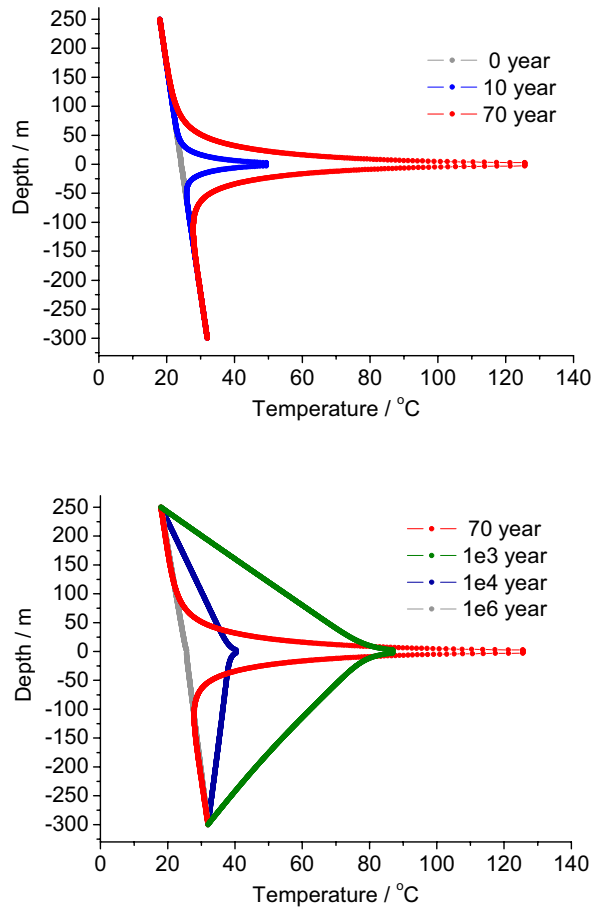
Figure 18. Temperature evolution along z-profile.
(top for 0~70 years, bottom for 70~1e6years)

Evolution of Stress

Figure 19 shows that the *horizontal stress* at point V3 and H6 increases slowly over the first 50 years, but then sharply reaches the peak temperature after ending of forced ventilation. The peak stresses at V3 and H6 are about 35MPa and 13Mpa, respectively, corresponding to the thermal peak.

Figure 20 shows the *vertical stress* evolution along vertical and horizontal profiles.

Figure 21 shows that *vertical displacement* along the z-profile changes with time following the same trend as the stress evolution. The maximum displacement at the ground surface is 0.23m.
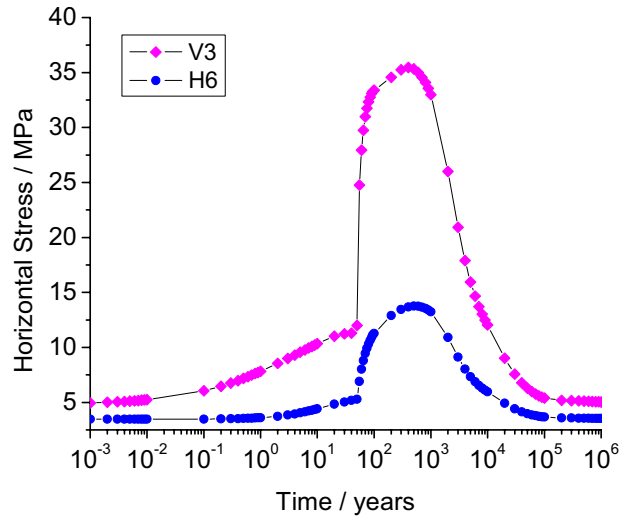
Figure 19. Vertical stress evolution at test points V3 and H6
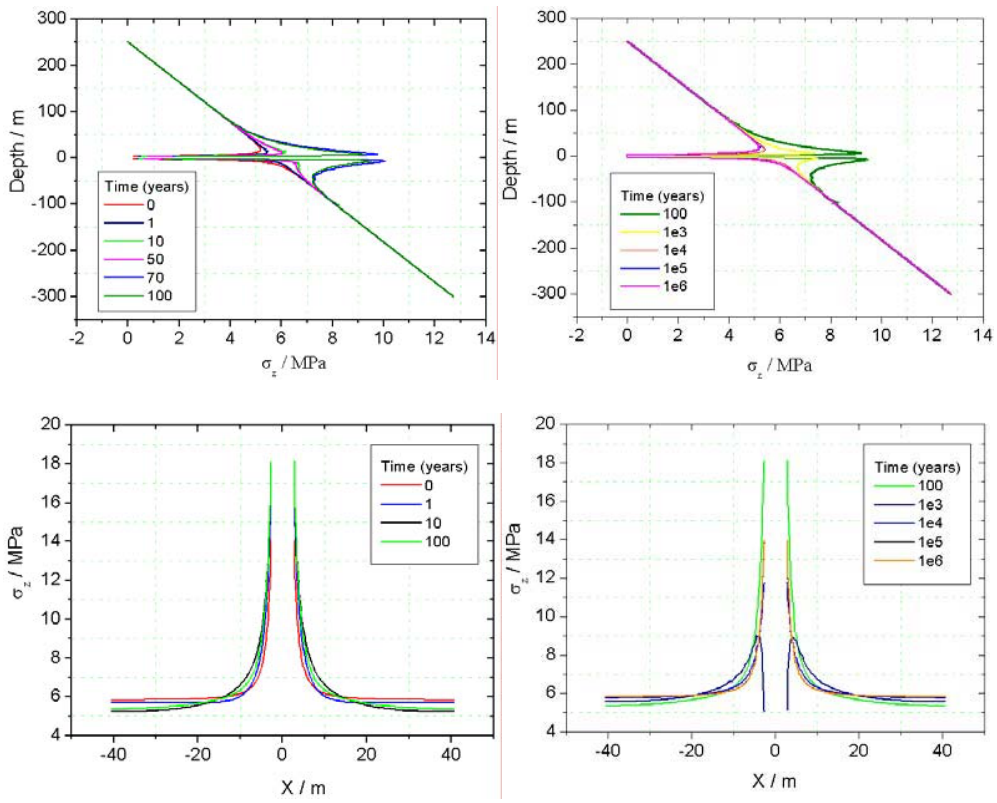
Figure 20. Vertical stress evolution along z-profile (top) and x-profile (bottom)
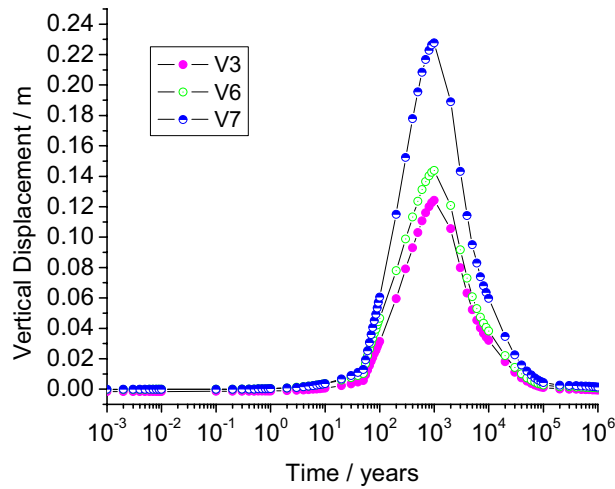
Figure 21. Vertical displacement evolution at test points V3, V6 and V7

Evolution of Water Saturation and Fluid Pressure

Figure 22 represents the evolution of *water saturation* in the rock near the drift surface. Rock dry-out occurs over hundreds years, which is due to water boiling at temperatures above 100^oC. For this modeling phase, we adopt a practical pore-water boiling model described in Figure 14. According to this model, water and vapor movements in the boiling zone are neglected.

During the simulation, there is always a unsaturated water flow downward in the entire rock column, and maintains a constant flux of 6mm/year in most areas away from the drift. Figure 23 represents the water flux along the x-profile at initial conditions (0 year of simulation time). The no-flux boundary at the drift wall causes increase fluxes near the drift surface, as water is diverted sideways and around the drifts. These fluxes remain steady in the entire area except for the immediate boiling zone according to the pore-water boiling model.
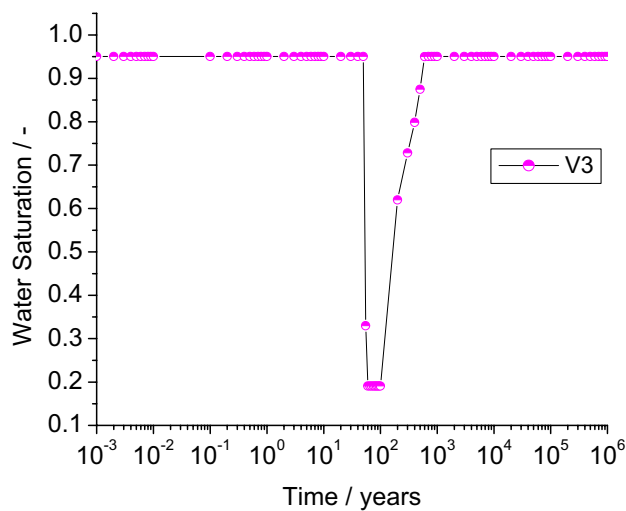
Figure 22. Water saturation evolution at test point V3
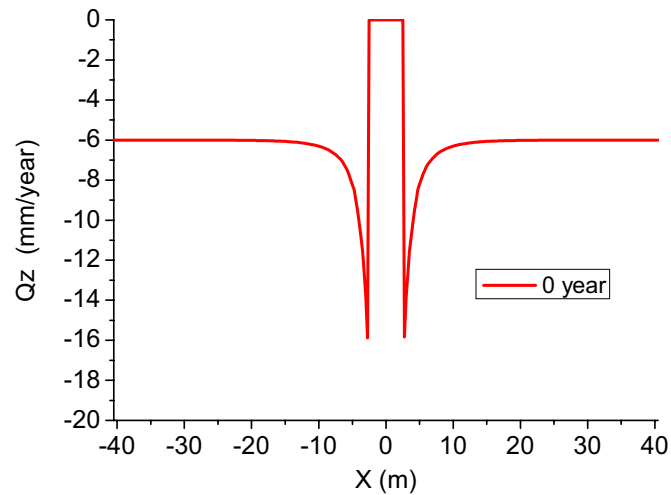
Figure 23. Simulation results of vertical flux through the repository horizon.

4 CONCLUSION AND DISCUSSTION

In this phase, we use a simplified practical model in both THM1 and THM2 simulations for comparison with other teams. It runs more stable and fast than a more complex 'physical' model. However the latter can include more flexible approaches for many classical physical processes, such as water flow in fractures and vapor transport. When the model calibration is finalized and all disagreements between international teams have been resolved, a more complex model should be used in our next step simulation, including a dual-continuum or an ECM model. We believe it will improve to analysis of the fracture system in the next modeling phase of Task D.

References

Barr D., Birkholzer J., Rutqvist J., and Sonnenthal E., 2004. Draft Description for DECOVALEX-THMC Task D: Long-Term Permeability/Porosity Changes in EDZ and Near Field.

Damjanac B., Brandshaug T.,Carranza-Torres C, Detournay C. and Perrochet P, 2000. An evaluation of local thermo-mechanical effects on seepage into waste disposal rooms at Yucca Mountain. Itasca Consulting Group Inc November 2000.

Jing L. 2003. A review of techniques, advances and outstanding issues in numerical modelling for rock mechanics and rock engineering. Int. J. Rock Mech & Min Sci., Vol.40, 283-353.

Nguyen, T.S. et al, 2003. Modelling the response of the bentonite in the FEBEX heater experiment. International conference on coupled THMC processes in geo-systems: fundamentals, modeling, experiments and applications, GeoProc2003,96-101.

van Genuchten, M. T., 1980. A closed-form equation for predicting the hydraulic conductivity of unsaturated soils. Soil Sci Soc Am J 44: pp. 892-898.

Appendix G

Status Report for D_THC

DOE Team

DOE Team THC1 Analysis

E. Sonnenthal, J. Rutqvist, J. Birkholzer

Lawrence Berkeley National Laboratory

I. INTRODUCTION

THC1 is a model of a generic repository located in saturated crystalline rock, where emplacement tunnels are backfilled with buffer material (FEBEX-type). The description of Task D_THC1 is based on data from Aspö and the Japanese program. Properties of the bentonite buffer material are based on a sample investigated by the Japanese program.

In Phase 1 of the THC1 simulation study, only mineral-water dissolution/precipitation reactions are considered. In Phase 2, the added effects of ion exchange and sorption will be considered (Barr et al., 2005). Volume changes owing to clay swelling and pore compressibility are included in Phase 1, but no mechanical effects are considered. Permeability and porosity changes owing to mineral precipitation/dissolution are also not considered in the Phase 1 simulations. Many simplifications are made regarding the geochemical set-up and processes considered in this analysis. Therefore, the model and results are intended only as a basis for comparison among groups modeling the same phenomena, and not as a realistic representation of the processes and parameters associated with an actual site or experiment.

TOUGHREACT (Xu et al., 2004) was used for all simulations discussed in this report. TOUGHREACT solves the conservation of heat and fluid mass for multiphase and multicomponent systems (including air, water vapor, and liquid), and diffusive and advective transport of aqueous and gaseous species. Mineral-water-gas reactions can be solved assuming either local equilibrium or using various kinetic formulations. Simulations were performed using the sequential noniterative scheme for the coupling between flow transport and reaction. Details regarding the mathematical formulations used can be found in the TOUGHREACT users manual (Xu et al., 2004) and in the TOUGH2 V2 users manual (Pruess et al., 1998). Results of TOUGHREACT simulations for DECOVALEX Task III can be found in Sonnenthal et al. (2005).

II. MODEL SET-UP AND INPUTS

II.1. Model Geometry and Numerical Grid

The model geometry is based on Figure 6.1 shown in Barr et al. (2005). A single continuum numerical grid was developed to reflect the geometry of the waste package, bentonite-filled drift, fractured granite host rock, as well as the observation points (Figure 1). The horizontal and vertical dimensions are 35m and 1000m, respectively. The canister is 0.9m in diameter and is discretized into 60 pie-shaped grid blocks. The emplacement drift is 2.28m in diameter. The full model domain consists of 7852 grid blocks. The side boundaries are considered as no-flux

boundaries. The upper and lower boundaries are given fixed pressure, temperature, and water composition.
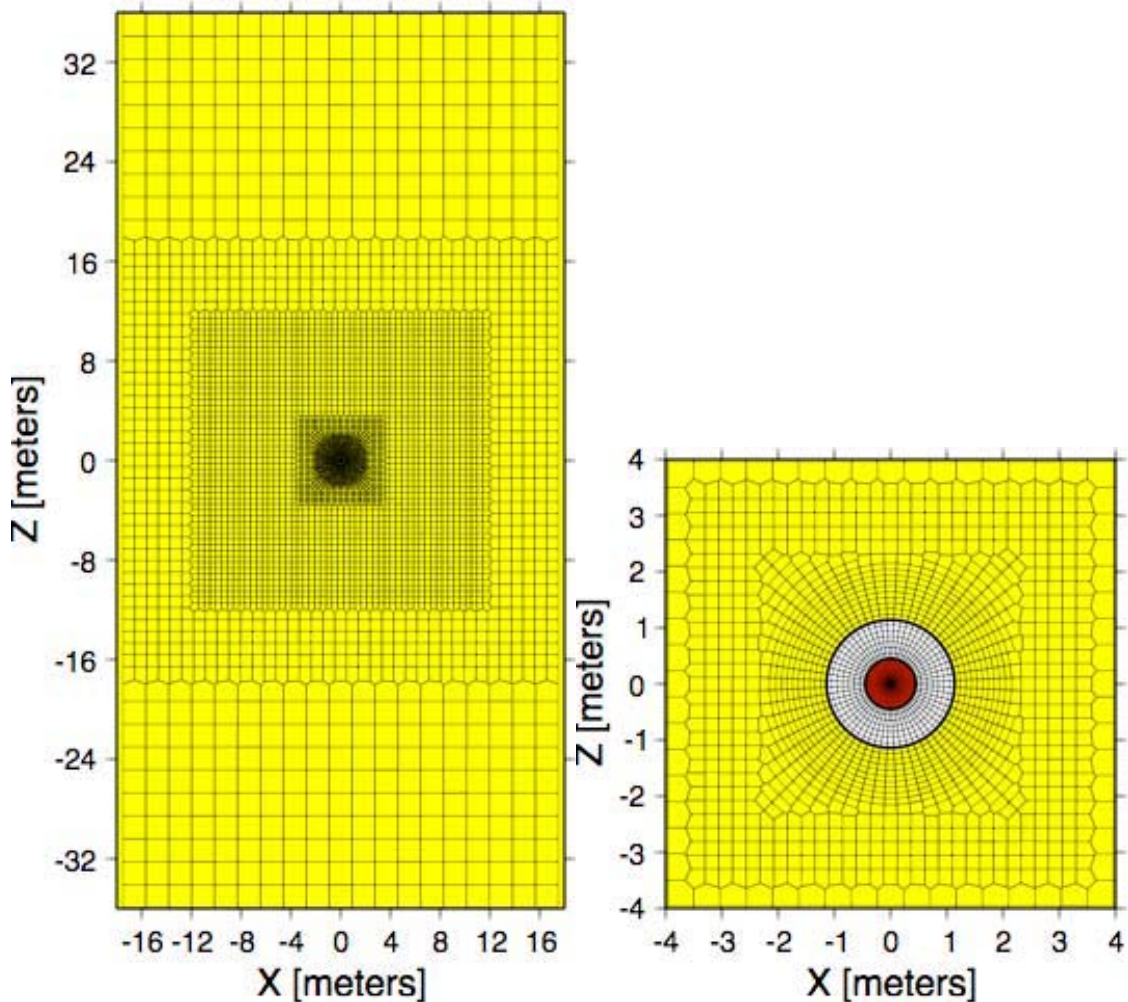
Figure 1.   Numerical mesh and enlargement of mesh showing waste canister (red), bentonite buffer (white), and drift wall boundary. Mesh extends 500m above and below the drift center, and 17.5m to each side.

II.2. Hydrological and Thermal Properties

Hydrological and thermal properties are listed in Table 1, as derived in part from Barr et al. (2005). Some parameter values were chosen for consistency with the DOE THM model parameter values. Some small inconsistencies still remain with regard to the values used by various teams which should be reconciled (i.e., van Genuchten parameters, porosity, pore compressibility, etc.).

Table 1. Granite and bentonite thermal and hydrological properties

Parameter	Granite	Bentonite
Grain density, [kg/m^3]	2700.	2700.
Porosity, [-]	0.01	0.41
Saturated permeability, [m^2]	$1.0 \cdot 10^{-17}$	$2.0 \cdot 10^{-21}$
Relative permeability, k_{rl}	$m = 0.6$, $S_{rl} = 0.01$	$k_{rl} = S^3$
Van Genuchten α [1/Pa]	$6.8027 \cdot 10^{-7}$	$3.3333 \cdot 10^{-8}$
Van Genuchten m	0.6	0.3
Compressibility, β [1/Pa]	$3.2 \cdot 10^{-9}$	$5.0 \cdot 10^{-8}$
Thermal expansion coeff., [1/°C]	0.0	$1.0 \cdot 10^{-4}$
Dry specific heat, [J/kg·°C]	900.	800.
Thermal conductivity [W/m·°C] dry/wet	3.0/3.0	0.5/1.3
Tortuosity	1.0	0.8

The heat input emanating from the decaying waste was derived from Barr et al. (2005), and is identical to that used in the DOE THM analysis (Rutqvist, this report).

II.3 Mineralogy

II.3.1 Mineralogy of Granitic Host Rock

Mineralogical abundances for the granitic host rock are based on data from the Smäland granite (Rhen et al. 1997) and listed in Table 2. Biotite was recalculated into the annite and phlogopite endmembers, with thermodynamic data from the Yucca Mountain EQ3/6 database (see Appendix 1 for thermodynamic data). Minor phases are neglected in Step 1, and mineral abundances are renormalized to 100%. Because the initial equilibrium system depends on the mineral assemblage and not on the initial abundances, the volume fractions of the phases were assumed to be equivalent to the mass fractions. Once kinetic simulations are carried in Step 2, requiring reactive surface areas, the abundances will be recalculated to volume fractions.

Table 2. Mineral abundances in the Smäland Granite (based on Rhen et al., 1997)

Mineral	Abundance (mass fraction)
Quartz	0.2756
K-Feldspar	0.2724
Plagioclase	0.3964
Annite	0.0489
Phlogopite	0.0067

II.3.2. Initial Mineralogy of the Kunigel V1 Bentonite

Kunigel V1 Na-bentonite is used as the buffer material, with mineral abundances given in Table 3 (Table 1, Ochs et al., 2004). In order to simplify the problem in Step 1, pyrite and other minor phases are not considered (thus, no redox reactions).

Table 3. Mineral abundances in the Kunigel-V1 bentonite (Ochs et al., 2004)

Mineral	Abundance (mass fraction)
Na-montmorillonite	0.475
Quartz	0.335
K-Feldspar	0.041
Calcite	0.0235
Dolomite	0.029
Pyrite	0.006

II.4. Water Chemistry

The initial water chemistry in the granite is based on data from Aspö. Laaksoharju (2002) described three cases in which water of different origins (shallow, deep, mixed) flowing toward the tunnel resulted in either calcite precipitation (shallow and mixed) in fractures or none (deep). For this case, the Litorina Sea composition was chosen as listed in Table 4. A water composition for the bentonite was derived from the Japanese program (Table 4). Although these compositions were used as input to the model, they were equilibrated with the granite and bentonite under in-situ temperatures prior to the full THC simulation (see Section III).

Table 4. Initial water chemistry in granite (Laaksoharju, 2002) and bentonite

	Litorina Sea (mol/kg H$_2$O)	Bentonite (mol/kg H$_2$O)
pH	7.7	8.4
Cl	1.833E-01	1.500E-05
Na	1.598E-01	3.600E-03
K	3.427E-03	6.200E-05
Ca	3.767E-03	1.100E-04
Mg	1.843E-02	5.500E-05
HCO$_3$	1.524E-03	3.500E-03
SO$_4$	9.265E-03	1.100E-04
SiO$_2$	---	3.400E-04
Total	4.110E-01	7.727E-03
Charge Balance (%)	1.032E+00	3.326E+00

III. THC1 SIMULATION RESULTS

Simulation results are shown for a fully saturated system, and for the bentonite initially at 65% water saturation. The following sections discuss the initialization steps and outputs, the temperature and saturation history, and followed by discussion of chemical changes to aqueous species and minerals for the saturated and unsaturated cases.

III.1. Initialization

A series of initialization steps were performed prior to the simulation of waste canister and accompanying THC processes. First, a steady-state pre-excavation flow simulation was performed, assuming that the entire rock column is granite. Boundary conditions were those given in Barr et al. (2005) (0.1 MPa and 10°C at the top, 9.0 MPa and 40°C at the base). These boundary conditions with the chosen properties result in approximately 3mm/yr of downward flow with a temperature at the 500m depth of slightly less than 25°C and a fluid pressure of approximately 4.5MPa.

For the fully saturated case, the drift was filled with bentonite, assuming the fluid pressure is identical to that in the pre-excavation granite. A post-excavation simulation was then performed for one time step to equilibrate the mineral assemblage with the initial water chemistry for the entire model domain. Therefore, prior to the THC simulation the system is at steady-state for water and heat flow and all grid blocks have water compositions equilibrated with the local mineral assemblage. The equilibrated water chemistry in Table 5 for the location V1 in the bentonite (~5cm above the canister surface) and in the granite at point V6 (~10cm above the drift crown).

Table 5. Equilibrated water chemistry in granite (V6) and bentonite (V1)

	Litorina Sea-Granite (mol/kg H_2O)	Bentonite (mol/kg H_2O)
Temperature (°C)	24.60	24.93
pH	8.497	7.060
Cl	1.839E-01	1.500E-05
Na	2.009E-01	4.758E-03
K	1.786E-04	3.362E-04
Ca	2.777E-03	2.747E-03
Mg	1.583E-04	5.500E-05
HCO_3	5.328E-04	5.105E-03
SO_4	9.270E-03	1.100E-04
SiO_2	3.336E-04	1.775E-04
AlO_2	7.644E-08	3.539E-08
Fe^{2+}	3.320E-07	9.999E-11
Total	4.110E-01	7.727E-03

Because the initial and potential secondary mineral assemblage was very limited in this simplified Step 1 simulation, the equilibrated water chemistry is quite different from the

measured initial water composition for most reactive species. For Steps 2 and 3, an attempt should be made to more accurately define the mineral assemblages, thermodynamic data, and kinetic data in order to start with initial water compositions closer to the measured compositions.

In the unsaturated case, the bentonite was assumed to have an initial liquid saturation of 0.65. A single time step was run to re-set the initial pressure distribution for an unsaturated system and to create input files for the TOUGHREACT EOS4 module that considers vapor pressure lowering due to capillary pressure.

III.2. Thermal and Hydrological Evolution

The temperature evolution at point V1 for the saturated and unsaturated cases is shown in Figure 2. Temperatures for the unsaturated case rise faster owing to the lower thermal conductivity of the air-vapor gas phase. Full resaturation occurs before the peak temperature is reached resulting in both cases having the same maximum temperature (~88°C). The temperature history is similar to that provided by the other teams, yet the peak temperature is about 2-4°C lower. The discrepancy in peak temperature appears to be due in part to the coarse time discretization of the heat input, and the lack of a prolonged post-excavation simulation (without heat), which would result in delayed rewetting of the bentonite. Other potential discrepancies, such as the thermal conductivity as a function of liquid saturation, may also play a role.
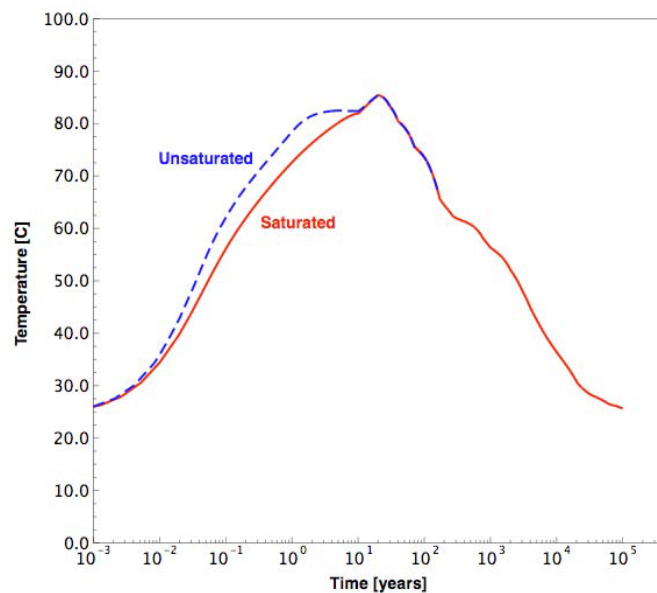
Figure 2.   Temperature history for fully saturated and initially unsaturated bentonite at point V1 adjacent to canister.

The evolution of liquid saturation at points V1 (in bentonite adjacent to waste package) and V2 (in bentonite adjacent

 to the drift crown) is shown in Figure 3. The dryout and resaturation behavior at V1 is similar, albeit reaching values slightly lower, than that observed by the other teams (except the BGR

THC1 simulation, which shows slightly less drying). Point V2 does not exhibit any drying, and shows fairly rapid rewetting since it is adjacent to the fully saturated granite and is directly below the drift crown.
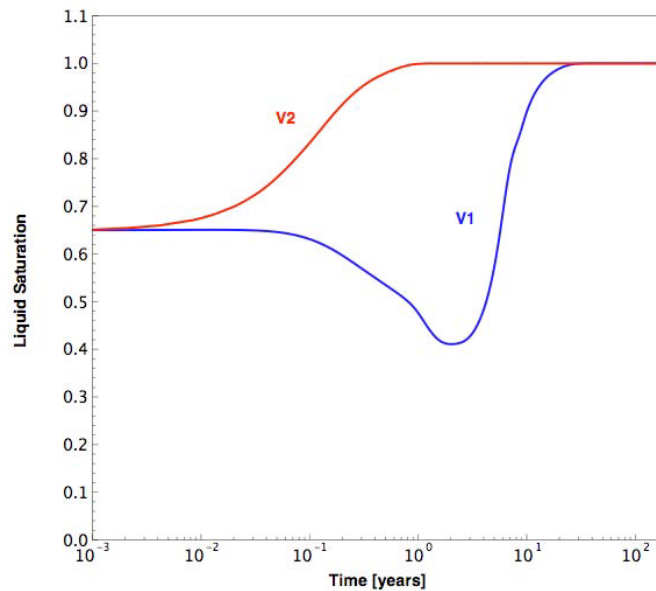
Figure 3. Liquid saturation evolution at points V1 (in bentonite adjacent to waste canister) and V2 (in bentonite adjacent to drift crown).

III.3. Geochemical Evolution: Saturated Case

Results for the saturated case are shown in Figure 4 from 0.01 to 100,000 years. The temperature rise is quite rapid, and diffusion of aqueous species is the dominant mechanism of transport between the granite and the bentonite owing to the very different initial water compositions. Some flow through the very low permeability bentonite is evident from the asymmetry of the concentration profiles above and below the drift by 1000 years (steeper gradient above owing to downward flow). Na and Cl show the strongest increase in the bentonite as a result of diffusion from the seawater and also slow flow into the bentonite. By 100,000 years there are no vertical changes in temperature or water composition, as a result of the complete replacement of the initial bentonite water by seawater and the equilibration of the mineral assemblages to this water composition at the ambient temperature.
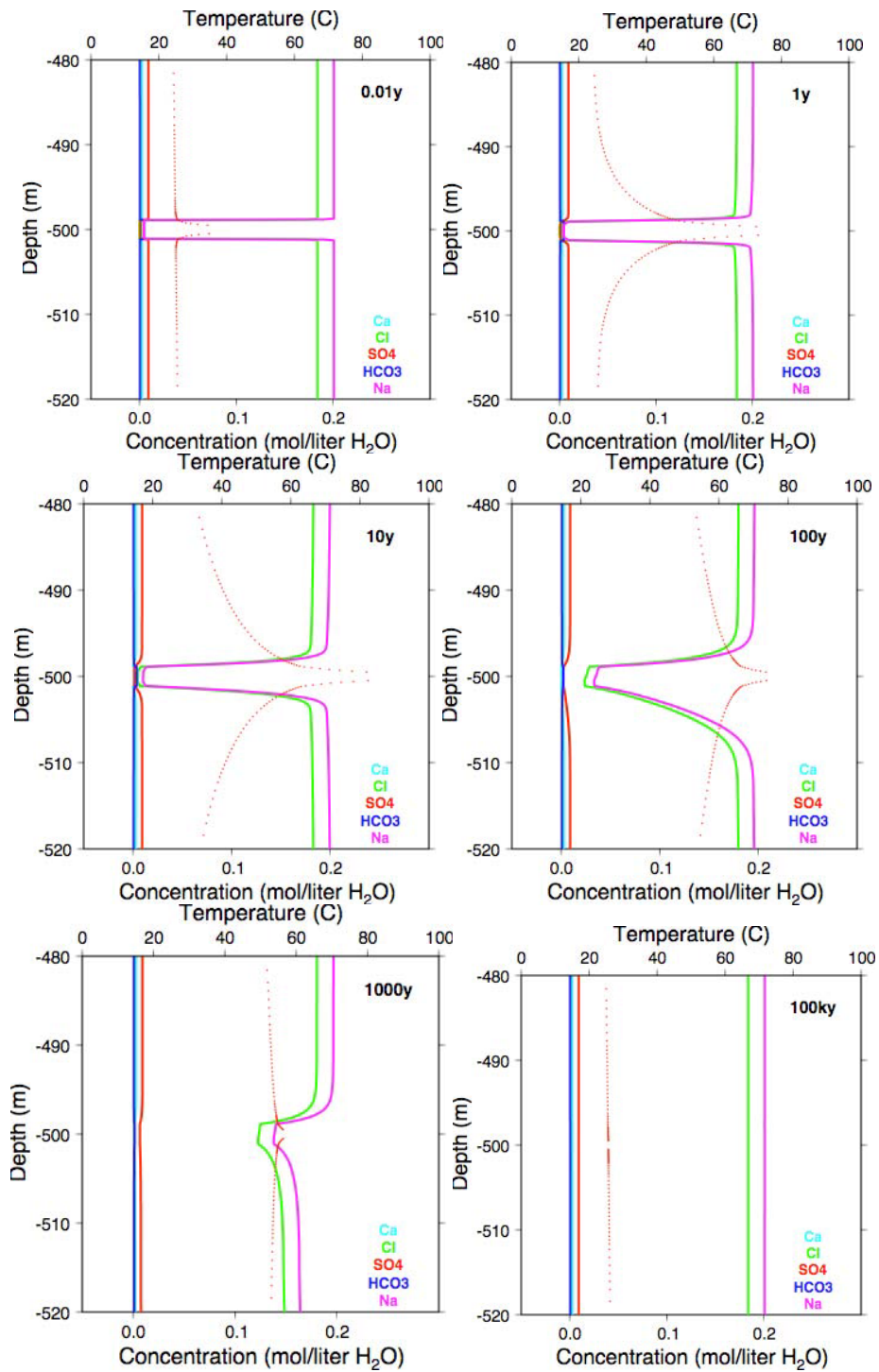
Figure 4. Vertical profile of selected aqueous species concentrations (total) and temperature through the drift center for the fully saturated case. Times shown are 0.01, 1, 10, 100, 1000, and 100,000 years.

Changes in mineralogy over a 100,000-year time span are shown in Figure 5. The vertical extent of the profile was reduced to 4 meters above/below the drift center to capture a region of strong mineralogical changes restricted to the granite at the contact with the bentonite and within the bentonite. The changes from the initial abundances are expressed in moles of mineral precipitated per m^3 of rock mass. In cases where the overall abundance may not differ appreciably, the changes to the mineral abundances allow mineral alteration effects to be readily observed. The results of the simulation show a region of strong mineralogical changes that is restricted to the granite at the contact with the bentonite and within the bentonite.

Initially, there are small changes in the abundances of some minerals in the bentonite owing to initial disequilibrium. The minor initial effects are overwhelmed by the heat- and transport-induced changes. By 10 years, the effects of aqueous species diffusion across the bentonite-granite contact are apparent, with albite dissolution and quartz+calcite precipitation in the granite. At this time, K-feldspar and calcite are dissolving in the bentonite near the margin of the granite, but are precipitating in the hotter zone adjacent to the canister. The complex interplay of diffusion across the contact and the strong temperature gradients result in sharp changes in mineral dissolution/precipitation behavior traversing from the granite to the canister. By 100,000 years there is some asymmetry in the albite dissolution in the granite (greater below the drift) but otherwise the patterns are fairly symmetric. Na-montmorillonite in the bentonite shows increased stability adjacent to the canister and also precipitates as a new secondary phase in the granite, but has dissolved in the bentonite at margin of the drift.
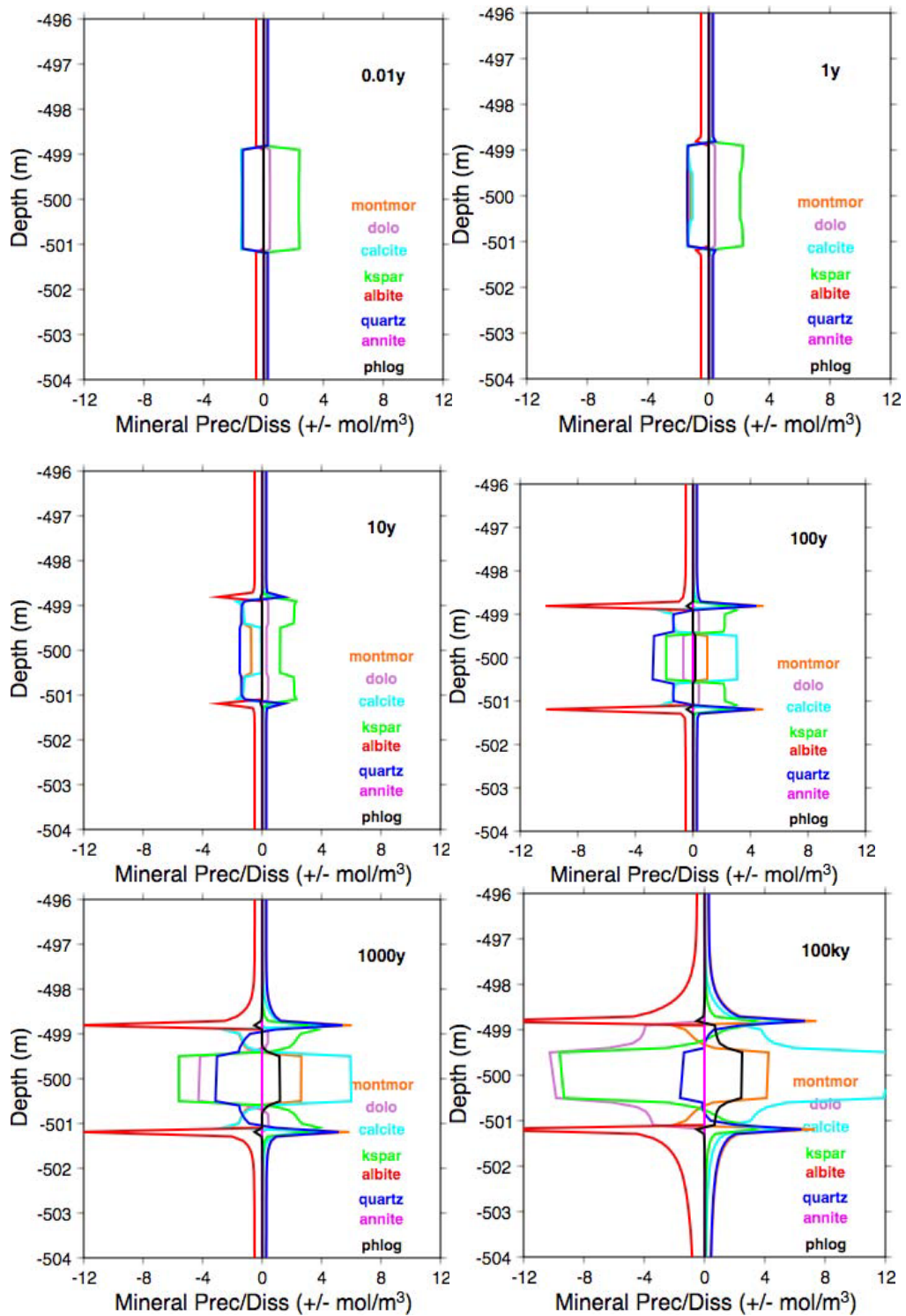
Figure 5. Vertical profile of changes in mineral abundances through the drift center for the fully saturated case. Times shown are 0.01, 1, 10, 100, 1000, and 100,000 years.

III.4. Geochemical Evolution: Unsaturated Case

The unsaturated bentonite was simulating using the same geochemical conditions as the saturated case. The main differences in THC processes between the saturated and unsaturated systems are due to (1) the smaller volume of water in the unsaturated bentonite thus reducing the extent of reaction required to maintain equilibrium between the aqueous species and minerals, (2) the drying effect near the canister, and (3) the larger influx of seawater through capillary-driven rewetting from the granite to the bentonite. Aqueous species concentrations for the unsaturated case are shown in Figure 6 from 0.01 to 100 years. The temperature rise is more rapid, and concentrations of Na and Cl rise more rapidly near the canister due to both the drying effect and to the influx of seawater via capillary suction. Small inflections to lower concentrations at ten years may be the result of evaporation near the canister and condensation in the cooler zone adjacent to the wetting front. After 100 years, the temperature and compositional trends are close to those displayed by the saturated system, since the unsaturated time period is relatively short.
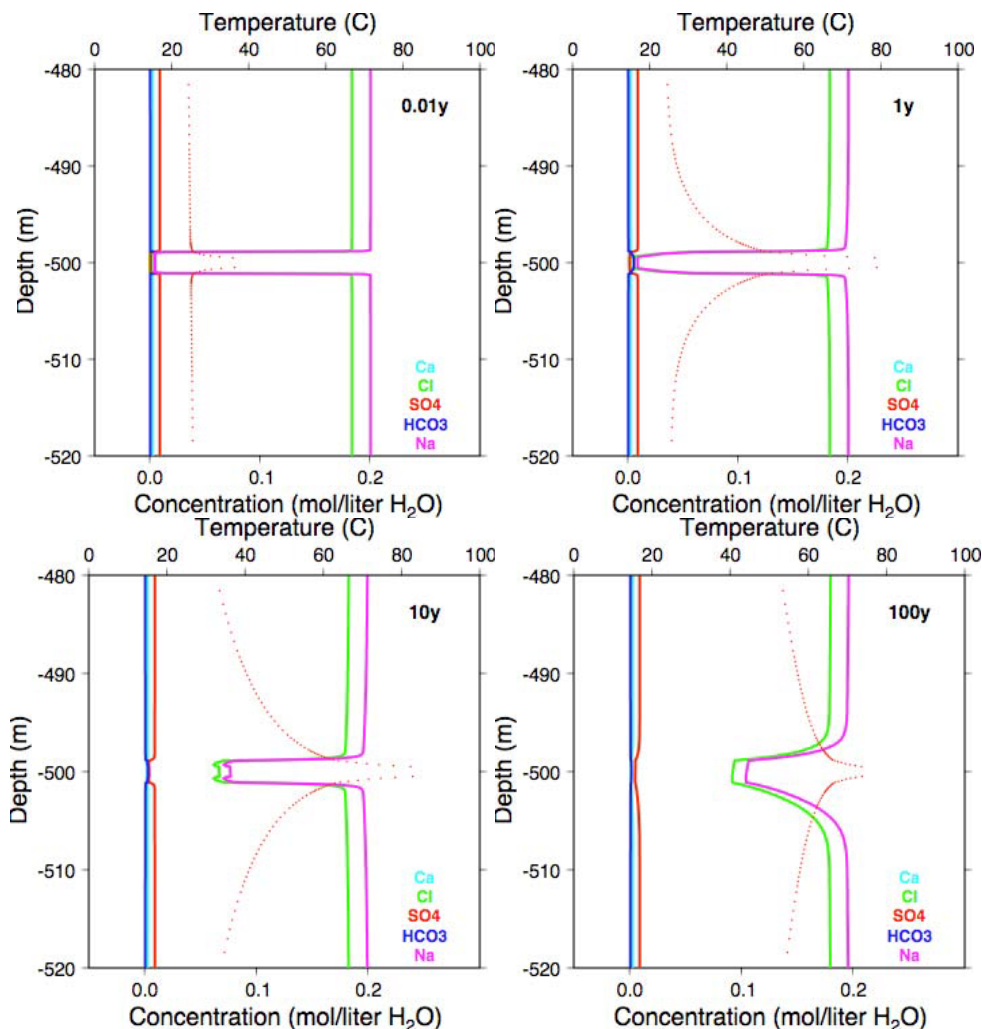
Figure 6. Vertical profile of selected aqueous species concentrations (total) and temperature through the drift center for the initially unsaturated case. Times shown are 0.01, 1, 10, and 100 years.

Changes in mineral abundances for the unsaturated case are shown in Figure 7 for 0.01, 1, 10, and 100 years. The mineralogical trends for the unsaturated case are similar to the saturated case; however, after 100 years the changes are smaller in the granite owing primarily to the greater influx of seawater into the bentonite, and to the lower saturation in the bentonite, thus reducing the effects of diffusion from the bentonite into the granite. In the bentonite, there is more calcite precipitation and less K-feldspar dissolution, a result of slightly higher temperature, lower liquid saturation, and seawater influx.
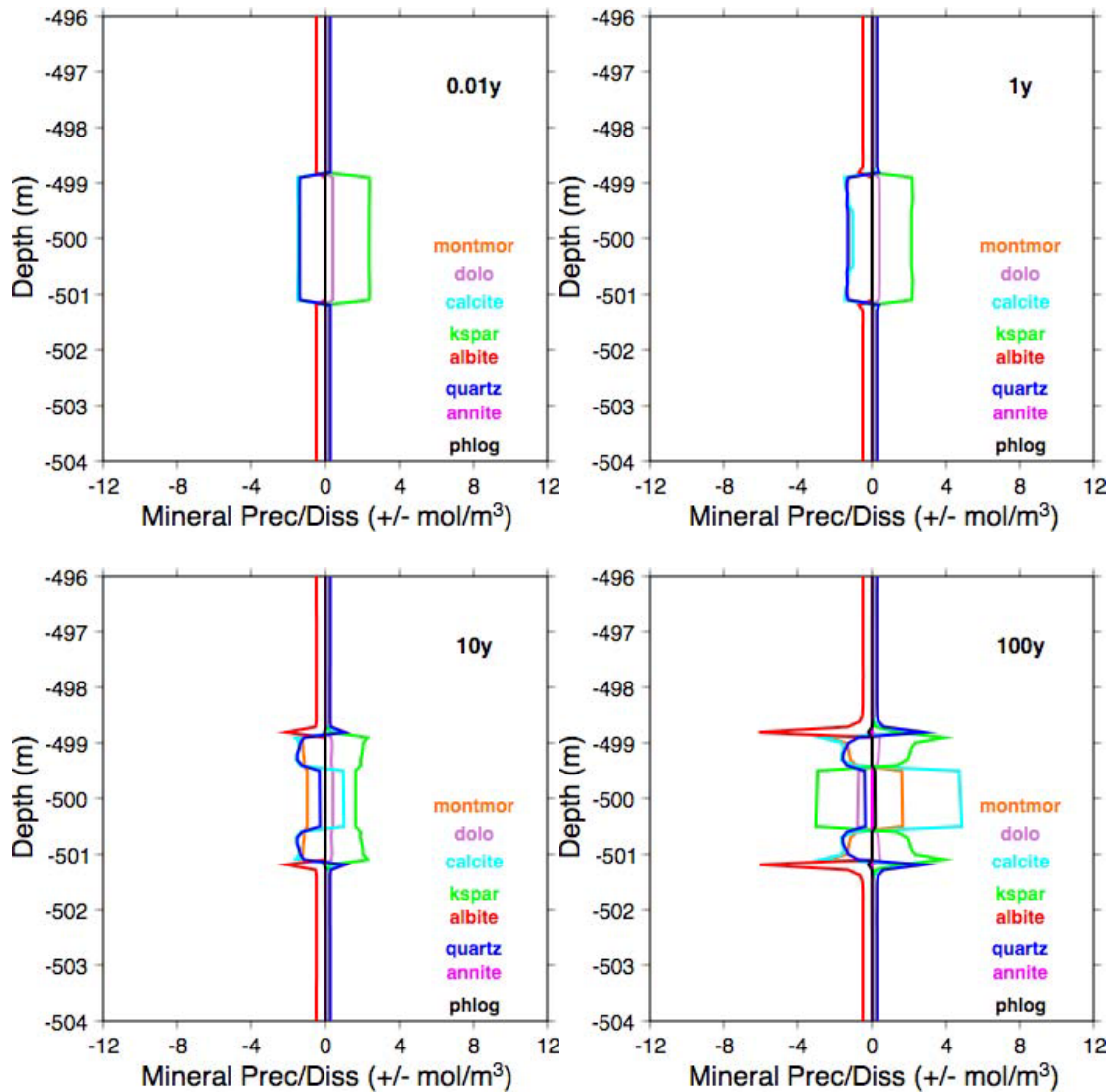
Figure 7. Vertical profile of changes in mineral phases (mol/m³ rock) through the drift center for the initially unsaturated case. Times shown are 0.01, 1, 10, and 100 years.

IV. CONCLUSIONS AND SUGGESTIONS FOR THC1 PHASES 2 & 3

As a result of contrasting mineralogy and water chemistry, and the rapid heating owing to the decay of radionuclides, significant mineralogical changes (dissolution and precipitation) take place over very narrow zones at the contact of the granite and the bentonite buffer and within the bentonite. The pattern and magnitude of the changes is a result of diffusion, slow rewetting processes, and the thermodynamic stability of the phases. In this first phase of THC1 simulations, all mineral-water reactions were assumed to take place at local equilibrium and the assemblage of potential secondary phases was very limited. Many assumptions were made in order to facilitate comparison between the groups; therefore, it should be emphasized the results are not be expected to realistically depict the evolution of the geochemical system.

In the following phases of Task D, more realistic geochemical reactions are to be treated, including ion exchange, kinetic rates of mineral reactions, and reactive surface areas for minerals in fractures and in the bentonite as a function of liquid saturation. Effects of mineral precipitation/dissolution on permeability and flow are an important aspect of DECOVALEX-THMC and will be treated in Phase 2. These are just among a few of the important phenomena/processes not treated in the Phase 1 simulations. Other simplifications include the use of a single molecular diffusion coefficient for all aqueous species, the lack of thermal diffusion of aqueous species, ignoring gas species transport (other than water vapor), and coupled mechanical and mechanochemical processes. Such complex phenomena will be up to the individual groups to consider in Phase 3 for which a more realistic treatment is expected.

V. REFERENCES

Barr D., Birkholzer J., Rutqvist J., and Sonnenthal E., 2005. *Draft Description for DECOVALEX-THMC TaskD: Long-Term Permeability/Porosity Changes in EDZ and Near Field, due to THM and THC Processes in Volcanic and Crystalline-Bentonite Systems.* REV01, August 2005 (see also in Appendix A).

Laaksoharju, M. 2003, *Update of the hydrogeochemical model 2002. GeoMod GW Report*, Aspö Hard Rock Laboratory, October 2003.

Ochs M., Lothenbach B., Shibata M. and Yui M. 2004, *Thermodynamic modeling and sensitivity analysis of porewater chemistry in compacted bentonite*, Physics and Chemistry of the Earth, Parts A/B/C, Volume 29, Issue 1, pp. 129-136.

Pruess, K., Oldenburg C. and Moridis G., 1999. *TOUGH2 User's Guide, Version 2.0*, Lawrence Berkeley National Laboratory Report LBNL-43134, Berkeley, CA.

Rhen I., Backborn G., Gustafson G., Stanfors R., and Wikberg P. 1997, *Results from pre-investigations and detailed site characterization. Summary report*. SKB Technical Report 97-03. ASPÖ HRL – Geoscientific evaluation 1997/2. Swedish Nuclear Fuel and Waste Management Company, Stockholm, Sweden.

Sonnenthal E., Ito A., Spycher N., Yui M., Apps J., Sugita Y., Conrad M., and Kawakami S., 2005. *Approaches to modeling coupled thermal, hydrological, and chemical processes in the Drift Scale Heater Test at Yucca Mountain*. International Journal of Rock Mechanics and Mining Sciences, 42:698-719.

Xu, T., Sonnenthal, E.L., Spycher, N., Pruess, K., 2004. *TOUGHREACT user's guide: A simulation program for non-isothermal multiphase reactive geochemical transport in variable saturated geologic media.* Lawrence Berkeley National Laboratory Report LBNL-55460, Berkeley, California, USA, 192 pp.

VI. APPENDIX: THERMODYNAMIC DATA FOR MINERALS

```
Temperature points:' 8   0.01  25.00  60.00  100.00  150.00  200.00  250.00  300.00
'quartz'              60.084   22.688   1  1.0000 'sio2(aq)'
'quartz'              -4.1605  -3.7501  -3.3553  -3.0132  -2.6679  -2.3823  -2.1490  -1.9822
'albite_low'          262.223  100.070   3  1.0000 'na+' 3.0000 'sio2(aq)' 1.0000 'alo2-'
'albite_low'          -21.0877 -19.3543 -17.6402 -16.1706 -14.7591 -13.6930 -12.9497 -12.6229
'k-feldspar'          278.332  108.870   3  1.0000 'k+' 3.0000 'sio2(aq)' 1.0000 'alo2-'
'k-feldspar'          -24.5774 -22.3941 -20.1690 -18.2496 -16.4229 -15.0570 -14.0934 -13.5997
'annite'       511.880 154.320   6  1.0000 'k+' 3.0000 'sio2(aq)' 4.0000 'h2o' 1.0000 'alo2-' -6.0000 'h+' 3.0000 'fe++'
'annite'               8.9412   7.3505   5.2377   3.2179   1.1722  -0.5646  -2.2287  -4.1080
'phlogopite' 417.260 149.660  6  -6.0000 'h+' 1.0000 'k+' 3.0000 'mg+2' 3.0000 'sio2(aq)' 4.0000 'h2o' 1.0000 'alo2-'
'phlogopite'          17.7331  15.3212  12.3023   9.5062   6.7570   4.5162   2.4815   0.3259
'montmor-na'         -37.5566 -34.6220 -31.7340 -29.3371 -27.1461 -25.5882 -24.5848 -24.2470
'montmor-na'           0.52488434E+03  -0.33950614E+04  -0.46020519E+00   0.19561066E+06  -0.13245975E+08
'calcite'            100.087   36.934   3  -1.0000 'h+' 1.0000 'ca+2' 1.0000 'hco3-'
'calcite'              2.2257   1.8487   1.3330   0.7743   0.0999  -0.5838  -1.3262  -2.2154
'dolomite'           184.401   64.365   4  -2.0000 'h+' 1.0000 'ca+2' 1.0000 'mg+2' 2.0000 'hco3-'
'dolomite'             3.4063   2.5135   1.3314   0.0944  -1.3493  -2.7744  -4.2968  -6.1006
```

Appendix H

Status Report for D_THC

JNC Team (Japan)

Progress on: DECOVALEX-THMC Task-D THC

JNC TEAM (Japan)

Japan Atomic Energy Research and Development Agency (JAEA) Team
Yoshihiro Oda, Kiyoshi Fujisaki, Tomoo Fujita (JAEA), Masakazu Chijimatsu (HZM)
e-mail address: Oda.yoshihiro@jaea.go.jp

1. INTRODUCTION

Interactions among thermal, hydrological, and mechanical processes are thoroughly studied in the DECOVALEX project. Chemical processes however, can also lead to changes in thermal, hydrological and mechanical properties, and can affect the integrity of the near field.

Some experimental studies are under way by the Japan Nuclear Cycle Development Institute (JNC) to build a database for the interaction between chemical processes and other processes, such as permeability and swelling properties of buffer materials saturated by saline water, and of buffer material reacting to cement. In the near future, we will incorporate this database into our research.

JNC has already developed the coupled thermal, hydraulic, and mechanical (T-H-M) model, and has initiated research on coupled T-H-M-C processes to predict the chemical evolution of buffer material and pore-water chemistry, as well as the chemical effects on other (thermal, hydraulic, and mechanical) processes. In this research, a numerical experimental system for coupled T-H-M-C processes is developed to predict the long-term evolution of the near field (the engineered barriers and surrounding host rock) for various near field repository designs and geological environments.

It is very difficult (in a short time) to construct a code for coupled processes by using individual process codes, because detailed modification for coupling is needed in each code. We have developed the coupling system COUPLYS (Neyama et al. 2002) that has shown to be very effective in improving the efficiency and quality for individual process-code linkage. Using COUPLYS, the prototype code for coupled T-H-M-C processes has been developed. The coupled T-H-M-C processes in the prototype code are analyzed by the coupled T-H-M code THAMES (Chijimatsu et al. 1999), mass transport code Dtransu-3D-EL (Nishigaki et al. 2001) and geochemical code PHREEQC (Parkhurst et al. 1999). This paper presents the prototype code development and typical results of exercises performed by the prototype code.

2. DEVELOPMENT OF THE COUPLED T-H-M-C MODEL

To develop the coupled T-H-M-C model, we sorted out the interactions for each process and built the conceptual model for the coupled T-H-M-C processes (Figure 1). Although many kinds of chemical processes are assumed in the near-field of a high-level waste (HLW) repository, our current focal point is to take into account the interaction between minerals and pore water in the compacted bentonite.
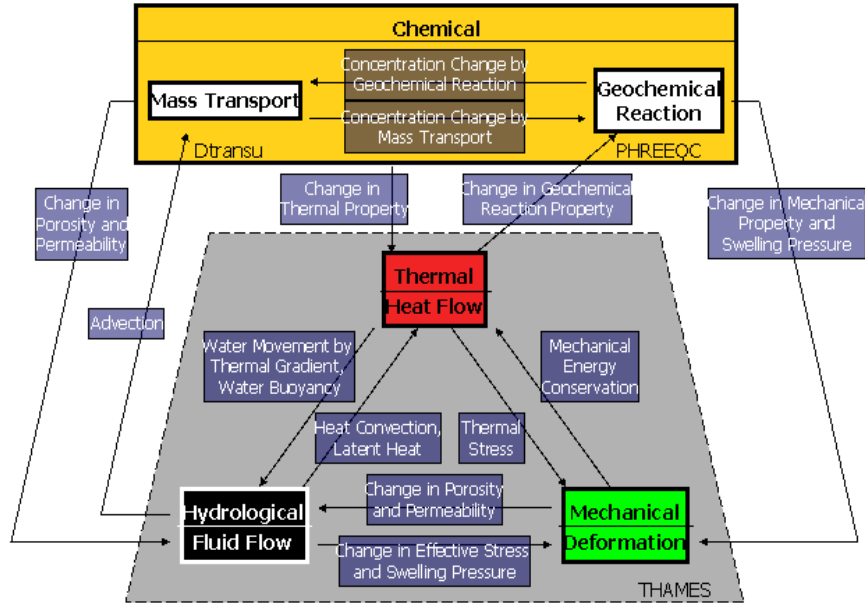
Figure 1. Conceptual model for coupled T-H-M-C processes

From the conceptual model, we have developed the coupled T-H-M-C model, based on a coupled T-H-M model (inside the broken line in Figure 1; Ohnishi et al., 1985; Chijimatsu et al., 2000) and reactive-mass transport model (inside the box named "Chemical" in Figure 1). This is a system of governing equations composed of Equations (1)–(9) (below), which couple heat flow, fluid flow, deformation, mass transport, and geochemical reactions in terms of following primary variables: temperature T, pressure head Ψ, displacement u_i, total dissolved concentration of the nth master species $C_{\langle n \rangle}$, and total dissolved and precipitated concentration of the nth master species $T_{\langle n \rangle}$. Here we set master species as the linear independent basis for geochemical reactions. Speciation in solution and dissolution/precipitation of minerals is calculated by a series of governing equations for geochemical reactions. Then we adopt an equilibrium model for geochemical reactions (Parkhurst et al. 1999), mainly because of the reliability and abundance of thermodynamic data for geochemical reactions.

$$\frac{\partial}{\partial x_i}\left(\rho_l C_l q_l T\right) - \frac{\partial}{\partial x_i}\left(\lambda_m \frac{\partial T}{\partial x_i}\right) + \frac{\partial}{\partial t}\left(\rho_m C_m T\right) = 0, \tag{1}$$

$$-\frac{\partial}{\partial x_i}\left[\xi \rho_l D_\theta \frac{\partial \theta}{\partial x_i} + (1-\xi)\frac{\rho_l^2 gK}{\mu_l}\frac{\partial(\psi+z)}{\partial x_i} + \rho_l D_T \frac{\partial T}{\partial x_i}\right] + \frac{\partial}{\partial t}\left(\rho_l nS\right) = 0, \tag{2}$$

$$\frac{\partial}{\partial x_j}\left[\frac{1}{2}C_{ijkl}\left(\frac{\partial u_k}{\partial x_l}+\frac{\partial u_l}{\partial x_k}\right) - \pi'\delta_{ij} - \frac{E}{1-2\nu}\delta_{ij}\alpha_s\left(T-T_0\right) + \chi\delta_{ij}\rho_l g\psi\right] + \rho_m b_i = 0, \tag{3}$$

$$\frac{\partial}{\partial x_i}\left(\rho_l q_l C_{\langle n \rangle}\right) - \frac{\partial}{\partial x_i}\left(\rho_l n S D_{ij} \frac{\partial C_{\langle n \rangle}}{\partial x_j}\right) + \frac{\partial}{\partial t}\left(\rho_l n S T_{\langle n \rangle}\right) = 0 \, , \tag{4}$$

$$\sum_{a=1}^{A}\left(z_a m_a\right) = 0 \, , \tag{5}$$

$$\sum_{a=1}^{A}\left(v_a m_a\right) = OPV + \sum_{p=1}^{P}\left(u_p MIN_p\right), \tag{6}$$

$$C_{\langle n \rangle} = \sum_{a=1}^{A}\left(c_{a,n} m_a\right) = T_{\langle n \rangle} + \sum_{p=1}^{P}\left(b_{p,n} MIN_p\right) \tag{7}$$

$$\sum_{n=1}^{N}\left[b_{p,n} \log\left(a_n\right)\right] = \log\left(K_p\right), \tag{8}$$

$$\log\left(a_a\right) = \log\left(K_a\right) + \sum_{n=1}^{N}\left[c_{a,n} \log\left(a_n\right)\right] \tag{9}$$

Table 1 shows the nomenclature in Equations (1)-(9). Equation (1), (2) and (3) are the governing equations of energy conservation for thermal process, of mass conservation of fluid for hydrological processes, and of momentum conservation for mechanical processes, respectively.

Table 1 Nomenclatures in equations

A	total number of aqueous species
a_a, a_n	thermodynamic activity of the a-th aqueous, and n-th master species
b_i	body force
$b_{p,n}$, $c_{a,n}$	stoichiometric coefficient of the n-th master species in the p-th mineral, and a-th aqueous species
C_{ijkl}	elastic matrix
C_l, C_m	specific heat of liquid, and medium
$C_{\langle n \rangle}$	total dissolved concentration of the n-th master species
D_{ij}	dispersion tensor
D_T, D_θ	thermal, and isothermal water diffusivity
E	young's modulus
g	acceleration of gravity
K	intrinsic permeability
K_a, K_p	thermodynamic equilibrium constant for mass action equation for the a-th aqueous, and p-th mineral species
m_a	molality of the a-th aqueous species
MIN_p	moles of the a-th p-th mineral transferred into aqueous phase

N	total number of master species
n	porosity
OPV	sum of operational valence of the speciation in the initial solution
P	total number of mineral
q_i	flux of liquid phase
S	degree of saturation
T, T_0	temperature, initial temperature
$T_{\langle n \rangle}$	total dissolved and precipitated concentration of the n-th master species
u_i	displacement
u_p, v_a	sum of operational valence of the constituents in the p-th mineral, and a-th aqueous species
z	elevation head
z_a	charge of the a-th aqueous species
α_s	linear thermal expansion coefficient of solid
δ_{ij}	Kronecker's delta
θ	volumetric water content
λ_m	thermal conductivity of medium
μ_l	viscosity of liquid
v	Poisson's ratio
ξ	unsaturated parameter (0: saturated, 1: unsaturated zone)
π'	swelling pressure contributing to swelling stress
ρ_l, ρ_m	density of liquid, and medium
χ	effective stress parameter
ψ	pressure head

Equations (4–9) are governing equations for chemical processes, as follows: Equation (4) is for mass transport, and the governing equation of mass conservation of each master species through mass transport. One series of equations (5–9) is for geochemical reactions, and the governing equations for electrical neutrality conservation of electrons, mass conservation of each master species through geochemical reaction, mass action for each mineral; and mass action for each aqueous species, respectively.

To predict precisely the near-field behavior for long-term performance analysis by inclusion of the near-field chemical evolution, we first integrate chemical processes into the interactive model for thermal, hydrological, and mechanical processes. After this step, we can introduce the interactive model for chemical process to other processes, and then we can realize a fully coupled T-H-M-C model.

3. DEVELOPMENT OF THE COUPLED T-H-M-C CODE

The coupling technique was selected after consideration of existing analysis codes, taking into account efficiency and quality in developing the coupling code. (We call it prototype code.) We also develop the coupling technique such that it is not dependent on the programming language of the existing analysis codes.

Coupling codes can be developed efficiently using this concept. An end-user defines the block of data definition based on coupling data information. This data definition includes variable name, type, dimension, and size for each variable by text format. This technique uses Data Definition Language (DDL) to describe the coupling data for each analysis code. A module of shared memory management prepares the reference table to access coupling data, and this module ensures memory area based on data definition by DDL. A reference table controls the correlation between variable name and address in the shared memory. An interface program functions to access coupling data between shared memory and each analysis code by using the commands "get" and "set," described in the source program of each analysis code. Then, this interface program transfers coupling data to each analysis code through shared memory.

This process management program controls the start-up/termination and pause/restart of each process, based on the input data of process management in text format, in which the executive order of the processes and termination conditions are described. This program has adopted "semaphore" to control the process of each analysis code. Semaphore is implemented on the UNIX machine as a standard; it is a general-purpose function that aims to synchronize various processes. COUPLYS adopted the semaphore set, which can use values from 0 to 32767, and is thus able take many processes into consideration.

Existing codes of THAMES, specifically Dtransu-3D-EL and PHREEQC, are used in the prototype code based on the concept. The prototype coupling system has the functions of start-up/termination and pause/re-start for each code, and commands of "get" and "set" for coupling data, as described in the source program of each analysis code.

The data files define variable name, type, dimension and size for coupling data by text file. The control file defines the procedure of coupled T-H-M-C analysis by each analysis code and coupling module. The coupling module contains the treatment necessary for coupling analysis.

4. PRELIMINARY ANALYSIS

We did some preliminary analysis based on the H12 Report repository design used by this T-H-M-C prototype code. This repository design was analyzed using the T-H-M capability by THAMES. For the chemical condition, PHREEQE was used on saturated bentonite, rocks, and some ground water.

4.1 Calculation Model and Conditions

This repository design consists of soft/hard rock, backfill, bentonite, overpack, vitrified waste and optional support concrete. The buffer material is a mix of 70% kunigel V1 and 30% silica sand, with a dry density 1,600 kg/m^3, which is the same as the bentonite used in the H12 Report of JNC. Other materials (backfill, soft, and hard rock) are also the same as in H12 Report.

Table 2   Parameters of materials

	Rock	Support	Backfill	Bentonite	Overpack	Vitrified Waste
Density [kg/m^3]	2.2×10^3	2.3×10^3	1.8×10^3 *	1.6×10^3 *	7.8×10^3	2.8×10^3
Young's modulus [MPa]	3.5×10^3	2.5×10^4	3.0	46.0	2.0×10^5	8.2×10^4
Poisson's ratio [-]	0.3	0.167	0.4	0.3	0.3	0.3
Initial porosity [-]	0.3	0.15	0.41	0.41	0.41	0.41
Hydraulic conductivity [m/s]	1.0×10^{-15}	1.0×10^{-21}	6.0×10^{-19}	4.0×10^{-20}	1.0×10^{-30}	1.0×10^{-30}
Thermal conductivity [W/m/K]	2.2	1.88	(1)	(1)	53.0	1.2
Specific heat [kJ/kg/K]	1.4	0.75	(2)	(2)	0.46	0.96
Thermal expansion [1/K]	1.0×10^{-6}	1.0×10^{-6}	1.0×10^{-6}	1.0×10^{-6}	1.64×10^{-6}	1.0×10^{-6}
horizontal dispersion	0.5	0.02	0.02	0.02	0.0	0.0
vertical dispersion	0.005	0.002	0.002	0.002	0.0	0.0
diffusivity of liquid	5.0×10^{-10}	5.0×10^{-10}	5.0×10^{-10}	5.0×10^{-10}	1.0×10^{-20}	1.0×10^{-20}
diffusivity of CO_2 gas	1.0×10^{-20}	1.8×10^{-5}	1.8×10^{-5}	1.8×10^{-5}	1.0×10^{-20}	1.0×10^{-20}
diffusivity of O_2 gas	1.0×10^{-20}	1.35×10^{-5}	1.35×10^{-5}	1.35×10^{-5}	1.0×10^{-20}	1.0×10^{-20}
retarded coefficient	1.0	1.0	1.0	1.0	1.0	1.0
attenuation constant	0.0	0.0	0.0	0.0	0.0	0.0

*: dry density

(1): $(34.1+4.18\omega)/(100+\omega)$

(2): $4.44\times10^{-1}+1.38\times10^{-2}\omega+6.14\times10^{-3}\omega^2-1.69\times10^{-4}\omega^3$

For the water retention of buffer material, the van Genuchten equation is employed, and the parameters used are $\alpha=8.0\times10^{-3}$ [1/m], $n=1.6$ [-], $\theta_s=0.403$ [-], $\theta_r=0.0$ [-]. The equation for thermal water diffusivity in buffer material is $D_T=D_{T0}\exp[\alpha(T-T_0)/T_0]$. Here, $D_{T0}=2.0\times10^{-11}$ [m^2/s/K], $\alpha_T=-0.2$ [-], and $T_0=10$ [°C].

Pore-water composition in buffer, fresh type (Fresh-Reducing-High-pH, FRHP) groundwater and saline type groundwater (Saline-Reducing-High-pH) are described in Table 3, and mineral compositions are given in Table 4. Buffer and backfill material are 21% O_2 gas and 0.0032% CO_2 gas.

Table 3. Composition of water

	pore	FRHP	SRHP
pH [-]	6.572	8.5	8.0
Eh [mV]	(pe=-2.173)	-281	-303
Na [mol/l]	4.1×10^{-1}	3.6×10^{-3}	6.2×10^{-1}
Ca [mol/l]	8.1×10^{-2}	1.1×10^{-4}	3.3×10^{-4}
K [mol/l]	3.1×10^{-3}	6.2×10^{-5}	1.1×10^{-2}
Mg [mol/l]	1.0×10^{-3}	5.0×10^{-5}	2.5×10^{-4}
Fe [mol/l]	4.7×10^{-3}	9.7×10^{-10}	3.9×10^{-8}
Al [mol/l]	6.2×10^{-1}	3.4×10^{-7}	3.2×10^{-9}
C [mol/l]	1.0×10^{-10}	3.5×10^{-3}	3.5×10^{-2}
S [mol/l]	2.0×10^{-3}	1.1×10^{-4}	3.0×10^{-2}
B [mol/l]	2.8×10^{-1}	2.9×10^{-4}	1.7×10^{-3}
P [mol/l]	1.0×10^{-10}	2.9×10^{-6}	2.6×10^{-7}
F [mol/l]	1.0×10^{-10}	5.4×10^{-5}	1.0×10^{-4}
N [mol/l]	1.0×10^{-10}	2.3×10^{-5}	5.2×10^{-3}
Cl [mol/l]	7.8×10^{-3}	1.5×10^{-5}	5.9×10^{-1}
Si [mol/l]	3.2×10^{-4}	3.4×10^{-4}	3.0×10^{-4}

Table 4. Mineral compositions [wt%]

	buffer & Backfill	FRHP Rock	SRHP Rock	support
smectite	32.9*			
chalcedony	26.6	14.29	16.67	
calcite	1.82	14.29	16.67	
pyrite	0.49	14.29		
albite		14.29	16.67	
kaolinite		14.29		
plagioclase	3.85*			
analcime	2.38*			
dolomite	1.96*		16.67	
muscovite			16.67	
microcline		14.29	16.67	
Magnetite		14.29		
Ca(OH)₂				49.0
SiO₂				51.0
Silica Sand	30.0*			

*: not included in geochemical calculation

Table 4b. Ion exchange, surface complexation ref. H12 report of JNC

cation exchange reactions on the fixed negative charge	cation exchange capacity [meq/100g]		60.1
	initial cation occupancies [meq/100g]	ZNa	51.4
		Z₂Ca	7.4
		ZK	0.6
		Z₂MG	0.7
	Gaines & Thomas selectivity coefficients (log $K_{G\&T}$)	2ZNa-Z₂Ca	0.69
		ZNa-ZK	0.42
		2ZNa-Z₂Mg	0.67
		ZNa-ZH	1.88
surface complexation reactions at the edge sites	protonation constant	log K(+) = 5.67	
	deprotonation constant	log K(-) = -7.92	
	site concentration for smectite [mol/g]	6.5×10^{-5}	
	specific surface area for smectite [m²/g]	29	

The mesh for initial and boundary conditions were shown in Figure 2. The mesh has 11,926 nodes and 9,993 elements. Figure 4 shows the time history of heat production for a waste package used in this analysis. It is assumed that the waste package has been stored for 50 years after reprocessing and before emplacement. The quantity of the heat product is defined as the quantity of heat generated per volume (per vitrified waste package). Here, we calculated three cases.

(1) Hard rock (HR) with FRHP. This is for reference and is the same as in the H12 Report.

(2) Soft rock (SR) with SRHP.

(3) SR + SRHP + Support. This is to distinguish the effect of support for the Horonobe *in situ* experiment.
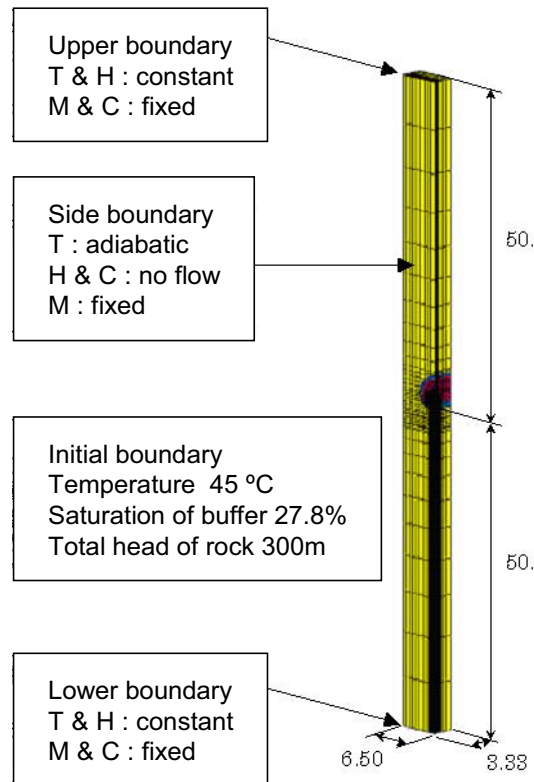
Figure 1. Total mesh
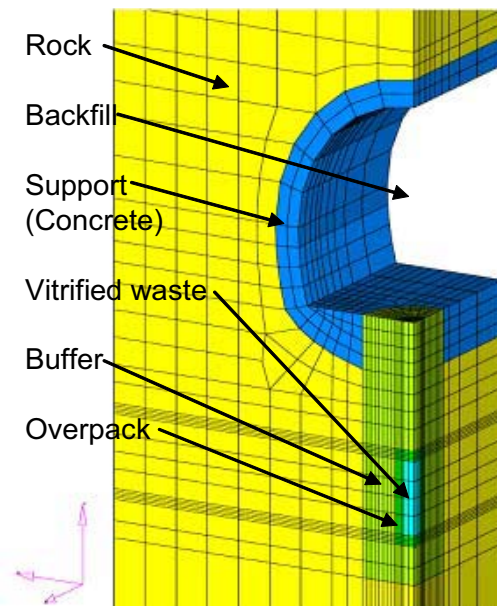
Figure 2. Mesh of H12 Report repository design for THMC Calculation
(overview and details around the vitrified waste)
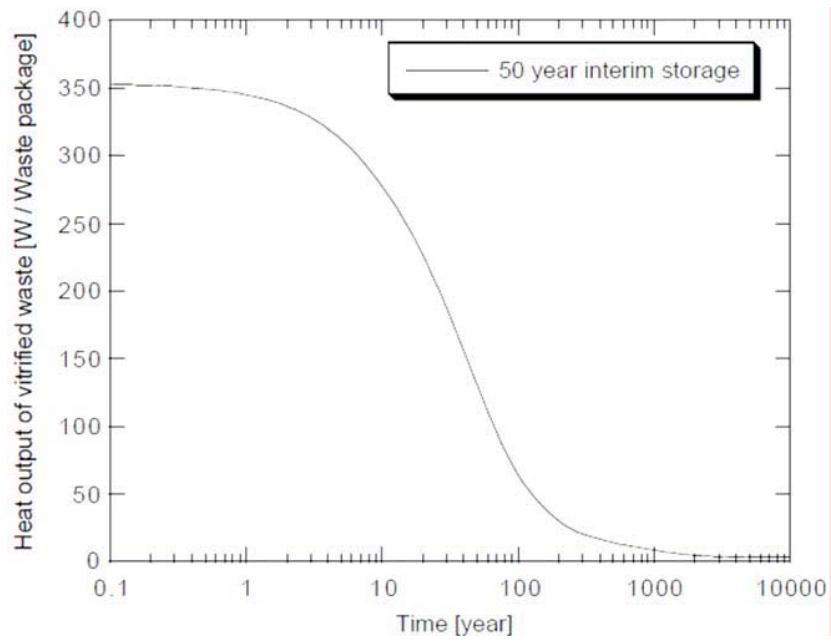
Figure 3. Vitrified waste heat outputs after the interim storage as a function of time

4.2 Results

Figures 4–6 show the contour plots of temperature, saturation, and pH distribution after 10 years. Figure 4 shows the temperature distribution around the vitrified waste. Each case shows almost the same distribution. It means that differences in groundwater, rock, or the existence of the support don't affect on the temperature distribution. Figure 5 shows the saturation. SRHP is the fastest of all, because the permeability of buffer material increases with the concentration of salt. On the other hand, SRHP + SR + support case is the slowest, because of the low hydraulic property of the support. Figure 6 is pH distribution. Around the support, a high pH region appears resulting from the reaction between the groundwater and the support. But the inner region surrounded by the support is still at low pH, because the groundwater did not reach there. The low pH region of FRHP + HR is slightly wider than the others, because sodium chloride diffused from the buffer material made the pH lower.
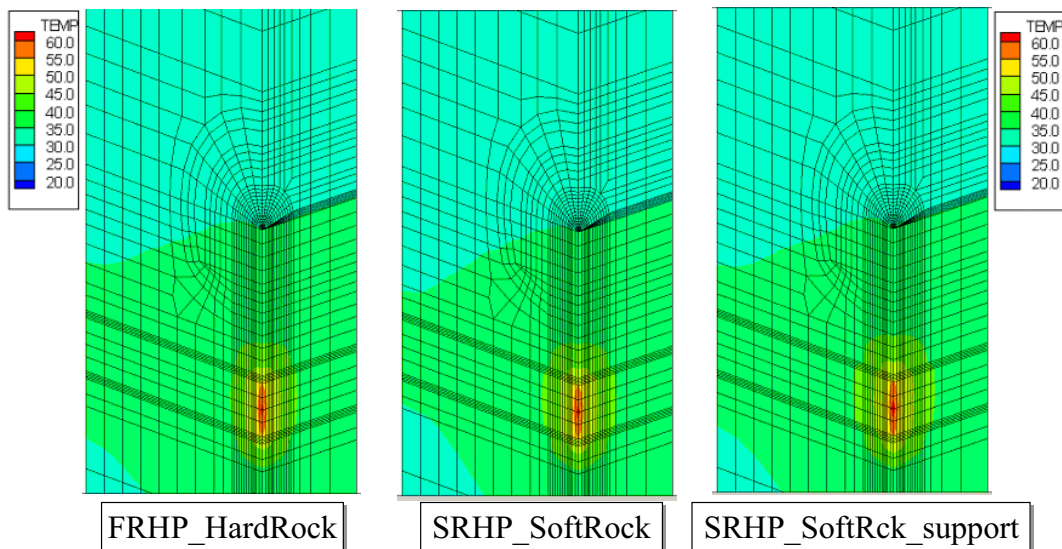
Figure 4. Temperature distributions after 10 years
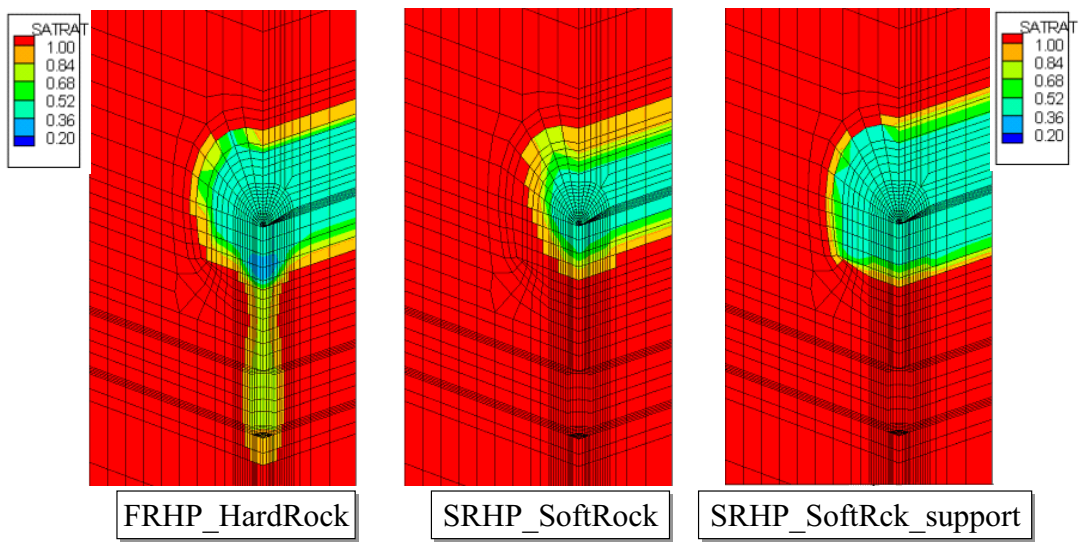
Figure 5. Saturation distributions after 10 years
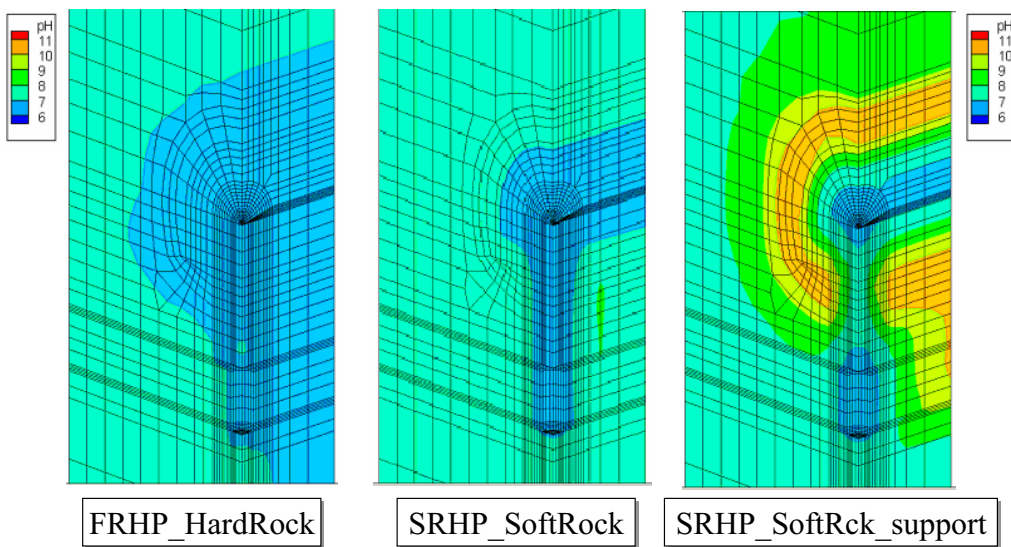
Figure 6. pH distributions after 10 years

5. COUPLE EXPERIMENT

COUPLE, which is the in-room equipment of ENTRY JNC Tokai, simulates coupled THMC processes in the near field of the engineered barrier system. It has an inner heater that simulates the overpack, outer heaters on the outer walls of the rock for boundary conditions, and outer jacks. The buffer material and rocks are installed optionally. (It is at 1/7 scale of our repository design.)

The objectives of the experiments are primarily to validate the coupled T-H by comparing observed and simulated values, and to measure pore-water pH in the buffer material. We finished the 1st experimental operation, and now are performing the 2nd experimental operation. In both operations, there is water over the mortal block with 0.1m depth. We capped and sealed the top of the bentonite to avoid water entering the bentonite directory.
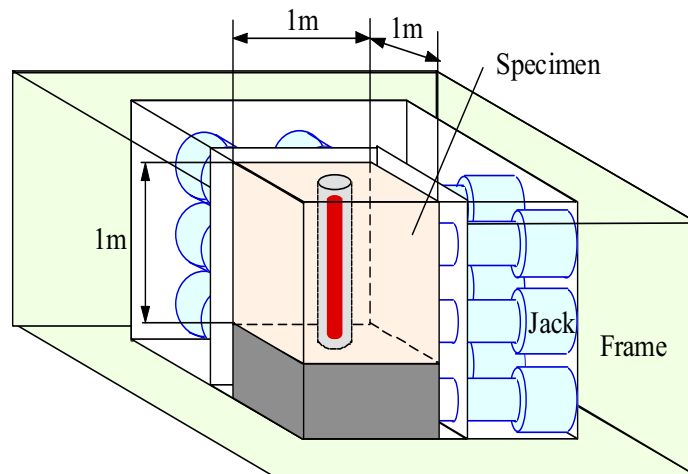
Figure 7. Overview of COUPLE equipment

Picture 1. Preparation from 2nd Operation

5.1 First operation

The first operation lasted 6 months (from June 3, 2003 to December 1, 2003). Outer heaters were kept stable at 70°C, as were inner heaters (90°C at their surface). In the first experiment, there was no outer stress to simplify the phenomena.

The simulated rock was made of the mortar, because we wanted to investigate the chemical effects especially from the outer mortar to the inner buffer material. The mortar block was of low cement content (1 m^3) to improve hydraulic permeability, and it was 1m^3. Buffer material was 70% Kunigel V1 with 30% silica sand. The dry density was 1,600 Mg/m^3. Buffer material and the inner heater were put into the center vertical hole of mortar.

5.1.1 THM Analysis by THAMES

The temperature and water content of the buffer material in the first experiment were estimated by THAMES. Initial conditions and some properties are shown in Tables 5 and 6. Other properties are the same as in Section 4. In the 1st operation, some THMC changes were expected to measure, but except for thermal measurements, sensors were broken month by month. Only some results could be compared with the THM simulation.
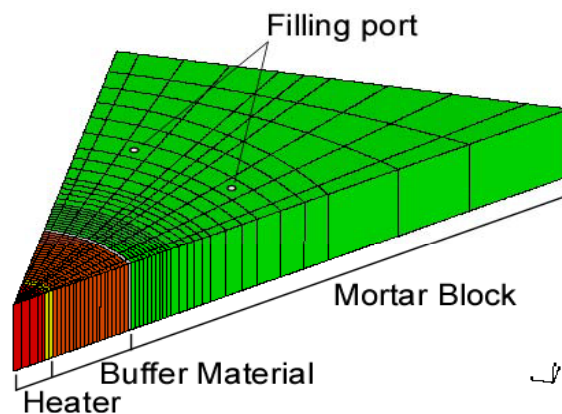
Figure 8. Mesh of COUPLE experiment for THMC Calculation

Table 5. Initial conditions

Buffer Material Temperature	20 °C
Degree of Saturation	50 %
Mortar Temperature	20 °C
Total Head	0.6 m (at the middle of COUPLE and add 10cm water head)
Inner Heater Boundary Condition Temperature	Fixed at 90 °C
Outer Boundary Condition Temperature	Fixed at 70 °C

Table 6. Properties

	Heater	Buffer	Mortar
Dry density [kg/m^3]	8,000	1,600	1,200
Intrinsic Permeability [m^2]	1.0×10^{-30}	4.0×10^{-20}	1.7×10^{-16}
Porosity [-]	0.0001	0.403	0.460
Thermal Conductivity [W/m/K]	16.0	1.0(Init.)~2.0(Sat.)	0.92
Specific Heat [kJ/kg/K]	0.50	0.7(Init.)~1.1(Sat.)	1.67
Water diffusivity [m^2/s]	-	Function of T&H	-
Thermal Water Diffusivity [m^2/s°C]	-	7.0×10^{-12}	-

5.1.2 Results

The temperature distribution generated by COUPLE showed good agreement with the THAMES simulation. However, the time history for swelling pressure indicated strange behavior. We think the stress sensor was moved when we installed the buffer. For saturation, we installed two types of sensors, but one was broken at high temperature and another was broken at high water content. For hydraulic behavior, the calculated saturation time of buffer material showed good agreement with observation, but it was necessary to calibrate thermal water diffusivity. For chemical reactions, only the pore-water pH of the buffer material could be measured as a THM coupled process.

From the results of pH distribution over time, the chemical influence was low for thermal and hydrological behavior. No secondary mineral was found in bentonite after x-ray diffraction, as well as scanning electron microscope (SEM), and Energy Dispersion X-ray Spectrometry (EDS). The cation distributions in the buffer that were measured after operation were very interesting: monovalente cations are at a high concentration at outer heaters and low at inner, but divalent cations showed in inverse distribution. We tried to simulate the chemical changes of buffer material using PHREEQC, but we have not yet been able to explain what occurred. Now we are trying to apply the THMC code to the 1st operation.
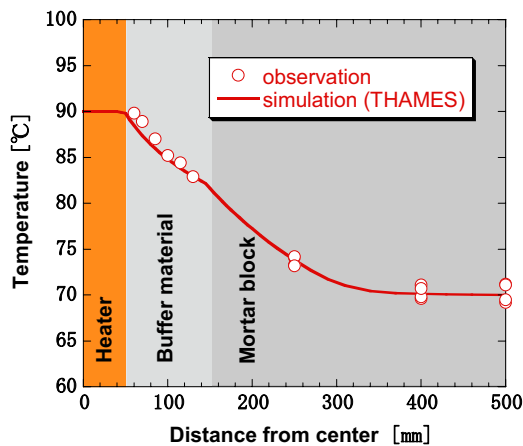
Figure 9. Temperature distribution   Figure 10. Swelling pressure
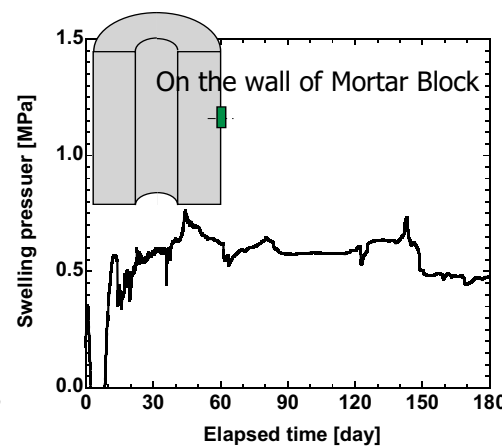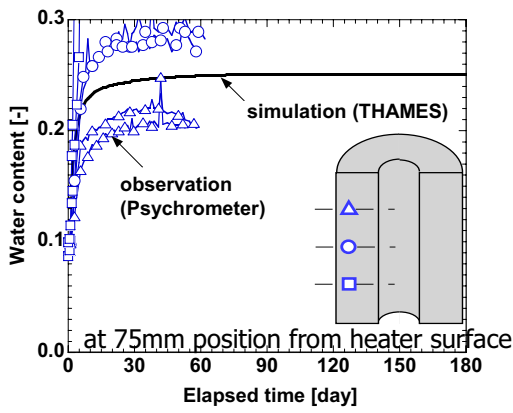
Figure 11. Water content
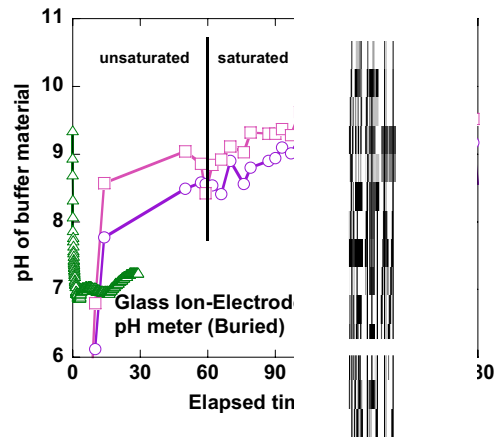
Figure 12. pH in buffer
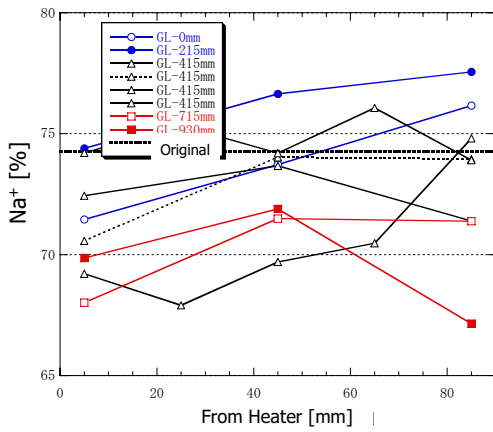
(a) Sodium distribution
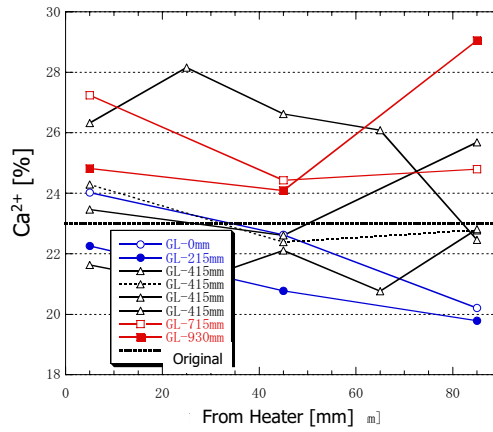
(b) Calcium distribution
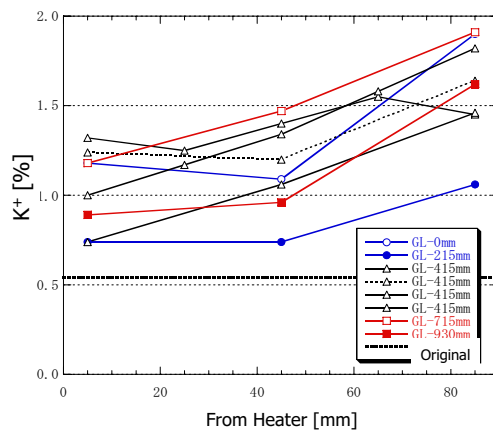
(c) Potassium distribution
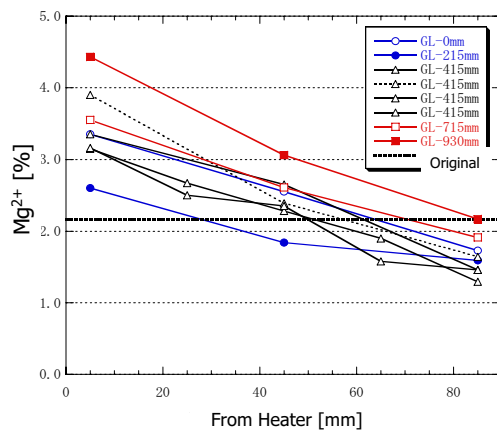
(d) Magnesium distribution

Figure 13. Cation distributions in the buffer after the 1st operation

5.2 Second operation

For the second operation, a mortar block is chosen for simulated rock again, but its water/cement ratio is larger than that of the previous operation, because the chemical influence on other phenomena is the most important issue in this operation. In this operation, we plan to have a longer experimental time and to keep a high pH in the water with N_2 gas bubbling to keep out the atmosphere (especially CO_2). Table 7 shows the differences in each operation.

(1) Choose a high ratio for cement to mortar block; it makes rich Na, K, and Ca ions in the mortar reaction water.

(2) To avoid calcite precipitate by CO_2, carry out N_2 gas bubbling of mortar-block reaction water to eradicate the influence of atmospheric air.

The high ratio cement to mortal block may make the permeability of mortar very small, so that our buffer material is then not saturated 3 months after the start of operation. The N_2 gas bubbling keeps a high pH and a high concentration of ions (Table 8).

Table 7. Basic conditions for each operation

	1st operation	2nd operation
Date from / to	Jun.3rd, 2003 / Dec. 1st, 2003	Apr. 1st, 2005 /
Temperature [°C] Inner / Outer Heater Surface	90/70	90/70
Displacement	constrain	constrain
Mortal (Water/Cement)	251/193 Ordinary Portland Cement	55/100 Ordinary Portland Cement
Bentonite	Kunigel-V1:Si-sand(70:30) 1,600 kg/m^3	Kunigel-V1:Si-sand(70:30) 1,600 kg/m^3
Initial Water	ground water	ground water
Atmosphere	the atmosphere	N2-bubbleing
Packing	Si-Sand	Kunigel-V1

Table 8. Chemical changes in covering water of COUPLE (2nd operation) [mg/L] (Covering water is kept 10cm depth with adding pure water.)

date	Na	Ca	Si	Al	Mg	K	SO$_4^{2-}$	HCO$_3^-$	pH
05/04/12	196	24.9	25.6	8.17	<0.01	345	54.5	0.4	11.9
05/05/11	251	7.92	60.0	11.1	<0.01	409	111	0.6	12.0
05/06/13	268	5.94	74.8	10.8	<0.01	418	112	0.8	11.9
05/07/12	281	5.26	84.2	10.2	<0.01	414	110	0.9	11.8
05/08/09	291	4.85	92.4	10.1	<0.01	423	112	0.9	11.9

6. SUMMARY AND DISCUSSION

A prototype T-H-M-C calculation code was developed, based on THAMES, Dtransu-3D-EL, and PHREEQC, and was applied to the H12 Report repository design. The saturation time is faster than that in the H12 Report, because the relation between permeability and the concentration of soluble salts is included in the prototype code. The chemical changes, as with pH distribution, are changed because this prototype code treats the unsaturated phase. But the difference between most T-H-M-C calculations and those of THAMES are not very large. We think it comes from the coupled model for geochemistry with others, which means the feedback from chemical changes to others are limited. The T-H-M-C prototype code needs a number of models to calculate a more realistic simulation. At present, we are trying to calculate a multitude of cases using our prototype code to understand coupled phenomena through simulation. On the other hand, we are also trying to apply the kinetic reaction for the oxidation of pyrite and the dissolution of smectite. We think they are important in evaluating the corrosion of overpack material and the maintenance of buffer-material function.

The in-room T-H-M-C coupled experiment started its 2nd experimental operation on April 1st 2005. This operation employs high cement concentration mortal and N_2 bubbling to keep a high pH in the water. They are expected to make clearer chemical changes than occurred in the 1st operation. Also during the 1st operation, some sensors were broken; we think research and development for sensors is important to T-H-M-C study. Finally, there was no evidence of secondary minerals in the buffer after the 1st operation. New analysis methods to understand the chemical changes after such operations are needed.

7. REFERENCES

Chijimatsu, M., Fujita, T., Kobayashi A. & Nakano, M. 2000. Experiment and Validation of Numerical Simulation of Coupled Thermal, Hydraulic and Mechanical Behaviour in the Engineered Buffer Materials. International Journal for Numerical and Analytical Methods in Geomechanics. Vol. 24: pp. 403–424.

Ito, A., Kawakami, S., Yui, M. & Chijimatsu, M. 2002. Numerical Analysis about the Mass Transport in Unsaturated Buffer Material under Thermal Gradient (in Japanese). Proc. the 57th Japan Society of Civil Engineers Annual Meeting. CS10-052: pp. 485–486.

JNC 2000. Second progress report on research and development for the geological disposal of HLW in Japan, Project overview report. JNC TN1410 2000-001.

Ohnishi, Y., Shibata, H. & Kobayashi, A. 1985. Development of Finite Element Code for the Analysis of Coupled Thermo -Hydro -Mechanical Behaviors of a Saturated-Unsaturated Medium. Proc. Int. Symp. on Coupled Process Affecting the Performance of a Nuclear Waste Repository, Berkeley: pp. 263– 268.

Parkhurst, D.L., Thorstnsen, D.C. & Plummer, L.H. 1980. PHREEQE - A Computer Program for Geochemical Calculations. U.S. Geological Survey. Water-Resources Investigations 80-96.

Stephansson et al., O. 1995. Thermo -Hydro -Mechanical Coupling in Rock Mechanics. International Journal of Rock Mechanics and Mining Sciences, 32(5).

Stephansson et al., O. 2001. DECOVALEX II. International Journal of Rock Mechanics and Mining Sciences, 38(1).

Chijimatsu, M., Fujita, T., Kobayashi, A. & Ohnishi, Y. 1999. Coupled Thermo-Hydro-Mechanical Experiment at Kamaishi Mine, Technical Note 16-99-03, Analyses of Task 2C, DECOVALEX II. JNC TN8400 99-031.

JNC 2000. Second progress report on research and development for the geological disposal of HLW in Japan, Supporting Report 2, Repository Design and Engineering Technology. JNC TN1410 2000-003.

Nishigaki, M., Hishiya, T. & Hashimoto, N. 2001. DENSITY DEPENDENT GROUNDWATER FLOW WITH MASS TRANSPORT IN SATURATED - UNSATURATED POROUS MEDIA. Proceedings of the First Asian-Pacific Congress on Computational Mechanics: pp. 1375–1380.

Neyama, A., Ishihara, Y., Yui, M. & Ito, A. 2002. Development of Process Coupling System for the Numerical Experiment of High Level Radioactive Waste. WSEAS Transactions on Mathematics. Volume 1. ISSN 1109-2769: pp. 186–191.

Parkhurst, D.L., Thorstnsen, D.C. & Plummer, L.H. 1980. PHREEQE - A Computer Program for Geochemical Calculations. U.S. Geological Survey. Water-Resources Investigations 80-96.

Yeh, G.T. & Tripathi, V.S. 1990. HYDROGEOCHEM: A Coupled Model of HYDROlogic Transport and GEOCHEMical Equilibria in Reactive Multicomponent Systems. ORNL-6371. Environmental Sciences Division Publication No. 3170. Oak Ridge National Laboratory.

Appendix I

Status Report for D_THC

BGR Team (Germany)

Center of Applied Geosciences
University of Tübingen

Geozentrum Hannover
Bundesanstalt für
Geowissenschaften und Rohstoffe

Progress on THC Analysis
(Phase I)

M. Xie, W. Wang and O. Kolditz (UT)
T. Nowak, H. Kunz and H. Shao (BGR)

Contents

1 INTRODUCTION

This report presents coupled thermal-hydrological-chemical (THC) simulation results for DECOVALEX-THMC, Task D, conducted by the Center for Applied Geoscience (ZAG), University of Tübingen, on the behalf of the Federal Institute for Geosciences and Natural Resources (BGR), Hanover, Germany. This task is described in detail by Barr et al. (2004) ([3]). The central point of this task is to explore various aspects of long-term, permanent changes (caused by THM and THC coupled processes) in hydraulic properties of bentonite and/or rock in the near field of a nuclear waste repository. This report presents results for the Task D THC1 Step 1 by using the object-oriented FEM simulator GeoSys/RockFlow.

2 THEORETICAL BACKGROUND

2.1 MATERIAL BEHAVIOR

2.1.1 Swelling

Porosity. With the increase of water content and/or decrease of pore-water ionic concentration, bentonite swells because of the interlayer porosity change, which can be described by the chemical swelling model presented by Xie et al., (2004), as summarized in Equations (1) and (2). According to this model, porosity in bentonite can be distinguished by interlayer (n_{IL}) and interparticle porosity (n_{IP}). The latter is of special importance for water flow and is called the effective porosity. During the moisture swelling process, the effective porosity, and consequently the effective permeability of bentonite, can increase in the case of free swelling or decrease under confined conditions. Of course, this subsequently influences the chemical transport process,

$$n_{\mathrm{IL}} = (S^l)^\eta \cdot \beta \cdot n_{\mathrm{IL}max} \tag{1}$$

$$n_{\mathrm{IL}max} = m S_0 \rho_d \left(\frac{\varepsilon \varepsilon_0 R T}{2 F^2 I \times 10^3} \right)^{\frac{1}{2}} \tag{2}$$

in which n_{IL} is the interlayer porosity, which represents the space occupied by diffuse double layers (DDLs); $n_{\mathrm{IL}max}$ is the maximum interlayer porosity, which represents the swelling potential of bentonite; S^l is the degree of liquid saturation; β represents the volume fraction of the expansive minerals, η is a dimensionless coefficient, R is the universal gas constant, T is the absolute temperature [K], F is the Faraday constant, ε is the dielectric constant, and ε_0 is the permittivity of free space. The ionic strength I is defined as (see e.g., Stumm and Morgan, 1996; Dzoonbok and Moul, 1990):

$$I = \frac{1}{2} \sum_i c_i z_i^2 \tag{3}$$

where c_i is the ith ionic concentration of the pore water [M] and z_i represents the valence of the ith ion.

The number of effective layers m within one particle of expansive minerals in bentonite is a mineral structural parameter defined as the number of layers contributing to the swelling effect. Because the montmorillonite particles are very small, the average m value is used. This value is calculated as the ratio of total specific surface area S_{total} in m^2/g (including the surface between layers, which can separate by swelling) to external specific surface area S_0 in m^2/g (only the surface of particles).

$$m = \frac{S_{total}}{S_0}$$

(4)

The value S_{total} is normally determined by the methylene blue and the Keeling hygroscopy methods. The value S_0 is normally measured using the BET (Brunauer, Emmet and Teller N_2 Adsorption) method (ASTM International, 2001a; 2001b; FEBEX Working Groups, 2000).

The quantity $n_{IL,max}$ represents the swelling potential of the montmorillonite minerals contained in a compacted bentonite; it depends on the soil properties of the sample, the mineral properties of montmorillonite, and the chemical properties of pore water. The amount of swelling calculated by Equation 1 depends on the initial water saturation and the change in water content, swelling conditions (confined or unconfined), and the variation in pore water chemistry.

Effective porosity. Effective porosity is the amount of interconnected pore space in a soil or rock through which fluids can pass, expressed as a percent of bulk volume (U.S. Bureau of Mines, 1997). Owing to electrostatic attraction, interlayer-water in compacted bentonite is practically immobile. Therefore, the effective porosity n_{eff} of compacted bentonite varies with the saturation and swelling processes. In the case of confined swelling, the effective porosity decreases with increased water saturation. Theoretically, it can be reduced to zero, which means the permeability reaches zero; however, this is not the case in practice. A part of the porosity, which is defined here as the minimal porosity, remains, how much depends on the swelling pressure and the compressibility of the sample. Therefore, the effective porosity of bentonite in the case of confined swelling can be derived from the initial porosity n_0, interlayer porosity $n_{IL,}$ and minimal porosity n_{min}:

$$n_{eff} = \begin{cases} n_0 - n_{IL} & , & n_{eff} > n_{min} \\ n_{min} & , & n_{eff} \leq n_{min} \end{cases}$$

(5)

In the case of free swelling, the volume change should be taken into consideration, which means the total porosity n_{tot} changes with swelling/shrinking. The effective porosity is:

$$n_{eff} = n_{tot} - n_{IL}$$

(6)

However, if the water content is below the shrinkage limit, free swelling/shrinking is limited. Macroscopically, volume change nearly vanishes. Microscopically, interlayer porosity variation changes the interparticle porosity. In this case, Equation (5) can be used for calculating n_{eff}.

2.1.2 Water in compacted bentonite

Bentonites contain a large quantity of montmorillonite (65–90wt.%), which determines the properties of bentonites (Bradbury and Bayens, 2003). Owing to the special mineral structure, relatively high net negative charge on the mineral surface, and the extremely high specific

surface of montmorillonite, water not only can flow through large pores but also enter into the interlayer spaces. Around the mineral surfaces, diffuse double layers (DDLs) can only build up completely under totally free-swelling conditions. Bradbury and Baeyens (2003) divided the water in bentonite into three types: interlayer water, double layer water and free water. Interlayer water is only one to four monolayers of water molecules thick (<1 nm), and differs from "free water" with respect to fluid properties (Newman, 1987; Schoen et al., 1989). Free water exists only in large pores. The rest is the double-layer water in the electric diffuse double layers. DDLs in highly compacted bentonite can overlap. Because diffusion and chemical reactions can also occur in the DDLs, the term "bentonite pore water" is defined herein as the double layer water plus free water.

2.1.3 Two-phase flow

Capillary pressure. The parameters $p_c(S)$ (capillary pressure) and $k_{rel}(S)$ (relative permeability) are key factors affecting multiphase flow. Capillary pressure is defined as the difference between partial pressures of nonwetting and wetting phases and is a function of degree of saturation (Helmig, 1997). The $p_c(S)$ value can be measured for a given soil with respect to various fluids.

Relative permeability. For porous media containing more than one fluid, relative permeability is a key parameter. It is used to calculate the effective permeability ($k^\gamma_{rel(S)}\mathbf{K}$) , which is described in the extended Darcy's law. Different relationships between k^γ_{rel} and S^γ, (i.e.; constant value, linear function, potential function) can be found in the literature. The van Genuchten model, in conjunction with the approach of Mualem, is one of them (van Genuchten, 1980; Helmig, 1997; Lenhard and Parker, 1987):

$$k^l_{rel} = S^{l\frac{1}{2}}_{eff} \left[1 - (1 - S^{l1/\alpha}_{eff})^\alpha \right]^2 \tag{7}$$

$$k^g_{rel} = (1 - S^l_{eff})^{\frac{1}{2}} \left[1 - (S^{l1/\alpha}_{eff}) \right]^{2\alpha} \tag{8}$$

$$S^l_{eff} = \frac{\theta - \theta_r}{\theta_s - \theta_r} \tag{9}$$

where α is the van Genuchten parameter, and s and r indicate saturated and residual values of the water content (θ) respectively. According to this definition, the value of both relative permeability values k^γ_{rel} is in the range of [0; 1].

In the experiment with FEBEX compacted bentonite, the relative permeability value for gas was found to be much higher than that for liquid. A dual relative-permeability model is presented by (Olivella and Gens, 2000), which is used here in the simulation.

Swelling relative permeability. A large number of studies have tried to generate methods to independently predict permeability of sedimentary rocks from the bulk porosity (Berg, 1970; Bloch, 1991; Neuzil, 1994). Measured permeabilities of clays and shales were found to vary over the range of 10^{-22} m^2 to 10^{-14} m^2. Oelkers (1996) suggested a correlation between intrinsic permeability and effective porosity for clays and shales, which is adopted here for highly compacted bentonite. Based on this, the swelling relative permeability k_{relsw} for highly compacted bentonite is defined as:

$$k_{\mathrm{rel}_{sw}}\mathbf{k} = 9.87 \times 10^{-12} e^{-10+8n_{\mathrm{eff}}} \tag{10}$$

2.1.4 Geochemical reactions

Ion exchange. Owing to the high permanent negative charge on the surface of montmorillonite, which is balanced by the preferential sorption of exchangeable cations to the surface, the exchange capacity of montmorillonites is very high. Ion exchange is an important interaction mechanism between ions dissolved in pore water and solid minerals, especially in highly compacted bentonite where the volume of pore water is small and the propertion of montmorillonites is large (Bradbury and Bayens, 2003). Consequently, porewater chemistry can be strongly influenced by ion exchange.

Dissolution/precipitation. With dissolution and precipitation processes, the porosity n may be changed and can be expressed as:

$$n = n_0 - \sum_{j=1}^{nm} V_j \Delta M_j \tag{11}$$

where n_0 is the original porosity, Mj is the mass concentration of mineral j in moles per unit volume of porous medium, Vj is the molar volume of mineral j, and nm is the number of minerals.

Temperature dependence. Owing to nuclei decay in the canister, heat is generated, and thus temperature in the buffer material changes with the time. Therefore, it is important to investigate the temperature influence on the geochemical reactions. Temperature dependence of reactions is taken into account in PHREEQC2 in the following two methods, both modified the equilibrium constant K as a function of temperature:

1. By using the van't Hoff equation:

$$ln(\frac{K_2}{K_1}) = \frac{\Delta H^0}{R}(\frac{1}{T_1} - \frac{1}{T_2}) \tag{12}$$

in which K_1; K_2 are reaction coefficients at temperature T_1; T_2 in Kelvin respectively. In the PHREEQC2 database, reference *logK* value is given at 25°C. For example, the *logK* values of the chemical reaction of Albite $NaAlSi_3O_8 + 8H_2O = Na^+ + Al(OH)_{4_i} + 3H_4SiO_4$ at different temperature are calculated using Equation (12). *logK* at 25°C is -18.002, while ΔH_0 25.896 kcal.

2. Using an analytical expression for the temperature dependence of log K for a reaction defined with:

$$log_{10}K = A_1 + A_2T + \frac{A_3}{T} + A_4 log_{10}T + \frac{A_5}{T^2} \tag{13}$$

Up to five coefficients A_i (i = 1; 2; $\ldots$; 5) for the equation may be given to calculate the *logK* value at a given temperature. In PHREEQC2, the second method is given priority if parameters for both methods are provided. The *logK* values of the chemical reaction of gypsum $CaSO4 : 2H_2O = Ca^{+2} + SO_{4-2} + 2H_2O$ at different temperature are calculated using Equation (13). *logK* at 25°C is -18.002, A_1, A_2, A_3, A_4 and A_5 are 68.2401, 0.0, -3221.51, -25.0627 and 0.0.

2.2 GOVERNING EQUATIONS

2.2.1 Mass balance equations

In the macroscopic model, Richards flow is captured. In general, there are two concepts from which to formulate the balance equations: phase-related and compositional approaches. The compositional approach is advantageous for multiphase-multicomponental processes with phase changes (Gawin et al., 1995; Gens et al., 1998, and is adopted for this study. In this approach, the porous medium is regarded as a three-component system, with components air, water, and soil. Each of these components can be present in three phases (gas, liquid, and solid phase). In this study, air and solid are treated as single pseudo components with averaged properties, even if they consist of several components.

Hydraulic processes resulting from pressure, frictional, and gravitational forces are described by the extension of Darcy's law for multi-phase flow. The mobility of the fluid phases is characterized by their relative permeability and capillary pressure, both of which are a function of saturation. The equation describing Darcy's law with multi-phase flow is:

$$n\frac{\partial}{\partial t}[S\rho^l + (1-S)\rho^v] + \nabla \cdot (\mathbf{q}_f^l + \mathbf{q}_v) = Q_f \tag{14}$$

where n is porosity, S is liquid-phase saturation, ρ^l is density of liquid phase, ρ_v is density of vapor; and q_f^l is liquid phase flux, which can be derived by the classic Darcy's law:

$$\mathbf{q}_f^l = -nS\rho^l[\frac{k_{rel}\mathbf{k}}{\mu}(\nabla p - \rho^l g\nabla z)] \tag{15}$$

in which k_{rel} is the relative permeability, k represents the permeability tensor, μ is the viscosity, g is the acceleration of gravity, and z is the elevation.

Another term, q_v, in Equation (14) considers the vapor mass flux relative to solid and can be derived (Rutqvist et al., 2001):

$$\mathbf{q}_v = -\rho^l(D_{Pv}\mathbf{I}\nabla P_l + D_{T_v}\mathbf{I}\nabla T) \tag{16}$$

in which D_{Tv} is the thermal vapor diffusivity, and Q_f is the source term.

2.2.2 Energy conservation equations

The general heat-balance equation for a porous medium that consists of three phases (solid, gas, liquid) is described by:

$$\frac{\partial}{\partial t}[(1-n)\rho^s u^s + nS^g\rho^g u^g + nS^l\rho^l u^l] + \nabla \cdot (\mathbf{q}_h^s + \mathbf{q}_h^g + \mathbf{q}_h^l) = Q_h \tag{17}$$

where u^γ is phase internal enthalpy, ρ^γ is phase density, and $J^\gamma h$ is total heat flux in phase γ(s-solid, l-liquid and g-gas); Q_h is the heat source term, i.e., the heat generation rate per unit volume. By considering the heat conductivity and convection, the simple expression of heat transport can be derived (Wang et al., 2005):

$$\sum^{phase}(\rho^\gamma C_p^\gamma)\frac{\partial T}{\partial t} - \nabla\mathbf{q}_h = Q_h \tag{18}$$

7

$$\mathbf{q}_h = -K_e \nabla T + n \sum_{\gamma}^{phase} (\rho^{\gamma} C_p^{\gamma}) T \mathbf{v}$$, (19)

in which Ke is the heat conductivity, and C$^{\gamma}$p is the heat capacity of phase γ.

2.2.3 Multicomponent transport

The balance equation for multicomponent mass transport in porous media is given by [13]:

$$\frac{\partial(nS_{\gamma}C_{i,\gamma})}{\partial t} = -v_{\gamma}\nabla C_{i,\gamma} + \nabla(nS_{\gamma}D_{i,\gamma}\nabla C_{i,\gamma}) + nS_{\gamma}Q_{i,\gamma} + nS_{\gamma}\Gamma_{i,\gamma}(C_{1,\gamma}...C_{n,\gamma})$$ (20)

where $C_{i,\gamma}$ is the concentration of the i-th component of an *n* component system in phase *γ*. v_{γ} is the Darcy velocity of phase *γ*, S_{γ} is saturation of phase *γ*, *D* is the diffusion-dispersion coefficient of component *i* in phase *γ*, $Q_{i,\gamma}$ is the source/sink term, and $\Gamma_{i;\gamma}(C_{1,\gamma}...C_{n,\gamma})$ is the source/sink term of component *i* in phase *γ,* due to equilibrium chemical reactions with all other species in the same phase.

This transport equation has to be solved for each component in each fluid phase separately. The reaction term couples all equations of one fluid phase together. A sequential noniterative approach is adopted to solve this system of equations. In the first step, conservative transport for each component and each phase is calculated. In the second step, all chemical reactions are calculated for each node of the model grid. For the reaction step, the geochemical program PHREEQC2 (Febex Working Groups, 2000) was employed. This program was coupled to the GeoSys/RockFlow code by the sequential approach (Bauer et al., 2004).

3 PROBLEM DESCRIPTION

Task D_THC1 is defined to deal with the so called FEBEX type repository: granite with bentonite backfill. The granite is assumed to be saturated before excavation. During the excavation, the granite near the cave is desaturated. After the backfilling of unsaturated compacted bentonite, pore-water in granite flows towards bentonite, owing to the capillary effect. The geometry and material property data are the same as for the THM analysis, which are described in Barr et al. (2004).

The chemical compositions of smaland granite, bentonite (Kunigel V1), and the related pore-water chemistry are listed in the following tables (Tables 1, 2, and 3).

Table 1: Mineralogical abundances in the Smaland granite (modified from Rhen et al., 1997)	
Mineral	Abundance
	(Weight fraction)
Quartz	0.2756
K-Feldspar	0.2724
Plagioclase	0.3964
Annite	0.0489
Phlogopite	0.0067

Table 2: Mineralogical abundances in the Kunigel V1 (modified from Ochs et al., 2004)	
Mineral	Abundance
	(Weight fraction)
Quartz	0.335
Na-mintmorillonite	0.475
K-Feldspar	0.041
Calcite	0.0235
Dolomite	0.029
Pyrite	0.006

Note that a geochemical reaction calculation was performed (once) using the above water chemistry and mineral composition data to obtain the values at equilibrium. The resulting systems (pore-water chemistry and mineral composition) of both granite and bentonite at 25°C were used for initial concentrations. The boundary condition of chemistry at the bottom was calculated using the same method at 40°C.

3.1 COUPLED PROCESSES CONSIDERED

Thermally driven coupled THC processes occur with the heat output of the decaying radioactive waste. The most important processes are:

- Heating of bentonite and granite (<100°C)
- Multi-phase flow in bentonite or/and granite
- Changes in water chemistry in bentonite
- Changes in water chemistry in granite
- Precipitation/dissolution in bentonite and granite and related porosity changes

Table 3: Initial water chemistry in granite and Kunigel V1	
Litorina Sea	pH=7.7
Element	Concentration (mol/kg H2O
Cl^-	1.838e-1
Na^+	1.598e-1
K^+	3.427e-3
Ca^{2+}	3.767e-3
Mg^{2-}	1.843e-2
HCO_3^-	1.524e-3
SO_4^{2-}	9.265e-3
Charge balance	1.032e-2

Kunigel V1	pH=8.4
Element	Concentration (mol/kg H2O
Cl^-	1.500e-5
Na^+	3.600e-3
K^+	6.200e-5
Ca^{2+}	1.100e-4
Mg^{2-}	5.500e-5
HCO_3^-	3.500e-3
SO_4^{2-}	1.100e-4
Cl^-	3.400e-4
Charge balance	3.326e-2

3.2 GENERAL MODEL GEOMETRY

A general two-dimensional model is suggested for tasks D_THM and D_THC (Figure 1). The size of the models is dependent on the type of repositories, described in Table 4. Based on such definitions, it would be easy for all research teams to compare their results.

Figure 1: General model geometry, boundary conditions, and locations of points, lines, and areas for model output (Barr et al., 2004).

10

The initial and boundary conditions (ICs, BCs) for D_THM1 are given in Barr et al., (2004) as shown in Figure 2. For D_THC1 simulation, the same ICs, and BCs will be set in addition to initial geochemical conditions. The excavation is treated as a short event; therefore, only Case (a) and (d) are considered.

According to the definitions, the most difficult simulations are clearly of the two apparently different geochemical systems under nonisothermal unsaturated conditions. To simulate the complex THC processes in THC1, we took two steps:

1. Two geochemical systems in saturated porous media
2. Two geochemical systems in unsaturated porous media
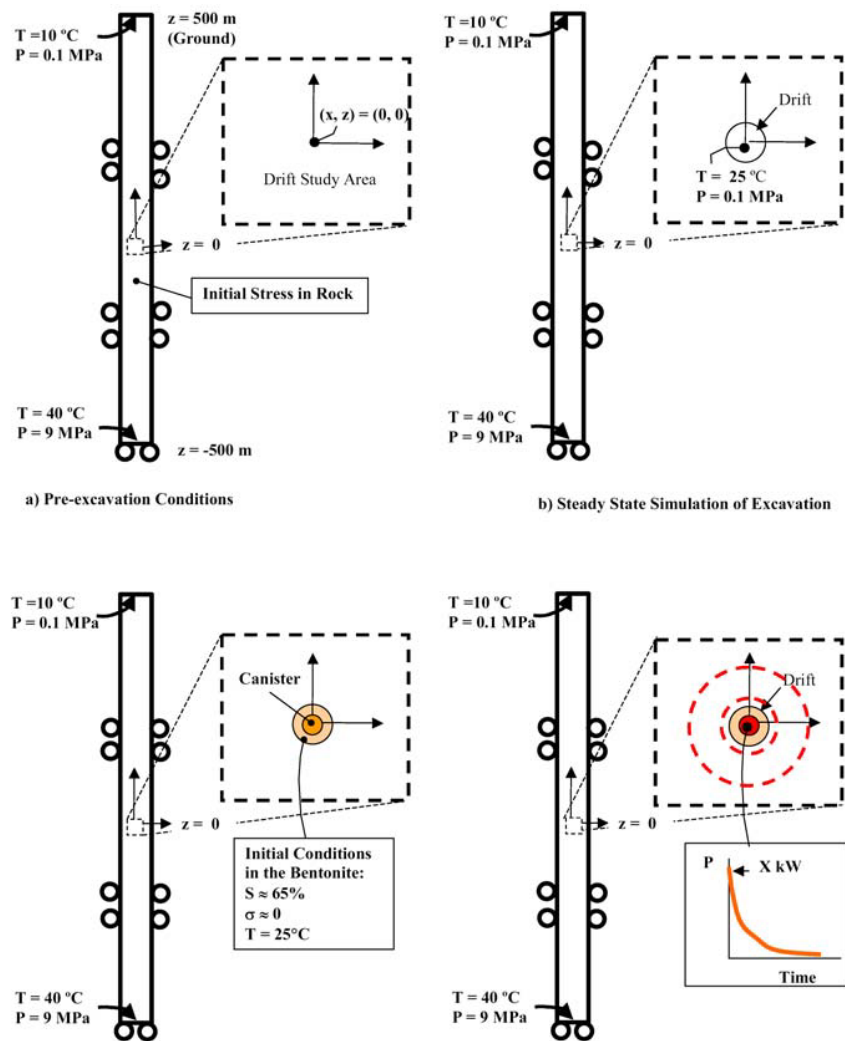
Figure 2. Special modeling sequence, boundaries, and initial conditions for Task D_THM1 (Kolditz, 2002)

Table 4: Size of model dimensions (in *m* in Figure 1)

Dimension	FEBEX-Type	Yucca Mountain Type
Vertical length, L_z	1000	550
Horizontal length, L_x	35	81
Drift diameter, d	2.28	5.50
Diameter of waste canister	0.9	1.7
Near drift study area, $3d \times 3d$	7×7	$16{:}5 \times 16{:}5$
Far field study area, $2/3Lx \times 2/3Lx$	25×25	54×54

All data from [3]

3.3 MATERIAL PARAMETERS FOR THC1 SIMULATIONS

The material parameters for granite and buffer are given in Tables 5 and 6, respectively.

Table 5. Material properties for granite

Parameter	Unit	Value
Density	Kg/ m^3	2700
Young's modulus	GPa	35.0
Poisson ratio	-	0.3
Biot's constant	-	1
Thermal expansion coefficient	-	1.0e-5
Thermal conductivity	W/mK	3
Thermal capacity	J/kgK	900
Porosity	-	0.01
Storativity	1/Pa	4.4e-10
Saturated permeability	m^2	1.0e-17

Table 6. Material properties for betonite

Parameter	Unit	Value
Density	Kg/ m^3	1600
Young's modulus	MPa	317
Poisson ratio	-	0.35
Biot's constant	-	1
Tortuosity	-	0.67e-5
Thermal expansion coefficient	-	1.0e-5
Thermal conductivity	W/mK	1.3
Thermal capacity	J/kgK	900
Porosity	-	0.389
Saturated permeability	m^2	2.0e-21

The relationship between capillary pressure and saturation for both rock and bentonite are depicted in Figure 3.
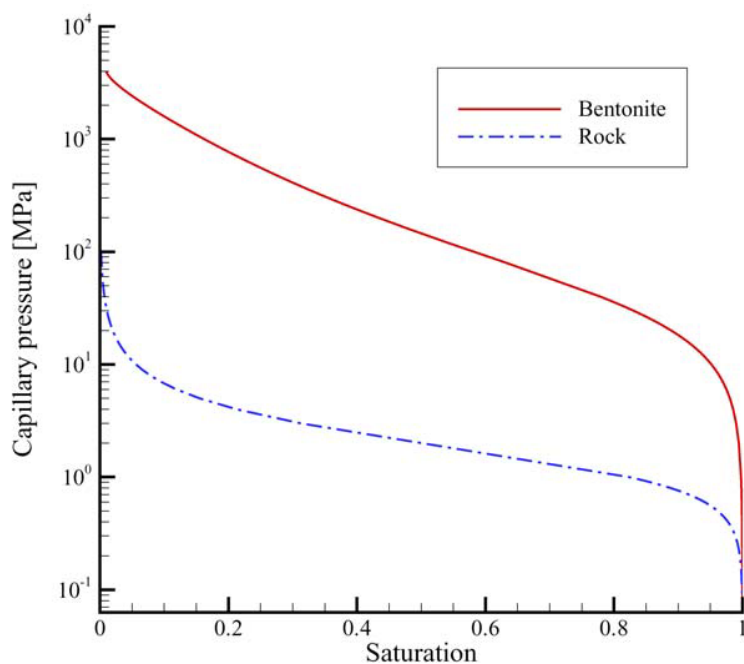
Figure 3: Capillary pressure vs saturation

The relationship between relative permeability and saturation is described in Figure 4

Figure 4: Relative permeability vs saturation

13
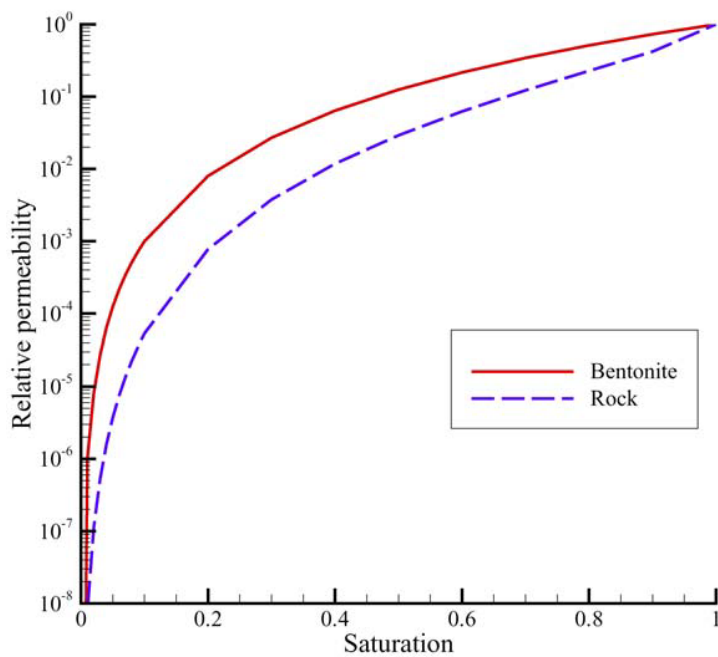
For mass transport, mass diffusion is included and the coefficients of mass diffusion for all ions and anions are assumed to be the same, 1×10^{-9} m^2/s. The minerals are immobile. The reactions included in the geochemical simulation can be found in the appendix.

3.4 CASE 1: SATURATED FLOW

To demonstrate the effect of two alternative geochemical systems, we conducted an intermediate simulation step using the assumption of saturated condition at the start time of THC simulation. Under this assumption, the initial liquid pressure (p^l) and temperature (T) is a linear distribution along depth. On the top, $p^l = 0.1$ MPa and T = 10°C. At a depth of 1,000 m beneath the ground surface, $p^l = 9.0$ MPa and T = 40°C. This results in a slow, downward liquid flow. This flow field remains almost unchanged over time. Temperature, however, changes with the heat source curve.

The temperature evolution is shown in Figure 5. The peak temperature at observation point V1 is 92.78°C, about 15 years after emplacement of waste.
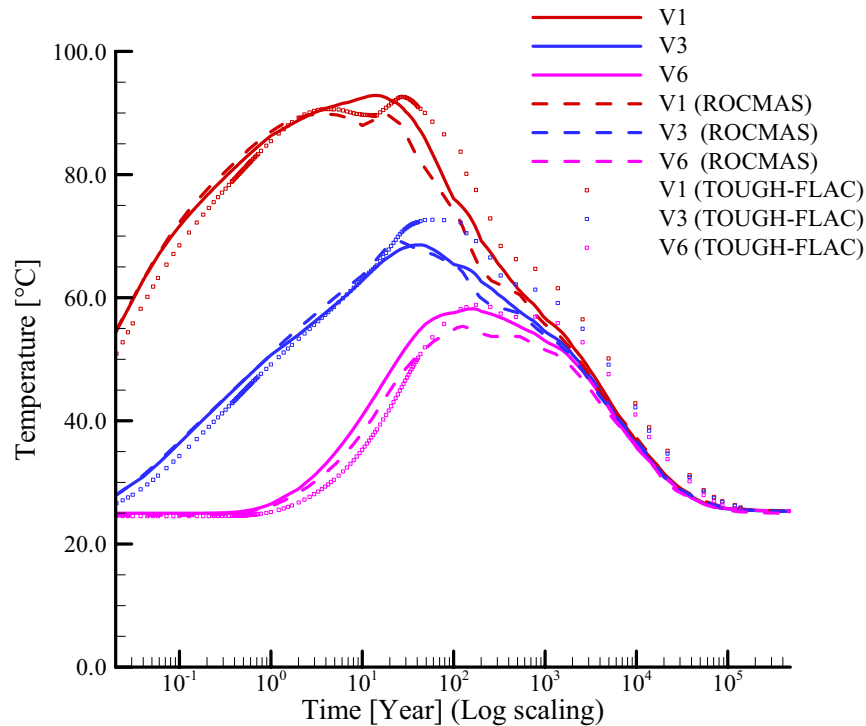
Figure 5: Temperature evolution and comparison with TOUGH-FLAC and ROCMAS simulation results

The aqueous species concentrations are shown in the vertical profiles near the canister from a depth of 480 to 520 m underground (Figures 6-11). There are quite different values of concentration for the two material groups (bentonite and rock) at 0.01 year. These values change with time, owing to diffusion and the very slow advection resulting from the initial hydraulic gradient, as well as the heat evolution effect.

14
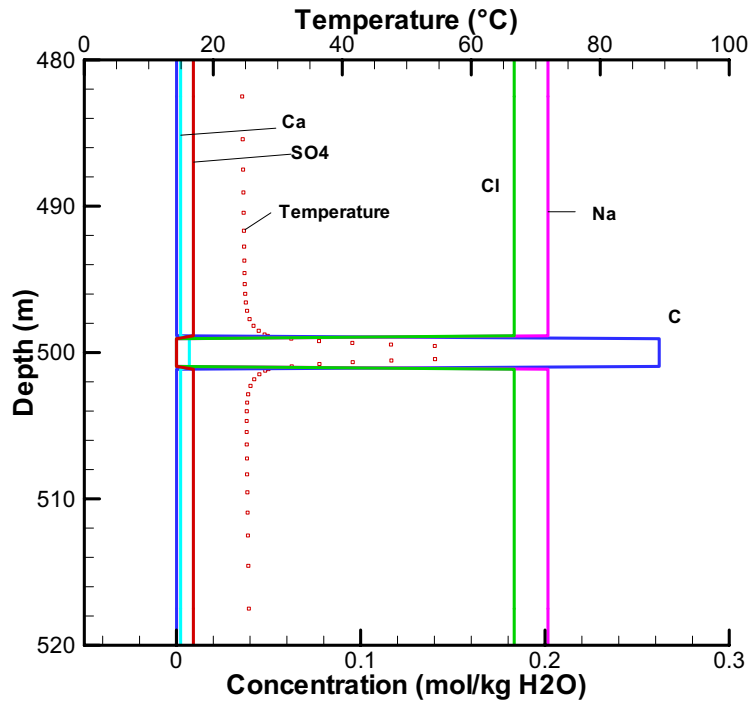
Figure 6: Vertical profile of aqueous species concentrations at 0.01 year

Figure 7: Vertical profile of aqueous species concentrations at 1 year

15
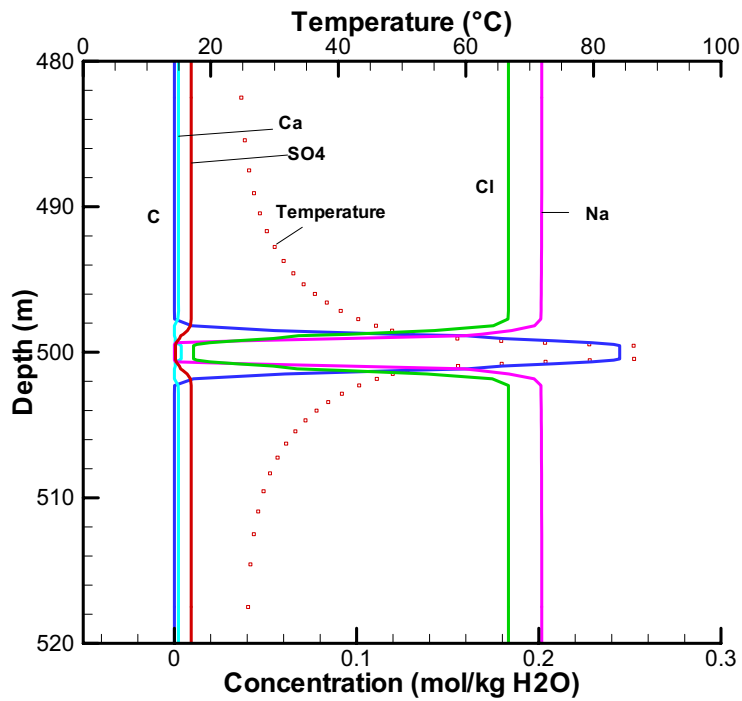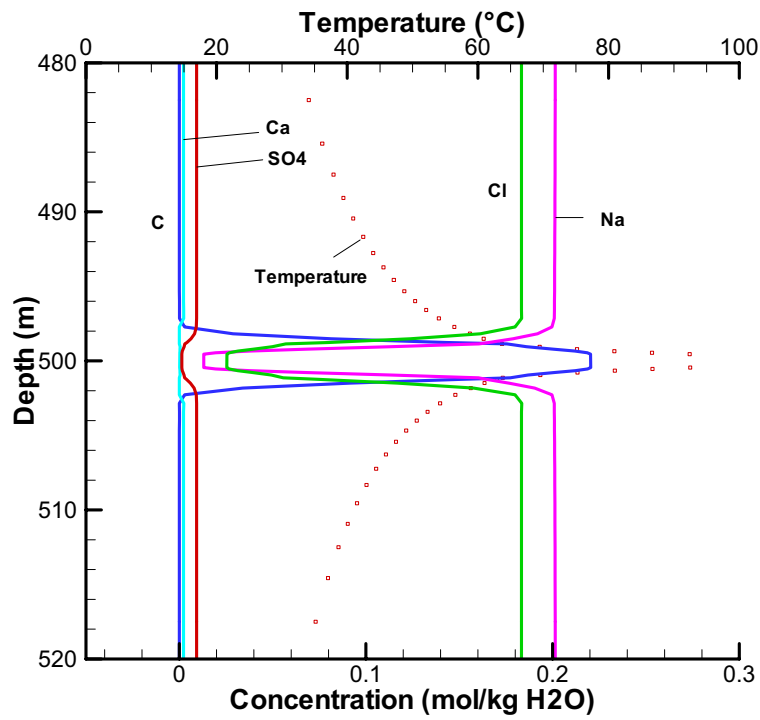
Figure 8: Vertical profile of aqueous species concentrations at 10 years
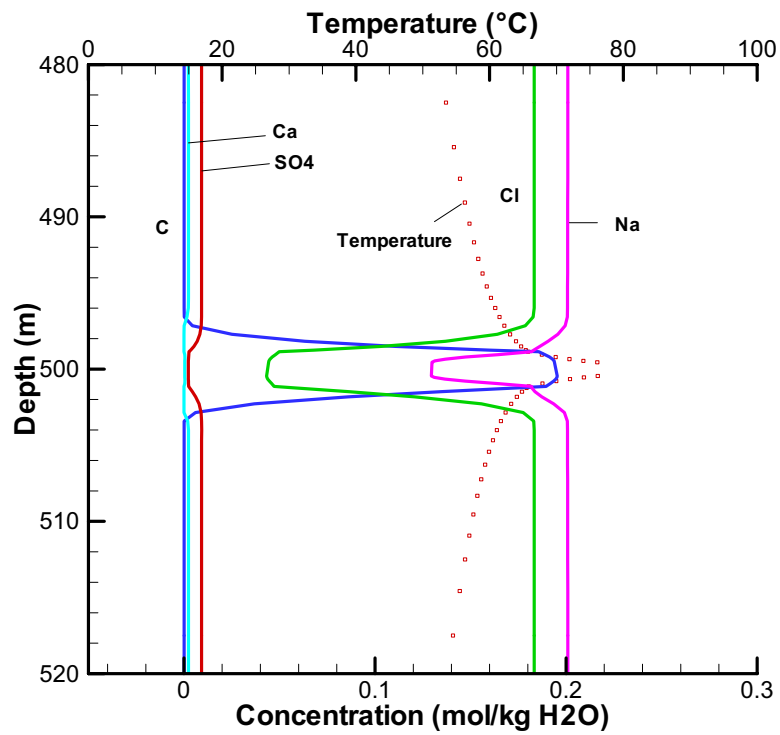
Figure 9: Vertical profile of aqueous species concentrations at 100 years

16
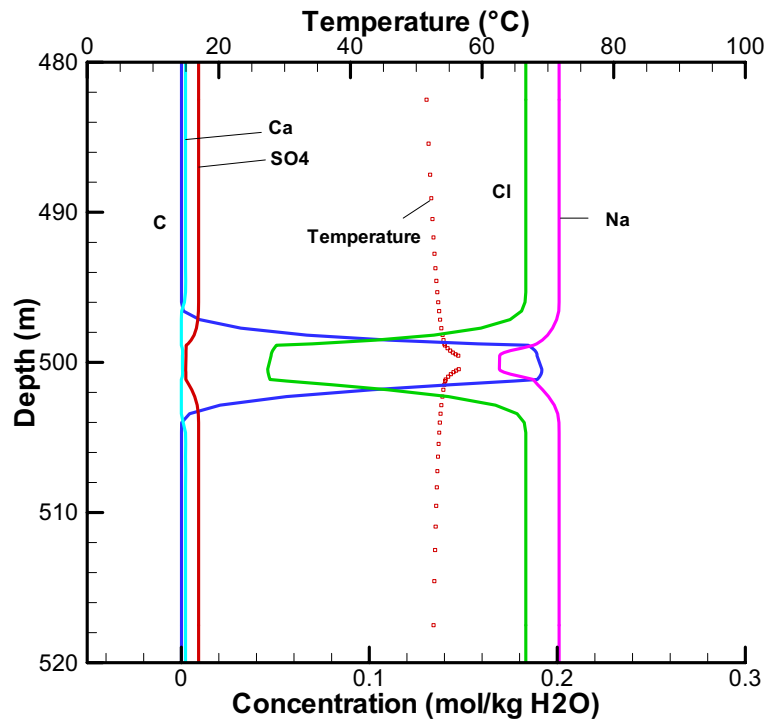
Figure 10: Vertical profile of aqueous species concentrations at 1000 years
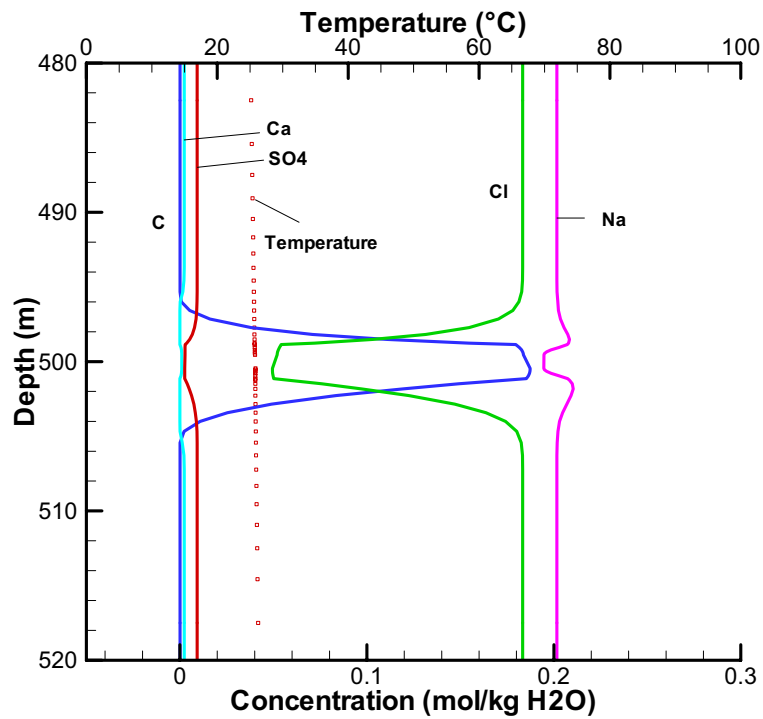
Figure 11: Vertical profile of aqueous species concentrations at 100,000 years

17

The mineral abundances along the vertical profile are shown in Figures 12, 13,14,15. The minerals are quite stable, and most of the dissolution or precipitation occurs in the adjacent area between the two materials.
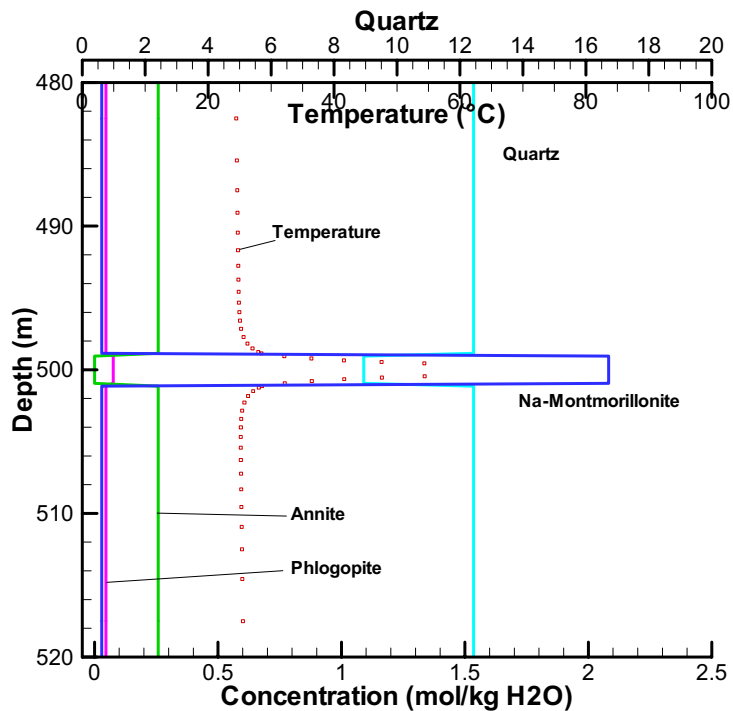
Figure 12: Vertical profile of mineral abundance at 0.01 year
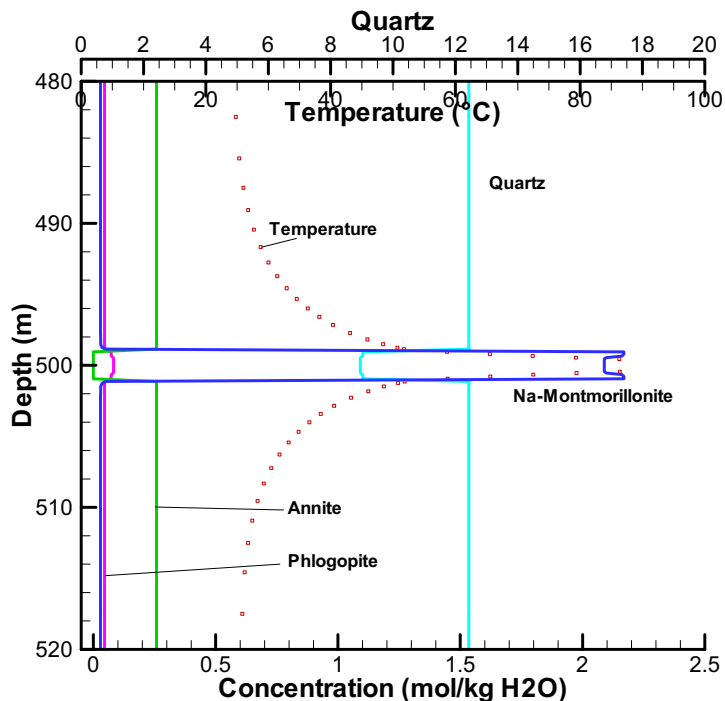
Figure 13: Vertical profile of mineral abundance at 1 year
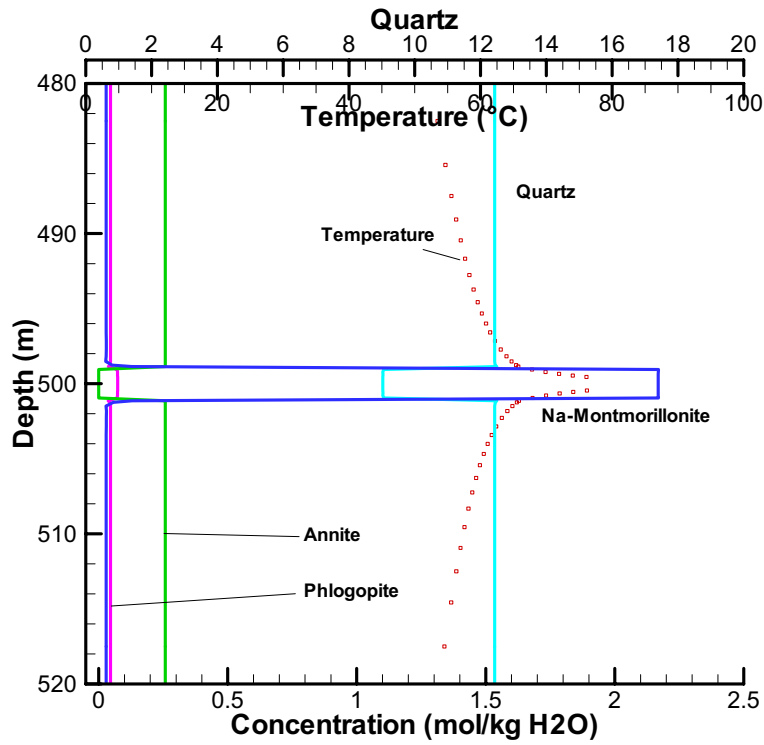
Figure 14: Vertical profile of mineral abundance at 100 years

Figure 15: Vertical profile of mineral abundance at 100,000 years

19
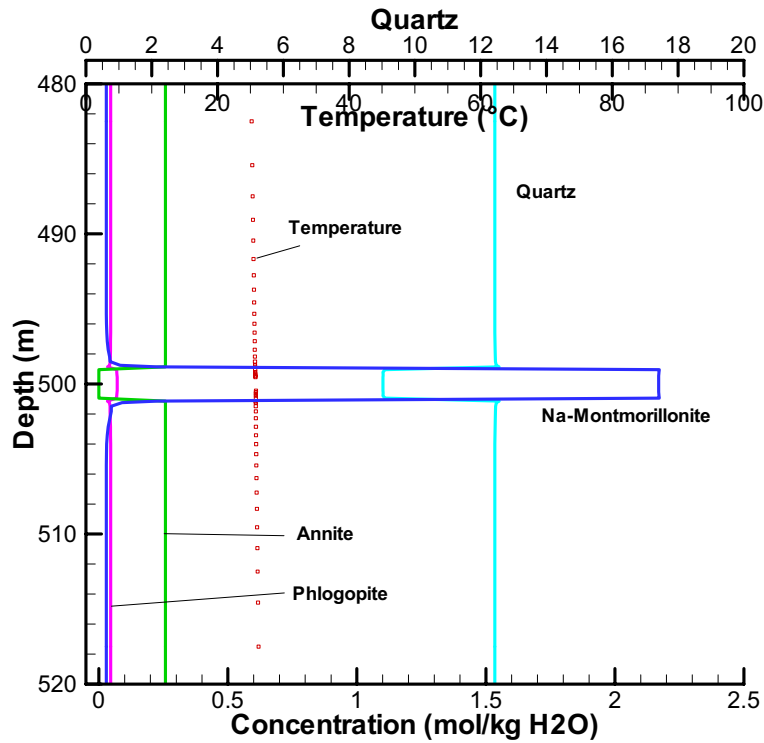
3.5 CASE 2: UNSATURATED FLOW

In this simulation, the bentonite is emplaced into the initially saturated rock mass at a saturation of about 65%.

3.5.1 Temperature evolution

The temperature evolution is shown in Figure 16. The peak temperature of 92.8°C occurs after 15 years. The temperature evolution is almost identical to the calculations using TOUGH-FLAC and ROCMAS (LBNL).
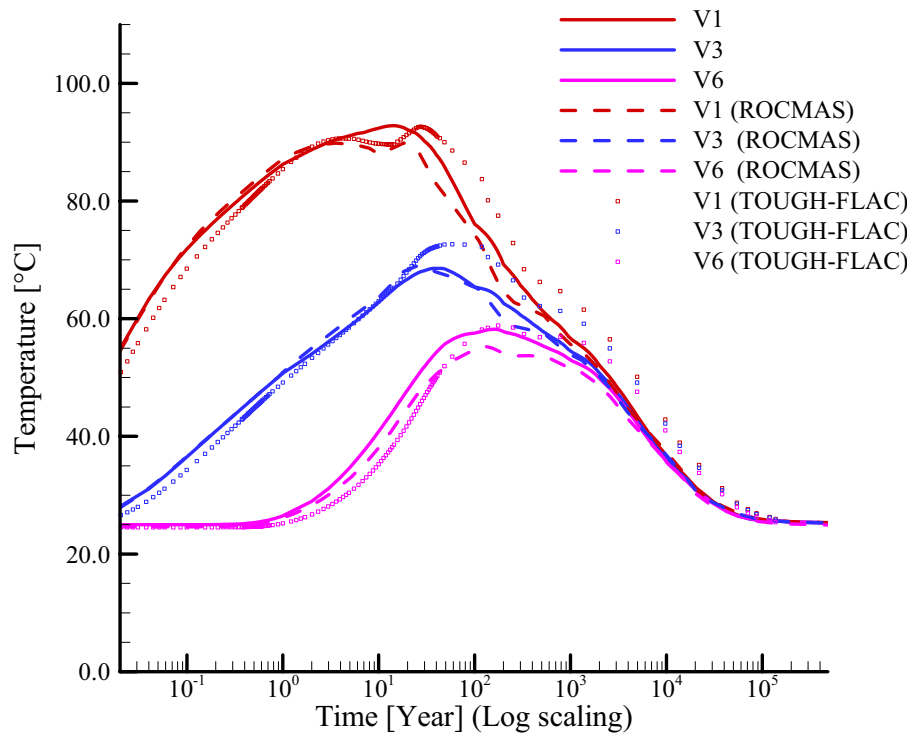
Figure 16: Temperature evolution and comparison with TOUGH-FLAC and ROCMAS simulation results

The temperature increases with depth, as shown in the local vertical profile (Figure 17). Near the canister, the temperature changes dramatically within 100 years. After 100,000 years, the temperature reaches the initial value. The same tendency can be observed in the horizontal profile (Figure 18).

20
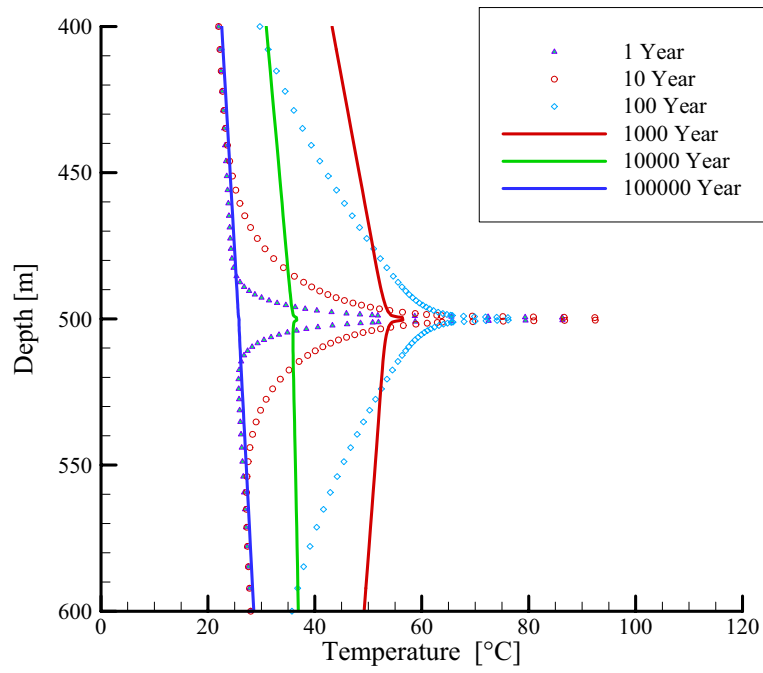
Figure 17: Vertical profile of temperature from 400 m to 600 m
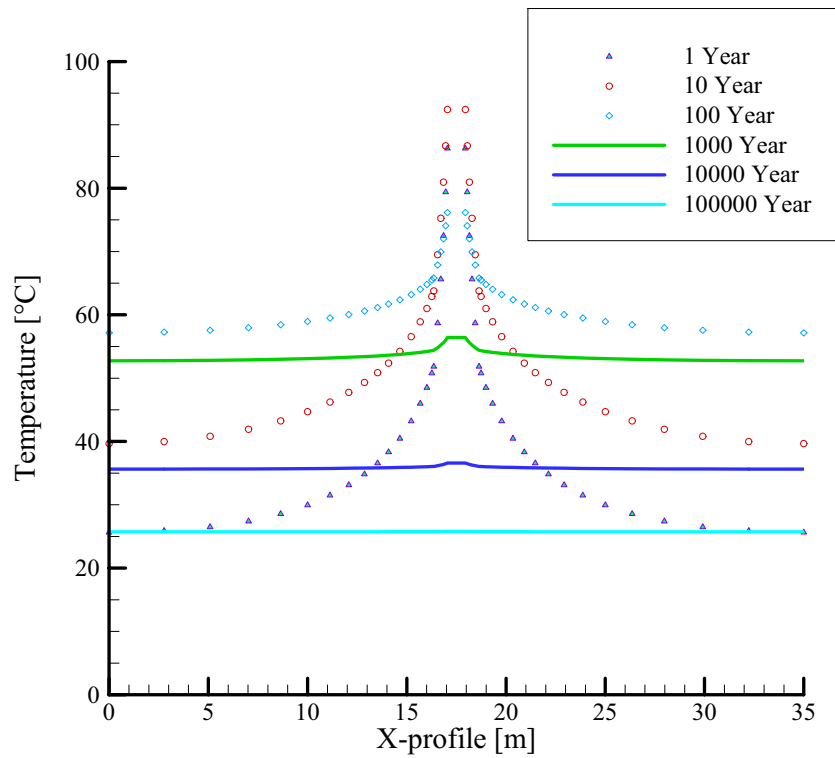
Figure 18: Horizontal profile of temperature

3.5.2 Saturation evolution

The evolution of saturation at Observation Point V1 (bentonite on contact canister) is shown in Figure 19. It is dry at the beginning,with the water saturation decreasing to 62.2% at about 1 year; after 25 years, the bentonite is saturated. This is not identical with the ROCMAS simulation results, because of the introduction of only one term for vapor diffusion, without mechanical coupling.
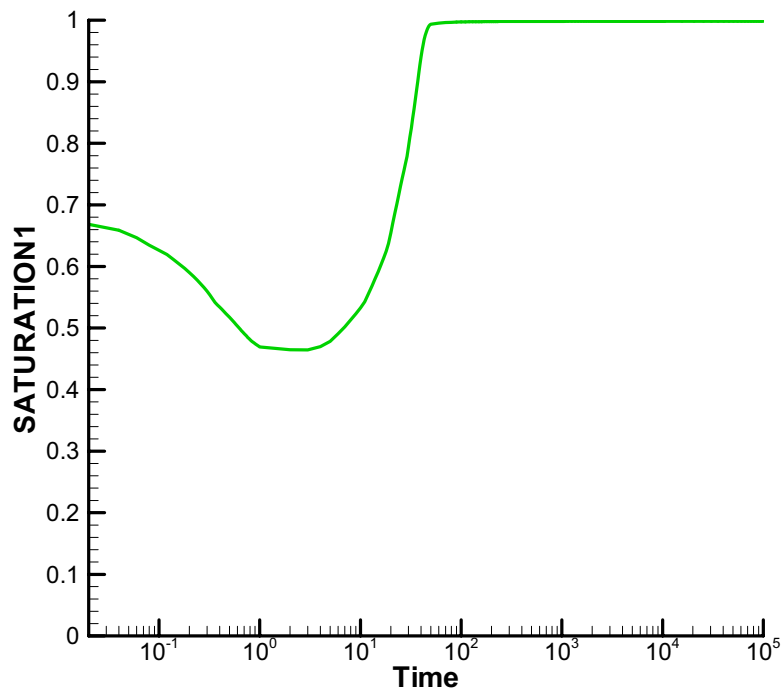
Figure 19: Water saturation evolution at point V1

3.5.3 Aqueous species concentrations and mineral abundance

The evolution of the aqueous species concentrations is shown in the vertical profiles (Figures 20, 21, 22, 23, 24). In comparison with the saturated case, the changes near the contact area of the two material groups (bentonite and rock) are much faster, owing to the capillary driving flow effect.
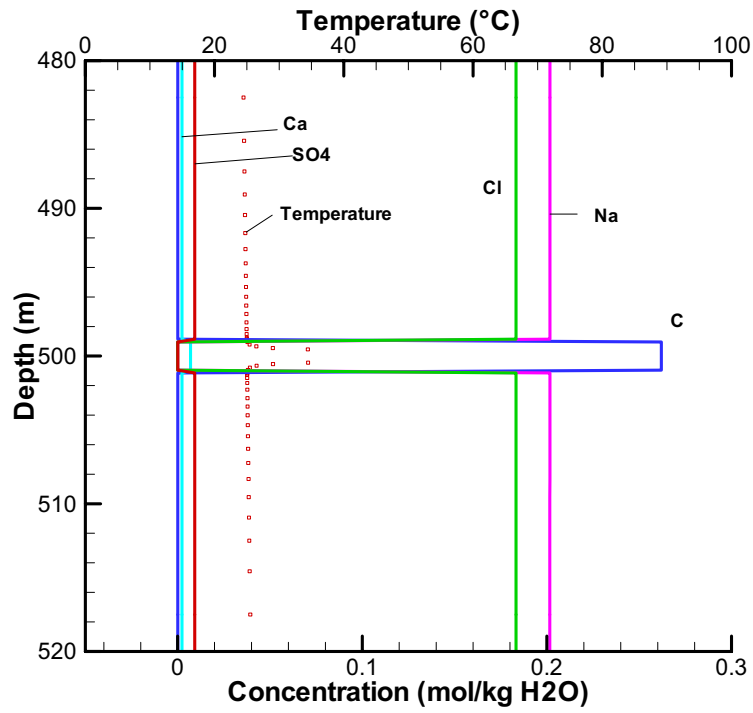
Figure 20: Vertical profile of aqueous species concentrations at 0.001 year
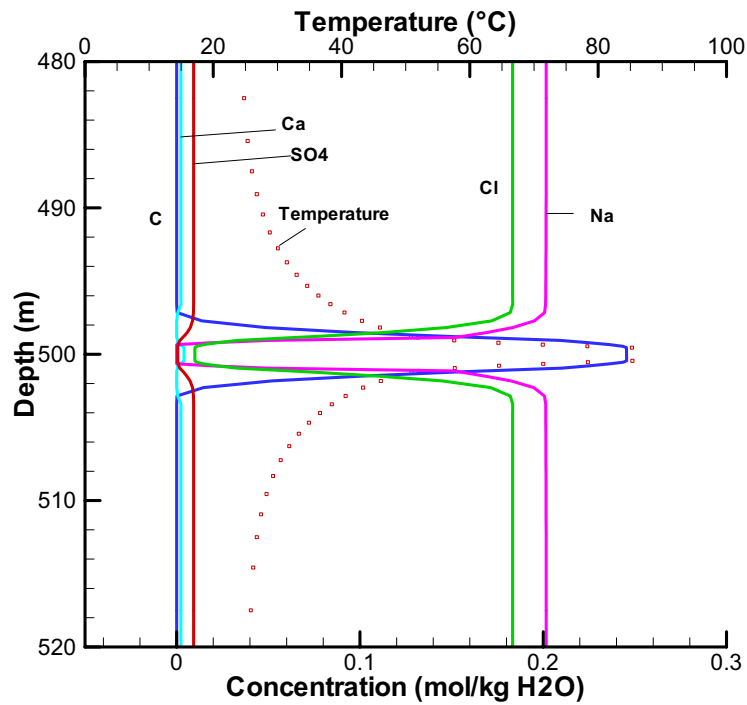
Figure 21: Vertical profile of aqueous species concentrations at 1 year

23
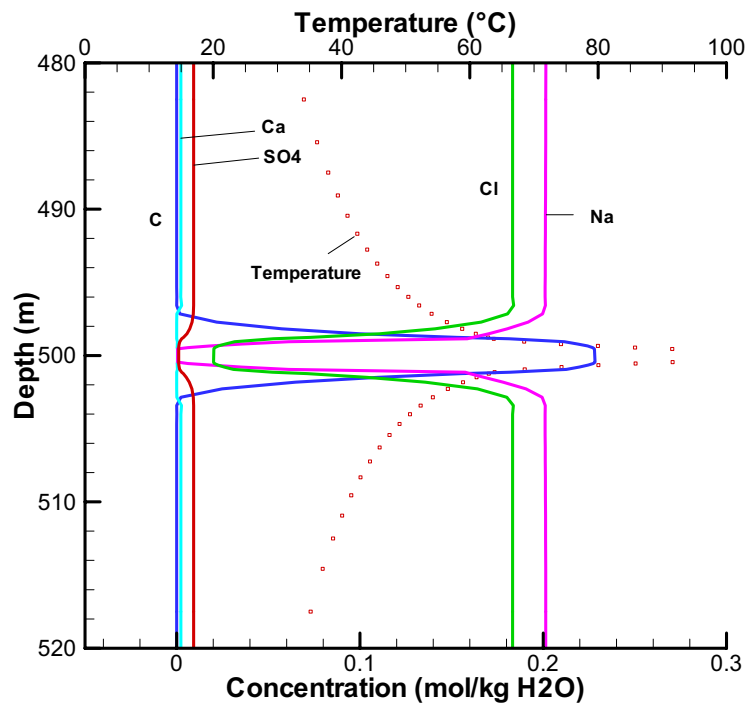
Figure 22: Vertical profile of aqueous species concentrations at 10 years
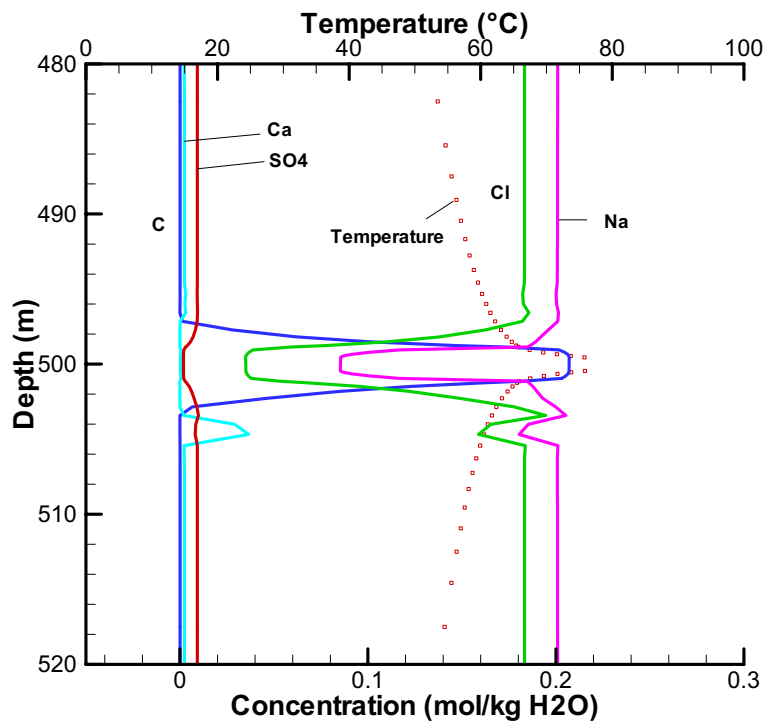
Figure 23: Vertical profile of aqueous species concentrations at 100 years

24
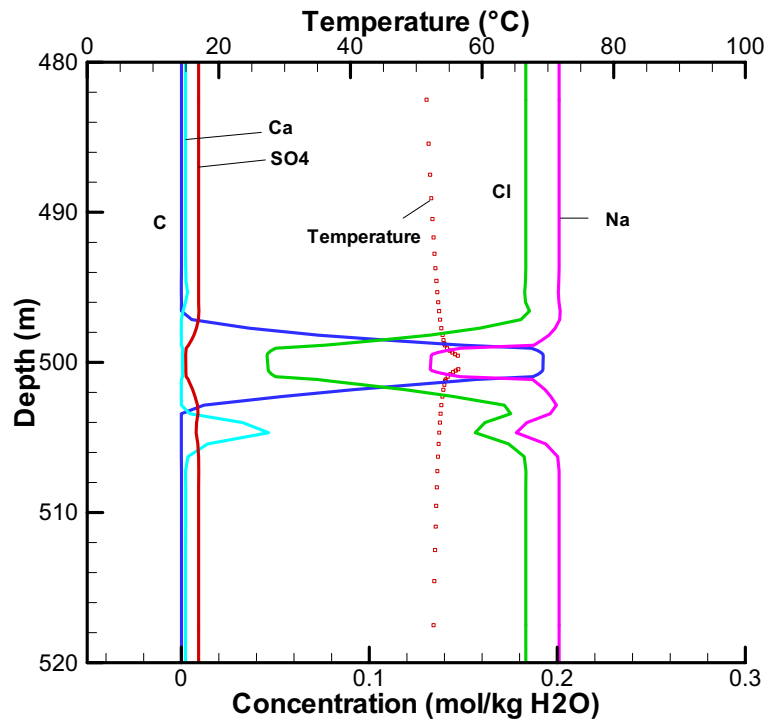
Figure 24: Vertical profile of aqueous species concentrations at 1000 years
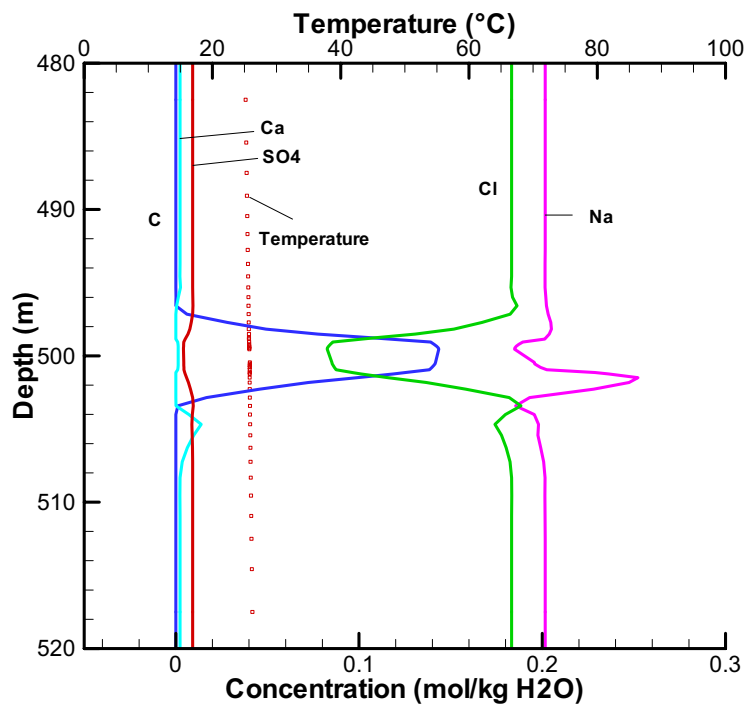
Figure 25: Vertical profile of aqueous species concentrations at 100,000 years

The mineral abundances along the vertical profile are shown in Figures 26, 27, 28, and 29. The minerals are also quite stable, and most of the dissolution or precipitation occurs in the adjacent area between two materials.
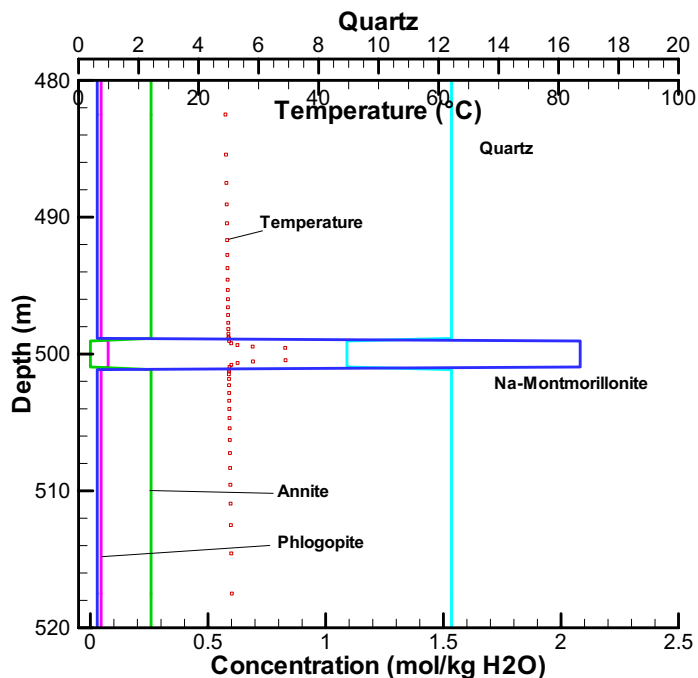
Figure 26: Vertical profile of mineral abundance at 0.001 year
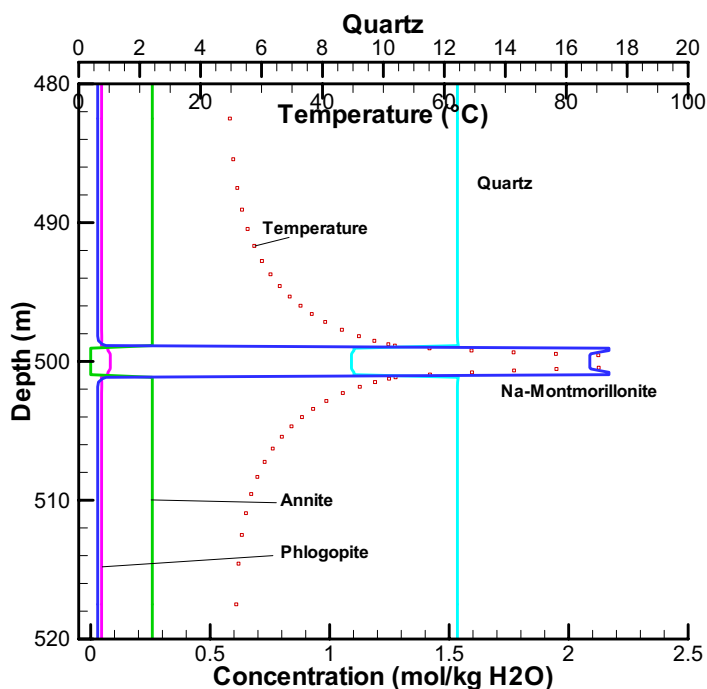
Figure 27: Vertical profile of mineral abundance at 1 year
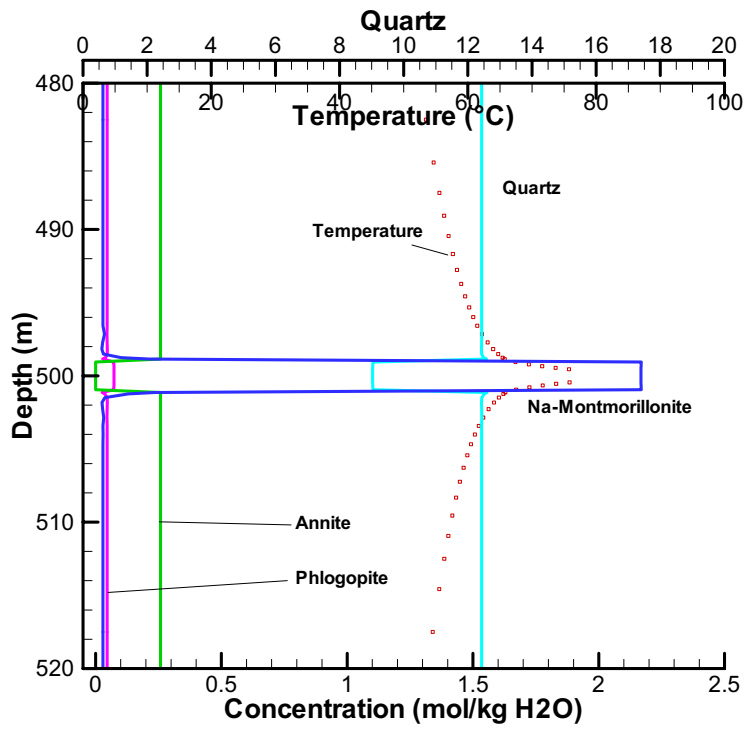
Figure 28: Vertical profile of mineral abundance at 100 years
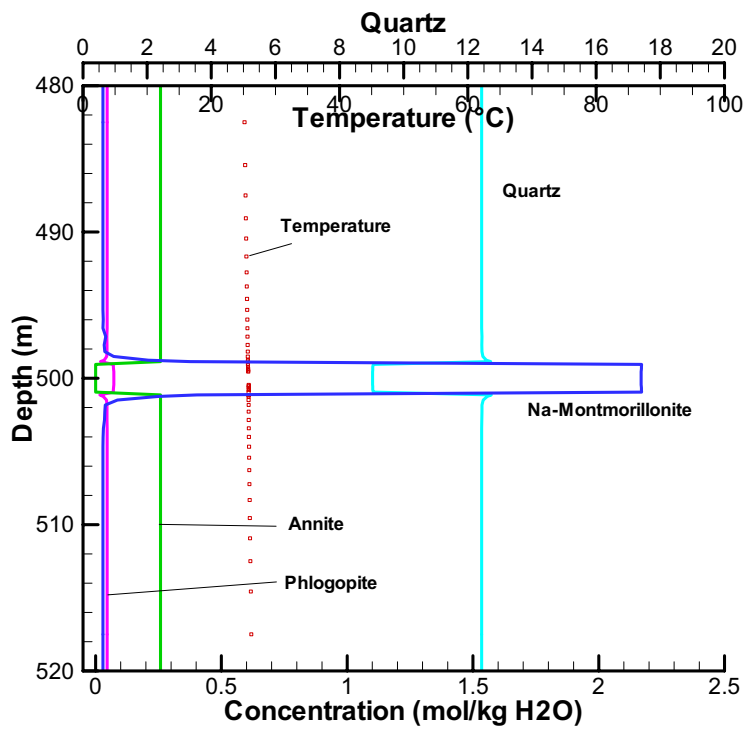
Figure 29: Vertical profile of mineral abundance at 100,000 years

The time evolution of minerals albite and K-feldspar at the observation points are illustrated in Figure 30 and Figure 31, respectively. There is no albite in the bentonite (Figure 30 point V1). Albite in granite dissolves over time, especially in the contact area (Figure 30 point V2) or near bentonite (Figure 30, Point V3). In the far field, there are little changes). K-feldspar in granite, however, precipitates with time at the observation points near the bentonite (Figure 31, Points V2, V3). K-feldspar in bentonite dissolves very quickly (Figure 31, Point V1).
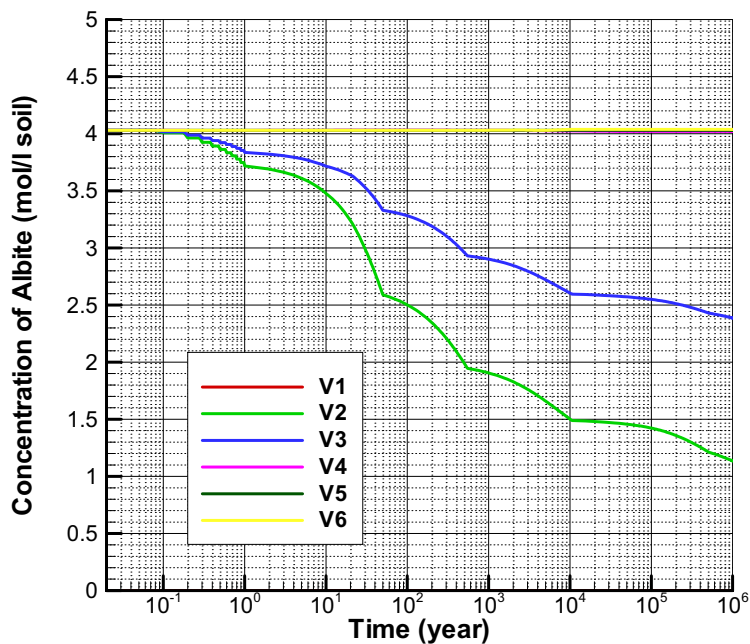
Figure 30: Evolution of mineral Albite
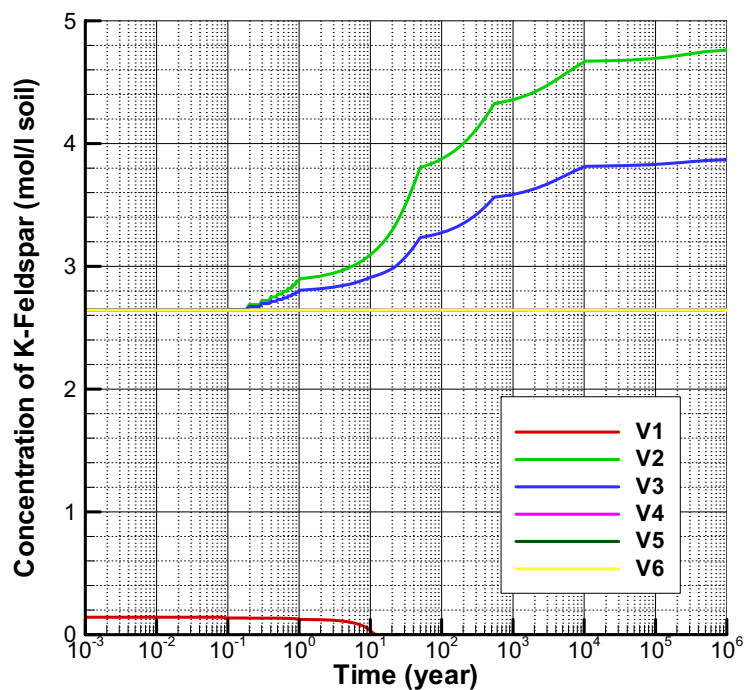
Figure 31: Evolution of mineral K-Feldspar

28

The time evolution of porosity owing to the dissolution/precipitation process can be seen in the Figures 32, 33 and 35. Changes also occur in the contact area, and the porosity of bentonite decreases. At earlier time, this change is much faster, because of the equilibrium assumption that no time-dependent geochemical reaction process is included.
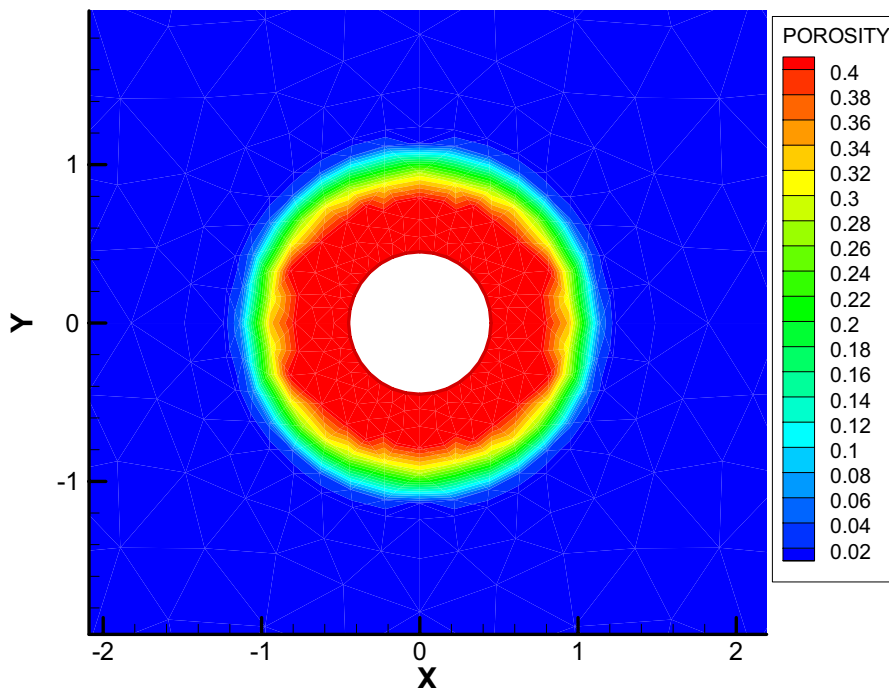
Figure 32: Porosity distribution at 0.001 year
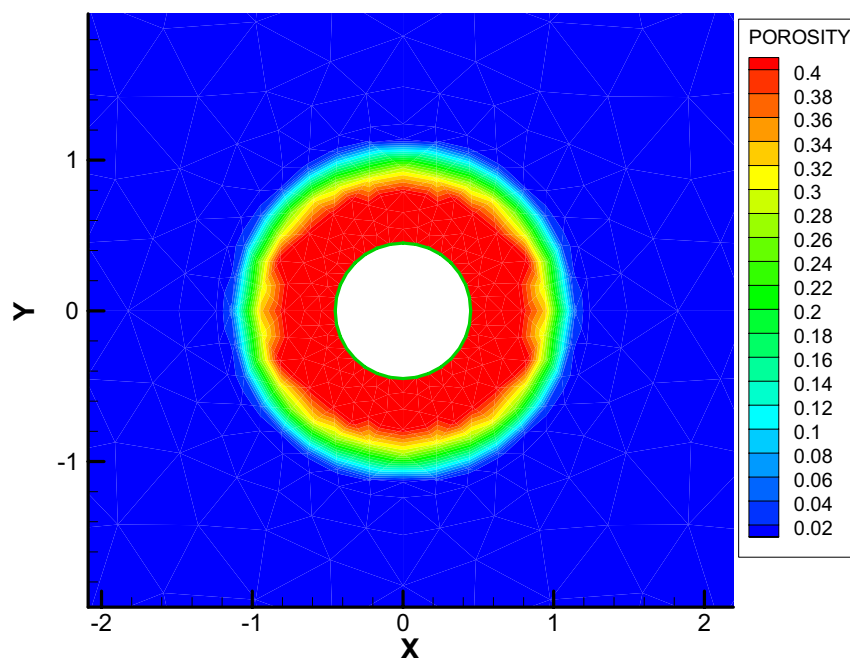
Figure 33: Porosity distribution at 100 years
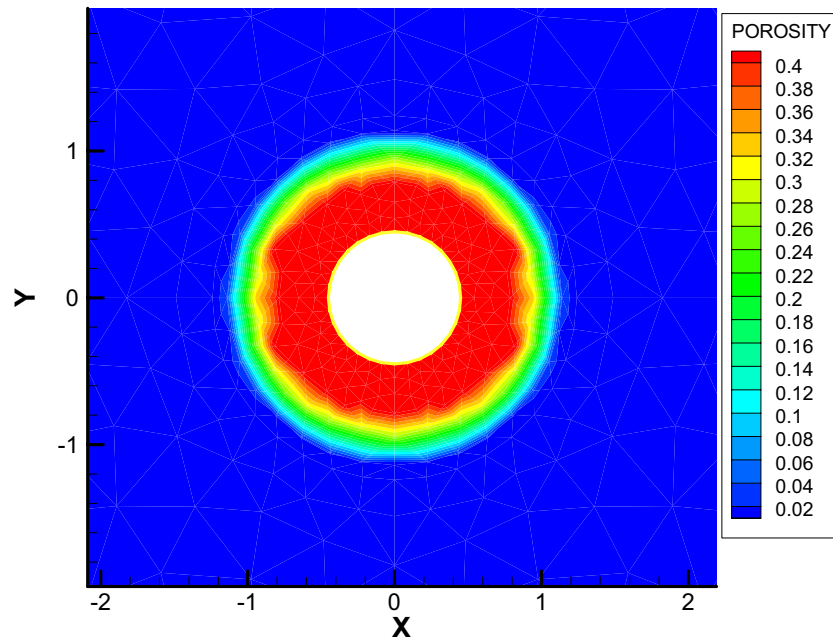
Figure 34: Porosity distribution at 100,000 years

The total effect of the mineral dissolution/precipitation can be seen from the vertical profiles of mineral abundance at different time in Figures 35, 36, 37 and 38.
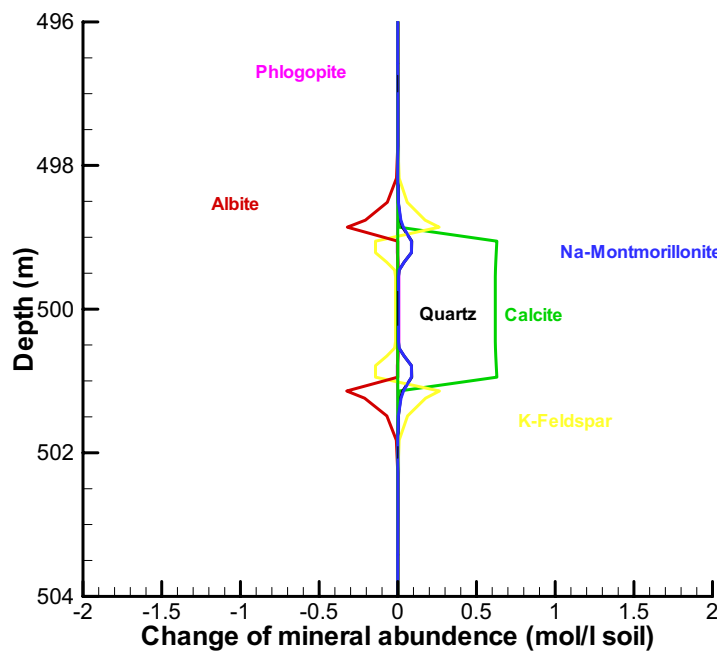
Figure 35: Vertical profile of mineral abundance at 1 year
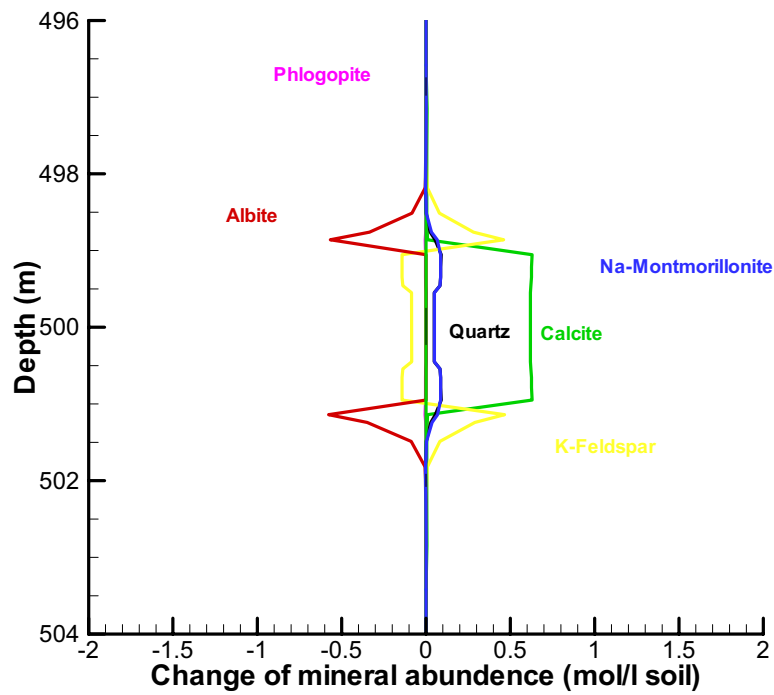
Figure 36: Vertical profile of mineral abundance at 10 years
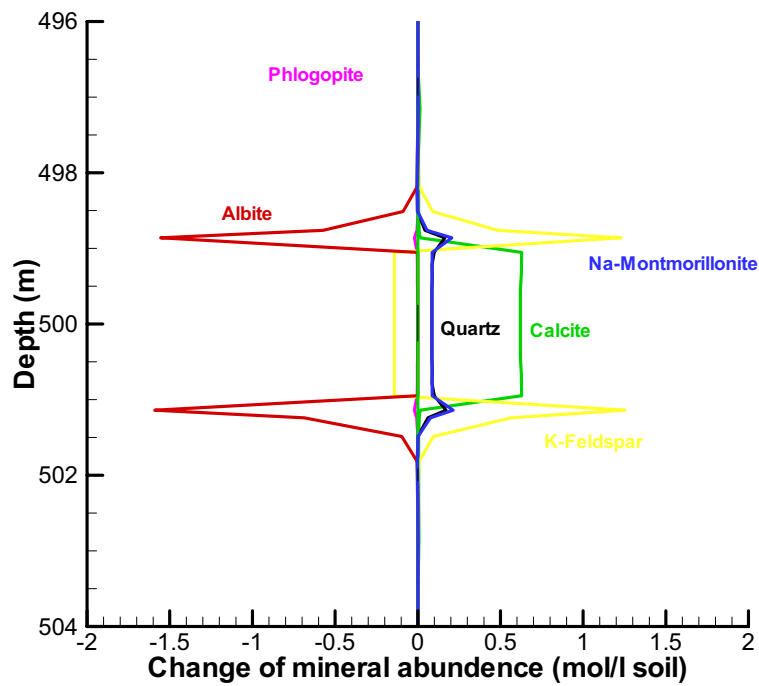
Figure 37: Vertical profile of mineral abundance at 100 years
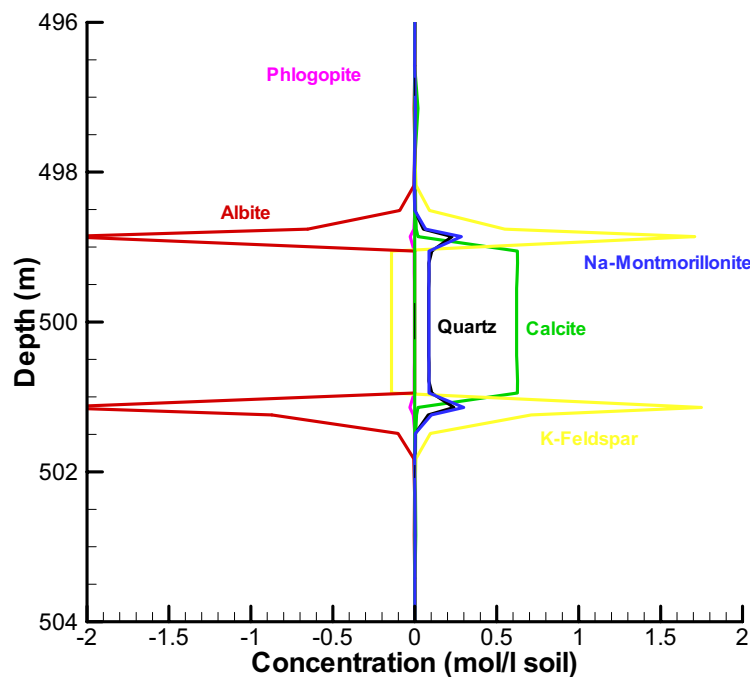
Figure 38: Vertical profile of mineral abundance at 1000 years

4. SUMMARY AND OUTLOOK

The nonisothermal reactive transport model of the object-oriented simulator GeoSys/RockFlow, which is able to simulate nonisothermal unsaturated flow and geochemical reactions through coupling to the geochemical reaction simulator PHREEQC2, is applied to simulate the DECOVALEX Task D_THC1 for the FEBEX-type repository (2D non-isothermal reactive transport in Case 1; [saturated] and Case 2; [unsaturated]). In the latter case, partially saturated bentonite was subjected to simultaneous heating by the canister and hydration with granite pore-water. The determination of reasonable reactions is essential for the simulation; the determination of the possible reactions can be reached using the initial chemical and mineral data and simple geochemical modelling (for example, by PHREEQC2).

Temperature affects not only multi-phase flow but also geochemical reactions. Especially at the initial stages, it was observed that the sample dried (due to evaporation) at the heated end where pore water from the formation had not yet arrived. Consequently, capillary pressure increased at the heated end, enhancing the flow rate. The effect on chemical reactions was also observed in the simulation. Changing the temperature caused variation of ionic concentrations in bentonite pore-water. Dissolution/precipetation of solid minerals is also closely related to the temperature change.

The swelling effect is an important phenomenon in bentonite. Under constrained conditions, effective porosity, and thus the effective permeability of the bentonite, will change. The swelling potential can also be influenced by variation in the chemical composition. But during this inception phase, such effects have not been included in the model.

32

ACKNOWLDGEMENT

BIBLIOGRAPHY

ASTM International, 2001a. Standard Test Method for Methylene Blue Index of Clay, C837-99. Ch. In: Book of standards, Volume:15.02.

ASTM International, 2001b. Standard Test Method for Precipitated Silica-Surface Area by Single B.E.T. Nitrogen Adsorption, D5604-96. Ch. In: Book of standards, Volume:09.01.

Barr, D., Birkholzer, J., Rutqvist, J., Sonnenthal, E., 2004. Draft description for DECOVALEX-THMC TASK D: long-term permeability/porosity changes in the EDZ and near field, due to THM and THC processes in volcanic and crystalline-bentonite systems. Tech. rep., Office of Repository Development, U.S. Dept. of Energy, and Earth Sciences Division, LBNL, USA.

Bauer, S., Xie, M., Kolditz, O., 2004. Prozess - Orientierung und objektorientierte Programmentwicklung für Mehrkomponenten-Transportmodelle im Grundwasser. In: Luckner, L. (Ed.), Modellierung und Prognose von NA und ENA-Prozessen, BMBF-Statusseminar des TV7. Dresden.

Berg, R., 1970. Method of determining permeability from reservior rock properties. Gulf Coast Assoc Geol Soc Trans 20, 303-317.

Bloch, S., 1991. Empirical prediction of porosity and permeability in sandstones. American Association of Petroleum Geologists Bulletin 75 (7), 1145-1160.

Bradbury, M., Baeyens, B., 2003. Porewater chemistry in compacted re-saturated MX-80 bentonite. J Contam. Hydrol. 61 (1-4), 329-338.

Dzombak, D., Morel, F., 1990. Surface Complexation Modelling; Hydrous Ferric Oxide. Wiley-Interscience, New York.

FEBEX Working groups, 2000. Full-scale engineered barriers experiment for a deep geological repository for high level radioactive waste in crystalline host rock. Final report.

Gawin, D., Baggio, P., Schrefler, B. A., 1995. Coupled heat, water and gas flow in deformable porous media. Int. J. Num. Meth. Fluids 20, 969-987.

Gens, A., Garcia-Molina, A. J., Olivella, S., Alonso, E. E., Huertas, F., 1998. Analysis of a full scale in situ test simulating repository conditions. International Journal for Numerical and Analytical Methods in Geomechanics 22, 515-548.

Helmig, R., 1997. Multiphase Flow and Transport Processes in the Subsurface. Springer, Berlin.

Kolditz, O., 2002. Computational Methods in Environmental Fluid Mechanics. Springer.

Lenhard, R. J., Parker, J. C., 1987. A model for hysteretic constitutive relations governing multiphase flow, 2. permeability-saturation relations. Water Resources Research 23, 2197-2206.

Neuzil, C., 1994. How permeable are clays and shales? Water Resources Research 30 (2), 145-150.

Newman, A., 1987. The interaction of water with clay mineral surfaces. In: Chemistry of Clays and Clay Minerals. Vol. 6. Longman Scientific & Technical, Harslow, Essex, pp. 237-274.

Oelkers, E., 1996. Physical and chemical properties of rocks and fluids for chemical mass transport calculations. Vol. 34. Ch. 2 in Reactive Transport in Porous Media, Reviews in Mineralogy (Mineralogy Society of America),P.H.Ribbe (Series Editor), pp. 130-191.

Olivella, S., Gens, A., 2000. Vapour transport in low permeability unsaturated soils with capillary effects. Transport in Porous Media 40, 219-241.

Parkhurst, D., Appelo, C., 1999. User's guide to PHREEQC (Version 2) - A computer program for speciation, batch-reaction, one-dimensional transport, and inverse geochemical calculations. Report 99-4259, U.S. Geological Survey, Denver, Colorado.

Rutqvist, J., Börgesson, L., Chijimatsu, M., Kobayashi, A., Jing, L., Nguyen, T., Noorishad, J., Tsang, C.-F., 2001. Thermohydromechanics of partially saturated geological media: governing equations and formulation of four finite element models. International Journal of Rock Mechanics and Mining Sciences 38, 105-127.

Schoen, M., Rhykerd, C. L., Diestler, D., Cushman, J., September 1989. Shear forces in molecularly thin films. Science 245, 1223-1225.

Stumm, W., Morgan, J. J., 1996. Aquatic Chemistry, third edition. John Wiley and Sons, New York.

US Bureau of Mines (Ed.), 1997. Dictionary of Mining, Mineral, and Related Terms, 2nd Edition. American Geological Institute.

van Genuchten, M. T., 1980. A closed-form equation for predicting the hydraulic conductivity of saturated soils. Soil Science Society of America Journal 44, 892-898.

Wang, W., Xie, M., Kolditz, O., Shao, H., Nowak, T., Kunz, H., 2005. Progress on THM analysis. DECOVALEX IV project, Task D Report.

Xie, M., Agus, S., Schanz, T., Kolditz, O., 2004. An upscaling method and numerical modelling of swelling/shrinking processes in compacted bentonite/sand mixtures. International Journal for Numerical and Analytical Methods in Geomechanics 28 (15), 1479-1502.

PHREEQC DATABASE FOR THC1 SIMULATION

```
SOLUTION_MASTER_SPECIES
#
#element        species alk     gfw_formula     element_gfw
#
H               H+      -1.0    H               1.008
H(1)            H+      -1.0    0.0
E               e-      0.0     0.0             0.0
O               H2O     0.0     O               16.0
O(-2)           H2O     0.0     0.0
Ca              Ca+2    0.0     Ca              40.08
Mg              Mg+2    0.0     Mg              24.312
Na              Na+     0.0     Na              22.9898
K               K+      0.0     K               39.102
Al              Al+3    0.0     Al              26.9815
Si              H4SiO4  0.0     SiO2            28.0843
Cl              Cl-     0.0     Cl              35.453
C               CO3-2   2.0     HCO3            12.0111
C(+4)           CO3-2   2.0     HCO3
Alkalinity      CO3-2   1.0     Ca0.5(CO3)0.5   50.05
S               SO4-2   0.0     SO4             32.064
S(6)            SO4-2   0.0     SO4
Ba      Ba+2            0.0     Ba              137.34
Sr      Sr+2            0.0     Sr              87.62
Tracer  Tracer          0.0     Tracer          1.0
Fe      Fe+2            0.0     Fe              55.847
Fe(+2)  Fe+2            0.0     Fe
Fe(+3)  Fe+3            -2.0    Fe
SOLUTION_SPECIES

H+ = H+
    log_k   0.0
    -gamma  9.0 0.0

e- = e-
    log_k   0.0

H2O = H2O
    log_k   0.0

Ca+2 = Ca+2
    log_k   0.0
    -gamma  5.0 0.1650

Mg+2 = Mg+2
    log_k   0.0
    -gamma  5.5 0.20

Na+ = Na+
    log_k   0.0
    -gamma  4.0 0.075

K+ = K+
    log_k   0.0
    -gamma  3.5 0.015

Al+3 = Al+3
    log_k   0.0
    -gamma  9.0 0.0
```

```
H4SiO4 = H4SiO4
    log_k   0.0

Cl- = Cl-
    log_k   0.0
    -gamma  3.5 0.015

CO3-2 = CO3-2
    log_k   0.0
    -gamma  5.4 0.0

SO4-2 = SO4-2
    log_k   0.0
    -gamma  5.0 -0.04

Fe+2 = Fe+2
        log_k           0.000
        -gamma    6.0000    0.0000


H2O = OH- + H+
    log_k   -14.0
    delta_h 13.362  kcal
    -analytic   -283.971    -0.05069842 13323.0 102.24447   -1119669.0
    -gamma  3.5 0.0

2 H2O = O2 + 4 H+ + 4 e-
    log_k   -86.08
    delta_h 134.79 kcal

2 H+ + 2 e- = H2
    log_k   -3.15
    delta_h -1.759

CO3-2 + H+ = HCO3-
    log_k   10.329
    delta_h -3.561  kcal
    -analytic   107.8871    0.03252849 -5151.79    -38.92561   563713.9
    -gamma  5.4 0.0

CO3-2 + 2 H+ = CO2 + H2O
    log_k   16.681
    delta_h -5.738  kcal
    -analytic   464.1965    0.09344813 -26986.16   -165.75951 2248628.9

SO4-2 + H+ = HSO4-
    log_k   1.988
    delta_h 3.85    kcal
    -analytic   -56.889 0.006473    2307.9 19.8858 0.0

Ca+2 + H2O = CaOH+ + H+
    log_k   -12.78

Ca+2 + CO3-2 = CaCO3
    log_k   3.224
    -analytic   -1228.732   -0.299440   35512.75    485.818
#   delta_h 3.545   kcal

Ca+2 + CO3-2 + H+ = CaHCO3+
    log_k   11.435
    delta_h -0.871  kcal
    -analytic   1317.0071   0.34546894 -39916.84   -517.70761 563713.9
    -gamma  5.4 0.0
```

```
Ca+2 + SO4-2 = CaSO4
    log_k   2.3
    delta_h 1.650   kcal


Mg+2 + H2O = MgOH+ + H+
    log_k   -11.44
    delta_h 15.952 kcal

Mg+2 + CO3-2 = MgCO3
    log_k   2.98
    delta_h 2.713   kcal
    -analytic   0.9910  0.00667

Mg+2 + H+ + CO3-2 = MgHCO3+
    log_k   11.399
    delta_h -2.771  kcal
    -analytic   48.6721 0.03252849  -2614.335   -18.00263   563713.9

Mg+2 + SO4-2 = MgSO4
    log_k   2.37
    delta_h 4.550   kcal

Na+ + H2O = NaOH + H+
    log_k   -14.18

Na+ + CO3-2 = NaCO3-
    log_k   1.27
    delta_h 8.910   kcal

Na+ + HCO3- = NaHCO3
    log_k   -0.25

Na+ + SO4-2 = NaSO4-
    log_k   0.7
    delta_h 1.120   kcal

K+ + H2O = KOH + H+
    log_k   -14.46

K+ + SO4-2 = KSO4-
    log_k   0.85
    delta_h 2.250   kcal


Al+3 + H2O = AlOH+2 + H+
    log_k   -5.0
    delta_h 11.49   kcal
    -analytic   -38.253 0.0 -656.27 14.327

Al+3 + 2 H2O = Al(OH)2+ + 2 H+
    log_k   -10.1
    delta_h 26.90   kcal
    -analytic   88.50   0.0 -9391.6 -27.121

Al+3 + 3 H2O = Al(OH)3 + 3 H+
    log_k   -16.9
    delta_h 39.89   kcal
    -analytic   226.374 0.0 -18247.8    -73.597

Al+3 + 4 H2O = Al(OH)4- + 4 H+
    log_k   -22.7
```

```
    delta_h 42.30    kcal
    -analytic    51.578   0.0 -11168.9    -14.865

Al+3 + SO4-2 = AlSO4+
    log_k    3.5
    delta_h 2.29 kcal

Al+3 + 2SO4-2 = Al(SO4)2-
    log_k    5.0
    delta_h 3.11 kcal

H4SiO4 = H3SiO4- + H+
        log_k   -9.929
        delta_h 8.935    kcal
        -gamma   4       0
        -analytical 6.368      -0.016346  -3405.9

Ba+2 = Ba+2
        log_k          0.000
        -gamma   5.0000    0.0000

Sr+2 = Sr+2
        log_k          0.000
        -gamma   5.2600    0.1210

HS- = S-2 + H+
        log_k          -12.918
        delta_h 12.1    kcal
        -gamma   5.0000    0.0000

SO4-2 + 9 H+ + 8 e- = HS- + 4 H2O
        log_k          33.65
        delta_h -60.140 kcal
        -gamma   3.5000    0.0000

HS- + H+ = H2S
        log_k          6.994
        delta_h -5.300   kcal
        -analytical  -11.17   0.02386  3279.0

Tracer = Tracer
        log_k          0.0

Fe+2 + H2O = FeOH+ + H+
        log_k          -9.500
        delta_h 13.200   kcal

Fe+2 + Cl- = FeCl+
        log_k          0.140

Fe+2 + CO3-2 = FeCO3
        log_k          4.380

Fe+2 + HCO3- = FeHCO3+
        log_k          2.0

Fe+2 + SO4-2 = FeSO4
        log_k          2.250
        delta_h 3.230    kcal

Fe+2 + HSO4- = FeHSO4+
        log_k          1.08
```

```
Fe+2 + 2HS- = Fe(HS)2
        log_k           8.95

Fe+2 + 3HS- = Fe(HS)3-
        log_k           10.987


Fe+2 = Fe+3 + e-
        log_k           -13.020
        delta_h 9.680   kcal
        -gamma    9.0000    0.0000

Fe+3 + H2O = FeOH+2 + H+
        log_k           -2.19
        delta_h 10.4    kcal

Fe+3 + 2 H2O = Fe(OH)2+ + 2 H+
        log_k           -5.67
        delta_h 17.1    kcal

Fe+3 + 3 H2O = Fe(OH)3 + 3 H+
        log_k           -12.56
        delta_h 24.8    kcal

Fe+3 + 4 H2O = Fe(OH)4- + 4 H+
        log_k           -21.6
        delta_h 31.9    kcal

2 Fe+3 + 2 H2O = Fe2(OH)2+4 + 2 H+
        log_k           -2.95
        delta_h 13.5    kcal

3 Fe+3 + 4 H2O = Fe3(OH)4+5 + 4 H+
        log_k           -6.3
        delta_h 14.3    kcal

Fe+3 + Cl- = FeCl+2
        log_k           1.48
        delta_h 5.6     kcal

Fe+3 + 2 Cl- = FeCl2+
        log_k           2.13

Fe+3 + 3 Cl- = FeCl3
        log_k           1.13

Fe+3 + SO4-2 = FeSO4+
        log_k           4.04
        delta_h 3.91    kcal

Fe+3 + HSO4- = FeHSO4+2
        log_k           2.48

Fe+3 + 2 SO4-2 = Fe(SO4)2-
        log_k           5.38
        delta_h 4.60              kcal

PHASES

Calcite
    CaCO3 = HCO3- + Ca+2 - H+
        log_k     1.8490
        delta_h   -24.5095
```

```
        -a_e   -6.401940E+01 -4.546451E-02 -2.312471E+03  3.266939E+01
5.637139E+05


Dolomite
    CaMg(CO3)2 = Ca+2 + Mg+2 + 2 CO3-2
    log_k   2.5135
    -analytic  -1.89E+03   -2.99E-01   1.06E+05    6.85E+02    -6.12E+06

Gypsum
    CaSO4:2H2O = Ca+2 + SO4-2 + 2 H2O
    log_k   -4.58
    delta_h -0.109 kcal
    -analytic   68.2401 0.0 -3221.51    -25.0627

Quartz
    SiO2 + 2 H2O = H4SiO4
    log_k   -3.98
    delta_h  5.990 kcal
#   -analytic   0.41    0.0 -1309.0 # Better for St.Paul:
    -analytic   1.8810  -0.00203 -1560.0


Pyrite
        FeS2 + 2 H+ + 2 e- = Fe+2 + 2 HS-
        log_k           -18.479
        delta_h 11.300 kcal

Albite
    NaAlSi3O8 + 8 H2O = Na+ + Al(OH)4- + 3 H4SiO4
    log_k   -18.002
    delta_h 25.896 kcal
    # David L. et al, 1999

K-feldspar
        KAlSi3O8 + 8 H2O = K+ + Al(OH)4- + 3 H4SiO4
        log_k           -20.573
        delta_h 30.820  kcal

Annite
    KFe3AlSi3O10(OH)2 + 10 H+ = K+ + 3 Fe+2 + Al+3 + 3 H4SiO4
    log_k       29.5523
    -analytic -3.12E+03   -4.31E-01   1.95E+05    1.11E+03    -1.11E+07

Phlogopite
    KAlMg3Si3O10(OH)2 + 10 H+ = K+ + Al+3 + 3 Mg+2 + 3 H4SiO4
    log_k       37.5250
    -analytic -3.21E+03   -4.39E-01   2.02E+05    1.14E+03    -1.13E+07

Na-Montmorillonite
    Na0.33Mg0.33Al1.67Si4O10(OH)2 + 6 H+ + 4 H2O = 0.33 Na+ + 0.33 Mg+2 +
1.67 Al+3 + 4 H4SiO4
    log_k   2.4583
    -analytic -3.05E+03   -4.06E-01   1.89E+05    1.08E+03    -1.18E+07
```